THE RELATIONSHIP BETWEEN ACTIVE FAULTING AND FLUVIAL GEOMORPHOLOGY: A CASE STUDY IN THE GEDIZ GRABEN, TURKEY.

by

EMIKO JANE KENT

A thesis submitted to Plymouth University

in partial fulfilment for the degree of

DOCTOR OF PHILOSOPHY

School of Geography, Earth and Environmental Science

Faculty of Science and the Environment

October 2015

ABSTRACT

THE RELATIONSHIP BETWEEN ACTIVE FAULTING AND FLUVIAL GEOMORPHOLOGY: A CASE STUDY IN THE GEDIZ GRABEN, TURKEY.

EMIKO JANE KENT

Identifying tectonically active faults and quantifying rates of movement is a key challenge in the Earth Sciences, in addition to this the interactions between active faulting and the landscape, specifically involving the fluvial network, is a relatively new area of study. Previous work has highlighted the value of understanding how the fluvial network responds to active tectonics, showing that a comprehensive understanding of the dynamic relationship between fluvial geomorphology and active tectonics is an important next step in geological research.

This study presents new information about the poorly constrained Quaternary tectonic history of the Gediz Graben, Turkey, providing the first quantification of rates of movement of the key fault array that presently controlling graben topography. The fluvial network has been investigated and the data has been used in order to add resolution to the tectonic history for the fault array, allowing for the quantification of post-linkage throw rates. The study then investigates the key controls on the behaviour of the fluvial network that cross the active topography building fault array in the Gediz Graben.

This study shows that there has been a linkage event occurring between 0.6 – 1 Ma, involving the three segments of the graben bounding fault array. The pre- and post-linkage throw rates are then extrapolated using data derived from the fluvial network, showing a faulting enhancement factor of 3 at the centre of the fault array, with the throw rate at the centre of the array predicted

to have increased from a pre-linkage rate of 0.6 ± 0.1 mm/yr to a rate of 2 ± 0.2 mm/yr. This research provides evidence that the fluvial network can be used in conjunction with other types of evidence to provide a greater resolution tectonic history.

Using both digital data and field studies this research presents an examination of the factors that influence the behaviour of bedrock rivers undergoing perturbation due to tectonics. Factors such as drainage area, tectonic throw rates and lithology have been investigated and the complicated interactions of these variables with the fluvial system have been quantified.

This study shows that the bedrock rivers are a significant source of information about tectonics, but further work is needed to resolve quantitatively how various factors influence how rivers adjust to tectonic perturbation, in a variety of tectonic situations, in order to enable river to be used as a primary tool for deriving information about tectonics.

.

TABLE OF CONTENTS

LIST OF FIGURES AND TABLES

TABLES

ACKNOWLEDGEMENTS

I owe a massive thank you to many people who have helped and supported my during my research at Plymouth University. I firstly need to thank my supervisory team for their support, encouragement, and inspiration throughout my PhD. I would like to say thank you to my director of studies, Dr Sarah Boulton, who has always been encouraging and supportive. Sarah has worked with me to, guiding me through the PhD process, while encouraging me to develop my thesis in a way that best suits my interests. She have been pivotal in helping me achieve my goals, and was always willing and available to talk about my ideas for my studies, and how best to develop them. In addition to this Sarah offered valuable emotional support during my years of study, and encouraged me when I felt disheartened.

Thanks also go to Professor Iain Stewart for his ability to find the best in any situation and help me see through my occasional stresses. Iains knowledge of faulting dynamics has led to some extensive and interesting conversations, helping me to develop my ideas. Thank you for always being interested in how I am feeling, and being willing to chat about it.

I owe many thanks to Dr Alex Whittaker and his exhaustive knowledge of fluvial geomorphology, I have learn a lot from him during my study. His thorough reviews of my work and enthusiastic discussions have been both incredibly helpful and inspiring. I must thank him for all of the extensive phone conversations we have had about my work and ideas, his guidance and knowledge has be pivotal in the success of my studies.

Thanks also to Prof. Cihat Alçiçek, for his advice on all aspect of Turkish geology. Cihats assistance in the field was very constructive, and he was always willing to help, be it with terrace mapping, OSL sampling, or measuring rivers in the field, he was enthusiastic without fail. His prompt feedback on my work was always insightful and helpful. I would also like to thank Chiat and his family, Hülya and Melis for their hospitality during my field work, they made me feel like one of the family.

There are many more people who have helped me to complete my studies. My PhD was funding was provided by Plymouth University, without which this research project would not have been possible. The Geology department has always been an enjoyable and friendly place to work, everybody is willing to help and support others. Sally Greenwood provided much practical support during my time at Plymouth University, she could always answer my questions about the day to day workings of the department and university. Shaun Lewin deserves many thanks for helping me to master aspects of ARC map, and dealing with my steep learning curve, I always had a lot of questions! He was always available to help in solving my sometimes,

seemingly endless computing problems. I would also like to thank Dr Jean-Luc Schwenninger for all his assistance with my OSL samples.

Thank you to Emre Esser and Emre Tuncel who helped me in the field with enthusiasm and kindness. Emre Esser patiently taught me to drive on Turkish roads, which were fairly intimidating to someone who has just passed their driving test. Thanks also to Emre Tuncel who helped with the driving and field studies and was very friendly and helpful.

I own a huge thank you to all my friends from the department, for always being sociable, friendly and supportive during my years at Plymouth University. Special thanks go to Madeleine who seemingly always knew when I felt like having a tea break, and shared my preference for ‘proper’ ice-cream breaks in the summers. I enjoyed sharing my office at various times over the years with Ahmed Omer, Waleed Hamed, Matt Meyer and Mohammed Chaanda. Thank you for the support and friendship during our shared experience.

I also need to say thank you to my mother and grandfather, who have always provided me with the support I have need and have always believed in me. My final huge thank you is for Sean, who has supported me in so many vital ways throughout these last few years. In particular while I have been writing up he has listening to my stress and worries, and encouraged me when it was getting me down.

AUTHOR'S DECLARATION

At no time during the registration for the degree of Doctor of Philosophy has the author been registered for any other University. Work submitted for this research degree at the Plymouth University has not formed part of any other degree either at Plymouth University or at another establishment.

This study was financed with the aid of a studentship form Plymouth University.

Relevant scientific seminars and conferences have been regularly attended during the course of this research and findings have been presented at conferences in the form of oral and poster presentations. Two manuscripts were prepared for publication.

During this research a number of awards were made to aid fieldwork, conference attendance and sample analysis:

- A travel grant of £200 from SOGES, Plymouth University for conference attendance.
- The Quaternary Research Association-RLAHA Luminescence Dating for up to 6 OSL dates, awarded 2013.
- £960 from the British society for Geomorphology postgraduate research award to fund a field season in Turkey.
- British society for Geomorphology postgraduate conference funding.

Presentation and Conferences Attended:

- Geological Society of London Frontiers Meetings: The Coupling Between Tectonics and Surface Processes (Geological Society of London, London). October 2011, **ATTENDANCE ONLY**.
- CRES Postgraduate annual conference, Plymouth, UK. November 2012. **ORAL PRESENTATION.**
- Tectonic Studies Group Annual Meeting (Edinburgh) January 2012 **ATTENDANCE ONLY**.
- CRES Postgraduate annual conference, Plymouth, UK. Session chair. November 2012 **ORAL PRESENTATION.**
- International Earth Science Colloquium on the Aegean Region (Dokuz Eylül University, Izmir, Turkey). October 2012, **POSTER PRESENTATION**
- British Society for Geomorphology 2013 Annual Conference (Royal Holloway University of London). September 2013. **ORAL PRESENTATION**

- Centre for Research in Earth Sciences (CRES), Plymouth, UK. Research seminar. February 2013. **ORAL PRESENTATION**.

External Contacts:

Dr Jean-Luc Schwenninger
Research Fellow, Luminescence Dating Research Laboratory for Archaeology and the History of Art
School of Geography and the Environment
University of Oxford
OUCE / Dyson Perrins Building
South Parks Road
Oxford, OX1 3QY

Word count of main body of thesis: 73,874

CHAPTER 1

INTRODUCTION

1.1: RATIONAL

Bedrock rivers originate in high altitude areas and typically incise into the underlying bedrock, exerting a fundamental control on landscape evolution in mountain catchments. They can set hill slope gradients, erode the landscape, control mass-wasting and transport material away from areas of high elevation, all of which significantly impacts upon topographic relief (Howard and Kerby, 1983; Howard et al., 1994; Tucker and Bras, 1998; Tucker and Whipple, 2002; Whittaker et al., 2007). Furthermore, bedrock rivers determine the distribution of mountain topographic relief and exhibit evidence of base level lowering through their longitudinal profiles (e.g. Tucker and Whipple, 2002).

Technological advances mean that bedrock rivers have received significant attention during the last two decades (e.g. Howard and Kerby, 1983; Howard et al., 1994; Snyder et al., 2000; Tucker and Whipple, 2002; Finnegan et al., 2005; Whittaker et al., 2010; Attal et al., 2011; Whittaker, 2011). There has subsequently been a realisation that bedrock rivers respond to changes in tectonic boundary conditions, as well as lithological and climatic variations. Rivers can then propagate these changes in the boundary conditions to the surrounding landscape (Tucker and Whipple, 2002; Finnegan et al., 2005; Whittaker et al., 2007; Attal, 2008; Attal et al., 2011). For example, uplift of a mountain range by active normal faulting (or an increase in the uplift rate) can send a wave of incision up a bedrock river, due to an increase in the incision rate (Tucker and Whipple, 2002; Van Laningham et al., 2006; Harkins et al., 2007; Whittaker et al., 2010; Whittaker, 2011).

Since the link between rivers and boundary conditions has been well constrained, work has focused on quantifying the impact of external factors (such as active faulting) upon rivers and the surrounding landscape, and consequently a number of landscape evolution models have been developed (Braun and Sambridge, 1997; Tucker et al., 2001; Willgoose et al., 1991; Hancock et al., 2002; Whipple and Tucker, 2002; Willgoose, 2005; Van De Wiel et al., 2007; Taylor-Perron and Fagherazzi, 2012). Fluvial-driven erosion features heavily in these models because a significant consideration of the models is to parameterise fluvial incision effectively. To achieve this goal it is necessary to be able to predict how channel slope, geometry and discharge control energy expenditure and shear stresses on the bed, and therefore modulate bedrock erosion in time and space (Lavé and Avouac 2001; Duvall et al. 2004; Whittaker et al., 2007b, Whittaker et al., 2008; Allan et al., 2012; Whittaker and Boulton, 2012; Mudd et al., 2014).

Investigation of river incision can be approached through simplified fluvial erosion laws. These will ideally include a suitable treatment of channel geometry that impacts upon incisional capacity (Whittaker et al., 2007b, Attal et al., 2008). Stream power laws are the most frequently used type of fluvial erosion law and are integrated into landscape evolution models (see section 3.5) and are commonly used to investigate river responses to tectonic perturbation (e.g. Duvall et al., 2004; Whipple, 2004; Finnegan et al., 2005). The detachment-limited (or bedrock) incision model (see Section 3.2.1) that is now often used to examine mountain rivers assumes that fluvial incision is proportional to stream power, which in turn is dependent upon the discharge and geometry of the river (Howard and Kerby, 1983; Seidl and Dietrich, 1992; Whittaker et al., 2007a; Attal et al., 2008; Attal et al., 2011). These studies

suggest that bedrock rivers can be adequately described by a stream power model in many circumstances.

However, there have been studies where the results indicate that the modelling struggles to reproduce field measured river geometries. For example, Whittaker et al. (2007a) studied rivers within the Italian Apennines and found that traditionally accepted hydraulic scaling relationships used to predict channel width of bedrock rivers break down under tectonic perturbation. As a result actual stream power values were approximately four times higher than those predicted using accepted relationships.

Furthermore, a number of studies have highlighted how bedrock lithology (e.g. Miller, 1991; Hancock et al., 1999; Stock and Montgomery, 1999; Crosby and Whipple, 2006; Cook et al., 2009; Whittaker and Boulton, 2012) and sediment flux in the river (Sklar and Dietrich, 1998; Sklar and Dietrich, 2001; Cook et al., 2014) may have an impact on how fast a river incises to counteract uplift. This effect could however be difficult to resolve as these factors are in practice bundled together in bedrock fluvial calculations of geometry and stream power (see Section 3.2.1).

Therefore, this study addresses the issue of lithological impact on steam power. As without a more complete understanding of how lithology affects fluvial modelling, it is unlikely that the modelling techniques will adequately predict values in areas where there is complex and varying lithology. This thesis aims to deal explicitly with the impact of the individual components of the bundled erodibility coefficient often used, and evaluate the potential impact on fluvial modelling of bedrock rivers of treating these variables in this way. This study has been made possible by the geology of the Gediz Graben located in the Western Anatolian Extensional Province (WAEP), Turkey.

The WAEP is an area of continental extension, much like the more studied Basin and Range Province of North America. Rates of extension across the graben systems in the WAEP have been estimated using GPS measurements (Barka and Reilinger, 1997; Aktuğ et al., 2009); however, historical and geological rates of fault motion are poorly constrained at best. Although the sedimentary sequence and history of graben evolution have been well documented (e.g. Çiftçi and Bozkurt, 2009; Oner and Dilek, 2011).

The Gediz Graben was selected as the study area, over other well constrained locations, due to the range of bedrock lithologies exposed in the footwall block. The lithologic variation along the Gediz Graben means that the rivers that drain the Bozdağ Range incise through different lithologies and different amounts 'hard' to 'soft' lithologies along the range, from 100 – 4% harder lithologies. In most areas of the range it is usual for the rivers to incise though gneiss and schist in the upper reaches and clastic sediments further downstream. There is a significant difference in the hardness of these rock types, which is obvious upon cursory examination in the field. In some areas there are no clastic sediments in the catchment, and in some locations there is a far greater variation in the lithology, including travertine and quartzite. This provides an excellent opportunity to try examine the lesser-studied and more controversial aspects of incisional modelling such as lithological and sediment flux impacts on river geometry and stream powers.

This study will make a significant contribution to the consideration of the ability of modelling to predict how bedrock rivers react to throw rate changes depending on additional influencing factors. It will then be possible to evaluate how well the current modelling allows for prediction of fluvial dynamics, which impact upon landscape development. This will be the first research to consider

fluvial responses to the active tectonics in the Gediz Graben, and will be one of a relatively small number of studies that examine predictions of river behaviour against field data.

1.2: AIMS AND OBJECTIVES

The contents of this thesis can be divided into four work packages that can be developed and written up for publication as individual papers, and additional discussions of the published theory. It is intended that the review of published literature will outline the state of research at this time, giving an overview of the data available for the Gediz Graben, and a generic understanding of fluvial networks in mountain ranges. Each of the subsequent chapters can stand alone but will also build progressively into a body of research examining the active of faulting of the Gediz Graben and how the knowledge of fluvial geomorphology can build upon existing tectonic knowledge.

This study investigates how the Gediz rivers are responding to the tectonic activity, the role of additional factors such as lithology in the measured response of the rivers, and the implications of field data on the predictive methods commonly used in fluvial geomorphology. The research into the dynamic fluvial network is designed to initially add to the understanding of the active graben faulting and distribution of erosion throughout the graben-bounding range. Then, significantly this study aims to further enhance the understanding and quantification of variables influencing river geometry, and evaluates the impact on the perceived ability of models to predict the behaviour of bedrock rivers.

The overall objective of this study is to test the hypothesis that rivers respond to tectonic perturbation in more complex ways than standard fluvial

modelling can account for; and that these differences will be rooted in the dramatic simplification of the combined effects of climate, lithology and sediment flux, which are subsumed into one numerical parameter (K) in fluvial models of bedrock rivers.

The aims of this thesis can therefore be broken down into five main areas:

1. Quantify the rates of faulting in the Gediz Graben using published data geological and structural data.
2. Use knickpoint theory to add to the resolution of structurally derived information for the Gediz Graben.
3. Consider how the rivers can be used to gather information about the faulting of the Gediz Graben when integrated with structural data.
4. To investigate impact of faulting on the behaviour of the Gediz rivers using field study of 6 rivers.
5. To consider the implications of not explicitly treating factors such as lithology and sediment flux on fluvial modelling of bedrock rivers using bedrock rivers within the Gediz Graben as an example.

These overall aims will be met by the objectives set out for each of the research chapters.

Chapters 2 and 3 provide overviews of existing data. Chapter 2 focuses on the geological history of the Gediz Graben, providing an overview of the timings and events that are key in the geological history of the western Turkish graben system. The chapter then goes on to review what is known about the present

day geology of the graben, giving a detailed description of faulting and lithology based on existing research.

Chapter 3 reviews published research on fluvial networks and fluvial geomorphology, with a focus on bedrock rivers that incise through uplifting mountains. This chapter outlines what is known about how bedrock rivers incise through the landscape, particularly in response to tectonic perturbation. It also examines how the behaviours of such rivers are modelled.

Chapter 4 focuses on deriving long-term (2 myr) estimates of fault throw rate on the graben bounding fault array, as the tectonic history of the Gediz Graben margin is currently poorly constrained. Data on the sedimentary units that infill the graben, forming both syn- and post-tectonic sediment packages, have been combined with pre-existing structural mapping of the faulting in the graben margin and published seismic lines and boreholes to aid in the estimation of throw rates. These published studies are combined with topographic data derived from digital elevation models (DEM) to produce time averaged throw rates along the active graben bounding normal fault.

Chapter 4 key objectives

(i) Produce the first quantitative data for fault motion along the active graben bounding fault array in the form of time averaged throw rates.

(ii) Make an assessment of the history of the active fault array determining whether or not the fault array has been linked.

(iii) Evaluate seismic hazard for this region of Turkey.

Chapter 5 presents a study of the terraces along the rivers and provides new optically stimulated luminescence dates (OSL) for a terrace level along three

rivers. The data for the Gediz Graben terraces are used to quantify the rate of incision that can be compared to the time averaged throw rates in Chapter 4.

Chapter 5 key objectives

(i) Determine the timing of T4 terrace formation along the rivers of the Gediz Graben.
(ii) Quantify incision rates on the rivers based upon OLS dating of terraces.

Chapter 6 examines the behaviour of rivers crossing the active graben bounding fault array of the Gediz Graben using digital methods. This chapter examines to what extent the rivers can be used to reveal details about the active tectonics of the fault array. The long-profiles and morphology of the rivers are studied in order to identify knickpoints, which are used to analyse the linkage of the fault array and (by combing this information with throw rates from Chapter 4) provide a present day throw rate. The chapter then studies the rate of knickpoint retreat in terms of throw rate and drainage area and compares the Gediz data to other areas with similar published data.

Chapter 6 key objectives

(i) Extract river long-profiles from DEM data, identify explicitly whether the rivers are undergoing a transient response to active tectonics.
(ii) Estimate the timing of the linkage event occurring on the graben bounding normal faults using river geomorphology.
(iii) Quantify present day throw rates on the graben bounding normal fault using information from the rivers.

(iv) Evaluate to what extent the throw rates are affecting the migration of the knickpoints upstream.

Chapter 7 presents a field investigation into six rivers draining into the Gediz Graben, focusing on the hydraulic geometry and stream powers within the studied rivers. This chapter examines whether the frequently used hydraulic scaling method can accurately predict the widths of the Gediz rivers and what effect this has on using accepted methods to predict stream powers for those rivers. The chapter then deals explicitly with the relative influences of lithology and sediment flux in relation to the variations between the rivers, considering the implications for not dealing with these variables independently when modelling of bedrock rivers.

Chapter 7 key objectives

(i) Quantify stream powers on rivers crossing the graben bounding fault using field data.
(ii) Evaluate the predictive powers of models that calculate width and stream power downstream from digital elevation models using real (field) data.
(iii) Evaluate the impact of lithology and sediment flux on the stream powers of the rivers, examine how important explicit treatment of these variables is to modelling and determine the accuracy of available prediction methods.

Chapter 8 provides a synthesis of the data presented in the previous chapters, in order to address the overall project aims. The chapter will bring

together the different types of evidence to summarise what is now known about the geological evolution of the Gediz Graben.

In addition, the chapter will evaluate the implications of the testing of common modelling practice on the ability of models to predict the behaviour of rivers and how this affects landscape modelling. The later parts of chapter 8 suggest suitable directions for further work based upon the findings of this this thesis and presents overall conclusions.

CHAPTER 2

GEOLOGICAL BACKGROUND OF THE GEDIZ GRABEN

2.1: CHAPTER HIGHLIGHTS

- The Gediz Graben was initiated as a half graben with a low-angle detachment in the south of the graben from16 Ma until 4 Ma.
- Around 2.6-2 Ma the dominant style of faulting controlling graben topography switched to high-angle normal faulting, this type of faulting is still active.
- The basement rocks of the Menderes Massive have been exhumed in the graben margins and in the southern margin are separated from syn-tectonic graben fill by the low-angle detachment fault.
- The high-angle normal faults displace the syn-tectonic sediments that are mainly conglomerates and sandstones of Miocene to Pleistocene age.

2.2: INTRODUCTION

As documented in Chapter 1 this study into the dynamic relationship between tectonics and rivers uses the Gediz Graben as a natural laboratory. The Gediz Graben is located within the actively extending Western Anatolian Extensional Province (WAEP). This chapter serves to provide a background to the broad areas of interest when it comes to the expression of extensional tectonics. The chapter also includes a detailed geological synthesis of the structure and sedimentology of the Gediz Graben (the study location for this investigation) in order to document the pre-existing constraints on geological processes that make the Gediz Graben an ideal area to study the dynamic

landscape reaction to tectonics. This chapter reviews past studies and presents currently accepted ideas about the formation of the graben and its current stratigraphic and structural configuration.

2.3: THE WESTERN ANATOLIAN EXTENSIONAL PROVINCE

The WAEP is the location of the western Anatolian Graben systems important to this study. The landmass of Turkey is formed from several continental fragments detached from the African Plate during the Permo-Triassic by rifting (Okay, 2008). These fragmented terrains were separated by the Tethys Ocean and Paratethys Sea during most of the Phanerozoic (Rögl, 1999); relics of these oceans can be seen today as ophiolites and accretionary prisms scattered around the complex geology of Anatolia. The fragments were amalgamated and accreted onto the southern margin of the Eurasian Plate from the Late Cretaceous to the Neogene during the Alpine Orogeny (Yerli, 2005); resulting in suture zones in the Pontide and Tauride mountains (figure 2.1).

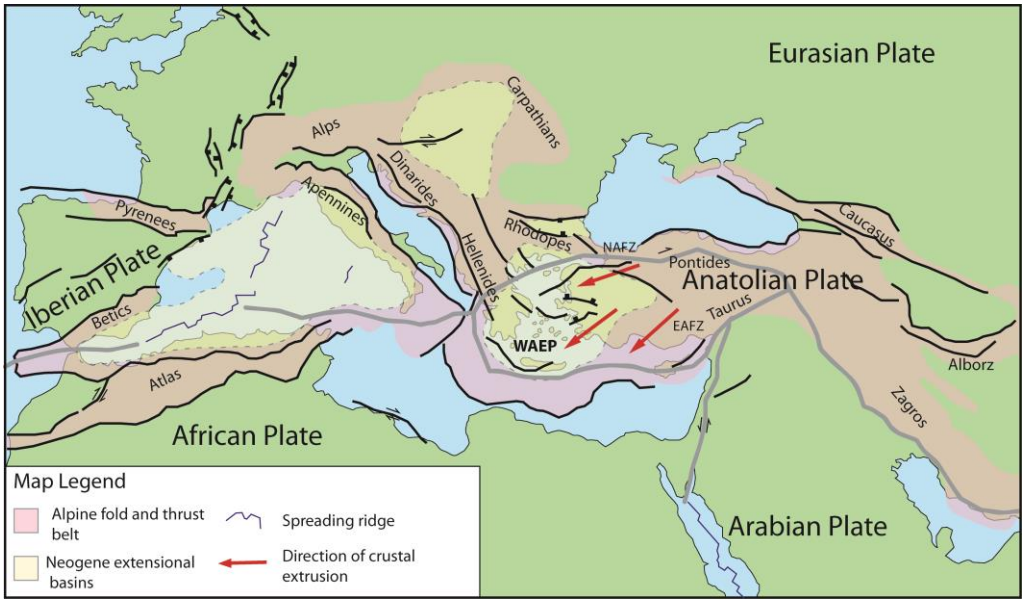

Figure 2.1: A map showing the extent of the Alpine fold and thrust belt. Areas of Neogene extension are highlighted along with significant mountain ranges. The Western Anatolian Extensional Province (WAEP) is highlighted and the direction of crustal extrusion of western Turkey is highlighted. NAFZ – North Anatolian fault zone. EAFZ – East Anatolian fault zone.

The tensional tectonics in the WAEP results from the switching of the Late Cenozoic collisional phase, to an extensional tectonic regime (Livermore and Smith, 1985). As a result, since the early Neogene western Turkey has been experiencing significant tectonic stretching over the WAEP (Sengor & Yılmaz 1981; Bozkurt & Mittwede 2001; Okay et al. 2001; Dilek & Pavlides 2006; Robertson & Mountrakis 2006; Ten Veen et al., 2009). The collisional forces led to anticlockwise extrusion of the Anatolian Plate to the west-south-west along the North Anatolian Fault Zone (NAFZ, figure 2.2) at a rate of approximately 20 mm/yr (figure 2.1, Westaway, 1994).

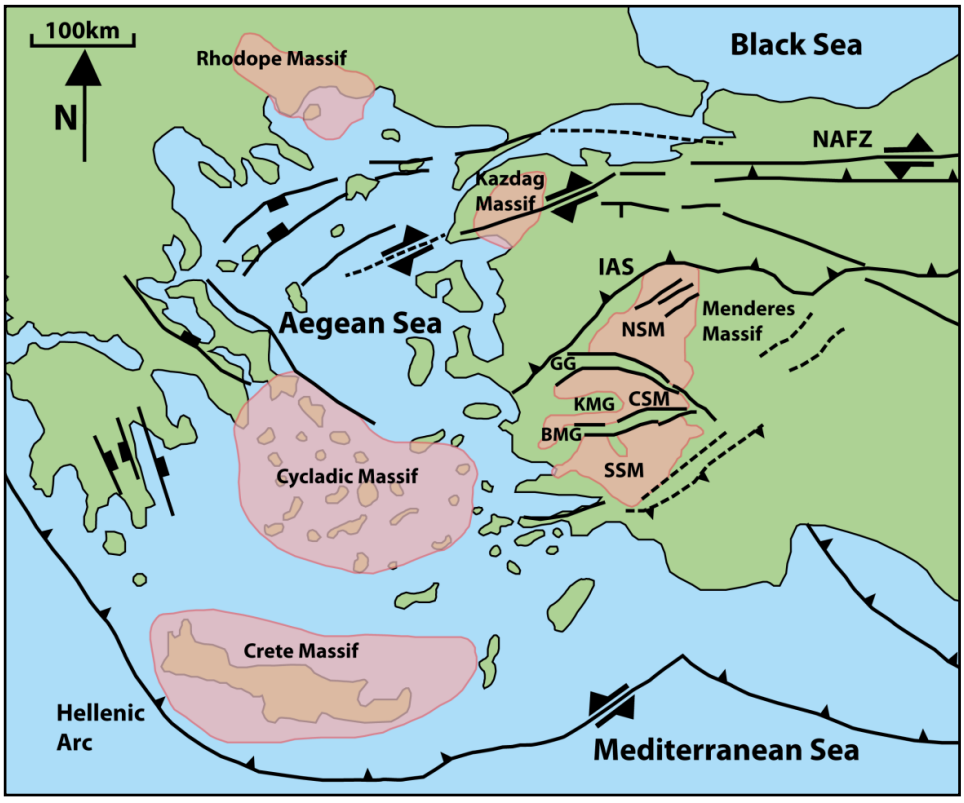

Figure 2.2: A map of the Aegean region showing the regional metamorphic massifs shaded in red. Sub-massifs of the Menders Massif: CSM – Central Menders Sub-massif; NSM – Northern Menders Sub-massif; SSM – Southern Menders Sub-massif. Grabens: BMG –Büyük Menderes Graben; GG – Gediz Graben; KMG – Küçük Menderes Graben. Fault zones: IAS – Izmir-Ankara suture; NAFZ – North Anatolian fault zone. Adapted from (Bozkurt 2003; Çemen et al., 2006).

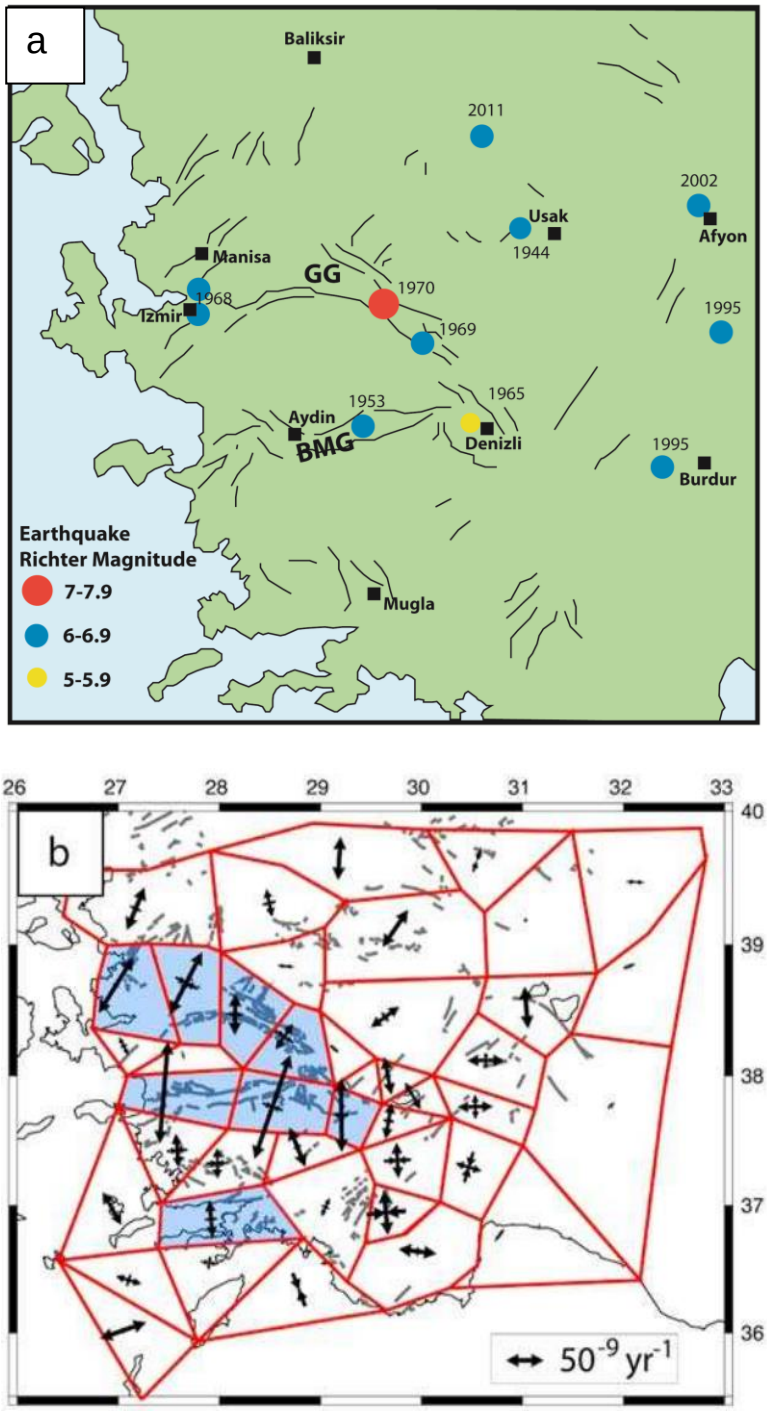

Figure 2.3: Tectonic data from the Gediz Graben A shows earthquakes above magnitude 5 occurring since 1950 in the Gediz Graben and surrounding area, three major earthquakes have occurred in the Gediz Graben (GG). Magnitude indicated by colour and size of dot. B shows the polygons used by Aktuğ et al. (2009), principle strain axes for each of the polygons are shown by arrows.

The extension and associated active faulting is still ongoing in the region and has led to significant historic earthquakes (Guidoboni et al., 1994; Guidoboni and Comastri, 2005) (figure 2.3). In 17 AD the Lydia earthquake caused extensive damage to the region, the city of Sardis, within the Gediz

Graben, was the most affected and suffered damage from which it never truly recovered (Guidoboni et al., 1994; Guidoboni and Comastri, 2005). Available historical records document up to fifteen towns and cities within the WAEP that were destroyed or damaged by the 17 AD earthquake, indicating widespread risk associated with earthquakes. The ancient city of Smyrna, near present day Izmir (figure 2.4), on the Aegean coast of Turkey was repeatedly destroyed by earthquakes (figure 2.3) including one in 2 AD and another in 178 AD (Guidoboni et al., 1994). Figure 2.5 shows the earthquakes above magnitude 5 between 1990 and 2010, there is a significant cluster in the extending area in western Turkey.

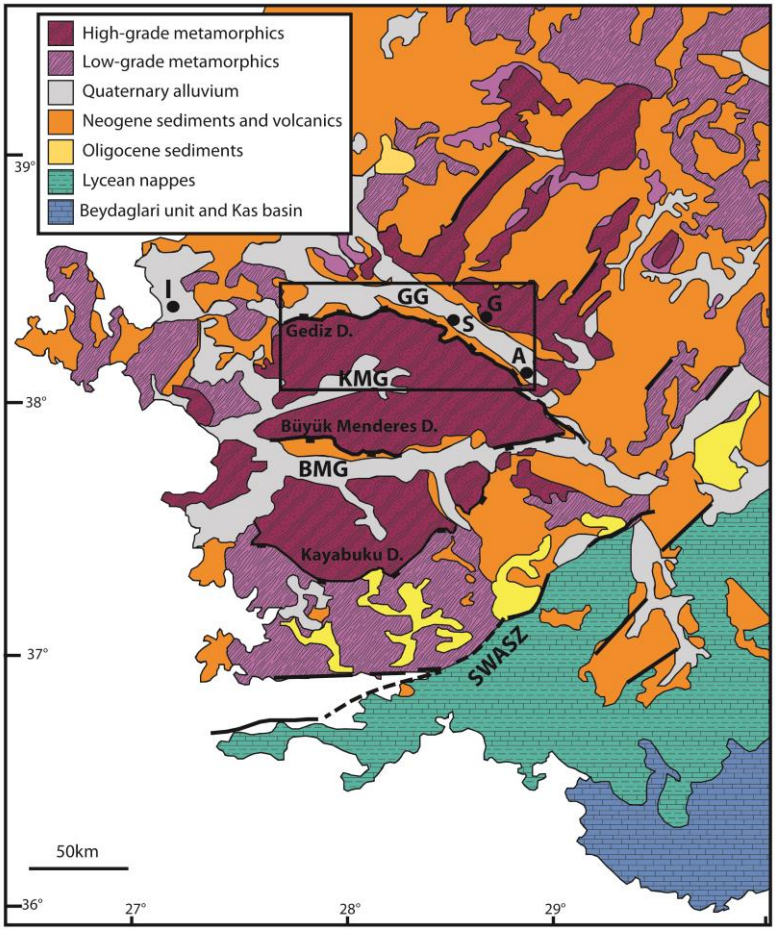

Figure 2.4: A map showing the regional geology of the extensional province in western Turkey. Grabens: BMG – Büyük Menderes Graben; GG – Gediz Graben; KMG – Küçük Menderes Graben. Locations mentioned in the text: A – Alaşehir; G – Gediz Village I – Izmir/Smyrna; S – Sardis. Adapted from Bozkurt, 2000; Bozkurt (2003); Çemen et al. (2006).

These recent and historical earthquakes illustrate that the WAEP is experiencing ongoing significant seismic activity (Bozkurt and Mittwede, 2005) (figure 2.5). As the region contains several towns and cities with populations between 50,000-150,000 this seismic hazard creates reasonable risk to the population centres as a result of active faulting.

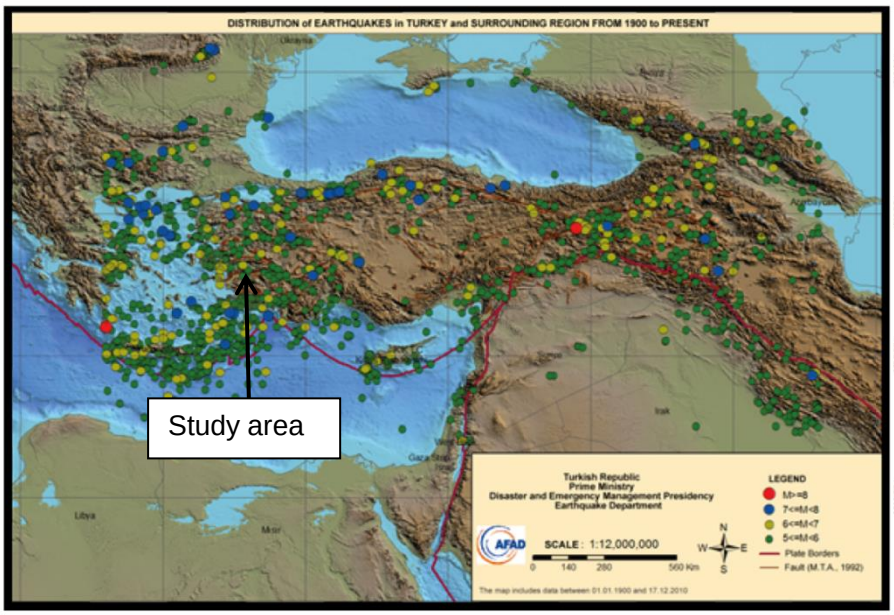

Figure 2.5: Earthquakes of above magnitude 5 from 1990 to 2010 in Turkey illustrating how the western Anatolian extensional province has a significant clustering of the earthquakes that have occurred. Adapted from imagery from the Turkey Ministry of Disaster and Emergency Management: earthquake department.

A number of competing mechanisms have been proposed as the cause of multiple phases of regional metamorphism and extensional deformation in western Turkey. These are: (i) subduction rollback along the Aegean-Cyprian trench (Le Pichon and Angelier, 1979; Kissel and Laj, 1988; Meulenkamp et al., 1988; Meulenkamp et al., 1994; Çiftçi and Bozkurt, 2009a); (ii) post orogenic collapse of over-thickened crust at the closure of the northern branch of the Neotethys (Dewey, 1988; Seyítoğlu and Scott, 1991; Seyítoğlu et al., 1992); (iii) westwards escape of the Anatolian micro-plate along the dextral North

Anatolian fault zone and sinistral East Anatolian fault system (Dewey and Sengör, 1979), and (iv) difference in convergence rates along the Aegean-Cyprian subduction zone (Doglioni et al., 2002; Çiftçi and Bozkurt, 2009a).

Of these mechanisms subduction rollback is the most widely accepted cause of the extension that is occurring in the WAEP. The extension is therefore thought to be a result of the slab roll back (from the subduction zone) in the west and push (from the convergence in the east), which causes the Anatolian plate (on which western Turkey is situated) to move in a SW direction, bounded by significant strike-slip fault zones such as the North Anatolian fault zone (NAFZ) and the East Anatolian Fault Zone (EAFZ, figure 2.1) forming the northern and southern plate margins, respectively (Çiftçi and Bozkurt, 2009a). The extension is expressed over the western Turkish landscape as a series of generally E-W trending grabens that dissect the metamorphic Menderes Massif, a significant metamorphic core complex within the area, which has been exhumed by active normal faulting.

Global Positioning System (GPS) studies yield insights into the rates of ongoing extension of the WAEP (e.g. Barka and Reilinger, 1997; Aktuğ et al., 2009)**.** For the WAEP, Barka and Reilinger (1997) estimated that Arabia is moving northwards with respect to the Eurasian Plate at 23 ± 1 mm/yr, 10 mm/yr of which is taken up by shortening within the Caucasus Mountains. Mueller et al. (1997) provide a similar rate of 22 mm/yr for extension over Anatolia. Extension within Western Anatolia is taken up largely on E-W and WNW-ESE trending graben systems, including the Gediz Graben (McKenzie, 1978) and the major normal faults that bound them.

Aktuğ et al. (2009) have also produced a study of GPS measurements in westernmost Turkey by dividing the area into polygons of around 10 km^2 and

calculating velocity gradients, assuming the gradient was constant within each polygon. Instead of providing one overall quantification (e.g. Barka and Reilinger, 1997) this method showed an increase in the rate of extension from east to west across the Anatolian Plateau and towards the Aegean coast, with the highest magnitude of extension occurring across the graben systems in western Turkey (Aktuğ et al., 2009). The available GPS data indicate 10 ± 5 mm/yr of extension across the Gediz and Büyük Menderes grabens (Barka and Reilinger, 1997; Aktuğ et al., 2009), which is distributed between the two grabens. These data yield an opening rate of 6 mm/yr for the Büyük Menderes Graben and 4 mm/yr for the Gediz Graben (Aktuğ et al., 2009).

2.3.1: THE MENDERES MASSIF

The Menderes Massif (figure 2.2) is a major metamorphic core complex within the WAEP, which records evidence of multiple phases of regional metamorphism and deformation spanning the Precambrian to the Eocene (Şengör et al., 1984; Bozkurt and Oberhansli, 2001; Çemen et al., 2006; Okay, 2008).

The Massif is bound by the Izmir-Ankara suture to the north, and by the Lycean Nappes (figure 2.4) to the south. The original studies of the metamorphic rocks within the WAEP divided them into cover and core sequences (e.g. Akkök, 1983). Subsequent studies have established however, that the Menderes Massif is composed of a core of Precambrian micaschists and gneiss intruded by metagranites in the latest Precambrian (Candan et al., 2001), overlain by series of nappes that have undergone Palaeozoic to Lower Cenozoic metamorphism (Çemen et al., 2006; Oner and Dilek, 2011). From the lowest to the highest they are the Bayindir, the Bozdağ and Çine nappes.

In the early to middle Miocene, NNE-SSW-directed extension initiated two detachment faults with opposing dip directions; the Gediz detachment dips to the north, while the Büyük Menderes detachment dips to the south (figure 2.3). It has been suggested that the faults which are now dipping at around 15° at the surface could have been higher angle, around 30°, when the faults were active (Busher et al. 2011). This arrangement of extensional faulting led to the formation of the east-west trending Neogene grabens subdividing the Menderes Massif into northern, central and southern sub-massifs (Iredale et al., 2013); these grabens are the Gediz Graben in the north, the central Küçük Menderes Graben and the Büyük Menderes Graben in the south (figures 2.2 and 2.4). Graben formation also generated accommodation space for the accumulation of sedimentary rock units of Neogene age to be deposited in the resulting basins, there are also significant areas of active deposition of Quaternary alluvium (Çiftçi, 2007; Çiftçi and Bozkurt, 2009a; Oner and Dilek, 2011).

The Northern Menderes sub-massif is located to the north east of the Gediz Graben, forming the northern bounding range of the graben. High grade metamorphic rocks have been dissected by NE-SW trending basins, the Gordes, Demirici, Selendi and Usak-Gure basins (Catlos and Çemen, 2005).

The Central Menderes sub-massif (figures 2.2 and 2.4) is delineated by two grabens, the Gediz Graben forms its northern boundary and the Büyük Menderes Graben bounds it to the south (Hetzel et al., 1998). Both of these grabens have provided accommodation space for deposition of Neogene sediments and are the site of current deposition (Çiftçi, 2007; Oner and Dilek, 2011).

The southern sub-massif of the Menderes basement rocks is bounded to the north by the Büyük Menderes Graben and associated Neogene to recent

sedimentation while in the south the Lycean nappes form the boundary with the high grade metamorphic rocks (figure 2.4) (Bozkurt and Satir, 2000; Iredale at al., 2013).

The Gediz Graben, the location for this study, is situated in an area of active extensional tectonics and the faults bounding the graben are currently active (Çiftçi, 2007; Oner and Dilek, 2011). Previous studies have mapped the area and so the geology of the graben has some significant constraints which allow the graben to be used to investigate the dynamic landscape reaction to tectonics (e.g Tahir, 1996; Koçyiğit et al., 1999 Lips et al., 2001; Çiftçi, 2007; Çiftçi and Bozkurt, 2009; Oner and Dilek, 2011). In the sections below the characteristics of extensional tectonics that are exhibited within the Gediz Graben will be reviewed. Following this the faulting and stratigraphy within the graben will be documented as these details are of importance to the subsequent chapters.

2.4: THE CHARACTERISTICS OF EXTENSIONAL TECTONICS

Extensional tectonic regimes, such as that operating within the WAEP, result in significant normal faulting. As mentioned in section 2.3.1 with reference to the WAEP, the extensional tectonics can be expressed as a series of grabens bounded by normal faults, trending broadly parallel to the direction of the subduction zone, if the crust is strong enough taking into account weakening by heat flow associated with subduction (Holdsworth and Turner, 2002). The basin and range topography expressed through normal faulting is typical of land based extensional tectonics (Twiss and Moores, 1992).

Within basin and range topographies faulting tends to occur commonly as moderate to high-angle normal faults although an increasing number of low

to very-low angle normal faults, some even approaching horizontal have been studied (Twiss and Moores, 1992). These faults serve to accommodate the extension occurring across the area (Collettini, 2011), emplacing younger rocks on top of older rocks leading to missing stratigraphy in vertical section. The low-angle faults, also known as detachment faults tend to separate the relatively unfaulted uplifted footwall, which can be often formed from basement rocks, and the faulted hanging wall undergoing subsidence (Twiss and Moores, 1992). Within the hanging wall of the low-angle normal fault the often high-angle faulting can form sets of imbricated faults, roughly parallel to each other (Twiss and Moores, 1992).

2.4.1: FOOTWALL UPLIFT AND HANGING WALL SUBSIDENCE ASSOCIATED WITH NORMAL FAULTING

Research on footwall uplift and hanging wall subsidence associated with normal faults suggests that ratios of footwall uplift to hanging wall subsidence may vary significantly between areas (e.g. Papanikolaou et al., 2010). Papanikolaou et al., (2010) found a ratio of 1:3 footwall uplift to hanging wall subsidence in Lazio-Abruzzo, Italy, using differential SAR Interferometry and GPS recordings from nearby field GPS stations. The 1:3 ratio falls within the value range presented by Stein and Barientos (1985) who stated that footwall throw should be a ratio between 1:1 and 1:5 over both coseismic and longer-term motions on a fault; in these ratios footwall uplift accounts for varying proportion of the total throw on the fault. Longer term motions in the Teton Range, North America (Byrd et al., 1994) and coseismic motions at the time of the Borah Peak earthquake (Stein et al., 1988) have yielded ratios of 1:2. On

the Xylokastro Fault in the Gulf of Corinth ratios of between 1:2.7 and 1:3.5 have been determined using plate models by Armijo et al. (1996).

2.4.2: PROPERTIES OF FAULTING WITHIN EXTENSIONAL TECTONIC REGIMES

Evidence suggests that normal faults are often planar and have dips varying between 30-60° (Jackson, 1987; Jackson and White, 1989). Collettini (2011) states that frictional fault reactivation theory predicts that slip on low-angle normal faults is unlikely, which is supported by the absence of moderate to large earthquakes of normal faults with dips of less than 30°. This view is supported by Twiss and Moores (1992) who state that there is no direct evidence for low-angle normal faulting in the brittle upper crust, although Crone and Harding (1984) show that in seismic profiles of Utah there are low-angle faults at depths of 2-3 km.

Low-angle normal faults or detachments have been recognised around the world associated with the exposure of metamorphic core complexes and within graben settings (Wernicke et al., 1987). This presents a paradox, as there is a lack of modern day active low-angle normal faults but there is evidence for displacement along these features. This paradox might be addressed by the work of Jackson and White (1989), who suggest that normal faults and faulted block must rotate about a horizontal axis over time, or a large gravity anomaly would be produced and the Moho discontinuity depressed. The implications of this theory are that presently inactive low-angle detachment faults would have rotated to low-angles where slip is not possible from actively slipping geometries.

The Gulf of Corinth has been used to illustrate how it is possible for surface expressed high-angle normal faults to decrease in dip with depth, i.e. listric (Jackson, 1987). There are additional areas that support the ability of normal faults to become listric with depth, for example the Gediz Graben, where the 1969 Alaşehir and 1970 Gediz earthquake are thought to have originated on a low angle normal fault at depth and been expressed at the surface along moderate to high-angle normal faults (Eyidogan and Jackson, 1985).

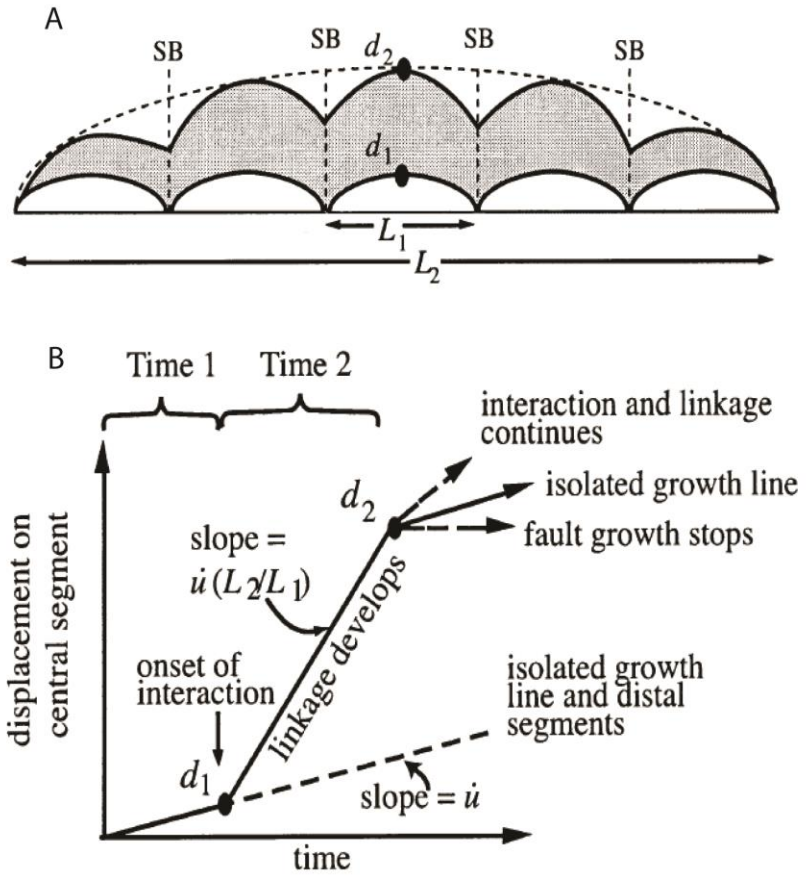

Figure 2.6: growth of an idealised fault array of N segments of equal length (L1) that link to form a total length. Segment boundaries are indicated by SB. (L2). A) The displacement profiles of the faults before and after interaction and linkage, d2 indicates the displacement after re-adjustment to interaction is complete. C shows the displacement as a function of time on the central fault in the array, time1 is the time prior to significant interaction, while time2 indicates the period of time over which slip rates vary along the array, linkage occurs during this time. Adapted from Cowie and Roberts (2001).

2.4.3: ALONG STRIKE TRENDS IN NORMAL FAULT ARRAYS

Normal faults bounding uplifted graben margins tend to occur in segments that combine to form a fault array. The normal fault array does not usually form a straight line, but has an overall along strike curved or sinuous surface trace, formed by the segments that can be either relatively straight or curved (Twiss and Moores, 1992). Normal fault segments have a distinctive pattern of throw value along strike as illustrated by work undertaken by Cowie and Roberts (2001). The typical distribution of throw along strike of a fault is that the greatest amount of slip and throw occur at the centre of the segment, with values decreasing to zero at the tips of the fault.

Cowie and Roberts (2001) present data showing the scaling relationships of slip and throw along strike on faults, demonstrating that slip and throw rates and therefore total amounts of slip and throw tend to be higher on faults located centrally in an array (figure 2.6). The work of Cowie and Roberts (2001) is supported by Roberts and Michetti (2004) who undertook a study of the Lazio-Abruzzo Apennines, Italy. Roberts and Michetti (2004) determined the location of non-linked faults by drawing a number of cross-sections across faults to determine where throw was reduced to zero. Their research shows that there can be two situations; the first, where a fault not interacting with other segments in an array gives a throw profile that is zero at the tips and reaches a maximum in the centre (figure 2.6). If, however the faults are interacting or linked the second situation occurs, where the greatest rate of throw, and accumulation of throw, shifts to the centre of the new linked length (figure 2.6). In this situation the previously existing, but now linked fault tips undergo an increase in throw rate to non-zero throw values.

2.4.4: INTERACTIONS OVER TIME IN NORMAL FAULT ARRAYS

Peacock (2002) presents the possible stages of fault evolution and interaction over time as documented in many other studies (e.g. Peacock and Sanderson, 1994; Childs et al., 1995; Gawthorp et al., 1997; Nicol et al., 1997; Cowie, 1998; Young-Seog and Sanderson, 2005). Stage one (figure 2.7) is non-interaction of fault strands even if they are overlapping. Stage two (figure 2.7) is the initiation of some degree of interaction between fault segments leading to tiled beds between the segments that form a relay ramp (Peacock and Sanderson, 1994). Stage three (figure 2.7) involves the breaking of the relay ramp as the faults increase interaction (Childs et al., 1995) after stage 3 the relay ramp is destroyed as the faults become linked. Peacock and Sanderson (1994) state that the fault at stage four should be irregular and have an along strike bend.

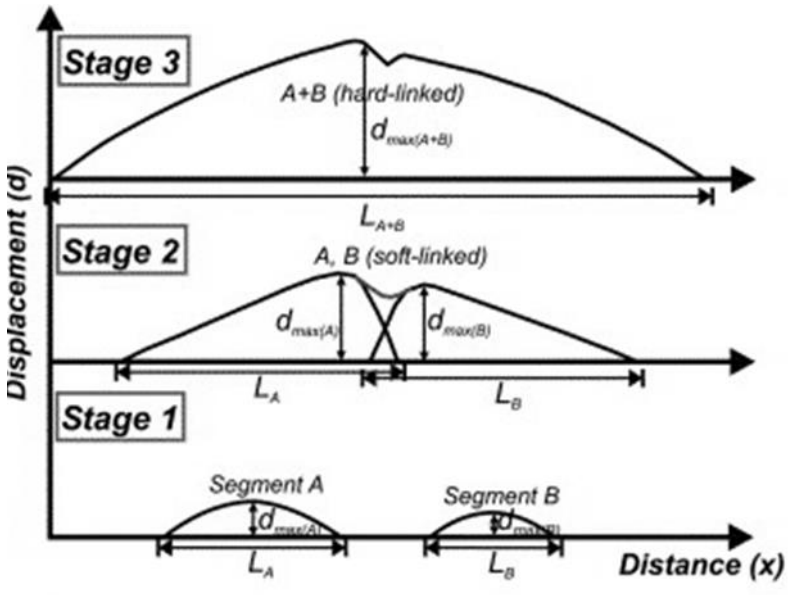

Figure 2.7: Shows three stages of fault interaction and linkage between two segments A and B. The development of displacement along strike of the linked fault array is shown. From Young-Seog and Sanderson, (2005).

During the time of interaction and linkage development the displacement on the fault increases in order to readjust to the new length of the fault (figures 2.6 and 2,7), During the period of interaction and linkage the whole fault zone re-adjusts displacement (d) to the rapid increase in length (L) until the scaling relationship $d = \gamma L$ is re-established. Normal faults therefore grow in a way that leads to significant variations in slip and throw along strike and through time.

2.5: STYLES OF FAULTING WITHIN THE GEDIZ GRABEN

The natural laboratory for this study is the WAEP, and specifically the Gediz Graben, a prominent expression of extensional tectonics within the WAEP. The topography of the Gediz Graben has been created by faulting that has been ongoing for about 16 Myr (Çiftçi, 2007; Buscher et al., 2013). Previous research has mapped the styles of faulting within the area so as to further understand the evolution of the graben and the present day situation in terms of seismic hazards.

Previous studies suggest at least three (Paton, 1992; Çiftçi and Bozkurt, 2009a, 2009b; Çiftçi and Bozkurt, 2010) and up to four styles (Oner and Dilek, 2011) of faulting within the Gediz Graben (figure 2.8). All the faults documented by the studies were considered to have been active during the graben evolution including: (i) the main low-angle detachment (Çiftçi and Bozkurt, 2009a; 2009b; Oner and Dilek, 2011); (ii) high-angle normal faults (Çiftçi and Bozkurt, 2009a; 2009b; Oner and Dilek, 2011); (iii) low-angle normal faults (Çiftçi and Bozkurt, 2009a; 2009b; Oner and Dilek, 2011), and (iv) oblique-slip scissor faults (Oner and Dilek, 2011).

2.5.1: LOW-ANGLE FAULTING

The Gediz Grabens southern margin is bounded by a low-angle normal fault with a dip of 15°-28° (figures 2.9), (Çiftçi, 2007; Oner and Dilek, 2011) that dips to the north and has a general E-W strike, although locally the fault varies in its strike (Çiftçi and Bozkurt, 2009a; Oner and Dilek, 2011). This normal fault has been variably named the Gediz detachment (Lips et al., 2001), the Karadut fault (Tahir, 1996) or the Çamköy detachment (Koçyiğit et al., 1999). This study will use the naming convention of Lips et al., (2001), calling the low-angle normal fault the Gediz Detachment.

The detachment fault separates the sedimentary graben fill and the metamorphic basement of the Menderes Massif, which is often exposed as a well-defined surface (figure 2.8) on the metamorphic rocks. The fault has been observed by Oner and Dilek (2011) to have a corrugated appearance over a lengthscale of 10's of m, which they propose are the result of NNE-SSW trending fold structures within the Menderes Massif basement.

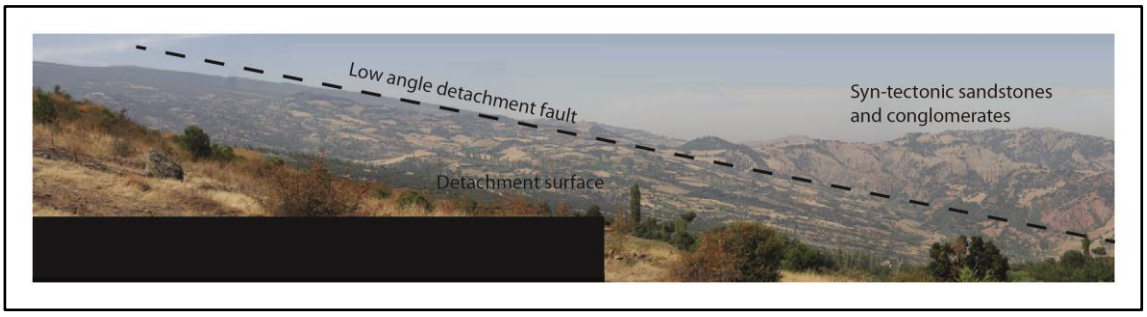

Figure 2.8: A field photograph of the detachment surface that can be seen as a regular slope of approximately 15° which is pervasive across much of the higher elevations of the range in the central and eastern thirds. The syn-tectonic sedimentary rocks are faulted against the basement rocks of the Menders Massif by the shallow dipping detachment fault.

Localised low-angle normal faults can be found in both the sedimentary graben fill and the metamorphic rocks of the Menderes Massif where they appear to have fairly similar dips and orientations to the detachment (Oner and

Dilek, 2011). These low-angle normal faults are best seen within the valleys of rivers flowing from south to north as this exposes cross sectional views and good exposures of the sedimentary units. The faults usually strike ENE-WSW with dips ranging from 10° to 25°; the faults are brittle, near surface structures with small amounts of offset (Cohen et al., 1995; Bozkurt and Sözbilir, 2004; Çiftçi and Bozkurt, 2009a; Oner and Dilek, 2011). These localised low-angle faults suggest that low-angle faulting did not occur solely on the regional-scale Gediz Detachment.

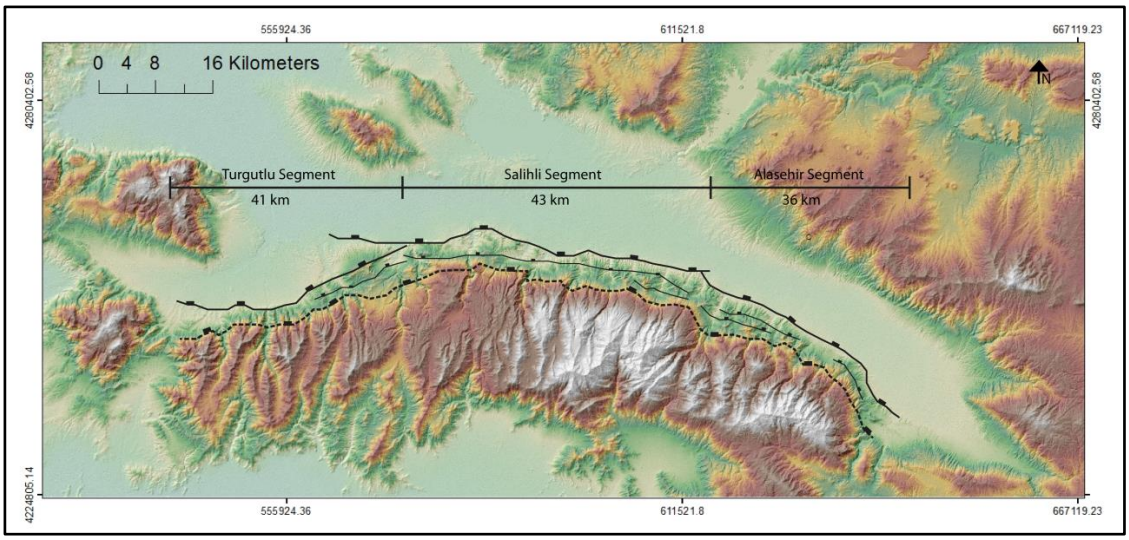

Figure 2.9: Digital Elevation Model (DEM) imagery of the Bozdağ Range. The main regional faults have been mapped onto 30m ASTER imagery and the map shows the low-angle normal fault (Gediz Detachment) is shown as a black line while the high-angle normal faults are shown in solid black lines. The Graben bounding normal fault is shown in a bold solid line while older high angle normal faults are shown as thinner lines. The graben bounding normal fault is segmented into three segments, the Turgultlu, Salihli and Alaşehir segments with their corresponding lengths stated.

2.5.2: HIGH-ANGLE NORMAL FAULTING

High-angle normal faults occur as major faults within the southern graben margin as well as the graben bounding normal fault (figure 2.4). Major high-angle faults within the graben generally strike WNW-ESE (Çiftçi and Bozkurt, 2009a) and have disturbed both the syn-tectonic sedimentary fill of the graben

and the metamorphic basement rocks of the Menderes Massif (Koçyiğit et al., 1999). When the southern graben margin is observed in plan view (figure 2.9), the major high-angle normal faults appear to be curvilinear and segmented along strike (Çiftçi and Bozkurt, 2007; 2009a). The major regional high-angle normal faults are some of the most prominent structural features within the graben and bound the present topographic graben (figure 2.9). The major regional high angle normal faults (figure 2.9) are of particular interest to this study; the faults are laterally extensive, spanning the length of the whole margin in two parallel arrays and so form the major high-angle controls on graben topography. The outer high-angle normal fault (labelled OHANF in figure 2.8) array is furthest from the present topographic graben and predominantly separates the lower and middle Miocene strata from the Pliocene-Pleistocene formations (figures 2.10 and 2.11).

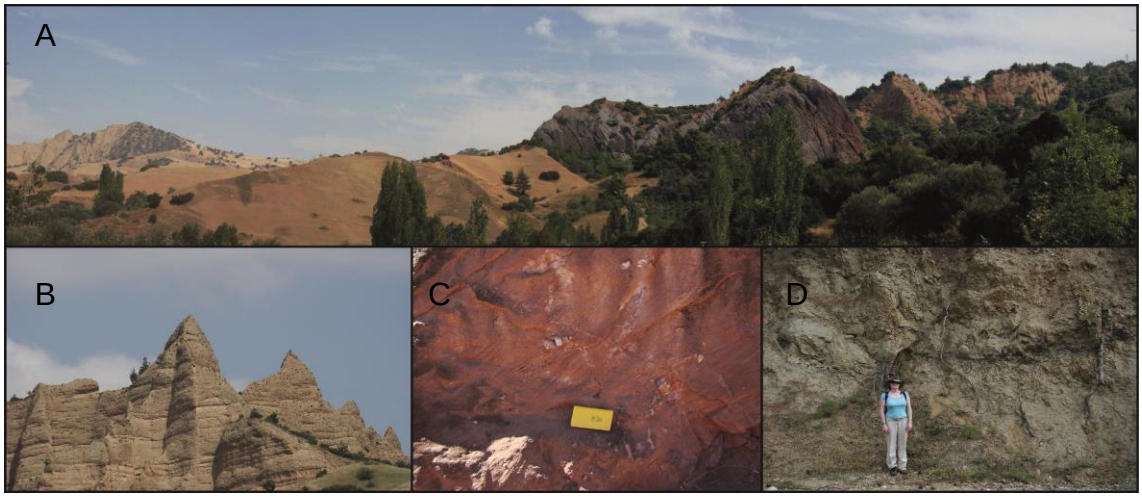

Figure 2.10: A selection of field photographs that illustrate the distinct characteristics of the clastic sedimentary rock formations that fill the Gediz Graben. A, shows the sedimentary unit succession from Miocene Alaşehir and Caltılık Formations (purple and red coloured rocks) at high elevations to the Plio-Pleistocene Gediz and Kaletepe Formations (orange and yellow rocks) at lower elevations within the graben. The Plio-Pleistocene sediments are faulted against the quaternary alluvium within the graben valley by the graben bounding fault. B shows the significant horizons within the Kaletepe Formation which is well exposed to the west of the graben. C shows the red colouring of the Caltılık Formation. D shows the Salihli Member of the Gediz Formation with the typical yellow to grey colouring and a darker organic rich layer typical of the formation.

The graben-bounding normal fault (GBNF, figure 2.4) array marks the boundary of the modern topographic graben, and juxtaposes the current topographic escarpment with the Quaternary alluvium in the graben axis (Koçyiğit et al., 1999; Lips et al., 2001; Çiftçi and Bozkurt, 2009a, 2009b). The graben-bounding fault normal fault array separates the present Quaternary alluvium of the topographic graben from the Pliocene formations and marks the start of the topographic relief (figure 2.11).

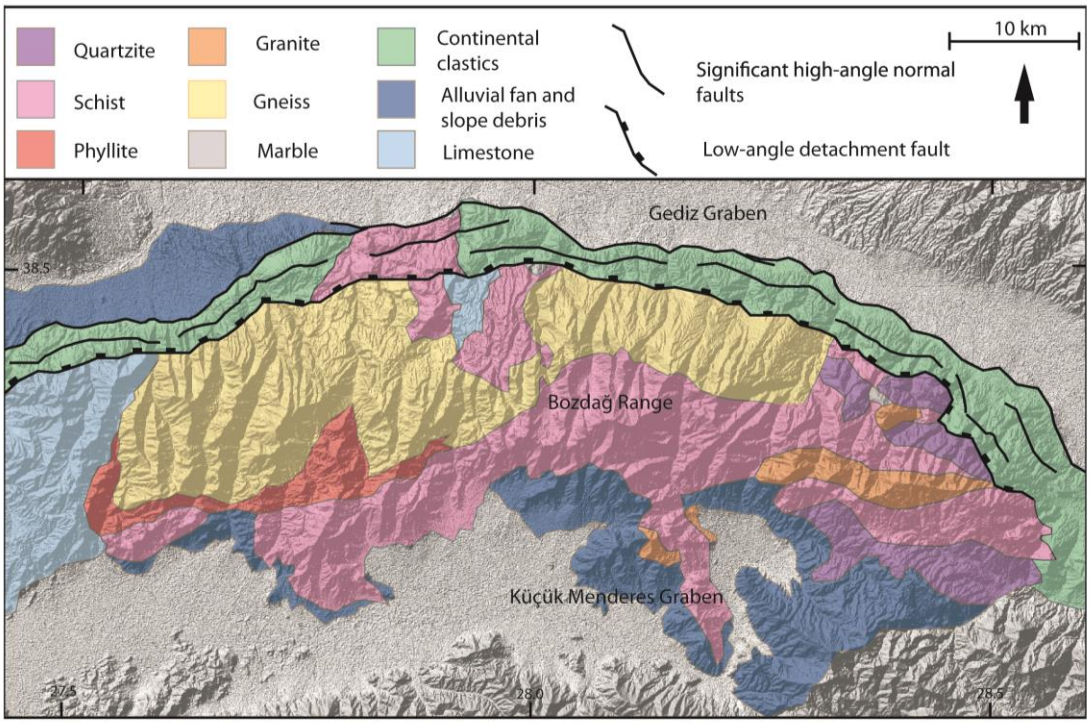

Figure 2.11: A generalised geological map of the Gediz Graben showing the lithologies that make up the Bozdağ Range and syn-tectonic sedimentary graben fill. The locations of the low-angle detachment and high-angle normal faults are also shown compiled from Şenel and Aydal, (2002); Çiftçi and Bozkurt, (2009a and 2009b); Oner and Dilek, (2011).

The fault is segmented along its length (figure 2.9) and for the purposes of this study the individual segments have been given names related to the major towns in the area: the Turgutlu strand to the west (41 km long), the central Salihli Segment (43 km long) and the Alaşehir Segment in the east (36 km in length). Oner and Dilek (2011) observed surface offset Quaternary alluvial

fans along the range front indicating that all three of the segments of the graben bounding fault have been active sub-recent times. This is supported by the seismic activity that is recorded on the faults, such as the 6.9 and 7.0 magnitude earthquakes that occurred within the Gediz Graben in 1969 and 1970 respectively (Arapat and Bingol, 1969; Mitchell, 1976).

In addition, there are additional associated small-scale synthetic and antithetic faults (Çiftçi and Bozkurt, 2009a). These are localised normal faults, with moderate to high-angle northwards dip, and additional localised normal faults that dip southwards. The southwards dipping faults tend to dip at higher angles (65-75°) than the secondary synthetic normal faults, at 60°-65° (Oner and Dilek, 2011).

Oner and Dilek (2011) in addition to the previous sets of faults also mapped oblique 'scissor', or hinge faults striking NNE-SSW and dipping around 65°. They reported seeing them most readily within stream valleys striking parallel to the valley. The scissor faults are unreported by other researchers, and this study failed to find convincing evidence for these structures. However, Oner and Dilek (2011) claimed the scissor faults are best preserved and most observable within the crystalline rock of the detachment footwall.

2.5.3: MODELS FOR THE DEVELOPMENT OF THE GEDIZ GRABEN THROUGH TIME AND THE RELATIONSHIP BETWEEN HIGH AND LOW-ANGLE NORMAL FAULTING

Previous work on the faulting within the Gediz graben has focused on the mapping and classification of the faults and how they interact with the sedimentology (e.g. Tahir, 1996; Koçyiğit et al., 1999; Çiftçi, 2007; Çiftçi and Bozkurt, 2009a, 2009b; Çiftçi and Bozkurt, 2010; Oner and Dilek, 2011). Until

recently attempts had not been made to quantify rates of movement on the faults so therefore little quantitative data such as slip rates and age constrains on faulting exists for the faulting with the Gediz Graben. However, qualitative studies have added to the knowledge of faulting by assessing cross-cutting relationships (Çiftçi and Bozkurt, 2009a, 2009b; Oner and Dilek, 2011).

It is widely accepted that the development of the Gediz Graben took place in two phases (e.g.; Koçyiğit et al., 1999; Oner and Dilek, 2011; Busher et al., 2013). Originally Koçyiğit et al. (1999) proposed a two stage formation for the graben based upon the sedimentary evidence of two contrasting graben fill sediment packages, which they state show differences in levels of deformation and lithology. Furthermore, Koçyiğit et al. (1999) document the age of the observed transition as Plio-Quaternary (around 2.6 Ma) from paleontological evidence. More recently Buscher et al. (2013) developed the model of graben formation dynamics based on structural evidence and differences in styles of faulting. Prior to 2.6 Ma, extension was accommodated on the low-angle detachment fault resulting in the exhumation of the high-grade metamorphic Menderes Massif (Buscher et al., 2013). Between 2.6 and 2 Ma significant high-angle faulting developed along the length of the graben, and from 2 Ma high-angle normal faulting becoming dominant resulting in the present day graben. Both the studies of Buscher et al. (2013) and Koçyiğit et al. (1999) infer a similar age for the transition from sedimentary and structural evidence, so 2.6-2 Ma will be used as the timing of the transition from phase 1, low-angle normal faulting to phase 2, high-angle normal faulting.

Buscher et al. (2013) used radiometric dating, in the form of He ages to constrain rates of rock exhumation for the Bozdağ Range and slip rates along the Gediz detachment fault. Their Apatite and zircon (U–Th)/He and fission-

track ages produced exhumation rates of 0.6–2 km Ma^{-1} beneath the Gediz detachment. Slip rates for the shallow-dipping Gediz detachment fault were determined to be 4.3 (+3.0 -1.2) mm/yr using zircon (U–Th)/He ages of c. 4–2 Ma in the footwall of the fault. The also produced ^{10}Be-based catchment-wide erosion rates of 80-180 mm/kyr in nine catchments. Buscher et al. (2013) concluded that tectonic denudation caused by low-angle detachment faulting rather than erosion is the dominant process in rock exhumation in the area. They constrain the age of initiation of the low-angle normal fault as 16 Ma and determined that this structure was active until 2 Ma.

The slip rates Buscher et al. (2013) produced is valid only the period of 2 – 4 myr, and suggests that this shows that the low-angle detachment underwent an acceleration in slip before becoming inactive. Using this rate Buscher et al., (2013) were then able to quantify vertical exhumation of the Bozdağ block assuming that the dip of the fault has remained at the present day dip of 15°. The resulting exhumation rate was calculated as 1.1 km/myr, which they state is a minimum that may be increased if the angle of the detachment fault has been steeper in the past.

The study by Buscher et al. (2013) also proposes that there was a transition in the style of faulting from extension taken up on the low-angle detachment fault into dominantly high-angle graben bounding normal faulting between 2.5 and 2 Ma. This in combination with the radiometric dating of Buscher et al. (2013) gives a possible post early-Pleistocene age for the initiation of the current graben bounding high-angle normal fault as the newest units are uplifted and back tilted compared to their equivalent in the graben fill. This evidence suggests that initiation of the graben may have occurred during

the Miocene but the modern graben configuration and much of its development has occurred during the Quaternary.

Eyidogan and Jackson (1985) proposed that the high-angle normal faults persist at depth until they link with the underlying low-angle detachment fault, forming a listric fault pattern (figure 2.12). The linking of the normal fault at depth has been suggested due to the 1969 Alaşehir earthquake which had a focal depth of 6 km and occurred on a fault plane that dips at approximately 32° to the NNE (Eydogan and Jackson, 1985). This places the focus of the earthquake on a deep, shallowly dipping fault, which is inferred to be the deeper extent of the detachment fault that now connects with the newer high-angle normal faults, which are actively uplifting the mountain rage in the footwalls. The research of Buscher et al. (2013) supports Eydogan and Jackson's (1985) linkage model. In addition they argue that a segment of the low-angle normal fault which underlies the high-angle normal fault is still active, while the low-

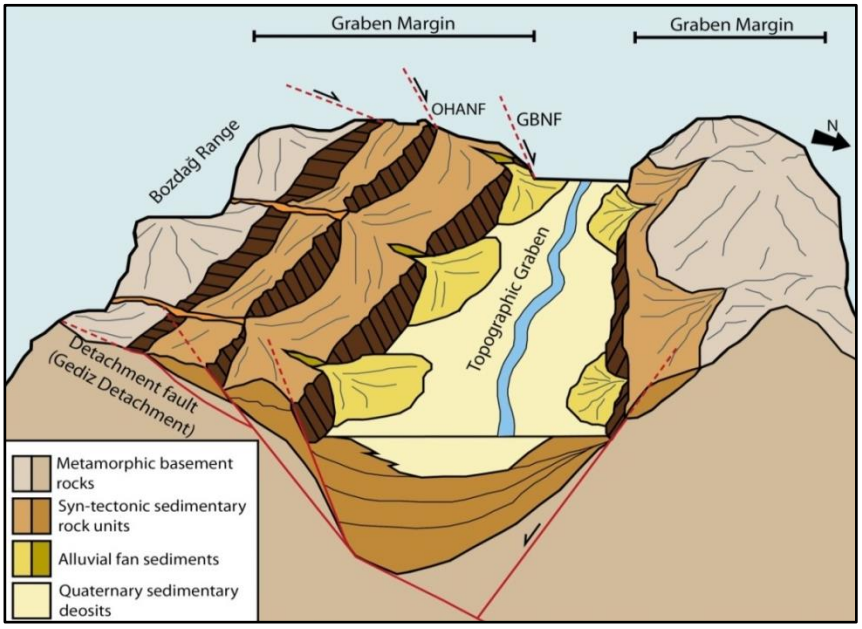

Figure 2.12: A schematic cross-section of the Gediz Graben that presents the hypothesis of Eydogan and Jackson's (1985) proposal that the high-angle normal faults persist at depth until they link with the underlying low-angle detachment fault forming a listric fault (figure adapted from Koçyigit et al., 1999 [faults shown in red]).

angle fault in the footwall of the high-angle normal faulting is inactive. Additional research has supported this arrangement of faulting, showing the high-angle normal faults in the graben margin linking at depth with the low-angle fault (Çiftçi and Bozkurt, 2010; Çiftçi, 2007).

2.6: STRATIGRAPHY AND SEDIMENTOLOGY OF THE GEDIZ GRABEN

The higher elevation areas of the Bozdağ Range are composed of the igneous and metamorphic rocks of the Menderes Massif while extension and high-angle normal faulting has been accompanied by sedimentation within the graben producing the current geology and configuration of the Gediz Graben (figure 2.12). The sedimentary history of the Gediz Graben (figure 2.13) has been studied over the past 30 years, resulting in an understanding of the depositional nature of both the syn- and post-tectonic sediment packages as well as facilitating age constraint of the stratigraphical units (e.g. İztan and Yazman, 1991; Cohen et al., 1995; Koçyiğit et al., 1999; Sarıca, 2000; Seyitoğlu et al., 2002; Purvis and Robertson, 2005; Ciftci, 2007; Ciftci and Bozkurt, 2009b; Oner and Dilek, 2011). This knowledge of the stratigraphy and sedimentology of the Gediz Graben (figure 2.13) is important because it provides a framework on which to base studies of both the active normal faulting and the rivers that incise into the sedimentary and metamorphic units. Palaeontological evidence provides the age constraints needed to work out the rates of movement on the faults cutting the sediments. Knowledge of the sedimentary character of the graben fill sediments is also useful in the study of the rivers draining the mountains. Lithology of the rocks that a rivers incises through can have an

impact upon how the river responds to changes in the active tectonics of an area (e.g. Miller, 1991).

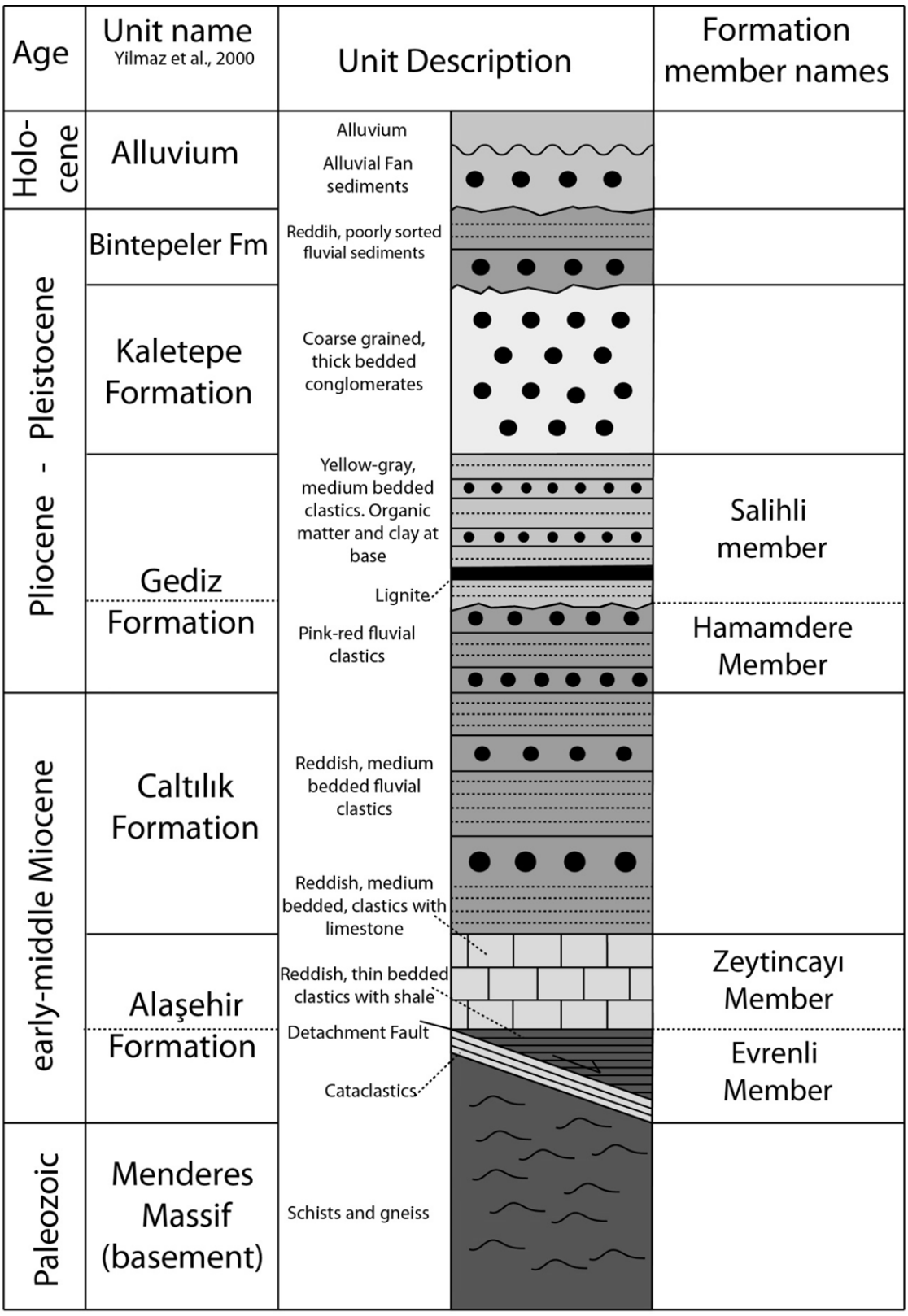

Figure 2.13: Unit descriptions and names for the syn- and post-tectonic sedimentary formations in the Gediz Graben.

Alluvial and fluvial sediments dominate the lithologies deposited within the Gediz Graben with units of Miocene and Plio-Pleistocene age forming the syn- and post-tectonic stratigraphy. The stratigraphic nomenclature for the graben fill sediments have varied in the literature, a stratigraphic correlation of the unit names used in past studies has been provided in figure 2.14. Previous researchers (İztan and Yazman, 1991; Cohen et al., 1995; Edinger, 1996; Seyitoğlu and Scott, 1996; Seyitoğlu and Benda, 1998; Koçyiğit et al., 1999; Sarıca, 2000; Seyitoğlu et al., 2002; Purvis and Robertson, 2005; Ciftci, 2007; Ciftci and Bozkurt, 2009; Oner and Dilek, 2011) have varied in their classification of sedimentary units, some particular units are referred to throughout the research as formations while other sedimentary units have been classified as both formations and formation members depending on the naming conventions used. Throughout this study the stratigraphic nomenclature of Ciftci and Bozkurt (2009b), Ciftci (2007) and Yilmaz et al. (2000) has been preferentially adopted as this has been most comprehensively mapped and described.

The majority of evidence for the age of the sedimentary infill of the graben comes from the fossil content of specific rock units, in particular sporomorph associations. Sporomorphs are the fossilised evidence of pollen and spores from plants, which can give a good age indication, and associations of sporomorphs can be used to date rock units in which they are found as the collection of plants are specific to a particular area and time. Figure 2.14 includes notes the paleontological and palynological evidence for the ages of the rock units found within the Gediz Graben compiled from a number of studies (e.g. Benda, 1971; Benda and Meulenkamp, 1979; Seyitoğlu and Benda, 1998;

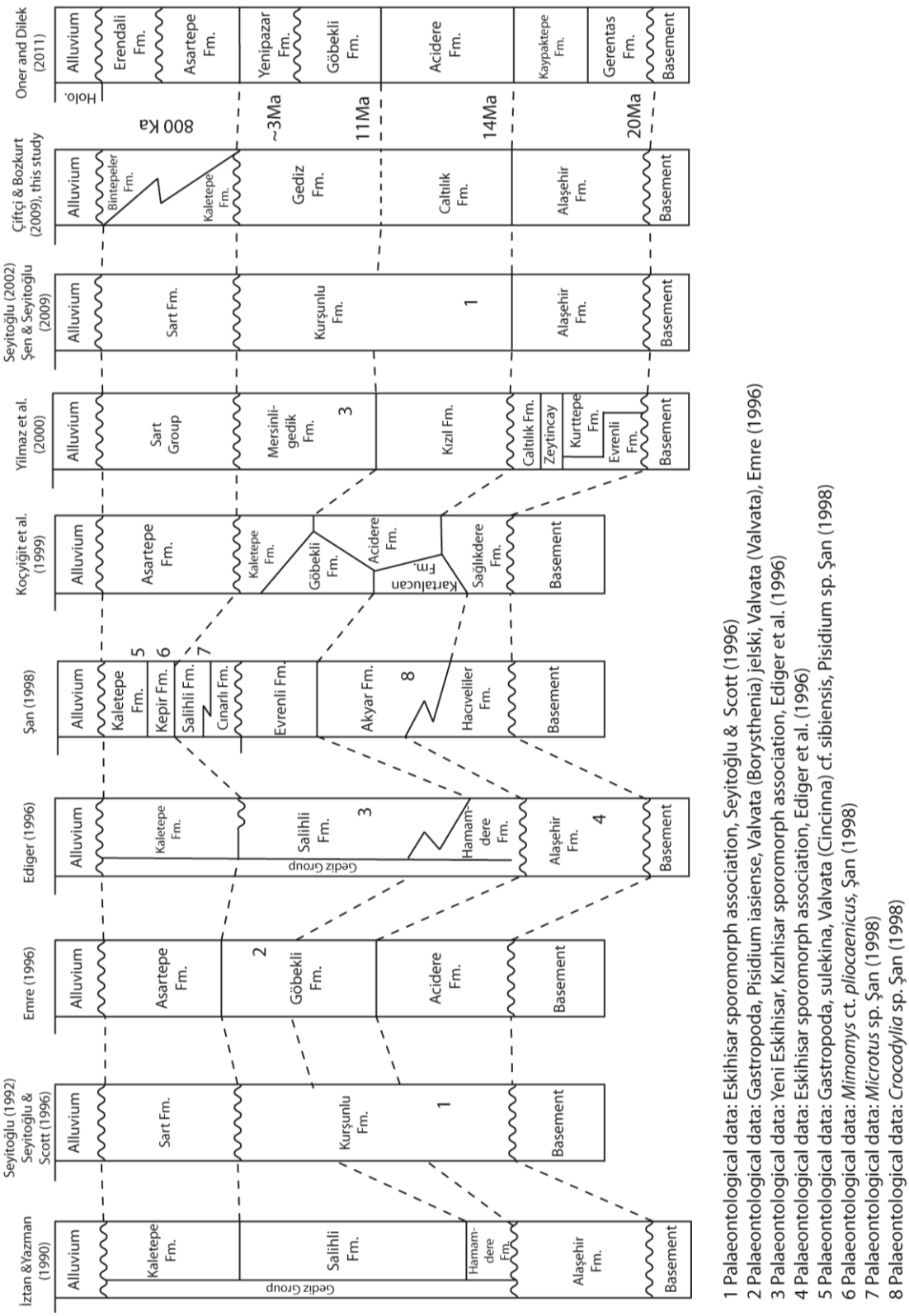

1 Palaeontological data: Eskihisar sporomorph association, Seyitoğlu & Scott (1996)
2 Palaeontological data: Gastropoda, Pisidium iasiense, Valvata (Borysthenia) jelski, Valvata (Valvata), Emre (1996)
3 Palaeontological data: Yeni Eskihisar, Kızılhisar sporomorph association, Ediger et al. (1996)
4 Palaeontological data: Eskihisar sporomorph association, Ediger et al. (1996)
5 Palaeontological data: Gastropoda, sulekina, Valvata (Cincinna) cf. sibiensis, Pisidium sp. Şan (1998)
6 Palaeontological data: *Mimomys* ct. *pliocaenicus*, Şan (1998)
7 Palaeontological data: *Microtus* sp. Şan (1998)
8 Palaeontological data: *Crocodylia* sp. Şan (1998)

Figure 2.14: A correlation of the naming conventions used for the syn- and post-tectonic sedimentary units of the Gediz Graben. Numbers represent the type of age constrain used for a particular rock unit in a variety of studies.

Ediger et al., 1996; Tahir, 1996; Purvis and Robertson, 2005; Richardson Bunbury, 1996; Sarica, 2000; Koçyiğit et al., 1999).

2.6.1: THE ALAŞEHIR FORMATION

The sedimentary basin fill of the Gediz Graben begins with the Alaşehir Formation which lies directly upon the detachment surface and basement rocks in the higher elevations ([Ağırbaş, 2006] figure 2.13) and dips at between 50-60°. It is separated into two members, the upper Zeytinçayı and lower Evrenli members (Çiftçi, 2007; Çiftçi and Bozkurt, 2009b).

The Alaşehir Formation has been dated by Edinger et al. (1996) as early to middle Miocene in age after palynological investigation identified an Eskihisar sporomorph association (Benda, 1971). The Eskihirsar sporomorph found within the rocks of the formation, and isotopic dating, particularly Ar-Ar dating on volcanic rocks on the northern margin allowed researchers to constrain the age of the Alaşehir Formation to 20-14 Ma (Edinger, 1996; Benda et al., 1974; Benda and Meulenkamp, 1979; Seyitoğlu and Benda, 1998; Richardson-Bunbury, 1996).

The Evrenli Member is older and is composed of red coloured shales, which alternate with a succession of conglomerates, sandstones and mudstones. These are overlain by the Zeytinçayı Member, composed of limestones and clastic sediments (Seyitoğlu et al., 2002; Çiftçi, 2007).

Observations of the oldest outcrops of the Evrenli Member in the Gediz Graben have described the formation as consisting of thick bedded, clast-supported, conglomerates with pebble to cobble-sized clasts and finely laminated sandstones and shales that exhibit a characteristic grey to beige weathered colour in field observation (Çiftçi and Bozkurt, 2009b; Oner and

Dilek, 2011). Within the conglomerate are found sub-rounded to sub-angular clasts including marbles, quartzite, granite, granite-gneiss and mica schist derived from the footwall of the detachment fault (Çiftçi, 2007; Cohen et al., 1995). The sandstones are observed to be well-sorted and well-bedded. Outcrop thickness of the Evrenli Member has been estimated as a maximum of ~600 m, and outcrops only in the vicinity of Alaşehir (Oner and Dilek, 2011).

The thickness of the Zeytinçayı Member does not appear to be more than ~200 m. The Zeytinçayı Member changes from greyish conglomerates in the lowermost layers to red-coloured conglomerates conformably above. The lower greyish conglomerates are formed from angular- to sub-angular clasts that sit conformably on top of the Evrenli Member. Overlying the lowermost conglomerate are fine-grained clayey limestones and red-coloured claystones. The uppermost Zeytinçayı Member consists of red-coloured, well-sorted and well-bedded sandstones, which alternate with well-cemented, poorly-sorted conglomerates (Yazman and İztan, 1990; Çiftçi and Bozkurt, 2008; Oner and Dilek, 2011).

The Evrenli and Zeytinçayı members are interpreted as being derived from a lacustrine-fan delta depositional environment (Oner and Dilek, 2011). Oner and Dilek (2011) propose that the rocks of the Evrenli and Zeytinçayı members were deposited in fault-bounded short lived playa lakes that were developed in the early stages of the supra-detachment basement evolution in the early Miocene.

2.6.2: THE CALTILIK FORMATION

The clastic Caltılık Formation generally conformably overlies the Alaşehir Formation (figure 2.13), although in isolated areas Oner and Dilek (2011)

observed the Acidere Formation lying directly on top of the low-angle detachment surface. Eskihisar sporomorph associations from the lower Caltılık Formation (figure 2.14) have yielded middle to late Miocene ages of 11-14 Ma for the age of the Formation (Seyitoğlu and Scott, 1996), while palynological data have also yielded Middle Miocene ages for formation.

At its lowermost level the Caltılık Formation is a characteristically red-coloured, medium to thickly-bedded and poorly-sorted conglomerate (Oner and Dilek, 2011; Oner, 2012). Clasts within the conglomerate are angular to sub-angular, pebble to boulder-sized metamorphic rocks; these are interspersed with well-sorted layers of sandstone. The conglomerate beds alternate with sandstone layers that are well-bedded and medium-grained with a muddy matrix (Tahir, 1996; Çiftçi and Bozkurt, 2009b).

Within the sandstone the clasts are principally quartzite, micaschists, gneiss, granites and some cataclastic rocks of coarse sand to coarse gravel grain size. Within the conglomerates of the Caltılık Formation sandstone and mudstone lenses can be observed, these contain visible bedding with cross-bedding structures. Upper parts of the Acidere Formation are composed of well-sorted, well-consolidated, clast-supported conglomerate with well-developed pebble imbrications and graded bedding (Tahir, 1996; Oner, 2012).

The predominant direction of dip, which varies between moderate to steep (35°-55°), in the conglomeritic rocks is S-SW with occasional northerly dip direction (Purvis and Robertson, 2004). The thickness of the Caltılık Formation is around 500 m in the vicinity of the village of Degirmendere to the west of the graben and in the east of the graben it is about 400 m thick (Oner and Dilek, 2011; Oner, 2012).

The characteristics of the Caltılık Formation are broadly indicative of an alluvial and fluvial depositional system (Ingersoll and Busby, 1995). Within the overall alluvial and fluvial depositional architecture there is alternation of moderate- to well-sorted conglomerates with massive and thick-bedded pebble and boulder conglomerates, which suggests significant fluctuations in the energy level within the fluvial system that produced the sediments (Oner and Dilek, 2011; Oner, 2012). Oner and Dilek (2011) have interpreted the unsorted, coarse-grained conglomerate as debris flows resulting from major faulting events resulting in additional uplift of the Menderes Massif metamorphic basement rocks.

2.6.3 THE GEDIZ FORMATION

The Gediz Formation of Çiftçi and Bozkurt (2009b) has been separated into two members, the Salihli and Hamamdere Formation (figure 2.13). The Hamamdere Member lies conformably on top of, although occasionally locally has a faulted contact with, the Caltılık Formation. The Gediz Formation has been dated by Ediger et al. (1996) propose a middle Miocene or late Miocene age based on the Kızılhisar (11–5 Ma) sporomorph association (Kayseri et al. 2008). In addition, the Gediz Formation has been dated using gastropod fauna including *Gyraulus arminienis Jekelius, Melanosis (Melanopsis) decollate Stoliczka, Pyrgula dacica Jekelius, Pyrgula sp.* and *Pseudomnicola sp*. (Tahir, 1996; Purvis and Robertson, 2005), that yielded an age of late Miocene (ca. 11 Ma) near the base of the formation.

The Salihli Member of the Gediz Formation is considered to be Plio-Pleistocene in age due to the documentation of plant fragments, pollen, gastropod and rare mammalian fossils within the middle stratigraphic sections

of the, these give an age of late Pliocene (~3 Ma) for the base of the Salihli Member (Sarica, 2000).

The Hamamdere is dominantly composed of layers of light grey and light red conglomerates, which alternate throughout the section (Oner and Dilek, 2011). At the base and in lower sections the Hamamdere Member is made up of conglomerate with cobble and pebble-sized clasts well-cemented in a fine sand to silt size, detrital muscovite rich matrix. Stratigraphically higher in the unit the conglomerate alternates with less resistant sandstone and sandstones with pebbles, which contain clasts of the underlying Caltılık Formation. The source rocks of the clasts within the Göbekli Member are in the majority metamorphic core complex with some granite and cataclastic rocks (Oner and Dilek, 2011). The Hamamdere Member generally has a moderate to shallow dip to the S, SW and SE but can be found to be dipping to the north in places (Oner and Dilek, 2011).

The Salihli Member is documented by Oner and Dilek as lying on top of the Göbekli Member of the Gediz Formation along the southern graben margin in all but the westernmost localities where it has a faulted contact with the lower to middle Miocene Caltılık Formation (Çiftçi and Bozkurt, 2009b; Oner and Dilek, 2011). This formation member is yellowish to brown in colour and consists mainly of poorly consolidated conglomerates, sandstones and mudstones. In the lower stratigraphic layers around the contact between the Hamamdere Member and the Salihli Member there are layers of mud, silt and sandstone that are interspersed with organic-rich layers such as bituminous coal and lignite and organic-rich muds (Oner and Dilek, 2011).

The Salihli Member typically exhibits a coarsening upwards sequence that ends in a combination of sandstones with micaceous matrix and dominant

conglomerates at the contact with the overlying Kaletepe Formation (Çiftçi, 2007). The source rocks of the clasts found in the Salihli Member vary a little from those of the older formations, mainly being derived from granite, quartzite, gneiss and schist, with significantly less cataclastic clasts than the lower formations of Miocene age (Oner and Dilek, 2011). Inclusion of clasts from older sedimentary formations can be seen most readily in the eastern part of the study area where red coloured, pebble-sized clasts of the Caltılık Formation and Hamamdere Member of the Salihli Formations can be seen within the Salihli Member of the Gediz Formation (Çiftçi and Bozkurt, 2009b). The maximum thickness of the Salihli Member is documented at 250 m by Oner and Dilek (2011).

The Hamamdere Member has been interpreted as being fluvially derived due to the sedimentary features within the unit (Çiftçi, 2007; Oner and Dilek, 2011;). The alternation between conglomerates and sandstones in the upper stratigraphic layers are indicative of alluvial fan formation. The sedimentology of the Salihli Member is indicative of deposition in a fluviolacustrine setting. The coal and organic-rich layers in the lower stratigraphic levels suggest deposition in playa lake environments, inferred to have been of limited size as the lignite and clay-rich layers are laterally discontinuous along strike (Oner and Dilek, 2011).

2.6.4: THE KALETEPE FORMATION

The Pleistocene Kaletepe Formation conformably lies over the Gediz Formation (figure 2.13), and is exposed extensively along southern range of the Gediz Graben (İztan and Yazman, 1990). Kaletepe Formation dips at around 30-35° with occasional higher dipping areas.

It is composed of massive to poorly-bedded, clast-supported, and yellowish coloured conglomerate (Oner and Dilek, 2011). The conglomerate alternates with sand to siltstone layers. The Kaletepe Formation is predominantly a coarse-grained formation with fewer fine-grained rocks than in the Yenipazar Formation. The clasts found within the Kaletepe Formation are composed of granite, gneiss, schists (Oner and Dilek, 2011; Çiftçi and Bozkurt, 2009b). The absolute thickness of the Kaletepe Formation is not known but the minimum thickness is considered to be around 500m (Oner and Dilek, 2011).

The upwards coarsening of the Kaletepe Formation, as well as documented rapid changes in clast lithologies between stratigraphic layers, is indicative of an alluvial fan depositional environment (Oner and Dilek, 2011; İztan and Yazman, 1990). Oner and Dilek (2011) suggest that rapid loading of the coarse-grained fan and debris flow sediments of the Kaletepe Formation into the basin may have caused burial and subsequent alteration of material deposited in the pre-existing playa lakes resulting in the lignite horizons within the underlying Yenipazar Member of the Gediz Formation.

2.6.5: BINTEPELER FORMATION

The Pleistocene Bintepeler Formation (figure 2.13) is the youngest formation within the Gediz Graben and it unconformably overlies the older Kaletepe Formation (Oner and Dilek, 2011; Çiftçi and Bozkurt, 2009b). The formation dips at between 30-40°. Field observations of *Cervus elapus* (Red Deer) and *Bos primigenius* (an extinct type of cattle) teeth and jaw bones within the units overlying the Gediz Formation, may suggest an even younger Late Pleistocene age (ca. 900-800 Ka) for the upper Bintepeler Formation.

The formation is composed of poorly lithified clasts of pebble to cobble size and is a light red colour. The Bintepeler Formation can be seen forming relict uplifted terraces and alluvial fans along the margins of the graben. Within the fine-grained layers of the Bintepeler Formation cross-bedding and graded-bedding are observable. The Bintepeler Formation has an estimated thickness of around 350 m to the east of the graben and 250 m in the western extent of the graben (Oner and Dilek, 2011). These types of sediments are typical of alternating alluvial fan and fluvial systems.

2.7: SUMMARY

Overall the is a reasonably wide range of information known about the geology of the Gediz Graben. The locations of the fault have been studied in depth, although the work has not focused on constraining throw rates. Sedimentation within the Gediz Graben has been ongoing for around 20 Ma, depositing a number of sedimentary units which have been well studied but naming conventions have been varied through studies. The Alaşehir Formation has bracketing ages of 20-14 Ma, overlain by the Caltılık Formation of 14-11 Ma. The Caltılık Formation is overlain by the Gediz Formation that may be 14-5 Ma at it base and as young as 2 Ma at the top of the formation. These formations are in turn overlain by the Kaletepe Formation and Bintepeler Formation which have a Pliocene to Pleistocene age possibly ranging from 2.5-0.7 Ma or possibly younger.

CHAPTER 3

A REVIEW OF PAST RESEARCH INTO FLUVIAL GEOMORPHOLOGY AND TECTONICS

3.1: INTRODUCTION

There is a dynamic relationship between rivers and landscape evolution that has been a significant and developing area of tectonic and geomorphic research over the last twenty years (e.g. Seidl & Dietrich, 1992; Whipple and Tucker, 1999; Snyder et al., 2000; Burbank and Anderson, 2001; Tucker and Whipple, 2002; Whipple and Tucker 2002; Whipple, 2004; Wobus et al., 2006b; Crosby and Whipple, 2006; Attal et al., 2011; Whittaker and Boulton, 2012 and others). What is now known about the relationship between the landscape, and the rivers that interact with it, is that rivers do respond in recognised ways to a variety of external and boundary conditions; one such process is tectonic perturbation and changes in base level. In this chapter a review of the literature surrounding bedrock river incision and studies that link tectonics to knickpoint retreat is first introduced. Based on this review, a quantitative analysis of the tectonic geomorphology of river systems draining the southern margin of the tectonically active Gediz Graben is presented in Chapters 6 and 7, with the aim of using our growing understanding of river response to tectonics to explore the tectonic and geomorphic history of the Gediz Graben. Specifically, how the landscape of this region has recorded the history of high-angle active faulting since the late Pliocene (2-2.6 Ma) will be investigated.

3.2: STUDIES OF FLUVIAL GEOMORPHOLOGY

River channels are of particular significance in landscape evolution as rivers fundamentally control the shape of the landscape in areas that have not experienced significant glacial activity. Rivers intensely dissect the landscape, eroding significant valley systems into the pre-existing topography. By forming a fluvial network the rivers determine the location and frequency of landsliding and other gravitational transport processes (e.g. Howard and Kerby, 1983; Howard et al., 1994; Tucker and Bras, 1998; Snyder et al., 2000; Willet and Brandon 2002; Whipple and Tucker, 2002; Tucker and Whipple, 2002; Attal et al., 2011). Fluvial systems are also major agents of erosion and transportation, especially in upland areas where the rivers incise into the bedrock. In these upland areas the fluvial processes are directly coupled with the hill slope processes, acting as a primary influence on mass-wasting processes and hillslope gradients. All of this means that rivers act as primary redistributors of sediment through the landscape. Moreover, rivers are patently sensitive to both tectonic and climatic variables through their discharge and channel gradient. As a result of their sensitivity to tectonic and climatic signals, and their integration with hillslope processes, the fluvial system is able to transmit the effects of changes in these boundary conditions to the surrounding landscape (Lavé and Avouac, 2001; Burbank and Anderson, 2001; Whipple and Tucker, 2002; Tucker and Whipple, 2002; Whipple, 2004; Attal et al., 2011; Whittaker and Boulton, 2012). Moreover, rivers should reflect tectonically induced uplift, changes in denudation and dynamic erosional processes through their geometry.

Given that rivers do respond in known ways to changes in boundary conditions (Howard and Kerby, 1983; Seidl and Dietrich, 1992; Tucker and

Whipple, 2002; Whipple and Tucker, 2002; Whittaker et al., 2008) they can be considered an archive of past events (Wobus et al., 2006a). In this way rivers prove to be a valuable tool in the analysis of past events if the temporal evolution of river systems and the landscape can be established. Therefore, a key challenge in tectonic geomorphology is to determine how rapidly landscape responds to changes in tectonic boundary conditions, such as climate change, tectonic perturbation or sediment erosion and transport, because this would control how long fluvial landscapes might "record" tectonics over time (e.g. Crosby and Whipple, 2006; Whittaker and Boulton, 2012).

To address these questions effectively, it is necessary to be able to quantify the rate of fluvial erosion over geologically meaningful timescales (i.e. 10^5 or 10^6 years). Consequently over the last 30 years a number of fluvial erosion 'laws' have been formulated, (e.g. Howard and Kerby, 1983; Seidl and Dietrich, 1992;; Howard et al., 1994; Sklar and Dietrich, 1998; Tucker and Whipple, 2002; Whipple and Tucker, 2002; Attal et al., 2008). Despite their differences, they share a common goal of describing the long-term rate of channel erosion as a function of important variables such as catchment size and channel gradient. They are intentionally simplistic because it is not possible to know the detailed hydrodynamics of individual river channels over million year periods (Howard and Kerby, 1983; Willgoose et al., 1991; Sklar and Dietrich, 1998; Carretier and Lucazeau, 2005). A number of these fluvial erosion laws have subsequently been incorporated into landscape evolution models (e.g. Willgoose et al.,1991; Howard,1994; Tucker and Slingerland, 1994; Braun and Sambridge, 1997; Coulthard, 2001; Tucker and Bras, 2000; Carretier and Lucazeau, 2005), which may also include hillslope erosion laws and may take account of additional factors such as lithology and landsliding, and may be

driven by tectonic or climatic variables (Densmore et al., 1998; Lancaster et al., 2001; Fletcher et al., 2006; Cohen et al., 2009).

3.2.1: MODELLING LANDSCAPE EVOLUTION

Geomorphology aims to explain the origins, diversity and terrain of the Earth's surface and the ability to do this is based upon; 1) quantitative qualification of the terrain, 2) the improving theory describing the dynamic modification of topography and the variables that control it (Tucker and Hancock, 2010). The theories of landscape evolution have advanced in sophistication from the 1980's to the present day (Tucker et al., 2001; Tucker and Hancock, 2010). Typically, the equations governing landscape evolution are complex and cannot often be solved using closed form and require a numerical solution method, resulting in the current understanding of a landscape evolution 'model' incorporating both the underlying theory and the computer programs that calculate solutions to the equations (Tucker and Hancock, 2010). Landscape evolution models contain a variety of components, these include; a statement of continuity of mass, geomorphic transport functions to describe the generation and movement of sediment and solutes on hillslopes, a representation of runoff generation and its routing across the landscape and geomorphic transport functions for erosion and transport by water and water-sediment mixtures (Dietrich et al., 2003). They also contain numerical methods to iterate forward in time to obtain approximate solutions to the governing equations (Tucker and Hancock, 2010). These variables allow for consideration of the initial and boundary conditions on the system, which include climate forcing, base level (tectonic) controls and substrate (lithology). As these

landscape evolution models are partly dependent on fluvial processes it is vital to quantitatively understand these aspects of the models.

Howard (1980; 1987; 1998) and Howard et al. (1994) defined five types of channels, with primary emphasis on bed morphology: (1) live bed sand alluvial; (2) live bed gravel alluvial; (3) threshold gravel alluvial; (4) mixed bedrock-alluvial; and (5) bedrock. These channel types are usually categorised into three dominant categories, which have specific fluvial erosion laws; transport-limited, detachment-limited and hybrid. The transport-limited (alluvial) channel model types (1 and 2), are characterised by a system in which the channel gradient is set principally by sediment flux. In such rivers sediment flux is equal to, or greater than, the capacity of the river to transport it. Models 4 and 5 are detachment-limited (bedrock); the incision into bedrock is modelled as a function of the shear stress on the bed (Howard and Kerby, 1983; Whipple and Tucker, 1999), total stream power (Seidl & Dietrich, 1992) or unit stream power (Whipple and Tucker, 2002). The intermediate category (3) is a hybrid of the two end members.

Stream power (Ω) is defined as the rate of energy dissipation on the banks and bed of a river for a unit of downstream length. Specific stream power per unit area (ω), which is measured in W/m^2 is particularly considered to influence fluvial processes such as erosion, transport and deposition (Sklar and Dietrich, 1998; Knighton, 1999). Stream power is determined by the power of water which is determined by the work of water (W_w) over a distance (ΔZ) (Knighton, 1998):

$$W_W = F\Delta Z = V\rho_W g\Delta Z \quad (\textbf{eq. 3.1})$$

Where: F = force

ΔZ = distance

ρ_w = density of water

g = gravitational acceleration (9.81 m/s^2)

V = volume of water

The power, P_w, exerted by the water, is the work done over a given time (Δt)

$$P_W = W_W/\Delta t = V\rho_W g\Delta Z/\Delta t \quad \textbf{(eq. 3.2)}$$

The discharge (Q) of a river is the volume of water over a given time, which can be substituted in the equation:

$$P_w = \rho_W gQ\Delta Z \quad \textbf{(eq. 3.3)}$$

Consequently, if we consider the power of water per length of channel (Δx), we obtain the total stream power Ω (e.g. Seidl and Dietrich, 1992):

$$\Omega = P_W/\Delta x = \rho_W\, gQ\Delta Z/\Delta x \quad \textbf{(eq. 3.4)}$$

as a change in distance over length can be considered to be the channel slope (S):

$$\Omega = \rho_W gQS \quad \textbf{(eq. 3.5)}$$

Because channels of different geometrical size can have identical total stream powers, stream power per unit area, ω, is often thought to best model fluvial processes, such as erosion, transport and deposition (e.g. Whipple and Tucker, 1999; Montgomery and Gran, 2001). Unit stream power can be considered the intensity of stream power over a unit area of the channel bed (A_{cb}), a factor which can be related to the channel width (W) and unit length, Δx (Attal et al., 2008):

$$\omega = P_W / A_{cb} = \rho_W g Q \Delta Z / W \Delta x \quad (\textbf{eq. 3.6})$$

Again substituting in the slope component:

$$\omega = \rho_W g (Q/W) S \quad (\textbf{eq. 3.7})$$

Consequently, the unit stream power exerted by a channel is directly proportional to its discharge and its gradient, but inversely proportional to the channel width.

Equation 3.7 forms the basis for most detachment-limited “erosion laws”. (Howard and Kerby, 1983; Seidl & Dietrich, 1992; Whipple and Tucker, 2002; Whittaker et al., 2008). This standard model contains three main assumptions:

1) The rate of long-term stream incision is linearly proportional to stream power per unit area, or the local streambed shear stress, which can be derived in an analogous way to the equations given above (Tucker and Whipple, 2002).

2) The ability of the river to detach parts of the river bed is a limiting factor and the sediment load carried in the channel can be neglected (Whipple, 2004).
3) Catchment drainage area, A, which is easy to calculate, can be used as a proxy for catchment discharge, which is often unknown. In this case, $A = dQ^y$, where d is a constant that depends on climate, and y is an exponent that is often assumed to be 1 (Whipple and Tucker, 2002).
4) Channel width, where unconstrained, can be considered a function of discharge or drainage area (i.e. $W \sim cQ^b$, where c is constant that varies in different settings and b is approximately a half) (Whittaker et al., 2007a).

These assumptions and derivations have given rise to what is known as the "stream power" family of erosion laws. The erosion law (Whipple and Tucker, 1999) can be expressed as a power law function of drainage area (A) and the slope of the channel (S):

$$E = KA^m S^n \quad \textbf{(eq. 3.8)}$$

In this case, m and n are parameters that are either empirically found, or are derived from theoretical considerations, and K (the dimensional coefficient of erosion) incorporates many variables such as climate, lithology, channel geometry and sediment supply (Hack, 1957; Seidl & Dietrich, 1992; Whipple and Tucker, 1999; Snyder et al., 2000; Tucker and Whipple, 2002). The values chosen to represent the constants m and n vary depending on the stream power law used to derive them. If the rate of incision is proportional to unit stream power, ω, and assumptions 2-4, above, are correct, then m = 0.5 and n

= 1 (e.g. Whipple and Tucker, 1999; Montgomery and Gran, 2001). If erosion is modelled as a power law function of total stream power (Ω) m = 1 and n = 1 (Seidl and Dietrich, 1992), and using fluvial shear stress m = 1/3 and n = 2/3 (Howard and Kerby, 1983).

In contrast alluvial rivers possess channels that typically have channel beds and banks covered in a layer of transportable sediment. In alluvial systems incision rate is determined by the capacity of the river to transport sediment downstream (Tucker and Whipple, 2002). As the channel of alluvial rivers are covered in a layer of sediment it is hard for the river to erode into bedrock; bedrock erosion will occur when more sediment is transported downstream from the area in question than the sediment load from upstream, incision occurs and the gradient of the river is adjusted to optimise sediment transport (Tucker and Bras, 1998). Incision into bedrock can occur within transport-limited river channels but it is limited in extent; most incision will be into sediment not bedrock, and is controlled by the sediment carrying capacity of the river (Howard, 1998). A sediment transport law has been produced for transport-limited (alluvial) rivers (Willgoose et al., 1991; Whipple and Tucker, 2002). In a transport-limited river the incision rate is proportional to the downstream divergence of the sediment flux, which in reality is represented by a 3D derivative of vectors. A transport-limited sediment transport law can be expressed in similar way to a stream power law and gives the rate of sediment transport (Q_s) as a result of a given relationship between slope (S) and the peak discharge per unit width (q) and the sediment transport coefficient, K_s, and the empirically derived constants m and n with values greater than 0 (as in equation 3.9).

The peak sediment discharge per unit area can be calculated using channel width (W) and discharge (Q) in the relationship q = Q/W (e.g. Willgoose et al., 1991; Montgomeray and Foufoula-Georgiou, 1993; Whipple and Tucker, 2002):

$$Q_S = K_S(Q/W)^m S^n = K_S q^m S^n \quad \textbf{(eq. 3.9)}$$

Hybrid rivers lie somewhere on the continuum from the alluvial to bedrock end member models. These rivers are generally characterised by a combination, or alternation between, the extreme of a pure bedrock channel and environments of alluvial sediment deposition. As this model contains influences from both end-members of the model continuum it takes into account both sediment transport capacity and resistance to detachment of the bedrock material. The hybrid model is representative of an entire continuum of characterised river channels, and could represent the transition from one extreme of the spectrum to the other (Sklar and Dietrich, 1998). In such hybrid models, the effects of sediment flux on erosion rates are typically incorporated into a traditional stream power erosion law by including a function, f(Qs),that depends on the precise sediment transport and erosional dynamics (equation 3.10). (Sklar and Dietrich, 2004; Cowie et al., 2008): This can be expressed as:

$$E = dz/dt = f(Qs)KA^m S^n \quad \textbf{(eq. 3.10)}$$

When f(Qs) is approximately constant, this hybrid law behaves identically to a standard detachment-limited erosion law.

3.3: STEADY-STATE

A steady-state landscape is an important concept in geomorphology with fundamental work done by Hack (1960). Hack (1960) discussed landscapes in dynamic equilibrium and established the idea that landscape morphology could remain fixed in space if the rate of rock uplift was equal to the rate of erosion. In short landscapes can erode at the same rate, but the interaction of uplift and erosion could then maintain a steady-state topography. One method for assessing landscape equilibrium is through the river long profile (figures 3.1 and 3.2), which plots the distance downstream at points along the rivers path against the bed elevation at that point. This provides a visual method of determining features of interest in studies of river perturbation. In steady-state situations concave river profiles reflect a downstream decrease in slope that compensates for the increased discharge of rivers (Montgomery and Gran, 2001). By contrast, in a transient landscape, uplift rate and erosion rate are not equal; for example, uplift rate could outpace erosion due to ongoing-movement on faults.

Research in different field areas around the globe has shown that true steady-state conditions can be problematic to identify because of the transient nature of many geomorphic features that occur within the landscape due to conditions such as lithology or base level change (e.g., Snyder et al., 2000; Goldrick and Bishop, 2007; Whittaker et al., 2007). Consequently, some researchers have suggested that despite the theory of a steady state landscape, it may be practically unachievable due to the ability of conditions such as climate and tectonics to undergo rapid change (e.g. Snyder et al., 2000; Whipple, 2001; Whipple, 2004). Nethertheless, steady-state conditions have been clearly indicated in a few environments (Castillo-Rodríguez, 2011), being

documented in areas such as Taiwan (Whipple, 2001), and the Southern Alps in New Zealand (Crosby and Whipple, 2006). In other areas, whether the landscape is in steady state is subject to greater debate. For example Montgomery and Gran (2001) interpreted the Oregon Coastal Range, USA, as being in steady-state, yet Van Laningham et al., (2006) state that they have identified transient rivers, highlighting how methods can impact on conclusions when used differently or slightly varying criteria are used. In other areas such as Tibet it has been determined that the situation is nearly steady-state (e.g. Ouimet, 2007; Ouimet et al., 2009) but it cannot be concluded with conviction that steady state conditions have been reached.

Rivers modulate landscape responses to transient conditions and determine the shape and tempo of landscape evolution (Whipple and Tucker, 1999). The first studies into landscapes in steady state and rivers were carried out in alluvial rivers (e.g. Willgoose et al., 1991) with later research beginning to focus on bedrock rivers (e.g. Whipple and Tucker, 1999).

As there is a dynamic relationship between the fluvial erosion rate and the rate of uplift within tectonically active areas it is possible to define the rate of change of the river bed elevation (dz/dt) as the difference between the rate of uplift (U) and the rate of erosion (E):

$$\mathrm{dz/dt} = \mathrm{U} - \mathrm{E} \quad (\textbf{eq. 3.11})$$

Where uplift rate is equal to erosion rate the rate of change of the river bed elevation, which can be expressed in the form of any erosion model, is equal to 0 (dz/dt = 0). As a result of this under steady-state conditions the

different erosion models predict concave up river profiles (Whipple and Tucker, 2002).

As in tectonically active areas, uplift rate competes with erosion rate relative to a given base level so the rate of change in elevation of the river bed (dz/dt) can be expressed in the form of any erosion law (equations 3.11 and 3.12), containing the variables drainage area (A) and the slope of the channel (S), in which m and n are two empirically derived constants and K is a dimensional coefficient of erosion:

$$dz/dt = U - KA^m S^n \quad \textbf{(eq. 3.12)}$$

Under steady-state conditions dz/dt = 0 so the uplift and the erosion rate are the same, and since erosion rate is hypothesised to be equal to stream power, the uplift rate should be equal to the stream power.

$$U = KA^mS^n \quad \text{so} \quad E = KA^mS^n \quad \textbf{(eq. 3.13)}$$

If U and K are uniform along a channel, the exponent m and n control the concavity of the river, with m/n known as the concavity index (θ), which modulates the rate of change of a river channel gradient with increasing drainage area. If channel slope is expressed as a function of drainage area, as derived above, then the coefficient in equation. 3.14, $(U/K)^{1/n}$, controls the steepness of the river channel and is known as the steepness index (k_s). Both θ and k_s can be extracted from DEMs by linear regression on a log-log slope-area graph (Sklar and Dietrich, 1998; Snyder et al., 2000; Kirby et al., 2003). Taking into account θ and k_s slope can be expressed as:

$$U/K = A^m S^n$$

$$U/K * 1/A^m = S^n$$

$$S^n = U/KA^S$$

$$S = (U/K)^{1/n} A^{-m/n}$$

$$S = k_s A^{-\theta} \quad \textbf{(eq. 3.14)}$$

Typically values for θ lie between 0.4 and 0.7 but both larger and smaller values have been occasionally measured (e.g. Sklar and Dietrich, 1998; Snyder et al., 2000; Kirby et al., 2003; Boulton and Whittaker, 2009). A value of 0.5 for θ is considered to be reliable as values of around 0.5 seem to be typical in many locations (Hack, 1957; Sklar and Dietrich, 1998; Stock and Montgomery, 1999; Snyder et al. 2000; Whittaker et al., 2007). For example Snyder et al. (2000) studied rivers under steady-state conditions in northern California, where θ was relatively uniform giving and average value of 0.43. Whittaker et al. (2007) show that concavities exert a fundamental control on the long profiles of rivers because channel elevation against distance downstream (L) is a power-law function of drainage area ($L \approx Ka^{0.5}$ as shown by Hack [1957]). As a result of this most channels should produce a concave up profile in topographic steady-state, on the condition that K is uniform through the catchment (Whittaker et al., 2007).

Due to the uniformity of concave up profiles in steady-state conditions with unvarying K, research focuses on studying variation from the accepted standard concavity values and varying trends in steepness index, which equation 3.14 shows is related to uplift rate, U.

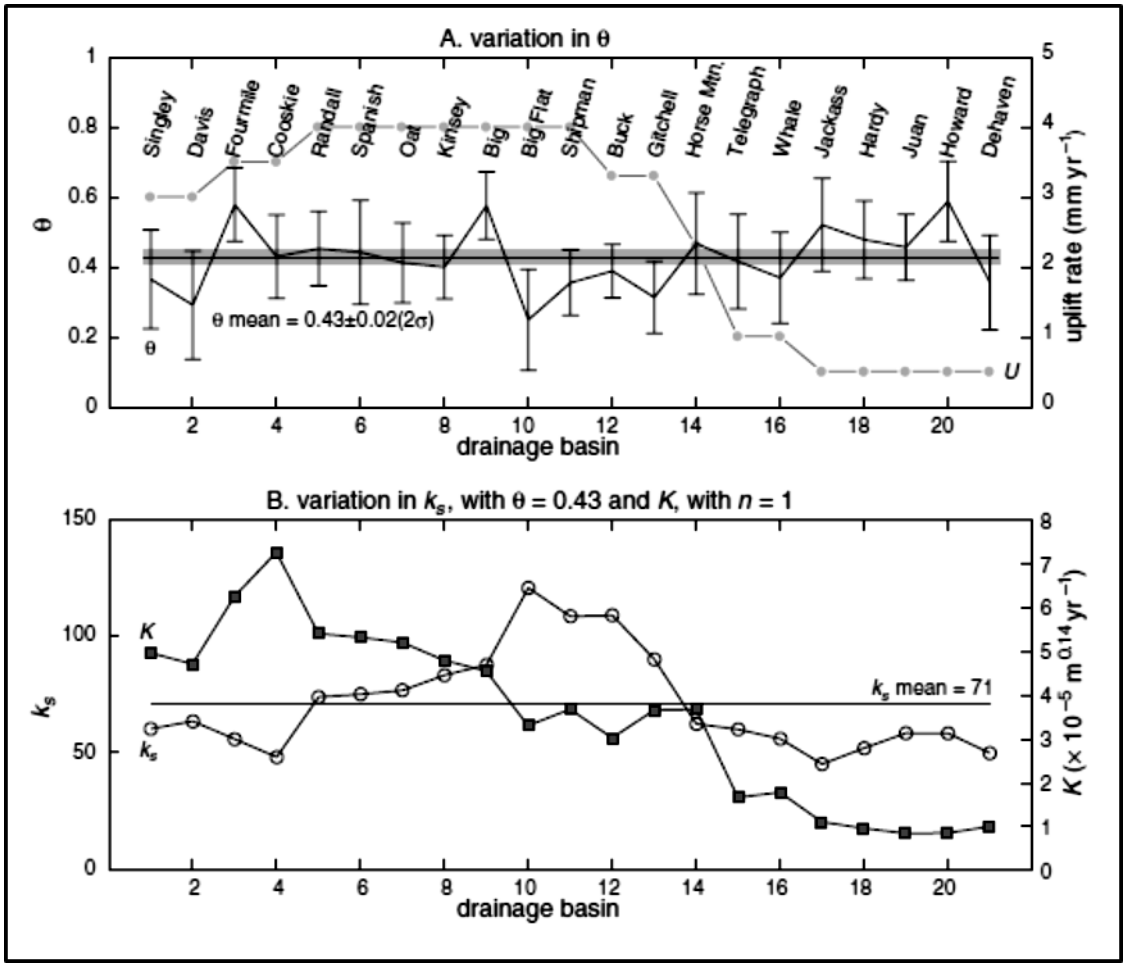

Figure 3.1: Figure showing a study of 21 river channels in the Mendocino triple junction area, California. Concavity and steepness index were compared to uplift rate, which is superimposed on the upper section of the graph as a grey line. Snyder et al. (2000) show that the steepness index is higher in areas of higher uplift rate, suggesting that steepness index is influenced significantly by the rate of uplift on faults that the rivers cross. From Snyder et al. (2000).

Snyder et al. (2000) studied rivers under steady-state conditions located in northern California, where they have been influenced by the movements of the Mendocino triple junction (figure 3.1). In this area the uplift rate varies between 0.5 and 4 mm/yr and the steepness index varies in line with the changes in uplift rate. Kirby et al. (2003) also determined that the areas of highest uplift rate had higher steepness indices, while ruling out significant effects from sediment flux, precipitation and drainage area. This study also

ruled out significant effects from lithology, which is important because rock resistance to erosion is also subsumed into steepness index via the parameter K, leaving uplift as the isolated main influence on steepness index. These results show that it is clear that steepness index includes information on uplift. Kirby and Whipple (2001) also investigated how channels respond to variations in uplift rate, after theoretically predicting results. They suggested that when channels flow towards areas of increased uplift, the concavity should be reduced, which when flowing towards areas of reduced uplift the concavity should increase. They then sought to test their predictions in the Siwaliks Hills, Nepal. A suggested weakness of their predictions is that concavity values do not appear to vary significantly between areas of varying uplift rate and those with uniform uplift rates (Kirby et al., 2003), although steepness index does.

Another approach to steepness index analysis is the use of a normalised steepness index (k_{sn}) (Duvall et al., 2004; Wobus et al., 2006a; Whittaker et al., 2007), which suggests that a reference concavity can be set, at around 0.5 based upon the uniformity of measurements from case studies. This technique can be used to examine which normalised steepness index values are typical for a region, because otherwise concavity and (un-normalised) steepness index co-vary (e.g. Hurtrez at al., 1999; Snyder et al., 2000). This is illustrated by Wobus et al. (2006a), who recognised a linear relationship between the normalised steepness index and uplift rates in Nepal. However, normalised steepness indices are very sensitive to the value of the reference concavity chosen in the analysis (Whittaker et al., 2007). Additionally, the assumption that steepness index implicitly reveals trends in uplift rates relies on the assumption that the landscape is in topographic steady-state and this may well not be the case in tectonically active areas (Whittaker et al., 2007).

In fact much research has endeavoured to investigate river channels that are being perturbed by tectonics (e.g. Tucker and Whipple, 2002; Whipple and Tucker, 2002; Crosby and Whipple, 2006; Attal et al., 2008; Whittaker et al., 2008; Boulton and Whittaker 2009; Whittaker and Boulton, 2012). A key result of these studies is to show that river channels in detachment-limited rivers can be expected to show variation from the 'equilibrium' concave-up profile when encountering an increase in uplift rate. In these circumstances the definition of equilibrium employed by tectonic geomorphologists applies; where a river crossing an area of increased uplift adjusts its ability to incise at all points so that it matches rock uplift (Willet and Brandon, 2002; Whittaker et al., 2007).

3.4: TRANSIENT LANDSCAPES

An important finding of research in the last 10 years is that while different erosion models predict similar steady-state fluvial landscapes (Whipple and Tucker, 2002), each model end-member is expected to respond differently to changes in boundary conditions, such as changes in the rate of movement along faults, uplift or base level fall (e.g. Whipple and Tucker, 2002; Tucker and Whipple, 2002 and others). Numerical models of fluvial landscapes incorporating both transport-limited and detachment-limited erosion behaviours suggest that in reaction to tectonic perturbation, the alluvial end member is expected to display a diffusive behaviour in response to changes in boundary conditions upstream from the location of localised perturbation, such as increased uplift as a result of faulting (Howard et al., 1994; Whipple, 2004). Profile adjustment is dispersed through the stream network as the channel responds to the perturbation, with the upper reaches of the stream able to react to the change in boundary conditions before full adjustment of lower reaches to

the increased rate of fault slip (Schumm et al., 2002). Under steady-state and transient conditions this reaction produces similar responses (Whipple and Tucker, 2002).

By contrast, bedrock river channels are characterised by a break in slope, known as a knickpoint (e.g. Howard et al., 1994; Snyder et al., 2000; Whipple and Tucker, 2002; Tucker and Whipple, 2002; Whipple, 2004; Whittaker et al., 2008; Boulton and Whittaker, 2009; Whittaker and Boulton, 2012). An increase in relative uplift rate, or a relative base level fall, will instigate a response of incision in bedrock rivers upstream of the fault that steepens the river channel, this response then passes up the river as a wave (Snyder et al., 2000; Whipple and Tucker, 2002; Harkins et al., 2007; Whittaker et al., 2010). The knickpoint is defined as the area of the channel with the highest change in gradient between the steepened reach below and the yet-to-steepen channel above (Crosby and Whipple, 2006). In this way the detachment-limited river can be divided into the channel below the knickpoint, which is responding to the new rate of uplift, and the channel above the knickpoint that is yet to be perturbed. This knickpoint (and hence the area of the river channel responding to the new boundary conditions) moves upstream in a predictable way, resulting in the migration of the knickpoint, and landscape response to the new rate of uplift moving upstream, away from the origin of the perturbation (Whipple, 2004). The section of the river below the knickpoint is responding to the new base-level or relative uplift-rate conditions, through processes such as channel steepening, channel narrowing and associated increases in stream power (Snyder et al., 2000; Whipple and Tucker, 2002; Crosby and Whipple, 2006), while the area above the knickpoint is in disequilibrium with the new conditions.

The differences between the processes of adjustment to transient conditions in alluvial and bedrock end members, outlined above, means that bedrock rivers are easier to identify when in a transient state (Whipple and Tucker, 2002); they display distinct breaks in slope in long-river profiles, and these can be measured in the field. The responses of the detachment- and transport-limited erosion laws to changes in base level fall or relative uplift rates suggests that only in the response of bedrock rivers to the changes in boundary condition will there be an abrupt change in channel morphology (Whipple and Tucker, 2002).

The response of the fluvial system to perturbations should be seen through the fluvial network of the area and in a variety of different ways within the fluvial systems. For example, Whittaker et al. (2007) shows that predominantly bedrock rivers respond to increases in fault throw rates by developing: significant long-profile convexities; a loss of hydraulic scaling; channel aspect ratios that are a strong non-linear function of slope; narrow valley widths; elevated coarse fraction grain-sizes, and reduced downstream variability in channel planform geometry.

The rate of this basin-wide transient response determines a number of things: the landscape response time to external forcing; the sediment delivery to depositional centres, and the dynamic relationship between tectonics, climate, and erosion - a coupling that is hypothesized to affect landscape evolution (e.g. Howard and Kerby, 1983; Howard et al., 1994; Seidl et al., 19940; Skylar and Dietrich, 1998; Tucker and Whipple, 2002; Whipple and Tucker, 2002; Attal et al., 2008).

As explained above the transient response of bedrock rivers to base level changes can differentiate competing fluvial erosion models (Whipple and

Tucker, 2002; Tucker and Whipple 2002). Tucker and Whipple (2002) suggest that it seems unlikely that any of the erosion laws that have been proposed are universal. They go on to say that it is important to identify suitable test cases for erosion laws. This is illustrated by some of the recent studies into bedrock erosion. Some studies suggest that transient river long-profiles can characterized by a transport-limited erosion model (Loget et al., 2006; Cowie et al., 2008; Valla et al., 2010), while conversely, other researchers have suggested a detachment-limited model explains their field data (e.g., Stock and Montgomery,1999; Whipple et al., 2000; Kirby and Whipple, 2001; Attal et al., 2011). Attal et al. (2011) addressed these contrasting findings and suggest that the differences are due to the relative volume of sediment being transported through the fluvial system. In this study they tested the capability of transport and detachment fluvial erosion models to reproduce the already well-documented evolution of three river catchments in the central Apennines, Italy, which have independently constrained increases in relative uplift rate. They found that the transport-limited model could not reproduce the catchment response to an increase in uplift rate, while a detachment-limited model could, consistent with the low sediment supply in the channels (Attal et al., 2011).

What is clear from the previous works is that the study of transient responses of rivers to base level change requires additional case study sites that can provide a snapshot of a transient response to a quantified base level change. These areas should be used to place constraints on the dynamic response of fluvial systems (Tucker and Whipple, 2002).

3.5: KNICKPOINT THEORY

Studies of the fluvial geomorphology in bedrock rivers have utilised the river long profile extensively to identify changes in slope along the river profile (e.g. Knighton, 1998; Burbank and Anderson, 2001; Crosby and Whipple, 2006; Whittaker et al., 2008) (figures 3.2 and 3.3). The long profile provides a visual method of determining features of interest in studies of river perturbation. As a consequence of a change in boundary conditions, such as a decrease in base level, the typical concave-up river profile will be perturbed if the river is detachment-limited or hybrid-type river, developing the distinct break in slope already referred to as a knickpoint (figure 3.2). As a result of this perturbation, areas of the channel develop a localised of steepening, a convexity, referred to as a knickzone (Tucker and Whipple, 2002; Whittaker and Boulton, 2012). The knickzone extends from the area of initial perturbation (i.e. a fault) to the knickpoint, which represents the point at which there is the greatest change in slope gradient (Tinker and Wohl, 1998).

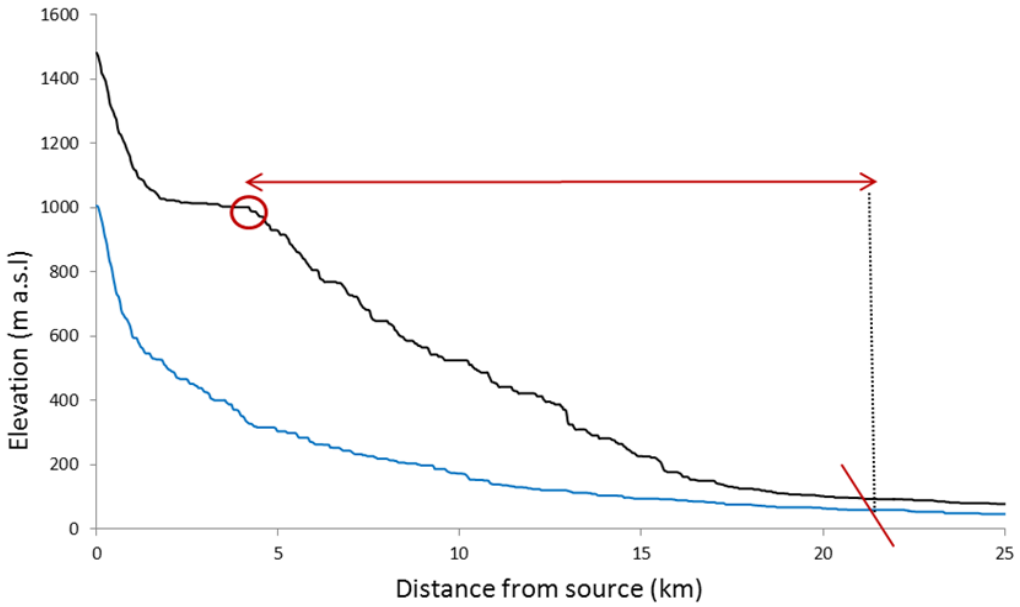

Figure 3.2: Representative examples of river long profiles. The blue profile exhibits the smooth concave up shape of a river presumably in equilibrium with its boundary conditions. The black profile exhibits a knickpoint (red circle) and a knickzone (indicated by the red arrow), indicating channel has been perturbed.

This knickzone is transferred up the river stepwise (figure 3.3), which can be explained by the influence of change in slope on stream power. When the slope is steepened the stream power is also elevated, this causes increased erosion of the bedrock and this process continues up the river towards its source. This suggests that as there is a link between stream power erosion laws and knickzone migration the stream power erosion laws can be useful tools in quantification of knickzone migration. This potential to quantify knickzone retreat in relation to the forcing mechanisms is a key consideration in tectonic geomorphology.

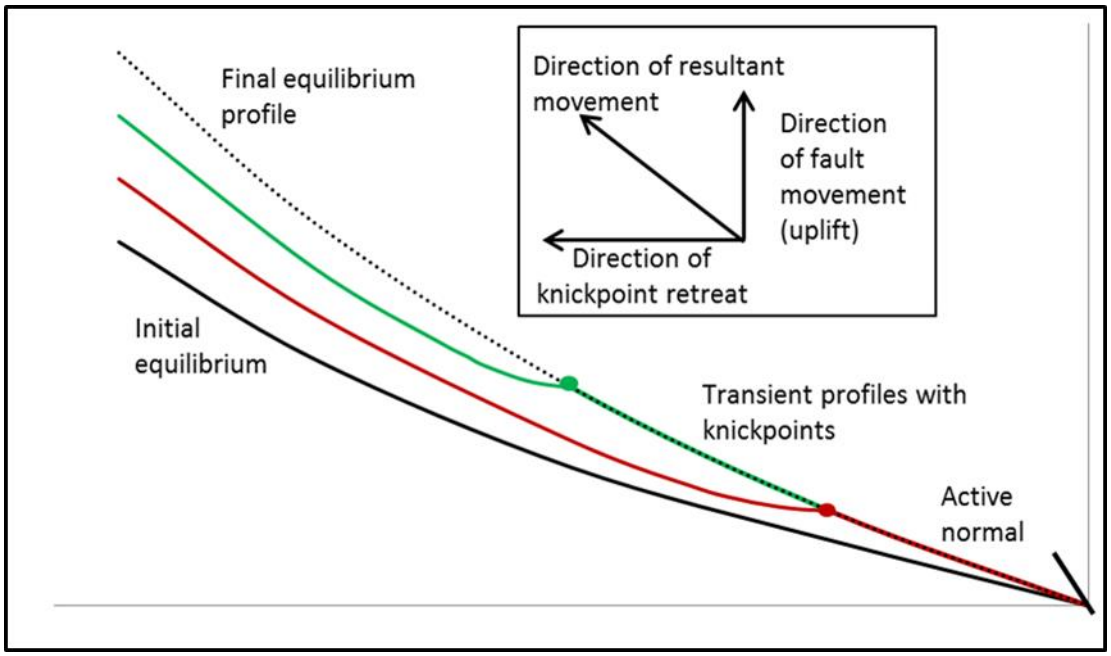

Figure 3.3: A schematic graph showing the evolution of a detachment-limited channel in response to perturbation by movement of a normal fault. The channel evolves from the black line through the red and green lines to the dotted line over time with a knickpoint that migrates backwards up the channel.

To quantify the relationship between the boundary conditions and river profile adjustment the average rate of knickzone retreat (V) can be calculated (**eq.15**) by dividing up-stream distance between the fault and the knickzone (Δx) by time since the initiation of faulting or increase in fault movement (Δt) (Crosby and Whipple, 2006; Whittaker and Boulton, 2012).

$$V = \Delta x/\Delta t \quad \textbf{(eq. 3.15)}$$

This method may provide a first order quantitative measure but the situation in reality is more complex than this simple relationship, because lithology (Anthony and Granger, 2007) and catchment size (Bishop et al., 2005) have been illustrated to influence the rate of knickzone migration. It has been suggested that catchments in Italy and Turkey can be described by a unit stream power law which enables the rate of knickpoint retreat to be deduced (Whipple and Tucker, 2002; Whittaker et al. 2007, 2008; Boulton and Whittaker, 2009). Expressing the erosion rate E and Slope, S in a stream power erosion law as partial differentials of elevation, z, time, t, and stream-wise distance, x, we can write:

$$E = dz/dt = KA^m(dz/dx)^n$$

Consequently as $S^n = S \times S^{n-1}$, we obtain:

$$dz/dt = KA^m(dz/dx)(dz/dx)^{n-1}$$

Re-arranging, this gives:

$$(dz/dt)(dx/dz) = KA^m(dz/dx)^{n-1}$$

This can be simplified to:

$$(dx/dt) = KA^mS^{n-1}$$

and as dx/dt is a velocity, we predict that the knickpoint retreat rates should scale as:

$$V \sim \Psi A^{m} S^{n-1} \quad \textbf{(eq. 3.16)}$$

The Ψ parameter serves to substitute for K and contains variables such as bedrock strength, climate, sediment flux, channel geometries and tectonics. This formula describes knickpoint retreat rates as being heavily influenced by drainage area to the power m, with larger drainage areas producing a faster retreat rate. Slope is also considered, but is eliminated when n=1, as obtained for a unit stream power model. Knickpoint retreat rates can be split into horizontal and vertical retreat rates, which is significant because the vertical retreat rate is dependent upon the difference between the uplift rate and vertical incision, while the equations 3.15 – 3.16 pertain to the horizontal knickpoint retreat rate, taking into account the drainage area of the river and to some extent the slope of the river channel. Whittaker and Boulton (2012) investigated the influences on knickpoint retreat rates in relation to equation 3.16 on rivers in southern Turkey (figure 3.4). They considered rivers with similar drainage areas and different fault slip rates and found that even while controlling for drainage area variations in this way there was still a six to seven fold difference in knickpoint retreat rates. This shows that that beyond the simple assumptions and maths in equation 3.16, the Ψ parameter varies also with fault slip rate.

The vertical propagation of knickpoints is dependent upon the difference between uplift rate and vertical incision (Whittaker, 2012). Theory and numerical modelling of vertical knickpoint propagation has suggested that the vertical movement of the knickpoint through a landscape should be independent of the

discharge and therefore drainage area of a river. It should instead respond to a relative uplift rate perturbation, such as in the situation when a river crosses a fault which has undergone a change in its slip rate, or a reduction in the fluvial rate of erosion (Crosby and Whipple, 2006). For example, Whittaker et al. (2008) show how the vertical elevation of long-profile convexities in transient channels in the Central Apennines, Italy, appear to scale with the magnitude of uplift rate increase both between different faults in the Apennines, with a

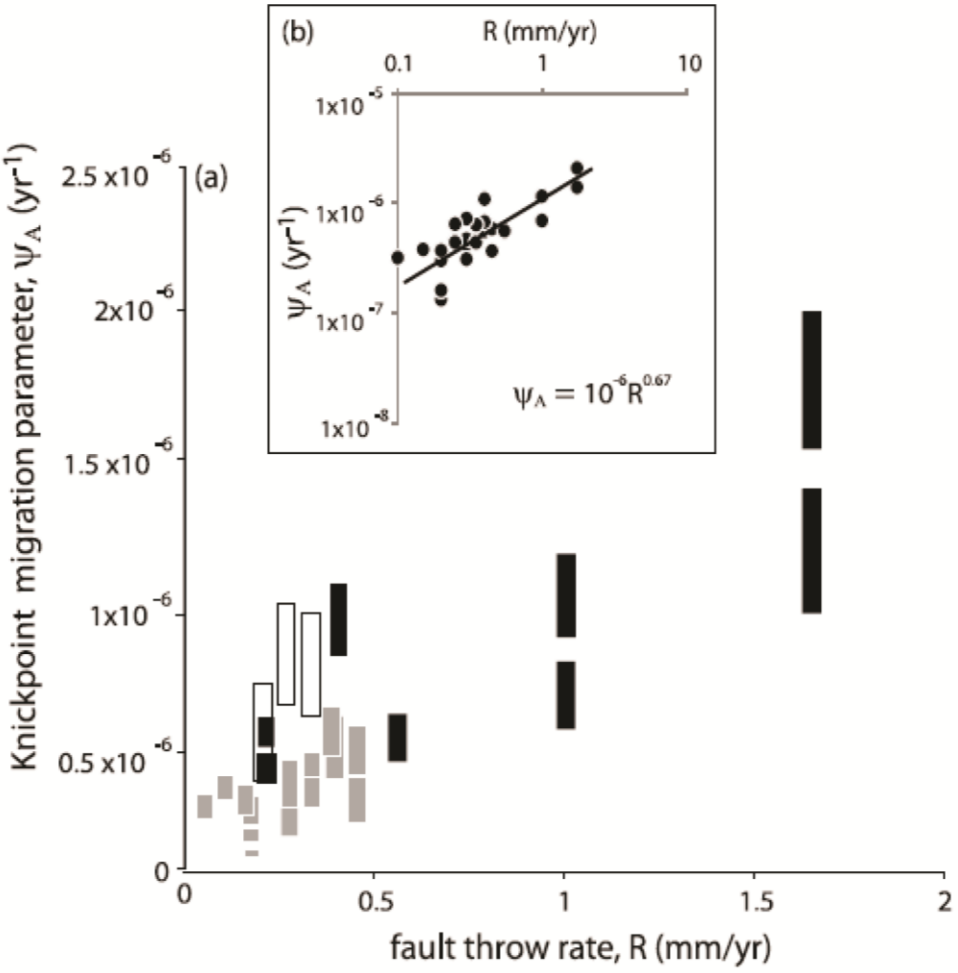

Figure 3.4: (a) Shows a plot of drainage-area-normalized knickpoint migration rate parameter, ΨA, against fault throw rate, R, for catchments in Turkey (gray bars) and Italy (black bars). Bars span a range of ΨA values for fault acceleration at 0.7–1 Ma in Italy, and 1.2–1.6 Ma in Turkey. White bars show ΨA estimates for Italian catchments crossing active normal faults. (b) Log ΨA against log R for maximum knickpoint migration rates for all channels. Line of best fit is a power law regression through the data, with the best fit equation shown. From Whittaker and Boulton (2012).

doubling of throw rate resulting in a factor of around two increase in knickpoint height. Further to that, Boulton and Whittaker (2009) produced study of knickpoints in southern Turkey which corroborated the findings that the height of the knickpoint above the active fault mirrors the local throw rates. Whittaker at al. (2008) concluded that there is a linear relationship between the throw rate, and the uplift rate increase, which is the difference in throw before and after the throw rate increase. The response of the knickpoint height to the uplift rate increase is thought to be due to the steepening of the channel bed in response to the perceived uplift, which it turn increases the fluvial incision rate leading to upstream migration of the knickpoint (Whipple and Tucker, 2002; Whittaker et al., 2008). Overall, Whittaker et al. (2008) suggest that the size of the convexity within the channel is a function of both the magnitude of the perturbation and the speed at which the knickpoint moves upstream. The relative motion of the knickpoint upstream is therefore a result of the interplay between the horizontal component of movement and the vertical component of movement. This suggests that measurement of the height of knickpoints above the active fault is a useful tool in the determination of throw rates.

3.5.1: KNICKPOINT RETREAT AND TECTONICS AND BASE-LEVEL CHANGE

Knickpoints resulting from base level variations (e.g. tectonic uplift on a fault, and/or eustatic sea-level change) are believed to be the dominant mechanism by which the dynamic relationship between tectonics and climate is conveyed to the landscape (Whipple and Tucker, 1999; Bishop, 2007). When a fall in base-level occurs owing to fault movement, a knickpoint is formed at the fault location that propagates headwards (Whipple and Tucker, 1999). The

derivation of fault-influenced knickpoint retreat rates are complicated by factors such as lithology and climate, encapsulated within the K value, that are not yet fully understood. Despite this, on-going research has attempted to reproduce detachment-limited channel incision in response to a lowering of base level (e.g., Howard, 1998; Whipple and Tucker, 1999; Snyder et al., 2000). In what can now be considered pioneering work into river profiles within the Himalaya, Seeber and Gornitz (1983) proposed that anomalously high channel gradients represent locally high uplift rates. Since 1983 geodetic surveys have been carried out (Jackson and Bilham, 1994) that have supported this initial suggestion and in recent years work into the influence of tectonics on river profiles has intensified. Whittaker and Boulton (2012) compared river long profiles and boundary conditions of rivers in the Central Apennines of Italy, and in Southern Turkey in an attempt to evaluate the relative effects of fault movement on the profiles of detachment-limited rivers in both areas. They observed several notable trends in the data, concluding that the response times of landscapes are strongly linked to the tectonic perturbations occurring on faults cutting across the rivers. Specifically they refer to the magnitude of the tectonic perturbation, concluding that higher throw rate leads to a higher rate of knickpoint migration. Their data show that for rivers with similar drainage areas, an order of magnitude difference in fault throw rate can lead to a six to seven fold difference in the rate at which the knickpoint moves.

Thus rivers perturbed by a greater degree of fault movement will regain their steady state conditions more quickly than those rivers with a smaller rate of uplift on faults. The dependence of knickpoint retreat rate on fault slip rates can be explained by the effect of dynamic channel adjustment to the faulting (Attal et al., 2008; Whittaker and Boulton, 2012), because the Turkish and

Italian rivers documented by Whittaker and Boulton (2012) show narrower and steeper channels in the rivers that cross faster-moving faults.

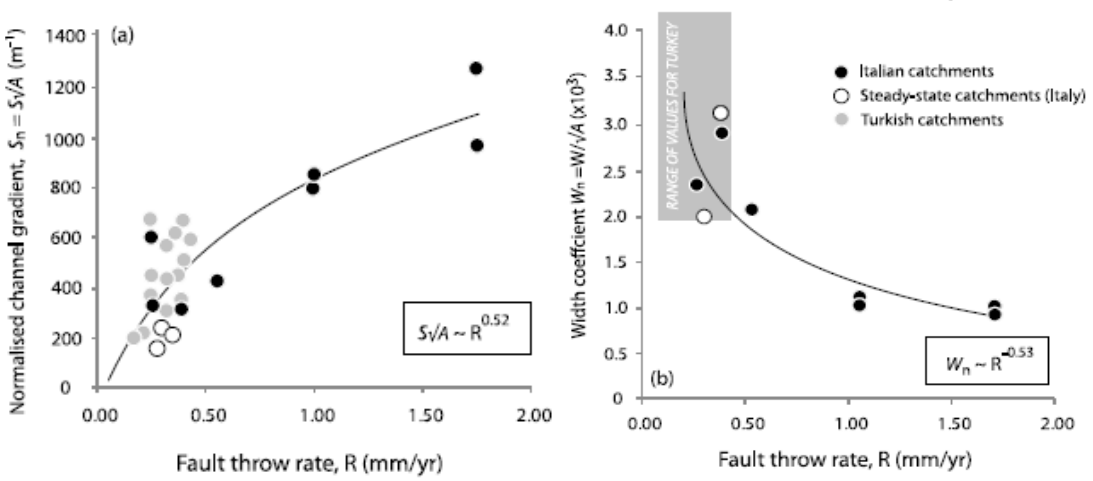

Figure 3.5: (a) Shows a plot of drainage area normalized channel slope, Sn =S√A against fault throw rate, R. Line shows best fit power law dependence of Sn on R. (b) Mean knickzone channel width, Wn, normalized for drainage area at the fault, against fault throw rate, R, for Italy (points) and Turkey (box shows data range). Line shows best fit power law dependence of Wn on R. From Whittaker and Boulton (2012).

3.6: EFFECTS OF CLIMATE ON RIVER GEOMORPHOLOGY

Climate has proven to be a difficult variable to examine in terms of rivers and landscape evolution. Climate can play a significant role in the amount and variability of run off and erosion thresholds, also in the growth or absence of anchoring vegetation that can in turn affect landscape evolution both by varying the rate at which landscapes are modified and by altering the pattern landscape changes (Whipple, 2004; Kent, 2011; Whittaker, 2012). Climate change can also create major eustatic change which would in turn affect sea level and so base levels in some areas.

Wobus et al. (2010) present an argument for differing characteristics for climatically driven and tectonically influenced changes in landscape evolution.

They propose that tectonically driven perturbation travels upstream in a wave from the site of the initial change in conditions while a climatically induced change in incision would produce a downstream wave of incision. This climatic effect is driven by an increase in the amount of water delivered to a river system, resulting in the downstream migrating wave of incision and a relaxing of the channel gradient.

Whittaker and Boulton (2012) concluded that climate can have a significant influence on the rate of knickpoint movement using data from the rivers they studied in Turkey and Italy, which have different climatic settings. Notably, there is a factor of two difference in the aridity in the two study areas with the Hatay region of Turkey being significantly more arid. For the Italian rivers studied, the drainage-area-normalised knickzone migration rate was found to be twice as fast as the rate for the more arid Turkish rivers. Whittaker and Boulton (2012) put forward the explanation that climate plays a major role in driving this difference. When the unit stream power model is adjusted to take into account precipitation and groundwater influences, a doubling in these factors would indeed be expected to lead to a four-fold increase in the speed of knickpoint migration.

3.7: EFFECTS OF LITHOLOGY AND SEDIMENT FLUX ON RIVER GEOMORPHOLOGY

A potentially important but often neglected influence in determining the rate and style of bedrock river response to a change in relative base level is bedrock lithology (Stock and Montgommery, 1999; Reneau, 2000; Anthony and Granger, 2001; Bishop et al, 2005; Brocard et al., 2006). A more resistant lithology in a river channel should theoretically require a higher stream power to

keep pace with tectonic uplift on a fault than an identical river incising across a weaker lithology. As such, the nature of the control exerted on knickpoint retreat and bedrock incision by lithology is an outstanding issue (Castillo-Rodríguez, 2011, Crosby and Whipple, 2006; Anthony and Granger, 2007; Haviv et al., 2010; Whittaker and Boulton, 2012). Lithology is often identified by researchers as being of particular significance in modulating bedrock river response to tectonics because it affects K in any stream power erosion law (Goldrock and Bishop, 1995; Anthony and Granger, 2007; Cook et al., 2009; Allen et al., 2013; Ferrier et al., 2013; Croissant and Braun, 2014). However, there is currently little consensus as to the magnitude of this effect nor is there currently an easy way to link measurements of bedrock type or strength directly to the K value used in either numerical models or empirical field studies. Consequently, while acknowledged as a complicating factor, it is often ignored in many geomorphic studies (Castillo-Rodríguez, 2011, Crosby and Whipple, 2006; Anthony and Granger, 2007).

Nevertheless, a few studies have tackled this question, with mixed results: Stock and Montgomery (1999) investigated rivers from Kauai (Hawaii), Australia, California and Japan and they found varying relationships between lithology and knickpoint retreat when using a stream-power-derived equation. They found that taking into account the lithologies of the areas mentioned, volcaniclasic rocks, granitoids and metasediments the value for K can vary over 5 orders of magnitude. Anthony and Granger (2007) proposed that progress of the knickpoint upstream in the tributaries of the Upper Cumberland River, USA was significantly influenced by lithology. Major differences in knickpoint retreat rates, which vary from 4000 mm/yr to 100 mm/yr, were observed in river between karstic lithology and other rock types. The authors suggest the

standard models for fluvial erosion laws are not sufficiently descriptive for karstic environments. They propose this insufficiency could in part be due to the substitution of the drainage area for the discharge because in this situation as the drainage area and discharge are not, in this case, linearly related. The important issue identified in the study by Antony and Granger, (2007) is that that certain lithologies may affect knickpoint migration in an obvious way associated explicitly with the lithology.

Others (e.g. Cook et al. 2009) have found that, in general, the properties of the lithology in addition to hardness may be important in determine the influence of lithology on erosivity. Cook et al. (2009) show that the orientation of the lithological layers may also provide a significant cause for knickzones and influence the speed at which they move. Cook et al. (2009) studied the Colorado River around Lee's Ferry, the location of a significant knickpoint (Wolkowinsky and Granger, 2004; Karlstrom, 2008). The authors modelled river profiles and incision rates using cosmogenic dating methods and propose that a recent pulse of incision is the result of headward propagation of incision in combination with the influence of an upstream dipping lithological boundary. They conclude that the combination of these effects is causing a complex pattern of adjustment in the Colorado River. However, recently Whittaker and Boulton (2012) found no significant influence of rock hardness on knickpoint retreat rate using Schmidt hammer measurements and the Selby rock mass strength measurement technique for transient catchments in both the Hatay Graben of Turkey and the Italian Apennines. This is despite the fact that rock hardness is often suggested as a factor exerting high influence on the velocity of knickpoint retreat by studies (Miller, 1991; Hancock et al., 1999; Stock and Montgomery, 1999; Crosby and Whipple, 2006). An additional problem is that

climate effects can also be subsumed into the value of K, with limited work (e.g. Whittaker and Boulton, 2012) having addressed this outstanding challenge

Another way in which lithology can influence the ability of a river to incise into the bedrock is sediment availability in the channel. Two effects have been documented by which sediment supply could influence fluvial erosion (Gilbert, 1877; Sklar and Dietrich, 1998; Sklar and Dietrich, 2001). If the sediment flux coming from upstream is low, incision rates are likely to be limited, due to the presence of few clasts in transport. These impact and abrade the channel bed and consequently increased sediment flux in the river leads to higher erosion rates, because more 'tools' are supplied from upstream to erode the channel bed. However, when sediment flux is too high the opposite becomes the case and large amounts of sediment can cover the bedrock channel and shield the bed from impact and abrasion wear. This 'cover effect' protects the channel base from erosion and any subsequent increases in sediment supply would serve to reduce erosion rates further still (Sklar & Dietrich, 1998; Sklar & Dietrich, 2001).

The ability of the 'tool effect' to increase abrasion at intermediate sediment supplies has been illustrated through experimental techniques using abrasion mills (Sklar & Dietrich, 2001; Cowie et al., 2008; Turowski and Rickermann, 2009; Meshkova, 2012). Sklar and Dietrich (2001) also state that the rock erosion rate declines rapidly with decreasing grain size in their experiments. This suggests that suggests that finer sediments carried within the water are inefficient tools eroding bedrock river channel, compared to the coarser sediments that are transported as bed load. Jansen et al. (2011) studied knickpoint retreat rates in rivers in western Scotland and found that knickpoint retreat rates have decreased by two orders of magnitude since the

early to mid- Holocene. They inferred that this slowing in postglacial knickpoint retreat was due to the depletion of paraglacial sediment supply over the Holocene, which lead to a deficiency of “tools” for bedrock erosion. The models for bedrock incision that do not take into consideration the tools effect can therefore over-predict incision rate for low sediment supply rates (Sklar and Dietrich, 2006).

To derive the effect of lithology and sediment supply on channel response to active tectonics, and important next step is to establish case studies in where the nature of both the tectonic forcing and the transient response of the river to this forcing are temporally and spatially well-constrained. Such case studies would allow for (i) the observation and modelling of hydraulic scaling adjustments to tectonic forcing; (ii) the comparison of river response to active faulting where lithological variation can be compared explicitly and (iii) where the differences between modelled, predicted and ‘real’ erosivities can be contrasted effectively.

3.8: WHERE ARE WE NOW?

Much progress has been made into understanding the dynamic relationship between rivers and landscape over the last fifteen to twenty years (Howard, 1998; Whipple and Tucker, 1999; Snyder et al., 2000; Tucker and Whipple, 2002; Whipple and Tucker, 2002; Crosby and Whipple, 2006; Attal et al., 2008; Whittaker et al., 2008; Boulton and Whittaker, 2009; Whittaker and Boulton, 2012 and others).

In order to understand the landscape response to external forcing mechanisms such as tectonics and climate ‘landscape evolution models’ have been produced. A key breakthrough of these models, such as CHILD (Tucker

et al., 2001), is that they allow the modelling through time of the evolution of a topographic surface by fluvial and hillslope erosion and sediment transport. Since the development of the landscape evolution models, work has begun to focus on how to best parameterise the upland river systems in terms of the behaviours, geometry and erosive processes that operate within the river systems, as fluvial erosion is a significant component of landscape evolution models. Being able to select an appropriate fluvial erosion model (detachment-limited, transport-limited and hybrid) is key, given that at topographic steady state the landscape evolution models can produce similar results for the three erosion models. As the assumption of steady state proved ineffective for this problem, a major breakthrough was made with the realisation that studying rivers undergoing transient responses to tectonics could yield more promising results (e.g. Howard et al., 1994; Snyder et al., 2000; Whipple and Tucker, 2002; Tucker and Whipple 2002; Whipple, 2004; Whittaker et al,, 2008; Boulton and Whittaker, 2009; Whittaker and Boulton, 2012). Under transient conditions alluvial rivers should respond diffusively while detachment-limited rivers should develop long-profile convexities (Whipple and Tucker, 2002). It has only recently been shown that rivers are responding unambiguously to tectonic perturbation and since been established that bedrock rivers do respond in a transient way to tectonic perturbation (Whittaker et al., 2008). This has been a key breakthrough, in fact it is now widely accepted that the response of detachment-limited rivers respond to tectonics can be understood to first order by the use of the stream power family of incision models (Kirkby and Whipple, 2012).

For example, it is now possible to exploit the measured vertical heights of knickpoints to investigate tectonics as it has been shown that knickpoint heights

scale with relative uplift (e.g. Boulton and Whittaker, 2009). It is also possible to predict how far a knickpoint will travel upstream, based upon the size of the rivers drainage area. The progress made on the links between drainage area and knickpoint celerity mean that knickpoint data, when combined with drainage area information, can provide useful constraints on causes and timing of knickpoint initiations when studying multiple rivers.

Consequently, it is now possible to focus on using well-constrained field sites to answer detailed questions such as the major influences on knickpoint celerity, such as climate and lithology which are currently subsumed into the K parameter in erosion laws. Identifying detachment-limited rivers, in areas with well constrained geological variables is therefore a key endeavour.

Another current key question within earth sciences is to what extent is it possible to gather tectonics information directly from the fluvial system. As discussed above, there have been a number of studies that have attempted to collect tectonic information from fluvial networks, and they have had some success in analysing systematic information about river systems and extracting from it patterns of active deformation in the study area (e.g. Seeber and Gornitz, 1983; Merrits and Vincent, 1989; Lavé and Avouac, 2001). The limits on this research are currently set by a lack of calibration of the model parameters (Duvall et al., 2004). It is therefore necessary to consider real geological constraints; for example it is vital to have a well quantified tectonic signal, such as throw rate, when undertaking studies into how bedrock rivers respond to changes in climate and tectonics.

As such, the ability to extract tectonic information from the fluvial system requires an understanding and quantification of the relationship between such factors as channel gradients, lithology, and uplift rates. What is now needed is

the identification of case study sites that can provide a snapshot of a transient response to a quantified base level change. These areas must allow for independently quantified uplift rates, and well constrained lithology, combined with in-depth field and computational measurement of fluvial morphology. This will enable the analysis and quantification of the nature of the transient responses occurring within perturbed bedrock river systems.

CHAPTER 4

TIME AVERAGED, LONG-TERM, RATES OF FAULT MOTION FOR THE GEDIZ GRABEN

4.1: CHAPTER HIGHLIGHTS

- The faulting within the Gediz Graben has been two phase: Low-angle normal faulting dominated the formation of graben topography between 16 – 2.6 myr, high-angle normal faulting has been dominant since 2 myr.
- This study quantifies the rate at which throw has been occurring over the last 2 myr, with rates varying between 0.4 mm/yr and 1.5 mm/yr along strike.
- The distribution of different rates along strike of the graben bounding fault array suggests that the fault segments have become linked during the last 2 myr.
- The further study of the graben bounding fault arrays suggest that an earthquake occurring along the fault array could have a predicted Mw of 6.3 to 7.9, depending upon how much of the array ruptures.

4.2: INTRODUCTION

This chapter discusses the ways in which previous researchers have quantified the rates of active faulting, discussing aspects of the method such as the time periods over which specific methods can be used and what pre-existing features are needed to make the method useful in a given area. The

advantages and disadvantages of the techniques will be discussed in order to determine the best method to use in the Gediz Graben.

The chapter then reviews what is known about the active tectonics of the Gediz Graben and highlights the gaps in the current knowledge of the active tectonics of the region. In order to address the highlighted issues and knowledge gaps, this study then presents new throw rates on the high-angle normal faults using a combination of established and novel methodologies. The Gediz Graben was chosen for this study as the rates of throw on the active normal faults that control the topographic evolution of the area are unknown but there is a well constrained structural and stratigraphic framework as well as seismic and borehole data. This study will take into account the implications of these novel throw rates on the hazards to the surrounding area produced by the new data set.

4.2.1: FAULTING AND SEISMICITY WITHIN THE GEDIZ GRABEN

The Gediz Graben has been inhabited, with significant built infrastructure, since at least 472 BC (Hanfmann et al., 1983). The ancient town of Sardis, which can still be seen near the modern town of Sart, was the capital of the ancient kingdom of Lydia and one of the most important cities in the Persian Empire. In 17 AD the Lydia earthquake caused extensive damage to the region including the city of Sardis, sustaining damage from which it never truly recovered (Ambraseys, 2009). The damage can still be seen in the ruins of the city today.

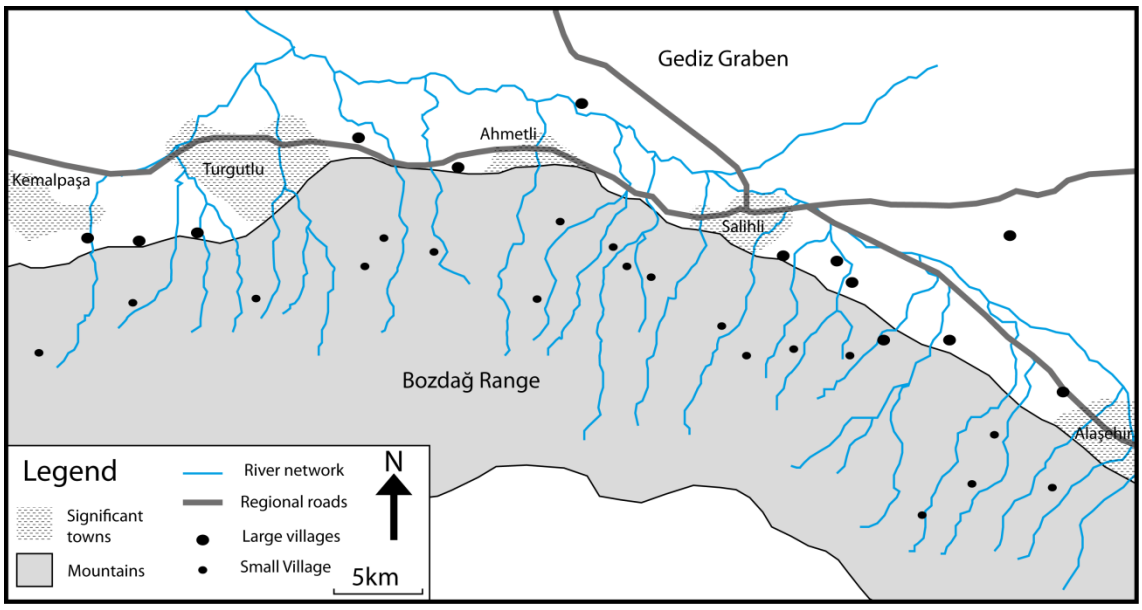

Figure 4.1: A map of the southern Gediz Graben showing the high elevation area (grey) and the valley areas (white); the black line represents the limit of the topographic elevations and the approximate location of the graben bounding faults. The river and road networks are marked on with the rivers (blue) illustrating the streams draining out of the mountains and into the Gediz valley. Significant population centres are marked with a hatched pattern and additional settlements are marked with black dots dependent on size. The larger towns and villages are in a position very close to the graben bounding fault array and there are a significant number of smaller villages within the mountains.

The Gediz Graben has been continually inhabited since the time that Sardis was a significant seat of power, and the modern graben is now the location of several towns with significant populations of around 50-150,000 people (figure 4.1 [http://www.turkstat.gov.tr/]), notably, Turgutlu (122,383 urban population of 2012), Salihli (98,618 urban population of 2012) and Alaşehir (48,147 urban population of 2012). There are also many villages of populations of over 1000 people situated between the major population centres and many others situated along the river valleys and around the locations of significant regional high-angle normal faults within the graben margin (figure 4.1). These villages persist up to the higher altitudes, some being situated on the detachment surface. A common feature of all of these settlements irrespective of size is their proximity to active faulting, is that many of the major towns and villages are built on or next to active faults, that bound the Bozdağ Range.

The risk to these settlements is illustrated by the recent earthquakes that have occurred the Gediz Graben and surrounding region; including three earthquakes of over M_w 5.0 in the last twenty five years (Eiodogan and Jackson, 1985; Buscher et al., 2013). A significant earthquake of magnitude 6.9 occurred in 1969, creating a surface rupture of around 30 km (Arpat and Bingol, 1969). Another earthquake occurred within the Gediz Graben in March 1970, this 7.2 magnitude earthquake left thousands homeless and over 1000 people dead; it led to the total relocation of the village of Gediz (Mitchell, 1976). Additional large-magnitude earthquakes occurred in 1866 and 1944 (Ambraseys and Jackson 1998). Outside of the graben, the 2011 Kütahya earthquake, of 5.8 M_w, caused shaking of buildings in the Gediz Graben (Yılmaz and Avşar, 2013).

This evidence of destructive earthquakes shows both that there are ongoing active tectonics within the Gediz Graben, and that population centres are at risk from the active faulting. In the Gediz Graben, it would be advantageous to have quantified fault movement rates of the graben bounding normal faults as there are currently no estimates for fault slip along the 120 km extent of the high-angle normal faults on, or near, which the large settlements in the graben are built (figure 4.1).

4.2.2: FAULTING AND THE LANDSCAPE

Faults show significant variations in their properties such as length, dip and depth to which they propagate (e.g. Twiss and Moores, 1992); this variation in properties leads to differences the earthquake potential of the fault as well as in the development of the seismic landscape (e.g. Koons and Kirby, 2007; Hovius and Von Blanckenburg, 2007; Wobus et al., 2006a). Due to these variations, and the ability of faults to fundamentally control landscapes, it is

useful to know as much about faults as possible, especially when they coincide with populated areas.

The current understanding of landscape response to external forcing indicates that the rate of erosion resulting from changing boundary conditions is controlled by a variety of factors including annual rainfall, bedrock lithology, base-level drop, rate of rock uplift, and fluvial and hill slope processes (e.g., Howard et al., 1994; Sklar and Dietrich, 1998, 2004; Whipple and Tucker, 1999; Whipple et al., 2000; Simpson and Schlunegger, 2003; Densmore et al., 2003; Dorsey and Roering, 2006). Therefore, faults are an important factor in landscape evolution because they allow for uplift of rock units, thereby impacting on hillslope processes. Uplift of rock units within the footwall of the normal faults, for example forms significant topography in landscapes, creating areas of high escarpments and ranges juxtaposed with low valleys.

In this way, normal faults can significantly impact the erosion, transport and deposition of sediment in the area by creating hillslopes and allowing for the formation of significant river networks that drain the high-elevation areas and generally flow into a principle river within the valley. Topography like this can be found in many mountainous with significant regional normal faulting.

4.2.3: FAULTING AND SEISMIC HAZARD

Gaining greater insight into the activity of the faults within the Gediz Graben is important because factors such as fault geometry and movement rates are of use in the consideration or seismic hazard (Wesnousky, 1986; Bilham et al., 2001; Sutherland et al., 2013). Determining whether or not faults are active is important for planning and seismic hazard mitigation, for example in California it is not permitted to construct new building on or near faults that

have been actively moving within the last 11,000 years (Hart and Bryant, 1997). Building regulations such as those used in California are of less use when settlements already exist such as in the Gediz Graben. In these situations possessing a greater amount of information about the faults in the area is necessary if seismic hazard is to be considered, and if strategies for dealing with risks to settlements caused by tectonic hazards are to be assessed.

An understanding of the manner in which a major fault is segmented into an array of fault strands is considered an important aspect in understanding the hazard posed by a fault. Observations have shown that long faults do not usually rupture along their whole length during seismic events (Geophysics Study Committee, 1986; Schwartz and Coppersmith, 1986). Key questions that arise from the understanding that faults tend to rupture only along part their length are: 1) to what degree is the location of rupture random, or does it reflect segmentation? 2) Can these segments be identified using geologic, seismologic or geophysical data? Surface geology and changes in fault geometry commonly appear to have a one-to-one correlation as a result of rupture processes occurring at seismogenic depths (Schwartz and Coppersmith, 1984). Because of this it should be possible to use geologic and geophysical data to define segments.

Quantifying rates of movement on faults is an important consideration in the analysis of seismic hazard because the rates can be used to compare the relative activity of faults. Schwartz and Coppersmith (1986), however, caution against the use of fault movement rates these do not necessarily correspond to earthquake potential in a direct way. Faults with high rates of motion can produce large earthquakes, but it is also possible for faults with lower rates to produce large earthquake events too.

Despite the ambiguity between slip rates and the size of the associated earthquakes it is recognised that although the slip does not correspond with the magnitude of the earthquake, faults that are moving faster will produce more frequent earthquakes than slower moving faults (Cowie and Roberts, 2001; Roberts et al., 2004) .

4.3: PREVIOUS WORK CALCULATING FAULT MOVEMENT RATES AND THE METHODS USED

There are many different ways that researchers have addressed the question of rates of fault displacement, which are applicable over different time scales and have varying degrees or reliability. Methods for analysing fault movement generally fall into four categories; 1) Geomorphic methods, which use topography and surface features; 2) Stratigraphic, which use the offset of geological strata; 3) remote sensing methods, which utilise analysis of digital imagery such as DEM's and LIDAR; 4) Geophysical methods, which use tools such as exploration surveys (e.g. seismic reflection) to observe the arrangement of rock units in the subsurface (McCalpin, 2009).

Several aspects of fault movement can be calculated; many studies quantify fault slip, or displacement on the fault plane (e.g. Peacock and Sanderson, 1994; Michetti et al., 1996; Willemse et al., 1996; Monaco et al., 1997; Piccardi et al., 1999) represented by the relative displacement of piercing points. However, caution must be used when studying oblique-slip faults, as separation (i.e. the offset of a fault) could be erroneously identified as displacement. The throw and heave can also be measured; these correspond to the vertical and horizontal components of movement along the fault plane (e.g.

Monaco et al., 1997; Cowie and Roberts, 2001). Throw is useful for examining the amount of uplift occurring within mountainous areas.

These quantifications have been used to provide estimates of the hazards posed by active faulting. That said, there are currently few areas where movement rates are known with enough certainty to allow for explicit evaluation of seismic hazard, which is particularly hampered by a scarcity of data and the ambiguity of data derived using different methods.

The issue of determining fault movement rates is complicated by the recognition that the amounts of slip and throw vary over the length of a fault segment (figure 4.2), with higher amounts of movement at the centre of the fault segment, and also that displacement can be modulated by adjacent active fault segments (Harris and Day, 1993; Gupta and Scholz, 2000; Nicol et al., 2002). This highlights the need for high-resolution displacement data along fault arrays, rather than single estimates, to aid in the comprehensive understanding of faulting and seismic hazard within a given area.

All of the methods used to quantify rates of fault movement include inherent sources of error specific to the process in question that add varying degrees of uncertainty to the estimate. Indeed, different methods to quantify slip rates have been shown to produce different results for the same fault. Possibly because they address slip rate quantifications over different time scales (Cowie and Roberts, 2001). For example, in the Italian Apennines geomorphic evidence, such as triangular facets and scarps along range fronts (Piccardi et al., 1999) and trenching and radiometric dating of fault scarps (Michetti et al., 1996; Galadini et al., 1997) yield differing results.

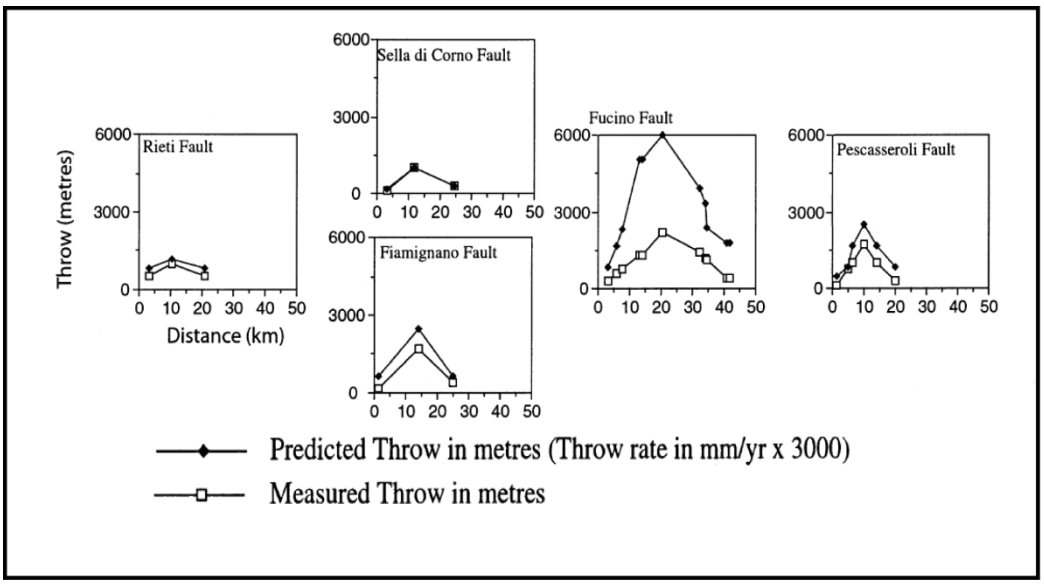

Figure 4.2: Cowie and Roberts (2001) presented throw rate data from a fault array in the Italian Apennines that shows how throw rates vary along strike, with the highest rates in the centre of the fault segment.

Despite the variations in movement rates produced by different methods, the ability to work out the rate of movement of faults over different time scales can be useful in analysing the past activity of a fault system. Independent methods offer evidence from a variety of sources, and so allow for quantification of fault movement rates in a wider range of areas. The following sections (4.3.1 to 4.3.6) outline the methods commonly used to determine rates of fault movement and summarise their applicability within the Gediz Graben.

4.3.1: USING GEOMORPHOLOGY TO QUANTIFY RATES OF MOVEMENT ON NORMAL FAULTS

Offset geomorphic features are increasingly being used to assess rates of fault movement beacuse the methods to extract dates from them have become more accurate. Prior to the 1990s the methods to date landforms were centred on relative dating, such as degree of soil development, rock varnish and lichenometry (e.g. Harden and Matti, 1989, Rockwell et al., 1990). These

methods have a significant weakness in that they are based upon surface alteration so there are many variables that can affect the speed of the alteration, such as rainfall, temperature and lithology (McCalpin, 2009).

Despite the ambiguity provided by surface alteration, progress has been made with the use of cosmogenically produced isotopes found within rock surfaces, Isotopes such as ^{36}Cl, ^{10}Be and ^{26}Al have been used to date surface stabilisation and have allowed for more accurate and precise age estimates (Rockwell et al., 1990; Ritz et al., 1995; Brown et al., 1998; Gosse and Phillips, 2001; Daëron et al., 2004; Van Der Woerd et al., 2006). In addition, methods such as palaeomagnetism can be used to constrain the age of faulted volcanic features such as offset lava flows (Walker and Jackson, 2002).

A variety of landscape features can be useful for quantifying vertical movement and slip rates. The most commonly used are offset alluvial fans and steams, uplifted river terraces and past glacial features. Offset alluvial fans have been successfully used to quantify rates of movement on normal fault systems using a range of methods. For example a study of the Altai Mountains of western Mongolia (Nissen et al., 2000) estimated late Quaternary slip rates by measuring scarp heights and dating alluvial fans with Optically Stimulated Luminescence (OSL). Difficulties encountered were the uncertainty in measurements of fault dip due to lack of scarp exposure, and the inherent situational inaccuracies of the OSL dating method. Offset landslides (McGill et al., 2010) and offset stream channels within fan surfaces can also be used to restore landforms (Walker and Jackson, 2002) so as to measure offsets, alongside quantified ages to yield rates.

River terraces lend themselves to the study of rates of fault movement in areas with vertical movement, with both depositional cut and fill terraces and

erosional strath terraces used. OSL dating of terraces uplifted above the current river level by active faulting has become common as the dating methods have improved (e.g. Rockwell et al., 1984; Zuchiewicz et al., 2004; Shyu et al., 2006). The increasing use of OSL for dating river terrace sediments means that the maximum time limits of slip rate estimates are around 300 ky years, which corresponds to the typical maximum range of OSL dating. Radiocarbon dating can also be used but the limitations constrain the usefulness of this method to anything likely to be 40 ky or younger (Taylor, 1997).

Glacial features have also been used to assess rates of fault displacement, notably within the Apennines of Italy, where landforms dating back to the last glacial maximum, 20,000 years ago, are readily preserved (Roberts and Michetti, 2004; Giraudi and Frezzotti, 1997; Giraudi, 1995; Blumetti et al., 1993). These studies have looked for offsets in moraines and fluvioglacial fans associated with glacial retreat that have good time constraints. During glacial maximum and glacial retreat stages sedimentation and erosion rates are high relative to the fault slip rates, but in postglacial periods the rate of erosion and sedimentation can be reduced (Roberts and Michetti, 2004). Reduced sedimentation causes fault scarps to be preserved, which results in offsets in the smoother glacial surfaces cut during earlier, more erosive times. The fan surfaces and bedrock slopes are often covered in a datable post-glacial organic-rich soil, which contains abundant palaeo-vegetation and volcanic ash.

The methods for investigating offset glacial features such as moraines and channels are similar to those for assessing fault displacement of alluvial fan surfaces and other drainage features. Dates are acquired for the displaced feature and the offset distance is measured allowing for calculation of rates (e.g.

Roberts and Michetti, 2004; Giraudi and Frezzotti, 1997; Giraudi, 1995; Blumetti et al., 1993).

To summarise, the use of geomorphic features in the quantification of throw and slip rates is dependent upon the availability of appropriate landforms and features that can be identified and measured in the field. It is also necessary for the features to contain datable material, or to have existing reliable time constrains in order to utilise the features for rate analysis. Therefore, a limitation of this method for quantifying throw and slip rates is that while the method is useful over shorter time scales of around 100 yr - 300 ky, the dating methods that can be used in each situation are limited by materials at the site of investigation that can be dated, and then in turn, the age range of the dating method.

4.3.2: USING STRATIGRAPHY TO QUANTIFY RATES OF MOVEMENT ON NORMAL FAULTS

Geological cross-sections based upon lithological and structural maps can be used to analyse fault slip rates and also allow for isolation of vertical throw and horizontal heave displacement components. The amount of slip, throw or heave can be estimated from sediment thickness of graben infilling sedimentary rock units in combination with the orientation of tilted strata (e.g. McLeod et al., 2000; Nicol et al., 1997). Cross-sections provide estimates of fault slip rates over time scales of $>10^5$-10^7 years. The cross-sections appear to produce more stable estimates of fault movement rates, compared to methods that derive movement rates over shorter (~200 kyr) time scales, which appear to have greater variability (Nicol et al., 1997). By constructing cross-sections using available data, such as maps, sedimentary logs and geophysical surveys a

reliable model can be created. Piercing points identified on the cross-section can then provide dependable estimates of fault displacement rates, if the age of the relevant rock unit is known and the mapping reliable. This method has been used by Cowie and Roberts (2001) to estimate total throw in Abruzzo, (Italy) and the Gulf of Corinth, (Greece). According to this study cross-section construction may be the best way to resolve long-term fault slip rates and seismic hazard, although such data are sparse and often of insufficient quality in many actively deforming regions (Cowie and Roberts, 2001).

The reliability of cross-sections in the quantification of movement rates is dependent upon the veracity of the data from which they are constructed. An accurate cross-section requires constraints on the location and dips of faults, and if possible, information about the subsurface dip of the faults, as they may not remain planar. To quantify the rates from the cross-section it is also necessary to have access to reliable age data for stratigraphic units. The use of cross-sections to quantify throw rates is therefore limited by the availability of a combination of pre-existing structural, stratigraphic and geophysical data, or the ability to acquire these data before constructing the cross-section. One way of acquiring a cross-sectional view of the evidence for faulting is trenching.

Trenching (figure 4.3) has been widely used to quantify fault slip rates (e.g. Schwartz and Coppersmith, 1984; Michetti, et al., 1996; Sébrier et al., 1997; Litchfield et al., 2006;) and involves excavation of a trench across active faults in order to study (pre-)historic earthquakes (figure 4.3). Whilst surficial features might provide evidence of only the latest earthquake through the currently exposed fault scarp, a fault trench can reveal evidence of older fault movement. The trenching method falls foul of the limitations on methods used

to assign dates, and additionally the type of material used for dating can have implications for the age derived from analysis (Niemi and Hall, 1992).

However, trenches are fairly versatile, and can be used to gather data on either palaeoearthquake recurrence or palaeoearthquake displacement and the type of information required from trenching influences the location of the trench (e.g. Swan et al., 1980; Sieh, 1981; Schwartz and Coppersmith, 1984). In terms of fault displacements trenches dug perpendicular to the active fault to provide information about the vertical movement of the fault and parallel to the fault to provide data on the horizontal motion component (McCalpin, 2009).

The location of the trench is dependent upon two main factors; the location of the fault must be known accurately, to within a few metres and ideally precisely. The second consideration should be the setting of the site to be trenched as the location should be one that favours sedimentation on both sides of the fault, in order to preserve a record of tectonic activity (McCalpin, 2009). A significant problem with trenching is that trench penetration may not be great enough to expose the larger vertical scarps, although this problem can be partly addressed by digging of larger, tiered and supported trenches (Olig et al., 2005).

Özkaymak et al., (2011) quantified the slip rate along the Manastır Fault in the Manissa fault zone (Turkey) by examining the cumulative displacement across the fault. Assuming a maximum time interval of 5 Ma for the deformation, a minimum slip rate of 0.3 mm/yr was quantified for the Manastır Fault.

Another example of where trenching has been used to quantify displacements on a normal faults is the Wasatch Fault, Utah (figure 4.3), which has been the site of several studies (e.g. Swan et al., 1980; Schwartz and Coppersmith, 1984; McCalpin et al., 1994; Olig et al., 2005). For example,

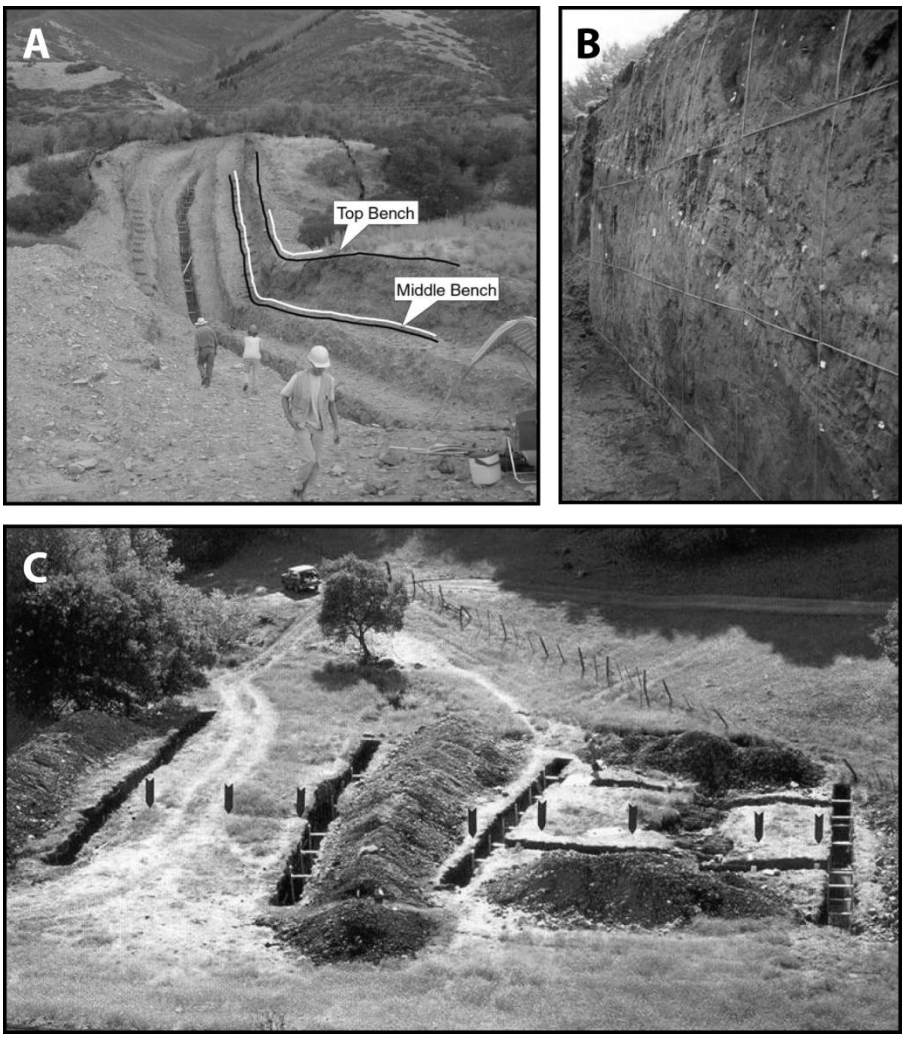

Figure 4.3: Figures to illustrate the trenching method of fault analysis. A) The Mapleton 'mega trench', a large benched trench across a 23 m normal fault scarp in the Wasatch fault (Buddensiek, 2004). B) A trench wall showing the delineated reference net used for logging the trench sides (Pantosti et al. 1993). C) The trenching method is use on the Rogers Creek strike slip fault, California. The fault runs across the image, indicated by black arrows, showing how multiple trenches in different orientations can provide information on both vertical and horizontal movement (Pantosti et al. 1993).

Schwartz and Coppersmith (1984) dug trenches on the Wasatch Fault and measured displacement per event has been from 1.6 to 2.6 m with an of average of around 2 m. Swan et al., (1980) also trenched the Wasatch fault, north of Salt Lake City, and measured 10 to 11 m of cumulative net vertical tectonic displacement since the middle Holocene. They determined that displacement for individual faulting events ranged from 1.7 to 3.7 m. These

studies have highlighted that trenching can be a very valuable in quantification of slip and throw values although there are a few significant caveats.

Firstly, trenching requires the locations of the fault that is to be trenched to be known with high degree of accuracy, the past work has shown that trench location is critical and that often success or failure of an investigation is determined by location of the trench (McCalpin, 2009). Secondly, if a suitable site is found there must then be appropriate materials for dating offset units within the trench in order to provide age constraints for the measured offset. If these limitations are overcome trenching can yield a high resolution fault movement data.

4.3.3: THE ROLE OF DIGITAL IMAGE ANALYSIS IN THE QUANTIFICATION OF RATES OF MOVEMENT ON NORMAL FAULTS

Use of digital aerial imagery can enable quantification of fault slip and throw rates (McCalpin, 2009). Aerial photography was a commonly used method for identifying faults up until the 1990s. For example, 298 measurements of vertical throw were made on the Wasatch fault zone by Nelson and Personius (1993) and Nelson et al. (2006). The measurements were made from 35 year old black and white photographs using an analytical stereoplotter. For the Wasatch Fault studies measurement of throw from aerial imagery was a very efficient method of measuring fault movement; the measurement of vertical throw took far less time than measuring from areal imagery than it would have to measure them all in the field (McCalpin, 2009).

The disadvantage of aerial photography is that a lot of the photographs are unrectified and within unrectified images the vertical scale is not constant

within the image. Also the analysis of aerial photographs in highly vegetated areas is difficult as the vegetation obscures surface features (McCalpin, 2009).

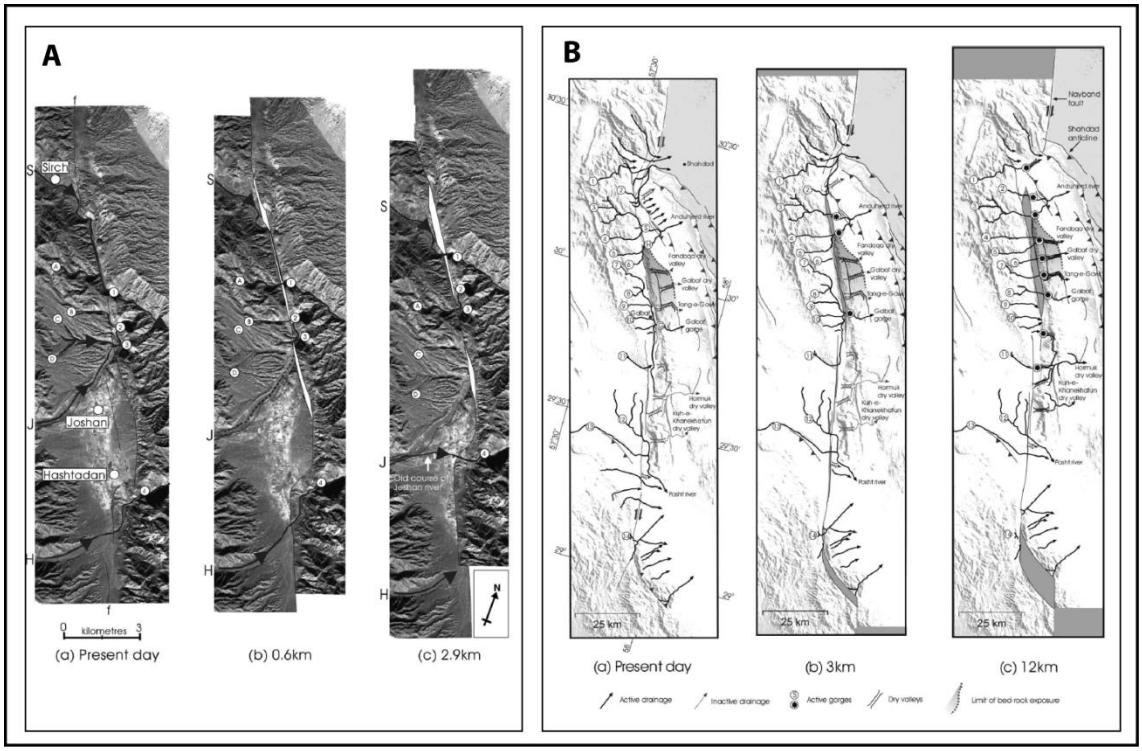

Figure 4.4: The use of digital elevation imagery to reconstruct movement on faults illustrated by using the Gowk Fault, Iran. Offset stream channels in old fan surfaces were reconstructed and the displacement measured, this was combined with age contains on the fan surfaces to quantify slip rate. A) shows the imagery of the fan surfaces and B) shows the specific channels used to reconstruct the fans (Walker and Jackson, 2002).

Digital elevation models (e.g. figure 4.4) which are a representation of a terrain's surface created from terrain elevation data, are gradually surpassing the number of studies using photographs. This is due to the wider availability and benefits of digital image data, such as the data contained within them and the variety of information they can yield through analysis (e.g. Walker and Jackson, 2002; Frankel et al., 2007). Using DEMs has increased significantly in the last decade and many studies are now being conducted in areas of low slip rates and increasingly subtle surface expressions of deformation. DEMs allow users to recognise these subtle features using image analysis and manipulation such as exaggeration of topography and draping satellite images.

Digital elevation data can be obtained for the majority of the Earth's surface, at several resolutions. The GTOPO30 global dataset has a 1 km resolution. Shuttle Radar Topography Mission (STRM) data has nearly global coverage at a resolution of 90 m. Advanced Spaceborne Thermal Emission and Reflection Radiometer (ASTER) elevation data are now available globally at 30 m resolution. Higher resolution data, which is generally available in the USA and some other regions, are important if small-scale features are being examined. The digital elevation data are usually available for free, and are downloadable from the internet. Due to the inexpensive nature of digital elevation data the use of such imagery in investigations is highly common; generally used in conjunction with another method such as a dating technique to quantify rates of fault movement. Addition imagery is frequently used in the planning of other methods such as trenching.

In the analysis of fault movement DEMs have proven to be very useful in the examination of offset features on strike slip faults. Walker and Jackson (2002) studied the Gowk Fault, (Iran) where they measured 12 km of cumulative offset on stream channels in old fan surfaces. This combined with age contains on the fan surfaces using K-Ar dating of offset basalts enabled them to quantify a slip rate of 1.5 –2.4 mm/yr.

Given that DEM imagery can be readily acquired (free or for a fee) and easily manipulated it is a valuable tool in fault analysis. However, a limitation of using imagery for quantifying rates is that if movement rates are required additional information must be known about the stratigraphy, a time constraint is vital in the calculation of rates. This may be an easy issue to overcome if the area has been extensively mapped, but if mapping is patchy or non-existent it

would require original mapping and most likely a form of dating to establish the ages of the stratigraphy units studied in the imagery.

4.3.4: USING SEISMIC INVESTIGATION TO QUANTIFY RATES OF MOVEMENT ON NORMAL FAULTS

Seismic investigation methods have become progressively more widely used as the equipment and expertise have improved. Increasingly, researchers are seeing geophysical exploration as a worthwhile expense; for example, employing geophysical methods before trenching will allow a more advantageous location for the trench (McCalpin 2009).

Seismic methods are useful for quantifying slip and throw rates in terrestrial environments as it allows for imaging of faults in the subsurface, yielding a greater amount of information that surface mapping alone. Thus a reliable extension of known fault dips at the surface to any depth below the surface can be achieved (McCalpin 2009). Then two methods used to characterise subsurface strata and define piercing points for slip and throw measurements are seismic reflection and refraction surveys.

In seismic reflection the waves travel downward initially and are reflected at some point back to the surface, the overall path of the waves is essentially vertical. Whereas, in seismic refraction the principal portion of the wave-path travels along the interface between layers and is approximately horizontal.

Seismic reflection is useful for calculating the rates of vertically movement on faults in areas such as grabens due to its ability to image horizontal and dipping reflectors (McCalpin 2009). In general seismic refraction does not have as high resolution as reflection surveys and as a consequence it can be limiting, yielding information about larger scale features. For example

Pelton et al. (1985) used seismic refraction on the surface rupture of the 1983 Borah Peak earthquake but were only able to identify the larger faulted units.

Since the 1990s high resolution seismic reflection techniques have been employed to greater success than seismic refraction techniques (Miller et al., 1990; McCalpin et al., 1994; Sheley et al., 2003; Mattson, 2004; Buddensiek et al., 2008). Where both methods can be used seismic reflection generally has better vertical resolution and can more easily be used to target a greater array of features such as dipping contrasts. Comparisons of high resolution seismic reflection surveys which have been compared to trench logs show that most details within the trench can be imaged with reflection surveys (Zilberman et al., 2005; McCalpin, 2009).

Seismic surveying methods require a large input of expertise, finance and equipment, each of which could be a limiting factor for the applicability of the method to fault analysis. An estimate of the financial output required for a seismic reflection or refraction survey can be up into hundreds of pound per day depending upon the site. In addition to this the ability to quantify rates from geophysical data is controlled by the access to reliable data on the age of strata to be imaged in the surveys.

4.3.5: USING GLOBAL POSITIONING SYSTEM (GPS) AND COMPUTATIONAL METHODS TO QUANTIFY RATES OF MOVEMENT ON NORMAL FAULTS

GPS has been used to determine contemporary strain accumulation rates of the Wasatch fault, Utah, and have the results have been used to provide key data for evaluating normal fault behaviour and related earthquake hazard assessment (Chang et al., 2006). The GPS network spans the 300-km

long and 200-km wide area of the Wasatch fault zone and includes 8 permanent GPS stations that have been operating continuously 1997. Measurements indicate a principal horizontal extension rate of 24 ± 6 nstrain/yr with the direction nearly perpendicular to the fault (Chang et al., 2006), the strain rate corresponds to a horizontal displacement rate of 1.6 ± 0.4 mm/yr. GPS has also been used to analyse rates of strain accumulation in the area affected by the 1908 Messina earthquake, southern Italy (Serpelloni et al., 2010). Modelling of the GPS velocities was used to infer slip-rates of 3. 5 mm/yr + 2.0 − 1.3 and 1.6 mm/yr + 0.3 − 0.2 mm/yr for the dip–slip and strike–slip components of the fault zone respectively.

GPS studies have become routinely used to assess regional strain rates over a decadal time scale (Aktuğ et al., 2009; Barka and Reilinger, 1997; Clarke et al., 1997), which can be useful when studying ongoing tectonic activity. The geographic range of the strain rate estimates can vary based upon the density of the GPS monitoring sites, and as a consequence may be broadly useful over wider areas (Clarke et al., 1997). However, GPS may struggle to provide accurate estimates of fault movement over specific faults systems, unless GPS stations are specifically aimed at measuring movement on that particular fault system.

In terms of quantifying rates of fault motion, GPS measurement could be useful if GPS stations were specifically placed to analyse movement over certain faults; in this case the availability and positioning of GPS stations is a limitation of the method. As GPS monitoring works in real time the estimates of fault slip and throw rates could be accurate for a very short amount of time but would not give representative long-term movement rates.

As a result of this inaccuracy caused by scale and resolution of study geodetic measurements of strain rates often appear to overestimate the rates of movement seen on specific faults in areas of extension (Cowie and Roberts, 2001). Additionally this method measures strain and not the movement of features due to localised fault movement so the results are converted to estimates of closure rates over a fault or fault array.

4.3.6: METHOD APPLICABILITY WITHIN THE GEDIZ GRABEN IN RELATION TO THE DESIRED OUTCOMES OF THE INVESTIGATION:

Many of the methods examined in sections 4.3.1 to 4.3.5 provide very localised results, specific to a certain area of the fault such as cross-section analysis and reconstruction methods. The aim of this chapter is to produce a high-resolution, data set on fault throw rates to aid in analysis of the landscape development of the Gediz Graben. The requirements of the method or methods used to quantify throw rates in the Gediz Graben are:

1. It will yield a high resolution data set; providing multiple throw rate estimates along the fault, at last one per every 10 km.
2. It requires little financial input; a low-cost method has the potential to be useful in many areas around the world where funds are not plentiful for fault investigations.
3. It must fit within the expertise of the research involved in this project, which are within the stratigraphic, structural and geomorphologic areas.
4. It must be accomplished in a reasonable amount of time.
5. It must provide estimates of rates over the last 2 Myr.

Ideally the methodology used should take into account the pre-existing data available for the Gediz Graben. As documented in chapter 2 there has been high-resolution mapping of most of the graben, which contains the surface locations and dips of the different stratigraphic units. The stratigraphic units have good age constraint based mainly on paleontological data. Along with the stratigraphic knowledge, the locations of the faults have been documented to a reasonable degree of accuracy, and dips of the faults at the surface have been recorded (refer to section 2.5 for more detail). In addition to the mapping that has been carried out in the Gediz Graben, there is 270 km of 2D seismic reflection survey data and three accompanying borehole logs available for a portion of the graben of around 40 km in the extreme east near Alaşehir due to hydrocarbon exploration (Çiftçi, 2007). These have provided resolution of the sub-surface stratigraphy within the topographic graben.

Although the locations of the faults are known, more details on their precise location and the ability to locate significant fault scarps would be needed to allow trenching to be an applicable method. In the Gediz Graben the sedimentary rocks within the footwall are very soft and reasonably unconsolidated. As a result of the footwall lithology the fault planes are poorly exposed, although their locations can be determined. In addition to the structural limitations within the Gediz Graben trenching in time intensive and can be fairly expensive to carry out and so can be ruled out for use in the Gediz Graben. GPS measurements are also impractical within the Gediz Graben as GPS stations in the area are very sparse. Additionally the time scales that GPS measurements are utilised over are very short and this chapter aims to quantify faulting over the last 2 Myr.

Uplifted river terraces are present along the rivers draining the Bozdağ Range, but it is unlikely that these would yield throw rates over the 2 Myr period required. The terraces will therefore be documented in chapter 5 to provide time constraints on incision and possibly more recent rates of throw.

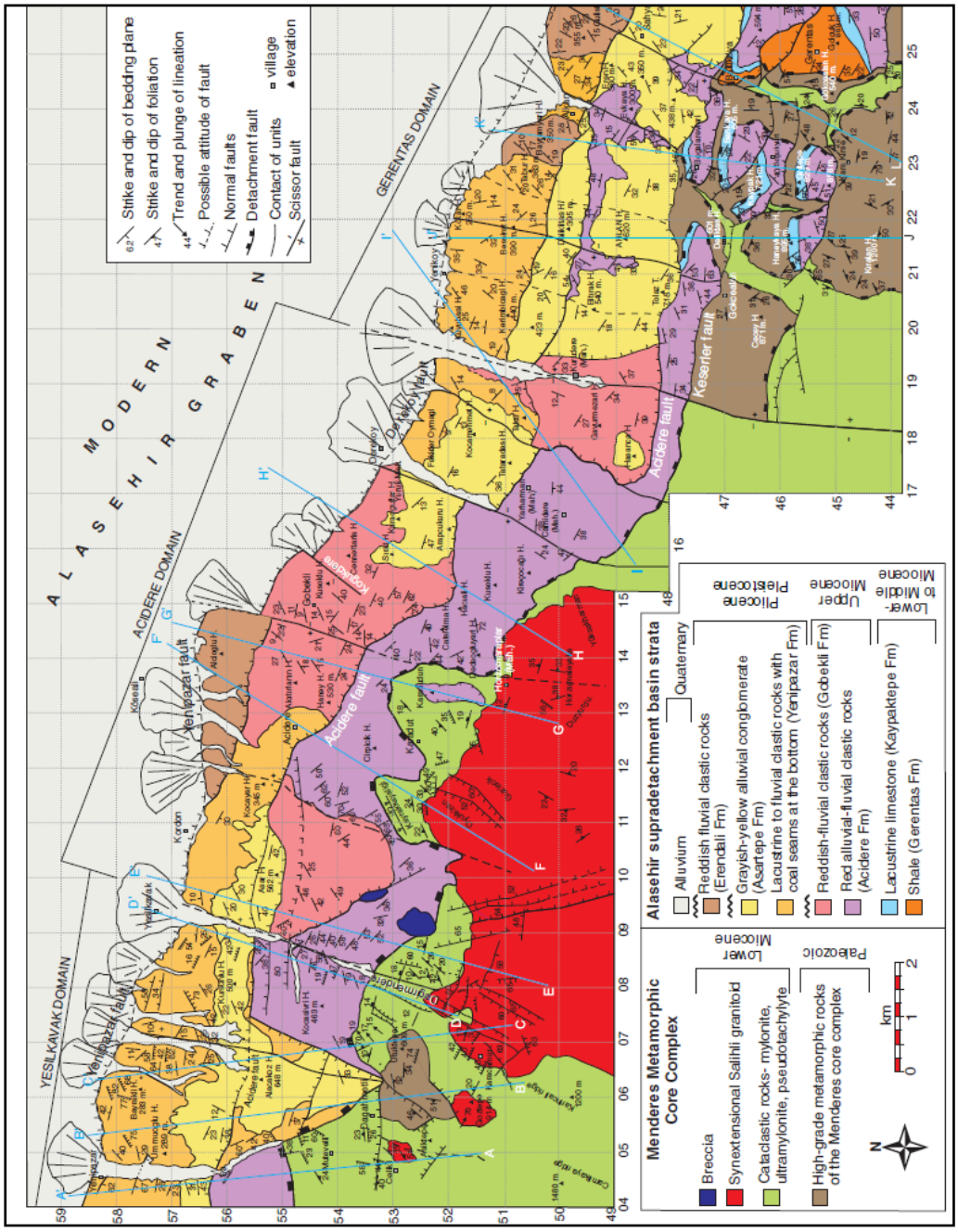

Figure 4.5: The geological map produced by Oner and Dilek (2011) showing surface mapping of the stratigraphy of the Gediz Graben. This maping was was in the construction of cross-sections (figure 4.11). Strike and dip information is also mapped onto the outcropping units.

A key combination of structural and stratigraphic mapping (Oner and Dilek, 2011 [figure 4.5]) and borehole and seismic survey data (Çiftçi, 2007 [figure 4.6]) makes cross-section analysis a useful desirable to this study; cross-sections can be constructed with little expense and low time requirements, they are also flexible in terms of location, and can be constructed as many times as needed along the range where data allows.

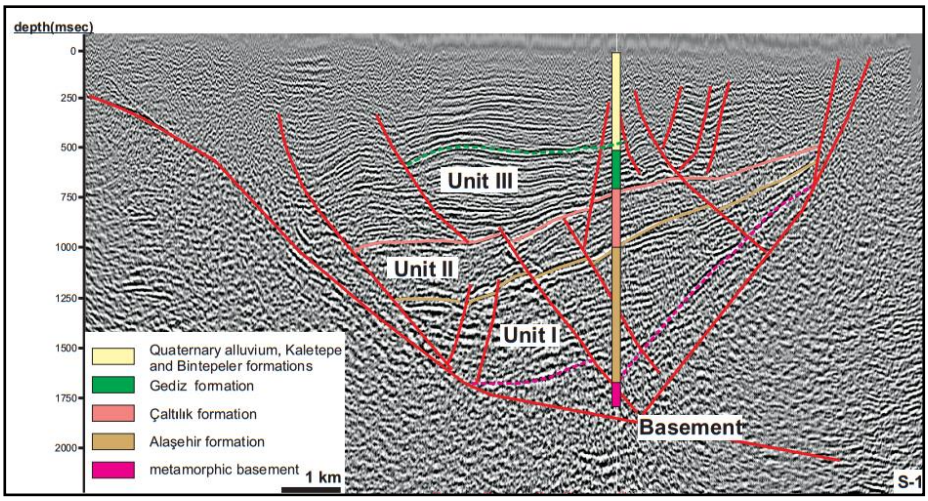

Figure 4.6: An example of one of the seismic reflection surveys and correlating bore hole for the Gediz Graben (from Çiftçi, 2007).

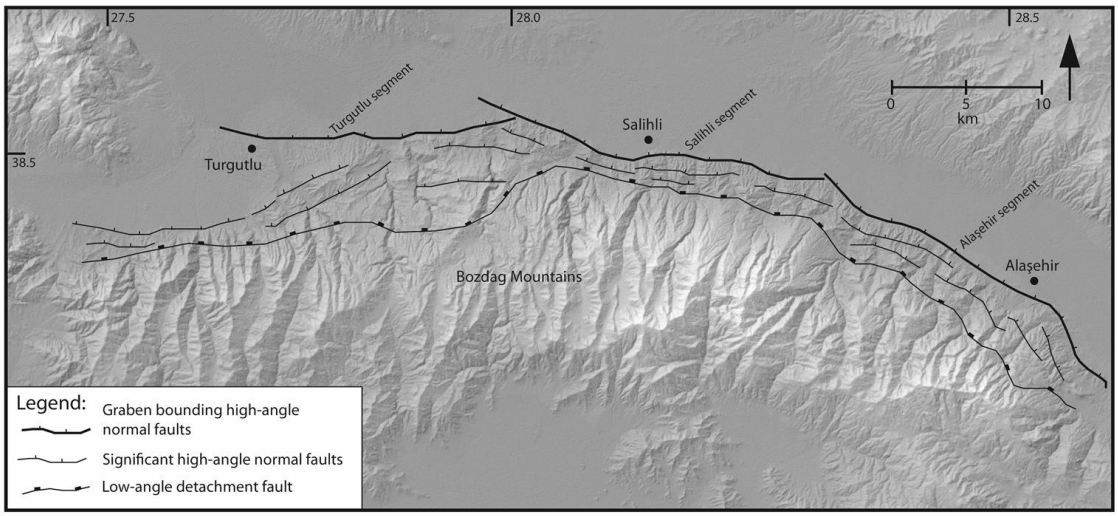

Figure 4.7: A topographic map showing the main styles faults within the Gediz Graben. The map displays the low-angle detachment fault and the significant high-angle normal faults on the southern Bozdağ Mountains. The youngest faults that bound the present day graben are shown with bold lines.

As the ASTER data (NASA https://wist.echo.nasa.gov/api/) is free and has 30 m resolution within the Gediz Graben, in areas not covered by the three complimentary data sets digital image analysis will be used to explore throw rates.

4.4: FAULTING WITHIN THE GEDIZ GRABEN

As documented within chapter 2 (section 2.5) the Gediz Graben exhibits two dominant styles of faulting. A major low-angle normal fault (the Gediz Detachment). The hangingwall of which is composed of syn-tectonic sedimentary packages, described in section 2.6. The low-angle normal fault was active between 16 myr and 2 myr (Buscher et al., 2013). Buscher et al. (2013) produced estimates of slip rate for the low angle fault between a period of 4 – 2 Myr, after which they propose that the low angle fault became inactive, a view also supported by other studies into the two-stage evolution of the graben (Koçyiğit et al., 1999; Bozkurt and Sözbilir, 2004).

Additionally there is an array of high-angle normal faults bounding the modern topographic graben valley. This faulting has been active since 2.6 – 2 Ma. (e.g. Koçyiğit et al., 1999; Bozkurt and Sözbilir, 2004; Çiftçi and Bozkurt, 2009a; Çiftçi and Bozkurt, 2009b; Çiftçi and Bozkurt, 2010; Oner and Dilek, 2011; Busher et al., 2013). The major faulting in the area is accompanied by minor faults in the same styles (Çiftçi and Bozkurt, 2010; Oner and Dilek, 201).

The principle concern in this study is the high-angle normal faults (figure 4.7), which occur along the whole 120 km length of the graben and crop out at lower elevations than the low-angle Gediz Detachment. Of particular interest to this chapter are the three laterally extensive fault segments that form a high-

angle graben-bounding normal fault array (GBNF, figure 2.6, refer back to this figure for a review the terminology used to describe the major high-angle normal fault arrays) that separates syn-tectonic sediments from the Quaternary fill of the Gediz Graben valley. Also considered is an outer high-angle normal fault array (OHANF, figure 2.6), striking parallel to the syn-tectonic sediments, running parallel to the outer normal fault array. The GBNF array is curvilinear and visually segmented into three strands (Çiftçi and Bozkurt, 2007; 2009a): the Turgutlu strand to the west (41 km long), the central Salihli Strand (43 km long) and the Alaşehir segments in the east (36 km) (Oner and Dilek 2011).

The commonly accepted model of graben formation in western Turkey is two stage (Koçyiğit et al., 1999; Bozkurt and Sözbilir, 2004; Busher et al., 2013), and in the Gediz graben this is supported by sedimentological evidence of unconformity separating the Miocene-Pliocene and Pliocene-Quaternary sediments.

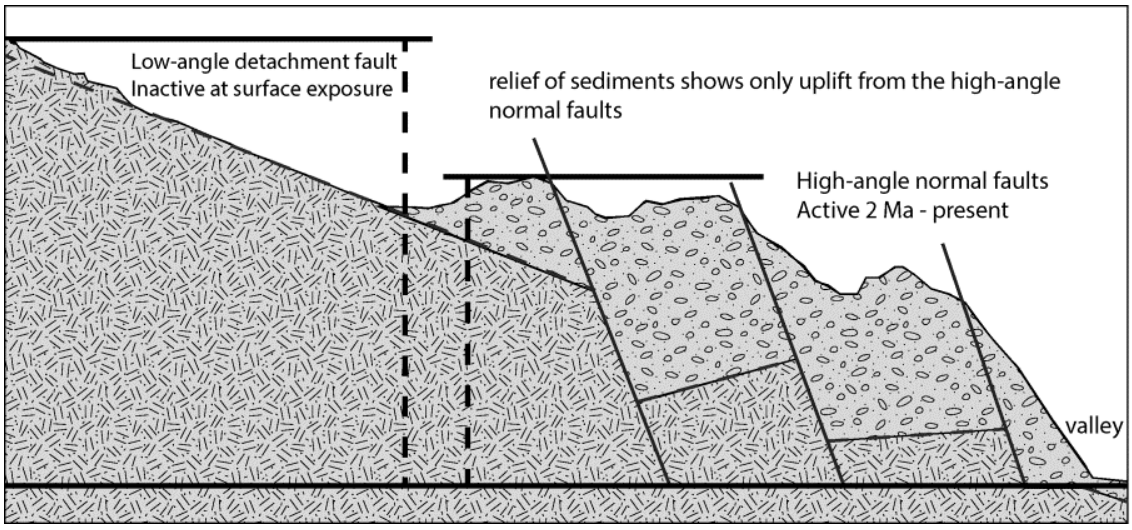

Figure 4.8: Schematic cross-section of the Bozdağ range from the drainage divide to the valley of the Gediz Graben. This image shows the two options for relief measurements using swath analysis. A large relief value can be obtained by taking the relief of the whole mountain range up to the exposed basement rocks in the peaks including the low-angle (phase 1) faulting. A smaller value can be derived by looking at the high-angle normal faults (phase 2 faulting) causing uplift of the sedimentary rocks.

For the period of dominant high-angle normal faulting of around 2 myr to present day, from here on referred to as phase 2 faulting (figure 4.8), there has been no work undertaken to quantify the rates of throw (or slip) on the faults of the Gediz Graben. The period of low-angle faulting occurring between 16 myr and 2 myr will be referred to as a phase 1 faulting in accordance with previous work (Koçyiğit et al., 1999; Bozkurt and Sözbilir, 2004; Buscher et al., 2013).

4.5: WHY CALCULATE THROW RATE OVER THE LAST 2 MYR?

This research derives values for vertical throw rates on the active graben bounding high-angle normal faults on the southern and most actively deforming margin of the Gediz Graben. This study specifically seeks to initially quantify the vertical throw component of fault movement rather than total slip displacement on the fault plane. That is because the throw component of fault movement is the significant influencing factor on knickpoint migration and will enable the comparison of fault movement to landscape evolution through river systems (see section 3.4 and 3.5 for a review of the literature), and throw fundamentally builds relief and topography. In order to compare the rates of fault movement in the Gediz Graben with other high-angle normal fault arrays where there only slip rates have been produced the quantified throw rates have also been converted to slip rates.

The time phase 2 high-angle faulting (2 – 0 myr) in the Gediz Graben, dominated by high-angle normal faulting is likely to have resulted in a higher rate of topography building over a 2 myr time scale compared to the preceding low-angle phase. High-angle normal faults result in a much larger uplift component of movement than low-angle normal-faults and so can have a

greater impact of the landscape over similar and even shorter time scales than low-angle faults even at slower slip rates.

There are significant differences in the field measurements of the dip of the two fault types, dip is approximately 15° for the low-angle faults and around 40-60° for the high-angle faults in the Gediz Graben (Koçyiğit et al., 1999; Çiftçi and Bozkurt, 2009a; Oner and Dilek, 2011; Buscher et al., 2013). Despite the differences in length of activity for the high- and low-angle faults, around 2 myr and 14 myr respectively, it is likely that the phase of high-angle normal faulting has created significant topography within the graben. It is also likely that the activity of the high-angle normal faults is responsible in large part for the present day form of the graben.

The present day activity on the main graben boundary fault is less well constrained than the episode of low-angle faulting. There has been some work that has attempted to provide some constraint, including the structural and sedimentological studies of Oner and Dilek (2011) and the radiometric dating of Buscher et al. (2013). The spatial distribution of early continental deposits in the hanging wall of the low-angle detachment indicates that high-angle normal faulting has shifted progressively northwards, giving a possible post early-Pleistocene (~700 Ka) age for development MGBF.

As there is uncertainty over the period of activity for the MGBF and the OHANF (see figure 2.6), and limited means by which throw can be estimated in all locations along the entire fault array the method used (see following sections) will need to be pragmatic and take an overall value of relief on the range in order to gauge throw rates. This means that the rate will need to encompass all activity on high-angle normal faulting over the last 2 Myr, as without constraints on the timing of both arrays it will not be possible to

determine the proportion of relief build by movement on the MGBF and the OHANF. This will by necessity create rates over the whole 2 myr history of high-angle normal faulting.

The last 2 myr is an appropriate time over which to evaluate fault movement when comparing to rivers currently responding to faulting. 1 – 3 myr is time it thought to be the time taken for bedrock rivers to fully respond to faulting through the whole river system (Miller et al., 2009; Whittaker and Boulton, 2012).

4.6: METHODS

As the amount of data available for the calculation of throw rates varies along strike, the pragmatic method used to calculate throw rates take advantage of various pieces of information at different stages. A flow diagram (figure 4.9) has been created to summarise the steps of the method.

4.6.1: CROSS-SECTIONS

Initially the geophysical survey information (Çiftçi, 2007 [figure 4.6]) was used in conjunction with structural and field verified published geological mapping (Ediger et al., 1996; Seyitoğlu and Scott, 1996; Şan, 1998; Çiftçi and Bozkurt, 2009a; Çiftçi and Bozkurt, 2010; Oner and Dilek, 2011 [figure 4.5]) to construct cross-sections in the eastern areas where all three sets of information were available. The lithologies were mapped onto the topography using the structural and geological maps of the Gediz Graben (Çiftçi, 2007; Çiftçi and Bozkurt, 2009a; Oner and Dilek, 2011 [figures 4.5) and the dips (figure 4.5) and unit thicknesses (Çiftçi, 2007; Oner and Dilek, 2011 [see section 2.6]) were used to propagate the units into the subsurface. Six cross-sections of the southern

bounding margin of the Gediz Graben were constructed (figure 4.9 step 2) in the east of the graben (figure 4.10 and 4.11).

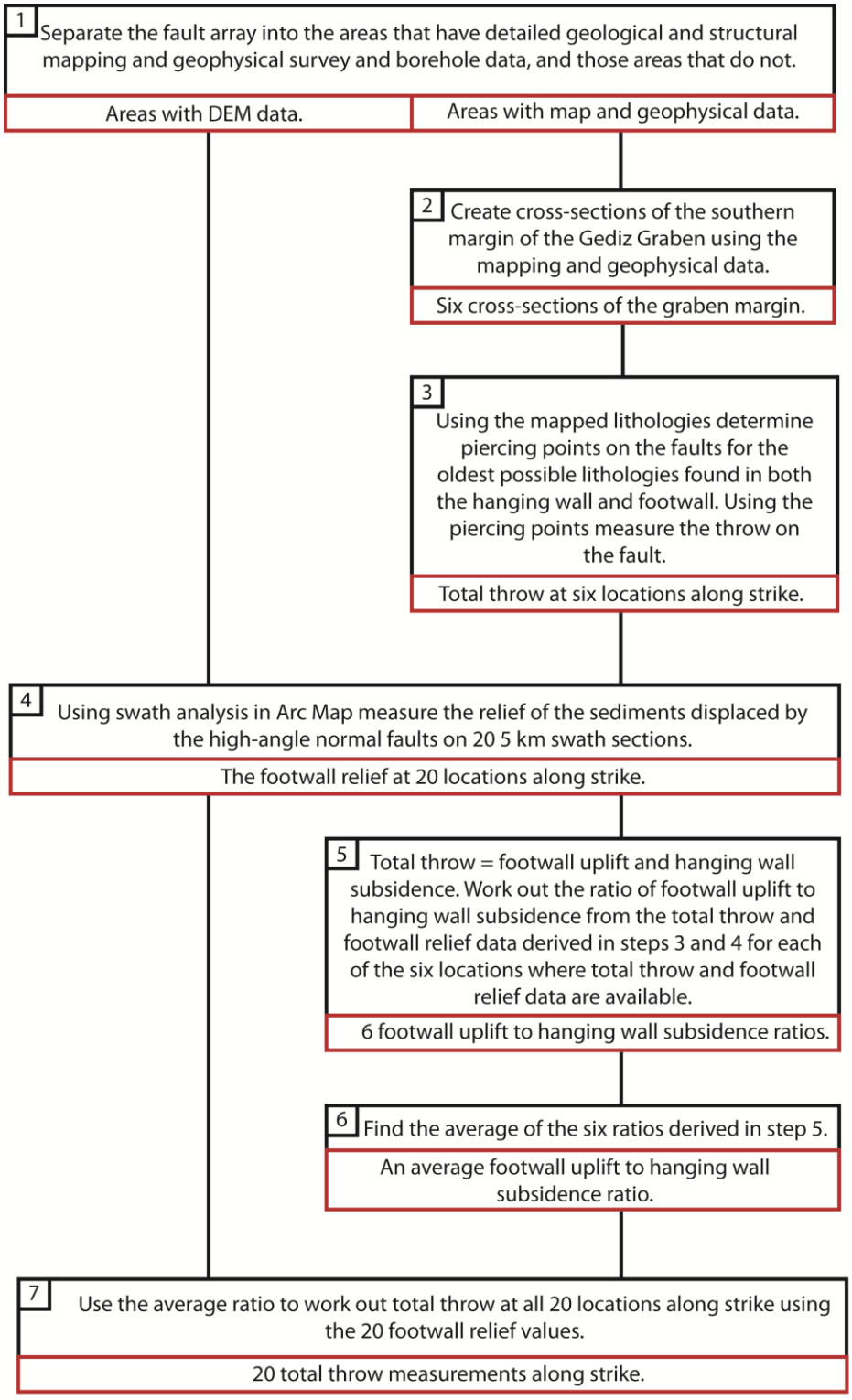

Figure 4.9: A flow diagram that summarises the methods used to calculate the time averaged throw rates along strike. The flow diagram distinguishes between areas when geophysical and bore hole data is supported by detailed mapping, and areas when DEM data and low-resolution mapping is available. The black box summarises the method and the red box details the product of that step. The joining lines show what type of data and which portion of the along strike is used step.

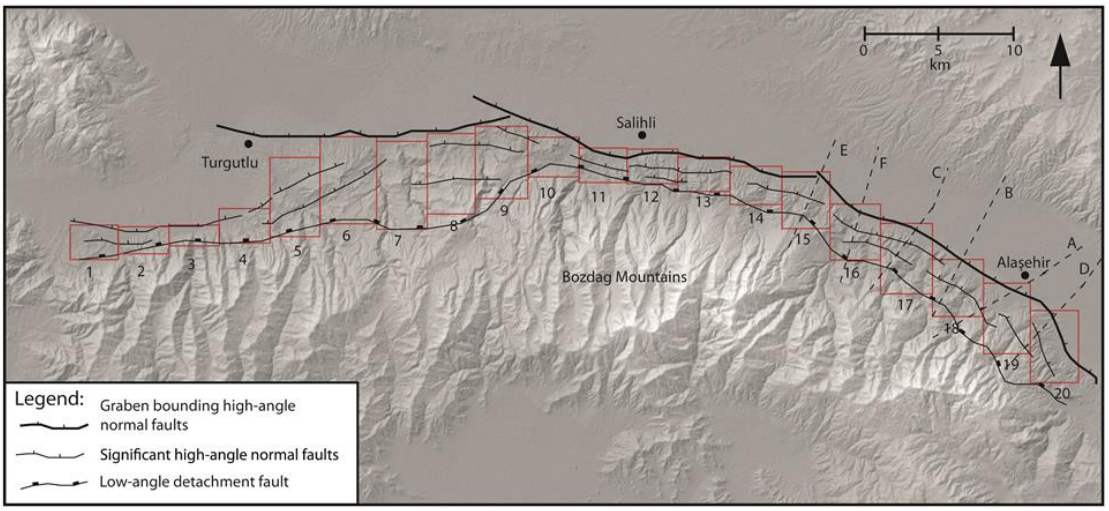

Figure 4.10: A map showing the cross-sections and swath analysis locations. This map shows the six cross-sections (A-F) created from structural, stratigraphic and geophysical evidence. It also shows the 5 km wide areas used for swath analysis, the red box shows the area of DEM that was used in the swath analysis for each section (1-20).

Using stratigraphic piercing points on the cross-sections within the sedimentary units of the syn-tectonic sediments, the amount of throw on the Turgutlu, Salihli and Alaşehir strands of the fault array within the southern graben margin have been calculated (figure 4.9 step 3). Throw was measured on the MGBF and the OHANF using piercing points. The method is illustrated on cross-sections B and F (figure 4.11). The piercing points for the vertical measurements were the base of sedimentary formations which were the most confidently mapped. The values provide a pragmatic quantification of cumulative footwall uplift on phase 2 high-angle normal faults over the last 2 myr.

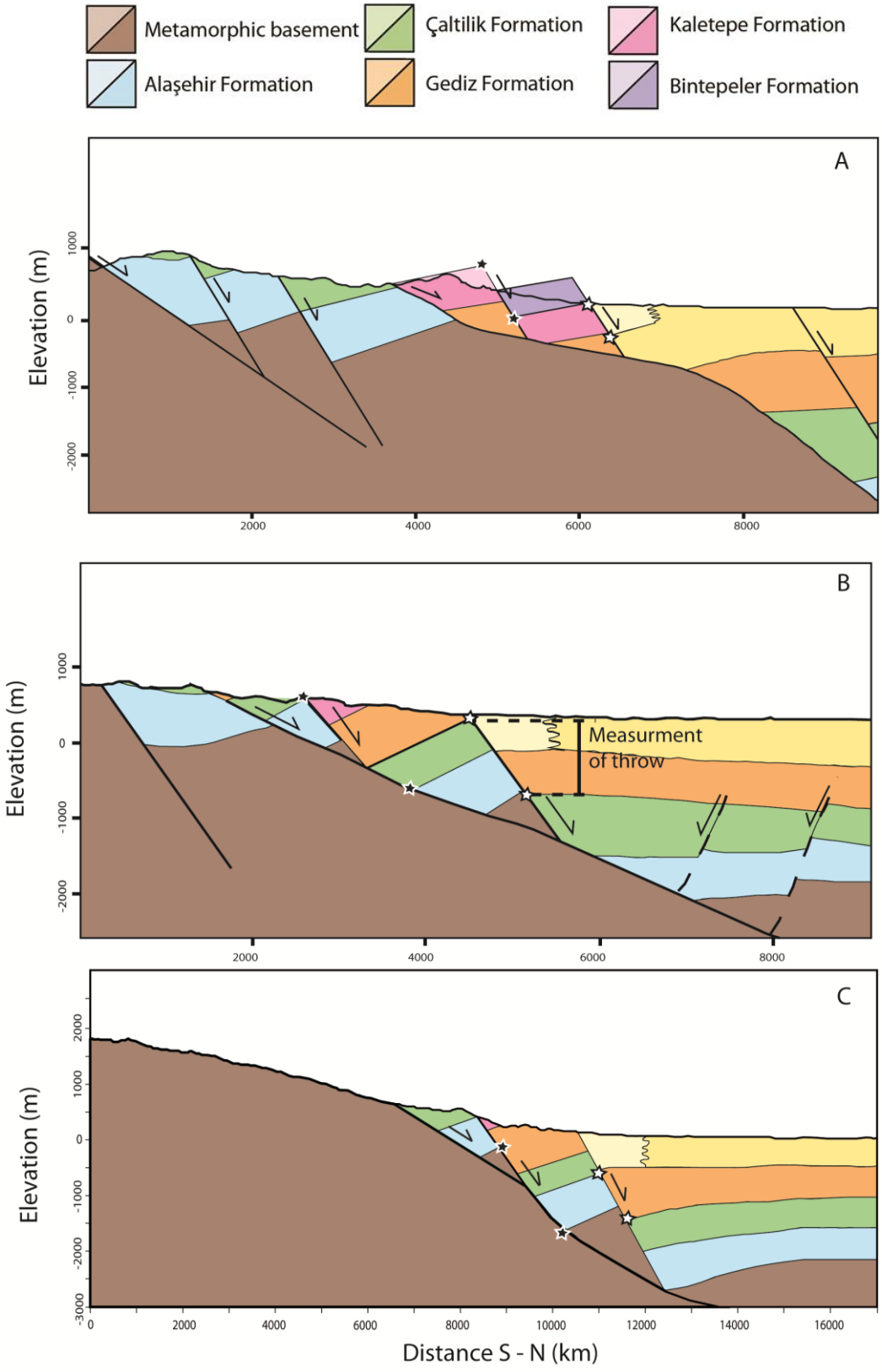
Metamorphic basement
Çaltilik Formation
Kaletepe Formation
Alaşehir Formation
Gediz Formation
Bintepeler Formation
A
B
C
Elevation (m)
Measurment of throw
Distance S - N (km)

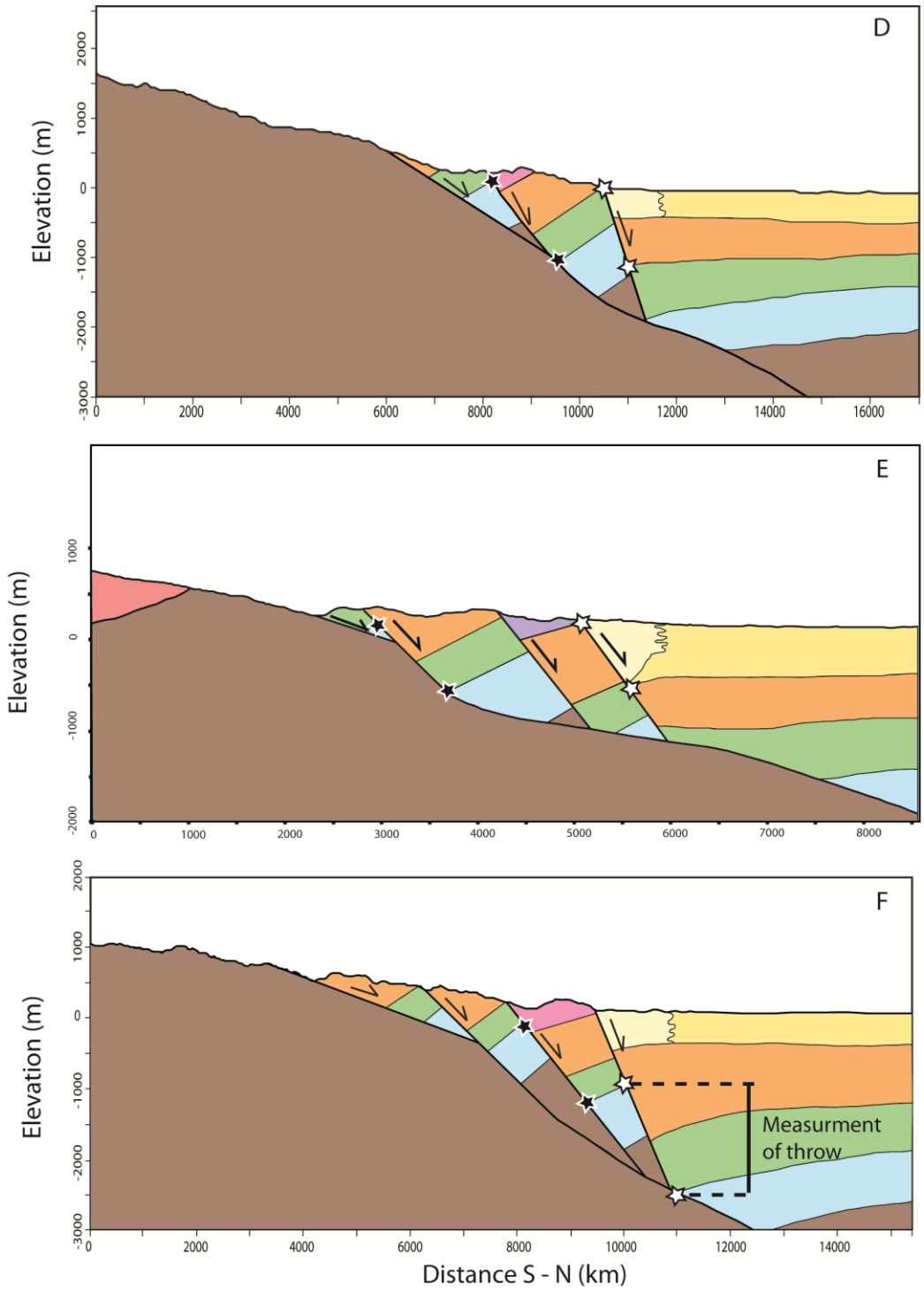

Figure 4.11: Cross-sections A – F constructed using published and field-checked structural information from; (Çiftçi and Bozkurt, 2009a; Çiftçi and Bozkurt, 2009b; Oner and Dilek, 2011) and sub-surface seismic from Çiftçi (2007). Stars indicate the piercing points used to determine throw and displacement on the outer and main graben boundary faults. The location of each cross-section is shown in figure 4.10. The yellow lithology is the Quaternary graben fill. Black stars show measurement on GBNF and white stars show the measurement on the OHANF.

4.6.2: THROW RATES ALONG THE ENTIRE LENGTH OF THE GRABEN BOUNDING FAULTS

To provide a high resolution throw rate data set over the whole of the graben bounding range, the available DEM imagery and structural and stratigraphic mapping data was used in conjunction with the measurements of throw gained from cross-section analysis (table 4.1) to expand the data set to areas without geophysical data. The total throw values were compared to values of footwall uplift derived from measurements of topographic relief obtained by swath analysis.

A 30 m ASTER DEM of the southern bounding range of the Gediz Graben was divided up into a series of twenty north-south oriented swaths of 5 km width (figure 4.10). The maximum elevation of the syn-tectonic sedimentary rocks formations was then extracted along each swath profile to produce the relief (the elevation difference between the graben floor and the summit elevation) for each of the twenty swath sections (figure 4.9 step 4).

A swath analysis allows for extraction of the relief of a mountain range and this study uses relief to gain information footwall uplift. Footwall uplift is a component of total throw on the normal faults, which is made up of a combination of footwall uplift and hanging wall subsidence. Subsequently the value of relief cannot be used as a direct proxy for total throw on the normal faults, but can be used as a proxy for footwall uplift. One caveat of this pragmatic method is that conventionally footwall uplift and hanging wall subsidence are defined relative to a non-moving datum. In this study such a datum is not practical and so graben valley floor level is used. This will level will naturally adjust through time due to deposition in the hanging wall, producing small variation over time and through space through the times used. But as this

is a pragmatic method an awareness of this possibility is required but it does not negate the potential usefulness of the method.

It is a realistic assumption to suggest that any elevation above the regional valley level is due to uplift processes and it is reasonable in a location of active uplift to estimate this value using the relief above the valley floor. This method of quantifying footwall uplift has a possible source of error in that it does not account for denudational processes within the range, although this should not cause large inaccuracies as the erosion within the bounding range is concentrated within the river valleys rather than the highest areas of elevation (Willgoose et al., 1991). A river with increased stream power leads to greater erosion within the river channel, and within the relatively unstable over steepened hillslopes caused by the downward incision (Willgoose et al., 1991). The high elevation areas that do not become included in the river induced hillslope remain relatively stable undergoing slower erosion and denudation, remaining at higher elevations.

The most significant decision that had to be made was, given there is a two stage history of graben formation, what is what the most appropriate relief to extract via the swath is for this investigation? One option was to extract the total relief of the Bozdağ Range (the bounding range), to the highest topography. The alternative was to divide the graben margin into two areas based upon whether low- or high-angle faulting was dominant in creating the present topography(figure 4.8). The total range relief represents a combination of vertical movement caused by the low- and high-angle faulting. The alternative, which will be used in this study is to consider the hangingwall of the low-angle normal fault, the location of the significant high-angle faulting and

syn-tectonic sediment accumulation. The relief of the uplifted sediments will be the best option to isolate the uplift on the high-angle faults (figure 4.8).

As the aim of this study is to quantify rates of phase 2 high-angle normal faulting over the last 2 myr this study uses the relief of the sediment packages uplifted by the high-angle normal faults; taking the relief from the metamorphic rocks in the higher elevations would yield an overestimate of footwall uplift as it incorporates the additional uplift caused by the slip of the low-angle detachment over a longer period of time.

The total throw values derived for the six cross-sections were then analysed with the footwall uplift values for the swath sections in which the cross-section lie (figure 4.9 step 5). Assuming that relief is a good proxy for footwall uplift over this time period, the ratio of footwall uplift to hangingwall subsidence, and the ratio of footwall uplift to total throw can then be calculated for each cross-section and swath analysis pair (c.f. Whittaker and Walker, 2015). Previous research suggests that ratios of footwall uplift to hangingwall subsidence may vary between areas (e.g. Papanikolaou et al., 2010). For example, Papanikolaou et al. (2010) found a 1:3 footwall uplift to hanging wall subsidence ratio in Lazio-Abruzzo, Italy, using differential SAR Interferometry and GPS recordings from nearby field GPS stations. On the Xylokastro Fault in the Gulf of Corinth ratios of between 1:3 and 1:4 have been determined using plate models by Armijo et al. (1996). Similar values of 1:3 were found for faults in the Sperchios Graben in central Greece (Whittaker and Walker, 2015).

The average ratio for the Gediz Graben was 1:4 as derived from the 6 cross-sections, which falls within the range of previous estimates. Additionally, if footwall relief were largely controlled by denudational processes, it would expected that the ratio of throw would vary considerably along strike, with very

high values obtained where cumulative throw is large but topography erosionally-limited (c.f. Densmore et al., 2004). The data do not show this, we therefore concluded that footwall relief in the Alaşehir fault segment is recording the variation in fault throw along strike with an acceptable degree of fidelity, and therefore this averaged ratio is used to estimate total throw along the MGBF along strike from the cross-section data.

The ratios for all six pairs were then averaged (figure 4.9 step 6) and using the footwall uplift to total throw ratio it was possible to work out the total throw from only the footwall component of vertical movement.

The cross-section method for analysing fault throw rates is considered one of the most accurate techniques for quantifying displacement rates over several million years when based upon precise and accurate data (Cowie and Roberts, 2001). Therefore the results from the analysis of the six cross-sections in the eastern Gediz Graben and the ratio calculated from them in combination with footwall data derived from imagery analysis can be considered a useful numerical device to access fault throw rates in the areas of the graben without 2D seismic reflection surveys.

4.6.3: EXTRACTING DATA FROM AREAS WITHOUT 2-D SEISMIC SURVEY DATA

The derived footwall uplift-total throw ratio was then used in conjunction with the footwall uplift component to derive the hangingwall subsidence and therefore the total throw on the normal faults for all twenty swath sections along the southern bounding range (figure 4.9 step 7). By using the ratio and the footwall component it was possible to calculate a value for the hanging wall subsidence using the swath extracted footwall uplift, to get total throw value for

each swath location. After throw values were derived for each swath location the throw rate was calculated using a time span of 2 myr.

To then facilitate comparison to other areas where only a slip rate data is available rather than the vertical throw the derived throw values for the Gediz Graben were converted to give the slip and slip rate values on the faults in those swath locations (table 4.1). Slip rate data was measured for the six cross-section locations but a method was required that would give values in each of the 20 locations calculated in a uniform way. The method used was documented in Nicol et al. (1997) where they state that throw on a fault is on average 75% of the slip on the same fault.

	outer fault	**error**		**MGBF throw (m)**	**error**		**total throw (m)**	**error**		**footwall from swath**	FW:TOTAL THROW RATIO			FW : HW RATIO		
		-	**+**		**-**	**+**		**-**	**+**			min	max		min	max
a	950	200	150	700	50	75	**1650**	250	225	541	**3.0**	2.6	3.5	**2.0**	1.6	2.5
b	1400	75	100	1250	50	80	**2650**	125	180	618	**4.3**	4.1	4.6	**3.3**	3.1	3.6
c	1800	100	75	1650	25	50	**3450**	125	125	472	**4.8**	4.6	4.9	**3.8**	3.6	3.9
d	1250	200	100	1200	50	75	**2450**	250	175	290	**3.8**	3.4	4.1	**2.8**	2.4	3.1
e	1000	150	50	800	50	50	**1800**	200	100	618	**3.7**	3.3	3.9	**2.7**	2.3	2.9
f	1800	50	150	1500	50	100	**3300**	100	250	487	**4.8**	4.6	5.1	**3.8**	3.6	4.1
										average	**4.1**	3.8	4.3	**3.1**	2.8	3.3

Table 4.1: Throw data derived from the analysis of cross-sections A - F. All data is provided in meters.

4.7: RESULTS AND DISCUSSION

4.7.1: THROW ON THE HIGH-ANGLE NORMAL FAULTS

Using the cross-section method (outlined in section 3.6.1) the total throw on the high-angle normal faults that have been active over the last 2 myr was quantified in six locations in the east of the graben. The method used piercing points for the vertical measurements defined by the base of sedimentary units

available in the footwall and hangingwall of the faults. Table 4.1 shows throw values and subsequently derived throw rates for the total high-angle normal fault throw in the Bozdağ range at each cross-section location over 2 myr. Total throw measured on the cross-sections ranges between 2000 m and 3900 m. Of this total the outer high-angle normal fault in each cross-section has accumulated the largest throw value.

The errors on the throw values (Table 4.1) were quantified by measuring the possible vertical differences of distance between piercing points caused by slight dip variation and unit thickness variations, based on the unit thicknesses as described in the literature (e.g. İztan and Yazman, 1990; Ediger et al., 1996; Tahir, 1996; Seyitoğlu and Scott, 1996; Koçyiğit et al., 1999; Çiftçi and Bozkurt, 2009b; Sen and Seyitoğlu, 2009; Oner and Dilek, 2011). This gives vertical errors of between + 425 -175 m and – 250 m -100 m on the total throw amounts.

4.7.2: FOOTWALL UPLIFT VALUES ALONG STRIKE

The swath analysis method outlined in section 4.6.2 was used in conjunction with constraints calculated from the cross-sections to quantify footwall uplift in 20 locations along the high-angle normal faults in the graben (figure 4.10). Relief of the uplifted syn-tectonic sedimentary units within the graben margin varies from 217 m to 724 m with two distinct sections to the range, the western third of the range contains the majority of the lower relief areas with higher relief to the east.

The eastern 80 km of the range has swath profile reliefs that vary between 420 m and 697 m while the western 45 km has a relief values ranging from 244 m to 420 m at the westernmost extent. Figure 4.10 shows that the

relief and therefore footwall uplift generally increases from west to east, with higher uplift values in the central area of the range and continuing towards the eastern extent, then decreases further to the east. When the three active graben-bounding normal fault segments are displayed with footwall uplift values (figure 4.12 and Table 4.1) there is an overall trend to higher footwall uplift values in the centre of the range within the Salihli Segment with the lowest values on the Turgutlu fault segment. Uplift values fall to lower values at the edges of the fault segments, although they do not fall to zero, this is particularly notable where the Salihli fault segment ends and the Alaşehir segment begins, at 80 km along strike of the range.

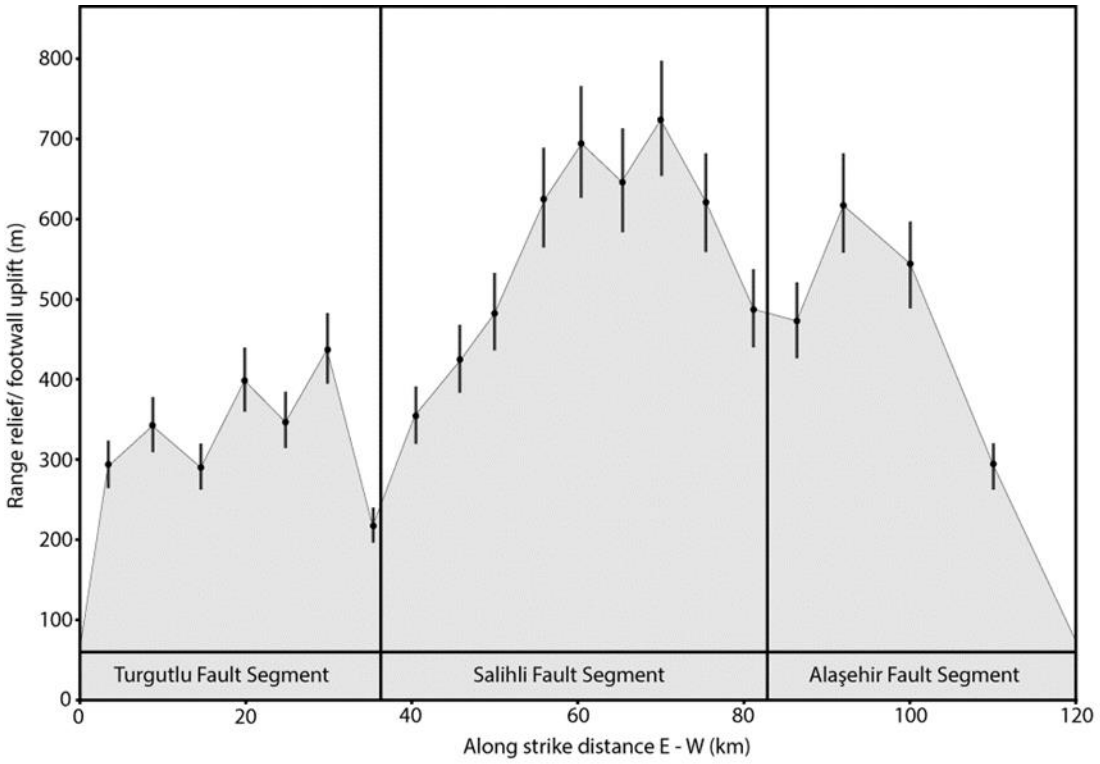

Figure 4.12: Graph showing the relief of the Bozdağ Range. This graph shows the range relief as a proxy for the footwall uplift component of total vertical throw. Superimposed onto the graph by vertical lines are the three mapped fault segments.

4.7.3: TOTAL THROW VALUES ALONG STRIKE

Using the values of footwall uplift and the total throw value derived from the cross-sections a footwall uplift to hanging wall subsidence ratio of 1:3 $^{(+/-0.3)}$ was produced. Previous research, discussed in chapter 2 (section 2.4.1) suggests that ratios footwall uplift to hangingwall subsidence may vary significantly between areas (e.g. Papanikolaou et al., 2010) but the ratio for the Gediz Graben falls within previous estimates. In addition to the footwall uplift to hangingwall subsidence ratio it was also possible to calculate an average footwall uplift to total throw ratio of 1:4 $^{(+/-0.3)}$ using the cross-sections.

Fault seg.	Swath no.	Cross-sect.	Distance along strike (km)	Footwall relief (m)	Total throw using 1:4.1 ratio	Throw Rate mm/yr using 2.6myr	Throw Rate mm/yr using 2myr	Displacement (m)	Slip rate (over 2ma)
	1		3.4	295	1209.5	0.47	0.60	1612.7	0.81
	2		8.7	342	1402.2	0.54	0.70	1869.6	0.93
	3		14.5	290	1189	0.46	0.59	1585.3	0.79
T	4		19.7	398	1631.8	0.63	0.82	2175.7	1.09
	5		24.7	348	1426.8	0.55	0.71	1902.4	0.95
	6		29.8	437	1791.7	0.69	0.90	2388.9	1.19
	7		35.3	217	889.7	0.34	0.44	1186.3	0.59
	8		40.4	354	1451.4	0.56	0.73	1935.2	0.97
	9		45.7	424	1738.4	0.67	0.87	2317.9	1.16
	10		50.3	483	1980.3	0.76	0.99	2640.4	1.32
	11		55.6	625	2562.5	0.99	1.28	3416.7	1.71
S	12		60.3	694	2845.4	1.09	1.42	3793.9	1.90
	13		65.3	646	2648.6	1.02	1.32	3531.5	1.77
	14		70.3	724	2968.4	1.14	1.48	3957.9	1.98
	15	E	75.4	618	2533.8	0.97	1.27	3378.4	1.69
	16	F	81.2	487	1996.7	0.77	1.00	2662.3	1.33
	17	C	86.3	472	1935.2	0.74	0.97	2580.3	1.29
A	18	B	91.9	618	2533.8	0.97	1.27	3378.4	1.69
	19	A	100	541	2218.1	0.85	1.11	2957.5	1.48
	20	D	110	290	1189	0.46	0.59	1585.3	0.79

Table 4.2: Throw and slip rate data for the 20 along strike swath sections of the Bozdağ Range, Gediz Graben. The Fault segments (fault seg.) labelled are Turgutlu (T), Salihli (S) and Alaşehir (A). Slip calculated from throw values using the Nicol et al. (2007) assumption of throw being 75% of slip on the same fault.

After derivation of the average 1:4 ratio the footwall uplift values for all 20 swath sections were converted to total throw values (Table 4.2). The total throw values share the same along strike trends as the footwall uplift; the maximum throw value at the centre of the Salihli fault segment is 2968 m, with values decreasing to zero at the eastern and western extremes of the range, but not at the locations of fault tips internal to the whole fault array.

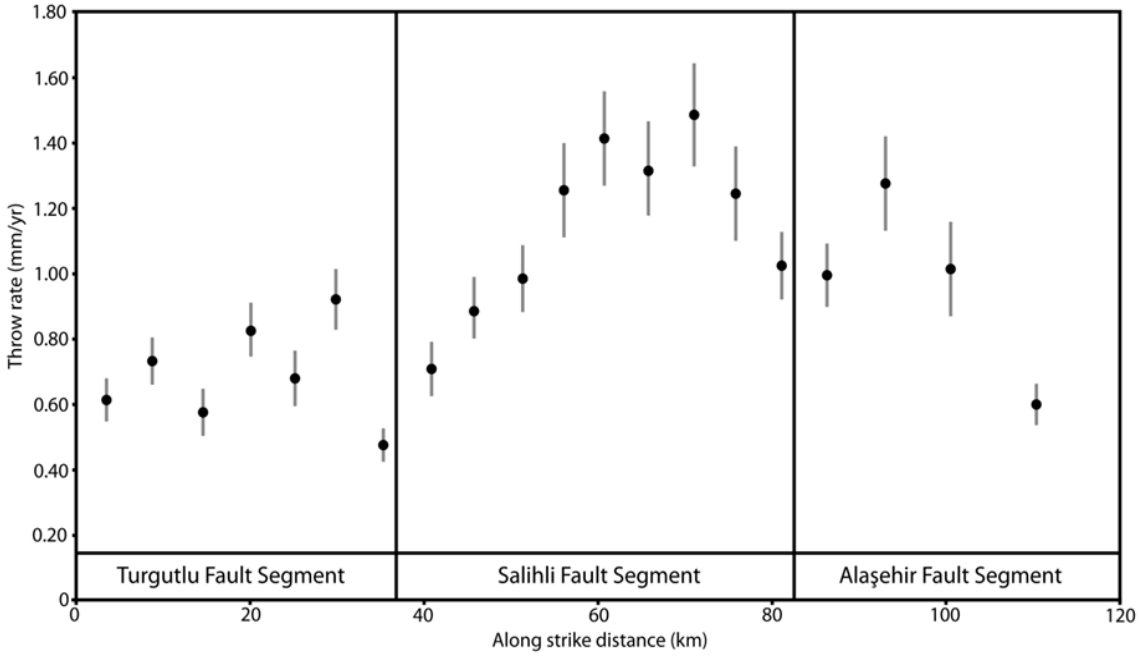

Figure 4.13: Throw rates for the high-angle normal faulting in the southern graben margin. The throw rates in mm/yr have been divided according to fault strands mapped from the 30m ASTER imagery. The errors are based upon a maximum of 10% variation in total throw over 2 myr.

The throw values have three peaks, located at approximately the centre of each fault segment with an overall peak within the centre of the fault array. The largest throw value of 2968 m is found within the Salihli fault segment around 70 km along the Bozdağ Range, additional segment peaks of 1790 m for the Turgutlu Segment and 2533 m for the Alaşehir Segment have been identified at around mid-way along each segment. It is notable that the peaks

within the Turgutlu and Alaşehir segments tend to lie off centre of the strand towards the direction of the Salihli segment in the centre of the array.

Throw rates calculated over 2 myr using the derived total throw rate vary between 0.4 ± 0.04 and 1.5 ± 0.15 mm/yr (figure 4.13) at the 20 locations along strike. The throw rates are at a minimum towards the edge of the range with rates lying within the 0.4 – 0.6 mm/yr range. The swath sections in a more central location along the mountain range have higher values and can reach values around three times those in the more peripheral swath sections with central swath sections lying on the Salihli fault segment yielding throw rates ranging from 0.7± to 1.5 ± 0.15 mm/yr. There is a maximum throw rate value within each fault segment of 0.9 ± 0.17 mm/yr for the Turgutlu Segment, 1.5 ± 0.15 mm/yr for the Salihli Segment and 1.3 ± 0.12 mm/yr for the Alaşehir Segment.

4.7.4 SLIP VALUES CALCULATED FROM THE DERIVED THROW DATA

Slip values calculated using the Nicol et al. (1997) method range between 1186 m and 3957 m along strike. The values for each of the 20 locations are documented in table 4.2 along with calculated slip rates which range from 0.6 mm/yr to 2.0 mm/yr. Overall the slip rates are less in the western extent of the graben margin and higher from the centre to the east, the Turgutlu Segment has an average slip rate of 0.9 mm/yr, the Salihli Segment has an average slip rate of 1.5 mm/yr and the Alaşehir Segment was calculated to slip at an average rate of 1.3 mm/yr.

4.7.5: THE RATES OF THROW AND SLIP AND HOW THEY COMPARE TO RATES OF MOVEMENT ON OTHER FAULT ARRAYS

The throw rates of between 0.4 and 1.5 mm/yr for the whole of the Gediz Graben southern margin when calculated over each of the three fault strands give average throw rates for the Turgutlu Salihli and Alaşehir fault segments of 0.7 mm/yr, 1.2 mm/yr and 1.0 mm/yr respectively. When these values are compared to measurement of throw rate on faults from Italy and Greece they fit well within the range of throw rates other studies. Normal faults within the Lazio-Abruzzo Apennines in Italy yield calculated throw rates in the range of 0.4 – 2 mm/yr (Roberts and Michetti, 2004) while Papanikolaou et al. (2007) produced throw rates of 0.4 – 3 mm/yr for the same area.

Throw rates of 0.1 – 0.28 mm/yr were calculated for the area between the Xilokastro and South Alkyonides Fault Segments in the Gulf of Corinth over the last 126 kyr as constrained by raised-beach-shoreface sediments (Morewood and Roberts, 1997). Fault slip rates from the centre of fault segments in the Gulf of Corinth range from 1 mm/yr (Pantosti et al., 1996) to 8 mm/yr (Armijo et al.,1996). Morewood and Roberts (1997) have suggested that the higher rates of slip derived in the Gulf of Corinth are an over estimations due to the effects of localised warping of the surrounding rock being included in the rate quantification.

Throw rate data has been quantified in other Turkish graben systems, within the Hatay Graben, eastern Turkey the normal faults have a present-day maximum throw rate of 0.4 – 0.5 mm/yr (Boulton et al., 2006; Boulton and Whittaker, 2009). The values for time averaged normal fault throw within the Gediz Graben therefore fall within the expected range of rates for vertical throw, they also appear to be 2.5 times higher than those in the Hatay Graben.

Nicol et al. (1997) have stated that up until around 1990s quantification of throw and slip rates on faults was mainly concentrated on neotectonic faults with rates averaged over time scales of 200 kyr or less (Wallace, 1984; McCalpin, 1985; Coppersmith and Youngs, 1989; Nicol et al., 1997). McCalpin (1985) calculated the rate of slip rate on normal faults and the results of the studies on faults over 200 kyr lie between 0.01-1.61 mm/yr (McCalpin, 1985). The results of a variety of slip and throw rate studies that calculated the rate over approximately 200 kyr time periods are variable and was assumed that this would be true of results for older time averages as well (Nicol et al., 1997). Nicol et al. (1997) go on to conclude that over time scales of 1 - 40 myr the long-term normal fault throw and slip rates are markedly more stable than those of the short-term estimates. This has implications for the new data presented in this study as the new throw rate data should be a reliable source from which seismic hazard can be assessed.

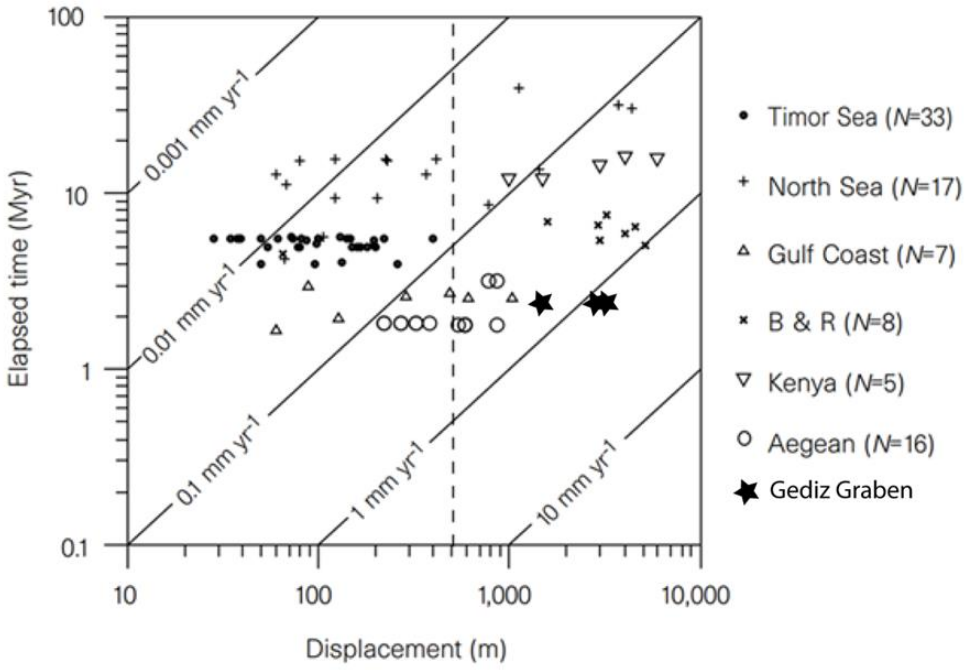

Figure 4.14: A graph showing the relationships between, time elapsed, displacement and slip rate for a variety of fault arrays taken from Nicol et al. (1997). The values for the Turgutlu, Salihli and Alaşehir fault segment of the Gediz Graben have been added.

Nicol et al. (1997) have published data that shows the elapsed time plotted against maximum slip for 86 faults from six regions on a log–log plot (figure 4.14), slip rates on the fault surfaces vary according to the location of the fault and with fault size. Slip rates for individual faults in their study is ~ 0.004 - 1.2 mm/yr. The values for slip rate that were calculated from the throw rate data for each of the Turgutlu, Salihli and Alaşehir fault segments have been added to the data set (figure 4.14) with slip rate values of 0.9, 1.5 and 1.3 mm/yr respectively the fault segments fall towards the higher slip rate values for the Aegean region data points with a horizontal linear trend. The data for the Gediz Graben does appear to be similar, if a little higher than the data from the Basin and Range Province, which is a comparable tectonic setting. According to Nicol et al. (1997) data distributed along a line parallel to the displacement axis (horizontal) indicates a direct relation between fault size and slip rate. This relationship appears to hold true for the Gediz Graben and general Aegean region showing that in general larger faults with greater slip values tend to have a higher slip rates than smaller faults.

In addition to the direct comparison of slip and throw rates the relationships between maximum displacement (D) and fault length (L) can also be evaluated. For the Turgutlu segment the D/L ratio is 0.033, for the Salihli Segment is it 0.084, and for the Alaşehir Segment the D/L is 0.080. These values lie firmly within the range of D/L expected from normal faults (e.g. Yin and Groshong 2006). This suggests that the pragmatic methods used to quantify throw rates have been reasonably successful in accomplishing that aim.

4.7.6: ALONG STRIKE TRENDS IN THE GEDIZ GRABEN

The Gediz fault array is 124 km long with the longest fault segment being the central Salihli segment, at 47 km in length, the Alaşehir segment has a length of 42 km, and the shortest segment is the Turgultu segment at 35 km in length. As has been previously discussed (section 2.4.3) the highest values of throw should be found near the centre of the fault while the throw should reduce to zero at the fault tips (e.g. Barnett et al., 1987; Cowie and Roberts, 2001; Kim and Sanderson, 2005).

The Salihli segment exhibits the largest throw values of any of the fault segments with the largest towards the central region reaching throw values of 2284 - 2968 m centrally and to the east of centre along the segment. The smallest values for throw on the Salihli Segment are located at the fault tips but do not reduce to zero.

Within the Alaşehir Segment of the fault there is a peak in the throw rate in the central third of the fault segment and similarly to the Salihli Segment the minimum values are at the end of the fault segment. There is reduction of throw to zero to the eastern fault tip but the western end of the fault has a non-zero value. The Turgutlu Segment shows broadly the same trends but with more variation on the throw values along the segment length. There are a series of peaks to the data with a maximum value of 0.69 mm/yr lies off-centre, closer towards the Salihli segment of the fault array. There is a zero value for throw at the western fault tip and a non-zero value for throw at the eastern end of the fault strand near to the western extent of the Salihli segment.

This distribution of throw value magnitudes along strike of the fault segments is in agreement with the research on fault length and throw scaling,

(section 2.4.3) although there is an absence of zero throw values at the ends of segments where the fault lies next to another segment.

It is well documented that in areas of extension, large faults form through the linkage of smaller faults in an array (e.g. Walsh and Watterson, 1988; Nicol et al., 1997; Hancock, 1994; Gawthorp et al., 1997; Cowie, 1998; Gupta and Scholz, 2000; Roberts and Michetti 2004) and research has suggested that linked faults towards the centre of the array should have higher throw rates than those peripheral in the fault array (e.g. Roberts and Michetti, 2004). The trend in the data for the Gediz Graben across the whole 124 km fault array is that the highest values for throw rate are found towards the centre of the fault array at around 60-75 km along strike; the highest value of 1.48 mm/yr is found 72 km along strike, within the centre third of the fault array. Linkage of the fault strands is supported by the non-zero throw and throw rate values at both tips of the central Salihli segment (figure 4.13 and table 4.2) suggesting the all three fault segments are linked, causing the Gediz high-angle normal fault array to have grown in steps caused by the linkage events. A relay ramp has been observed in the locations of suggested linkage between the Turgutlu and Salihli fault segments (Çiftçi, 2007). The fault array also has an along strike bend of approximately 40° from east to west, which adds additional support for the linkage of the fault segments which bound the modern topographic graben as curvature would result from the linkage of two faults that were not completely parallel (Fossen, 2010) .

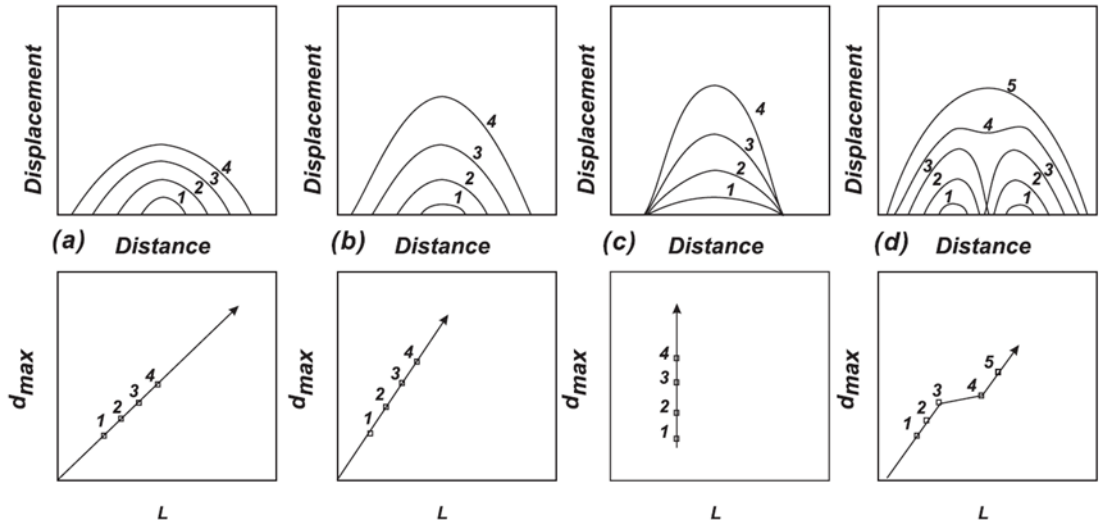

Figure 4.15: Fault growth models illustrated by the relationship between length and displacement on faults over time: (a) Constant length to maximum displacement ratio. (b) Increasing length to maximum displacement ratio. (c) Constant length model. (d) Fault linkage model, which is the likeliest mode of growth for the Gediz Graben fault array. Models adapted from Kim and Sanderson (2005); Walsh et al. (2002); Kim et al. (2000); Cartwright et al. (1995); and Peacock and Sanderson (1991).

If the faults in the Gediz Graben are linked it appears that they may not have been linked for long as the fault segments still maintain individual peaks while having the central and most significant array throw peak. Research suggests that as faults undergo linkage the maximum rates of throw on the previous independent faults shift towards the new centre of the soft linked fault array (Cowie, 1998; Roberts and Michetti 2004; Kim and Sanderson, 2005 [figure 4.15]). As faults link there would be a gradual complete convergence of the maximum throw rate to the centre of the new longer fault (Kim and Sanderson, 2005) erasing the evidence of segment peaks over time.

These data from the Gediz Graben suggests that the fault segments acted independently before a linkage event that occurred at a time between 2 myr to present. The data shows the typical pattern of fault linkage, the overall central peak in throw and throw rate.

4.7.7: IMPLICATIONS FOR SEISMIC HAZARD ANALYSIS IN THE GEDIZ GRABEN

The observations of the Gediz Graben area indicate that faulting is still active with the well-developed modern topographic graben abruptly meeting significant uplift of the graben margin, with recent alluvial fan formation and faceted spurs (Çiftçi, 2007; Oner and Dilek, 2011). The calculated slip rates also suggest that the high-angle normal faulting has been ongoing at a fairly high rate for active normal faulting for the last 2 myr. The occurrence of large earthquakes such as the 6.9 magnitude Alaşehir earthquake in 1969 indicates that large earthquakes occur. Seismic hazards associated with active normal faulting are commonly mapped using instrumental and historic records of seismicity (Robets and Michetti, 2004). Several researchers have suggested that this method may not be an accurate indicator of present or future seismic hazard. Clarke et al. (1997) state that relative or complete seismic quiescence is not a reliable indicator for future activity in an area and Roberts and Michetti, (2004) support this view giving the reason that the historical and instrumental record fails to take into account the fundamental determinant of seismic hazard. Cowie and Roberts (2001) have specified that earthquake recurrence intervals tend to decrease as slip rate increases, this means that significant information useful to analysis of seismic hazard comes from a high resolution record of the rates of fault movement. Cowie and Roberts (2001) go further to say that seismic hazard can vary along the length of a fault array based upon the magnitude of fault throw along strike. The implications of this are that in order to provide a useful assessment of seismic hazard complete with spatial variation, a high resolution record of throw rates in a number of locations along strike of the fault array is needed (Roberts and Michetti, 2004). This study therefore

provides a higher resolution indication of seismic hazard than has previously been published for the Gediz Graben.

Construction of a detailed seismic hazard map for the Gediz Graben is beyond the scope of this thesis but the Republic of Turkey Disaster and Emergency Management Presidency have prepared an earthquake zoning hazard map of Turkey (figure 4.16). It is possible to calculate the maximum magnitude of an earthquake in the Gediz Graben to compare to their mapping. The maximum magnitude for a fault can be calculated using surface rupture length. Between one half and one third of the total length of the fault is thought to rupture in a seismic event (Mark, 1977).

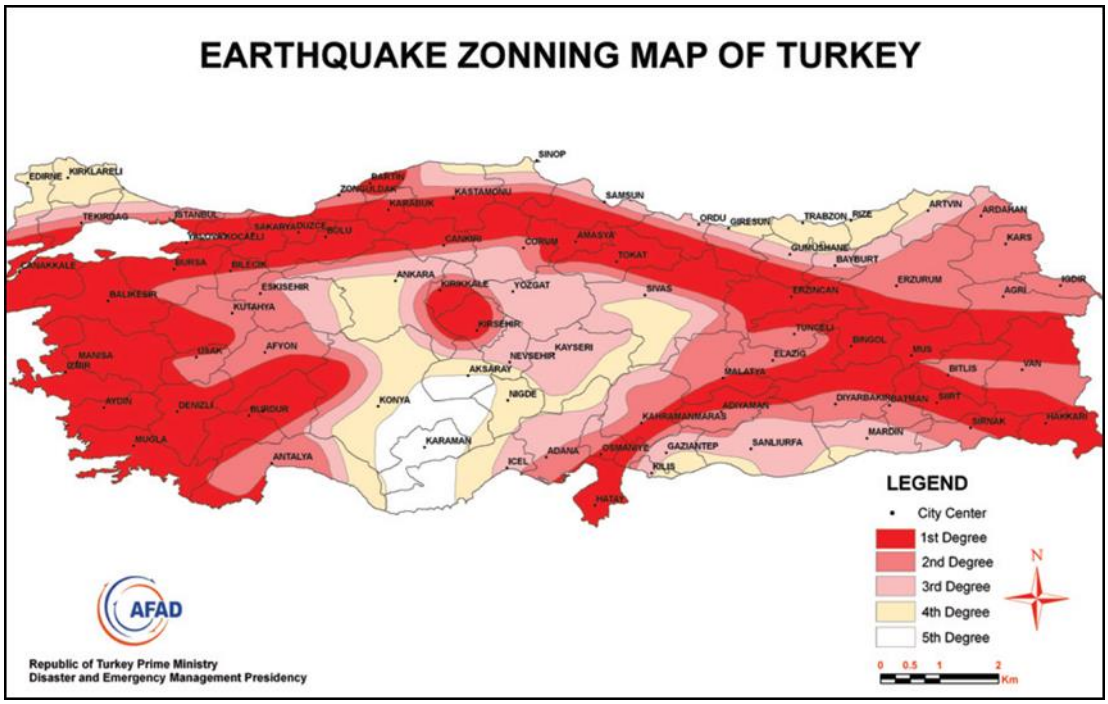

Figure 4.16: The earthquake zoning map of Turkey produced by the Republic of Turkey Disaster and Emergency Management Presidency (AFAD).

Following Wells and Coppersmith (1994), the moment magnitude (Mw) this can be expressed, for a normal fault, as

$$Mw=4.86+1.32\log L \quad \textbf{(eq. 4.1)}$$

where L is fault rupture length (in km).

The fault array that bounds the Gediz Graben is linked in two areas along strike with three segments of around 40 km in length, giving a total length of 120 km. A rupture that occurs along the whole of one of the 40 km segments would produce an earthquake of predicted magnitude 6.9. If the rupture was to occur over one half to one third of the segment this would produce an earthquake with predicted Mw of 6.3 to 6.5. As the fault segments have linked it is possible that the fault array could act as one longer fault of 120 km. If the whole of the array were to rupture the predicted Mw is 7.6. A rupture of one half of the array, 60 km, would produce a predicted Mw of 7.2. A rupture of on third of the array (40 km) would be expected to produce an earthquake with Mw of 6.9. It is also possible that because the sedimentary units of the Gediz Graben are fairly unconsolidated the effects of an earthquake would be increased in these areas.

The Gediz Graben and surrounding region have experienced some large earthquakes over Mw 5.0 in the last twenty five years (Eiodogan and Jackson, 1985; Buscher et al., 2013), including a destructive earthquake of magnitude 6.9 in 1969, (Arpat and Bingol, 1969). Another earthquake occurred within the Gediz Graben in March 1970, this earthquake had a magnitude of 7.2 and left thousands homeless and over 1000 people dead, it lead to the total relocation of the village of Gediz (Mitchell, 1976). The historical evidence supports the magnitude prediction with documented earthquakes ranging from 5 – 7.2 Mw. The calculated possible magnitude for earthquakes within the Gediz Graben does suggest significantly that an even larger earthquake could occur if enough of the fault length ruptured.

4.8: CONCLUSIONS

These new data show that in the Gediz Graben the throw rates vary from 0.4 to 1.2 mm/yr along the fault array as this is mirrored by the relief. The graben bounding faults have undergone a two stage history with a change in the throw rate at a period of fault linkage at two locations around 40 and 65 km along strike of the fault, which has increased the rate of movement in locations along on the high angle normal faults.

These results are important as they not only provide novel quantification of throw rates of the bounding faults of the southern margin of the Gediz Graben, providing greater insight into the active tectonics of the area, but it also highlights the potential impact to studies of past tectonics of the use of geomorphic data alongside the traditionally used geological data. The key point arising from this study is that currently available geological data on its own does not give much information about the graben tectonics and how they change through time. By combining geologic data with the geomorphic data from topographic studies more data about the active faulting within the Gediz Graben has been produced and quantified.

CHAPTER 5

OSL DATING OF MAPPED RIVER TERRACES TO EXTRACT MODERN DAY INCISION AND THROW RATES

5.1: CHAPTER HIGHLIGHTS

- Fluvial terraces were examined along three rivers draining the southern margin of the Gediz Graben; within these river valleys, terraces were found at 6 elevations (T1 – T6 terrace levels) above the present channel.
- OSL sampling reveals that aggradation of the terraces in the T4 Gediz Graben likely started around 84 kyr T4 terrace, with OSL dates yielding ages of between 83.79 ± 7.19 – 7.06 ± 0.59 kyr.
- These data produce incision rates of between 0.24 – 3.96 mm/yr, although the 0.24 ±0.02 mmy/yr rate is likely to be the most representative incision rate and the use of the other ages is likely to overestimate the incision rates.

5.2: INTRODUCTION

This chapter studies the fluvial terraces within the southern margin of the Gediz Graben. The terraces documented along the rivers within the Bozdağ Range appear in flights of different elevations above the current elevation of the river channel, this suggests that the river may be responding to tectonic activity, as well as climatic variables. This chapter assigns ages to the some of the terraces observed along three different rivers draining the range using optically stimulated luminescence (OSL) dating and provides relevant river terrace mapping. These age data are then combined with measurements made in the

field relating to terrace heights, combining these variables enables rates of incision to be quantified. Incision rates have been used to estimate recent, short-term, uplift rates associated with graben bounding high-angle normal fault in those locations valid over 15 Kyr.

5.3: BACKGROUND INFORMATION ON RIVER TERRACE STUDIES

River systems are among the most important geomorphic agents in the landscape (Vandenberghe and Maddy, 2001), as they preserve records of environmental changes, geology, geomorphology, climate, hydrology, vegetation and tectonics (Schumm, 1977; Blum and Törnqvist, 2000; Rittenour, 2008). The fluvial deposits of these rivers therefore act as potential archives for changes in climate and tectonics (Wallinga, 2002a; Rittenour, 2008). As rivers are such important agents of change in the landscape, and produce archival deposits, it is unsurprising that fluvial sediments receive a lot of attention from geologists, sedimentologists, geomorphologists and geographers (Wallinga, 2002a).

5.3.1: RIVER TERRACES

Fluvial terraces (figure 5.1) are common landforms found around the world, located on the flanks of river valleys in a wide range of tectonic and climatic settings (Bull, 1991; Westaway et al., 2009; Stokes et al., 2012). Terraces are a key observable feature for studies into fluvial processes, active tectonics, and paleoclimatology. Analysis can provide ages and the terraces can be used as geodetic markers to analyse tectonic and climatic process rates (e.g. Törnqvist et al., 2000; Cheong et al., 2003, Chen et al., 2003; Zuchiewicz et al., 2004; Rittenour et al., 2005; Mahan, 2006; Mason et al., 2006; Rodnight

et al., 2006; Amos et al., 2007; Mukul et al., 2007; Tooth et al., 2007). Terraces record the unsteadiness in the rate of vertical incision of a channel predominantly caused by fluxes in sediment and the amount of vegetation showing geomorphic, and hydrologic responses to climate.

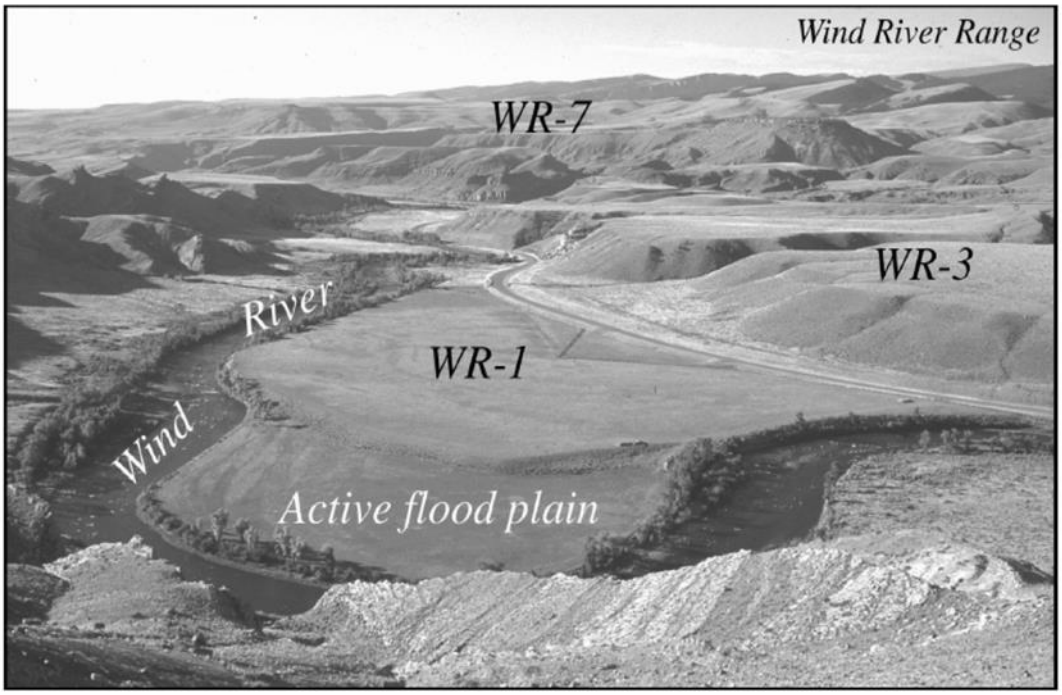

Figure 5.1: An example of river terraces from the Wind River, Wyoming. A flight of three terraces can be seen above the current flood plain, labelled WR-1, WR-3 and WR-7. Photo from Hancock and Anderson, (2002).

Fluvial terraces form as either strath (figure 5.2C) or fill terraces (figure 5.2D). Fill terraces are formed when a significant amount of sediment enters the fluvial system, and subsequently the amount of sediment within the river is far greater than the amount of sediment the river is capable transporting through the system (Pederson et al., 2006). This causes the river channel to aggrade, depositing the sediment on, and raising the level of, the floodplain. When the amount of sediment within the river system declines the river has an elevated floodplain (Gibbard and Lewin, 2009; Westaway et al., 2009; Stokes et al.,

2012). Strath terraces are formed when the river channel incises laterally into bedrock. This occurs when the sediment being transported by the river is less than the amount the river is capable of moving (Fairbridge, 1968). The sediment in the channel acts as tools to move the channel laterally, the resulting floodplain is the strath terrace.

5.3.2: THE RELATIONSHIPS BETWEEN CLIMATE AND TECTONICS AND RIVER TERRACES

Fluvial terraces can occur in flights up the valley sides of a river (figures 5.1 and 5.2) and the flight can span time scales of several tens to hundreds of thousands of years (Bridgland and Westaway, 2008a; Gibbard and Lewin, 2009; Westaway et al., 2009; Stokes et al., 2012). This gives terraces great potential as a widely available resource for investigating aspects of geology and geomorphology such as climate change, tectonic uplift and base level changes over both recent timescales and over hundreds of thousands of years.

The controls on river terrace formation by climate have been studied in great detail in terms of the aggradational and incisional processes needed for terrace formation in a variety of climatic settings (e.g. Bull, 1991; Gibbard and Lewin, 2002). Sediment aggradation occurs when valley slopes are relatively unstable and a limited amount of vegetation allows for the erosion and transport of sediment to the valley floor. Incision occurs when the valley sides are stable due to the effects of more sediment anchoring vegetation, and hence there is reduced sediment transported to the valley floor (Stokes et al., 2012). In the Quaternary this generally means that aggradation occurs during glacial times and incision in interglacial periods (Vandenberghe, 2008). However, there have been studies (Van den Berg, 1996; Van den Berg and Van Hoof, 2001;

Bridgland and Westaway, 2008b; Pazzaglia, 2013) that suggest that the designation of aggradation in glacial periods, and incision in interglacial periods is an over simplification, and that timing of incision and aggradation compared

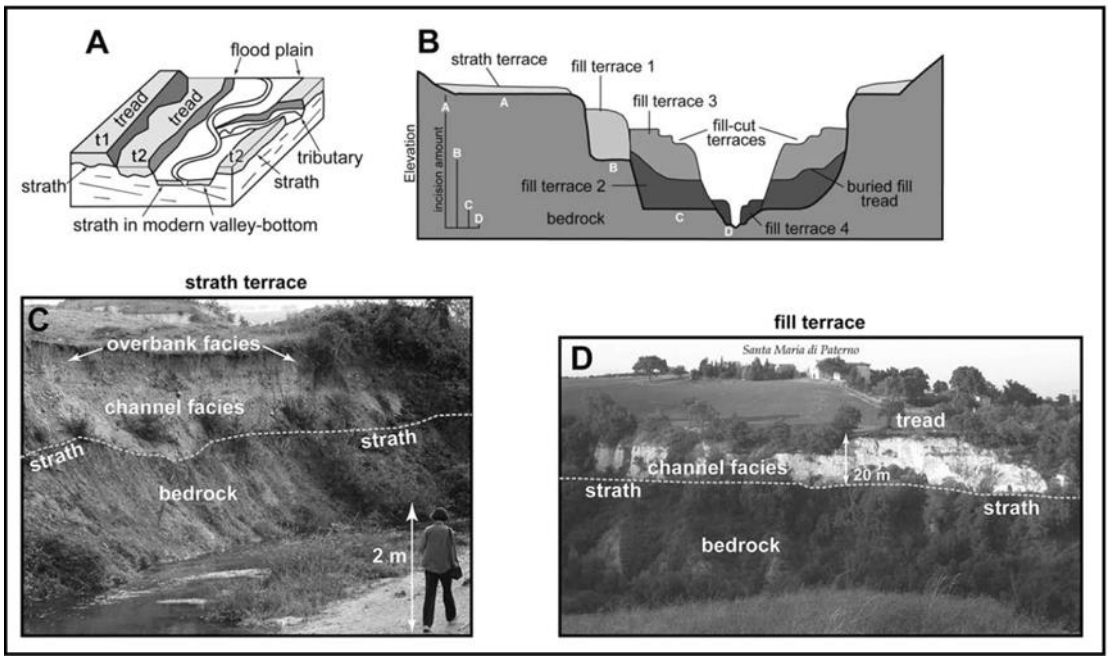

Figure 5.2: A cartoon and photograph representation of the relationships between terraces, terrace deposits and incision–aggradation history from the study of Romagna and Marche Apennines Italy (Wegmann and Pazzaglia, 2009). 5.2A Shows a schematic diagram illustrating the relationships between terraces t1, t2, straths, floodplain, and valley bottom in the study. 5.2B Shows a hypothetical cross-section showing geometry of the strath and fill terraces and an idealized complex sequences of fill (aggradational) and fill-cut (degradational) terraces (Strath surfaces are labelled A–D). Strath surfaces (e.g. 5.2C) are can be used to measure the amount and rate of fluvial incision. With strath terraces it is generally assumed that the overlying sediment is intimately associated with the bevelling of the strath surface and the age of the overlying sediments can be used as a proxy for the age of the strath surface itself. For fill terraces (e.g. 5.D), the age of the overlying sediments may be much younger than the underlying strath. For fill terraces, a minimum strath age can be determined from the oldest radiometric age obtained from basal fill deposits.

to climatic events varies depending on latitude. Rivers within Mediterranean and arid/semi-arid climates become loaded with sediment during the transition from glacial to interglacial conditions, rather than at peak glacial conditions (Bull, 1991; Blum and Valastro, 1994; Ritter et al., 2000) as there tends to be more vegetation during the (wetter) glacial times. The vegetation can be quickly removed as the climate warms, liberating sediment (Pazzaglia, 2013). Climate

change has therefore been established as an important control on terrace formation, providing sediments for aggradation.

Climate is an important factor in river terrace creation but it cannot explain the formation of terrace flights (staircases). The mechanism for the formation of terrace flights must invoke a base-level lowering trend such as sea-level change or tectonic movements (Bridgland, 2000; Bridgeland and Westaway, 2008a; Bridgeland and Westaway, 2008b; Gibbard and Lewin, 2009; Stokes et al., 2012).

On a river that crosses an active fault, where uplift occurs upstream, the terraces that line the river valley can provide information about the localised tectonics as the height of the terraces should broadly correlate with the magnitude of displacement (Burbank and Anderson, 2001). A long-term terrace flight should allow quantification of the long-term displacement history of a fault with higher terraces recording tens to hundreds of metres of vertical movement (Burbank and Anderson, 2001).

Despite the evident usefulness of fluvial terraces in geological studies it is apparent that the interplay of climatic and tectonic processes needs to be carefully considered if accurate information is to be extracted from the terrace record. Active tectonics provides a compelling mechanism for the formation of multiple terraces levels, but the variations between incision and deposition of sediment provided by influences such as climate provide some uncertainty in the analysis of terrace formation (Stokes et al., 2012). In addition, climate can impact further on the availability of materials for dating in terrace deposits, for example, in glaciated areas it is common to form terraces (Pazzaglia, 2013) but it is also common for glacial advances to remove evidence of older terraces through erosion (Stokes et al., 2012). Disruption of the sedimentary record held

in terraces can be a problem for analysis and can affect the reliability of results, for example bioturbation by organisms and Anthropogenic influences can disturb or modify the landforms. Fluvial transport of sediments deposited in terraces also requires considerations which are mentioned in more detail in section 5.6.2. Overall though, fluvial terraces have been provided a wealth of information for studies of fluvial response to sea-level change (e.g. Maddy et al., 1998; Törnqvist, 1998; Blum and Törnqvist, 2000; Rittenour et al., 2007), climate change (e.g. Leigh et al., 2004; Schokker et al., 2005; Brook et al., 2006; Sohn et al., 2007) and palaeoseismic reconstruction (e.g. Personius, 1995; Pazzaglia and Brandon, 2001; Chen et al., 2003; Cheong et al., 2003; Zuchiewicz et al., 2004; Mahan, 2006; Amos et al., 2007; Mason et al., 2007; Mukul et al., 2007).

5.3.3: MEASURING UPLIFT AND INCISION RATES USING RIVER TERRACES

Despite the important information that fluvial sediments can contain, the dating of these deposits can be problematic. Radiocarbon dating has been traditionally the most widely used method in geochronology, but it is not always appropriate for fluvial sediments (Wallinga , 2002a; Rittenour, 2008). In many cases there is a lack of available material to enable the use of radiocarbon dating, particularly as radiocarbon dating can date materials with a maximum age of ~35 kyr. There can also be problems with the reworking of old carbon within many fluvial sediments (Blong and Gillespie, 1978; Gillespie et al., 1992; Sowers et al., 2000).

Other radiometric methods used to date fluvial materials, include Uranium series or Potassium-Argon dating. Both these methods however, are

limited in their applicability to fluvial deposits (Wallinga, 2002a), but in certain situations they can provide ages for sediment deposition or landform abandonment (Gosse and Phillips, 2001). Uranium Series Dating requires uranium bearing deposits within closed systems in which the radiometric material is neither gained nor lost after deposition. This method has been used effectively on speleothems and other calcareous precipitates (e.g. Fouke et al., 2002; Sharp et al., 2003; Sierralta et al., 2010), and is therefore well suited to dating travertines but cannot be used for other types of fluvial deposits. Potassium-Argon dating is widely applied to date igneous rocks (Richards and Smart, 1991). This method requires fluvial sediments to be intercalated with tephras or lava flows to constrain the ages of fluvial sequences (e.g. Gansecki et al., 1996; Karner and Renne, 1998; Westaway et al., 2004; Westaway et al., 2006a)

Optically stimulated luminescence (OSL) is useful for dating inorganic sediments, such as those from fluvial or aeolian environments, where suitable materials for dating by methods such as radiocarbon are not found (Blong and Gillespie 1978, Stanley and Hait, 2000). This method has the benefit of providing direct dating of the time of sediment deposition and as a result has enabled greater use of dating in geological studies (e.g. Stokes, 1999). Despite OSL dating having its own specific caveats (documented in section 5.6.1 – 5.6.2) many researchers have successfully applied OSL to the dating of river terrace deposits (e.g. Törnqvist et al., 2000; Cheong et al., 2003, Chen et al., 2003; Zuchiewicz et al., 2004; Rittenour et al., 2005; Mahan, 2006; Mason et al., 2006; Rodnight et al., 2006; Amos et al., 2007; Mukul et al., 2007; Tooth et al., 2007).

As a river terrace is an elevated abandoned flood plain of the active river that has responded to changing conditions by incising, it is possible to estimate the rate of incision over the time since terrace formation by utilizing the height of the terrace above the modern river level assuming negligible surface erosion (Burbank and Anderson, 2001; Stokes et al., 2012). There have been many examples of these type of studies as the methods for allowing accurate dating of the terrace have been developed (e.g. Berryman et al., 2000; Maddy et al., 2000; Hsieh and Knuepfer, 2001; Mathew et al., 2006; Cunha et al., 2008; Gibbard and Lewin, 2009; Martins et al., 2009). The studies have utilised a variety of different dating methods to quantify incision but OSL is particularly common, for example Martins et al. (2009) used OSL dating to constrain the ages of 4 terrace levels along the Tejo River, in an actively uplifting area of Portugal. Incision rates of 0.13 m/kyr to 0.53 m/kyr were calculated using the terrace ages and the height of the terrace. Cunha et al. (2008) also utilized OSL to estimate incision using the same method in the Rodão Graben section of the Tejo River, providing a rates of between 1 mm/yr and 0.1 mm/yr depending on the period of time over which the estimate was time averaged.

It has been proposed that tectonic uplift rates can be calculated from the relative heights of terraces with respect to the modern river flood plain by the use of fluvial incision rates as a proxy for rock uplift (e.g. Personius, 1995; Burbank et al., 1996; Maddy 1997; Pazzaglia and Brandon, 2001; Mathew et al., 2006; Srivastra and Misra, 2008). Tectonic controls on terrace formation have been widely reported, particularly in Europe (e.g. Brunnacker and Boenigk, 1983; Van den Berg et al., 1996; Maddy, 1997; Bridgland, 2000; Maddy et al., 2001). Maddy (1997) suggests that attributing the vertical difference between the terrace and the present flood plain is a valid method for

evaluating rates of uplift, if the study basin is situated far enough inland to negate the effects of base level fall. Maddy (1997) tested this method on terraces in the Upper Thames Valley (England) where a rate of uplift of 7 cm/Ka was calculated, which is in good agreement with previous estimates based on raised beach deposits (Preece et a., 1990), aminostratigraphy (Bowen, 1995) and magnetostratigraphy (Rose et al., 1999), which produce age estimates of around 1.8 Ma for the deposits.

Westaway et al. (2006b) used fluvial terraces from the Solent River to reconstruct the uplift history of central southern England. They made the assumption that fluvial incision was in direct response to surface uplift, they also conclude that climatic forcing controls the precise timing of terrace formation. Therefore, the height of the terrace gravels above the modern river is a result of uplift since deposition. The archaeological record was used to constrain the dates of the terraces, specifically the first appearances of bout coupé hand axes, as markers for marine isotope stages (MIS). Westaway et al. (2006b) show that most of the Solent region has uplifted by 70 m since the late Early Pleistocene and by 150 m since the Middle Pliocene.

The caveats of assuming that the height of the terrace above the river is a purely a function of uplift are highlighted by Maddy (1997) and others (e.g. Hsieh and Knuepfer, 2001; Wegmann and Pazzaglia, 2002; Litchfield and Berryman, 2006), for example the uplift rates produced cannot be attributed to steady rates of uplift and the final uplift rate could hide any changes in uplift rate. Therefore using fluvial incision rates as a proxy for uplift rates might lead to inaccurate uplift rate quantification, and the lack of independently quantified uplift rates might hinder the evaluation of such a problem (Litchfield and Berryman, 2006). Furthermore, fluvial incision rates can vary significantly

through time due to changes in external variables such as climate and tectonics and human influence that cause changes in the steepness of the stream gradient, the amount of sediment contained in the river, and the total amount of water flowing through the system (Bull, 1991; Hsieh and Knuepfer, 2001; Wegmann and Pazzaglia, 2002).

Litchfield and Berryman (2006) set out to test the validity of the incision rate proxy using the Hikurangi Margin (New Zealand). By examining terraces, deriving incision rates and comparing them to uplift rates they found that the calculated post-glacial incision rates are 1.5 times greater than the Quaternary uplift rate and 5 times greater than the long-term uplift rate (which could be partially accounted for by periods of tectonic quiescence).

Therefore, it is evident that fluvial incision rates have potential as proxies for uplift rates, but these data must be interpreted with caution and be regarded as an approximation of averaged uplift rates.

5.3.4: OSL STUDIES IN TURKEY

The study of fluvial terraces, and specifically the use of OSL to date fluvial deposits, has proliferated in the last 15 years due to advancements in the methodological techniques (Stokes, 1999; Wallinga, 2002a; Rittenour, 2008). Despite this there have been relatively few studies that use OSL to date fluvial terrace deposits carried out in Turkey, and fewer still that use incision rates gained from analysis of river terraces to analyse uplift rates. In addition, there is a complete absence of studies that examine the rate of uplift in the study area through incision and fluvial terrace studies. The majority of the studies carried out on river terraces within Turkey are based in the south-east, for example, a synthesis of terrace deposits along the Euphrates River encompassing some of

south-eastern Turkey to elucidate uplift rates (Demir et al., 2007). Additionally, Bridgland et al. (2007) have worked on the terraces on the River Tigris, also in south-eastern Turkey.

A number of studies have focused on the upper reaches of the Gediz River, near to the town of Kula (Westaway et al., 2004; Maddy et al., 2005; Westaway et al., 2009). This area is in northern bounding mountain range of the Gediz Graben (the site of this study is the southern range). The land surface here has uplifted by ~400 m since the Middle Pliocene in the upper reaches of the Gediz River. It was possible to derive the uplift rate because the river terraces are capped by basalt flows that have been K–Ar and Ar–Ar dated. The basalt flows allow for time constraints of up to ~1264 kyr to be examined in five areas with known net incision. This allowed Westaway et al. (2009) to suggest that the local uplift rate in the Kula area is ~0.2 mm/yr.

5.4: CONSTRAINTS ON REGIONAL AND TURKISH CLIMATE

Climate is a central consideration in studies of fluvial terraces, as climate is the primary control on the periodic availability of sediment loads within rivers enabling and constraining incision and aggradation episodes. Rivers are able to aggrade when they cannot transport the sediment load within them, such as when the ratio of sediment load to discharge is high (Maddy et al., 2001). Rivers also aggrade when vegetation growth is inhibited, this allows more sediment to be transported into the river system and melt water and/or precipitation allow the sediment load to be carried in the rivers (Maddy et al., 2001; Westaway et al., 2003). These conditions are expected to occur at transitions to and from glacial conditions (Maddy et al., 2001; Westaway et al., 2003).

In order to examine the relationship between the terrace deposits in the Gediz Graben and the overall climate of the Mediterranean the following section give details of climatic studies that have focused on Late Pleistocene to Holocene climates; the focus on this age range of data is due to the ~150 kyr limit for the use of OSL, the method utilised in this study.

U-Pb dating of speleothems form the Negev Desert has given an insight into humidity around the Mediterranean over the last ~ 3 Ma (Vaks et al., 2013). The record shows that the Mediterranean was humid around 3.1 Ma and this was followed by a general trend towards aridity over the last 3 myr. The increased aridity was punctuated by periods of increase humidity starting from around 1.7 Ma and occurring intermittently at 980 Ka, 959 Ka, 693 Ka, 621 Ka, 600 Ka, and 79 Ka.

In addition, Schulte et al. (2002, 2008) have studied the River Aguas basin in southeastern Spain (figure 5.3), producing a record of fluvial archives and travertine and slope deposits over the last 170 kyr. They have utilised U/Th and OSL dating indicate a dominant aggradational regime from 169 to 26 kyr. They show that this has been punctuated by at least four incision events between 167 – 148 kyr, 148 – 110 kyr, around 95 kyr and at 71 kyr.

There are a variety of high-resolution ice-core records from Greenland (Dansgaard et al., 1993; Grootes & Stuiver, 1997) that suggest the climate into and during the Holocene was characterised by a marked stability in the northern hemisphere. The records seem to show that the post-glacial interval was relatively stable, with a single global and rapid climate change event 8.2 Ka ago (Alley et al. 1997; Alley & Agustsdottir, 2005; Nicoll and Küçükuysal, 2013). However, there are an increasing number of studies based on ocean core records from the North Atlantic Ocean and Mediterranean Sea that demonstrate

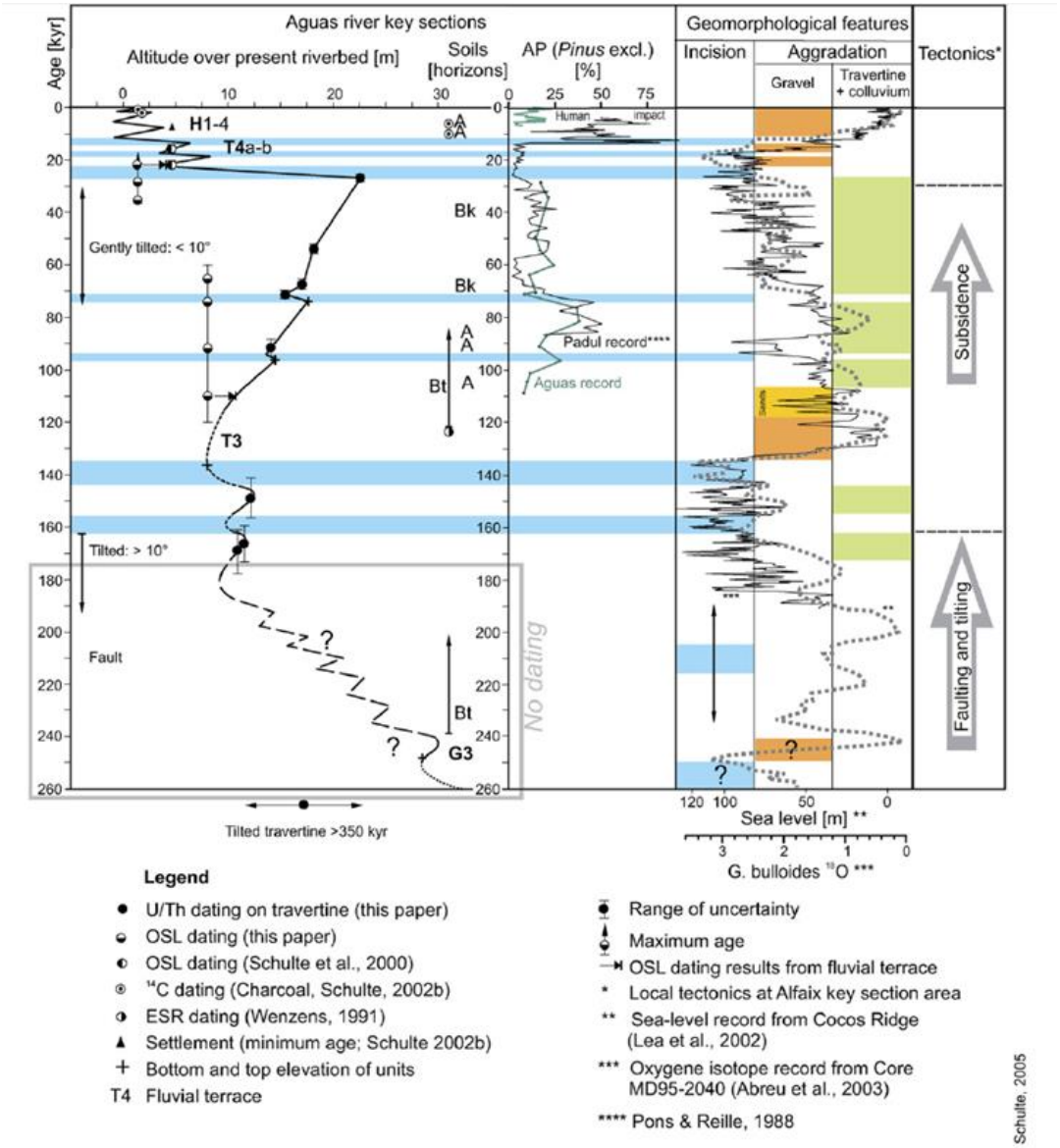

Figure 5.3: A correlation between the River Aguas sequences and regional proxies, showing periods of dominant aggradation and incision From Schulte et al. (1998).

that there was significant variation in Holocene climate (e.g., Ariztegui et al., 2000; Sbaffi et al,. 2004, Kotthoff et al., 2008a; Kotthoff et al., 2008b; Peyron et al., 2011; Schmiedl et al., 2010; Nicoll and Küçükuysal., 2013). The cooling at 8.2 Ka is the strongest short-term climate anomaly within the Holocene and produced rapid terrestrial ecosystem turnover as far south as the Mediterranean, shown by Pross et al. (2009), who studied pollen data from northeastern Greece.

Combourieu-Nebout et al., (2013) produced a high-resolution, multiproxy study of the Adriatic marine core MD 90-917, which provides a review of the vegetation and climate in the Southcentral Mediterranean (figure 5.4). The reconstruction shows the Preboreal oscillation around 11.3 – 11.2 Ka, is linked to increasing river inputs from Adriatic rivers recorded by increase in clay mineral contribution to marine sediments. Temperature, inferred from pollen, declines during the early–mid Holocene and then then increases during the mid–late Holocene. Several short vegetation and climatic events are shown in the record. The study also reconstructed summer precipitation and shows a regional maximum between 8.0 and 7.0 Ka. Two important changes in vegetation are shown at 7.7 Ka and 7.5 – 7.0 Ka that Combourieu-Nebout et al., (2013) correlate with increased river inputs around the Adriatic. During the mid-Holocene a homogenous precipitation regime was initiated by year-round moisture and after 6000 Ka summer precipitation decreases towards present-day values while winter precipitation rises.

Lake studies in regional E-W transect from Greece to Iran, from the Ioannina, Abant, Golhisar, Eski Acigol, Van, Zeribar, and Mirabad lakes (Roberts et al. 2011). Around 7.9 Ka $\delta^{18}O$ values indicate that the hydro-climatic conditions were wetter than the present day (Roberts et al., 2011; Nicoll and Küçükuysal, 2013). A trend towards aridity was noticed in some of the lakes by around 6.6 Ka, indicated by a shift to more positive $\delta^{18}O$ values which are indicative of high evaporation, and more arid climates (Eastwood et al., 2007). Between 6.0 and 3.0 Ka, the lake isotope data indicate wet-to-dry oscillations, accompanied by a general trend towards regional dryness (Roberts et al., 2011). Enhanced drought is indicated by the lake records during the periods 5.3 Ka to 5.0 Ka, 4.5 Ka to 4.0 Ka and 3.0 Ka to 2.8 Ka, with the dry episodes

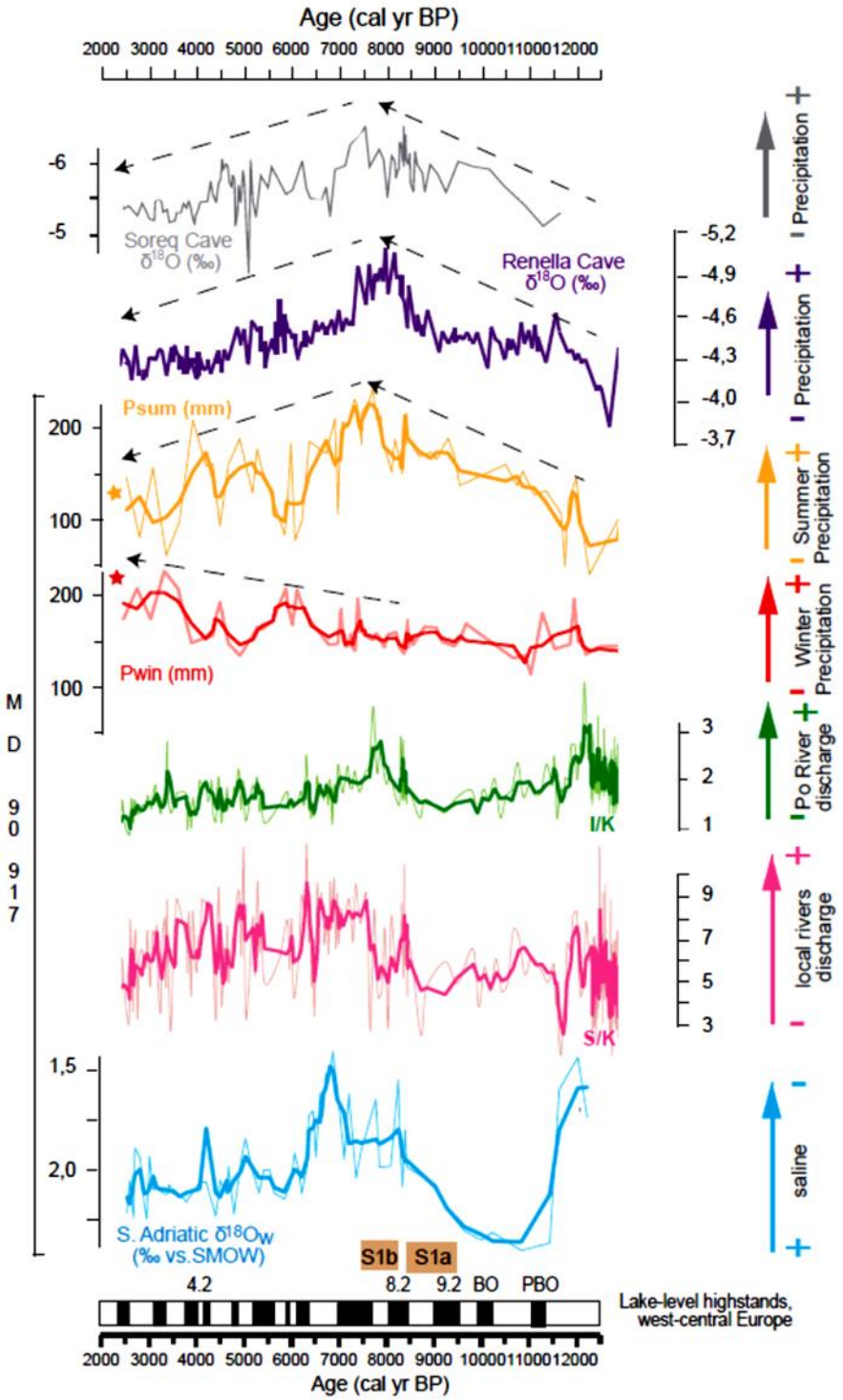

Figure 5.4 A comparison of the data from the multiproxy study of the Adriatic marine core MD 90-917. From bottom to top: lake level highstands in western Europe; sea surface salinity, Local river discharge, Po River discharge and precipitation data. From Combourieu-Nebout et al., (2013).

punctuated by short periods of elevated moisture availability. A significant period of increased moisture availability is the period from 4.0 Ka to 3.3 Ka,

which was a significant wet phase within the overall trend towards drier and cooler conditions since the mid-Holocene (Roberts et al. 2011; Küçükuysal, 2013).

5.5: FIELD DATA COLLECTION METHODS

Terrace maps were made for three rivers within the southern bounding margin of the Gediz Graben (figure 5.5), the river valleys were examined for preserved, undisturbed, uplifted terraces along their length (figure 5.6). In order

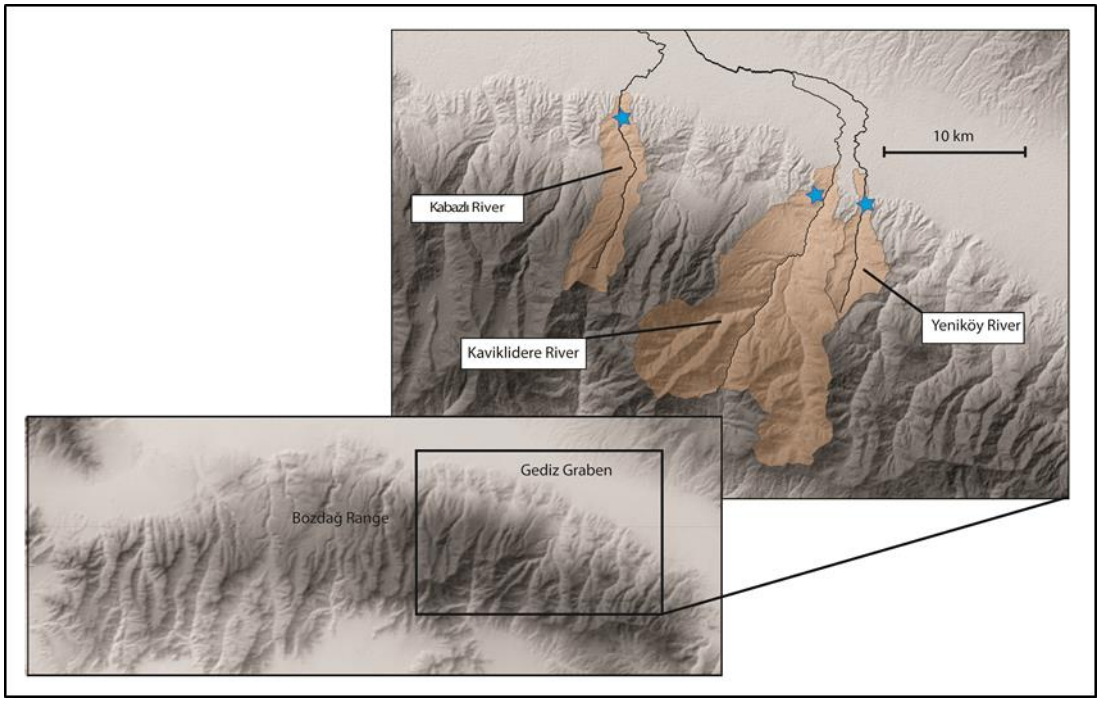

Figure 5.5: A map of the Kabazlı, Kaviklidere and Yeniköy rivers where the terrace levels were mapped and the five OSL samples were taken. The blue stars show the locations of the samples along each river.

to create a terrace map a contour base map was made from the ASTER imagery in ArcMap. An initial observation of possible terraces was made using the slope analysis tool in Arc Map to isolate areas where the slope was fairly low and constant over a reasonable area. Due to the 30 m resolution of the ASTER imagery only the larger terrace areas could be identified in this way so it was necessary to complete the remaining mapping of terraces in the field.

Figure 5.6: Field photographs from the study rivers. A) The T2 and T3 terrace levels as seen from a distance on the Kabazlı River. B) the T4 terrace that was sample on the Yeniköy River. C) A close up of the terrace deposits samples from the T4 terrace on the Kavikladere River, with the Gamma Spectrometer in use. C) A close up of the terrace deposits samples from the T4 terrace on the Yeniköy River, with the Gamma Spectrometer in use.

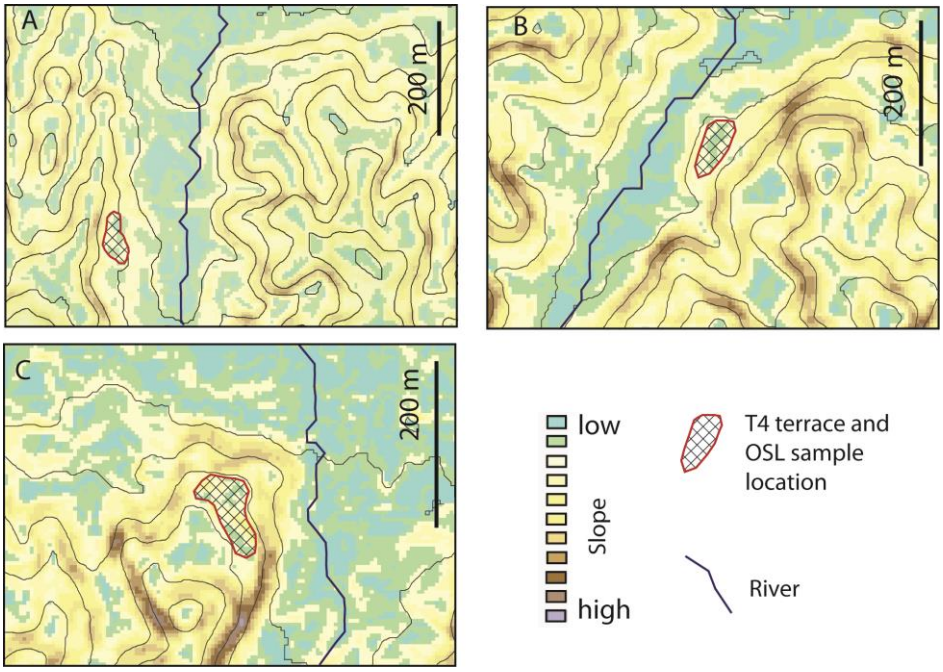

Figure 5.7: Slope maps of the study rivers showing the T4 terrace sampled. A) Kabazlı Kabazlı River, B) Kaviklidere River, C) Yeniköy River. Contours represent 10 m of elevation change.

Terraces were mapped within the sedimentary units along the river and within the lower elevations of the metamorphic rocks further upstream. Where areas of low, uniform slope were identified further features were identified which indicate the presence of a terrace including the presence of typical terrace sediments such as channel deposits and fine and medium-grained sands. The height of the terraces above the current elevation of the river level was measured and attention was paid to possible terraces at the same elevation across the river in order to identify the presence of paired and single terraces.

The elevation of the terraces was recorded in the field using a TruPulse laser rangefinder. The laser range finder emits infrared energy pulses and determines the distance of an object by measuring the time it takes for each pulse to travel from the rangefinder to the target, and then back again. The TruPulse is sufficiently sensitive to detect distances using both reflective and non-reflective targets. When shooting distance measurements to a non-reflective target, the maximum measurement distance is approximately 1,000 meters. There are a number of factors that will affect the value of the error on the distance measurements. To provide the most accurate measurements using the laser rangefinder the following should be considered with respect to the target and environment: 1) colour of the target; 2) target finish; 3) angle of shooting, and 4) lighting conditions. A bright, matt target and shooting perpendicular to a target in overcast conditions will both maximise the maximum possible distance measurement and the accuracy of the distance measurement. Errors range from 0.1 m for a very good target and conditions to 1 m for a very bad target in bad conditions.

Terrace deposits were found along three rivers (figures 5.5, 5.7 and 5.8), In total 6 terrace elevations relative to modern day river level, were mapped

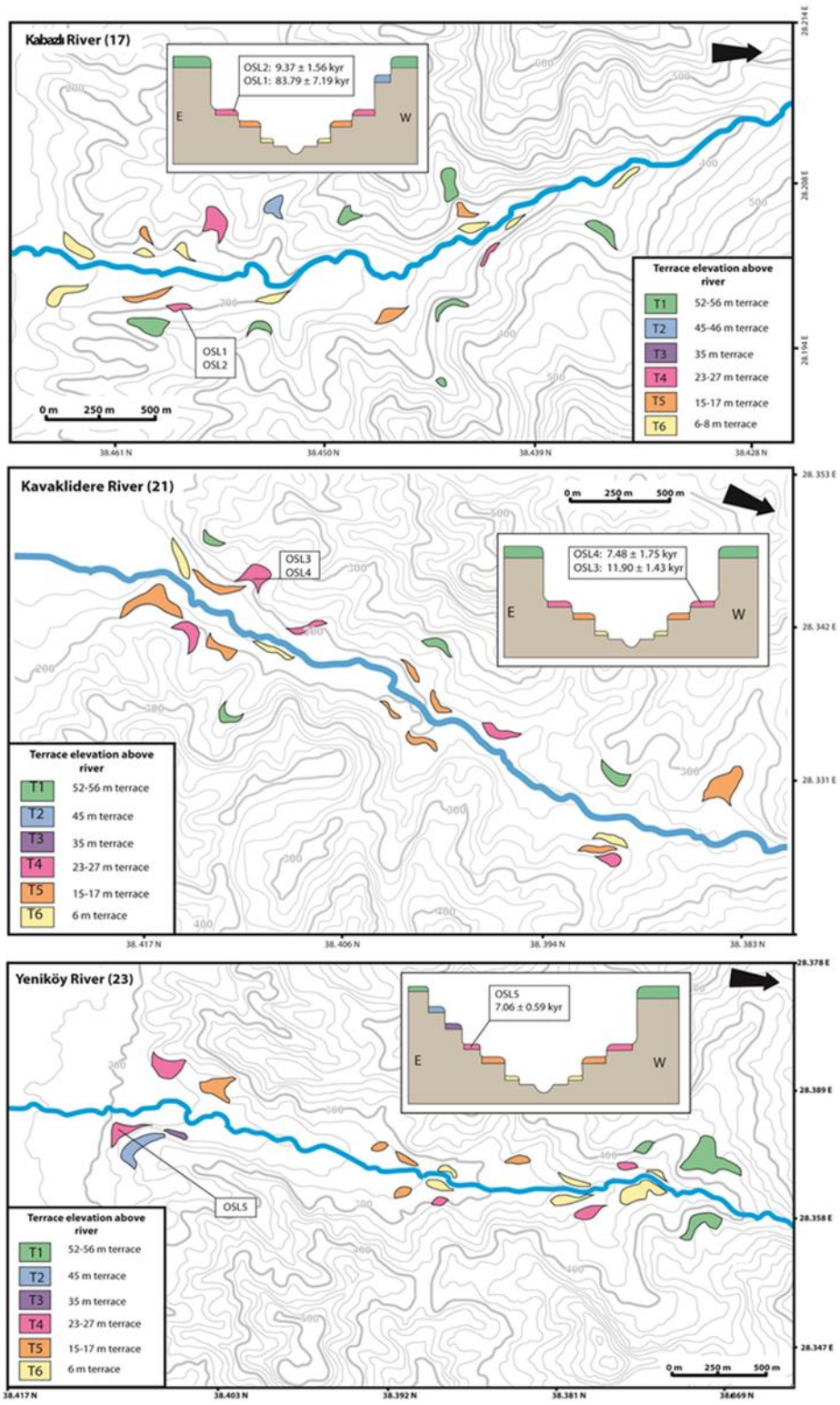

Figure 5.8: Terrace maps for the Kabazlı (top), Kavikladere (middle) and Yeniköy (bottom) rivers. In each location six terrace levels were mapped, T1-T6. An inset in the terrace maps shows which of the terrace levels were present in each side of the river valley.

along the Kabazlı, Kavaklıdere and Yeniköy rivers (figure 5.7). The terrace heights are 52 m – 56 m (T1), 45 m (T2), 35 m (T3), 23 m – 27 m (T4) 15 m - 17 m (T5) and 6 m (T6) with not all terrace heights being present along all three rivers (figure 5.8). The presence of terrace staircases on the rivers indicates that the rivers have been experiencing uplift throughout the time since the formation of the highest terrace (Maddy et al., 2000).

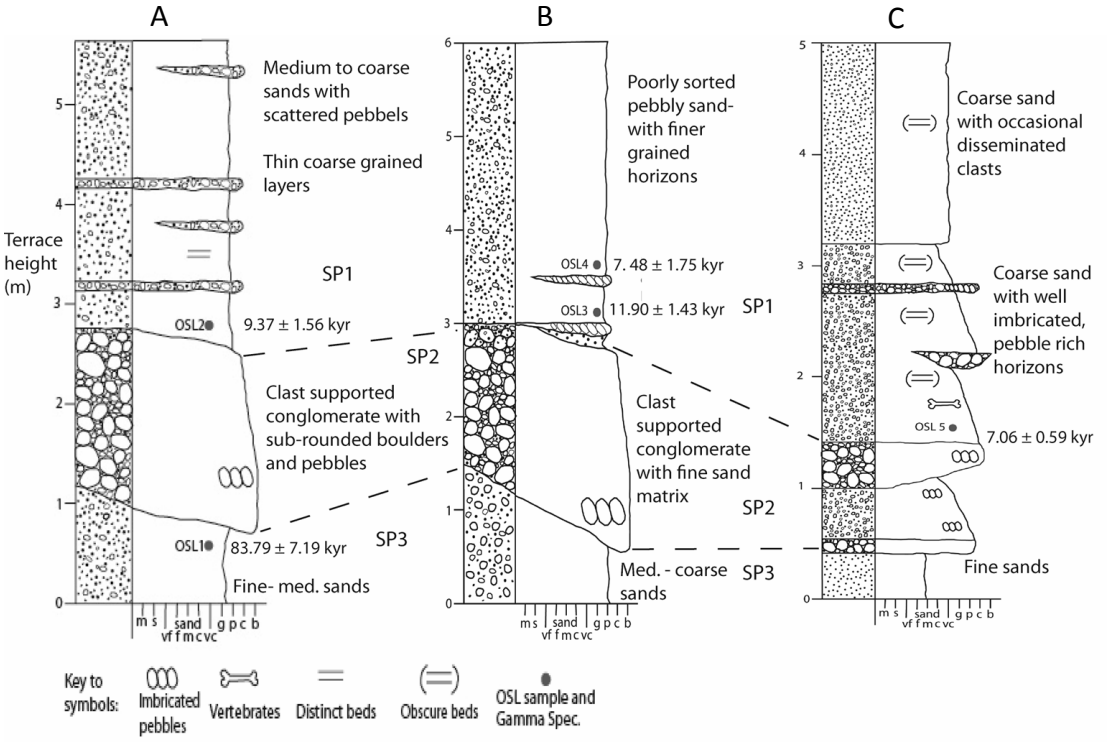

Figure 5.9: Stratigraphic logs of the T4 terrace locations on the (A) Kabazlı, (B) Kavikladere and (C) Yeniköy river valleys where the OSL samples were taken. The locations of the OSL samples are marked on and sediment packages interpreted to have originated by similar events around similar times have been correlated with dashed lines and result in three sediment packages (SP1-SP3).

When suitable terraces and sample locations were identified stratigraphic were drawn up (figure 5.9), samples were then taken. The sampling strategy was to source samples from one terrace level, in order to make comparisons

between rivers. Due to this the T4 terrace was picked as on all three rivers as this terrace level provided the most accessible and appropriate material in the valley of all three rivers. Ideally samples would be taken from the top and bottom of the terrace deposits to allow for the dating of the whole terrace sequence, but in reality the sampling of the top of the terrace was restricted by the height at which samples could be taken. It was necessary to sample from lithologies that were dominantly medium to coarse sand with as few large clasts as possible as they would hinder the sampling process. In selecting these lithologies from the specific locations within the sedimentary sequence the aim was to sample specific lithology breaks.

In total five OSL samples were collected from the logged terraces using metal pipes, which were sealed to prevent light contamination. *In-situ* radioactivity measurements were then made using a gamma mass spectrometer, to aid in the calculation of ages from OSL dating.

5.6: OSL DATING

OSL is part of a family of dating methods that relate to radioactive decay, measuring the relocation of electrons at defects with crystalline materials (Stokes, 1999). OSL dating specifically uses the optical properties of quartz and feldspar (Rittenour, 2008) found in sediments such as sand and silt, in order to enable calculation of the date that this sediment was last exposed to sunlight (e.g. Aitken, 1985; Aitken, 1992; Aitken, 1998; Wagner, 1998; Stokes, 1999; Wallinga, 2002a; Bøtter-Jensen et al., 2003), and therefore provides a deposition or burial date. The OSL dating method (figure 5.10) is based upon the premise that as the minerals are transported to the site of deposition the

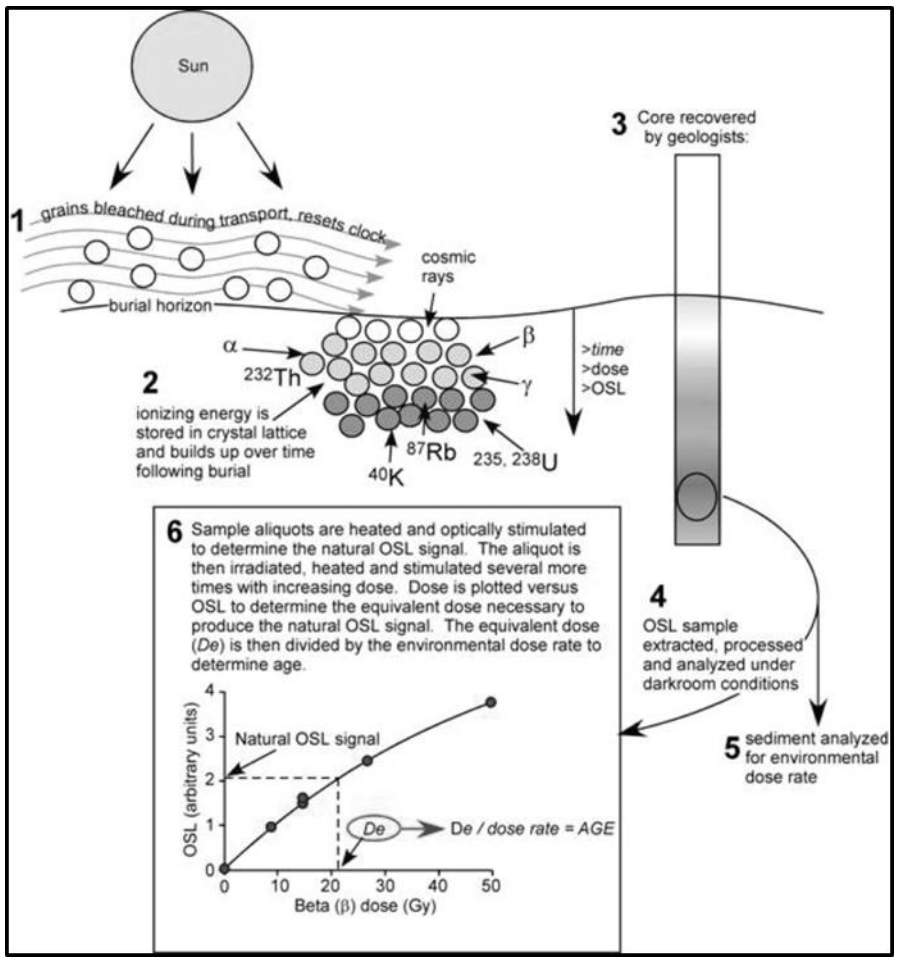

Figure 5.10: A schematic diagram showing the main features of optically stimulated luminesce dating (OSL). Step 1, how the grains are bleached during transport; step 2, how ionising energy is stored in the crystal lattice during burial; step 4, the taking of a sample in the field; step 4 the processing of the sample in the lab; step 5, the determination of the background radiation conditions for inclusion in calculations. Step 6 shows how sample age is calculated using the determined equivalent dose. Taken from Mallinson, D. (2008).

luminescence stored within the mineral is reduced to zero, so that any luminescence revealed by dating is a function of the time since burial.

To determine the age of the sediment/last exposure to sunlight the following equation (Wallinga, 2002a) is used which combines the equivalent dose with the irradiation dose rate. A radiation dose, called the palaeodose, is accumulated during burial

$$\text{Age} = \frac{\text{Equivalent dose}}{\text{Dose rate}} = \frac{\text{P}_{\text{Gy}}}{\text{D}_{\text{Gy a}^{-1}}} \qquad \textbf{(eq: 5.1)}$$

The equivalent dose (measured in grays: P_{GY}) is the laboratory beta dose that induces the same amount of luminescence as low levels of ionising radiation (Aitken, 1985, 1998) from Uranium, Thorium and Potassium (K^{40}) within the surrounding sediment (e.g. Aitken, 1985, 1998; Wagner, 1998; Stokes, 1999; Wallinga, 2002a; Bøtter-Jensen et al., 2003) and a small amount of background radiation from cosmic rays (Stokes, 1999) that the mineral acquires since burial (the palaeodose).

The samples were taken using metal tubes to extract sediment from medium-grained sands forming the terraces; the tubes containing the samples were then immediately sealed to avoid light contamination. Once the sediment sample was removed a gamma mass spectrometer was used to determine the external gamma dose rate (units $D_{Gya\text{-}}{}^{1}$) from the concentrations of K, Th and U.

The OSL samples were processed at the University of Oxford Luminescence Dating Laboratory, enabled by the receipt of the Quaternary Research Association- Research Laboratory for Archaeology and the History of Art Luminescence Dating Award. The results were based on luminescence measurements of sand-sized quartz (180-255µm) extracted from the five provided samples using standard preparation techniques including, wet sieving, HCl (10%) treatment to remove carbonates, HF treatment (48%) to dissolve feldspathic minerals and etch the quartz grains and heavy mineral separation with sodium polytungstate to remove any additional unwanted minerals. The samples were measured in automated Risø luminescence readers (Bøtter-Jensen, 1988, 1997; Bøtter-Jensen et al., 2000) or a Lexsyg Research device using a SAR post-IR blue OSL measurement protocol (Murray and Wintle,

2000; Banerjee et al., 2001; Wintle and Murray, 2006). Beta dose rate calculations were carried out and were based on the concentration of radioactive elements (potassium, thorium and uranium) within the samples and were derived from elemental analysis by Inductively Coupled Plasma Mass Spectrometry/Atomic emission spectroscopy (ICP-MS/AES) using a fusion sample preparation technique.

The external gamma dose rate was determined from the concentrations of K, Th and U obtained from in-situ radioactivity measurements using a gamma mass spectrometer. The final OSL age estimates were produced to include an additional 2% systematic error to account for possible uncertainties in source calibration. The dose rate calculations are based on Aitken (1985) and incorporated beta attenuation factors (Mejdahl 1979), dose rate conversion factors (Adamiec and Aitken 1998) and an absorption coefficient for the water content (Zimmerman 1971). The contribution of cosmic radiation to the total dose rate was calculated as a function of latitude, altitude, burial depth and average over-burden density based on data by Prescott and Hutton (1994).

5.6.1: METHODOLOGICAL CONSIDERATIONS WHEN USING OSL DATING

OSL is useful for dating inorganic sediments, such as those from fluvial or aeolian environments, where suitable material for dating, by methods such as radiocarbon, is not found (Blong and Gillespie 1978, Stanley and Hait, 2000). As a result it has opened up wider areas to dating, but the method does not come without caveats of its own. The age range of OSL dating is from around a few years to 150 ky for quartz and 1 Myr for feldspar. The time limits of the OSL dating technique are determined by a number of factors: 1) the capability of the

dosimeter material (e.g. quartz or feldspar) to take up charge; 2) the rate at which trapped electrons are created within the lattice of the dated material, this has a direct link to the levels of radiation acquired from external sources; 3) the stability of the trapped electrons within the material (Stokes, 1999). At the lower end of the dating range the method is limited by the possibilities of incomplete resetting or zeroing of the sample before it is deposited (Wallinga, 2002a). At the upper end of the OSL dating range the limits are based upon the saturation of traps for free charge carrying electrons, which means that no more can be built up, effectively stopping the clock (Wallinga, 2002a).

Therefore, ‘saturation' of the signal is when the crystal lattice becomes 'full up', at which point the sample cannot acquire a greater luminescence signal. The point at which a sample becomes saturated depends on the dose rate of the sample. Samples subjected to a high dose rate will become saturated more quickly, and fully saturated samples will not record the full duration of their burial history. In these cases only a minimum age can be determined. A typical amount of absorbed radiation for sand dominated environments is 1-2 Gy kyr^{-1}, in environments with such levels of radiation dates of up to 150 Kyr have been achieved (Stokes et al., 1994). Owing to the limiting factor of saturation of available traps when levels of background radiation are lower, older dated ages can be measured (Huntley et. al., 1993).

The accuracy of OSL ages can be affected by a number of factors including: 1) mixing and bioturbation of the sediments, which can redistribute sediment causing mixing of older and younger sediments (Johnson et al., 2014). The mix of ages can result in a distribution of equivalent dose measurements and therefore significant uncertainty in the dating (Rodrigues, 2013); 2) β -dose heterogeneity, where the beta dose is not be received

uniformly by all grains within a sample. When some grains receive more β -dose than others this will contribute to spread into the equivalent dose distribution (Mayya et al., 2006; Morthekai and Reddy, 2012); 3) partial bleaching (partial resetting) of the luminescence signal can also cause inaccuracies in the derived age of the sediment. Partial bleaching occurs if the grains are not exposed to enough sunlight to cause total bleaching before they are buried (Rittenour, 2008). Partial bleaching can be a particular problem where the environment from which the sample can contains significant water, such as fluvial or glacial environments (Olley et al., 1998); 4) if the OSL signal is not fully reset before deposition and covering, an age overestimation can occur as there is additional luminescence signal included in the natural luminescence from before the sediment was buried.

5.6.2: USING OSL DATING IN FLUVIAL ENVIRONMENTS

When used within fluvial environments luminescence dating can be more prone to producing inaccurate ages for sediment burial. All techniques for OSL dating and the production of accurate ages rely on the assumption that any luminescence signal acquired before burial is removed by exposure to light prior to burial (Wallinga, 2002a; Rittenour, 2008). When OSL is utilised in fluvial environments incomplete bleaching can be a problem, this was more of a problem when using thermoluminescence, but the OSL signal now commonly used is more sensitive than the thermal signal (Duller, 1996; Aitken, 1998; Wallinga, 2002a), although it does not remove the issue completely.

Under full sunlight conditions the trapped charge within potential OSL samples is reduced by a factor of 10 in seconds (Godfrey et al., 1988; Wallinga, 2002a), the rate at which beaching is achieved is reduced significantly when the

sample is carried within or lies under water, the spectrum of light the sample receives is also restricted (Berger and Luternauer, 1987). Additionally, the suspended load of the river can increase this effect by shielding the sediment (Berger and Luternauer, 1987). The inclusion in the sample of partially beached gains can lead to an overestimate of ages due to large scatter on the dose distribution of the equivalent dose (Duller, 1994; Jacobs et al., 2003; Rittenour, 2008) and therefore scatter, and associated large errors on the equivalent dose distribution are a clear indication of incomplete bleaching (Wallinga, 2002b).

When considering using OSL dating in fluvial settings it is also important to consider the speed at which bleaching can occur. For example, Hansen et al. (1999) document ages from feldspars that were a factor of 2 greater than those from quartz for Holocene glaciofluvial environments. Additionally Wallinga et al. (2001) compared quartz and feldspar OSL ages from sub-modern fluvial sediments and the quartz grains yielded more accurate results. Overall the evidence suggests that carrying out OSL analysis on quartz will provide the most accurate results within fluvial settings (Wallinga, 2002b).

5.7: RESULTS

OSL samples were taken from the T4 terrace between 23 m – 28 m on all three rivers (figure 5.7 and 5.8). The samples were analysed at the labs in Oxford University (table 5.1) and provide constraining ages on the T4 terrace along the three rivers. Samples OSL1 and OSL2 were taken from T4 fill terrace deposits within the valley sides of the Kabazlı River (figures 5.8 and 5.9A). The stratigraphic log (figure 5.9A) shows that at the bottom of the terrace there is around 1 m of medium to coarse-grained sands with some pebbles and cobbles. Above this is approximately 1.5 m of clast-supported conglomerate

Sample	Burial depth (cm)	Water content (%)	Palaeodose (Gy)	Dose rate (Gy/ka)	OSL age estimate (ka)
OSL1	400	0.8 [0-60]	249.77 ± 15.16	2.98 ± 0.17	83.79 ± 7.19
OSL2	250	1.4 [0-6]	39.18 ± 6.06	4.18 ± 0.25	9.37 ± 1.56
OSL3	200	0.3 [0-6]	28.42± 2.96	2.39 ± 0.14	11.90 ± 1.43
OSL4	300	3.5 [0-6]	20.68 ± 4.67	2.76 ± 0.16	7. 48 ± 1.75
OSL5	150	4.2 [1-7]	21.42 ± 1.20	3.03 ± 0.18	7.06 ± 0.59

Table 5.1: The results of the OSL dating of samples from the Kabazlı, Kavaklıdere and Yeniköy rivers.

with sub-rounded pebble to boulder sized clasts and a course sand to pebble matrix. There are imbricated pebble and boulder clasts within the conglomerate. On top of the conglomerate is just over three meters, medium to sub angular, coarse-grained sands with scattered pebbles and boulders. The sands are distinctly bedded with beds ranging from ~ 2 – 20 cm. Within this sand sequence are scattered ~5 cm layers of coarser sand and pebbles. The terrace is 6 m in height, the top is ~28 m above the current river level.

OSL1 was taken from the fine to medium-grained sand units at the bottom of the terrace. The height of sample OSL1 above the current river channel is 22 m, and the burial age is 83.78 ± 7.19 Ka (table 5.2). OSL2 was taken from within the well bedded sands above the conglomerate. The elevation of OSL2 above the modern level of the river is 24.3 m and the age of the sample is 9.37 ± 1.56 Ka (table 5.2).

Sample	Age (kyr)	± (kyr)	Sample elevation above river (m)	Incision rate mm/yr	+ error on incision rate (mm/yr)	- error on incision rate (mm/yr)	Time averaged throw rate on fault (mm/yr)
OSL1	83.78	7.19	22	0.26	0.02	0.02	
OSL2	9.37	1.56	24.3	2.59	0.52	0.37	1.33
OSL3	11.9	1.43	25	2.10	0.29	0.23	
OSL4	7.48	1.75	25.5	3.41	1.04	0.65	0.99
OSL5	7.06	0.59	28	3.97	0.36	0.31	0.96

Table 5.2: Calculated incision/uplift rate for each of the OSL samples and the throw rate measured on the active fault averaged over 2myr.

Two samples, OSL3 and OSL4 were taken from a T4 fill terrace sequence in the valley of the Kavaklıdere River (figures 5.8 and 5.9B). The stratigraphic log (figure 5.9B) is similar to that of the Kabazlı River with a total T4 terrace height of around 6 m. At the bottom of the terrace is approximately 1 m of medium to coarse-grained sands with pebble and cobble clasts. This lithology appears to be bedded although the beds are not particularly obvious. On top of this there is around 1.5 m of clast-supported conglomerate with rounded to sub-rounded clasts of pebble to boulder size, and a coarse-sand to pebble matrix. On top of the conglomerate is three meters of poorly-sorted, indistinctly-bedded, medium to sub-angular, coarse-grained sands. Within the sands there are occasional scattered pebbles and boulders and thin (1 – 2 cm) horizons of finer sand and silt. There are also discontinuous layers of imbricated pebbles.

Both samples were taken from above the conglomerate unit, from within dominantly medium to coarse-grained, poorly-sorted, sands. OSL3 was taken at a height of 25 m above the river and has an age of 11.90 ± 1.43 Ka. OSL4 was taken 25.5 m above the river and has an age of 7.48 ± 1.75 Ka, the samples are

separated by an imbricated sub-rounded to rounded pebble horizon (table 5.2). A further 2.5 m of sand are above total terrace height of 6 m.

An additional sample, OSL5 was taken from a T4 fill terrace in the valley of the Yeniköy River (figures 5.8 and 5.9C). The stratigraphic log (figure 5.9C) of the T4 terrace shows 0.4 m of fine sands at the bottom of the terrace. On top of this there is a ~10 cm horizon of matrix-supported pebble conglomerate. Above this is a is a 0.5 m unit of coarse sands with a lot of pebble-sized clasts, within this unit imbrication of the pebble clasts was observed. Above this is another conglomerate unit around 0.4 m thick. It clast-supported with rounded to sub-rounded clasts of pebble to boulder-size and a sub-rounded course sand to pebble matrix. On top of the conglomerate is a 1.6 m unit of bedded, medium to sub-angular, coarse-grained sands. OSL 5 was taken from this unit form just above the conglomerate. Within the sands there are laterally-discontinuous imbricated pebble horizons. At the top of the terrace there is a bedded, dominantly medium-grained sand with disseminated larger clasts.

The height of OSL5 above the present river channel is 28 m and the age of the sample is 7.06 ± 0.59 Ka (table 5.2). In total the T4 terrace height on the Yeniköy River 5 m, giving the top of the terrace a height of around 31 above the river.

An error of ± 0.7 m has been assigned to all of the height measurements as the terraces are of medium to dark colour and matt finish and the conditions on the day of measurement were slightly cloudy skies and the angle of measurement with the laser range finder was not more than 45°.

5.8: DISCUSSION

5.8.1: AGGRADATION OF THE T4 TERRACE IN THE GEDIZ RIVERS

The stratigraphy (figure 5.9) can be used in combination with the ages acquired through OSL dating of samples (tables 5.1 and 5.2) to interpret aggradational and incisional episodes on the rivers. Stratigraphy is similar in the T4 terrace along each of the rivers, suggesting similar processes are depositing the sediment. These are divided into distinct lithological sediment packages, each of which are assigned a number for ease of reference in the discussion of the possible conditions of deposition (figure 5.9).

The sands overlying the conglomerate layer in each river are referred to as sediment package 1. The conglomerate unit has been designated as sediment package 2 and the sand below the conglomerate in each terrace is package 3.

Sediment package 1 (figure 5.9) shows significant similarities between all three rivers so these have been correlated. In each river package 1 is dominated by medium to coarse-grained sands with pebble clasts. Within the sands in each river are thin, laterally discontinuous layers of pebble sized material. Sediment package 3 has been dated in each of the three rivers with samples OSL2, OSL3 and OSL5 taken from just above the top of the conglomerates of package 2. The dates obtained from the base of package three are 9.37 ± 0.56 Ka, 11.90 ± 1.43, Ka 7.06 ± 0.59 Ka. An additional sample, OSL4 was taken from further up the terrace in the Kaviklidere River and provides a date of 7.48 ± 1.75 Ka.

From the sedimentology and morphology of the outcrop specific to package 1 it is likely that it represents hill slope deposits. There appears to have been a regional trend towards the deposition of hill slope material at a time of around 11- 7 Ka. The trend is evidenced by the very similar deposits found in

each of the rivers, in terms of sedimentology and morphology of the deposits and ages derived using OSL dating.

Sediment package 2 is present in all three rivers, with 1.5 – 2 m continuous packages found in the Kavaklıdere and Kabazlı rivers. In the Yeniköy River the conglomerate is smaller and is broken by coarse sand with plenty of pebble clasts. Despite this difference the conglomerates share many properties such as imbrication and clast-support as well as dominant large sub-rounded clast sizes. It is therefore reasonable to assume the same environment of deposition with some local scale differences. The base of sediment package 3 (figure 5.9) is constrained to around 84 Ka by OSL1 which was taken from the top of the underlying sediment package. While it is possible the younger dates for package 1 constrain the younger extent of the conglomerates to ~12 Ka, the hill slope processes responsible for the deposition of package 1 could have occurred at a significantly more recent time. The conglomerates therefore could account for up to ~72 Ka of aggradation between the ages of 84 – 12 Ka, although as previously stated the duration of aggradation could be less. Accordingly, the duration of aggradation could subsume into it both the last glacial, the last glacial maximum and the Younger Dryas (last glacial stade). The stratigraphy of this sediment package and the apparent suppression in deposition generally fit with the type of change in deposition that would be expected for a terrace deposit, and so sediment package 2 is determined to be the T4 terrace deposit with a thickness of approximately 1.5 m. A base date of 84 Ka also correlates with a period of aggradation in the Aguas River, Spain (Schulte et al., 2002).

Sediment package 3 (figure 5.9) is formed predominantly of sand with some larger clasts, and has been dated in the Kabazlı River as 83.78 ± 7.19 Ka.

The Kavaklıdere and Yeniköy rivers have similar lithologies to the Kabazlı at the base of their respective terraces. These similarities make it reasonable to assume that if their sediment packages were dated, a comparable date would be produced. This assumption is necessary as their higher large clast content precluded sampling. The grain size in sediment package 1 is relatively small with larger clasts and an age of 83.78 ± 7.19 Ka and so could be a relatively low energy deposits that occurred before the onset of significant terrace aggradation.

Overall it appears that climate could be influencing terrace formation, as the deposition of the T4 terrace conglomerates could be associated with the last glacial or younger Dryas. Although greater resolution of dating and better constraints on the T4 terrace would be needed to resolve the climatic influence. In addition the 83.78 ± 7.19 Ka date for T4 allows time for the formation of the younger T5 and T6 terraces found at elevations closer the modern day river level.

5.8.2: HOW DO THE AGGRADATIONAL TERRACE DATES FOR THE GEDIZ GRABEN COMPARE TO OTHER REGIONAL TERRACE SEQUENCES?

The studies of terrace sequences in Turkey has been fewer in number than those based in western Europe, but have increased in number recently (e.g. Demir et al., 2004; Westaway et al., 2004; Maddy et al., 2005; Westaway et al., 2006; Bridgland et al., 2007; Maddy et al., 2008; Seyrek et al., 2008; Bridgland et al., 2012). South-eastern Turkey has been the location for the majority of the recent studies on the Euphrates, Tigris and Orontes (e.g. Bridgland et al., 2003; Demir et al., 2007; Demir et al., 2008; Bridgland et al., 2012). There have been few terrace studies based in western Turkey, although

a notable study site is the upper Gediz River catchment around Kula, of which the studies by Westaway et al. (2004) and Maddy et al. (2005, 2008) are significant examples. Many of the terrace flights studied in Turkey are of Miocene to Pliocene age, and so cannot be correlated with the Pleistocene to Holocene sequences observed and measured in the Gediz Graben fluvial system. For example Seyrek et al. (2008) date up to seven terrace levels along the rivers of the Amanos Mountains, southern Turkey where the youngest dated terrace was 15 Kyr and the older terraces were dated to 140 Kyr to 640 Kyr.

The Ebro River in Mediterranean Spain has been the location of a number of studies that have dated fluvial terraces (Sancho et al., 2004; Sancho, 2003; Santisteban and Schulte, 2007). These studies have identified a Qt6 terrace level that has an age of 96 ± 16 Ka. The Qt6 Ebro River terrace therefore correlates broadly with the age of the T4 terrace on the Gediz rivers.

Furthermore, the timing of aggradation in the Gediz rivers correspond to the timings of aggradation within the Aguas River (Schulte, 2008). Figure 5.3 shows that between 90 – 60 Kyr the Aguas River had an aggradational regime which fits well with the age constraint on the aggradational terrace unit in the Gediz Rivers at 83.78 ± 7.19 Ka.

5.8.3: CALCULATED INCISION AND UPLIFT RATES

OSL1 has a burial age of 83.79±7.19 kyr, whilst the sample OSL2, from 2.3 m higher in the stratigraphy has a burial age of 9.37±1.56 kyr. As discussed in section 5.8.1 the age constraints in the overlying sediment package 1 are could produce a significant underestimate of the age of the top of the T4 terrace deposits of package 2. When the height above the river and the age of the

sample are considered, OSL2 provides an incision rate for the Kabazlı River of 2.5 +0.52 -0.37 mm/yr (table 5.2), which is therefore likely to be a fairly significant over estimate of incision. When the age defining the base of aggradation of sediment package 2 is used (83.78 ± 7.19 Ka from OSL1), and a height above the modern river of 22 m is factored in, the incision rate is lower, at 0.24 ± 0.02 mm/yr (table 5.2).

On the Kavaklıdere and Yeniköy Rivers the only available dates are from the hill slope deposits of package 1. These give incision rates that are of similar magnitude to that derived using the package 1 date from the Kabazlı River, 3.41 +1.04 -0.65 to 3.96 mm/yr +0.36 -0.31 mm/yr respectively (table 5.2).

As sediment package 2 has been determined to represent the T4 terrace deposits along the Gediz rivers the age constraints on this package will provide the most pertinent incision rate data. Therefore the incision rate of 0.24 ± 0.02 mm/yr is taken as a representative value for the three rivers studied. If sediment package 3 was dated in the Kavaklıdere and Yeniköy Rivers it would likely yield a similar result given the similarity of the stratigraphy. Overall the incision rates similar to the rates of 0.1 mm/yr – 1 mm/yr for the Tejo River in Portugal (Cunha et al., 2008; Martins et al., 2009).

As the dated terraces are part of terrace staircase sequences on each of the rivers, it follows that the footwall of the high angle normal faults that bound the topographic graben must be actively uplifting (see chapter 4 for more details).

The derived representative rate of river incision (table 5.1 and preceding parts of this section) can be used as a proxy for a Gediz generalised uplift rate (Personius, 1995; Burbank et al., 1996; Maddy 1997; Pazzaglia and Brandon, 2001; Mathew et al., 2006; Srivastra and Misra, 2008). Because the

determination of tectonic uplift requires some estimate of the geometry of the riverbed at the time the terrace was deposited (Lavé and Avouac, 2000). It may simply be assumed that the river has maintained a constant profile during deformation, with river incision counterbalancing tectonic uplift. Accordingly, tectonic uplift since terrace abandonment would then be equal to incision, and the difference of elevation between the abandoned terrace and the present river will give an uplift rate (Lavé and Avouac, 2000; Litchfield et al., 2007). However, this may not be an accurate way to represent uplift, and the uplift rate produced using incision rate as a proxy should considered a maximum.

It is possible to compare the uplift rate to the time average throw rates calculated in chapter 4. The calculated most representative incision rate of 0.24 ± 0.02 mm/yr can be compared to the average throw rate of the fault for the three rivers which is 1.1 mm/yr and to the rate on the throw rate of 1.33 mm/yr near the Kabazlı River (see chapter 4). The incision rate seems to under estimate the throw rates and it is therefore unclear how closely the incision rates represent the uplift rate in the Gediz Graben.

5.8.4: COMPARISION TO CATHMENT WIDER EROSION RATES

The terrace data can also be compared to spatially averaged erosion rates for river catchments that have been determined from the ^{10}Be concentration in sand samples taken from active streams (e.g. Granger et al., 1996; Norton et al., 2007). If a landscape approaches steady state, where hillslope erosion and rock uplift rates are relatively steady and locally similar, then it should be possible to quantify rock uplift rates from hillslope erosion rates (Cyr et al., 2010). To quantify spatially integrated catchment wide erosion rates in the Bozdağ block, Buscher at al. (2013) took stream sediment samples

at the outlets of nine catchments (figure 5.11) for which the erosion rates were calculated using ^{10}Be over the time period needed to remove an approximately 60 cm thick layer from the surface (10^3-10^5 years). The sand samples were taken from active streams at the boundary of the metamorphic basement rocks and the clastic sediments within the catchment of the river. Four of these samples were collected from the northern side of the Bozdağ Rage (from rivers flowing into the Gediz Graben). The samples were taken so that they contained only metamorphic rocks and cataclasites and not the Neogene sediments. Buscher et al. (2013) calculated that catchments draining into the Gediz Graben generally had catchment-wide erosion rates of between 0.08 and 0.181 mm/yr.

One of the catchment erosion rates derived for the Gediz Graben by Buscher et al. (2013) corresponds to the Kabazlı River from which samples OSL1 and OSL2 were taken. The T4 terrace yields an incision rate of 0.24 ± 0.02 mm/yr. The corresponding catchment wide erosion rate from Buscher et al. (2013) is 0.085 mm/yr. Clearly, their catchment wide erosion rate is much smaller than the terrace derived incision rates of the Kabazlı River. The disparity between the results provided by the two methods can be explained by investigating the geology and geomorphology of the river catchment (figure 5.12). The Kabazlı River contains a tectonic knickpoint that has incised into the metamorphic basement and the catchment wider erosion rate calculated by Buscher et al., (2013) does not take this into account. The distance from the downstream point at which the river starts to incise into the metamorphic rocks to the source of the river is 8.7 km with a drainage area of 19.6 km^2 of the total river catchment. The knickpoint has incised up from the point at which Buscher et al. (2013) sampled by 4.4 km, with a distance of 4.3 km remaining upstream

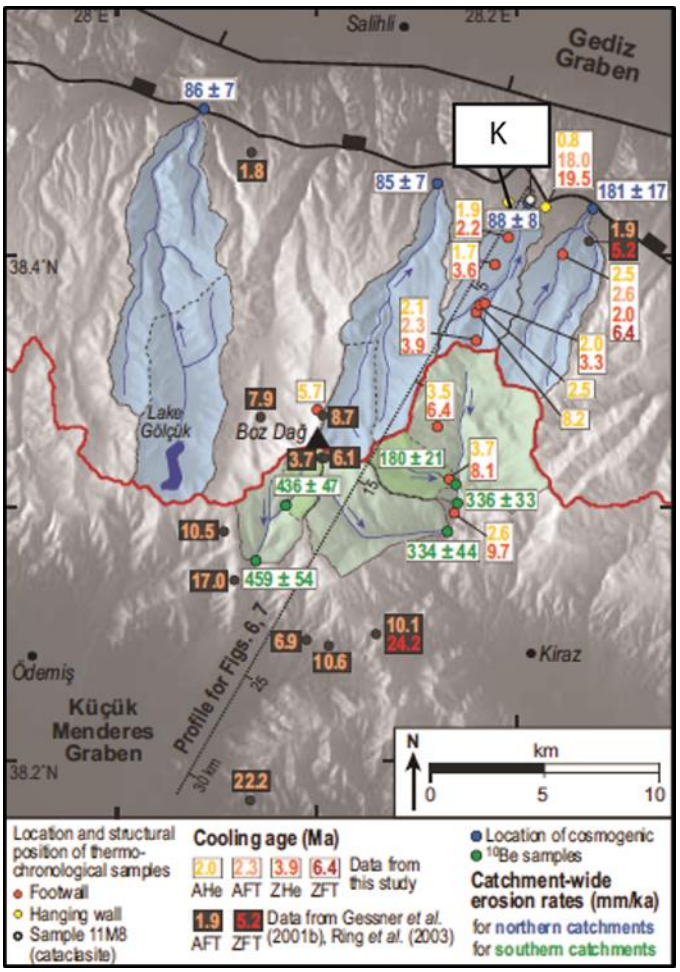

Figure 5.11: A map showing the catchment wide erosion rates (blue text) produced by Buscher et al. (2013). The red line indicates the location of the drainage divide and the blue dots show the location of the sand sample dated using ^{10}Be. The units for the catchment wide erosion rates are mm/ka. The river catchment for the Kabazlı River where the T4 terrace levels were dated using OSL in this study is labelled K (map adapted from Buscher et al. (2013).

and an upstream drainage area of 9.8 km^2. The knickpoint is associated with higher incision rates downstream, affecting 51.8% of the river channel distance and 50% of the catchment area, and lower erosion rates upstream.

Therefore, the catchment wide erosion rate is capturing an average of the catchment erosion above and below the knickpoint. In addition to not taking into account this differential erosion, the sample was also taken upstream of the highly erodible sedimentary rocks that make up the remaining 3.2 km of the river channel upstream of the active graben bounding fault. The rocks in this

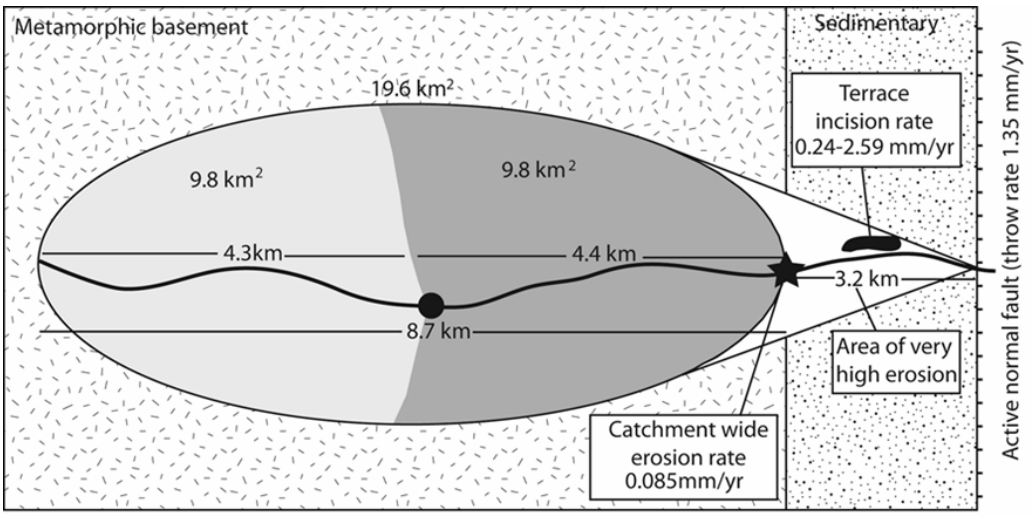

Figure 5.12: A schematic illustrating the different erosion and incision rates quantified for the Kabazlı River (catchment wide erosion rate from Buscher et al., 2013).The schematic shows the presence of a knickpoint in the river (black dot) which has a low erosion rate upstream (light grey shaded area) and a higher erosion rate down stream of the knickpoint (dark grey). The figure also shows an area of very high erosion (white) that is not taken into account in the catchment wider erosion rate (sample take from the black star) but is considered in the incision rate from the T4 terrace downstream.

part of the river valley are weak and have visibly undergone large amounts of incision. The field and OSL evidence shows that there has to have been significant incision occurring in this catchment during the Holocene especially within the downstream sediments; this is evidenced by the presence of the terrace and the incision rate of 0.24 ± 0.02 mm/yr. The catchment wide erosion rate of Buscher et al (2013), therefore must be a significant underestimate of the incision occurring in the total length of the Kabazlı River to the active fault.

5.9: CONCLUSIONS

A terrace flight preserved along three rivers draining the southern margin of the Gediz Graben indicates that there has been ongoing uplift along the graben bounding fault over at least the last 85 kyr. The OSL dating of the T4 sediment associated with the T4 terrace yielded ages of between 83.79 ± 7.19 –

7.06 ± 0.59 Ka. The sedimentology and stratigraphy indicates that the sediment package 2, which is dominantly conglomeritic is the T4 terrace sediment. The terrace is overlain by hill slope deposits, which have similar morphology and ages in each of the rivers. The climate record shows that the T4 terrace could be correlated with the last glacial stade and cooler Younger Dryas although additional investigation and dating would be required to clarify this issue. The maximum incision rates in the three studied rivers calculated for the OSL samples vary between 3.96 – 2.59 mm/yr although this study concludes that 0.24 ± 0.02 mm/yr is a more representative incision rate using the older OSL date. These rates are similar to other Mediterranean incision rates from terraces but low compared to similar rates in tectonically active areas of Asia. If the incision rate of 0.24 ± 0.02 mm/yr is considered a proxy for uplift in the Gediz Graben, the rate appears to underestimates the time average throw rates derived in Chapter 4 by around 0.75 mm/yr.

CHAPTER 6

THE INTERACTION OF ACTIVE TECTONICS AND RIVER GEOMORPHOLOGY WITHIN THE GEDIZ GRABEN

6.1: CHAPTER HIGHLIGHTS

- The rivers within the Gediz Graben all contain a single knickpoint initiated by an increase in throw rate on the basin-bounding fault.
- This increase in throw rate was caused by linkage of the three main fault segments of the high-angle graben bounding normal fault array at some time between 0.6 Ma and 1 Ma.
- The faulting enhancement factor has been calculated to be 3 at the centre of the fault array, with the throw rate predicted to have increased to 2 mm/yr.
- Drainage area variations and throw rate differences cannot explain the entirely of the variation of in knickpoint retreat rate within the Gediz Graben or in contrasting the data to other areas.
- Climate has been ruled out as an additional source of the variation in retreat rates, as has a dependence of Ψ on slope, but the differences may be caused by lithology, sediment flux or channel width relationships.

6.2: INTRODUCTION

It is now widely accepted that fluvial geomorphology can give qualitative and quantitative insights into tectonics. In steady state landscapes, channel steepness indices have been directly linked to surface uplift rates (Snyder et al., 2000; Whipple, 2001; Kirby et al., 2003; Oiumet et al., 2009). While in transient

landscapes responding to a tectonic perturbation, a considerable body of literature has addressed the way in which the fluvial system records changes in relative uplift rate in time and space (e.g. Whipple and Tucker, 2002; Whittaker et al., 2008; Whittaker and Boulton, 2012). In bedrock fluvial systems a knickpoint can be initiated following a change of boundary conditions, such as an increase in fault slip rate (Snyder et al., 2000; Whipple and Tucker, 2002; Crosby and Whipple, 2006; Whittaker et al., 2008; Whittaker and Boulton, 2012). The increase in channel steepness, caused by faster throw rates leads to an increase local river incision. Consequently, the knickpoint migrates upstream, and so the effects of the new tectonic boundary conditions are propagated throughout the catchment (section 3.5; Crosby and Whipple, 2006; Gasparini et al., 2006; Whittaker et al., 2008). The migration of knickpoints upstream can be split into a horizontal and vertical component. The progress of the knickpoints upstream in plan view is influenced by several factors such as drainage area and lithology (Whipple, 2004; Wobus et al., 2006a, 2000b; Whittaker et al., 2007, 2008; Attal et al., 2008), and can yield information about landscape response times; a primary control is known to be drainage area because this predictably influences the speed of knickpoint retreat, and this can be predicted analytically using the stream power erosion law (Seidl and Dietrich, 1992; Whipple and Tucker, 1999; Montgomery and Gran, 2001; Whipple and Tucker, 2002; Whittaker et al., 2008; section 3.5). Lithology is identified by some researchers as being of significance in determining the rate of knickpoint retreat because it should affect bedrock erodibility, hence K in any form of the classical stream power erosion law (section 3.5, Goldrick and Bishop, 1995; Anthony and Granger, 2007; Cook et al., 2009). Nevertheless a number of studies in recent years (e.g. Stock and Montgomery, 1999; Whittaker and

Boulton, 2012) have concluded that lithology seemingly has little relative influence on knickpoint retreat rates relative to other factors. Climate can also play a significant role in the amount and variability of run off and erosion thresholds, also in the growth or absence of anchoring vegetation, which can in turn affect landscape evolution both by varying the rate at which landscapes are modified and by altering the pattern landscape changes (Whipple, 2004; Kent, 2011; Whittaker, 2012). Recently, Whittaker et al., (2008) studied the plan-view migration of knickpoints in rivers in the Italian Apennines and their relation to active tectonics. This study quantified the drainage-area normalised knickpoint migration parameter (Ψ) upstream of faults that had increased their slip rate at the same time. Consequently, Ψ was expected to be similar for all rivers as lithology and climate were similar between study sites. However, it was found that Ψ was correlated with fault slip rates, suggesting that transient landscape responses were potentially controlled by rates of fault motion. Whittaker and Boulton (2012) noted the same relationships in both Italian and Turkish rivers. They observed the same links between the drainage area normalised knickpoint retreat parameter and the fault throw rates that they attributed to higher fault slip rates leading to channel narrowing, generating knickpoints that migrate faster upstream.

Furthermore, the vertical rate of knickpoint propagation upstream in a catchment is theoretically independent of drainage area, but dependent on the relative magnitude of tectonic perturbation generating the knickpoint (Wobus et al., 2006b; Crosby et al., 2006; Whittaker and Boulton, 2012). Consequently, if knickpoints are measured according to their vertical height above the source of tectonic perturbation (i.e. the active fault), their heights should scale with the throw rate on the active fault and should not be affected by the drainage area of

the river. Several studies have linked the heights of the knickpoints upstream to the rate of fault movement and have verified these general principles (Harkins et al., 2007; Boulton and Whittaker, 2009; Whittaker et al., 2008; Whittaker and Boulton, 2012). For instance, this latter study determined that the along strike trends in the height of knickpoints above active faults closely mirrors the fault throw rate along strike.

The time span over which rivers respond to these changes in tectonics, and pass these effects to the surrounding landscape is fundamentally determined by knickpoint migration rates (Whipple and Tucker, 1999; Whipple et al., 2000; Whipple, 2004; Wobus et al., 2006a). A number of studies have suggested that this process can take several million years (Merritts and Bull, 1989; Whipple, 2001; Snyder et al., 2000; Whittaker and Boulton, 2012). Consequently, this makes rivers ideal natural laboratories for evaluation of the landscape response to active faulting over Pliocene to Recent timescales.

Therefore this chapter addresses the evolution of the fluvial system of the southern margin the Gediz Graben from the late Pliocene to recent to examine the interaction between active faulting and landscape evolution in this tectonically-active area. In particular, this chapter exploits quantitative techniques from fluvial geomorphology to: 1) evaluate the differences in the longitudinal profiles of the rivers crossing the active high-angle graben-bounding normal faults; 2) identify knickpoints initiated by tectonic processes, and identify landscape transience; 3) determine to what extent drainage area and fault throw controls the progress of knickpoints upstream; 4) relate knickpoints heights to fault slip-rates and 5) determine the effects of differing boundary conditions (e.g. tectonics, climate, lithology) on landscape response times.

6.3: GEOLOGICAL AND TECTONIC BACKGROUND

The Gediz Graben in western Turkey lies within the Western Anatolian Extensional Province, an area of active extensional tectonics (Sengor & Yılmaz, 1981; Bozkurt & Mittwede 2001; Okay et al., 2001; Dilek & Pavlides 2006; Robertson & Mountrakis 2006; Ten Veen et al., 2009). GPS data shows that extension is still occurring in the Western Anatolian Extensional Province (WAEP) (e.g. Barka and Reilinger, 1997; Aktung et al., 2009). For the WAEP Barka and Reilinger (1997) estimated that Anatolia is moving northwards with respect to the Eurasian Plate at 23±1, 10 mm/yr. Mueller et al. (1997) provide a similar rate of 22 mm/yr for extension over Anatolia. The Available GPS data indicate 10±5 mm/yr of extension the Gediz and Büyük Menderes grabens (Barka and Reilinger, 1997; Aktung et al., 2009), which is distributed between the two grabens. These data yield an opening rate of 6 mm/yr for the Büyük Menderes Graben and 4 mm/yr for the Gediz Graben (Aktung et al., 2009). Further detail relating to the location and nature of the Gediz Graben and surrounding areas can be found in chapter 2 (figures 2.4, 2.8 and 2.10).

The basin is one of a series of grabens within western Turkey resulting from extensional tectonics in this area (Paton, 1992; Barka and Reilinger, 1997; Çiftçi and Bozkurt, 2009a; Çiftçi and Bozkurt, 2009b; Aktung et al., 2009 Çiftçi and Bozkurt, 2010). The modern topographic graben is 120 km long with a roughly E-W oriented graben axis. The geology of the southern margin, the Bozdağ Range, is dominated by the metamorphic central Menderes sub-massif and syn-tectonic sedimentary units (figure 6.1). These lithologies together form a mountain range that trends in a roughly W-E direction and reaches elevations of 2159 m at its highest peak, Bozdağ, in the centre of the range. The extensional tectonic regime of western Turkey has led to significant historic

earthquakes in the region (Guidoboni and Comastri, 2005; Guidoboni et al., 1994) (figure 2.3). An earthquake in 17 AD caused extensive damage to the region and the city of Sardis (located within the Gediz Graben) suffered damage from which it never truly recovered (Bauer, 2013). The ancient city of Smyrna, in present day Izmir (figure 2.4) on the Aegean coast of Turkey was repeatedly destroyed by earthquakes including one in 2 AD and another in 178 AD (Guidoboni et al., 1994). A significant earthquake of magnitude 6.9 occurred in 1969, creating a surface rupture of around 30 km (Arapat and Bingol, 1969) within the Gediz Graben. Another earthquake occurred in March 1970; this 7.2 magnitude earthquake left thousands homeless and over 1000 people dead (Mitchell, 1976). Additional large magnitude earthquakes occurred in 1866 and

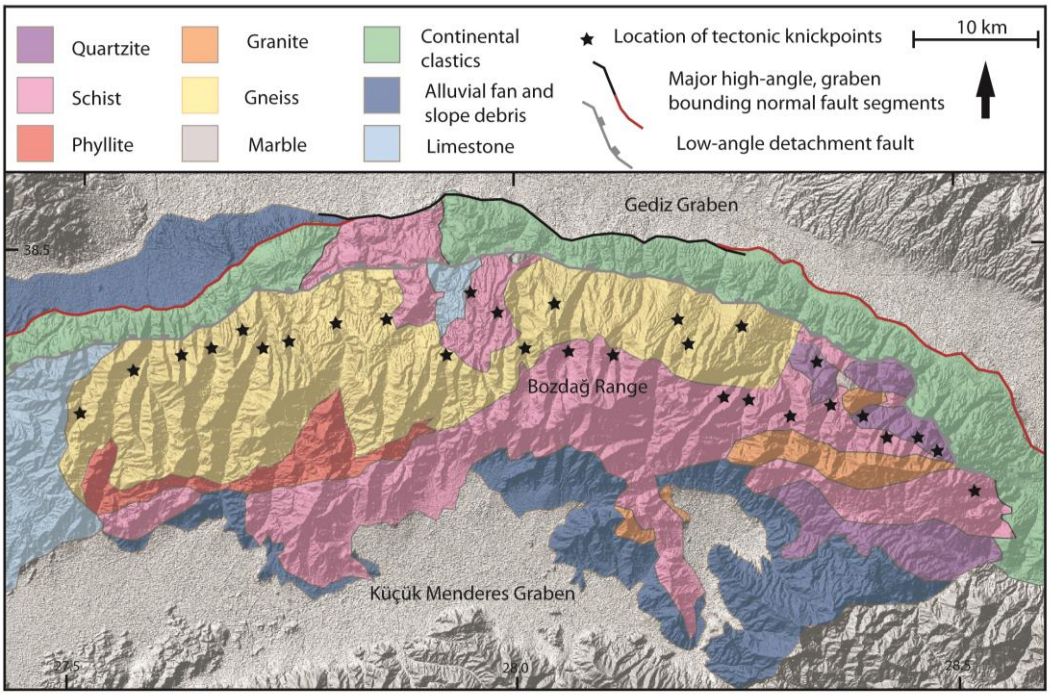

Figure 6.1: A simplified geological map showing the main lithologies in the Gediz Graben and the significant regional faults, a low angle detachment and an array of high-angle normal faults that bound the modern topographic graben. The tectonic knickpoints for each of the studied rivers are marked onto the rivers.

1944 (Ambraseys and Jackson 1998), these regional earthquakes illustrate how seismicity related to extension is affecting areas such as the Gediz Graben, creating significant seismic hazard.

The formation of the modern topographic Gediz Graben occurred as a two-stage process, which was initiated at 16 Ma with uplift and subsidence occurring primarily along a laterally continuous low-angle detachment fault in the southern graben margin (e.g. Buscher et al., 2013; Koçyiğit et al., 1999). Between 2.6 – 2 Ma the dominant style of faulting switched to high-angle normal faulting in both the northern and southern graben margins (Buscher et al., 2013; see chapter 2 for a review of the geology of the Gediz Graben). In the southern margin the high-angle normal faulting occurs on three segments that form the 120 km long array. The longest fault segment is the central Salihli segment at 47 km in length, the eastern Alaşehir segment has a length of 42 km and the shortest segment is the western Turgultu segment at approximately 35 km in length (figure 2.8). Although the existence and location of active faults are generally agreed, the rate, and relative magnitude of the faulting in along the graben margin has, until now, remained unconstrained. Chapter 4 presented stratigraphic and structural measurements to address some of these key questions. In particular, structural cross-sections, piercing point data and topographic swath profiles were used to constrain the geologic throw along the strike of the faults, and to quantify how this scaled with the variation in footwall relief along the basin margin (figure 6.2). Time-averaged throw rate data were calculated for the high-angle normal faults bounding the present day topographic graben, assuming these normal faults have been active from 2 – 2.6 Ma to the present day (Koçyiğit et al., 1999; Buscher et al., 2013). Time-averaged throw rates lie between 0.44 and 1.27 mm/yr along the fault array for

the whole of the Gediz Graben southern margin. When the average throw rate is calculated over each of the three fault strands rates for the Turgutlu Salihli and Alaşehir fault segments are 0.7 mm/yr, 1.2 mm/yr and 1.0 mm/yr respectively for the last 2.6 My (figure 4.11). The data presented in chapter 4 showed that the trend in the throw rate data for the Gediz Graben across the whole 124 km fault system was for the highest values of throw rate to be found towards the centre of the fault array. The highest time-averaged rate of 1.48 mm/yr is found at 72 km along strike and the lowest values are at the ends of the whole fault array (figure 4.11).

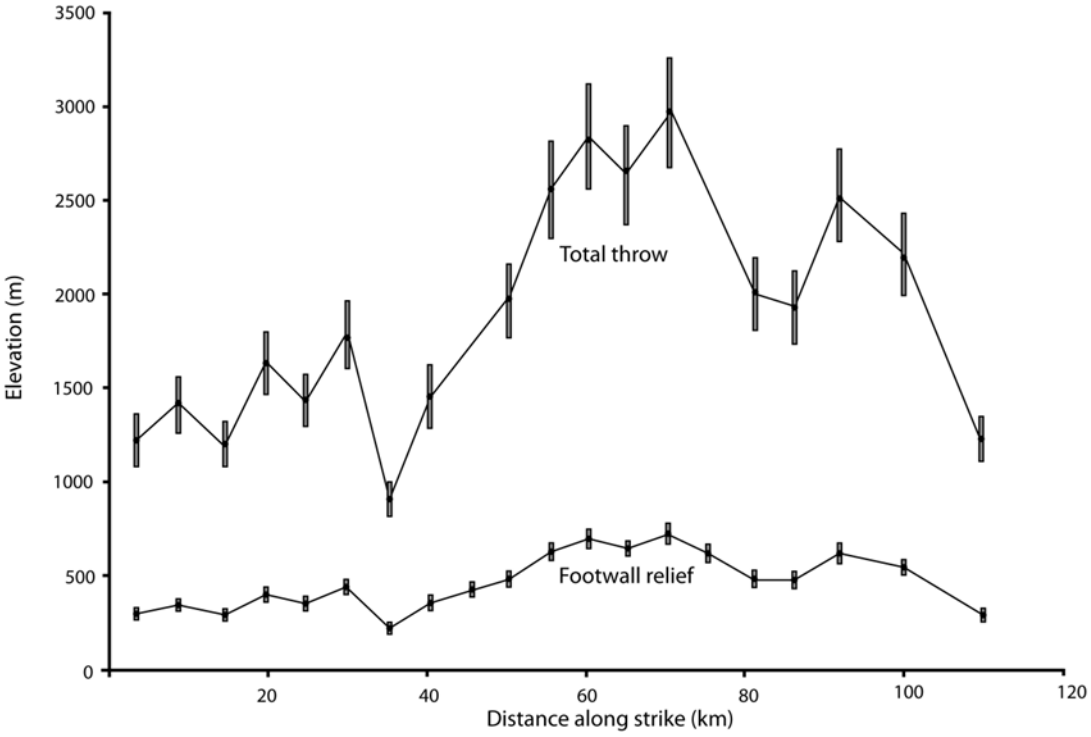

Figure 6.2: Total throw and footwall relief along strike. The errors on the values are 10%, as within 5km of the measurement site the value did not vary by more than 10% of the measured value.

However, the data presented in chapter 4 also suggest that at least one fault linkage event has occurred between the fault segments at some stage since fault initiation. It has been well documented that on a fault segment the highest values of throw should be found near the centre of the fault while the throw should reduce to zero at the fault tips (e.g. Kim and Sanderson, 2005; Cowie and Roberts, 2001; Barnett et al., 1987). However, where the mapped extent of the eastern and western segments meet the central fault segment, there are non-zero values for the fault throw. Moreover, the existence of three fault strands can be clearly seen in measures of footwall relief (section 4.7). Additionally, seismic data supports the existence of three depo-centres, where during the Late Pliocene-Early Pleistocene sediment was deposited within the hanging wall of the high-angle fault array (Oner and Dilek, 2011; Çiftçi and Bozkurt, 2009). However, from the late Pleistocene to the present day the graben acts as a single depo-centre (Çiftçi and Bozkurt, 2009). Linkage of the fault strands in the Gediz Graben is therefore supported by the non-zero throw values at the mapped areas of the central Salihli segment furthest from the centre and the overall trends in throw rate along strike suggesting the all three of the fault segments are linked (see chapter 4 for detailed information).

6.4: METHODS

The analysis conducted in this chapter centres on data extracted using Digital Elevation Models (DEMs). These data were analysed using ArcGIS (Arc Map) and RiverTools software. Topographic data were acquired from the Advanced Spaceborne Thermal Emission and Reflection Radiometer (ASTER) DEM data, with a 30 x 30 m resolution (NASA https://wist.echo.nasa.gov/api/).

Vertical errors on ASTER data are stated at 7 – 14 m in terms of standard deviation (ASTER GDEM Validation Team, 2009).

6.4.1: EXTRACTION OF RIVER PROFILES AND CATCHMENT INFORMATION FROM ASTER IMAGERY

The Bozdağ Range that bounds the Gediz Graben contains a well-developed drainage network of rivers that have their source at the drainage divide and incise through the mountains, into the Gediz Graben, all joining the trunk Gediz River, which drains the graben. The drainage network and catchment areas of the Gediz Graben were analysed using the DEM data. Rivers were selected that originate at the divide and become the main trunk river of the catchment. This was important as the aim of this study is to evaluate how the impact of active tectonics is transferred through a bedrock river system to the entire catchment. To address these aims, 24 catchments (figure 6.3)

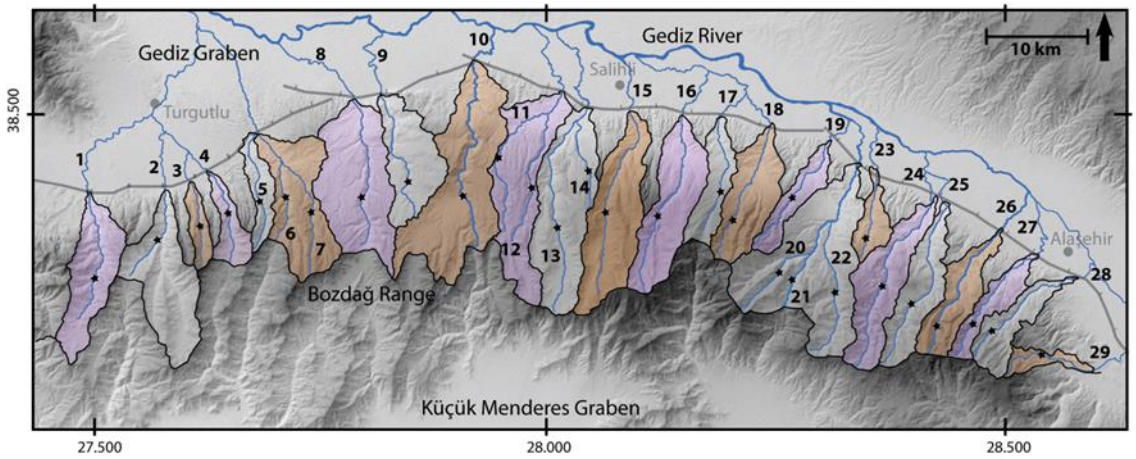

Figure 6.3: A topographic map of the southern margin of the Gediz Graben (the Bozdağ Range). The rivers and catchments extracted for this study are mapped onto the image. All the extracted rivers flow into the main Gediz trunk river, flowing through the Gediz Graben in a westerly direction. The black stars show the location along the channels of the identified tectonic knickpoints. The grey lines show the location of the active graben-bounding normal fault array.

containing 29 rivers (figure 6.4), including some significant tributaries of trunk rivers that cross the active normal fault, were identified and extracted using the Arc hydrology tool box and the RiverTools software suite.

DEMs typically have isolated sinks that need to be filled to create a hydrologically consistent surface. This process is done using the spatial analysis hydrology 'fill' tool in the Arc Toolbox. The flow directions on the DEM were then analysed using the 'Flow direction' hydrology tool which utilises a D8 algorithm. A D8 flow grid (Jenson and Dominque, 1988) is a grid of flow directions defined for each cell as the direction of the one of its eight adjacent or diagonal neighbours with the steepest downward slope. Flow direction is reported as 'no data' for grid cells adjacent to the edge of the DEM. In flat areas, flow directions are assigned away from higher ground and towards lower ground using the method of Garbrecht and Martz (1997).

Once the flow directions have been analysed it is possible to calculate the flow accumulation using the 'Flow Accumulation' hydrology tool. This calculates the drainage accumulated to a specific cell in the flow path. Using the flow accumulation grid, the stream network was defined by identifying pixels that have a large number of other pixels draining into them, using the Spatial Analyst tool Conditional option and 'Con' command. Within this command, it is possible to stipulate the amount of pixels that need to be draining into a subsequent pixel to create a stream network. A threshold value of 300 pixels gives a stream-forming drainage area threshold of 270000 m^2 (0.27 km^2), which is a realistic value that we confirmed against "blue-lined" streams on conventional topographic maps. The raster output from the 'Con' command kept only the cells which had a flow accumulation greater than 300 with all other pixels being assigned a null value.

To create a properly-defined stream network, the raster above was used in conjunction with the flow direction raster using the ‘Stream order’ hydrology tool. Strahler ordering was used in this step (Strahler, 1952). Streams of the first order have no tributaries and stream order increases downstream, only when streams of the same order intersect. The stream ordering raster was finally converted into vector data using the flow direction raster to provide line based coverage; this was done using the ‘Stream to feature’ command in Arc Toolbox.

To extract, at the basin-bounding fault, the watershed boundaries for each catchment draining the Bozdağ Range a point shapefile was used to represent the ‘pour point’, which is the outflow of the catchment and is found by selecting a pixel along the river at the selected outlet of the catchment. All the major outflow valleys, picked at the bounding fault were analysed in this way. The watershed for each valley (using the specified ‘pour point’) was extracted from the flow direction raster using the ‘Watershed’ tool in the hydrology toolbox (figure 6.3).

River profile data for each of the main streams draining the Bozdağ Range and crossing the active fault were extracted using RiverTools software. The 30 m ASTER tiles were imported and then mosaicked using the Patch RTG DEMs option to create a RiverTools Information (RTI) file. To extract the river profile data, several key steps are followed in RiverTools; in most respects these steps are analogous to the creation of a stream network in ArcGIS described above. The initial step is the construction of the D8 flow grid, which requires the pits and flats in the DEM to be resolved; a depressionless DEM is created from the mosaicked DEM using the ‘fill all depressions’ option within the FlowGrid (D8) from the extract menu. The D8 flow grid is then created through the option of ‘iterative linking’.

RiverTools was then prompted to extract a vector formatted tree file from the constructed flow grid using the 'Extract RT Treefile' function. RiverTools then create a 'drainage tree' based on the previously extracted flow grid directions to the edge of the DEM. This step created a RiverTools Vector (RTV) file containing the topology of the river network from the existing raster data. The final step was the extraction of the river network using the 'Extract River Network' which distinguishes between flow vectors on hill slopes and channels in a river network. The flow vectors on the hill slopes were pruned using the Horton–Strahler method (Horton, 1945; Strahler, 1952; Strahler, 1957) as in ArcGIS hydrology toolbox, and the resulting stream channel vector data is extracted from this. This process creates and stores a suite of files containing information such as upstream end pixel ID, downstream end pixel ID, Strahler order, straight line slope, along channel slope, total length of all channels upstream, relief, absolute sinuosity, drainage density, number of links per stream, and number of tributaries of various orders. RiverTools can extract a longitudinal profile from any point on the drainage network that the user defines. For our purposes, it was therefore important to identify the point furthest upstream on the extracted drainage network. The extracted data files contain data taken every 0.02 km to 0.03 km along the channel, and at each location the latitude, longitude, elevation, downstream distance and upstream drainage area were recorded.

6.4.2: LONGITUDINAL PROFILES AND CHANNEL GRADIENTS

The long profiles of each river (figure 6.4), and their channel slopes, S, and drainage areas, A, as a function of downstream distance, L were derived from the RiverTools data output. Reach-average channel gradients were calculated using elevation differences of 15 m. Linear regression was

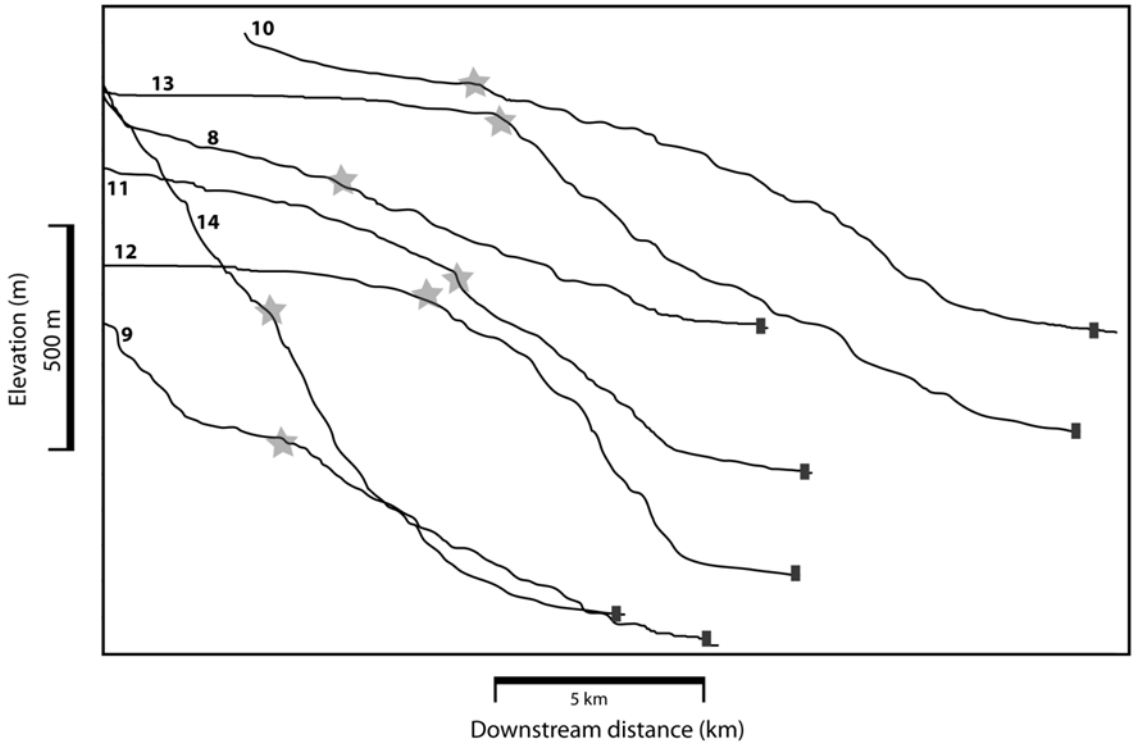
10
13
8
11
14
12
9
Elevation (m)
500 m
5 km
Downstream distance (km)

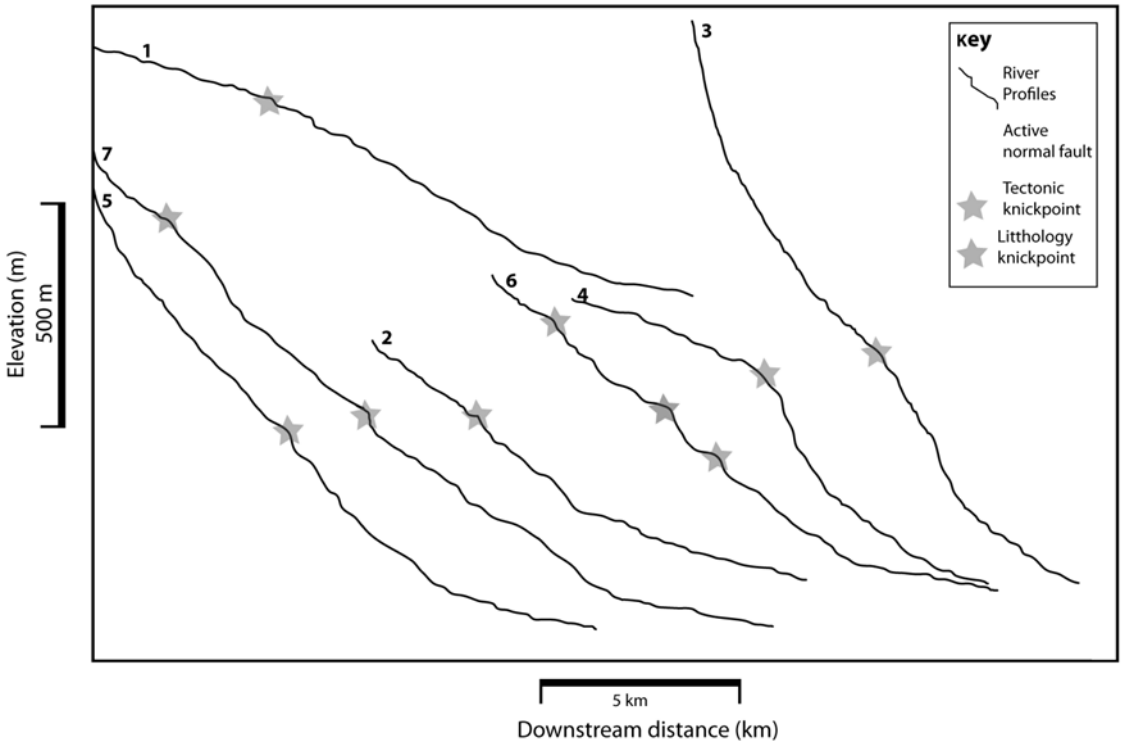
1
3
7
5
6
4
2
key
River Profiles
Active normal fault
Tectonic knickpoint
Litthology knickpoint
Elevation (m)
500 m
5 km
Downstream distance (km)

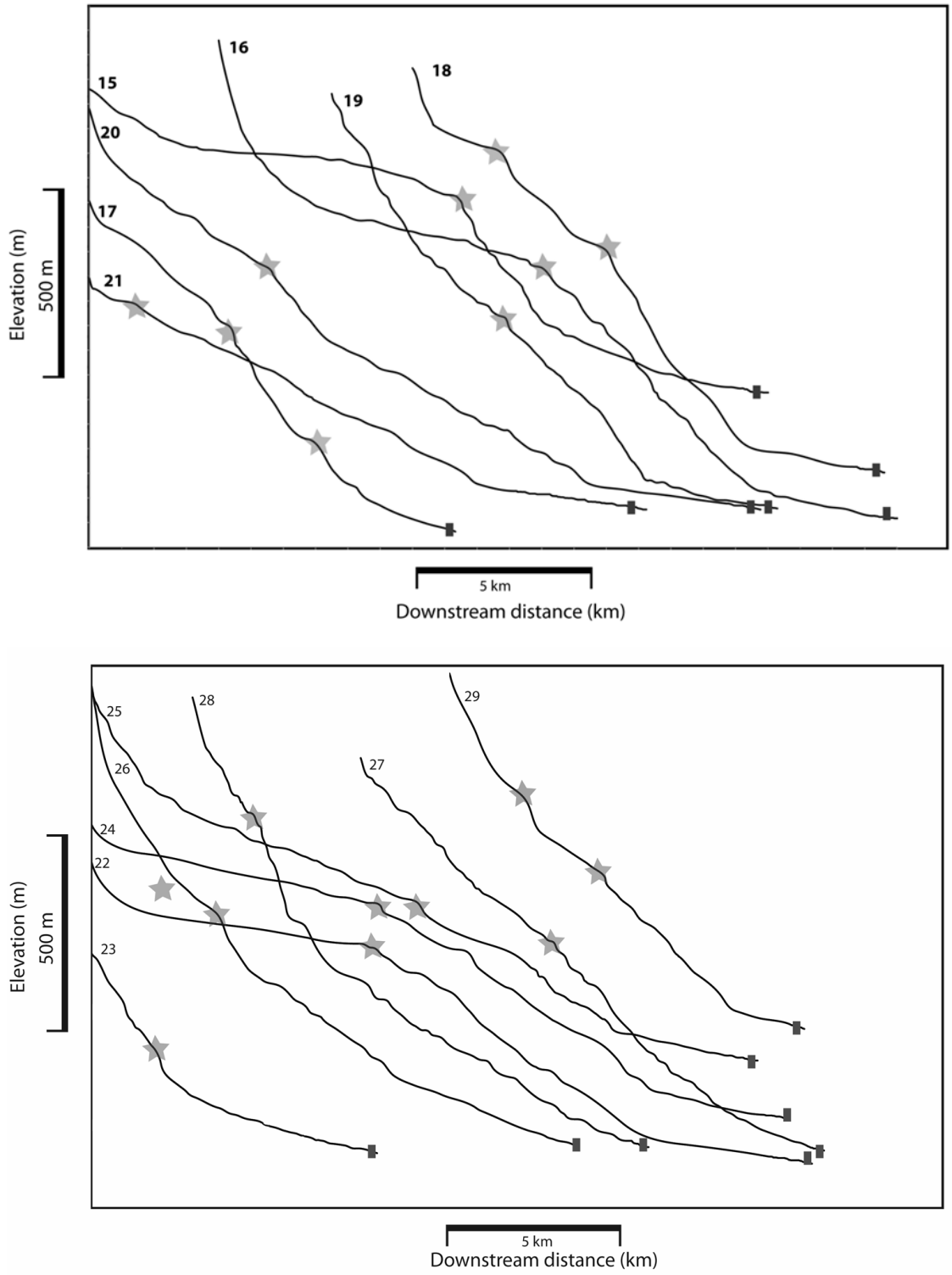

Figure 6.4: Long profiles for the 29 rivers extracted that drain the Bozdağ Range and cross the active high-angle normal fault array. The catchment locations for each of the rivers are shown in figure 6.3. The location where the river intersects the active normal fault is shown with a dash and the position of the tectonic knickpoint for each river is marked with a star, any lithology knickpoints are marked with a grey star.

undertaken on log-log slope-drainage area plots for each river in order to calculate normalised channel steepness index, k_{sn} where,

$$S = k_{sn} A^{-\theta} \quad \textbf{(eq. 6.1)}$$

and θ is the channel concavity. A standard concavity of 0.45 was used to derive the normalised steepness index (c.f. Wobus et al., 2006) to enable comparison between different rivers in the graben that vary in terms of their absolute concavity. Where knickpoints were present in the long profile (section 6.4.3), normalised steepness indices were derived for (i) upstream of the fault and downstream of the knickpoints and (ii) upstream of the knickpoint and downstream of the drainage divide.

6.4.3: KNICKPOINT IDENTIFICATION

A knickzone can be defined as a large-scale convexity in a river longitudinal profile, and a knickpoint as the precise profile break where the rate of change of the channel gradient is greatest in the river profile (Kirby et al., 2003; Crosby and Whipple, 2006; Wobus et al., 2006; Pederson and Tresler, 2012; Whittaker and Boulton, 2012). The presence or absence of knickpoints in the river long profiles upstream of the active faults was noted for each river. The knickzones identified here, and consequent convexities in the river profiles extracted, are large in scale (hundreds to thousands of metres), and thus influence significant portion of each catchment by length. It is stressed that this study is not concerned with small-scale or localised waterfall-type gradient changes in the river channels. Two methods were used to isolate and confirm the location of knickpoints along the river profile. The initial method was a visual

inspection of the longitudinal profile of each river. Any large-scale knickzones, clearly apparent from a visual inspection of the profile, were marked (e.g. Pederson and Tresler, 2012; Whittaker and Boulton, 2012). However, in many cases the precise downstream position of the knickpoint is not always easy to see within a convex-upward long profile. To avoid ambiguity in the location of the knickpoints, the reach-averaged slope data were plotted against downstream distance for each profile and the river profile overlaid. These graphs were used to derive robust knickpoint locations in each of the study rivers. Having constrained knickpoint locations in each river, the knickpoint data was extracted from the DEMs, including the vertical height of the knickpoint above the active fault, the upstream drainage area at the knickpoint, the downstream distance of the knickpoint, the total length and drainage area of the river and the along-strike position, relative to the graben margin, where the river flows across the active fault.

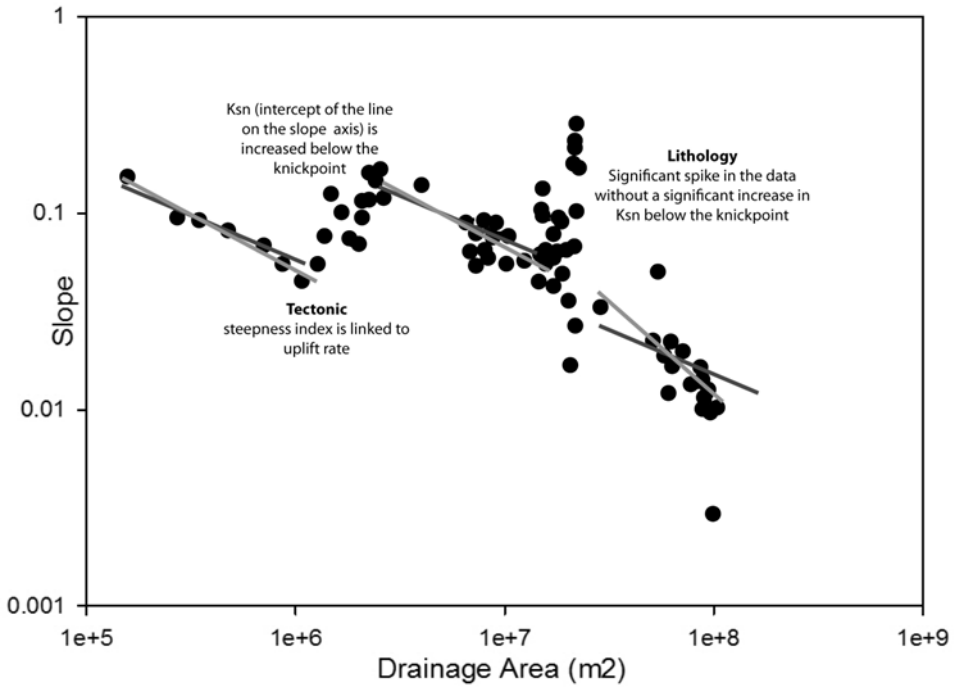

Figure 6.5: An example of a slope-drainage area plot in log-log space, using river 7. The morphology of the data that indicates both tectonics and lithology induced knickpoints is annotated. Slope-drainage area graphs for all other rivers are available in appendix 1.

It is accepted that lithology can cause knickpoints to form through differences in erodibility (e.g., Snyder et al., 2000; Baldwin et al., 2003; Duvall et al., 2004; Goldrick and Bishop, 2007; Anthony and Granger, 2007; Whittaker et al., 2007). Consequently, it was necessary to identify any lithology-instigated knickpoints so that they could be excluded from the analysis of knickpoints reacting to fault movement. Knickpoints initiated by lithology were identified through the use of a log-log plot of drainage area against slope (e.g. Haviv et al., 2010; Pederson and Tresler, 2012) and verified by determining where the rivers cross boundaries between different lithologies using geologic maps (Çiftçi and Bozkurt, 2009; Oner and Dilek, 2011). When knickpoints are present in a channel, they are necessarily indicated by break in the trend of the data in a log-slope log-drainage area plot. The morphology of the data break in this log space is important as it potentially yields information about the cause of the observed knickpoint (Wobus et al., 2006a). A “slope-break” knickpoint can be identified by an offset scaling relationship in the drainage area-slope plot. Consequently, two linear regressions with different intercepts (steepness indices) can be fitted to the data upstream and downstream of the knickpoint (Wobus et al., 2006a). As the steepness index is theoretically related to uplift rate (Sklar and Dietrich, 1998; Snyder et al., 2000; Kirby et al., 2003 and see section 3.2.3) and an increased steepness index is indicative of increased uplift rates, knickpoints associated with k_{sn} differences are good candidates for having a tectonic origin (figure 6.5). However, there are also ‘vertical-step’ knickpoints which appear on the drainage area-gradient plots as peaks or spikes in the data (Goldrick and Bishop, 2007). The intercept of the regression line on the slope axis in this case does not increase between the regressions, so k_{sn} does not change. Typically, vertical-step knickpoints are caused by

differences in the strength of rock at the channel bed. All the river profiles were plotted as log-log slope-area plots and the knickpoints were classified as either tectonically induced or caused by lithology, based on the process outlined above. The knickpoints classed as lithology-induced were cross-referenced against geological maps to verify if any of these corresponded with a lithological change. Any verified lithological knickpoints were excluded from consideration in this study. The reasonable assumption was made that the knickpoint (the top of the convex reach) upstream of the active normal faults in each long profile is the distance upstream that the wave-like response to tectonic perturbation has travelled (Crosby and Whipple, 2006; Whittaker et al., 2007b, 2008; Berlin and Anderson, 2009; Attal et al., 2011).

6.5: RESULTS

All the extracted rivers drain in a broadly northern direction into the Gediz River that runs along the axis of the Gediz Graben. The length of the rivers vary between 7.8 km and 24.1 km, with the longest rivers lying within the centre of the range, and shorter rivers occurring at the range margins. There is a corresponding variation in the size of the catchment area for each river from 7.7 km^2 to 119.1 km^2 (table 6.1).

The Bozdağ Range displays a marked topographic asymmetry with the shallow dipping Gediz Detachment to the north creating a wide, gently sloping range up to the drainage divide in the Gediz Graben and steep topography forming the southern part of the range bounding the adjacent Küçük Menderes Graben. The drainage divide throughout most of the mountain range is situated close to the Küçük Menderes Graben, although it is more central in the eastern part of the mountains. The catchments within the Gediz Graben are elongate

River	Dist. along strike (km)	drain age area (km2)	length to fault (km)	Active fault elev. (m)	Area at KP (km2)	KP height above fault (m)	KP dist down stream (km)	KP dist. from fault (km)	ksi 1 (linkage 1 myr)	ksi (linkage 0.6 myr)	ksi ratio	KP reatreat rate (linkage at 1 myr)	KP reatreat rate (linkage at 0.6 myr)	ksn upstream	ksn down stream	ksn ratio	Throw rates over 2 myr (mm/yr)	Footwall relief (m)	Throw from sediments (m)	KP retreat rate (linkage at 0.6 myr)	KP retreat rate (linkage at 1 myr)
1	5.6	49.1	14.7	144	20.84	381	5.35	9.35	1.59E-06	2.66E-06	1.67	11.22	18.69	43.08	63.07	1.46	0.7011	342	1402	15.58	9.35
2	12.8	63.94	10.77	173	5.99	346	2.67	8.1	1.56E-06	2.59E-06	1.67	12.45	20.74	52.68	84.14	1.60	0.5945	290	1189	13.50	8.10
3	15.3	9.57	9.16	187	5.88	483	4.9	4.26	1.50E-06	2.50E-06	1.67	4.65	7.75	41.26	79.70	1.93	0.5945	290	1189	7.10	4.26
4	17.7	18.26	10.29	170	11.52	449	4.76	5.53	1.41E-06	2.35E-06	1.67	6.01	10.05	21.57	34.78	1.61	0.8159	398	1632	9.22	5.53
5	22.7	18.5	12.5	170	5.27	428	4.89	7.61	2.35E-06	3.90E-06	1.66	13.30	36.73	57.42	74.19	1.29	0.7134	348	1427	12.68	7.61
6	22.7	63	12.04	147	16.2	403	4.52	7.52	1.40E-06	2.34E-06	1.67	11.17	18.61	34.12	65.40	1.92	0.7134	348	1427	13.13	7.88
7	22.7	90.04	16.8	147	14.2	465	6.6	10.2	1.87E-06	3.12E-06	1.67	14.94	24.89	60.52	103.08	1.70	0.7134	348	1427	17.00	10.20
8	32.9	79.53	16.38	105	20.59	415	5.56	10.82	1.64E-06	2.75E-06	1.68	14.62	24.50	56.15	140.48	2.50	0.89585	437	1792	18.03	10.82
9	35.4	46.71	15.1	97	11.64	548	4.75	10.35	2.04E-06	3.42E-06	1.67	13.96	23.38	53.10	141.69	2.67	0.44485	217	890	17.25	10.35
10	44.6	105.2	22.2	88	19.2	697	5.62	16.58	2.10E-06	3.50E-06	1.67	21.57	35.93	17.81	67.00	3.76	0.8692	424	1738	27.63	16.58
11	53.4	73.22	18.24	119	12.58	562	8.51	9.73	1.91E-06	3.18E-06	1.67	16.33	27.22	23.10	50.84	2.20	0.99015	483	1980	16.22	9.73
12	53.4	73.49	17.18	119	27.2	661	9.8	7.38	1.19E-06	1.99E-06	1.67	10.20	16.99	21.09	46.89	2.22	0.99015	483	1980	12.30	7.38
13	56.3	82.74	24.1	117	29.41	885	9.4	14.7	2.09E-06	3.49E-06	1.67	19.04	31.74	32.70	90.10	2.76	1.28125	625	2563	24.50	14.70
14	56.3	82.72	12.8	116	4.2	834	4.12	8.68	2.60E-06	4.34E-06	1.67	28.36	47.27	27.90	82.30	2.95	1.28125	625	2563	14.47	8.68
15	60.3	71.11	21	125	37.08	820	10.66	10.34	1.39E-06	2.32E-06	1.67	11.75	19.58	38.74	77.05	1.99	1.4227	694	2845	17.23	10.34
16	65.4	59.78	20.2	127	26.93	1029	9.79	10.41	1.71E-06	2.84E-06	1.67	13.19	21.98	95.38	317.00	3.32	1.33045	649	2661	17.35	10.41
17	69	26.97	11.86	200	9.8	924	4.3	7.56	1.68E-06	2.80E-06	1.67	8.36	13.94	87.67	314.14	3.58	1.33045	649	2661	12.60	7.56
18	73.7	47.8	14.6	177	7.9	863	5.6	9	2.03E-06	3.38E-06	1.67	13.81	23.02	63.70	248.00	3.89	1.4842	724	2968	15.00	9.00
19	79.2	22.03	13.7	157	8.47	680	6.05	7.65	2.10E-06	3.49E-06	1.67	9.79	16.32	59.00	187.00	3.17	1.2669	618	2534	12.75	7.65
20	79.8	118.62	20.77	153	7.03	978	5.53	15.24	2.60E-06	4.34E-06	1.67	28.36	47.27	74.59	239.04	3.20	0.99835	487	1997	25.40	15.24
21	79.8	118.62	17.21	153	16.52	557	5.94	11.27	1.40E-06	2.33E-06	1.67	15.25	25.42	71.80	87.83	1.22	0.99835	487	1997	21.68	13.01
22	82.8	119.2	21.4	153	24.6	777	8.6	12.8	1.76E-06	2.94E-06	1.67	19.19	31.98	62.20	78.26	1.26	0.99835	487	1997	21.33	12.80
23	85	14.97	8.42	194	2.06	408	1.7	6.72	2.22E-06	3.70E-06	1.67	8.56	14.26	61.91	107.85	1.74	0.99835	487	1997	11.20	6.72
24	90	53.43	20.52	175	20.44	710	8.66	11.86	2.00E-06	3.33E-06	1.67	14.61	24.35	28.40	59.02	2.08	0.9676	472	1935	19.77	11.86
25	91.5	42.72	19.01	185	16	685	7	12.01	2.31E-06	3.86E-06	1.67	15.20	25.33	84.98	208.20	2.45	0.9676	472	1935	20.02	12.01
26	97.2	34.31	14.49	236	3.8	764	3.7	10.79	2.52E-06	4.20E-06	1.67	11.84	19.73	101.00	151.90	1.50	1.2669	618	2534	17.98	10.79
27	100.9	22.27	13.17	224	8.07	730	4.5	8.67	1.61E-06	2.68E-06	1.67	7.56	12.60	73.48	81.82	1.11	1.10905	541	2218	14.45	8.67
28	105.1	29.12	13.56	215	6.36	795	5.8	7.76	1.64E-06	2.73E-06	1.67	8.84	14.74	78.91	160.63	2.04	0.5945	290	1189	12.93	7.76
29	110	7.7	7.8	354	5.9	427	5.1	2.7	9.24E-07	1.54E-06	1.67	2.54	4.23	84.00	159.00	1.89	0.5945	290	1189	4.50	2.70

Table 6.1: Data extracted for the 29 rivers considered in this study. The knickpoint (KP) data in this table is for the tectonically induced knickpoints identified n each river and the active normal fault that they cross.

with their long axis parallel to the regional extension in a NNE-SSW direction (figure 6.3). Within the higher elevations of the range, near to the drainage divide, small sedimentary basins have formed that are drained by the elongate northward flowing rivers.

It is significant that all rivers draining the Bozdağ Range and crossing the margin-bounding fault of the graben all have convex long profiles. Associated knickpoints, defined using the methodologies discussed above are identified in each of the rivers studied (figure 6.4 and table 6.1). All rivers contain at least one non-lithologic knickpoint, identified from slope-area analysis. However, additional knickpoints, such as those found in rivers 6, 7, 17, 18 and 29 were not associated with substantial offset in steepness index using slope-area analysis. In each of the cases the location of these knickpoints was verified against geologic maps of the area; these lithology-associated knickpoints are often pinned to a contact between the sedimentary graben fill and the metamorphic basement or the boundary between metamorphic lithologies of differing hardness (figure 6.6). Consequently, these knickpoints are excluded from the subsequent analysis.

The existence of non-lithological knickpoints upstream of the active faults is clearly suggestive of a transient response of the fluvial network to active faulting in the Gediz Graben. For these tectonic knickpoints the resulting convexity starts directly upstream of the fault, and we make the reasonable deduction that these knickpoints have been generated from the fault, either when the fault started moving, or due to a later slip-rate increase.

Figure 6.6: The long profiles of the river that contain lithological knickpoints. The lithologies that the channel incises through are displayed under the profile, and both the lithology and tectonics knickpoints are marked on.

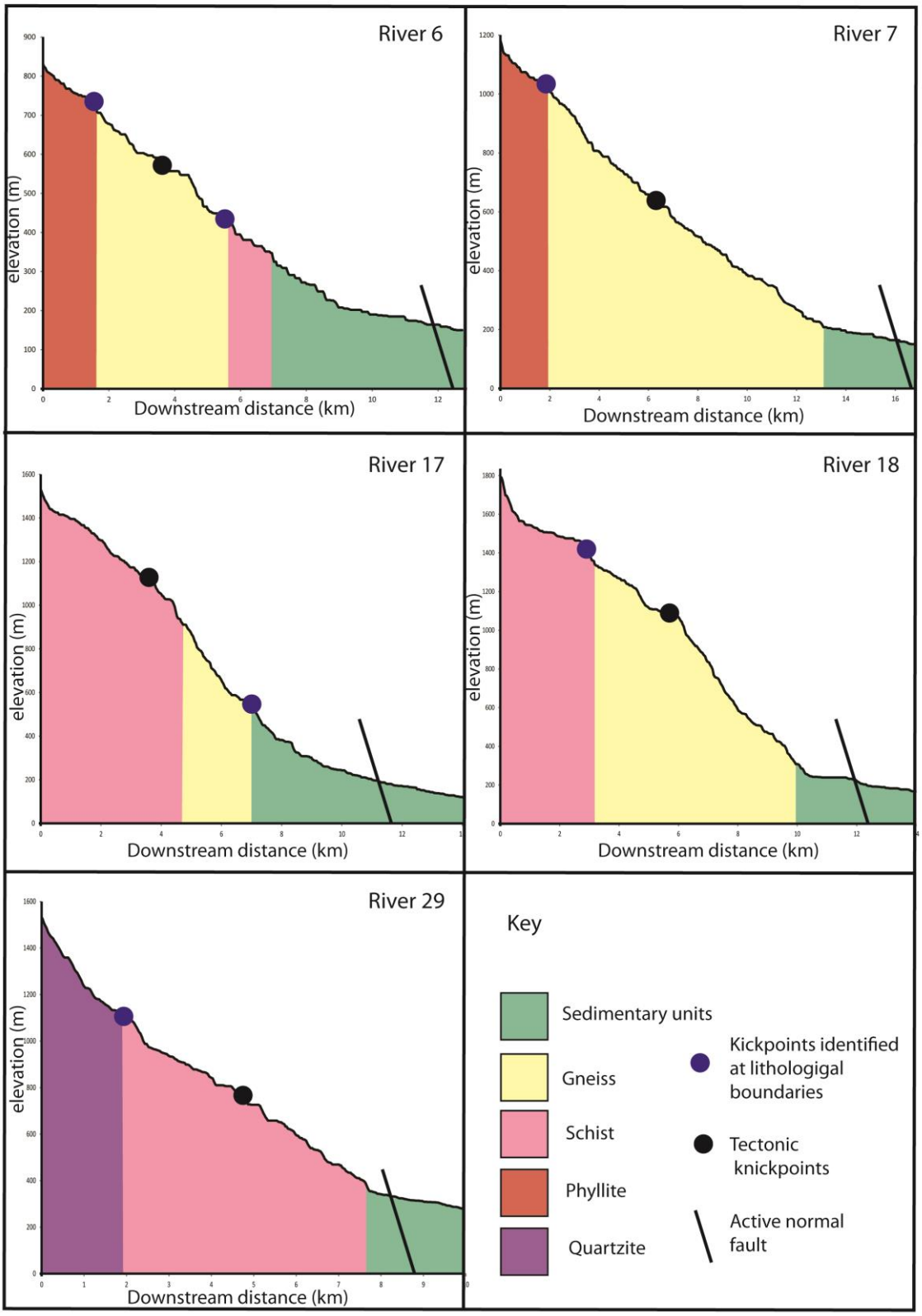

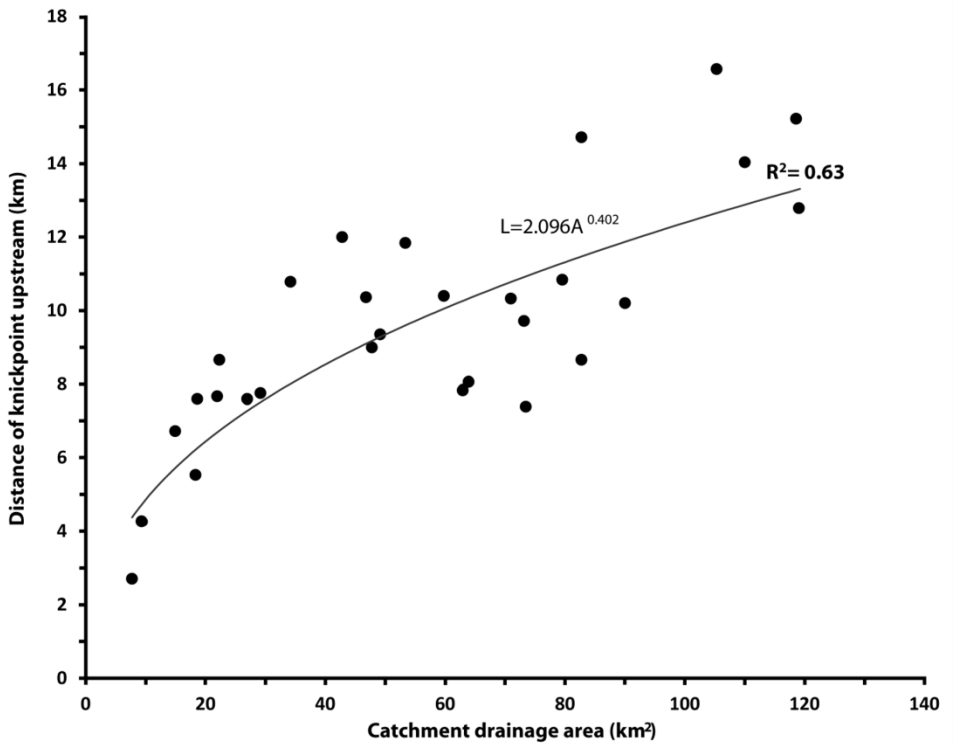

Figure 6.7: Graph showing the distance of the knickpoint upstream plotted against drainage area of the river catchment. The rivers with greater areas have knickpoints that have retreated further upstream. The relationship between the knickpoint upstream distance and the drainage area of $L \sim A^{0.41}$ is similar to the $L \sim A^{0.5}$. This suggests that knickpoints formed simultaneously as in rivers with greater the drainage areas the knickpoints can move upstream proportionally quicker than those with smaller areas.

The plan-view distance upstream that the tectonic knickpoint in each river has migrated varies along strike of the mountain range. However, when the distance of each knickpoint upstream of the fault is plotted against the drainage area, A, of each river catchment (figure 6.7), it is evident that the knickpoints within the channels with the largest catchments can be seen to have travelled further upstream from the fault. For example, river 10 has a catchment drainage area of 105.2 km^2 and the knickpoint has travelled 16.58 km upstream, while river 4, which has a drainage area of 18.26 km^2, has a knickpoint that has travelled only 5.5 km upstream. Studies of knickpoint behaviour in detachment-limited bedrock systems (e.g. Howard and Kerby, 1983; Seidl et al., 1994; Snyder et al., 2000; Tucker and Whipple, 2002; Whipple and Tucker, 2002; Anthony and Granger, 2007; Sklar and Dietrich, 2008; Boulton and Whittaker,

2009; Jansen et al., 2011; Whittaker and Boulton, 2012) suggest that all other factors being equal, the rate of knickpoint retreat upstream should scale with drainage area in a predictable way, being proportional to $A^{0.5}$ for a simple unit stream power model. (Tucker and Whipple, 2002; Bishop et al., 2005; Crosby and Whipple, 2006; Whittaker et al., 2008; see section 3.2). A line of best fit through this data reveals that the distance upstream that the knickpoint has travelled, L, scales as $A^{0.41}$. Figure 6.7 therefore shows that simple variations in drainage area do explain, to first order, the distance upstream the knickpoints have retreated. Importantly, such a relationship would be expected if the knickpoints in all of the rivers were initiated at the same time (Bishop et al., 2005; Castillo et al., 2013). Additional factors, such as lithological differences in bedrock erodibility, and differing distributions of drainage area with upstream channel distance from the fault may explain some of the residual.

The vertical heights of knickpoints, measured relative to the location and elevation of the basin bounding fault in each catchment vary systematically along the strike of the Gediz Graben (figure 6.8). The greatest knickpoint height is 1029 m above the fault occurring in river 16, at 65.4 km along strike of the range front, and approximately half-way along the length of the fault. The smallest knickpoint heights are found at the western end of the range where the knickpoints are found at heights of 346 m to 550 m above the fault. At the eastern end of the range the knickpoint heights are greater, and lie in the range of 427 m to 800 m (figure 6.7; table 6.1). The height of the knickpoints above the fault correlates well with the relative values of footwall relief and total throw on the active high-angle normal faults, which were derived in sections 4.72 and 4.73 of this thesis. The total throw increases towards the centre of the fault array by a factor of 3 compared to the extent of the mapped normal fault array

(figure 6.7) as does the height of the knickpoint above the active fault in the centre of the range compared with the margins. Significantly, although the three fault segments are clearly expressed in the footwall relief profile along strike of the fault, and are marked by throw minima at 38 km and 85 km along strike respectively, these segment boundaries have knickpoints with vertical heights of several hundred metres. The knickpoints documented here at segment boundaries are therefore likely to be related to the growth and interaction of the basin bounding faults, as opposed to the initiation of faulting.

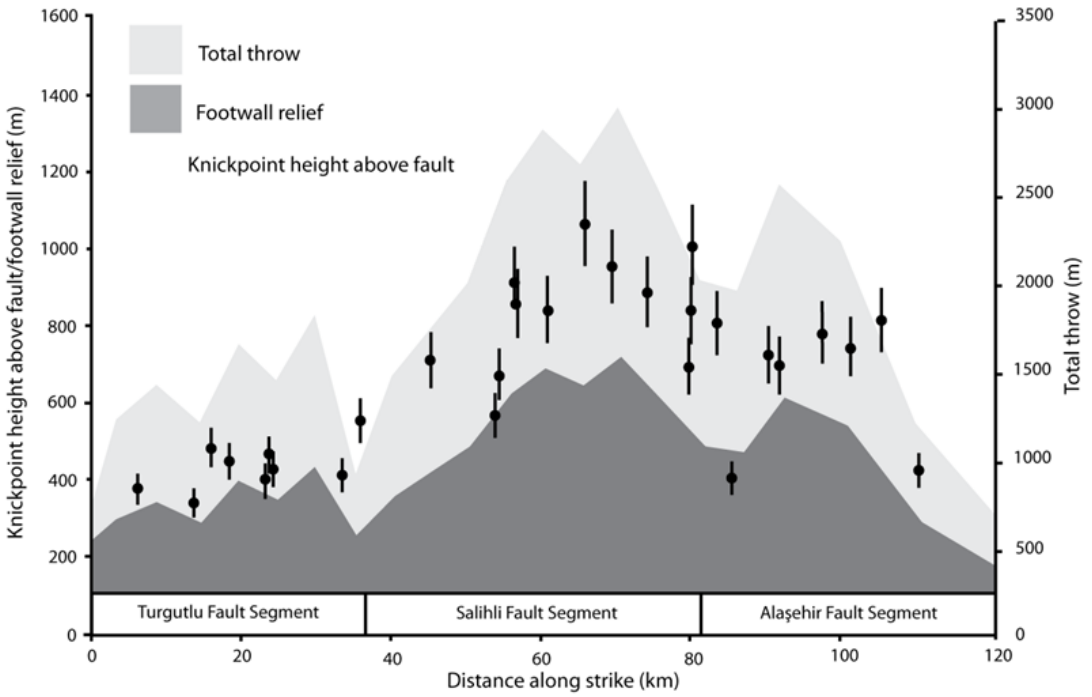

Figure 6.8: The heights of the knickpoints above the active fault plotted along strike, with the total throw and footwall relief superimposed. An error of 10% has been assigned to the knickpoint data to account of the variations in knickpoint placement between methods. The data shows that the heights of the knickpoints mirror the trends in the total throw and footwall relief.

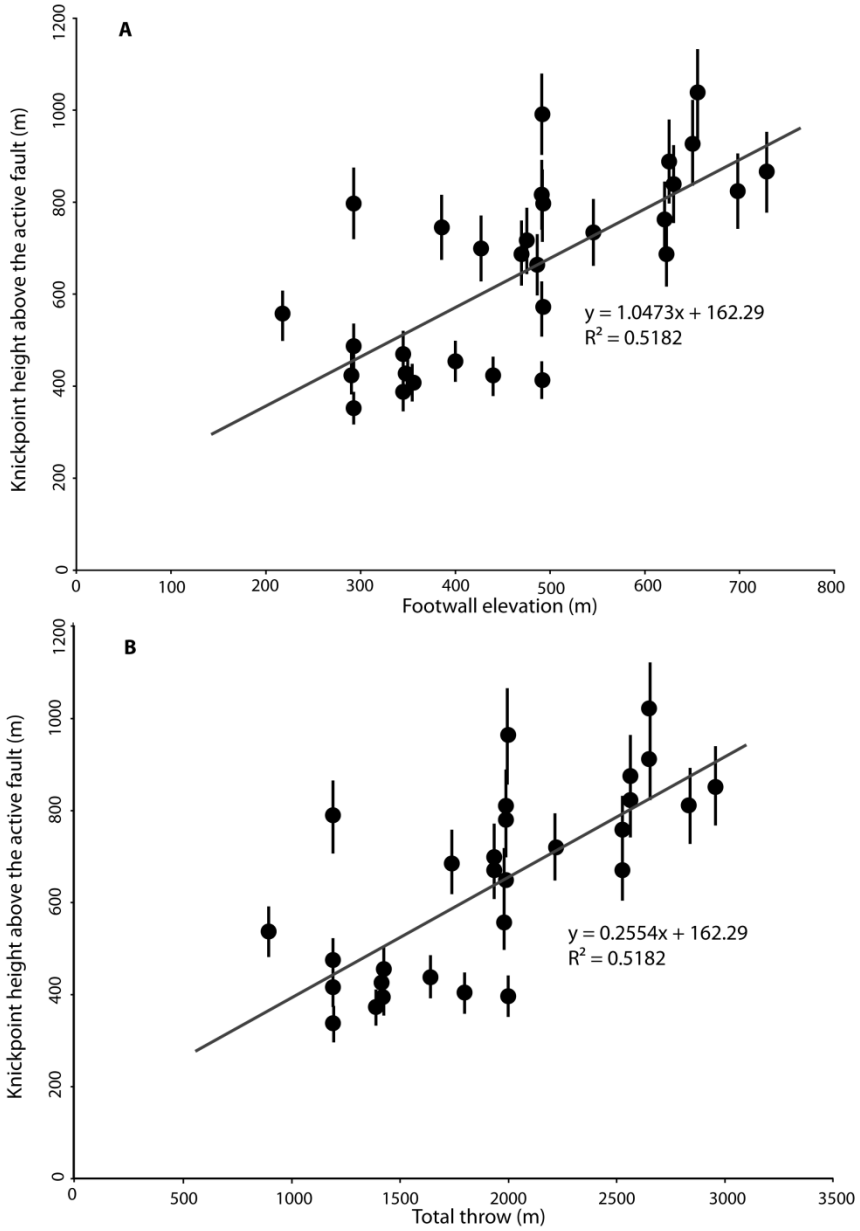

Figure 6.9: Plots of knickpoint height above the fault against (A) the extracted relief of the footwall and (B) the calculated total throw on the active normal faults. The red lines represent a linear regression. There is a trend towards greater height of the knickpoint above the fault with higher topography.

To test the relationship between knickpoints heights and the magnitude of the active normal faulting, knickpoint heights above the fault are plotted against the high-angle normal fault footwall relief and the derived total throw (figure 6.9). These data show that knickpoints height can be related to both relief and total throw with a linear relationship (r^2 = 0.52). The data suggest that both increases in relief and total throw due to movement of the high-angle

normal faults produce an increase in the knickpoint height. The equation of the linear best fit line for the plot of knickpoint height above the fault-footwall relief has a gradient of ~1, and therefore knickpoints heights are generally similar in magnitude to the footwall relief (figure 6.9a). However knickpoints heights are only a small fraction of the total geological throw (35% on average). The data in figure 6.9 illustrate how the knickpoints record both footwall uplift and total throw variations with a reasonable degree of fidelity, and suggest that they are recording variations in the magnitude of faulting along the strike of the basin-bounding structure.

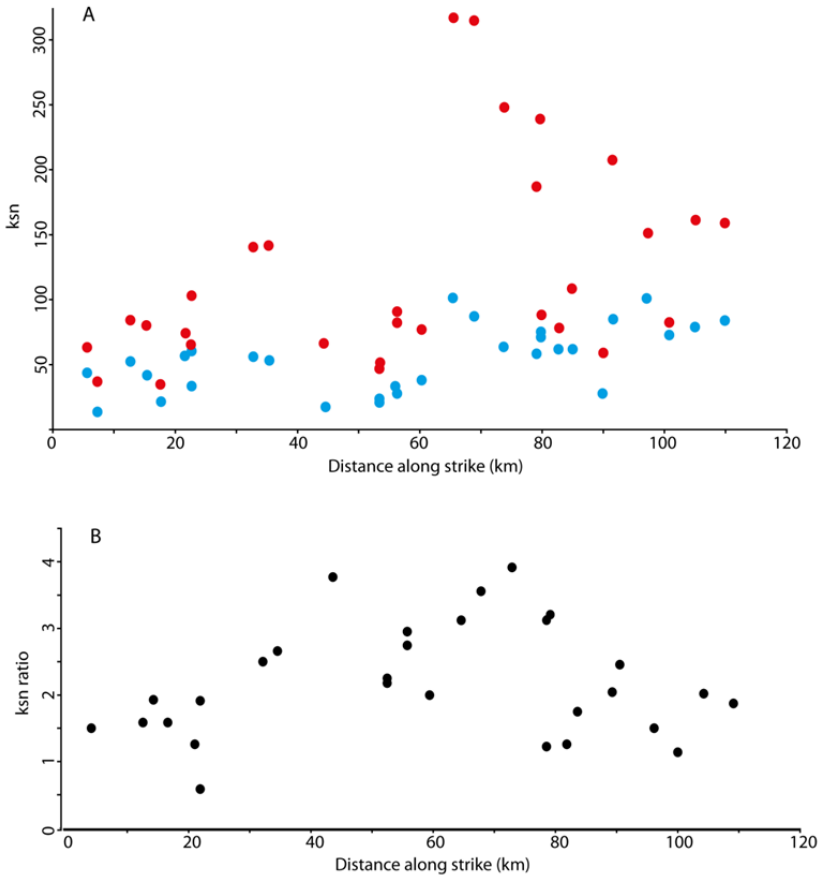

Figure 6.10: Along strike plots of concavity normalised steepness index (K_{sn}). The reference concavity used was 0.45. A) shows the K_{sn} values above the knickpoint (blue data points) on each river and the corresponding K_{sn} below the knickpoint (red data points). B) shows the ratios of K_{sn} above and below the knickpoint plotted along strike with black data points.

Channel steepness indices (k_{sn}) for each study river were also derived for channel reaches upstream and downstream of each of the knickpoints (figure 6.10a); these show significant variations between each data set. Upstream of the knickpoints, the k_{sn} values for each river range between 17.8 $m^{0.9}$ and 95.3 $m^{0.9}$ (blue points, figure 6.10a). However, there is little systematic variation in k_{sn} along the strike of the fault. In contrast, the values of k_{sn} downstream of the knickpoints, but upstream of the fault are consistently higher than the upstream value for the respective river; the average k_{sn} value upstream of the knickpoints is 55.5 $m^{0.9}$ while downstream of the knickpoints it is 124.2 $m^{0.9}$. However, there appears to be a general trend in the downstream k_{sn} data of significantly higher k_{sn} values in the centre of the fault array, with k_{sn} values reaching > 300 $m^{0.9}$ at 70 km along strike**.** In contrast, noticeably lower values of channel steepness in the downstream reaches of the rivers are consistently recorded towards the mapped extent of the fault array.

The disparities in channel steepness index upstream and downstream of the knickpoints on the channels can be effectively explored by the considering the ratio of the k_{sn} values along the strike of fault (figure 6.10b). This ratio increases to higher values in the centre of the fault array meaning that the k_{sn} values downstream of the knickpoint within rivers crossing the active normal fault the centre are larger than the upstream values by a greater amount. The ratio values in the centre of the fault array range from 2.5 – 3.89, while at the mapped extent of the fault array values of 1.1 – 2 are typical. As k_{sn} is commonly taken to scale with uplift rate (Kirby and Whipple, 2001; Kirby et al., 2003; Wobus et al., 2006), these data indicate that the relative uplift rate change responsible for creating the knickpoints must lie in this range and may have had a greater magnitude near the centre of the fault.

6.6: DISCUSSION

6.6.1: LANDSCAPE RESPONSE TO ACTIVE NORMAL FAULTING

A key aim of this study is to determine whether fluvial geomorphology can add to the resolution of structural data and a key part of this is to determine whether the fluvial system draining the Bozdağ Range are responding in a transient way to active faulting, and if so, to determine how this is recorded in the landscape. Chapter 4 presented evidence for ongoing faulting on high-angle normal faults bounding the Gediz Graben, and reported on a high resolution data set for along strike trends in throw.

The results presented in this chapter show that rivers within the Bozdağ Range all contain one tectonic knickpoint upstream of the active graben bounding faults, including in areas upstream of the fault segment boundaries (figure 6.8). The knickpoints in the Gediz Graben cannot be due to lithology as the dominant lithology changes along strike have been mapped (figure 6.1), and any lithology-related knickpoints identified (figure 6.6) were deliberately excluded from the subsequent analysis; the remaining knickpoints do not sit at lithological boundaries. There has also not been a regional base level fall or incision of sediment out of the graben valley that could account for the formation of knickpoints. Climate is not the cause of the knickpoints or their documented height variation along strike, as precipitation rates do not vary significantly along the Bozdağ Range (Sensoy et al., 2008). Consequently, active faulting is the most likely mechanism for the creation of the knickpoints observed in the rivers, and the fact that they are still observable in the landscape suggests that the rivers draining the Bozdağ graben are indeed recording a transient response to

tectonics. Figure 6.7 shows that the drainage area of each river is a key determinant of how far the knickpoints have moved up stream. In rivers with greatest drainage area the incisional wave associated with the knickpoint has reached greater distances upstream from the fault. The relationship between the upstream channel distance that the knickpoints have migrated, and their catchment drainage area ($L \sim A^{0.41}$) is very similar to the theoretical predictions from simple stream power models if the knickpoints had all started at the same time ($L \sim A^{0.5}$) (Whittaker and Boulton, 2012). Therefore, the simplest explanation for this relationship is that these knickpoints were generated by the same tectonic event.

Two potential tectonic events that could explain the formation of the knickpoints are therefore either; (i) the initiation of active faulting in the Pliocene, or (ii) a subsequent fault slip rate increase along the fault array, due to the interaction and linkage of previously isolated fault segments (e.g. Densmore et al., 2007; Boulton and Whittaker, 2009). The existence of fault linkage is discussed in chapter 4, and is clearly evidenced by the pattern of throw along strike of the fault, with non-zero values of throw at the fault segment boundaries where zero throw would be expected if the faults were acting independently. The existence of knickpoints in the channels upstream of segment boundaries also suggests that these knickpoints formed due to the linkage. Additionally, it would be expected that there would be two sets of knickpoints in each channel if fault initiation was being recorded, in addition to a later linkage event.

The heights of knickpoints along the strike of the fault array mirrors the pattern in throw and footwall relief measurements (figure 6.8) with maximum values of both throw and knickpoint height in the centre of the fault. Whittaker et al. (2008) proposed that the magnitude of the difference in throw rate before

and after fault linkage was the root cause of a similar relationship documented for knickpoints upstream of active faults in the central Italian Apennines. An increase in throw rate in the Gediz Graben is one result of fault interaction and linkage, as the centrally-located areas where fault segments meet that were experiencing very low to zero throw rates would suddenly (in geological terms) increase as they now be situated within a longer fault structure (Cowie, 1998; Cowie and Roberts, 2001).

This interpretation is also consistent with our estimates of normalised channel steepness index, which should reflect variations in relative uplift rate along the strike of the fault (Duvall et al., 2004; Wobus et al., 2006a; Whittaker et al., 2007; Boulton and Whittaker, 208; Whittaker and Boulton, 2012). As a channel is perturbed by increased slip on the basin-bounding fault, the river attempts to keep pace with the new rate of throw, leading to the steepening of the channel and the migration of a knickpoint upstream. A greater rate of throw should therefore increase the k_{sn} value below the knickpoint by a greater amount than a lesser throw rate increase, and this is reflected in the data from the Gediz Graben when considered along strike (figure 6.8). Assuming that uplift rates are linearly proportional to $k_{sn,}$ and channel steepness upstream and downstream of knickpoints is recording the erosional response to an uplift rate change (Wobus et al., 2006a; Whittaker et al., 2012; Kirby and Whipple, 2012) the ratio of k_{sn} upstream and downstream of the knickpoints suggest a maximum relative uplift rate difference of 3 – 4 in the centre of the fault.

The ratio of k_{sn} values above and below the knickpoint vary along the fault array from 2.5 – 3.89, at the centre, while values of 1.1 – 2 at the mapped extent of the fault array are typical. This may reflect the differences in uplift rate given that the areas with the highest ratio are also the areas with the highest

time averaged total throw as calculated from the total throw rates. As the k_{sn} ratio is linked to an increased uplift rate, this data strongly suggests that the differences in the k_{sn} ratios along strike are linked to the throw rates and how they vary along strike. The k_{sn} ratio data for rivers in the Gediz Graben suggest that there has been an enhancement of the amount of throw occurring on the faults since the linkage event.

6.6.2: CONSTRAINING FAULT THROW RATES

A caveat of using the derived geological throw to produce throw rate estimates along strike of the basin-bounding fault, as presented in chapter 4, is that the rate produced is necessarily time averaged over a timescale of 2 Myr. However, fault arrays that have undergone linkage tend to preferentially accumulate throw at the centre of the new longer fault array with minimal changes in throw rates at the tips of the faults. Consequently, the time-averaged throw rate values for the centre of the Gediz fault array are likely to under-estimate the present day throw rate as the time-averaged rates incorporate both the pre- and post-linkage rates. In contrast, the eastern and western extent of the fault array should have throw rates broadly similar to those that were produced using the time averaged method given that they are close to the tips of the fault array. Moreover, as knickpoints are transient features created due to a relative change in uplift rate or base level, their generation is linked to post-linkage throw rate, not the time averaged value. The steepness index data (figure 6.10) clearly show that the value of k_{sn} is higher below the knickpoints and above, and that the 'downstream' k_{sn} data are the greatest at the centre of the fault. More importantly, the use of time averaged rates may lead to the under-estimation of seismic hazard.

To overcome this problem it is possible to: (i) calculate the range of times for which fault acceleration could have occurred, given geological estimates of footwall relief and fault throw (figure 6.8); and (ii) estimate the throw rate enhancement factor likely associated with the documented fault linkage event along the array.

To solve this issue, we use estimates of when high-angle active faulting first occurred in the Gediz Graben and the footwall relief accumulated since that time to iteratively calculate all possibilities for throw rates before and after linkage. These values can then be compared with the times and throw rates required to grow knickpoints of the size found in the Gediz Graben. Overall, this will provide an estimate of both present day throw-rates and the timing of fault linkage and interaction (Whittaker et al., 2007; Boulton and Whittaker, 2008; Whittaker and Walker, 2015).

Chapter 4 presented the key constraints for this. In brief, between 2.6 and 2 Myr significant high-angle faulting developed along the length of the graben, and from 2 Myr high-angle normal faulting becoming dominant resulting in the present day graben. Both the studies of Buscher et al. (2013) and Koçyiğit et al. (1999) infer a similar age for the transition from sedimentary and structural evidence, so 2.6-2 Myr will be used as the timing of the transition from phase 1, low-angle normal faulting to phase 2, high-angle normal faulting.

The increase in throw on the faults can be examined using a fault enhancement factor, which quantifies how much enhancement of fault displacement there is at the centre of the fault array following fault linkage. This is reflected in the k_{sn} ratio data for rivers in the Gediz Graben and can also be quantified using fault interaction theory (Cowie and Roberts, 2001). This theory assumes that the displacement profile of the fault array is triangular in shape,

with a maximum value at the centre decreasing linearly to zero at the tips. The validity of the triangular approximation has been tested by Cowie and Roberts (2001) who showed that the greatest inaccuracies are at the tips of the fault array. Additionally, throw rate enhancement factor at the centre of the array is more important for our purposes, as we wish to estimate the maximum throw rate on the fault. Equation 6.2 shows how the fault enhancement factor, *E* (Boulton and Whittaker, 2008), for the centre of the Gediz fault array can be calculated by considering the length of the fault segment (Li) and the distance between the mid-point of the segment to the mapped extent of the post-linkage array (Ri):

$$\mathrm{E} = 2 \times (\mathrm{Ri}/\mathrm{Li}) \quad \textbf{(eq.6.2)}$$

The lengths of the three fault segments in the Gediz Graben are 41 km, 43 km, 36 km from west to east with a total array length of 120 km. For the Gediz Graben this equation yields a throw enhancement factor of ~3 at the centre of the array as a result of fault interaction and linkage, using our inference that the fault strands linked at the same time. This value is very similar to the enhancement factor of 3 – 4 deduced from k_{sn} ratios at the centre of the fault system in section 6.5.

The evidence presented so far supports the interaction and linkage of the high-angle normal faults at some point since their initiation at ~ 2.6 Ma. The analysis presented here points to this happening in one event, as there is only one tectonic knickpoint on each channel, and the distances the knickpoints have moved upstream are consistent with their being initiated at the same time (figure 6.7). Consequently, to estimate the timing of linkage (D), given

geological estimates of 2800 m of fault throw at the centre of the fault, all the possible solutions for the following equation are initially found, which equates the total throw (T) to the time and slip rates pre and post linkage:

$$T = (r_1 \times t_1) + (r_2 \times t_2) \quad \textbf{(eq. 6.3)}$$

In this case, r_1 and r_2 are the original and post linkage throw rates respectively and t_1 is the time between fault initiation and fault linkage, and t_2 is the time taken after the throw rate increase, the combination of which led to formation of the present day topography. $t_1 + t_2$ is therefore equal to 2.6 Myr. Additionally, we know that

$$r_2 = Er_1 \quad \textbf{(eq. 6.4)}$$

where E is again the throw rate enhancement factor. For the Gediz Graben we use a throw enhancement factor of 3 in the centre of the fault, consistent with both fault interaction theory and ratios of channel steepness index presented above. Using these equations and the estimate of total throw, the range of all possible slip rates before and after linkage were calculated, each of which is associated with a specific linkage time.

Figure 6.11 plots all the throw rates on the normal faults both pre- (blue diamonds) and post-linkage (red squares) for any time since linkage (t_2) that can satisfy the required accumulated 2800 m of throw at the centre of the fault over a time frame of 2.6 Myr. This allows for a throw rate difference to be worked out and plotted (black line) for the calculated pre- and corresponding

post-linkage throw rates difference, as knickpoints grow in in response to a differential throw rate.

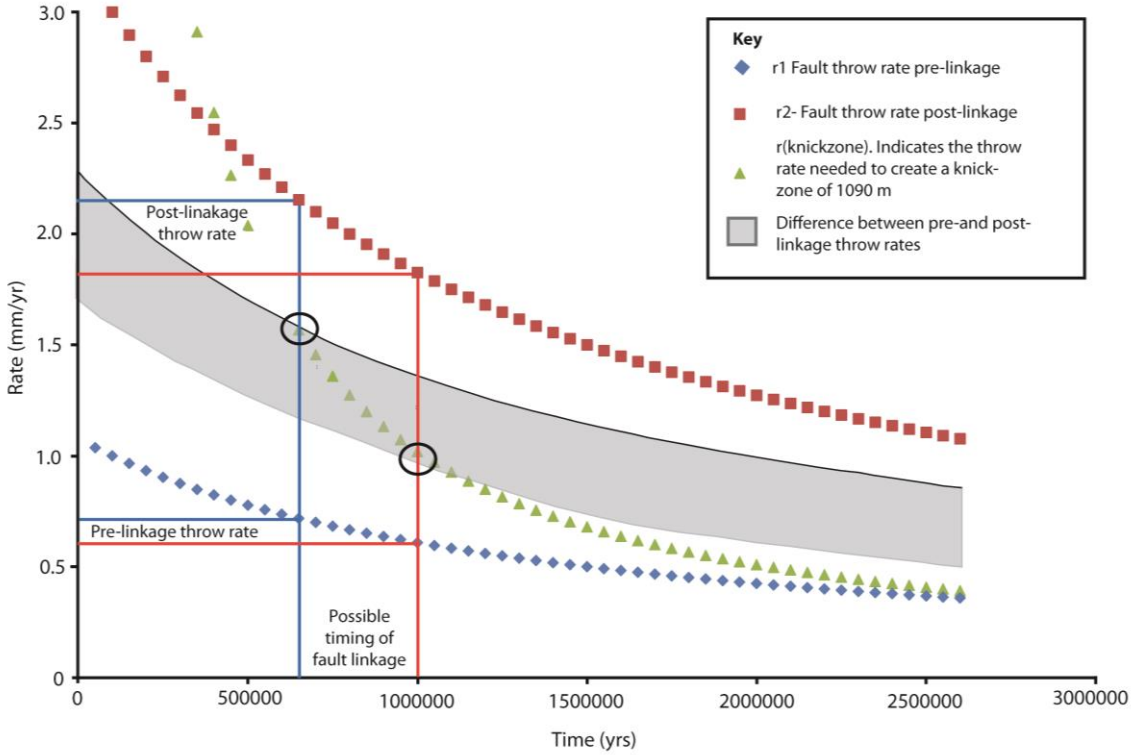

Figure 6.11: Calculation of possible throw rates for the centre of the active normal fault array in the Gediz Graben before and after linkage as predicted by equation 6.3. Given a displacement of T = 2800 m, all the combinations of the pre- and post-linkage throw rates that could account for the 2800m of displacement have been plotted. The blue diamonds show the required throw rate before linkage (r1), and red diamonds show the paired throw rate after linkage (r2), as a function of time since the throw rate increase (t2). The green triangles show the throw rate needed to generate a 1019 m high knickzone since linkage time (rknickzone). The black solid line shows difference between pre- and post-linkage throw rates, which is what the knickpoints respond to. As there has been deposition of graben fill sediments in the hanging wall a grey shaded area has been added to account for a reduction in perceived throw rate difference due to ~1 km of sediment deposition. This analysis yields a range of times for fault linkage of around 600 Kyr to 1 Ma.

However, the time and magnitude of the throw rate should also be consistent with the time taken to grow the knickpoints measured in the rivers (e.g. Boulton and Whittaker, 2009; Whittaker and Walker, 2015). Whittaker et al. (2008) showed through modelling and theoretical studies that the vertical height

of knickpoints should scale directly with the throw rate difference since the causal perturbation. This means that

$$H = t_2(r_2 - r_1) \quad \textbf{(eq. 6.5)}$$

The locus of points satisfying this relation is shown in green in figure 6.11, for one of the knickpoints in the centre of the fault array, which has a height of 1019 m. As the rate and hence time to grow the knickpoint should be consistent with a predicted differential throw rate pre- and post- linkage, it is therefore possible to estimate both the timing of this event, and the present day throw rate (c.f. Boulton and Whittaker, 2009; Whittaker and Walker, 2015). Our best estimate for the time of linkage is derived from the point at which the knickpoint data set (green triangles) crosses the throw rate difference data set (black line). A simple analysis therefore suggests that a linkage event at ~600 Ka explains the data well. However, as the knickpoints grow in response to a relative base level change, consideration needs to be given to the amount of graben fill in the subsiding hanging wall of the normal faults as this can reduce the differential throw rate increase “perceived” by the river. The sedimentation rate in the hangingwall of the fault is not precisely known, but this can be taken into account by considering up to 0.5 mm/yr of sediment accumulation to account for the presence of > 1000 m of sediment filling the graben depo-centre (Çiftçi, 2007). This will effectively reduce the throw rate experienced by the rivers. This has been represented on figure 5.11 as a grey bounding zone rather than a line; taking the lower bound for this, a maximum time for the linkage event is ~ 1 Ma.

Figure 6.11 can also provide an estimate of the rates of fault throw both pre- and post-linkage. The throw rate values yielded by the calculations are representative of the centre of the fault and therefore are range-maximum values. In accordance with the behaviour expected in normal faults the throw rates will decrease from the centre towards the fault tips with minimum throw rates will occurring at the fault tips. The calculations presented here therefore provide a present (post-linkage) throw rate of 2 ± 0.2 mm/yr and a pre-linkage rate of 0.6 ± 0.1 mm/yr at the centre of the fault array. The method undertaken provides a good quantification of throw rates at the centre of the fault array, but does not provide direct quantification other throw rates along strike. The values for throw rate for the areas along strike between the centre and the mapped extent of the normal faults, where throw rate is small compared to the centre, could be quantified by extrapolating along a straight line that joins the peak and minimum values for throw rate, where the distribution of throw rates along strike is modelled as a triangle (c.f. Cowie and Roberts, 2001) with its peak at the centre of the fault array.

The calculated post-linkage throw rate different to the throw rates gathered from time-averaged geological data (for detailed methods and results see chapter 4). Throw rates averaged over 2 myr and derived from cross-sections, seismic reflection surveys and geomorphic analysis give a maximum time-averaged throw rate of 1.4 mm/yr at the centre of the fault array. This results in an underestimation of present day throw rate by 0.6 mm/yr based on the post-linkage 2 mm/yr value estimated here using the time average value. This is expected if fault linkage has taken place, because underestimation at the centre of the fault is inherent in the time-averaged method.

6.6.3: CONSTRAINING KNICKPOINT RETREAT RATES

Having determined that there has been a tectonic perturbation due to fault linkage in the Gediz Graben, a significant question to consider is how fast the fluvially-sculpted landscape is responding to the interaction and linkage of the faults.

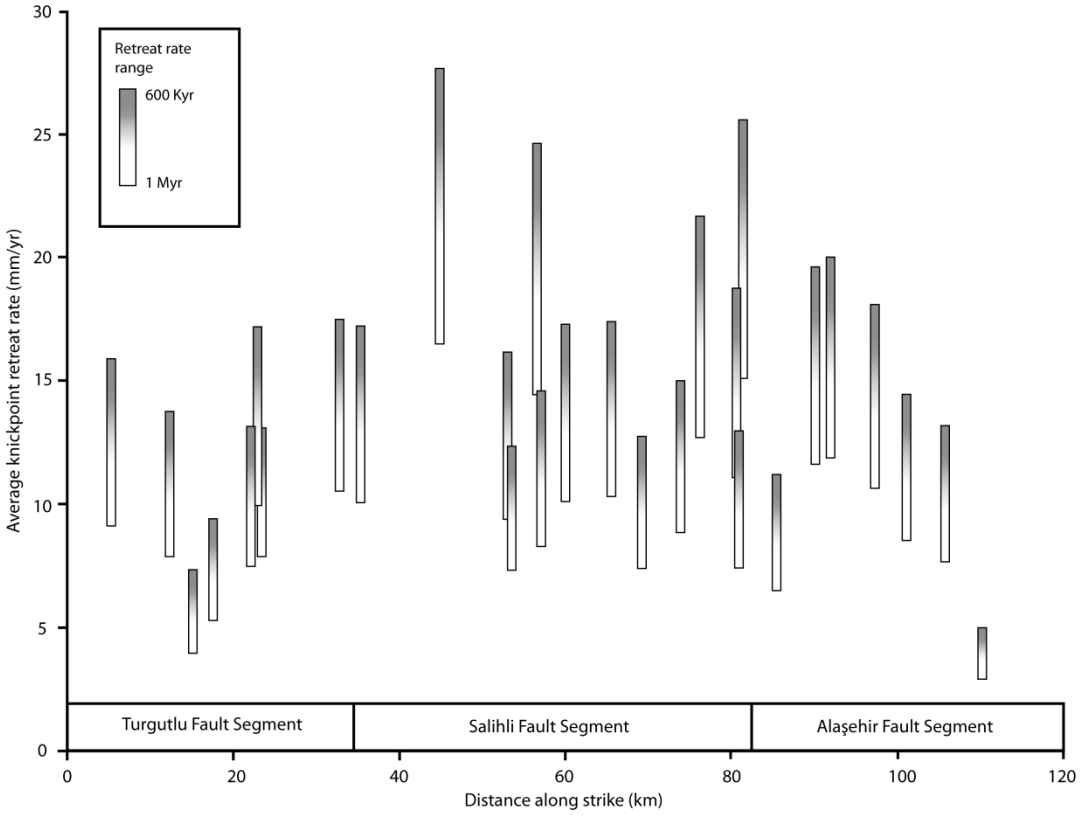

Figure 6.12: Time average retreat rates (calculated using plan-view knickpoint retreat) for knickpoints in the Gediz Graben plotted along strike. The range of the values is determined by the calculated range of time for fault linage induced knickpoint initiation of 1 to 0.6 myr.

As knickpoints retreat upstream, they transmit the effect of a relative base-level or uplift rate change to the catchment as a whole (Tucker and Whipple, 2002; Harkins et al., 2007; Whittaker et al., 2010; Whittaker and Boulton, 2012). Consequently, knickpoint retreat rates play a fundamental role in determining landscape response times in non-glaciated terrain (Whittaker and Boulton, 2012). Knickpoint retreat rates can be calculated by dividing the plan view upstream distance the knickpoint has moved from the fault by the time

since the linkage event (e.g. Bishop et al., 2005; Berlin and Anderson, 2007; Jansen et al., 2011; Whittaker and Boulton, 2012). A widely-used measure of landscape response time is the time taken for knickpoints to reach the headwaters of their catchments (e.g. Crosby et al., 2006; Harkins et al., 2007; Whittaker and Boulton, 2012). In the Gediz Graben the knickpoint retreat rates vary along strike significantly (figure 6.12). The lowest average retreat rates are found in the Turgutlu and Alaşehir Segments, with minimum values at each end occurring within the half of the segment nearest to the edge of the fault array. The minimum value within the Turgutlu Segment is 7.6 mm/yr with linkage at 600 Ka and 4.3 mm/yr with linkage at 1 Ma, while the minimum for Alaşehir with linkage at 600 Ka is 4.5 mm/yr and with linkage at 1 Ma is 2.7 mm/yr. The maximum average knickpoint retreat rates are found within the Salihli Segment and are 27.6 mm/yr and 16.6 mm/yr for linkage at 600 Ka and 1 Ma respectively. These knickpoint migration rates are comparable to those quoted in other studies over the same time periods. For example Jansen et al., (2010) calculated knickpoint retreat rates in response to galciostatic rebound of 20 mm/yr to 200 mm/yr in study sites in France. Hayakawa and Matsukara (2003) calculated retreat rates of 1.3 mm/yr to 270 mm/yr for Japanese rivers responding to ongoing tectonic uplift. The knickpoint retreat rates can also be compared to retreat rates derived for knickpoints that formed in response to an increase in normal fault throw rate for catchments located in areas of well-constrained active normal faulting in the Hatay Graben, Turkey and the central Apennines of Italy (Whittaker and Boulton, 2012). In the Gediz graben knickpoints are retreating at time-averaged rates of 2.7 mm/yr to 27.6 mm/yr. In contrast, the Hatay Graben knickpoints are retreating at rates between 0.3 mm/yr to 2.7 mm/yr. While in the Central Apennines, the knickpoints are known

to be retreating at between 1.4 and 10.7 mm/yr since a fault interaction event at ~0.8 Ma (Whittaker and Boulton, 2012). This shows that the knickpoints within the Gediz graben are moving up to 2.5 times as fast as those in the Central Apennines and 10 times as fast as those in the Hatay Graben.

However, these values may reflect differences in catchment size amongst other variables. It has been well established that the form of any stream power law (section 3.2) is a nonlinear kinematic wave with a wave celerity that can be used to represent the knickpoint retreat rate (Tucker and Whipple 2002; Whipple and Tucker, 2002; Wobus et al., 2006a, 2006b; Whittaker et al., 2008; Whittaker and Boulton, 2012). The Celerity (C_E) can be represented as

$$C_E = \Psi A^m S^{n-1} \quad \textbf{(eq. 6.6)}$$

Where Ψ is a parameter that represents all of the other controls on the knickpoint retreat velocity, including K, which embeds lithology and width narrowing that is not described by traditional hydraulic scaling assumptions (Attal et al., 2011). The dimensions of Ψ are dependent on the power exponents m and n (Tucker and Whipple, 2002, Whittaker et al., 2008; Whittaker and Boulton, 2012). When the erosion rate is dependent upon the rate of energy expenditure per unit width, (unit stream power [section 3.2]) and hydraulic width scaling is subsumed into the exponent on A, m = 0.5 and n =1, C_E should then be a function of the square root of the drainage area (Tucker and Whipple, 2002; Whittaker and Boulton, 2012). Consequently, rivers with greater drainage areas and hence discharges have knickpoints which retreat faster in a predictable way (e.g. Tucker and Whipple, 2002; Whitaker et al., 2008;

Whittaker and Boulton, 2012). As the Italian catchments are generally smaller than those in the Gediz Graben it would be expected that the Gediz Knickpoints could retreat more quickly.

If A is the dominant control on knickpoint retreat rate, the value of Ψ, which can be thought of as a drainage-area normalised knickpoint retreat parameter should be the same for all the rivers if lithology and other factors are equal.

Using the data derived from DEM analysis, the Ψ value for all the rivers in the Gediz Graben were calculated iteratively (table 6.1) by solving the following relation for the upstream position of the knickpoint, $L_{knick:}$

$$L_{knick} = L_{fault} - \frac{(\Psi\sqrt{A_{f(L)}})}{t} \qquad \textbf{(eq.6.7)}$$

Here L_{fault} is the distance downstream of the fault and t is the time since throw rate increase. A key factor of this equation is that it allows for the slowing of knickpoint retreat as a result of progressively declining drainage area upstream (Whittaker et al., 2008). Note that for similar rivers of different catchment sizes the time taken for knickpoints to reach the headwaters of a catchment should actually be the same if they all have the same Ψ. This is because bigger catchments should have faster-retreating knickpoints, but they also have proportionally longer trunk rivers, providing they follow the same L ~ √A catchment geometry scaling proposed by Hack (1957).

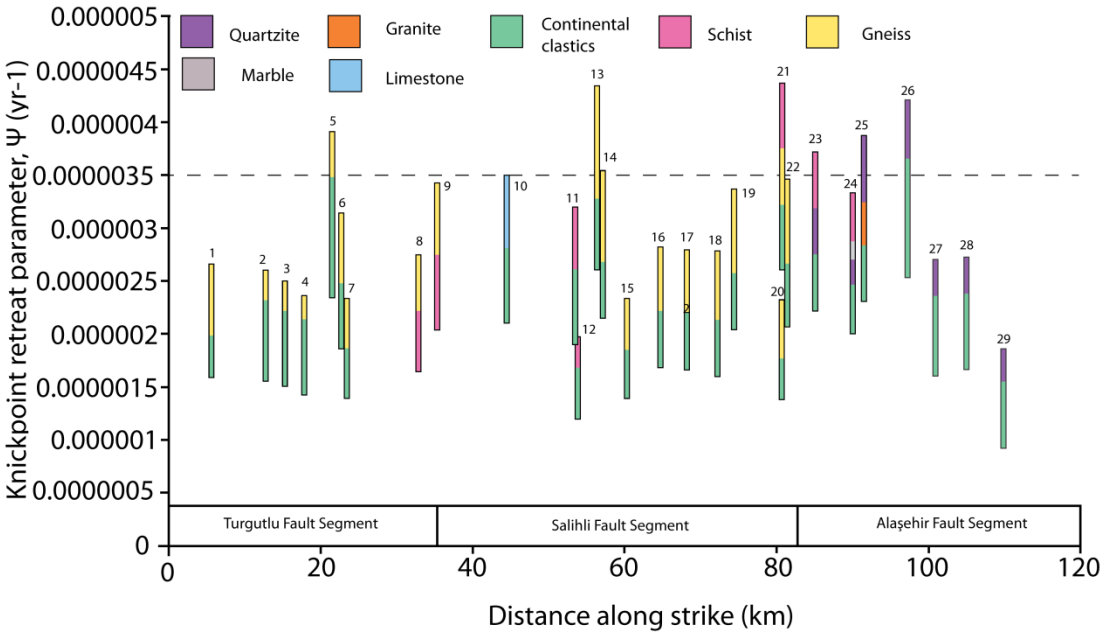

Figure 6.13: The knickpoint retreat parameters for knickpoints in the Gediz Graben plotted along strike, showing a bar range based on an oldest and youngest age for linkage at 1 to 0.6 Myr. The fill of the bars is determined by the lithologies that the knickpoints in the rivers have retreated through, up to the current position of the knickpoint in the channel.

In figure 6.13 the knickpoint retreat parameter for all the rivers is presented with the range for each river defined by the possible fault initiation timing of 1 Ma to 600 Ka. The Ψ values along strike vary by around a factor of 6, between $9.24x10^{-7}$ yr^{-1} at a linkage time of 1 Ma to $4.34x10^{-06}$ yr^{-1} when scaled for drainage area (figure 6.13). Consequently, although drainage area does explain some of the absolute differences in knickpoint retreat rate, the 6 fold variation in Ψ in the Gediz Graben shows that drainage area is not the only influence on the knickpoint retreat rate. The Ψ values for the rivers can be used to calculate typical landscape response times for the rivers in the Gediz Graben using a theoretical catchment with a 50 km^2 drainage area (an average value appropriate for the Gediz Graben rivers). Assuming that such a catchment obeys hacks scaling law (Hack, 1957) and assuming fault linkage at between 1 Myr and 600 Kyr the calculated landscape response time in the Gediz Graben

would be between 1.6 Myr and 2.7 Ma to propagate the knickpoint to within 1 km of the headwaters.

Other parameters that may influence these rates include channel gradient, if n > 1 in the stream power erosion law, lithology (i.e. bedrock erodibility) (Hack, 1973; Hack 1975; Goldrick and Bishop, 1995; Stock and Montgomery, 1999; Antony and Granger, 2001; Cook et al., 2009), sediment flux (Jansen et al., 2011) and dynamic channel narrowing effects (Attal et al., 2011).

Local climate differences can be ruled out immediately as a cause of the variation we see here, because there is no difference in precipitation rates across this small study area. However, Whittaker and Boulton (2012) suggested that knickpoint retreat rates may be sensitive to fault throw rates, even when drainage area differences have been taken into account, either because faster fault throw rates steepen the channels more effectively, and if n > 1, this would make any knickpoints migrate more rapidly, or because fault-driven channel steepening leads to dynamic channel narrowing which has a similar effect on knickpoints migration rate, even if n = 1. To assess whether Ψ scales with channel slope it is necessary to test the validity of the n=1 assumption in the celerity equation (e.g. 6.6). If n = 1 the speed of knickpoint retreat (V) is given by eq. 3.16. (Whipple and Tucker, 2002; Whittaker et al., 2007, 2008; Boulton and Whittaker, 2009) and is independent of slope. However we must now consider the validity of this assumption as for example, if n is 1 + f, where f is a positive number, it would be expected that $V = k A^{0.5} S^{f}$. The calculated Ψ values would not include this potential additional S^{f} factor. However, the drainage areas of the Gediz rivers vary between 8 km^2 and 119 km^2 and it is known that the slope of a channel is strongly controlled by drainage area as

slope decreases predictably as the drainage area gets larger as S ~$A^{-0.5}$ (Willgoose et al., 1991; Howard et al., 1994; Schorghofer and Rothman, 2002). Therefore, in order to examine for a relationship of Ψ ~S^f the effect of drainage area on channel gradients near the fault must be taken into account. Obtaining these channel slopes from the channel longitudinal profiles, and correcting them as $S\sqrt{A}$, we find that Ψ does not change significantly as drainage-area-normalised-slope increases. Consequently, we conclude that channel gradient S is not controlling Ψ, and that our assumption that n = 1 is valid (figure 6.14).

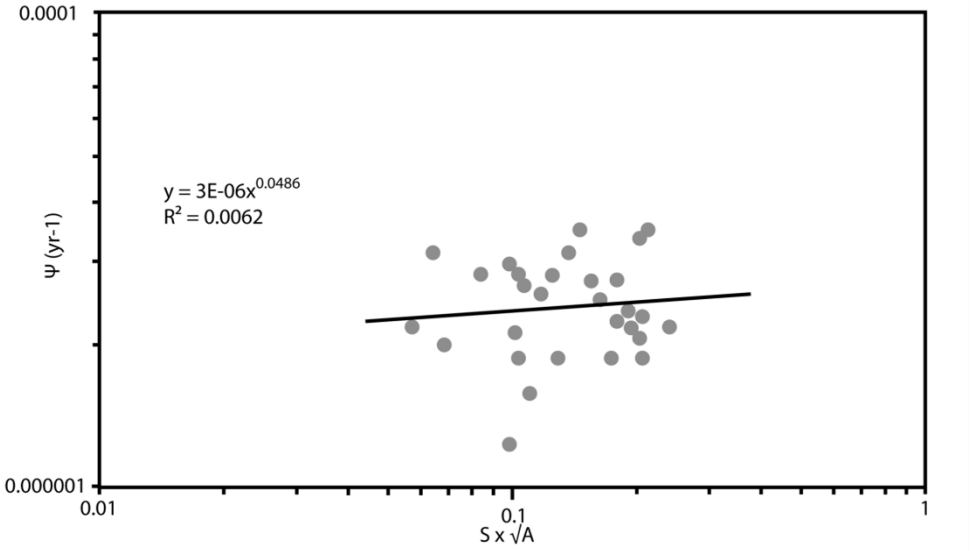

Figure 6.14: A graph showing a plot of Ψ against drainage-area-normalised-slope on a log-log plot. The graph shows that for the rivers in the Gediz Graben Ψ ~ (S√A) 0.05, with n = 1.05 for Sn-1. This relationship doesn't fit the data well. We can therefore confidently conclude that slope is not controlling Ψ, and the assumption that n = 1 is valid.

Additionally, figure 6.15 presents the Ψ data from the Gediz Graben as a function of modern (post-linkage) throw rates. Unlike the drainage area normalised slope data, it can be seen that there is a weak trend towards higher values for Ψ at higher throw rates. At calculated post linkage throw rates under 1 mm/yr for linkage at 600 Kyr the average Ψ is 2.95x10^{-06} yr^{-1}, and with a

linkage time of 1 m/yr the average Ψ value is $1.77x10^{-06}$ yr^{-1}. For higher post linkage throw rates from 1 mm/yr to the maximum of 2 mm/yr average Ψ values are $3.27x10^{-06}$ yr^{-1} for linkage at 600 Kyr and $1.96x10^{-06}$ yr^{-1} for linkage at 1 myr. This relationship was explained by Whittaker et al. (2008) as being related to channel narrowing effects which were driven by throw rate, and we propose the same effects may apply here.

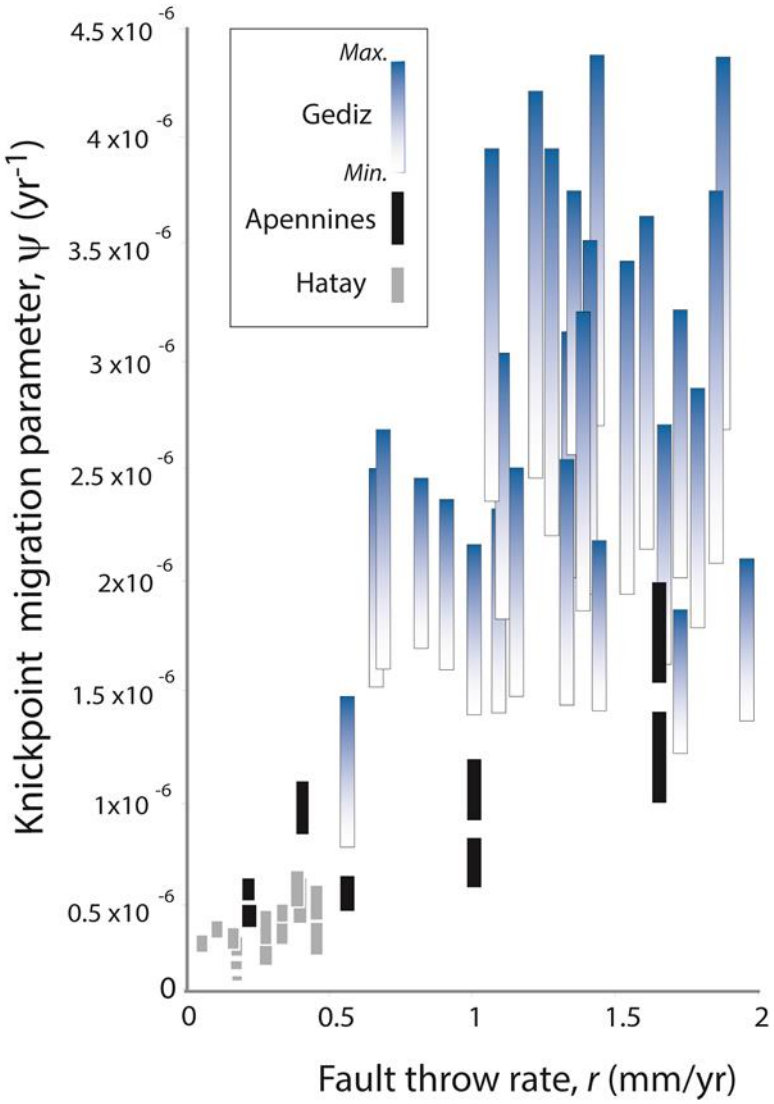

Figure 6.15: The knickpoint retreat parameter for the Gediz graben plotted against throw rate with maximum and minimum values based on linkage between 1 and 0.6 myr. The data for The Italian Apennines and Hatay Graben, Turkey, are included as black and grey bars. Additional data from Whittaker et al. (2008) and Whittaker and Boulton (2012).

It possible that the unexplained cause of the trends in knickpoint retreat rate and Ψ is a lithology effect. The Turgutlu segment and the Alaşehir Segment have retreat rates which seem to be higher than the calculated throw rates would suggest if throw rate was the main control.

In the Turgutlu segment the rivers incise through clastic sediments and gneiss (figures 6.1 and 6.13). In figure 6.13 a line has been fitted at $3.5x10^{-06}$ yr^{-1} to highlight the rivers that have a particularly high Ψ value. River 5 (figure 6.13) within the Turgutlu segment lies over this line. In river 5 the knickpoint has retreated through a channel that, by length, is around 2/3 clastic sediments and 1/3 gneiss. The distribution of gneiss and sediments in the rest of the rivers in the Turgutlu segment is similar in proportion (averaging around 45% gneiss) and location along the river and so the rock type does not appear to provide an indication of the cause of the higher Ψ value in this case. Within the Salihli Segment three rivers cross the line indicating higher values of Ψ (figure 6.13). Rivers 13 and 14 have knickpoints that have retreated through almost 2/3 gneiss and around 1/3 sediments. River 21 has a knickpoint that has retreated through 1/3 each of sediments, gneiss and schist. The lithologies in the river channels of the Salihli Segment do not seem to give an indication of why rivers 13, 14 and15 have higher Ψ values than the other rivers in the segments as the lithologies and amounts of particular lithologies do not differ from those in the rivers with smaller Ψ values. In the Alaşehir segment, rivers 23, 25 and 26 have Ψ values higher than $3.5x10^{-06}$ (figure 6.13). Each of these rivers has a knickpoint that has retreated through around 1/3 quartzite with various proportions of clastic sediments and schist, and in one river about 1/4 granite. As in the Salihli segment the rivers with higher Ψ values do not seem to have

different lithologies of amounts of lithologies than the rivers with smaller Ψ values.

Given that there few differences in the lithologies that the rivers incise through along strike between the rivers with Ψ values higher than $3.5x10^{-06}$ and the other rivers it is not clear that lithologies could be the cause of the differences in knickpoint retreat rates along strike. This does not explicitly rule out lithology as a cause of the variation; although it does mean that the differences cannot be attributed to lithologies determined from regional mapping. It is possible however, that the existing mapping of the geology does not accurately represent the lithologies found within the channels of the rivers. Additionally it could be that the lithology is not a good predictor of intrinsic rock hardness which accounts for other factors such as foliation and jointing. These differences can be highlighted in the field using measurements such as rock mass strength (Selby, 1980).

6.6.4: REGIONAL COMPARISON AND LANDSCAPE RESPONSE TIMES

These drainage area normalised knickpoints retreat (Ψ) values can be compared to existing studies both in the Hatay Graben of Turkey and in the Central Apennines of Italy (Whittaker et al., 2008; Whittaker and Boulton, 2012) (figure 6.15), both of which have rivers that incise through dominantly limestone lithologies. The most significant observation is that Ψ is much greater and therefore landscape response times are faster in the Gediz Graben than in the other two study areas. It can be seen that Ψ values for the Gediz Graben are at least a factor of two larger than those published for the Italian Apennines. The lowest Ψ values for the Gediz Graben rivers are as large as the highest values for the Italian Apennines. All the Ψ values for the Gediz Graben are significantly

greater than those from the Hatay Graben with a typical difference of a factor of 7.

Another significant observation is the relationship between throw rate and Ψ. The throw rates in the Hatay graben are all significantly less than those of the Gediz Graben, but the Gediz Graben rates are comparable to some of the rates within the Apennines. The average throw rate on the faults within the Gediz Graben is 1.4 mm/yr, while in the central Apennines and Hatay Graben the average throw rates are 0.7 mm/yr and 0.3 mm/yr, respectively. The average throw rate in the Gediz Graben is therefore double that of the Central Apennines and four times that of the Hatay graben. Ψ can be compared for rivers crossing faults with similar throw rates in the Gediz Graben and the Italian Apennines. For the Apennines the maximum Ψ of a river crossing a fault with a throw rate of 1.8 mm/yr is 1.41×10^{-6}, for a Gediz Graben river crossing a fault with a throw rate of 1.7 mm/yr the maximum Ψ is 2.79×10^{-6}. For a river crossing a fault with a throw rate of 1 mm/yr in the Apennines the maximum Ψ is 1.17×10^{-6}, in the Gediz Graben for a throw rate of 1.1 mm/yr the maximum Ψ is 3.12×10^{-6}. This shows that Ψ values in the Gediz Graben are around 2 – 2.5 times those for the same throw rates in the Apennines.

The data does appear to show that higher throw rates in the Gediz Graben leads to higher knickpoint retreat rates, but there is an important difference between the Hatay Graben and central Apennines data and the Gediz Graben data (figure 6.15). In the Hatay Graben and Central Apennines the throw rate variation can lead to a 7 fold difference in the knickpoint retreat parameter (Whittaker and Boulton, 2012), whereas in the Gediz, the throw rate variation of 0.4 mm/yr to 1.27 mm.yr gives around a maximum of a 4 fold variation.

Nevertheless, given that knickpoints crossing faults with a similar throw rate in each of the three study areas have quite different drainage area normalised retreat rates, at least one additional factor is therefore necessary to yield the variations in Ψ between the regions. One additional factor affecting knickpoint migration rate between the study areas is climate. Knickpoint celerity is scales, in reality, with discharge (for which drainage area is commonly used as a proxy). Discharge (Q) encompasses drainage area (A) and precipitation rate(p)

$$Q = pA \quad \textbf{(eq. 6.8)}$$

If knickpoint celerity (C_E) is then considered in terms of discharge, where k is constant, similar to Ψ, we can write:

$$C_E = k\sqrt{(pA_f)} \quad \textbf{(eq. 6.9)}$$

Consequently, as our Ψ is normalised for drainage area only, it implicitly includes precipitation variations which could cause differences in the Ψ values between the different areas. An inspection of equation 6.9, reveals that as the Ce scales with √p, so a factor of four difference in precipitation would be needed to produce the higher (doubled) Ψ values of the Gediz Graben compared to the Hatay Graben and Central Apennines.

The climate along the Bozdağ range today is uniform and fairly arid with modern precipitation rates varying from 500 mm/yr to 1000 mm/yr in the highest parts of the range (Turkish State Meteorological Service, 2014), while in the Apennines the precipitation varies between 750 mm/yr in L'Aquilla to up to 1500

mm/yr in the high Apennines (Whittaker and Boulton, 2012). In the Hatay Graben annual precipitation varies between 500 mm/yr to 1500 mm/yr (Whittaker and Boulton, 2012). The present day precipitation data clearly cannot explain the differences in Ψ between the areas; the Hatay Graben rainfall is not dissimilar to the Gediz Graben while the factor of 1.5 times in the precipitation rate between the Central Apennines and Gediz Graben would generate a knickpoint retreat rate 1.2 times quicker than that in the Gediz Graben, which the data shows is far from the reality.

In the past the Hatay Graben was twice as dry as it is in the present while Central Apennines was 2 – 4 times wetter than present day, and this accounted for the two fold differences drainage area normalised knickpoint retreat rate documented by Whittaker and Boulton (2012). So in order to account for the difference between the Gediz Graben and Apennines data (which has larger Ψ values than the Hatay Graben) we would require very significant increases in precipitation in the past in the Gediz Graben. Data suggests that a 4 fold increase in precipitation level within the Gediz Graben is the maximum possible difference that could have occurred in the last 5 Myr (Eronen et al., 2012). This gives a maximum past annual precipitation of around 3000 mm/yr for the Gediz Graben. The minimum estimate of precipitation an increase of 2 times present day precipitation in the past for the high Apennines gives past precipitation levels of around 3000 mm/yr. Given that a factor of 4 increase in precipitation is required to achieve the 2 fold difference in Ψ, it is not possible to precipitation to account for the total differences in Ψ.

Other possible sources of the inter-area variation include lithology and sediment flux variations (Cowie et al., 2008). The geology of the Hatay Graben and the Apennines is dominated by limestone. In contrast the Gediz Graben

has greater variation in the lithologies that form the Bozdağ Range. All but two of the 29 rivers studied have upwards of 1.5 km of continental clastic sediments directly upstream of the fault. Test of uniaxial compressive strength have shown the clastic sediments are consistently very soft (and presumably easily erodible) when compared to the metamorphic rocks found in the catchments. This significant erodibility is juxtaposed against the hardness of the lithologies that form the higher elevations of the Bozdağ Range and the majority of the river channels upstream of the fault array. These harder lithologies are dominated by schists and gneisses with additional granite, phyllite and quartzite. Although all rock types are significantly harder than the sediments they have different properties such as fractures and foliation which could theoretically lead to large differences in the intrinsic hardness and erodibility of the rocks. The following chapter will address this in more detail using field studies of rivers from the Gediz Graben to examine more specifically what might be causing the high retreat rates of the knickpoints compared to areas with similar throw rates.

6.7: CONCLUSIONS

The rivers within the Gediz Graben all contain a single knickpoint, which this study concludes were generated by active normal faulting and specifically, an increase in fault throw rates during the Pleistocene. This increase in throw rate is interpreted to have been caused by linkage of the three main fault segments of high-angle graben bounding normal fault array at some time between 600 kyr and 1 myr. The linkage event produced a faulting enhancement factor of 3 at the centre of the fault array, and the present day throw rate at the centre of the array is now estimated to be approximately 2 mm/yr. The Gediz graben has experienced significant historical earthquakes, a

notable example of which destroyed the ancient city of Sardis, and some notable earthquakes in the Alaşehir area in the 1960s. Within this study there has been an increase in throw rate at the centre of the fault to 2 ± 0.2 mm/yr from a pre-linkage rate of 0.6 ± 0.1 mm/yr. This represents around a tripling of throw rate, which should increase the frequency of seismic activity in the area. Given that chapter 4 proposes that earthquakes of up to M_w 7.6 could be expected (see 4.7.7 for details), the linkage of the faults likely increased the frequency and magnitude of significant seismic activity in the Graben.

This chapter shows that when the dependence of knickpoint retreat rate is normalised for drainage area effects there are still significant differences in the knickpoint retreat parameter along strike. Within the Gediz Graben there is a trend towards higher retreat rates with higher throw rates, although the significant increase in throw rate cannot account of all of the variations along strike in the Gediz data. The typical landscape response time implied for these rivers is between 1.6 Ma and 2.7 Ma.

When drainage-area-corrected knickpoint retreat data for the Gediz Graben are compared to other regional data from the Hatay Graben (western Turkey) and the Apennines (Italy) it is clear that the knickpoints in the Gediz Graben are retreating twice as fast on average than data published for the Central Apennines of Italy (Whittaker et al., 2008) and up to 7 times as fast as knickpoints in the Hatay Graben (Boulton and Whittaker, 2009; Whittaker and Boulton, 2012). While climate is relatively similar between the study areas, a possible source of the differences between the two areas is lithology. In the Hatay Graben and the Apennines the dominant lithology is limestone, while in the Gediz Graben lithologies are dominated by schists and gneisses. The following chapter will address this further uncertainty using field studies of rivers

from the Gediz Graben to examine more specifically what might be causing the high retreat rates of the knickpoints compared to areas with similar throw rates.

CHAPTER 7

TECTONIC AND LITHOLOGICAL CONTROLS ON FLUVIAL RESPONSE TO ACTIVE FAULTING, GEDIZ GRABEN

7.1: CHAPTER HIGHLIGHTS

- The rivers in the Gediz graben are responding transiently to the active uplift on the graben bounding fault, but the absence of fault scarps in the channel show that the incision in the rivers is keeping pace with uplift.
- Traditional hydraulic scaling models for channel width prediction, and alternative width prediction methods that include a channel gradient, fail to predict geometry of channels responding transiently to active faulting in the Gediz Graben.
- Peak measured stream powers within the metamorphic lithologies within the river channel in general scale predictably with throw rate.
- The clastic lithologies directly upstream of the active fault are, on average, 2.5 times weaker than the metamorphic rocks.
- Lithology has a significant effect on the stream powers measured at the fault when rivers incise through sedimentary rocks, reducing the stream power needed to keep pace with uplift by a factor 1.5 to 3.
- The Yeniköy River, which has abundant sediment in transport, has much lower stream power than the other rivers, even when corrected for fault throw rate and the increased erodibility of the clastic units. As the river is nonetheless incising rapidly in the Holocene (3.96 mm/yr +0.36 -0.31 mm/yr , Chapter 5), and there is no fault scarp developed in the channel,

this is interpreted as a product of sediment-flux dependent incision (a 'tools' effect *sensu* Sklar and Dietrich, 2004).

7.2 INTRODUCTION

In order to consider the impact of external factors, such as active faulting, upon bedrock rivers and their surrounding landscape, a number of landscape evolution models have been developed (Braun and Sambridge, 1997; Tucker et al., 2001; Willgoose et al., 1991; Hancock et al., 2002; Whipple and Tucker, 2002; Willgoose, 2005; Van De Wiel et al., 2007; Taylor-Perron and Fagherazzi, 2012). Due to the importance of rivers in driving erosion in these models, it is vital to be able to parameterise fluvial incision effectively. To do this, it is necessary to be able to predict accurately how channel slope, geometry and discharge and additional factors such as lithology and climate control energy expenditure and shear stresses on the bed, and thus modulate bedrock erosion in time and space (Lavé and Avouac 2001; Duvall et al. 2004; Whittaker et al., 2007b, Whittaker et al., 2008; Allan et al., 2012; Whittaker and Boulton, 2012; Mudd et al., 2014).

The detachment-limited (or bedrock) incision model (see section 3.2.1 for more information), which is usually used to model rivers incising into bedrock in mountainous regions assumes in its simplest form that fluvial incision is proportional to stream power, which in turn is dependent upon the discharge and geometry of the river. The detachment-limited model has gained support through field and modelling studies (e.g. Howard and Kerby, 1983; Seidl and Dietrich, 1992; Whittaker et al., 2007a; Attal et al., 2008; Attal et al., 2011) have suggested that bedrock rivers can be adequately described by a stream power model in many circumstances.

It is widely agreed that both hydraulic geometry and stream power are fundamental to how a river reacts to external forcing (Finnegan et al., 2005; Alto et al., 2006; Attal et al., 2008; Turowski et al., 2008; Allan et a., 2013; Ferrier et al., 2013; Cyr, 2014). Although "real" channel geometry has often been neglected in favour of empirical scaling relationships, this has led to a vigorous debate over how to best consider downstream river channel morphology within mountainous areas (e.g. Duvall et al., 2004; Tucker, 2004; Wohl, 2004; Wohl et al., 2004; Finnegan et al., 2005; Whittaker et al., 2007a; Attal et al., 2011; Ferrier et al., 2013; Cyr et al., 2014).

In detachment-limited settings, the rate of stream incision, ε, is generally modelled as being dependent only on stream power per unit area of the bed, ω,

$$\varepsilon \sim \omega \sim \rho g Q S / W \quad \textbf{(Eq. 7.1)}$$

where ρ is the water density (kgm^{-3}), Q is the discharge (m^3s^{-1}), S is the channel slope, and W is the channel width (m) (Howard et al., 1994; Whipple and Tucker, 1999; Whittaker et al., 2007a). Often, river incision laws are analysed with respect to hydraulic scaling relationships used to define downstream river morphology (e.g. Leopold and Maddock, 1953). Therefore channel geometry (e.g. W) is modelled using power-law functions of drainage area, A, which is typically used as a direct proxy for discharge, Q (Whipple and Tucker, 1999; Montgomery and Gran, 2001). Consequently, one can write

$$W = k_1 A^b \quad \textbf{(Eq. 7.2)}$$

where b is an exponent that controls the rate of widening with drainage area and k_1 is coefficient whose units depend on b. Substituting this relationship into equation. 7.1, and assuming that Q is linearly proportional to A implies that stream power scales as $KA^{0.5}S$, where K is an erodibility co-efficient that subsumes all other relevant parameters.

In landscape models this results in the assumption that slope, S, is the main variable that will respond to tectonic forcing (Willgoose et al., 1991; Hancock et al., 2002; Whipple and Tucker, 2002; Willgoose, 2005; Van De Wiel et al., 2007; Taylor-Perron and Fagherazzi, 2012). Although this model has achieved some success, it evidently neglects the role of channel width in governing fluvial erosivity, which is an important component of the response of rivers to tectonic forcing (Duvall et al., 2004; Finnegan et al., 2005; Whittaker et al., 2007b; Whittaker and Boulton, 2012),

However, Studies suggest that in reality, under the effects of tectonic perturbation, bedrock-river hydraulic geometry, in particular channel widths, can be strongly decoupled from the discharge of the river (Finnegan et al., 2005, Attal et al., 2011). In order to evaluate this possible source of error in landscape modelling this chapter will investigate the theoretical modelling of width evolution in bedrock rivers by comparing measures field values to predicted data of the sort often used in theoretical studies. One study that has contributed to this uncertainty of the prediction value of hydraulic scaling prediction of width in bedrock rivers is Whittaker et al. (2007a). They studied rivers within the Italian Apennines and found that there was a breakdown of traditionally accepted hydraulic scaling relationships where $W \sim A^{0.5}$, and subsequently the rivers had unit-stream power values around 4 times higher than those predicted using the scaling $A^{0.5}S$. These results show that modelling stream power based

on hydraulic scaling assumptions for steady-state rivers may under-predict 'real' fluvial erosivity in transient settings. This study aims to investigate the concequences of models that fix $W \sim A^{0.5}$, allowing only S to drive incision, in the Gediz Graben. They pothesis to be tested is that hydraulic scaling may not be able to capture the real response of rivers to tectonic perturbation. This is a significant concern as an increasing number of studies show that within areas of active tectonics bedrock river geometry can narrow significantly (e.g. Harbor, 1998; Lavé and Avouac 2001; Duvall et al. 2004; Whittaker et al., 2007b, Whittaker et al., 2008; Allan et al., 2012; Whittaker and Boulton, 2012; Fischer et al., 2013; Mudd et al., 2014). Consequently, constraining the circumstances in which dynamic width narrowing modulates landscape response to active tectonics remains and outstanding challenge.

An additional and important but neglected area of study is the role of bedrock lithology in determining the rate and style of bedrock river response to a change in relative base level (Stock and Montgommery, 1999; Reneau, 2000; Anthony and Granger, 2001; Bishop et al, 2005; Brocard et al., 2006). For instance, a more resistant lithology in a river channel should theoretically require a higher stream power to keep pace with tectonic uplift on a fault than the case where an identical river incises across a weaker lithology. As such, the nature of the control exerted on knickpoint retreat and bedrock incision by lithology is an outstanding issue (Castillo-Rodríguez, 2011, Crosby and Whipple, 2006; Anthony and Granger, 2007; Haviv et al., 2010; Whittaker and Boulton, 2012). Lithology is often identified by researchers as being of particular significance in modulating bedrock river response to tectonics because it affects K in any stream power erosion law ([see section 3.7 for more information] Goldrock and Bishop, 1995; Anthony and Granger, 2007; Cook et al., 2009;

Allen et al., 2013; Ferrier et al., 2013; Croissant and Braun, 2014). However, there is currently little consensus as to the magnitude of this effect nor is there currently an easy way to link measurements of bedrock type or strength directly to the K value used in either numerical models or empirical field studies. Consequently, while acknowledged as a complicating factor, it is often ignored in many geomorphic studies (Castillo-Rodríguez, 2011, Crosby and Whipple, 2006; Anthony and Granger, 2007).

The difficulty in analysing the effect of lithology on river channel geometry lies in determining the relative scale of the influence of lithology from all other possible influences in the parameter K, as currently lithology is bundled in to the K parameter along with several other variables. Another related issue is that the fluvial erosion laws may not adequately treat lithology in order to quantify incision accurately. The implication is that there can be a significant difference in the influence of the hardness of the lithology and the influence of overall rock strength, which also takes into account the presence of features such as fractures, joints and ground water flow. Consequently there is debate about which lithological parameters are most important for determining resistance to erosion. (Howard, 1998; Stock and Montgomery,1999; Whipple et al., 2000b; Sklar and Dietrich, 2001; Von Blankenburg, 2005; Jansen, 2006; Whittaker et al., 2007a; Allen et al., 2013). This study will contribute to this debate by testing they hypothesis that the softer rocks within the Gediz Graben impact significantly on the bedrock rivers by reducing the stream powers developed in rivers in response to active uplift in a way that modelling does not explicitly allow for prediction of. The variety of lithologies in the Gediz Graben make it a great place to compare and contrast between lithologies of differing hardness.

Another way in which lithology can influence the ability of a river to incise into the bedrock is sediment availability in the channel ([see section 3.7] Gilbert, 1877; Sklar and Dietrich, 1998; Sklar and Dietrich, 2001; Cook et al, 2014). If sediment flux coming from upstream is low, incision rates are limited, as there is little sediment to act as tools on the bed of the river. However, when sediment flux is too high large amounts of sediment can cover the bedrock channel and shield the bed abrasion (Sklar & Dietrich, 1998; Sklar & Dietrich, 2001).

The 'tool effect' has been illustrated through experimental techniques using abrasion mills (Sklar & Dietrich, 2001; Cowie et al., 2008; Turowski and Rickermann, 2009; Meshkova, 2012) and Sklar and Dietrich (2001) state that the rock erosion rate declines with smaller grain size in experimental situations.

With this in mind deriving the effect of lithology and sediment supply on channel response to active tectonics, and analysing how well this effect is accounted for in modelling is important. It is therefore vital to establish case studies in where the nature of both the tectonic forcing and the transient response of the river to this forcing are temporally and spatially well-constrained. Such case studies would allow for (i) the observation and modelling of hydraulic scaling adjustments to tectonic forcing; (ii) the comparison of river response to active faulting where lithological variation can be compared explicitly and (iii) where the differences between modelled, predicted and 'real' erosivities can be contrasted effectively.

This chapter addresses this challenge by presenting data on the hydraulic geometry, stream powers and substrate lithologies of six rivers draining the Bozdağ Range gathered through field study. The tectonic boundary conditions faced by these rivers have been comprehensively quantified in Chapters 4, 5 and 6 of this thesis.

In this chapter, empirical predictions of hydraulic scaling are compared to channel geometries measured in the field, and the transient response of rivers draining into Gediz Graben across active normal faults is evaluated. This will allow for comparison of the rate of uplift on the normal faults with both predicted and actual channel planforms. The predicted and measured stream power for each of the six rivers crossing the active fault will also be investigated, to evaluate how appropriate erosion-rate predictions based on hydraulic scaling relationships are to rivers responding transiently to active tectonics. This will yield detailed insights as to how the rivers in the Gediz Graben are adjusting to compensate for the increased rate of relative uplift since the mid Pleistocene. Significantly, to develop further the work in Chapter 6, the role of lithology in modulating the erosional response of rivers in the Gediz Graben will be examined, as a low-resolution evaluation of the lithology did not highlight an impact on knickpoint retreat rates, but field studies have allowed for much higher-resolution lithology mapping around the river channels. This will allow for quantification of the effect of erodibility differences between bedrock lithotypes, and the differences will be explicitly evaluated.

7.3: STUDY AREA AND TECTONIC BOUNDARY CONDITIONS

The Gediz Graben is an ideal natural laboratory to study the fluvial response of the landscape to active faulting, as the geological and tectonic influences on the system are well-constrained (see Chapters 2-6).

The Bozdağ Range forms the southern bounding range of the Gediz Graben, uplifted from the topographic graben floor by an active high-angle normal fault array, and previously (before 2 Ma) a low-angle detachment fault. To the south of the drainage divide of the Bozdağ Range the range slopes

steeply into the Küçük Menderes Graben, also bound by an active normal fault array. The range is steeper on the southern side, with the drainage divide in places offset towards the Küçük Menderes Graben, giving the range a slightly asymmetric profile (figure 7.1). The Küçük Menderes Graben experiences similar sizes of earthquakes to the Gediz Graben, the last significant earthquake in the Küçük Menderes Graben was the Torbalı earthquake, in 1928, which had a magnitude of 6.5 (Papoulia and Gülkan, 2001). Pertinent to the stream power studies is that to the presence of active faulting on both the north and south margins of the range the Bozdağ Range is a horst and the tectonic uplift across the block can be modelled to first order as being approximately uniform.

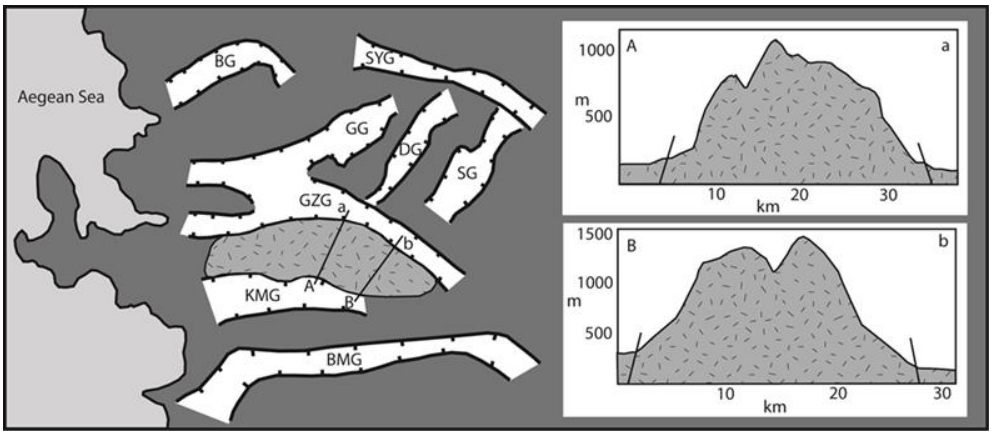

Figure 7.1: A map of the graben systems in southern Turkey. The stippled area between the Gediz Graben (GZG) and the Küçük Menders Graben (KMG) is the Bozdağ Range. The two inset profiles follow transects A-a and B-b, showing a profile of the Bozdağ Range at those points. The active normal faults on each side of the range are shown as black lines. Gördes Graben (GG), Demır Graben (DG), Selendİ Graben, Simay Graben (SYG), Bergama Graben (BG), Büyük Menders Graben (BMG).

To document river adjustment to the tectonic boundary conditions, six rivers have been selected for study (figure 7.2). The rivers were chosen to represent a variety of boundary conditions in terms of their throw rate and lithologies, and were also selected based on the level of accessibility, as field data with good spatial resolution is needed to test hydraulic scaling predictions.

The selected rivers have a three-fold spread of quantified post-linkage throw rates on the 6 rivers, ranging from ca. 0.7 mm/yr to 2 mm/yr (figure 7.3 and table 7.1).

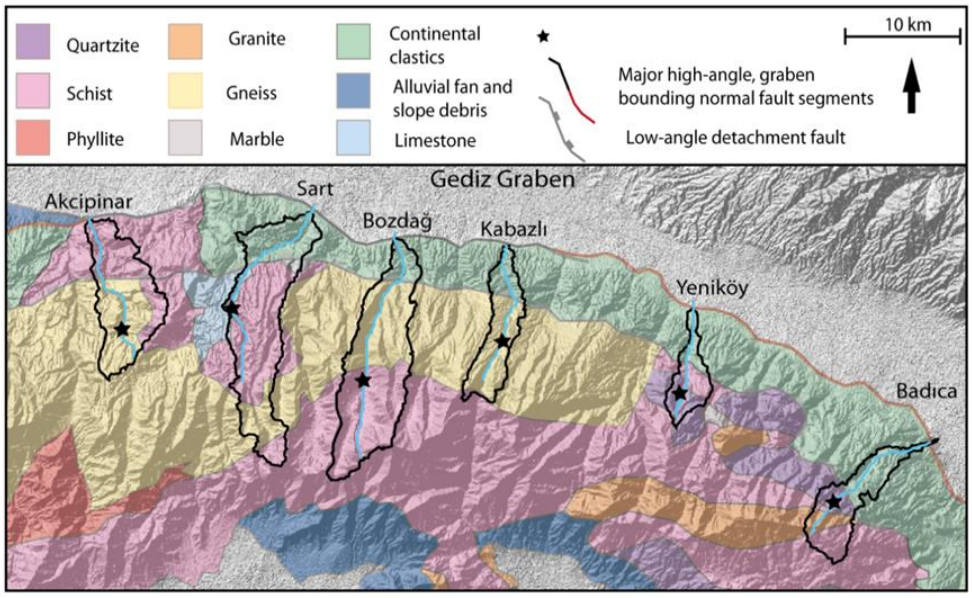

Figure 7.2: A generalised geological map of the Gediz Graben showing the location of the 6 river catchments (outlined in black) studied in the field. Black stars represent the knickpoints initiated by enhanced throw rate on the graben bounding normal fault due to fault linkage.

River	Distance along strike (km)	River length (km)	Catchment area (km^2)	% of catchment sediment	% of channel length in sediments	Whole river av. Selby (0-100)	Whole river av. rock hardness (0-100)	SRMS 2km av. upstream of fault (0-100)	Hardness 2km av. upstream of fault (0-100)	Present day throw rate (mm/yr)
Akcipinar	35.2	14.7	46.7	0	0	65	50	62	38	1.41
Sart	53	18.3	73	18	11	55	37	52	20	1.84
Bozdag	60.3	23	70.5	9	5	56	40	57	21	2
Kabazli	69	12.7	26.3	22	26	46	56	48	20	1.74
Yenikoy	85	8.2	14.5	30	44	55	40	53	20	1.37
Badinca	105.1	13.8	28.8	4	10	61	39	52	22	0.72

Table 7.1: A table of the boundary condition for each of the river studied in the field.

The highest throw rates are found in the middle section of the basin-bounding fault, around 60 km along strike, while the lowest throw rates are found towards the fault array tips. The rivers selected are a good representation of the varying distribution of throw rate in the footwall; a rate of 0.7 mm/yr is

found on the Badınca River, this is representative of a relatively distal position on the array, (figure 7.2). A throw rate of 2 mm/yr is found at the Bozdağ River, which represent the highest throw rates at the centre of the array. The other 4 rivers represent a sample of the throw rates between these extremes; the Akcipinar River crosses the fault with a throw rate of 1.5 mm/yr. The throw rate is 1.8 mm/yr for the Sart River; 1.7 mm/yr at the Kabazlı River; 1.4 mm/yr at the Yeniköy River and (figure 7.3).

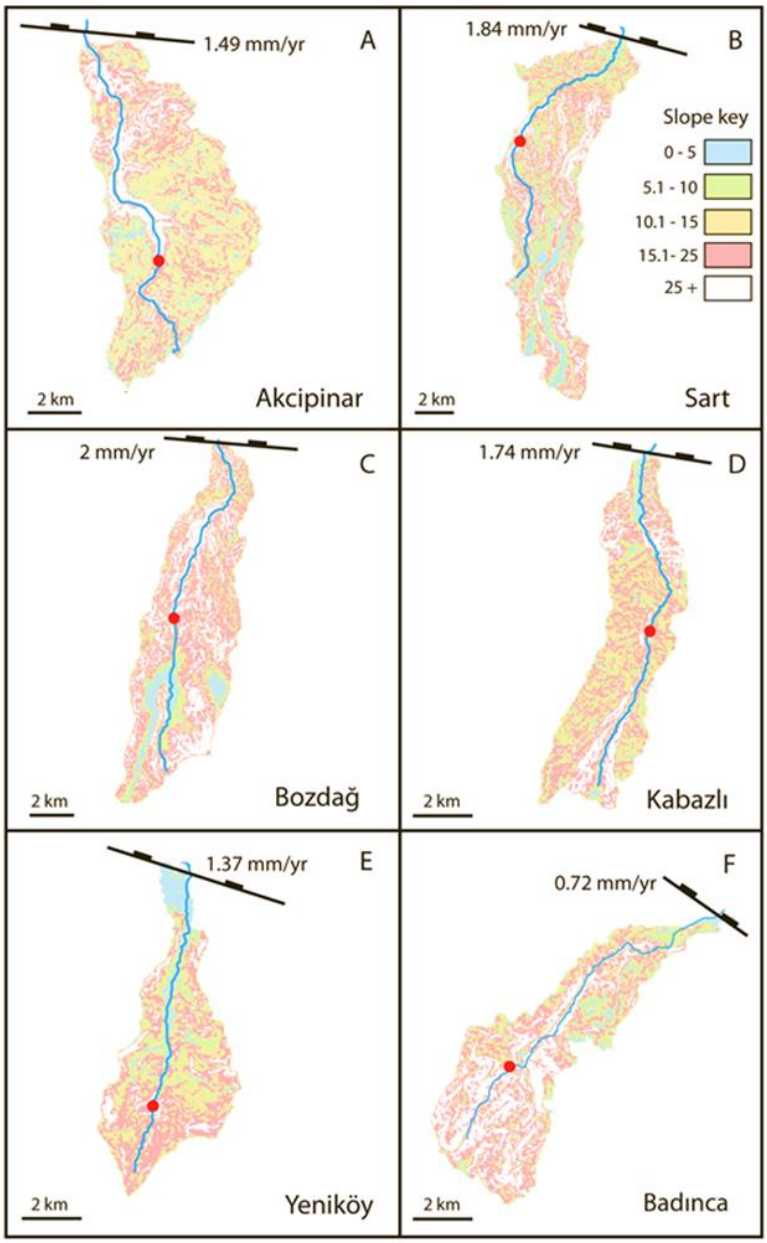

Figure 7.3: Slope maps of the catchments of the six rivers studies in the field. The maps show the location of the studied river and the position of the knickpoint in the channel. River shown along strike from west to east: A) Akcipinar River, B) Sart River, C) Bozdağ River D) Kabazlı River, E) Yeniköy River, F) Badınca River

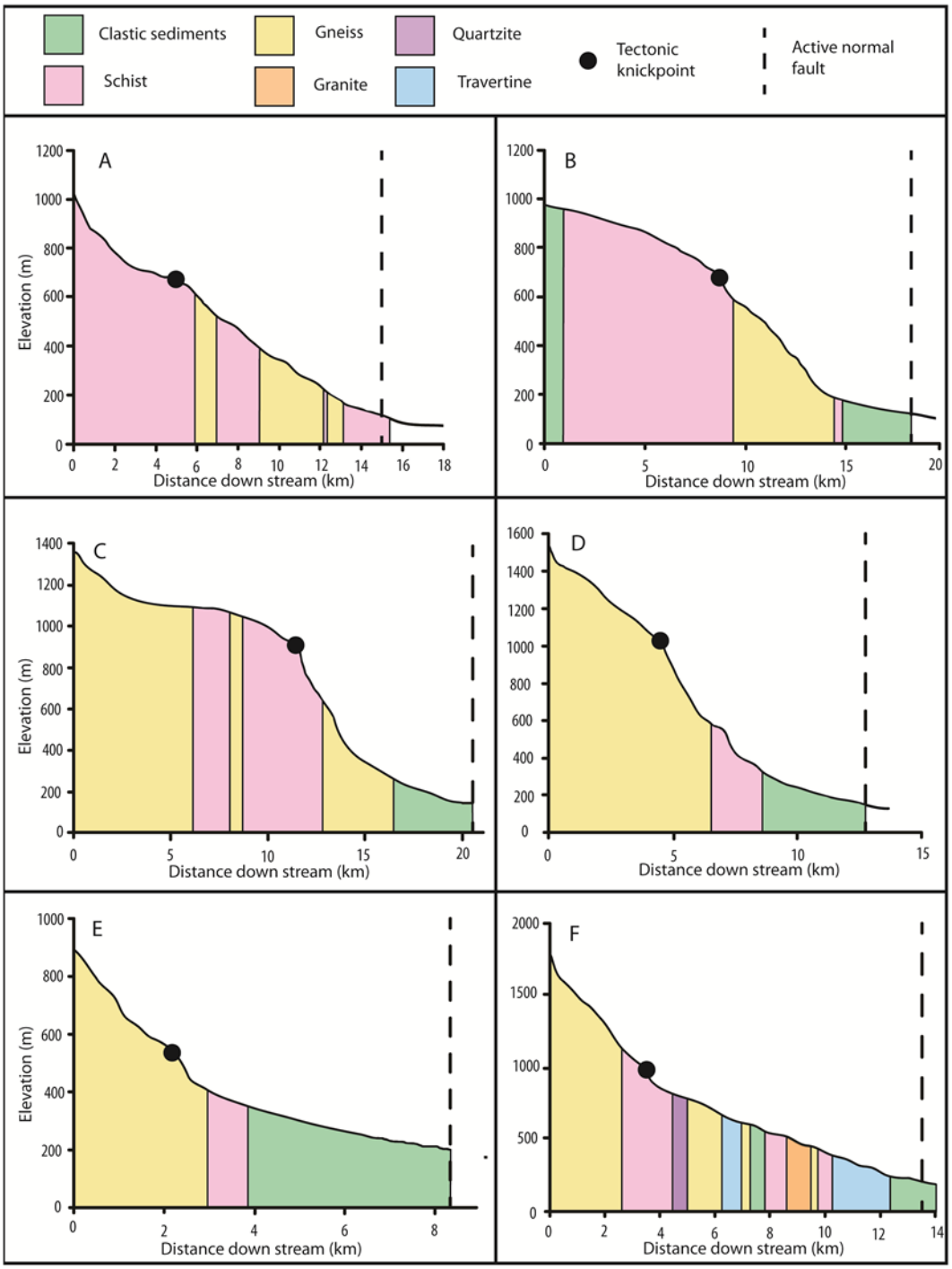

Figure 7.4: Graphs showing the river long profile for each of the river studied in the field. The area beneath the profile is shaded to represent the lithology that the river incises through. The knickpoint is marked on as a black circle and the fault is a black dashed line. A) Akcipinar River, B) Sart River, C) Bozdağ River D) Kabazlı River, E) Yeniköy River, F) Badınca River.

There are a range of lithologies along the six river channels (figures 7.2 and 7.3), including gneisses, granites, schists and clastic sediments (Ciftci,

2007; Oner and Dilek 2011). The distribution of these lithologies has also been mapped downstream for each channel based on these published maps (figure 7.3). There is considerable variety of lithologies between the channels: for instance, the Akcipinar River incises only through the metamorphic basement rocks upstream of the fault (figure 7.4), while all five of the remaining rivers incise through varying amounts of clastic sediments (figure 7.4). Some of the rivers are dominated by schist and gneiss while the Badınca River incises through quartzite in areas of the channel (figure 7.4).

7.4: METHODS

7.4.1: EXTRACTION OF CATCHMENTS AND RIVERS

Digital Elevation Model (DEM) data, was analysed using ArcGIS (Arc Map) and Rivertools software to extract key information about the selected study catchments. Topographic data was acquired from the Advanced Spaceborne Thermal Emission and Reflection Radiometer (ASTER) DEM data, with a resolution 30 x 30 metres (NASA https://wist.echo.nasa.gov/api/). Vertical errors on ASTER data are stated at 7 – 14 m in terms of standard deviation (ASTER GDEM Validation Team, 2009). Standard computational methods for extracting river long profiles, watersheds, and knickpoints locations were implemented (see chapter 6) and these were used to guide field data acquisition. In both Rivertools and Arc Map a stream network for the Bozdağ Range was created from the DEM using constructed flow directions and flow accumulation. This allowed for the selection, using RiverTools, of specific rivers that drain the flanks of the Bozdağ Range and flow into the Gediz Graben. Longitudinal profiles for the 6 study rivers were extracted from the drainage

network along the stream profile, allowing the latitude, longitude, elevation, downstream distance and upstream drainage area of study sites to be cross-referenced with DEM output.

7.4.2: FIELD MEASUREMENTS

The selected rivers were traversed in the field from the source to an elevation where the river crosses the active graben-bounding fault, entering the modern day topographic graben. Detailed channel measurements (found in appendix 2) were taken every 200 – 500 m downstream; study locations were mapped using a hand-held GPS with a spatial precision of ± 5m. In the field the following variables were measured (see appendix 2 for full data tables):

1) bankfull channel width (W_b),

2) maximum channel depth (H),

3) local channel slope (S),

4) valley width (Wv),

5) Percentage of the channel covered in sediment.

Hydraulic geometry (1 – 4) was measured using a TruPulse laser range-finder. The main source errors associated with the use of the laser range-finer to measure W_b and H are associated with selection of the surface used to measure (Whittaker et al., 2007a). The width and height of the channel were measured at bankfull stage (Leopold and Maddock, 1953; Knighton, 1998). The widths and depths measured for bankfull conditions were estimated from channel features such as the limits of active abrasion, vegetation boundaries, the highest levels of bleaching on boulders and water-washed surfaces, and the remains of high stage flood debris, following the methodologies of previous workers (e.g. Montgomery and Gran, 2001; Snyder et al., 2003; Whittaker et al.,

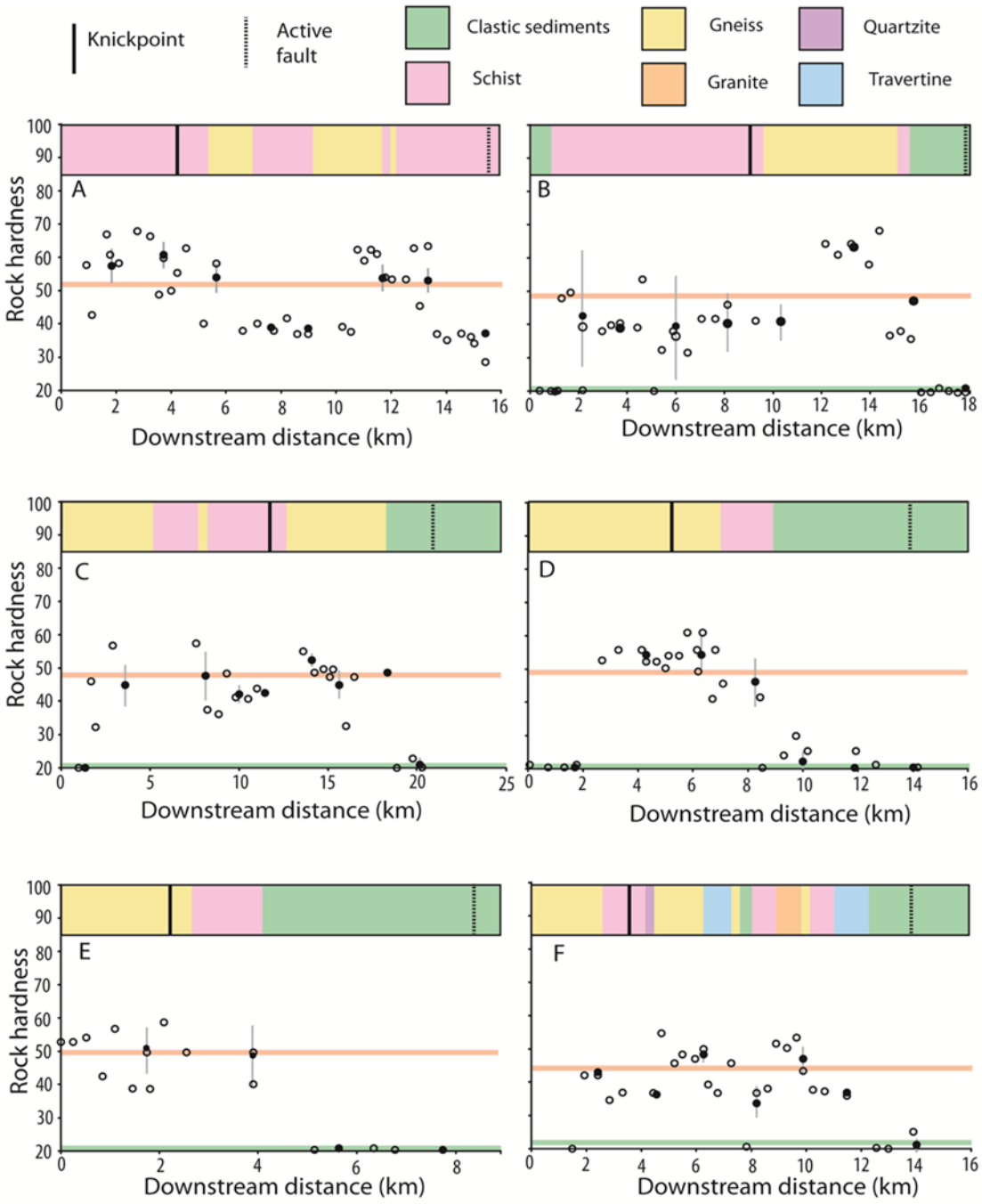

Figure 7.5: A graph showing the hardness of the rock as measured in the field (hollow circles) and hardness averaged over 2 km adjusted to lithological boundaries (black full circles). The error bars on the average measurements are 1 standard deviation. The coloured bar over the graphs shows the lithology the river incises through at that point in the channel. Also shown are the location of the tectonic knickpoint (solid black line) and the downstream distance of the active fault (dotted line). An orange line has been added to each set of river data to represent the average hardness for the metamorphic rocks, while a green line represents the average hardness of the sedimentary lithologies. Overall throughout the region the metamorphic rocks are ~2 times harder than the sedimentary rocks. A) Akcipinar River, B) Sart River, C) Bozdağ River D) Kabazlı River, E) Yeniköy River, F) Badınca River.

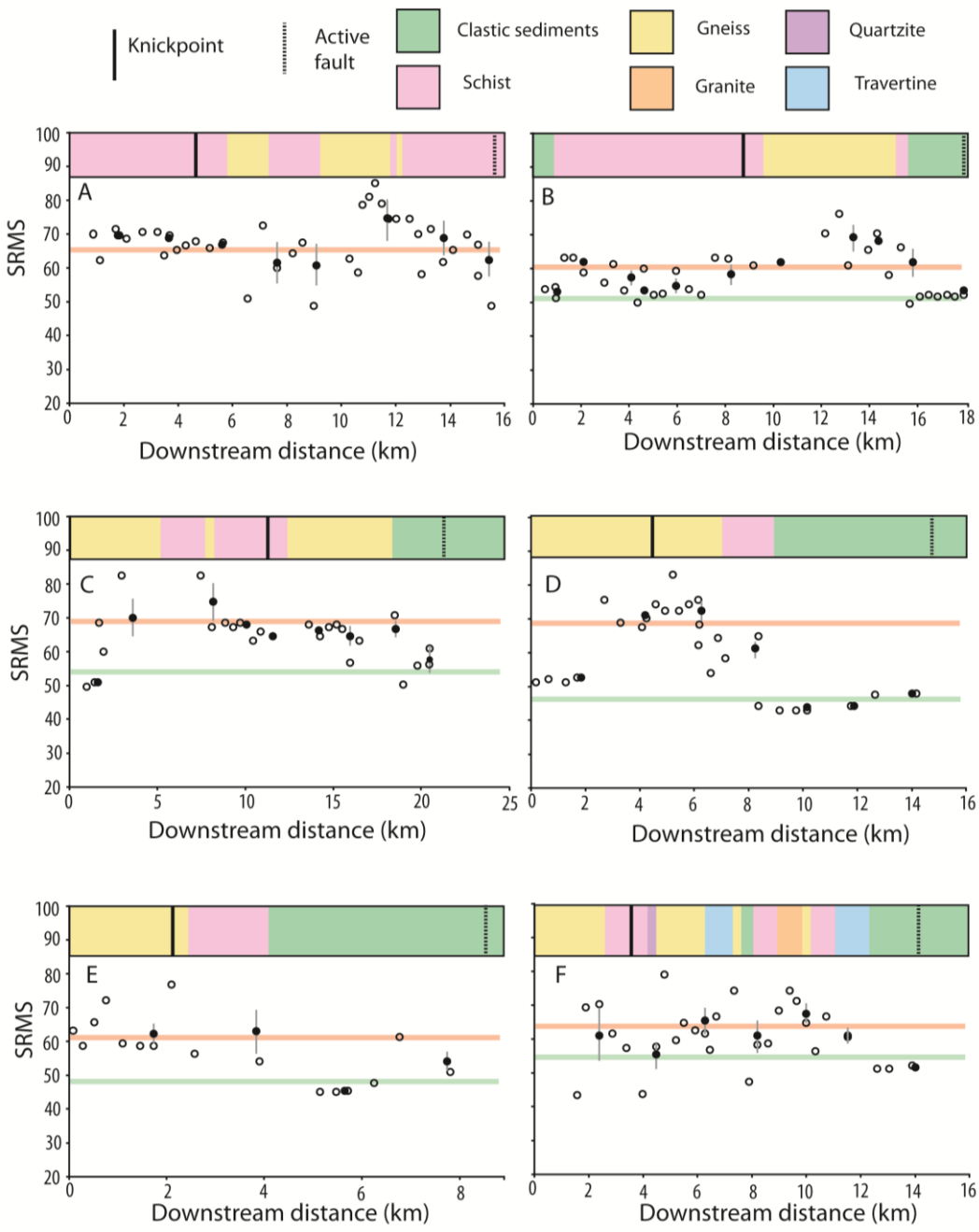

Figure 7.6: A graph showing the Selby Rock Mass Strength (SRMS) of the rock as measured in the field (hollow circles) and SRMS averaged over 2 km adjusted to lithological boundaries (black full circles). The error bars on the average measurements are 1 standard deviation. The coloured bar over the graphs shows the lithology the river incises through at that point in the channel. Also shown are the location of the tectonic knickpoint (solid black line) and the downstream distance of the active fault (dotted line). An orange line has been added to each set of river data to represent the average SRMS for the metamorphic rocks, while a green line represents the average SRMS of the sedimentary lithologies. A) Akcipinar River, B) Sart River, C) Bozdağ River D) Kabazlı River, E) Yeniköy River, F) Badınca River.

2007a). Based on these precedents, it is assumed such measurements reflect active conditions in the channel. Valley widths were measured at a standard height of 2 – 2.5 m above the bankfull depth of the river. The channel slope measurements were taken using a TruPulse laser range-finder. The measurement is representative of 10 – 30 m as appropriate for the location in which they were taken. Variation associated with hitting the target downstream with the laser range-finder gives an error of ± 0.2°; these reach level measurements were subsequently complemented with channel gradient data extracted from the DEM.

In each location where exposure allowed, the type of exposed bedrock is documented and the rock mass strength (hardness) is measured (figure 7.5). Intact rock strength was determined using a Schmidt hammer, which essentially measures the uniaxial compressive strength of the rock and can be taken as a measure of rock hardness (Selby, 1980). From this the Selby rock mass strength index (figure 7.6 [SRMS]) was also calculated (Selby, 1980). The Schmidt hammer rebound readings were made 22 times at each location and after the highest and lowest value were removed as outliers, the mean value was calculated from the remaining 20 measurements. This was subsequently corrected for the inclination of the hammer during use. The Selby index represents a semi-quantitative assessment of rock mass strength based not just on rock strength but also the degree of weathering and ground water saturation, and the orientation and size of joints and bedding. Values for the Selby index can range from 0 – 100 with soils and unconsolidated rock having values of values under 25 (Sklar and Dietrich, 2001; Whittaker, 2007). The Schmidt hammer does not easily or readily differentiate between lithologies of hardness from 0 – 20 and therefore 20 is the minimum reading recorded in this study,

representing soft and reasonably unconsolidated rocks. Because it highlights relative differences in intact rock strength and hardness (Sklar and Dietrich, 2001), it therefore gives an indication of the bedrocks resistance to erosion. This is important because intact rock strength may be a poor indicator of erodibility in heavily jointed lithologies (Whipple et al., 2000a).

7.4.3: CHANNEL WIDTH PREDICTION

In order to test how well channel width estimates predict the measured channel widths of the Gediz rivers the widths measured in the field are directly compared to the widths predicted using three different width scaling prediction methods. The three sets of predicted channel widths are based on power-law scaling relationships between catchment area and/or slope. Firstly, as many landscape evolution models and field studies assume $W \sim A^{0.5}$ (c.f. Leopold and Maddock, 1953), channel width was predicted using the hydraulic scaling introduced in section 7.1 (eq. 7.2).

Secondly, channel width was predicted using a scaling relationship proposed by Finnegan et al. (2005), which allows channels to narrow in areas of high slope:

$$W_f = k_2(A^{0.38}S^{-0.19}) \quad \textbf{(eq. 7.3)}$$

Finally, the empirical width scaling relationship derived for rivers eroding carbonate and crossing active faults in the Central Apennines of Italy, initially, proposed by Whittaker et al. (2007a) was used to predict the width of the Gediz Graben rivers:

$$W_w=k_3(A^{0.38}S^{-0.44}) \quad \textbf{(eq. 7.4)}$$

In this latter case, channel slope is modelled to be as important as drainage area in setting channel width. Each scaling relationship was used to calculate the downstream evolution of width that would be predicted for the channel using the drainage area of the river at that point in the channel and the local slope. The values of the prefactors (k_1 – k_3) for each scaling relationship were determined by selecting a k value that best fitted the downstream evolution of width as measured from field data.

7.4.4: HYDRAULIC SCALING AND UNIT STREAM POWER CALCULATIONS

Unit Stream power, ω (eq 7.1), the rate of energy dissipation against the bed and banks of a river or stream per unit downstream channel width is commonly used as an incision rate proxy for detachment-limited channels and has been used to track variations in erosivity in both quiescent and tectonically active areas (Dadson et al., 2003, Duvall et al., 2004; Whittaker et al., 2008). The width data measured in the field to calculate unit stream power for each of the six rivers measured in the field was used. Manning's equation (Manning, 1891 [eq. 7.5]) was applied to channel cross-sections measured near the fault in order to calculate fluid velocity (V) and therefore a discharge for the river at the fault.

$$V = \frac{\left(R_h{}^{2/3} \times S^{0.5}\right)}{M} \quad \textbf{(eq. 7.5)}$$

Where S is the slope of the channel or the linear hydraulic head loss, which is the same as the channel slope when the water depth is constant, M is the Manning coefficient, which is an empirical roughness coefficient. A standard roughness value of 0.03 was used for all rivers (e.g. Limerinos, J1970; Khayyun, 2008; Azamathulla and Jarrett, 2013). R_h is the hydraulic radius, which was calculated from the cross sectional area (A_{cs}) and the wetted perimeter (P), i.e.

$$R_h = A_{cs}/P \quad \textbf{(eq. 7.6)}$$

The resulting velocity estimate was multiplied by the cross-sectional area at that point to derive a discharge estimate. Because estimates of Q using this method are obviously sensitive to measurements of local channel slope and cross-sectional area, discharge variations upstream from the fault were derived by using the river drainage area to scale the predictions of Q elsewhere in the catchment. This method is more robust than applying Manning's equation independently to every study locality as discharge should vary predictably with down-system distance. The scaling of A for Q assumes that *A* is proportional to Q, which is reasonable for catchments of the size of those within the Gediz Graben (Sólyom and Tucker, 2004).

In order to compare the differences in stream power evolution between the six study rivers, the effect of varying ratios of discharge to drainage area for each river needs to be removed. To mitigate these intra-catchment variations in stream power (which imply differing effective precipitation rates), a regional median Q:A ratio from each of the six rivers was used to calculate stream powers for each channel in this study. This approach is reasonable, as rainfall rates do not vary greatly along the Bozdağ Range (Sensöy et al., 2008). This

method allowed us to calculate variations in realistic stream power between each of the rivers which were not conflating variations in implied Q:A scaling and were therefore directly comparable. The channel slopes used for the unit stream power calculations were taken from the DEM extracted data. The y/x change of the river channel over approximately 100m above and 100m below the filed measurement site were used in order to smooth out artefacts in the DEM. The unit stream powers were averaged over every 2 km of the channel, taking into account lithological boundaries in order to attain averages that are more representative of the variables along the channel.

7.5: RESULTS

All 6 of the rivers studied drain the uplifted Bozdağ Range horst block between bounding faults of the Gediz and Küçük Menderes Grabens (figure 7.1), and they enter the main Gediz River that runs roughly east-west through the Gediz Graben. Within each river a tectonically induced knickpoint has been identified; chapter 6 presented the evidence for the tectonic initiation and associated the knickpoint initiation with the linkage of the fault array. Figure 7.4 shows that the knickpoints do not correlated with lithological boundaries.

The 15 km long Akcipinar River is the trunk stream of a 47 km^2 catchment. The tectonic knickpoint is located approximately 5 km downstream (figure 7.4a). The river incises across the Gediz Graben bounding fault at a distance of 35.5 km along strike of the mapped extent of the fault, near to the town of Akcipinar. At this location the modern day throw rate after a linkage event between 0.6 – 1 Ma has been estimated at 1.5 mm/yr (figure 7.3a). The Akcipinar River incises through only metamorphic rocks exposed in the Bozdağ Range (figure 7.4a, 7.5a and 7.6a), which alternate between schist and gneiss

throughout the catchment. Schmidt hammer re-bound readings of intact rock hardness (figure 7.5a) the hardness of the metamorphic rocks varies from around 40 – 70, with somewhat weaker metamorphic rocks being found in the mid part of the stream. The Selby rock mass strength (SRMS) data (figure 7.6a), however indicate that there are limited differences in rock strength downstream for this river, with averaged values of between 60 – 70 for every 2 km adjusted to the rock type.

The Sart River is the 18 km long trunk stream of a 73 km^2 catchment. The river crosses the graben bounding fault 53.5 km from the western mapped extent of the fault, near the village of Sart and the ancient city of Sardis when the a modern day throw rate of ~ 1.85 mm/yr has been estimated. The linkage that has occurred on the fault array has resulted in a knickpoint at around 6 km downstream (figure 7.4). The Sart River incises through a combination of clastic Neogene and Quaternary sedimentary rocks which form the footwall of the fault and schist and gneiss at higher elevations within the catchment (figures 7.4b, 7.5b and 7.6b). The sediments form around 18% of the river catchment by area, while the river incises through sediments for 11% of its channel length to the fault (table 7.1). Schmidt hammer readings (figure 7.5b) indicate that the metamorphic rocks are 2 – 3 times harder than the sediments (green colours) and the Selby rock mass strength index (SRMS) of the metamorphic rocks is 1.2 times that of the sediments (figure 7.6b).

The Bozdağ River, 60 km along strike, is the 21 km long trunk stream of a 71 km^2 catchment, the source of the river is found near the village of Bozdağ. A knickpoint is located around 11 km downstream and the river crosses the graben bounding fault to the west of Salihli when the modern day throw rate is 2 mm/yr (table 7.1). The Bozdağ River incises through a combination clastic

sedimentary rocks for 5 % of the channel length (9% of the catchment) which lie close to the active bounding fault in the footwall and alternating schist and gneiss further up the catchment (figures 7.4c). Similarly to the Sart River the metamorphic rocks are on average 2.2 times harder than the sediments (figures 7.5c), while the average SRMS of the metamorphic lithologies is 1.3 times that of the sedimentary lithologies in the catchment (figures 7.6c).

The Kabazlı River is the 12 km trunk stream of a 27 km^2 catchment crossing the graben bounding fault near to the village of Kabazlı, 69 km along strike, where the modern day throw rate is 1.74 mm/yr (figure 7.3d). The tectonic knickpoint is located around 4 km downstream. The Kabazlı River incises through a combination of the softer clastic sedimentary rocks, for 22% of the catchment and 26% of the channel length (table 7.1), and significantly harder metamorphic rock which consist mostly of gneiss (figures 7.4). The metamorphic rocks are approximately 2.5 times harder than the sediments (figures 7.5d) while the average SRMS of the metamorphic lithologies is 1.4 times that of the sedimentary lithologies in the catchment (figures 7.6d).

The Yeniköy River, 85 km along strike, is the 9 km trunk stream of a 15 km^2 catchment, the source of the river is found near the village of Yeniköy. The knickpoint is about 5.5 km downstream and the river crosses the graben bounding fault near to Yeniköy village when the throw rate is 1.37 mm/yr and incises through a combination clastic sedimentary rocks which lie close to the active bounding fault in the footwall and alternating schist and gneiss (figure 7.3e). Similarly to the Kabazlı River the clastic sedimentary rocks and metamorphic rock which consist mostly of gneiss, in the case of the Yeniköy River the sediments make up around 30% of the catchment area and 44 % of the channel length (table 7.1). The metamorphic lithologies are approximately

2.5 times harder than the sedimentary rocks (figures 7.5e) and the average SRMS for the metamorphic rocks is 1.3 times greater (figures 7.6e)

The Badınca River, 105 km along strike, is the 14 km trunk stream of a 29 km^2 catchment. The river crosses the graben bounding fault to the east of the graben near to the village of Badınca, when the modern day throw rate is 0.72 mm/yr. The linkage event caused a knickpoint which is around 4 km downstream. The Badınca River catchment has the most complex geology and the river incises through occasional clastic sediments, gneiss, schist, granite, travertine and quartzite (figures 7.4f, 7.5f and 7.6f). Approximately 4 % of the catchment area is formed of the clastic sediments, which account for around 10% of the channel by length (table 7.1). The lithology is highly changeable in this catchment which leads to a variety of rock harness a values downstream between 20 – 50 (figure 7.5f). Overall the rocks appear to be a little softer than in some of the other rivers although the average SMRS values are comparable to the other catchments in the clastic sediments near the fault (figure 7.6f).

7.5.1: RIVER CHANNEL AND VALLEY WIDTHS DOWNSTREAM

A three point moving average is applied to the raw channel width data in Figure 7.7. In general, channel widths are highly variable downstream. In all rivers the averaged widths at the source of the river are significantly less than the width where the river crosses the active fault. The widths in the first 2 km of the rivers range from 0.5 m 3 m, while towards the fault in all rivers the channel width has climbed to at least 6 m. The smallest channel widths at the fault are found within the Akcipinar (figure 7.7a), Sart (figure 7.7b) and Badınca (figure 7.7f) rivers, which have an average width around the fault of 6 to 8 m. In the Bozdağ (figure 7.7c), Kabazlı (figure 7.7d) and Yeniköy (figure 7.7e) rivers, the

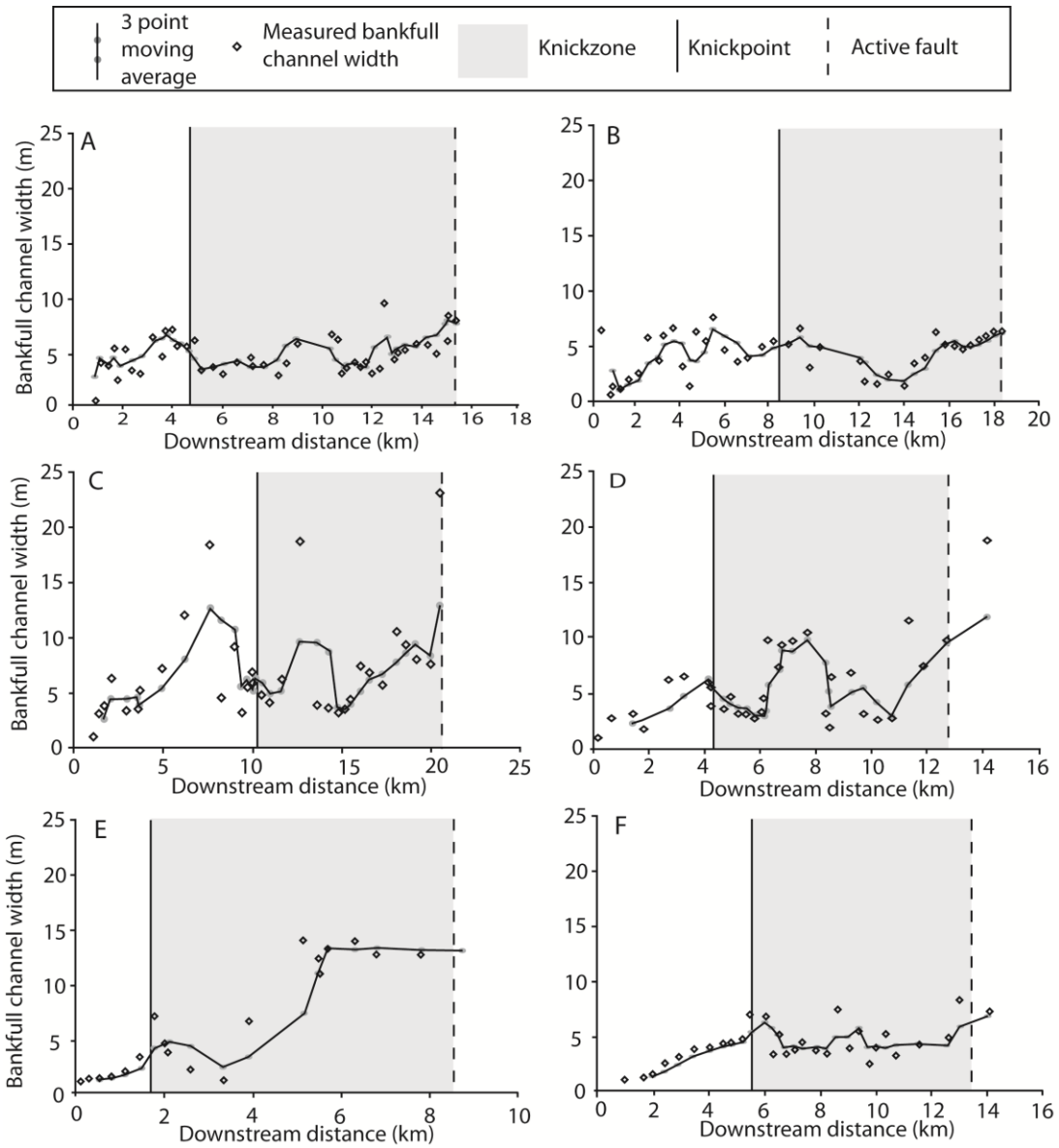

Figure 7.7: Bankfull channel widths (hollow diamond data points) measured in the filed with a laser rangefinder, and channel widths with a 3 point moving average applied (grey data points with black line) for the six studied rivers. River shown along strike from west to east: A) Akcipinar River, B) Sart River, C) Bozdağ River D) Kabazlı River, E) Yeniköy River, F) Badınca River.

channel widths at the fault range from 10 to 25 m. In general there is a lot of variation in channel width down system, but in all rivers there is a gradual climb in the river channel widths up to the knickpoint and then a significant narrowing directly around and downstream of the knickpoint, and within the knickzone upstream of the fault. The channel width plots then show a variable range of

narrow channel widths, but which subsequently increase towards the fault. The increase in channel widths within the knickzone from the initial suppression at the knickpoint coincides with the river incising through soft sedimentary lithologies lower in the catchment (figure 7.3).

The rivers within the Gediz Graben also exhibit a narrowing of valley width that varies by 10's of meters over distances of 200 – 400 m along the channel. Significantly, at the knickpoint the valley widths are low in all rivers (figure 7.8). The valleys widen through the knickzone as the sample locations approach the active fault in all rivers except the Akcipinar River, where the valley width widens significantly at the fault rather than in the approaching 2 – 4 km. This difference is likely to be due to the Akcipinar incising only through the hard metamorphic rocks, the other rivers having significant amounts of soft clastic sediments in the channel leading up to the fault. This is likely to be the reason the other river valleys widen over a greater distance, particularly the Yeniköy River, where around 30% of the catchment at lower elevations is made of sedimentary lithologies and where the channel widens predictably downstream towards the fault.

In summary these results show that there is a suppression of both channel width and valley with within the knickzone, where the values are lower than just above the knickpoint and gradually increase through the knickzone, widening significantly towards the fault. This can be seen by examining the widths in relation to the shades grey area that represents the knickzone in figures 7.7 and 7.8. The narrowing is most marked at the knickpoint and downstream. The widening in both channel and valley width coincides with the river incising into soft clastic sediments, which contrast in their hardness to the metamorphic basement rocks in the upper catchment (figure 7.5).

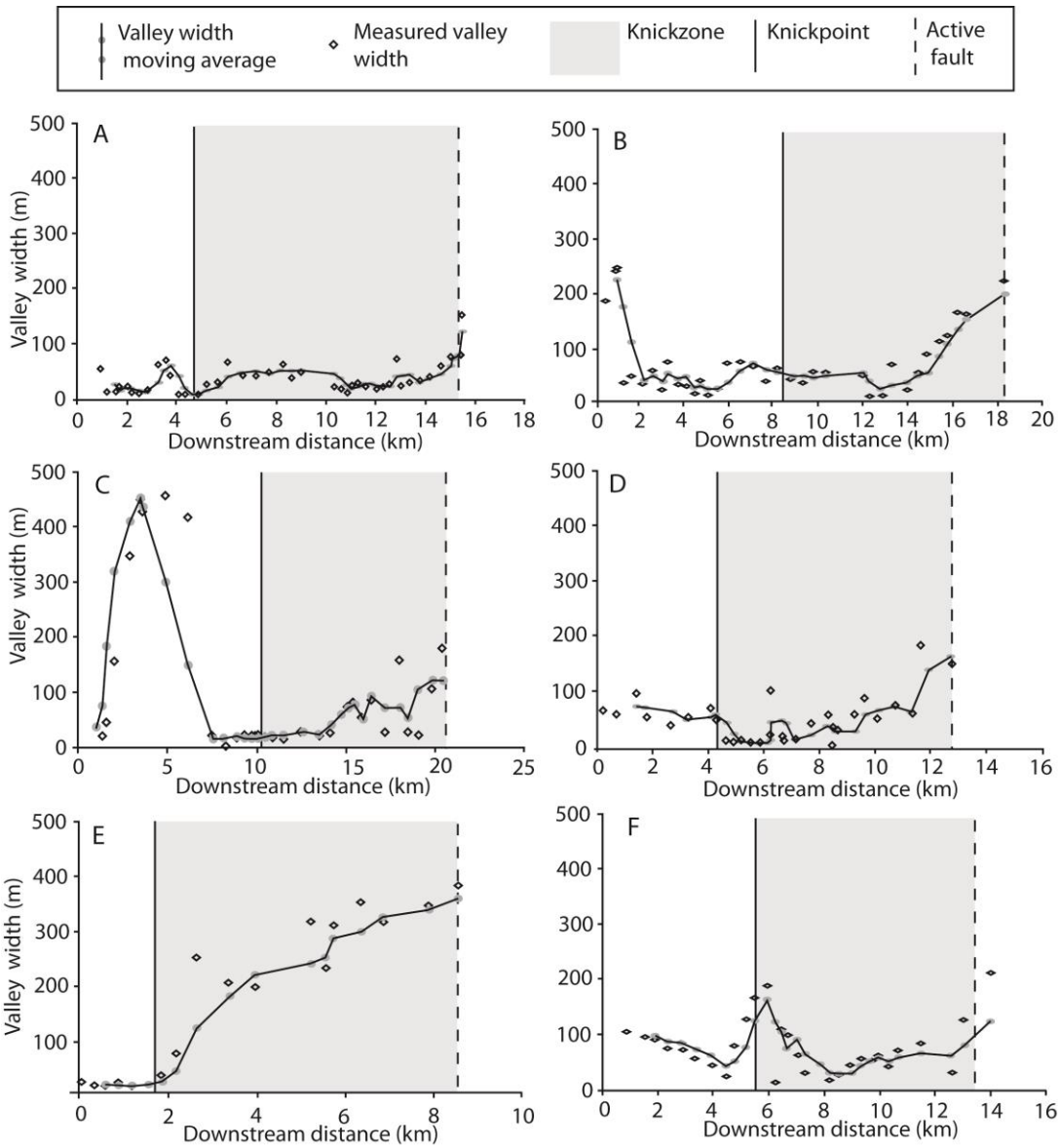

Figure 7.8: The valley widths measured in the field with a laser rangefinder (hollow diamond data points) and valley widths with a 3 point moving average applied (grey data points with black line) for the six studied rivers. River shown along strike from west to east: A) Akcipinar River, B) Sart River, C) Bozdağ River D) Kabazlı River, E) Yeniköy River, F) Badınca River.

7.5.2: DOWNSTREAM EVOLUTION IN STREAM POWER

The downstream evolution of unit stream power in each channel system gives a measure of how effectively each channel is keeping pace with the fault. For the Akcipinar River the stream power at the fault is 464 W/m^2 and the average stream power for around 2 km upstream of the fault is approximately 385 W/m^2 (figure 7.9a, table 7.2). The stream power grows progressively from

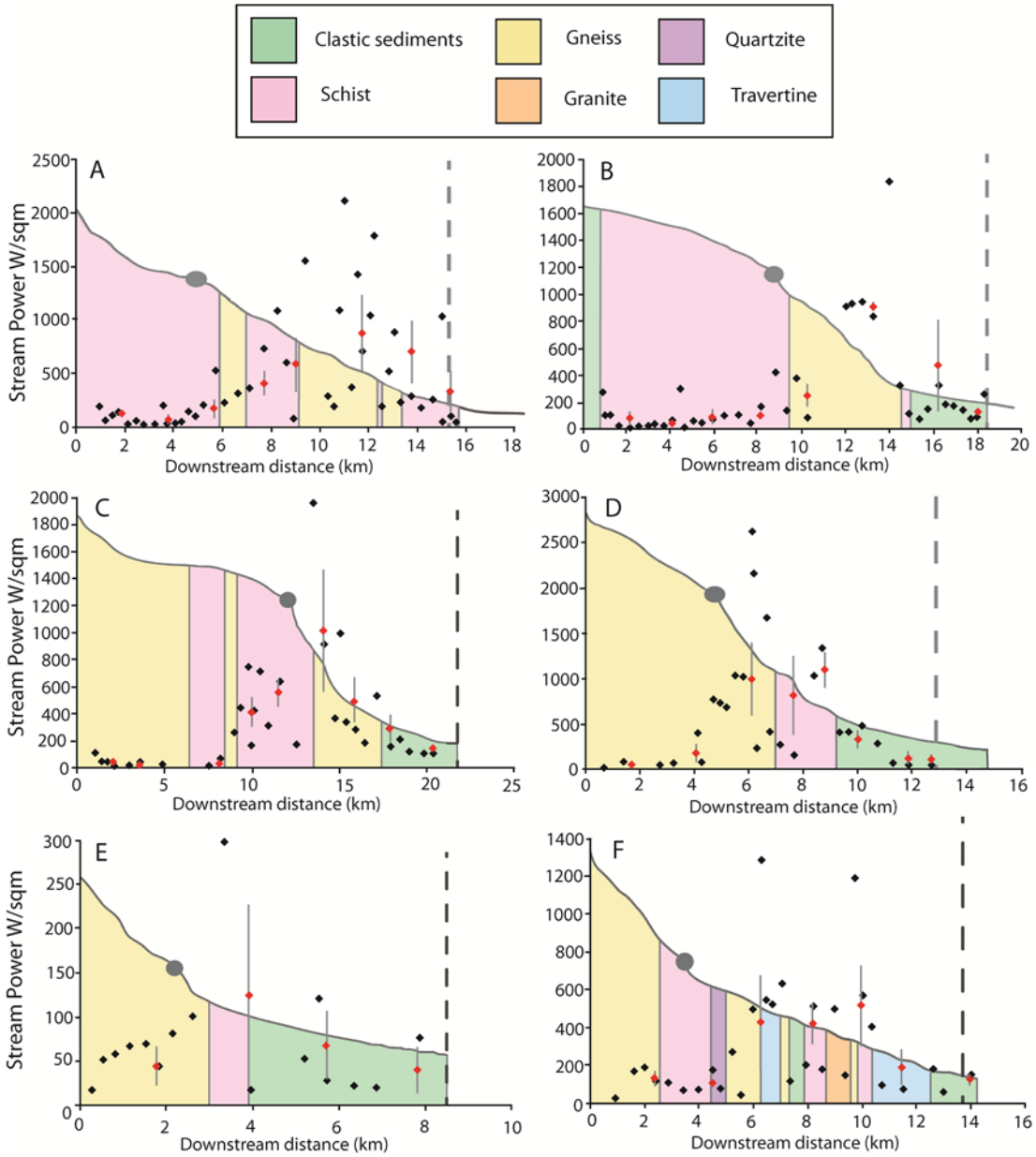

Figure 7.9: Graphs showing unit stream power calculated at all measurement locations along the rivers (black diamonds) and the unit stream powers averaged over 2 km adjusted for lithological boundaries (red diamonds). Stream power has been calculated using a regional median Q:A ratio. The average values have errors of one standard deviation. The stream powers have been superimposed over the river profile with a display of the lithologies that the river is incising though along the channel. The knickpoint is marked on as a black circle and the fault is a black dashed line. A) Akcipinar River, B) Sart River, C) Bozdağ River D) Kabazlı River, E) Yeniköy River, F) Badınca River.

minimum values of less than around 20 Wm^2 in the head waters to a maximum 2km average of 901 W/m^2 11 km downstream, and 5 km from the active fault. Clearly an obvious result of these stream power calculations is that channel

River	SP upstream of fault, 2 km av. (W/m^2)	Error (W/m^2)	SP at the fault (W/m^2)	Peak SP (W/m^2)	Peak SP, 2 km av. (W/m^2)	Error (W/m^2)
Akcipinar	384.5	133.7	463.5	2125.7	900.9	322.7
Sart	135.0	23.8	86.6	1844.9	907.7	23.0
Bozdag	143.7	25.5	114.7	2002.8	1030	459.7
Kabazli	115.6	58.8	49.4	2891	1000.0	392.2
Yenikoy	40.9	15.9	77.5	297.6	124.6	60.3
Badinca	131.5	33.5	157.3	1896.1	517	355.4

River	Throw rate increase/ decrease based upon Akcipinar	Predicted SP scaled to throw (peak SP)	Errors scaled to throw on Akipinar	FQs incisional efficiency in meta-morphic	Error assuming (~25% error on SP)
Akcipinar	1	900.9	322.7	1	0.3
Sart	1.3	1175.6	340.6	1.3	0.4
Bozdag	1.4	1277.9	652.1	1.2	0.4
Kabazli	1.2	1111.7	484.0	1.1	0.3
Yenikoy	1.0	875.3	58.6	7.0	2.1
Badinca	0.5	460.0	181.5	0.9	0.3

River	Throw rate increase relative to Badincia	Predicted SP scaled to throw rate for Badincia (W/m^2)	Error on SP scaled to Badincia (W/m^2)	FQs efficiency in sediments	Error on FQs (~25% error on Badinica SP)
Akcipinar	2.0				
Sart	2.6	336.1	84.0	2.5	0.6
Bozdag	2.8	365.3	91.3	2.5	0.6
Kabazli	2.4	317.8	79.4	2.7	0.7
Yenikoy	1.9	250.2	62.6	6.1	1.5
Badinca	1.0	131.5	32.9	1.0	0.3

Table 7.2: The measured stream powers (SP), at the fault, averaged over 2 km upstream of the fault, and 2 km averaged peak values within the metamorphic channel for the 6 rivers. The rest of the table shows the calculations performed for throw rate, lithology and sediment flux analysis.

erosivity increases towards the fault and drops significantly at the active fault. However, it is notable that stream powers are much lower upstream of the knickpoint, and only start to increase significantly downstream of the knickpoint, rising by a factor of ~9 between 5 and 12 km downstream.

The Sart River shows a similar evolution of stream power downstream to the Akcipinar. The stream power at the fault is 86.6W/m^2 and when averaged over 2 km upstream of the fault the stream power is 135 W/m^2 (figure 7.9b, table 7.2). Minimum values of around 20 W/m^2 are found in the head waters, upstream of the knickpoints but stream power increases significantly downstream of the knickpoint, progressively increasing to >900 W/m^2 at approximately 5 km downstream of the knickpoint, and 5 km upstream from the active fault. The values decrease after the peak towards the fault, corresponding to the river channel eroding through sediments (figure 7.9b). As the sediments have lower hardness and SRMS values than the metamorphic rocks in the Bozdağ Range this could be having a significant effect on the stream powers produced.

The Bozdağ River again shows a similar increase in stream power downstream with the peak values occurring around 15 km downstream and then declining with increasing proximity to the fault (figure 7.9c, table 7.2). The stream powers in the head waters are low where average stream power is 58 W/m^2, the values then generally increase towards and below the knickpoint. The maximum stream power values of 1030 W/m^2 are reach around 7 km upstream of the fault, Stream power is reduced to 115 W/m^2 at the fault and 144 W/m^2 over a distance of 2 km upstream of the fault. The sudden decrease in stream powers coincides with the incision through sediments (figure 7.9c), in a similar way to the Sart River.

For the Kabazlı River the stream power at the fault is 49.4 W/m^2 at the fault and 115.6 W/m^2 when average over the 2 km upstream of the fault (figure 7.9d, table 7.2). The stream powers are an average of 48 W/m^2 in the head waters and the values tend to increase downstream from around the knickpoint with a peak average for 2 km of the channel of 1198 W/m^2. The peak values occurs around 4-5 km upstream of the active fault. The stream powers decline from this point onwards, in a similar way to the other rivers with sediments in the channel, declining significantly at the boundary between the sediments and the metamorphic rocks.

The Yeniköy River has a stream power of 78 W/m^2 at the fault and 41 W/m^2 when averaged over a distance of 2 km upstream from the active fault (figure 7.9e, table 7.2). The stream powers in the head waters of the Yeniköy River are around the same than those near the fault with a 2 km average of 45 W/m^2 Yeniköy River. An increase in stream power occurs gradually from the headwaters with the peak value of 125 W/m^2 averaged over 2 km, occurring downstream of the knickpoint, after which the stream powers reduce significantly. The reduction in stream power occurs in the channel as it incises through sediments. However, it is noted that the magnitude of the stream powers developed in the Yeniköy River are considerably lower than for the other catchments in this study, despite the fact that the drainage area and bedrock lithologies are broadly comparable, this issue is returned to in the discussion

The Badınca River has a unit stream power at the fault 157 W/m^2 and the 2 km average upstream of the fault yields a stream power of 132 W/m^2 (figure 7.9f, table 7.2). The lowest stream powers are found in the head waters where there is an average unit stream power of 107 – 129 W/m^2. There is an overall

increase in the stream powers downstream, and significantly downstream of the knickpoint as shown by the 2 km average values in (figure 7.9f). The peak stream power of 517 W/m^2 over 2 km is at around 8 – 10 km downstream, and 6 km downstream of the knickpoint. In the 4 km immediately upstream of the active fault there is a reduction in stream power.

A noticeable trend in the stream powers for all the rivers is that they show significant increases downstream of the knickpoint, and then they decline rapidly at or towards the fault if and when soft sediments are encountered (figure 7.9). This is important when the trend is compared to the uplift field of the Bozdağ. The throw rate, and therefore uplift in the footwall of the active fault is best modelled as uniform as the Bozdağ Range can be considered to be undergoing horst block uplift due to the presence of active high angle faulting on the other side of the range, in the adjacent graben. The rivers have low stream powers upstream of the knickpoint within the channel and then elevated stream powers downstream of the knickpoint, and it is evident that the rivers are keeping pace with fault uplift due to the absence of fault scarp in the channel. Therefore, the distribution of stream power in the rivers relative to the uplift field indicate that the rivers are undergoing a transient response to tectonics.

A significant observation from the combination of data presented above that may complicate the interpretation of the stream power distribution is that the downstream development of stream power may be significantly influenced by lithology of the catchments and river channel. If the Akcipinar River is compared to the other rivers there is a measureable difference between the stream powers at the fault (table 7.2). In the Akcipinar the 2 km averaged stream power upstream of the fault is approximately 385 W/m^2, this is markedly higher than the other rivers, for example the Sart River, 135 W/m^2 and the

Bozdağ River, 115.6 W/m^2 have stream powers that are less than half that of the Akcipinar, as do the Kabazlı, Yeniköy and Badınca rivers (table 7.2). When mapped in the field it is apparent that there are dfferences between the distribution and amounts of lithologies in the rivers that are not clear from regional mapping. In particular there is a significant contrast between the lithologies of the Akcipinar and the other rivers, the Akcipinar incises through predominantly schist and a little gneiss along its whole length while the other rivers incises through weak clast sediments in varying proportions of catchment area and channel length. This raises an important question, to what extent does the high-resolution lithology of the catchment modulate the stream powers of the Gediz rivers given?

7.6: DISCUSSION

7.6.1 LANDSCAPE TRANSIENCE?

In rivers responding transiently to tectonics it is expected that hydraulic geometry will show some noticeably deviation from a downstream evolution for steady-state “equilibrium” rivers, such as valley and channel widths becoming narrower upstream of the fault and downstream of the knickpoint. Section 7.5.1 showed that both the channel and valley widths are lower below the knickpoint that would be expected given the values above the knickpoint, this suppression of width extends downstream towards the fault, with increases occurring rapidly in the few km above the fault.

Additionally, it has also been established that bedrock rivers respond transiently to changes in tectonic boundary conditions in a number observable and quantifiable ways (Keller and Pinter, 1996; Whipple, 2004; Whittaker et al.,

2007a; Attal et al., 2011; Whittaker, 2012; Kirby and Whipple, 2012; Castillo et al., 2013; Finnegan et al., 2014). Spikes in unit-stream power much shorter than the wavelength of the imposed uplift field are typically found in rivers responding transiently to tectonics. The Bozdağ Range forms a host block between the normal fault bounded Gediz Graben, and Küçük Menderes Graben, where both bounding normal fault arrays are currently active (figure 7.1). Due to the nature of the horst block, the uplift across the range can be modelled to first order as uniform uplift with a relatively constant throw. The stream power distribution downstream for the 6 rivers studied here show how the steam power increases from the drainage divide and peaks within the metamorphic rocks up to 7 km from the active fault. The stream powers only significantly increase downstream of the tectonically induced knickpoint in each of the rivers, and are consistently high downstream, throughout the knickzone. This is a spike in unit stream power that is shorter than the uplift field and implies that the rivers in the Gediz Graben are responding transiently to the active tectonics creating graben topography.

These traits of the graben rivers have enabled the bedrock rivers to adjust their ability to erode in order to keep pace with active uplift on the graben bounding fault (Wohl, 2004; Finnegan et al., 2005; Duvall et al., 2006; Whittaker et al., 2007a; Attal et al., 2008). This is evidenced by the lack of a fault scarp in the river channel at the fault. This ability to increase erosion in pace with increased uplift allows rivers to continue on their existing path without being curtailed or re-routed. As it is widely agreed that both hydraulic geometry and stream power are fundamental to how a river reacts to external forcing the rest of the discussion will investigate these factors.

The lack of a fault scarp in any of the 6 rivers implies that the rivers have responded to the change in the rate of throw and uplift initiated by the linkage of the faults 0.6 – 1 Ma. The above observations and measurements suggest that the rivers are still responding transiently to the change in uplift, as evidenced by the suppression of channel and valley widths and the stream power trends which do not fit the tectonic uplift field.

7.6.2: TESTING METHODS OF PREDICTING CHANNEL WIDTH DOWNSTREAM

A measure of channel width is required to predict stream power downstream in a river channel. In most landscape evolution models hydraulic scaling is used constrain the channel widths (Leopold & Maddock, 1953), usually with a scaling exponent of 0.5. There have been some studies that have tested the hydraulic scaling approach to estimating channel widths by comparing the estimated width to real measured data and have found that, particularly within areas of active uplift the exponent is different to the theoretical 0.5 (e.g. Duvall et al., 2004; Finnegan et al., 2005; Whittaker et al, 2007a). An additional issue that these past studies have raised is whether it is appropriate at all to assume that channel width can be modelled with reference only to drainage area.

In order to assess the validity of the $W = A^{0.5}$ hydraulic scaling relationship to the measured data the channel width data was plotted against the upstream drainage area for each field measurement location (figure 7.10) a power-law relationship of for each river was plotted in the form of (Eq. 7.2). The derived drainage area scaling relationships are shown in Fig. 7.10 and are: a) Akcipinar River, $W_b \sim A^{0.14}$, r^2 0.18; b) Sart River $W_b \sim A^{0.15}$, r^2 0.12; c) Bozdağ

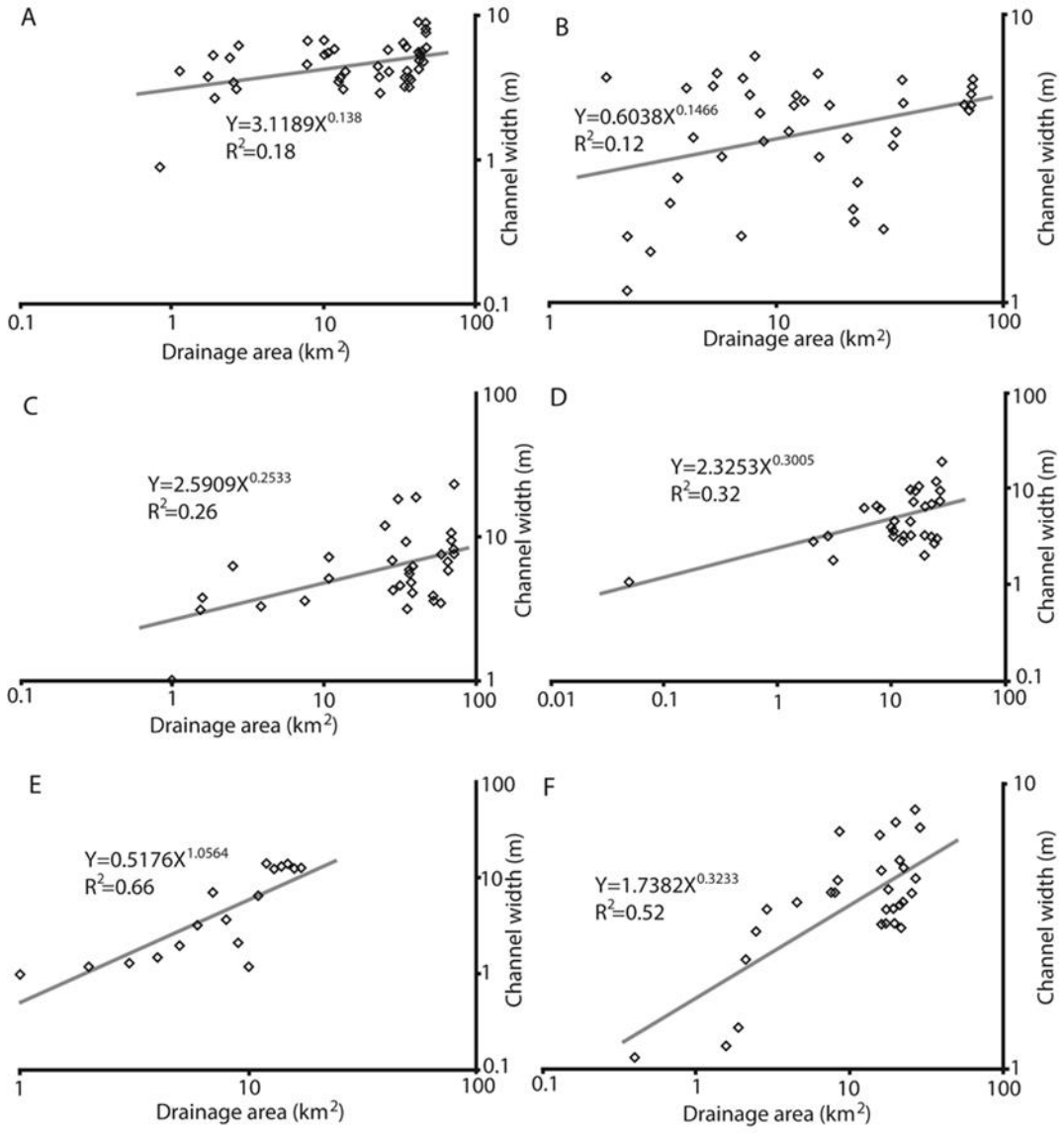

Figure 7.10: Log-log plots of the drainage area and width of the rivers at multiple points along the channel. The graphs show that the hydraulic scaling w = A0.5 does not adequately reproduce the downstream channel widths in the Gediz Graben. A) Akcipinar River, B) Sart River, C) Bozdağ River D) Kabali River, E) Yeniköy River, F) Badınca River.

River, $W_b \sim A^{0.25}$, r^2 0.26; d) Kabazlı River, $W_b \sim A^{0.3}$, r^2 0.32; e) Yeniköy River $W_b \sim A^{1.1}$, r^2 0.66; and f) Badınca River $W_b \sim A^{0.32}$, r^2 0.52. The r^2 values for the river are low and vary between 0.12 and 0.66 which shows that for the Gediz rivers a simple the discharge-based hydraulic scaling relationship is not a good way of modelling the width data for the Gediz Graben. The exponent varies significantly from the desired 0.5, the Badınca River with $A^{0.32}$ (figure 7.10f) is

the closest to 0.5, and in all cases but the Yeniköy River with $A^{1.1}$ (figure 7.10e) the exponent is smaller than 0.5.

As traditional hydraulic scaling is obviously a poor predictor of channel widths within the Gediz Graben, and subsequently would produce erroneous estimates the erosive power of the Gediz Rivers alternative methods of width prediction have been evaluated. The measured channel width from all six studied rivers have been compared to the widths predicted by two additional width scaling methods proposed and previously assessed by Finnegan et al. (2005) and Whittaker et al. (2007a). The additional width scaling relationships by Finnegan et al. (2005) and Whittaker et al. (2007a) are introduced in section 7.4.3 and use a modified form of the hydraulic scaling relationship that allows for inclusion of slope in the width predictions, allowing channel narrowing in areas of high slope.

The actual channel widths were compared to these two models by plotting the measured widths from field data against the best-fit predicted widths using the equations in section 7.4.3 (figure 7.11). If the width prediction methods accurately reproduce the measured widths of the river the line of best fit would have a gradient of 1 and an r^2 value approaching 1. The value of the k prefactor was changed to fit the line of best fit as close to a gradient of 1 as possible. In the case of the Whittaker method the r^2 values for all the rivers apart from the Yeniköy are negative and between -1.40 and 0.24. The r^2 value for the Yeniköy River was 0.6. For the Finnegan method the Yeniköy River again produces the best the r^2 value, 0.75, while the values for the other rivers are much lower, between -0.71 and 0.24. Overall it seems that all these width scaling methods are very poor predictors of river channel widths for the Gediz

Graben rivers, which are not only undergoing a transient response to tectonics but which also erode variable lithologies.

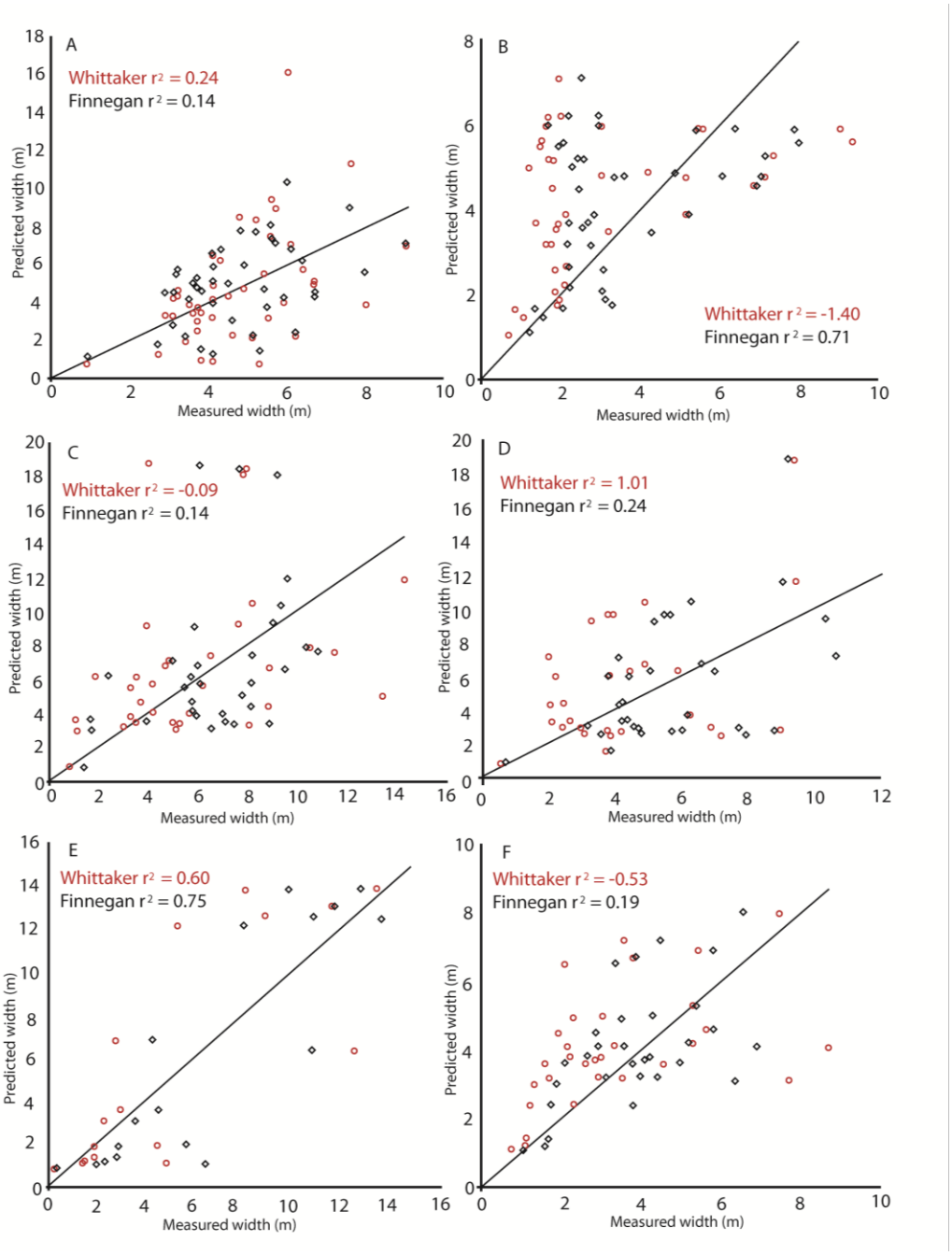

Figure 7.11: Channel widths measured in the field plotted against predicted widths using the Whittaker and Finnegan equations. The Line of best fit is set to a gradient of 1 and passes through the origin. The r2 value of the fit of the two data sets indicates how well the prediction methods match the actual data. The data shows that the methods are poor predictors of actual channel width, due to generally very low to negative r^2 values.

These results suggest that the use of hydraulic scaling and/or other width prediction techniques in landscape modelling are likely to lead to inaccurate

results when propagated through landscape models, and that existing modifications to hydraulic scaling laws do not translate well to other field areas. These data suggest that channel width measurements, derived from either field data and/or remote sensing methodologies must be made to properly model channel erosivity in areas of active faulting where footwall rocks are highly variable.

7.6.3: THE INFLUENCE OF THROW RATE ON THE STREAM POWERS OF THE GEDIZ GRABEN RIVERS

Fault scarps were not observed within any channels so it is clear that incision in the rivers is able to keep pace with tectonic uplift near the active graben-bounding fault. As it is clear that all the rivers studies are keeping pace with the uplift it is then possible to compare stream powers developed at the fault to evaluate the extent to which along-strike variations in throw rate can explain the differences in stream power. If the stream powers are not proportional to the throw values on the fault in the location of the river there must be other factors at play that modulate the response of the river on top of tectonics. In order to avoid very local peaks and troughs in stream power, and to gain a more representative view of the processes occurring with the rivers, 2 km averaged bins of unit stream power will be used for this analysis.

From observations in the field and measurements using a Schmidt hammer it is obvious that the clastic sediments within the catchment are much softer, and therefore more easily eroded. As seen in the plots of stream power downstream for each of the rivers (figure 7.9) in the rivers where there are sedimentary lithologies upstream of the active fault there is a significant reduction in the stream power, and this is returned to below. However, to

compare the effect of tectonic throw rate on the stream powers the peak 2 km average value will be examined as this lies within the harder metamorphic lithology in all cases. Data will be compared with respect to the Akcipinar river, where the catchment and channel bed comprises 100% metamorphic lithologies and therefore provides a good calibration point. In this analysis, the Bozdağ Range is assumed to be uplifted as a horst block (figure 7.1) and uplift rate is taken to be uniform across the horst block. Consequently, the rate experienced by the river in the area of peak stream power should be representative of the magnitude of the throw rate at the fault.

If the tectonic uplift occurring in the Gediz Graben is the only factor determining the stream power of the rivers (and hence their incision can be described a simple 'detachment-limited' erosion model) it would be expected that the stream powers would be proportional to the uplift rate estimated for the active normal faults. The present day throw rates determined in chapter 6 (table 7.1) show an approximately 3 fold difference in the throw rates between the rivers, so if throw rate is the only factor influencing stream powers in the rivers, it should be possible to observe a similar scaling in the stream powers. Assuming block horst uplift, the 100% metamorphic Akcipinar River's stream power can be scaled by the throw rate experienced by the other catchment to investigate this quantitatively.

In the Akcipinar River peak stream power is 901 W/m^2 for a throw rate of 1.4 mm/y (figure 7.12 and table 7.2). When the peak stream power value for the Akcipinar River is scaled to the throw rates on each of the other rivers, a predicted stream power that should be developed for each river within the metamorphic lithologies is obtained (table 7.2 and figure 7.12). A peak stream

power of 1278 W/m^2 would be expected for the Bozdağ River to account for the higher 2 mm/yr throw rate at the centre of the fault array (figure 7.12).

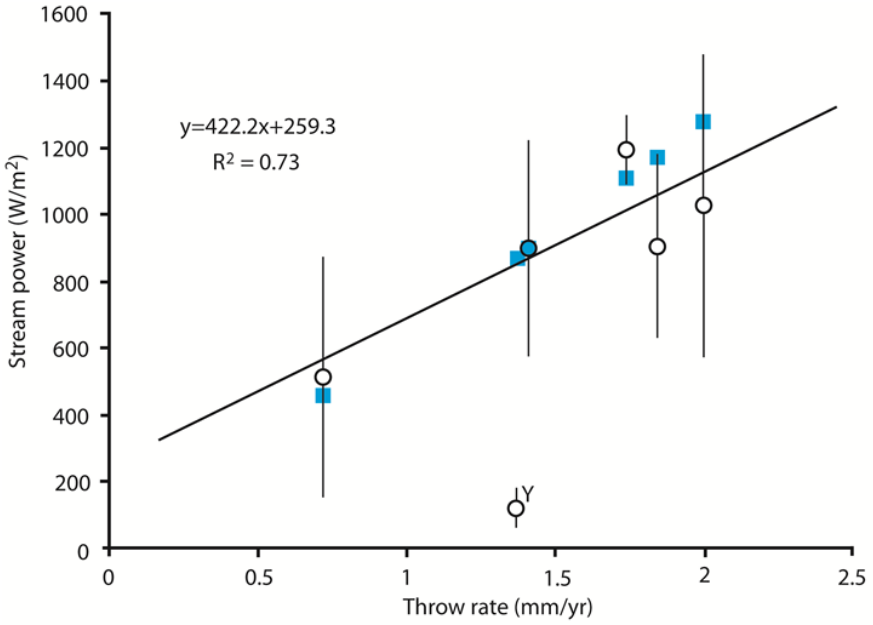

Figure 7.12: A graph showing the predicted stream power scaled to the fault throw plotted against the throw rate based upon using the 100 % metamorphic Akcipinar River peak steam power as a control (blue squares). Also plotted are the actual peak stream powers for each river, averaged over 2 km (hollow circles with a 1 standard deviation error). The peak stream power was used as this is the maximum stream power value, found within the metamorphic lithologies in each catchment, which makes the values comparable without the added influence of the rock hardness of different lithologies affecting the stream powers. A line of best fit has been plotted through the actual peak stream power data for all rivers excluding Yeniköy (indicated with a Y), as the Yeniköy River is a significant outlier to the data with another significant moderating factor in addition to tectonics.

Additionally for the lowest throw rate on the studied rivers, for the Badınca River a peak stream power of 460 W/m^2 would be expected due to the lower throw rate of 0.7 mm/yr (figure 7.12). When the Akcipinar River is used for as a guide for the expected stream power dependent on throw rate there is between a 0.89 and 7.03 fold difference between the predicted stream power values and the actual stream powers measured in the rivers near the fault (figure 7.12). For the Sart, Bozdağ and Kabazlı Rivers the peak stream powers scale well with throw rate, there is a 1.3, 1.2 and 0.9 factor difference between

the predicted and actual results respectively (figure 7.12). The Badınca River is has a 0.9 factor difference with a slightly higher peak stream power than would be expected, although in this river, there is a far more complex upstream geology than in the Sart, Bozdağ and Kabazlı Rivers that are formed only of gneiss and schist, this could explain the variation. In all cases, taking into account the spread in stream powers within the 2 km averaging interval, a linear dependency of stream power on throw rate is a good descriptor of the data. For a zero throw rate, a stream power of 259 W/mw is predicted, which would represent the 'background' stream power developed in rivers of this size, incising the same lithology, but which are not being perturbed by active tectonics.

The same type of analysis can be undertaken to examine the possible impact of sedimentary (clastic) bedrock on the stream powers of the rivers, assuming again that they are incising at a rate equal to the fault throw rate. For ease of scaling, the river with the slowest throw rate, the Badınca River (0.7 mm/yr) is used to conduct this analysis. If throw rate is a primary control on the stream power in the sediments the stream powers for other rivers incising through sedimentary lithologies would be expected to be higher in order to counteract the higher throw rates in the other rivers. Figure 7.13 shows the stream powers scaled to throw rate (blue squares) in a similar way to figure 7.12, but this time using the Badınca River stream power scaled to throw rate and the stream powers in the sedimentary rocks 2 km upstream of the fault (hollow circles). The Akcipinar River is included for comparison but is excluded from this aspect of the analysis as it has no sedimentary lithologies with its catchment.

The stream powers within 2 km of the fault in rivers incising through sediments do not appear to increase with throw rate in the way that the peak stream powers in the metamorphic rock do. All of the measured stream powers in rivers with sediments are lower than the stream power in the Badınca River, and within the errors on the values they actually do not scale with throw rate at all. This shows that the stream powers in the downstream areas of the catchment are not scaling to a factor of three difference in the throw rate as they do within the metamorphic rocks.

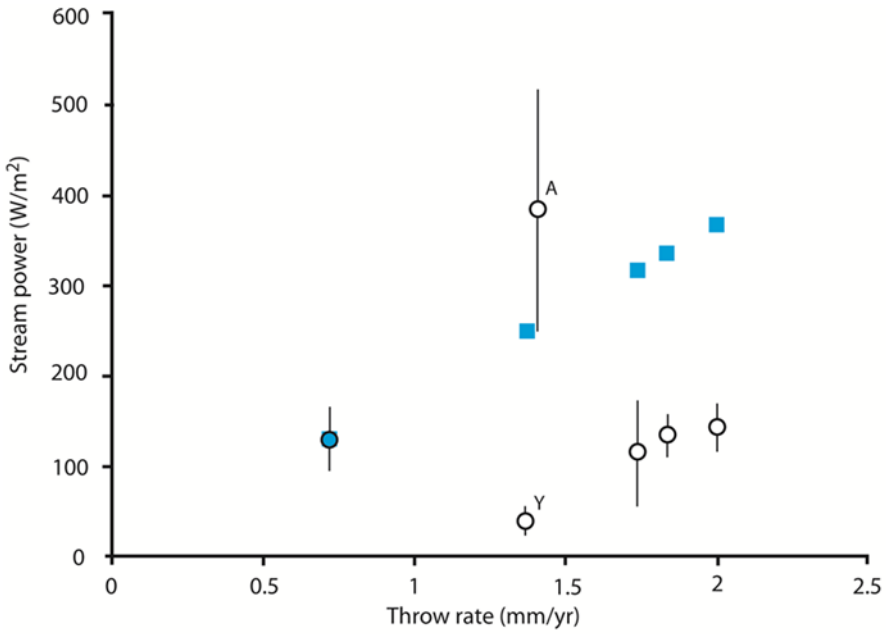

Figure 7.13: A graph comparing stream powers as a function of throw rate in the sedimentary rocks averaged over the 2 km upstream of the fault (hollow circles). The Badınca River has been used to create predictions of what the stream powers be in the other catchments dominated by sedimentary rocks at the fault (blue squares). The stream power in the Akcipinar catchment at the fault is also shown for comparison (A) and the Yeniköy River is marked Y. This graph shows that unlike in the metamorphic dominated upstream areas, stream powers in the downstream part of the catchment in the clastic sediments are not sensitive to a factor of 3 variation in throw rate.

Overall it is clear that the throw rates exert a first order control over the stream power within the metamorphic lithology present upstream in all rivers.

Figure 7.13 also shows that this primary modulation of stream power by throw rate breaks down when stream powers in the 5 rivers containing sedimentary rocks is considered. The lack of a fault scarp in the river channel shows that the rivers are incising at a rate that keeps pace with uplift, this means that tectonics exerts a significant influence over the stream powers developed in the rivers as the river have developed a stream power level that counteracts the uplift. But, that the sedimentary lithologies have a very significant impact of the stream powers of the rivers, overriding the effect of throw rate magnitude when they exist in the catchment.

The Yeniköy River is an outlier to the tectonic first order control over stream power development in the peak stream powers. There is a 7 fold difference between the predicted stream powers corrected for throw and calculated peak stream power values. The actual peak stream power developed is a lot smaller than would be expected (figure 7.12 and table 7.2) if throw rate was a primary control over the stream power in the Yeniköy River. However, as it is clear that the lower stream power still keeps pace with the uplift as there is no fault scarp in the Yeniköy River, there must be another factor at play that allows the Yeniköy River to keep pace with the uplift. There is a significant amount of clastic sediment in this river, around 30 % by catchment area and 44% by channel length within the catchment that vary significantly in their hardness form the metamorphic. The Akcipinar by contrast has a catchment and channel that is 100% metamorphic (figure 7.4 and 7.5). As all rivers but the Akcipinar have clastic sediment upstream of the fault is possible to investigate the effect that sediment is having on stream powers further in section 7.6.4.

7.6.4: THE INFLUENCE OF LITHOLOGY ON THE STREAM POWERS OF THE GEDIZ GRABEN RIVERS

Bedrock lithology is an important a factor in determining the rate and style of bedrock river response to a change in relative base level (Stock and Montgommery, 1999; Reneau, 2000; Bishop et al., 2005; Brocard et al., 2006; Anthony and Granger, 2007; Cook et al., 2009). The more resistant the lithology in the river channel the higher the stream power required to keep pace with the uplift on the fault. The precise nature of the control exerted on river response to tectonic perturbation is an outstanding issue that clearly requires additional work (Castillo-Rodríguez, 2011, Crosby and Whipple, 2006; Anthony and Granger, 2007; Haviv et al., 2010; Whittaker and Boulton, 2012). One of the most significant issues with this appears to be deciding on the relative scale of the influence of lithology, as currently lithology is bundled in to the K erodibility parameter, along with several other variables. Therefore the stream powers for the Gediz rivers can also be studied in light of the metamorphic and clastic lithologies that have been documented in the river channels to address how lithology can modulate stream powers in the study area (figure 7.14).

When the SRMS data for the metamorphic lithologies are examined there is little difference between the overall strength rating of the gneiss and the schist (figure 7.6). When only the Schmidt hammer reading for rock hardness are considered the measured hardness of the rocks vary significantly (figure 7.5), especially between the metamorphics and the sediments. Overall the gneiss and schist are of similar hardness although the schist appears to vary more, being slightly weaker than the gneiss in some areas, as illustrated by the averages and the lithology in figure 7.5. The areas of the channel more proximal to the active fault tend to incise through clastic sediments which have lower

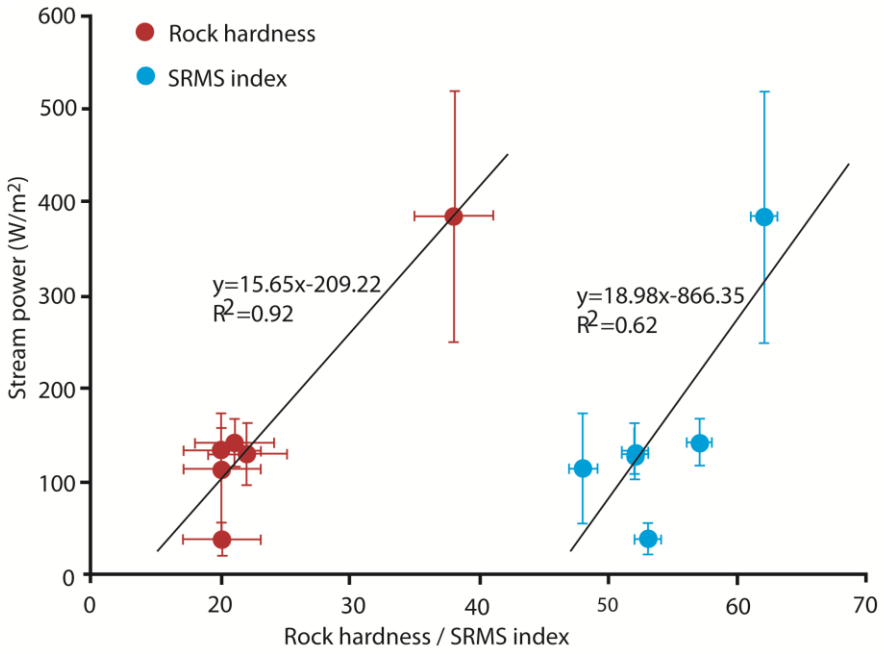

Figure 7.14: A graph plotting stream power averaged over 2km upstream of the fault against rock hardness measured, with a Schmidt hammer, and the SMRS index average for the 2 km channel length upstream of the fault. The graph shows that a factor of 2 reduction in rock hardness leads to an approximate 2.5 reduction in stream power, as the Akcipinar river (stream power of around 400) has an average hardness of around 40, compared to the majority of the rest of the rivers that have stream powers of around 150 and hardnesses of around 20. This indicates that indicating that the clastic sediments (present in all rivers apart from the Akcipinar) are at least 2.5x more erodible than the metamorphic rocks in the catchments.

SRMS ratings, 40 – 60, than the metamorphic SRMS values of 50 – 80 (figure 7.6). However the sediments vary significantly in hardness from the metamorphic basement rocks when measured with the Schmidt hammer (figure 7.5). Often they are too soft for the rebound hammer to register a meaningful reading, and in these cases are assigned a minimum 20 value, and they always have a lower hardness than 30. The metamorphic lithologies, which often have an average hardness measure of around 60 are on average 2 – 2.5 times harder than the sediments (figure 7.5).

Figure 7.14 quantifies the impact of rock hardness and SRMS on the stream powers of the rivers by plotting stream power at the fault against SRMS and Schmidt hammer rebound number. The results are not normalised by throw

rate as the figure 7.13 shows that stream powers at the fault in sedimentary catchments are not very sensitive to throw rate. There is at least a factor of two difference in the Schmidt hammer rebound hardness of the rocks from around an average of 40 in the metamorphic rocks of the Akcipinar river catchment to values of around 20 in the other river catchments in the sedimentary rocks. For this reduction in hardness, the data shows an approx. 2.5 reduction in stream power between the harder and softer lithologies. A similar result is found using the calculated SRMS index although with the SRMS data shows a little more scatter. Therefore it appear that a 2 fold difference in rock hardness is responsible for at least a 2.5x reduction in stream power between the rivers. This means K in a stream power law is varying by > 2.5 accounting for the differences between the metamorphic and sedimentary rock types. From this it seems evident that rock hardness might influence K in a non-linear way, with the halved rock hardness having a greater than 2x effect on increased erodibility.

The impact of lithology on the magnitude of K in this study is less than the 'orders of magnitude difference' in K that some authors have suggested. For example Stock and Montgomery (1999) have studied the effect of lithology on the K parameter in a simple unit stream power law where $E = KA^mS^n$. They noted that K parameter varies over 5 orders of magnitude between mudstones and volcaniclastic rocks from Japan and California (10^{-2} to10^{-5} m^2/yr) and granitoids and metasediments in Australia (10^{-6} to10^{-7} m^2/yr), but do state that the K variation due to climate is unresolved. They go on to conclude that that magnitude of variations in K would require the transient rate of denudation and time constants for landscape evolution to vary greatly with lithology. When this is compared to the data from this study the difference in erodibility between the

metamorphic rocks and the sediments is generally a factor of 2 – 3, and in the Yeniköy the difference is much larger, at around a factor of 7. Climate can be excluded from consideration in this study as the climate in the study area is uniform along strike and into the mountain range.

A caveat to this is that the Schmidt hammer may not be very accurate at measuring the appropriate hardness of rocks at the weaker end of the spectrum. The Schmidt hammer does not effectively take reading of rock hardness in rocks with a less than 20 reading, so hardnesses from 0 – 20 are all read as 20. This may partially explain why differences in throw rate in the sedimentary rocks cannot be differentiated, as the Schmidt hammer cannot elucidate differences in hardness less than 20.

An interesting feature of the data is that the Yeniköy River has similar rock strengths to the other rivers with sediments in the area near the fault, but it exhibits anomalously low stream powers, with actual stream power measurements at the fault at least three times lower than one would expect even if you corrected for the fact that bedrock lithology reduces stream powers by a factor of 2.5 . As the rock strength data is similar to the other rivers this is not likely to be an effect of the lithologies the river is incising through. So in all rivers lithology and erodibility contrasts can approximately explain the difference in stream powers developed in the metamorphic versus clastic rocks, but it does not explain differences in stream powers between catchments with differing throw rates eroding similar sediments near the fault.

7.6.5: THE POTENTIAL ROLE OF RELATIVE SEDIMENT SUPPLY

The substantially lower stream powers in the Yeniköy River, even taking into account the more erodible bedrock at the fault and adjusting for the fault

slip rate are surprising. One explanation for this is that the incisional capacity of this river can only be understood if sediment flux effects are taken into account (c.f. Cowie et al., 2008). In this case, there is a need to model sediment in transport directly influencing bedrock incision (E) through either enhanced erosion of exposed bedrock, via impact abrasion and plucking (a tools effect), or via inhibiting erosion by limiting the amount of bedrock exposed, a cover effect. This is known as the tools versus cover effect, where incision is a result of the dynamic interplay between tools and cover in the channel (e.g. Sklar and Dietrich, 2004).

It might be that the sediment flux and subsequent and tools verses cover effect is operating within the Gediz rivers to different extents. The Yeniköy River catchment may be supplying more tools than the rest of the rivers and is therefore more efficiently eroding the bedrock without having to steepen its channel slope leading to elevated stream power in order to incise at a rate that keeps pace with uplift (Cowie et al., 2008).

To test this idea, a stream power incision capacity enhancement factor f(Qs) has been calculated for each river, by dividing predicted stream powers, scaled to the tectonics ($\omega_{predicted}$) by actual 2 stream powers for each river, i.e.

$$f(Qs) = \omega_{predicted}/\omega_{measured} \quad \textbf{(eq. 7.7)}$$

Two sets of f(Qs) values have been calculated. For the first the ratios of predicted to actual peak stream powers in the metamorphic units (the values of which were presented in figure 7.12) are compared. In the second, a comparison of ratios of actual stream powers in the 2km upstream of the fault to

the predicted stream powers in the sedimentary units (as presented in figure 7.13) is made.

Sklar and Dietrich (2004) model sediment-flux-dependent incision as being dependent on the ratio long term average sediment supply (Qs) to the channel's transport capacity (Qc). While this can be measured relatively well in a flume setting and can be estimated for an individual flow (Sklar & Dietrich, 1998; Sklar & Dietrich, 2001), this ratio evidently varies in time and space. Indeed it is probably unknowable over a geologic timescale (c.f. Cowie et al., 2008). Consequently proxies need to be used for the sediment supply rate in the catchments. Two proxies are adopted. For the ratios of stream powers developed in the clastic sedimentary rocks, the proxy for Qs/Qc is the percentage of clastic sediments making up the catchment of the respective river. This is because our field observations show that much locally-derived sediment lying in the bed near the fault is clearly reworked from these Pliocene to Recent clastic rocks. For the ratios of stream powers developed in the metamorphic rocks, the estimated percentage of bedrock exposed (and thus percentage of bedrock covered by sediment) at each field measurement station is used. The average sediment cover on the bed upstream of the peak stream power is used as a proxy for the relative sediment supply.

The sediment flux controlled incisional enhancement capacity f(Qs) for the Sart, Bozdağ, Kabazlı and Badinca Rivers is between 1 and 2.7 (green squares in figure 7.14a), with the value of 1 relating to the Badınca river, which was used for calibration. This means that the Sart, Bozdağ and Kabazlı rivers are experiencing enhancement of incisional ability due to sediment supply of a factor of 2.5, 2.5 and 2.7 respectively. For the Yeniköy River, which has as significantly higher percentage of clastic sedimentary in the catchment the f(Qs)

is 6.1 (figure 7.15a). In this data series it can be seen that compared to the Badınca River, for the catchments with around 10-20% clastic rocks in the

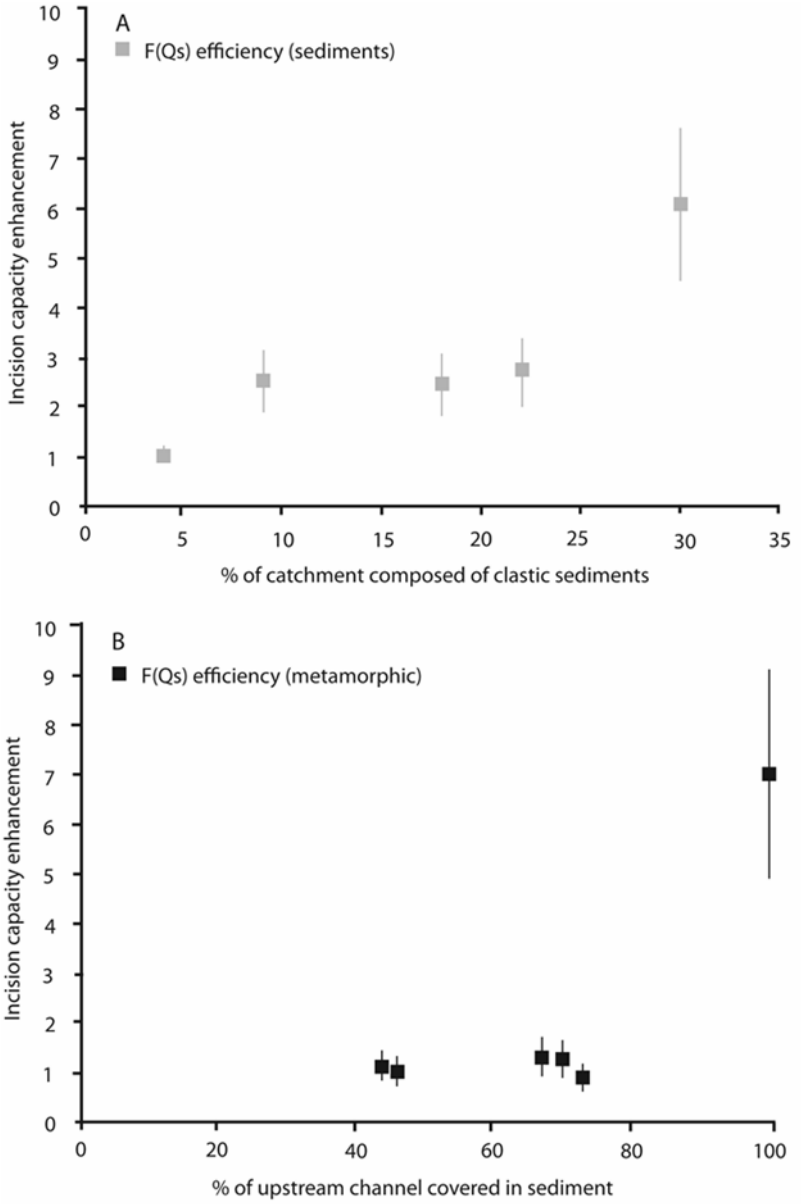

Figure 7.15: A) shows the incisional enhancement factor within the sediments (grey squares) plotted against the percentage of the catchment composed of soft clastic sediments. Plotted for all rivers where there are sedimentary lithologies within the catchment (so excluding the Akcipinar River) B) shows the incisional enhancement capacity in the metamorphic rocks (black squares) against the percentage of the channel upstream of the peak stream power that is covered in sediment.

catchment, the rivers are around two to three times as erosive as they would be if the detachment limited end-member stream power model is assumed. This increases to around a factor of 7 when the catchment is made up by more than

30% by area of clastic rocks. Figure 7.15a suggests that supply of clastic sediment from downstream from the metamorphic catchment area is boosting the erosive power of the rivers.

In the metamorphic rocks, the sediment flux enhancement factor, f(Qs) is around 1 for the five rivers which have a percentage upstream channel covered by sediment of 40 – 70 %. An f(Qs) of 1 means that sediment is not having a role in influencing bedrock incision rate, which fits directly with the fact that unit stream powers appear to scale with throw rate in these channels. Significantly, however, in the Yeniköy River the channel upstream of the peak in stream power is 100% blanketed in sediment, which is 25% more channel coverage than the highest value in the other rivers. The origin of the sediment may be isolated areas of sediment in the higher altitude of the range within the catchment of the Yeniköy River. This 25 % greater channel sediment coverage corresponds to around a 7 times increase in incision capacity f(Qs) in the upper catchment of the Yeniköy River compared to the other channels studied (figure 7.15b).

The rivers in the Gediz Graben are therefore consistent with being on the rising limb of the 'tools' effect mapped out by Sklar and Dietrich (2004). They plotted peak erosional efficiency for a dimensionless incision capacity enhancement factor around 7, which is similar to the value for the Yeniköy River, implying that the tool effect is at an extreme in the Yeniköy river (figure 7.16). This essentially means that the river can erode efficiently without steeping its long profile or narrowing significantly, allowing it to incise with less effective stream power than in the other rivers where the incision capacity enhancement factor is around 1 – 3. This accounts for the lower stream powers in the Yeniköy River than would be expected given the similarity in boundary

conditions to the other rivers. Sediment flux effects for the other rivers cannot be resolved where they incise metamorphic lithologies, but are potentially responsible for a 2 – 3 fold increase in incision capacity near the fault where all rivers except for the Akcipinar incision clastic sedimentary rocks. This may explain why there is not a simple dependence of stream power on throw rate near the fault for these channels.

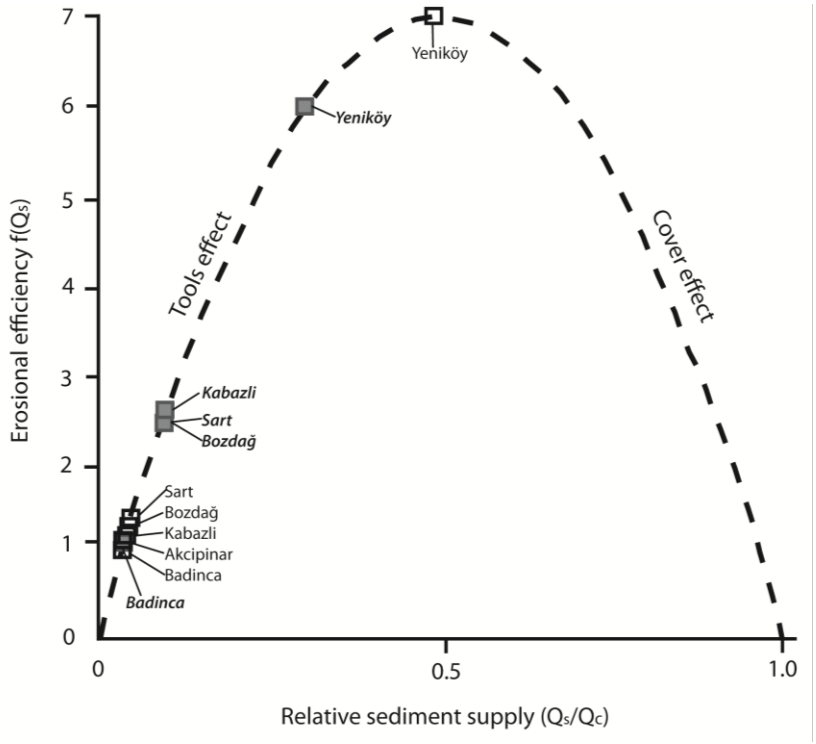

Figure 7.16: Material transported by a river influences incision rate, either through enhanced erosion bedrock, via impact abrasion and plucking by 'tools', or by inhibiting erosion by limiting the amount of bedrock exposed, known as the cover effect (e.g., Sklar and Dietrich, 2004). This effect can be modelled via the function f(Qs), where Qs is the volumetric rate of sediment supply if both tools and coverage effects are important, f(Qs) is expected to follow a parabolic-like function of Qs/Qc, where Qc is transport capacity. The data for the Gediz Rivers has been added to the parabolic tools-cover curve, which shows erosional efficiency increasing with increasing relative sediment supply but decreasing past a relative sediment supply that begins to shield the river bed. The grey squares labelled with the names of the rivers (in italic font) show the f(Qs) in the sedimentary stretches of the river bed for rivers with sedimentary bedrock in the channel (Akcipinar is excluded as the whole channel is metamorphic), the black hollow squares labelled with the appropriate river show the f(Qs) in the metamorphic stretches of the river. This shows that in the sedimentary stretches of channels there is an elevated 'tools' effect, which is particularly obvious in the Yeniköy River. In the Metamorphic channel stretches only the Yeniköy River shows significant impact of the tools effect, at the peak erosional efficiency proposed by Sklar and Dietrich, (2004). Adapted from Cowie et al., (2008).

Stock and Montgomery (1999 noted that K parameter varies over 5 orders of magnitude between mudstones and volcaniclastic rocks from Japan and California. In this study there is a difference in erodibility between the metamorphic rocks and the sediments of a factor of 2 – 3. In the Yeniköy the difference is much larger, at around a factor of 7, which has been attributed to sediment flux effects. An important result of this study is that in the Gediz Rivers it is possible to separate out forensically the differing effects of lithology and sediment flux in modulating incision capacity, both of which are typically subsumed into a K parameter in studies using simple stream power erosion laws (Hack, 1957; Seidl & Dietrich, 1992; Whipple and Tucker, 1999; Snyder et al., 2000; Tucker and Whipple, 2002).

7.7: CONCLUSIONS

A Field study of 6 rivers draining the Gediz Graben show that the channels are responding transiently to tectonic perturbation by changing their channel geometry and planform up and downstream of knickpoints in the rivers. The river channel and valley widths are generally supressed at and downstream of the knickzone, although they increase towards the active basin-bounding fault, in areas of the catchment with soft clastic sediments.

This chapter has shown that traditional hydraulic scaling relationships fail to predict the widths of the Gediz Graben rivers. An attempt to evaluate additional width prediction methods two other models were tested, which each give slope a varying importance in determining channel width (c.f. Finnegan et al., 2005; Whittaker et al., 2007) were tested and these also fail to predict river widths in all cases but for the Yeniköy River. Over all these results show that extreme care must be taken when predicting stream powers using widths

produced by hydraulic scaling algorithms, as the failure to predict width will propagate directly into estimates of river erosivity.

The unit stream powers of the field studied 6 rivers were calculated and evolve downstream in similar ways. In the head waters the stream powers are low, they stay reasonably low (under 150 W/m^2) until the knickpoint. Downstream of the knickpoint the stream powers rise significantly to peak values found within the metamorphic bedrock. When the channel enters the clastic sediments downstream towards the active fault the stream powers drop off. This study has determined that predominantly the rivers exhibit peak stream powers in the metamorphic rocks that scale with throw rate, suggesting that in detachment-limited models of erosion do an adequate job of predicting bedrock incision rate in this case.

The influence of lithology on modulating the river response to tectonic was then investigated. It was found that a 2 fold difference in Selby rock mass is responsible for at least a 2.5x reduction in stream power between the rivers. Meaning that K in a stream power law is varying by a factor of 2.5, showing that differences in rock hardness between metamorphic and sedimentary rocks affects erodibility in a non-linear way.

In the Yeniköy the difference between the erodibility caused by metamorphic and sedimentary lithologies is much larger, around a factor of 7, which has been attributed to sediment flux effects. A significant result of this study is the separation of the differing effects of lithology and sediment flux, which are typically subsumed into a K parameter in studies using simple stream power erosion laws.

CHAPTER 8: SYNOPSIS

8.1: OVERVIEW OF THE AIMS, METHODS AND SIGNIFICANT FINDIINGS OF THIS THESIS

The aims of this project were:

1. Quantify the rates of faulting in the Gediz Graben using published data geological and structural data.
2. Use knickpoint theory to and to the resolution of structurally derived information for the Gediz Graben.
3. Consider how the rivers can be used to gather information about the tectonics of the Gediz Graben when integrated with structural data.
4. To investigate impact of tectonics on the behaviour of the Gediz rivers using field study of 6 rivers.
5. To consider the implications of not explicitly treating factors such as lithology and sediment flux on fluvial modelling of bedrock rivers using bedrock rivers within the Gediz Graben as an example.

First, a synthesis of existing data such as geological mapping, geophysical surveys and topographic information (e.g. Çiftçi, 2007; Çiftçi and Bozkurt, 2009a; Çiftçi and Bozkurt, 2009b; Çiftçi and Bozkurt, 2010; Oner and Dilek, 2011; Busher et al., 2013) were used in a novel, pragmatic way to quantify rates of throw on the MGBF array of the Gediz Graben (Chapter 4). The chapter constrained the throw rates in the Gediz Graben to between 0.4 and 1.5 mm/y along strike, time averaged over 2 myr (figure 4.11). The throw rate distribution indicates that at some point during the history of the graben bounding fault array

the individual fault strands had undergone a linkage event. The linkage is suggested by the non-zero throw and throw-rate values at both tips of the central of the three segments of the graben-bounding fault array. The presence of an along-strike bend of approximately 40° from east to west, adds additional support for the linkage of the fault segments (Fossen, 2010).

Subsequently, rivers that incise across the active fault were studied, and this thesis presents evidence that they are undergoing a transient response to active faulting, demonstrated by the existence of tectonically-induced knickpoints within the river channels. These knickpoints were considered in line with existing knowledge on knickpoint theory and theoretical understanding of how rivers respond to tectonics (e.g. Howard and Kerby, 1983; Seidl & Dietrich, 1992; Whipple and Tucker, 1999; Whipple and Tucker, 2002; Whittaker et al., 2007a; Whittaker, 2012). There are knickpoints in the rivers that cross the fault at the ends of the main fault segments, where a zero throw magnitude would also be expected if these were unlinked fault tips. Therefore, the knickpoints identified in the river channels were caused by the linkage event on the graben bounding fault, causing an increase in throw rate. The knickpoints are not caused by fault initiation, as their elevations relative to the fault do not fit with this model.

The knickpoint parameters (e.g. elevation, upstream distance) provided data for calculations based on knickpoint and fault interaction theory that placed the timing of linkage at between 0.6 – 1 Ma, shedding new light on the evolution of this important fault system. Additionally, pre- and post-linkage throw rates at the centre of the fault could also be calculated. A post- linkage rate of 2 mm/yr and the pre-linkage rate of 0.6 mm/yr were determined for the centre of the

array. By contrast time averaged throw rates in the same location are 0.6 – 0.7 mm/yr (figure 8.1).

Chapter 7 then went on to document a detailed field study of six of the rivers from the Gediz Graben.

The chapter analysed the effectiveness and real life applicability of several aspects of predictive modelling of bedrock river using the Gediz Graben as a testing site. One aspect of modelling that was examined is whether prediction of channel width using the widely accepted hydraulic scaling methods produces results that replicate real life situations, or to what extent there is a disparity between the prediction and actual measurements. The results of the field study showed that the standard techniques of channel width predication are very poor predictors of the evolution of channel geometry downstream in tectonically perturbed bedrock rivers. The logical conclusion from this is that any unit stream power prediction made for the rivers using these hydraulically scaled channel is likely to be, and in the case of the Gediz Graben, does produce very inaccurate representations of the downstream evolution of stream powers.

That the predictions produce poor representations of real measurements of both channel width and stream powers in the Gediz Rivers was an important realisation and had implications for the rest of Chapter 7. The next part of the chapter went on to document the effects of local lithology on the stream powers developed in the rivers in response to tectonic uplift. Use of the predicted stream powers would, in the Gediz River have produced erroneous conclusions, as the predicted stream powers fail to exhibit any influence of the local channel lithology as the equations do not represent the real situation. Consequently the

stream powers calculated from the channel geometries measured in the field were compared to the local lithology at the point of measurement.

This type of study is not commonly done as the study of bedrock rivers in the field is often very time consuming and difficult. However, this part of the study produced some important results. In Chapter 6 the lithologies from mapping of the area by previous studies were compared to the river profiles, lithology apparently has a very minor impact on the river geometry and specifically the movement of knickpoints. However, chapter 7 studied the lithology at a far higher resolution and observed a direct and significant relationship between how easy it was to erode the bedrock lithology and the stream power developed in the river at that point. Specifically, a two fold difference in the hardness of the lithology measured with a Schmidt Hammer produces a difference of around 2.5 times in stream power developed. This shows explicitly that lithology can play a large role in the magnitude of stream power, and most likely in a non-linear way.

8.2: THE IMPLICATIONS OF THIS STUDY

This study has provided new data to constrain the tectonic evolution of the Gediz Graben. This is significant as this study has produced the first quantification of throw rates on the currently-active graben bounding fault array, which exceed 2 mm/yr in some places along the fault. Given that there are numerous settlements of 25-50,000 inhabitants situated near to, or on top of the active fault this information is very relevant and potentially useful in terms of preparedness for tectonic events.

The combination and analysis of the different data sets in this study shows that the graben has a two stage tectonic history with a transition from low to high-angle normal faulting around at between 2.6 – 2 myr. Between 2 – 1 myr the MGBF was initiated as a series of fault segments, creating a second parallel high-angle normal fault array, stepping out into the topographic graben. At some point between 1 – 0.6 myr a significant linkage event on the current graben-bounding normal fault occurred. These data show that the MGBF fault array is controlling the expression of topography in the Bozdağ Range, and is likely to have been the main control over at least the last 1 myr. This has impacted on graben topography, creating the present day topographic variations along strike and elevated the throw rates on the array. The increase in accumulated throw on the fault from this time could be what the previous research (e.g. Oner and Dilek, 2011; Buscher et al., 2013) labelled fault initiation.

The newly derived rates have also allowed for an estimation of the potential magnitude of earthquakes using the method of Wells and Coppersmith (1994). Earthquakes of magnitude of 6.9 – 7.6 Mw could be expected depending on how much of the fault array ruptures from 40 km segment, to the whole array (section 4.7.7). The Gediz Graben and surrounding region have experienced some large earthquakes over Mw 5.0 in the last twenty five years (Eiodogan and Jackson, 1985; Buscher et al., 2013), including a destructive earthquake of magnitude 6.9 in 1969 (Arpat and Bingol, 1969). Another earthquake occurred within the Gediz Graben in March 1970, this earthquake had a magnitude of 7.2 and left thousands homeless and over 1000 people dead, it lead to the total relocation of the village of Gediz (Mitchell, 1976). The historical evidence supports the magnitude prediction with documented earthquakes ranging from 5 – 7.2 Mw. The calculated possible magnitude for

earthquakes within the Gediz Graben suggest that an even larger earthquake could occur if enough of the fault length ruptured.

In addition to the increase in the knowledge of the active tectonics of the area this study has identification of rivers in the Gediz Graben that are responding in measured transient ways to tectonics perturbation and in the comparison of standardised models and theory relation to real life values. This has allowed several distinct and noteworthy contributions to be made in terms of furthering the information that can be gathered from a landscape and how it is used, and evaluation of the current methods of modelling fluvial geomorphology. Three of the most significant contributions of this thesis are detailed in the following sections (Sections 8.2.1 – 8.2.3).

8.2.1: INTEGRATING FAULT LINKAGE THEORY AND KNICKPOINT THEORY

Typically when information is required about historic or present day fault activity, studies utilise a well-known tool box of techniques from cross-sections to trenching and studies of imagery and dated surfaces (outlined in the introductory parts of Chapter 4). These methods can provide a large variety of information over different time scales (Cowie and Roberts 2001), and so are valuable tools which have allowed for the quantification of throw rates and the examination of pattern in the magnitude of throw along strike (Schwartz and Coppersmith, 1984; McAlpin et al., 1994; Nicol et al., 1997; Cowie and Roberts, 2001; Litchfield et al. 2006; Özkaymak et al., 2011). However, this study set out to test how a sophisticated understanding of geomorphology and transient landscape response could be integrated with fault interaction theory and

structural data, to improve constraints on fault slip rates where geological or geodetic data are sparse. It has been proposed widely that fluvial geomorphology can give qualitative and quantitative insights into tectonics, but this is one of the first studies to derive fault slip rates quantitatively from geomorphic analysis and this thesis shows that knickpoints are now a potential tool for examining tectonics (Snyder et al., 2000; Whipple, 2001; Kirby et al., 2003; Oiumet et al., 2009). Previously, studies have used this process in reverse, where they have taken a known tectonic template and then examined the landscape response to the tectonic rates (e.g. Howard et al., 1994; Snyder et al., 2000; Whipple and Tucker, 2002; Tucker and Whipple, 2002; Whipple, 2004; Whittaker et al., 2008; Boulton and Whittaker, 2009; Whittaker and Boulton, 2012). This study has reversed this process. Fault interaction theory has been combined with the sophisticated knowledge of geomorphology in the form of knickpoint theory to provide a detailed picture of the ongoing tectonic regime in the Gediz Graben. As a result in Chapter 6 the transient responses of the bedrock rivers have explicitly described and characterised. The knickpoint data was key in the dating of the linkage event evident from throw values to 0.6 – 1 Ma (figure 6.4), this also allowed for resolution of pre- and post-linkage rates at the centre of the array of 2 mm/yr and 0.6 mm/yr respectively. Without the in depth knowledge of geomorphology this information would have been inaccessible.

This is a significant step forward in both the study of faulting and fluvial geomorphology. Knickpoint theory has been the subject of an increased amount of attention and subsequent development with researchers documenting how rivers and in particular knickpoints respond to known throw rates (e.g. Howard et al., 1994; Snyder et al., 2000; Whipple and Tucker, 2002; Tucker and

Whipple, 2002; Whipple, 2004; Whittaker et al., 2008; Boulton and Whittaker, 2009; Whittaker and Boulton, 2012). In isolating the tectonic knickpoints in the rivers and combining the data with the available geological and structural, this study has pushed the applicability of geomorphology into a potentially very useful relationship with fault linkage theory. Without the integration of the methods it would not have been possible to derive details of the tectonic history in such high resolution, including throw rates pre- and post-linkage and assigning a timing of linkage.

This study highlights the usefulness the fluvial network in in constraining the fault evolution without the need for time-consuming effort and expensive trenching data and lab work. Much of the data is easily available by extraction from DEMs, and increasingly high resolution digital data could therefore be an efficient way to examine tectonics if the general relationships between rivers and tectonics are well understood and quantified.

It is obviously desirable to have as much information about fault movement in as high a resolution as possible, particularly in populated areas. It is possible, given the general state of knowledge on both knickpoint and fault linkage theories that knickpoint data could be used as the starting point for studies of tectonics from a surveying perspective. Figure 6.8 provides a plot of range relief and total throw along strike in the Gediz Graben, it also plots the data of vertical knickpoint height above the active fault. This study has shown that the knickpoint heights reflected both the range relief and the throw values along strike. If the general location of faults in known then this study suggests that it would be possible to extract knickpoint data at a very low cost and compare it to the known location of faults arrays and segments. This could, as figure 6.8 shows, provide significant information on the best places to study

increased rates of throw, and provide a very valuable source of data for very little cost.

8.2.2: CALIBRATING THE EFFECT OF LITHOLOGY ON TRANSIENT LANDSCAPE RESPONSE TIMES

Chapter 7 of this thesis presented a detailed field study of the geometry and erosivity of six rivers upstream of faults in the Gediz Graben for which well-constrained throw rates had been derived. The unit stream powers were compared between rivers with varying channel lithologies and importantly the results showed that lithology has a significant modulating influence on the response of the rivers keeping pace with uplift on the active fault. For example, a 2 fold reduction in rock hardness, measured *in situ* by multiple Schimidt hammer rebound tests, causes at least a 2.5x reduction in stream power between the rivers required to cut across the fault. This is interpreted as meaning that the K parameter in the widely-used stream power law also varies by a factor of 2.5. This result is important as it is often stated that lithology should have an influence on river responses to tectonic perturbation but there have been hardly any studies that set out to use comprehensive field data to quantify this explicitly. This study shows unequivocally that lithology can have a significant impact on modulating transient landscapes, and hence landscape response times.

The results suggest that even though tectonics is a primary influence on the response of the landscape through river incision, lithology must be seriously considered in field or numerical modelling studies, or predicted stream power predictions will be non-representative of the actual response of the landscape.

The implications of this for landscape modelling are clear. Lithology and sediment flux are currently subsumed into the K parameter in erosion laws. This study indicates that the treatment of the K parameter in these erosion laws must be carefully considered. Therefore this study suggests that to be able to accurately predict river geometries and stream powers, and therefore landscape evolution, the variables within the K parameter need to be explicitly defined. In Chapter 7 it is shown that both lithology and sediment flux can significantly alter the geometries and stream powers within rivers and neglecting this in models would significantly over or under predict stream powers at the fault. The Yeniköy River in the Gediz Graben is good example of this problem, where in reality much lower stream powers were required than would have been predicted to keep up with uplift, due to significant sediment flux effects.

This study has also highlighted the need to address how the lithological influence should be measured. In this study the rock hardness was measured using a Schmidt hammer, which takes reading of the uniaxial compressive strength of the rock. These readings were also combined with other lithological details such as joint spacing, orientation and dip of the rocks to produce the widely-used Selby Rock Mass Strength Index (SRMS [Selby, 1980]). The relative SRMS index ratings of the clastic sediments and metamorphic basement rocks did not always reliably record the visually very obvious differences in the erodibility of the two general rock types. However, the hardness measure using the Schmidt hammer produced a more reliable quantitative estimate of erodibility based upon the obvious field evidence of different amounts of incision between the sedimentary and metamorphic rocks.

This thesis therefore suggests that different methods for assessing hardness or rocks and rock erodibility may explain the equivocal results that

other workers have obtained when considering the influence of lithology on bedrock river erosion. This then raises the question of whether or not we have the right tools to really assess the impact of lithology.

The SRMS index is a good example of varying appropriateness of measurements. As already stated the SRMS index did not correlate well with the visible differences in incision in the field, and in addition, did not explain the differences in stream powers produced in response to and mitigating relative rates of active uplift along the fault array. In the SRMS the hardness is combined with other information such as the degree of weathering and ground water saturation, and the orientation and size of joints and bedding. The disparity between the representative ability of the hardness and the SRMS suggest that within the current method the level of weighting given to each variable may not be ideal for studying the erodibility of rocks. A suggestion to improve this is that future work should address the levels of weighting given to the properties of the lithology within the SRMS index calculations. The data presented in this thesis suggests that the hardness of the lithology should have a higher weighing in the calculation

Additionally, this study highlighted the problems of using a Schmidt hammer to measure poorly consolidated and very soft lithologies. In this study anything softer then a 20 reading on the Schmidt hammer was read as 20 as the sensitivity of the hammer below 20 is very poor. This could hinder the study of softer lithologies and produces poor resolution of the data for the softer rocks.

8.3: FURTHER WORK

This thesis has made a significant contribution to constraining the tectonic history of the Gediz Graben using a variety of methodologies.

Importantly it has combined an in depth knowledge of geomorphology with fault interaction theory to quantify rates of throw and the timing of linkage. The results of this study suggest that the extraction of knickpoints and knowledge of knickpoint theory can be used to quantify rates of fault throw and determine whether fault linkage has occurred, and provide possible dates for the event.

One suggestion for a further study would be to apply this method to other tectonically active areas with a range of fault slip rates and footwall lithologies. The strategy for the ongoing work could be to select two or three additional areas in which to replicate this study. The initial additional study areas should have a similar tectonic regime to the Gediz Graben, to allow for comparison of results from similar situations. The study areas would therefor need to have active normal faulting and graben-type topography. This study could therefore be conducted in a variety of areas, but could initially aim to concentrate the other grabens parallel to the Gediz, the Büyük Menderes and Küçük Menderes Grabens, as these study areas are very similar in their history and timings of formation as well as the general geology such as style of faulting and lithologies present. After the initial stage of the investigation depending on the results the study areas could become more diverse, the Basin and Range could be used for this study as the tectonic situation is still similar but there will be more variations in the other factors such as rates of fault movement and general geology of the area. This would allow for progressive testing of the hypothesis in a variety of more varied areas.

This would be important as it could lead to support for the proposed method of studying faulting put forward in this chapter. In this way there is then the possibility of conducting a study that looks at the easily extractable fluvial information and then uses the information to produce quantification of throw

rates. This geomorphology derived information could then be compared to information from other methods.

More specifically this study would aim to combine previous mapping for fault traces with knickpoint data extracted from DEMs. The data would consist of an extracted fluvial network with selected rivers extracted using available software. The river long profiles would then be studied both visually and with log-log slope-area plots to determine the locations and therefore heights of tectonic knickpoints. The knickpoint height data could then be compared to the mapped fault traces and data extracted from the DEM such as range relief , and used in conjunction with estimates of fault initiation to provide a quantification of pre- and post-linkage throw rates, and timing of linkage for areas where linkage has occurred.

Another suggestion for a further study is the issue of the influence of lithology on river response to active tectonics. In particular this thesis has highlighted that there needs to be more studies that use field derived data to analyse the influence of lithology. A particular aspect of this that needs work is the way that the erodibility of the lithologies around the river channel is quantified. In light of this a prosed study would identify an appropriate area where the lithology varies significantly both between rivers and also along the length of the studied rivers, in a similar way to the Gediz Graben. Obvious choices for the initial study are the Büyük Menderes and Küçük Menderes Grabens as they would allow that would allow for direct comparisons with data from the Gediz Graben, and show the same variations in comparable lithologies. The study would need to extract information about particular rivers using appropriate software and then a field study would need to be undertaken.

A minimum of five or six rivers should be walked in the field, measuring the river channel geometry. In addition to this, at each location of geometry measurements a suite of lithology data should be documented including Schmidt hammer hardness measurements and the additional characteristics of the rocks that contribute towards the SRMS index.

In addition to the data for the SRMS index additional methods of quantifying rock hardness would be tested. It is possible to estimate uniaxial compressive strength of rocks and relating grade assigned by Brown (1981) to particular ranges of compressive strengths (R6 = 250 MPa; R5 = 100- 250 MPa; R4 = 50-100 MPa; R3 = 25-50 MPa; R2 = 5-25 MPa; R1 = 1-5 MPa; R0 = 0.25-1 MPa). This can be done in the field using tables of rock properties that relate to given strength of rock. These properties relate to how easy it is to break the rock with either a hammer, pocket knife or finger nail. At each location that SRMS data is collected the Brown Grade should be assigned to the lithology using the required tool.

One additional reading of rock strength can be taken at each location using and Equotip reader. The Equotip uses the Leeb hardness principle, which is a rebound hardness measure typically used for testing metal in engendering context, although it is being used experimentally in the field for testing rock hardness (Viles et al., 2010). Viles et al. (2010) have tested the reading of a Schmidt hammer and Equotip and found that the readings are not necessarily comparable, although when the data is combined it can yield extra information.

The results of this study would allow for stream powers to be calculated in a similar way to this study, at multiple locations along the river channel. The study should then involve an analysis of the lithological data derived using Schmidt hammer, SRMS index, Brown grade and Equotip readings with respect

to the known stream powers. Advancing from this thesis the specific aim would be to analyse how different methods of measuring hardness or rebound strength of the lithology reflect the erodibility as determined through stream power analysis.

A thorough consideration of the individual hardness measures should be completed and as well as considering a combination of hardness measures and also alternative weighting within the components of the SRMS index. This should produce results that make it easier for future studies to accurately study the effect of lithology strength and erodibility on stream power, enabling the issues with current modelling documented within this thesis to be evaluated.

8.4: SIGNIFICANT CONCLUSIONS OF THESIS

- Geomorphic techniques can be used in conjunction with fault interaction theory to produced high resolution constraints on the rates of faulting and timings of linkage events on the active fault array in the Gediz Graben.
- The fluvial network of the Gediz Graben is unequivocally undergoing a transient response to the linkage event. Each river that was studied in chapter 6 shows a knickpoint interpreted to be due to the increase in throw rate caused by the linkage event. A transient response is also indicated by the supressed channel and valley width downstream of the knickpoint, and the short-wavelength of elevated stream powers upstream of the basin bounding faults.
- The typical landscape response time implied for these rivers is between 1.63 Ma and 2.73 Ma. Fluvial geomorphology therefore records tectonics over long time periods.

- Current channel width scaling methods used in extrapolative landscape modelling are poor predictors of actual channel widths as measured in the field as evidenced by data from the Gediz Graben. The implications of this result to landscape modelling is an issue that needs to be addressed in future research.
- In the Gediz Graben the steam powers in the rivers scale well with throw rates when they are measured within the relatively uniform, hard metamorphic basement rocks in the upper 2/3 of the catchments.
- The tectonic scaling breaks down when the stream powers in the lower catchments dominated by soft clastic sediments are considered.
- In the Gediz rivers it is possible to separate the differing effects of lithology and sediment flux in modulating incision capacity, both of which are typically subsumed into a generic K parameter in simple stream power erosion laws.
- A significant implication of this thesis is that the current treatment of a collection of variables within the K parameter is inappropriate for accurate landscape modelling. Variables such as lithology and sediment flux need to be treated individually and with more attention.

APPENDIX 1:

slope areas graphs used in chapter 6

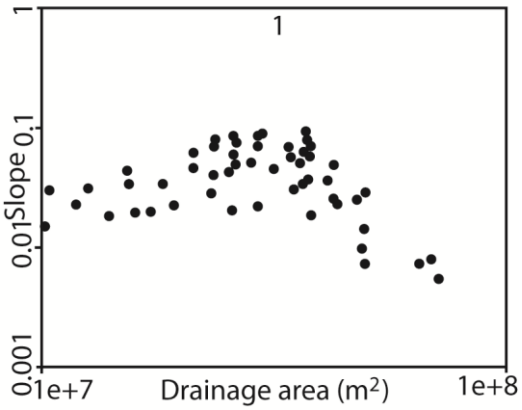

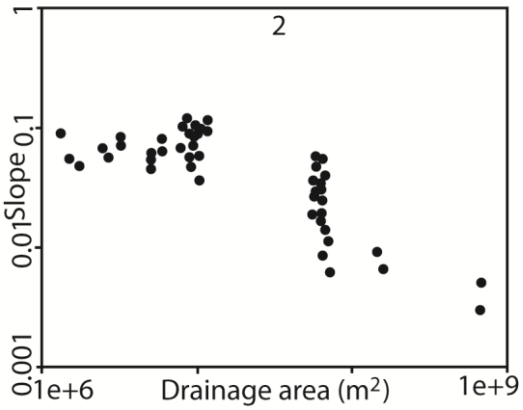

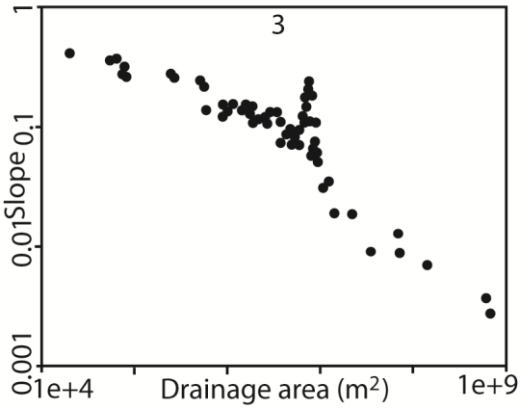

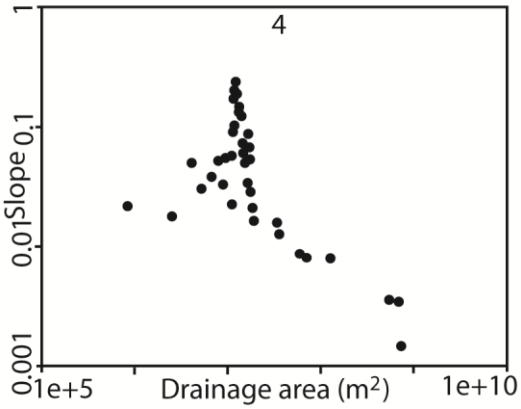

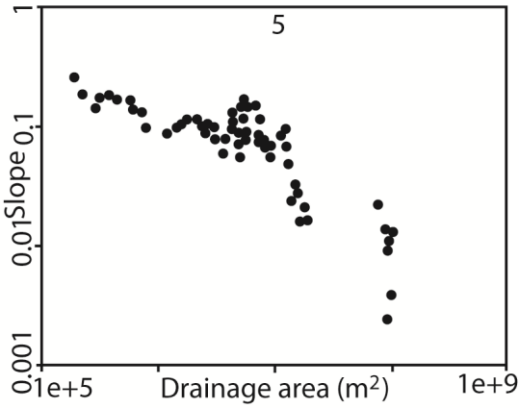

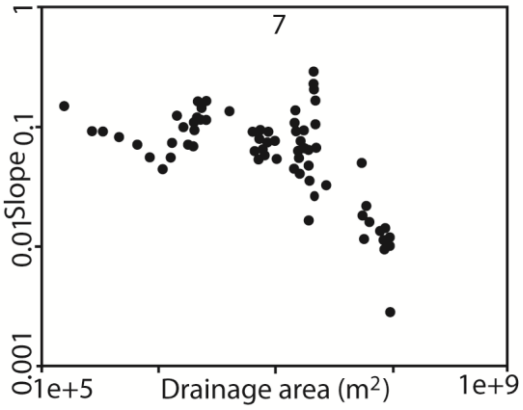

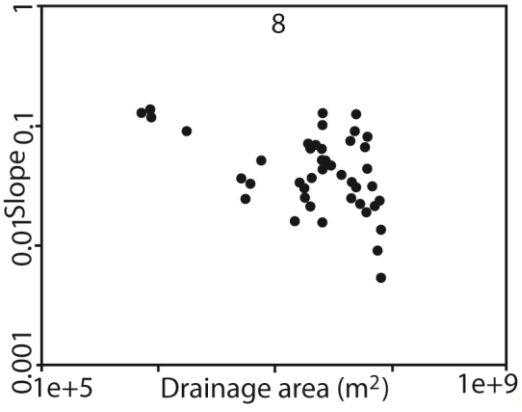

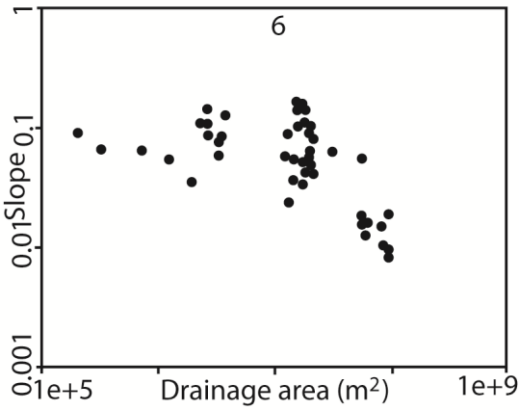

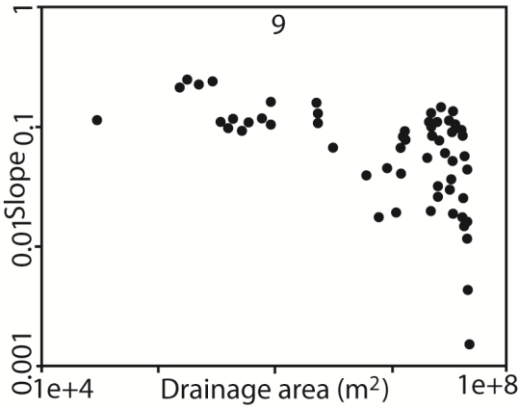
9
1
0.1
0.01
0.001
Slope
1e+4
Drainage area (m2)
1e+8

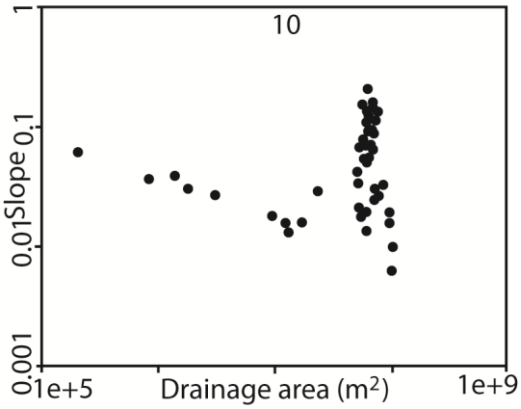
10
1
0.1
0.01
0.001
Slope
1e+5
Drainage area (m2)
1e+9

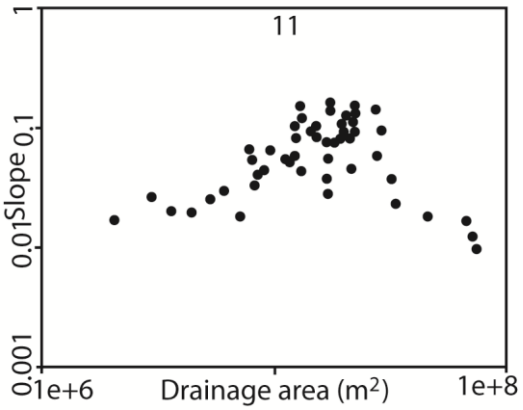
11
1
0.1
0.01
0.001
Slope
1e+6
Drainage area (m2)
1e+8

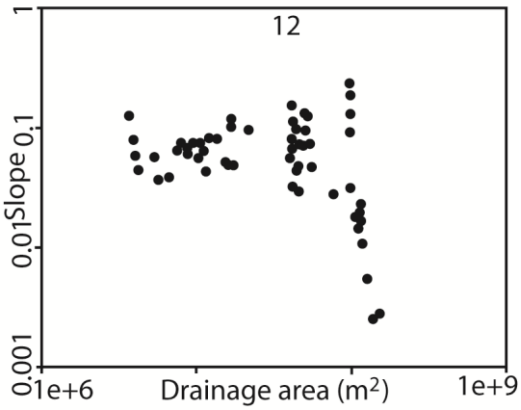
12
1
0.1
0.01
0.001
Slope
1e+6
Drainage area (m2)
1e+9

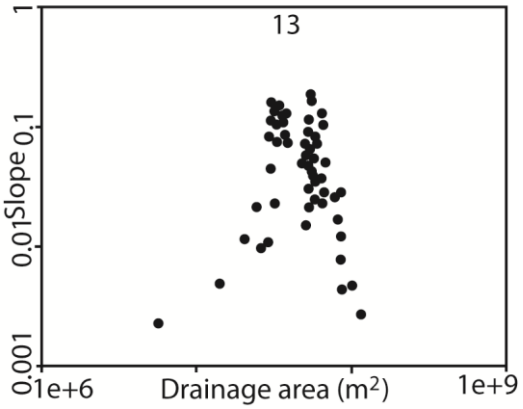
13
1
0.1
0.01
0.001
Slope
1e+6
Drainage area (m2)
1e+9

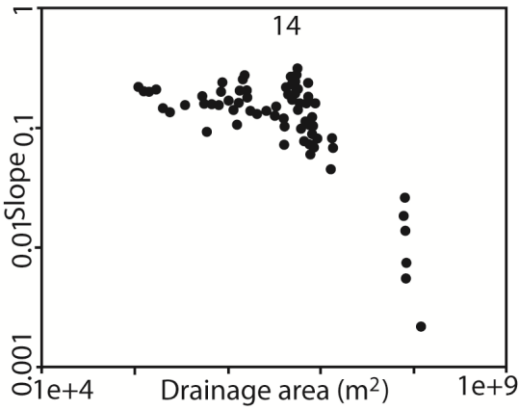
14
1
0.1
0.01
0.001
Slope
1e+4
Drainage area (m2)
1e+9

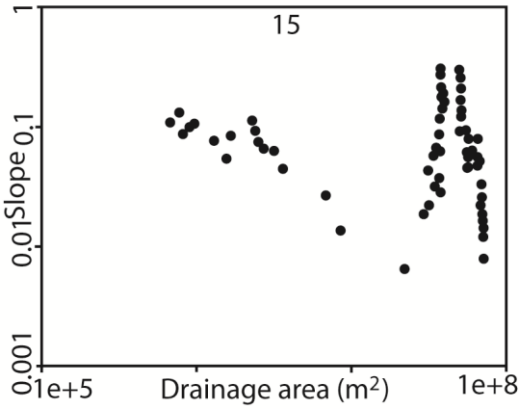
15
1
0.1
0.01
0.001
Slope
1e+5
Drainage area (m2)
1e+8

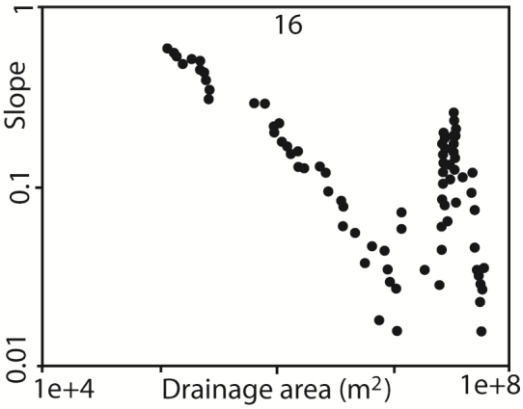
16
1
0.1
0.01
Slope
1e+4
Drainage area (m2)
1e+8

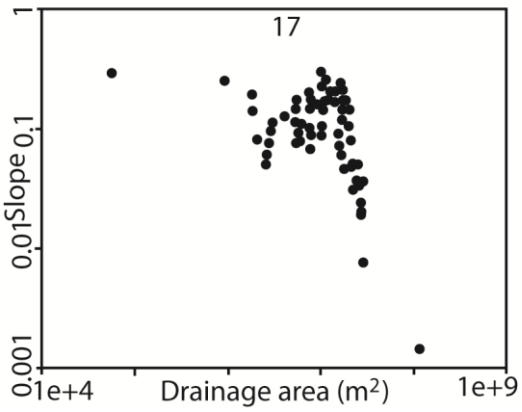
17
1
0.1
0.01
0.001
Slope
1e+4
Drainage area (m²)
1e+9

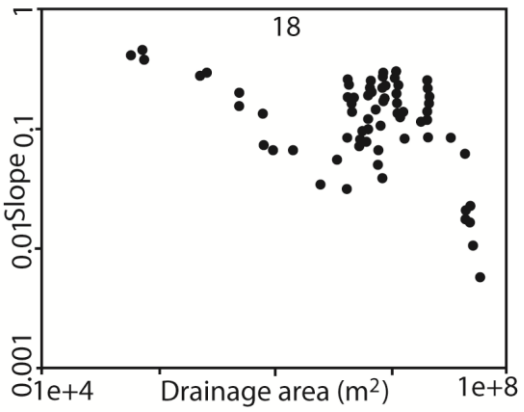
18
1
0.1
0.01
0.001
Slope
1e+4
Drainage area (m²)
1e+8

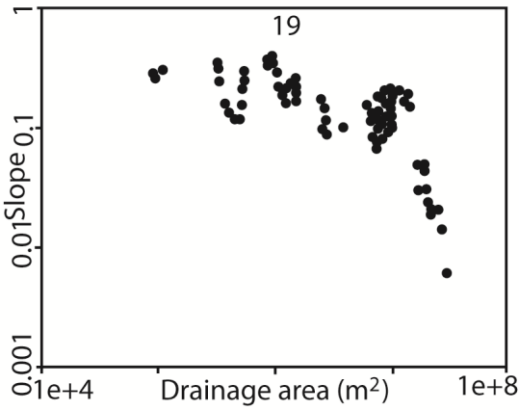
19
1
0.1
0.01
0.001
Slope
1e+4
Drainage area (m²)
1e+8

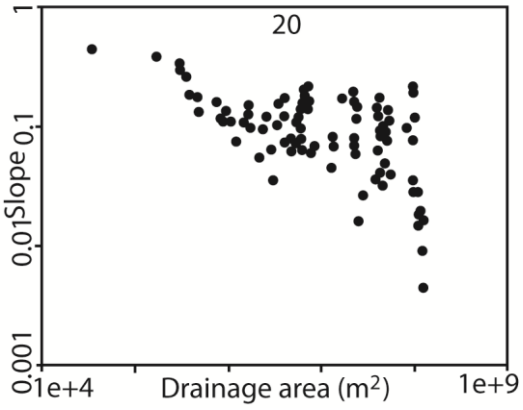
20
1
0.1
0.01
0.001
Slope
1e+4
Drainage area (m²)
1e+9

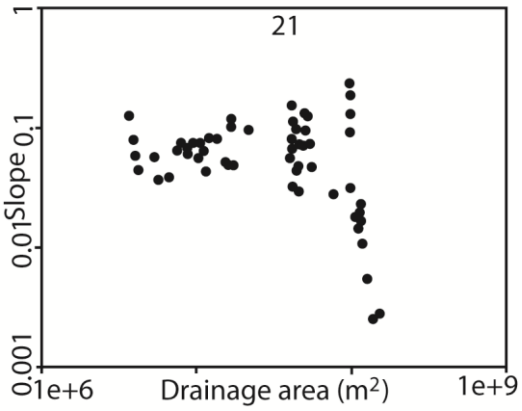
21
1
0.1
0.01
0.001
Slope
1e+6
Drainage area (m²)
1e+9

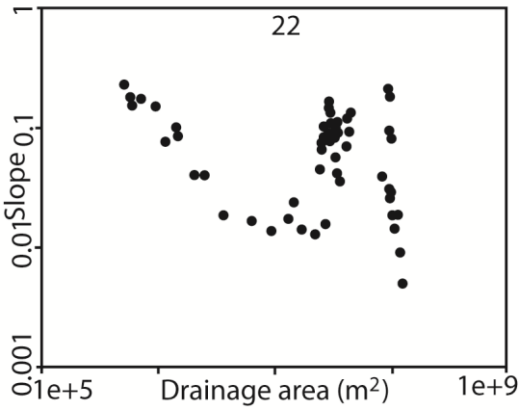
22
1
0.1
0.01
0.001
Slope
1e+5
Drainage area (m²)
1e+9

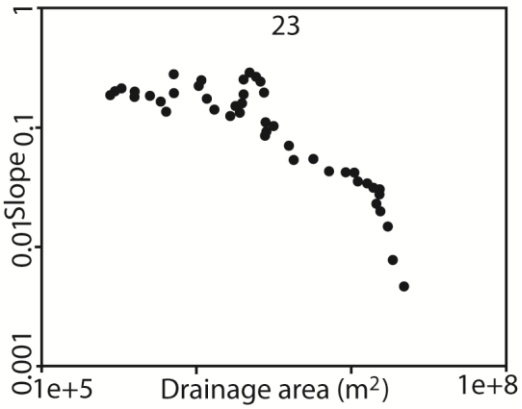
23
1
0.1
0.01
0.001
Slope
1e+5
Drainage area (m²)
1e+8

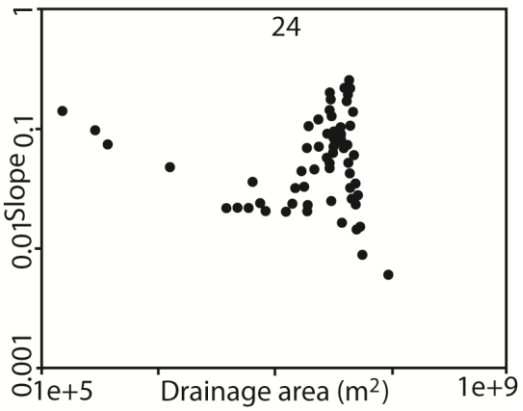
24
1
0.1
0.01
0.001
Slope
1e+5
Drainage area (m²)
1e+9

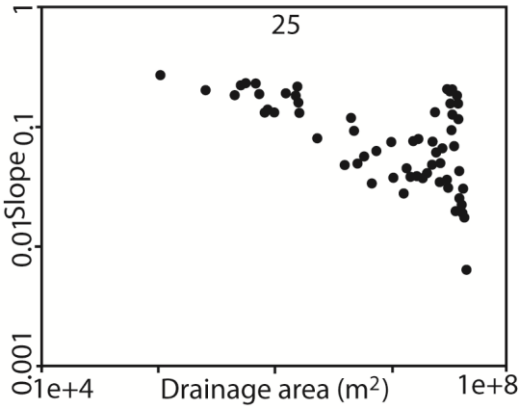
25
1
0.1
0.01
0.001
Slope
1e+4
Drainage area (m2)
1e+8

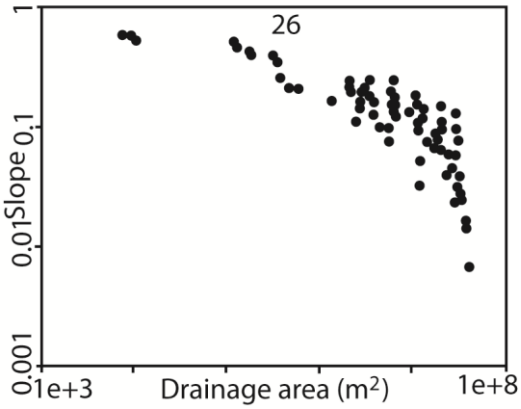
26
1
0.1
0.01
0.001
Slope
1e+3
Drainage area (m2)
1e+8

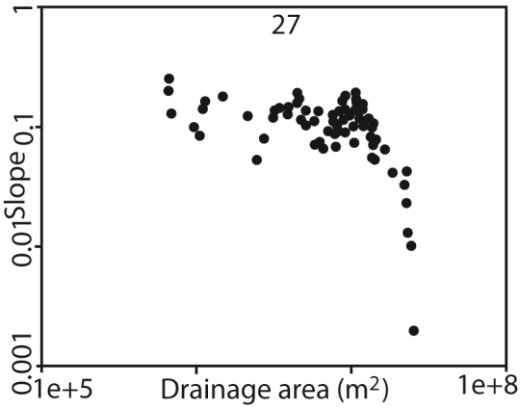
27
1
0.1
0.01
0.001
Slope
1e+5
Drainage area (m2)
1e+8

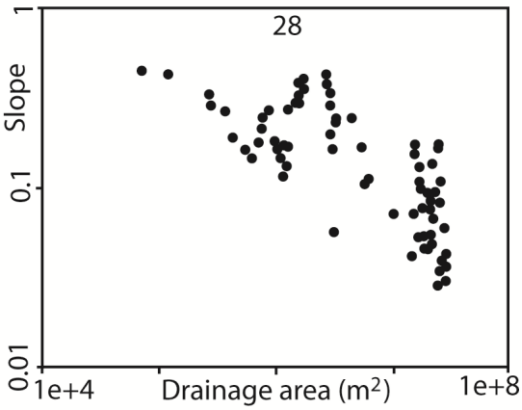
28
1
0.1
0.01
Slope
1e+4
Drainage area (m2)
1e+8

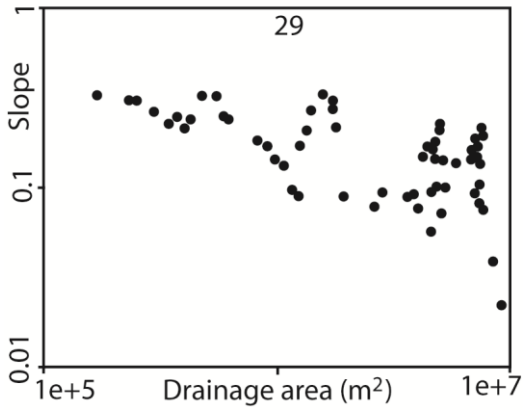
29
1
0.1
0.01
Slope
1e+5
Drainage area (m2)
1e+7

The Graph used to extrapolate present day throw rate

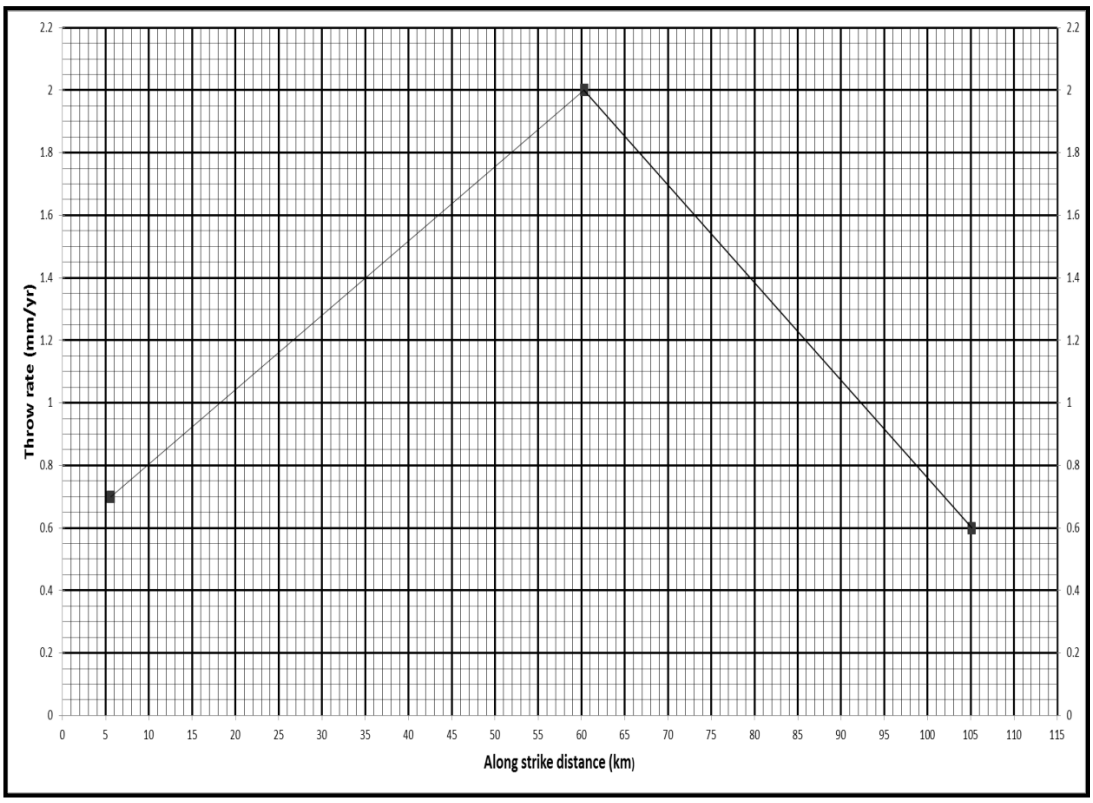

River #	Distance along strike (km)	Present throw rate extrapolated from timing data (mm/yr)	River #	Distance along strike (km)	Present throw rate extrapolated from timing data (mm/yr)
1	5.6	0.7	16	65.4	1.86
2	12.8	0.87	17	69	1.74
3	15.3	0.92	18	73.7	1.58
4	17.7	0.99	19	79.2	1.44
5	22.7	1.1	20	79.8	1.44
6	22.7	1.1	21	79.8	1.44
7	22.7	1.1	22	82.8	1.39
8	32.9	1.35	23	85	1.37
9	35.4	1.41	24	90	1.35
10	44.6	1.65	25	91.5	1.3
11	53.4	1.84	26	97.2	1.28
12	53.4	1.84	27	100.9	1.16
13	56.3	1.91	28	105.1	0.72
14	56.3	1.91	29	110	0.6
15	60.3	2			
16	65.4	1.86			

APPENDIX 2: ADDITIONAL DATA

Akcipinar River: Field data

Down stream distance (km)	Field location	Lat	Long	elevation (m)	Upstream area (km2)	Bankfull channel width (m)	Bankfull depth (m)	Valley width (m)	Slope measured with range finder (°)	DEM y/x	% bedrock in channel	Sediment % coarse	Sediment % med.	Sediment % fine
0.94	14	38.403	27.885	863	0.83	0.9	0.5	55	2	0.100	0	10	40	50
1.16	15	38.403	27.884	855	1.11	4.1	0.3	15.4	6.4	0.094	40	0	5	95
1.49	1	38.403	27.880	819	1.71	3.8	0.3	14.7	1.2	0.114	40	10	40	60
1.7	2	38.405	27.878	799	1.87	5.3	0.7	25	3.1	0.188	30	30	10	60
1.86	3	38.404	27.878	788	1.92	2.7	0.3	25	2.6	0.065	40	10	40	50
2.12	4	38.405	27.875	734	2.39	5.1	0.85	13.5	8	0.025	100	0	0	0
2.44	5	38.405	27.872	732	2.53	3.4	0.7	13.2	1.7	0.031	10	20	40	40
2.76	6	38.404	27.869	720	2.63	3.1	0.85	19	2.1	0.010	20	20	50	30
3.26	7	38.403	27.865	707	2.752	6.2	0.8	64	2.1	0.024	60	10	60	30
3.55	8	38.404	27.866	703	7.67	4.6	0.9	72	0.9	0.056	10	30	40	30
3.73	9	38.406	27.861	703	7.79	6.7	0.8	45	1.8	0.010	25	30	50	20
4.04	10	38.408	27.863	688	9.98	6.7	1.6	10.9	2.5	0.012	70	60	20	20
4.3	11	38.410	27.865	681	10.114	5.4	1.7	11.8	2	0.010	80	20	50	30
4.6	12	38.411	27.867	676	10.35	5.5	1.6	10.5	2.7	0.033	50	30	40	30
4.9	31	38.414	27.868	673	11.64	5.9	1.4	12.1	2.5	0.023	90	40	40	10
5.21	32	38.416	27.869	659	12.48	3.5	0.9	28	5.1	0.026	80	50	40	10
5.67	33	38.420	27.869	624	12.72	3.7	1.6	32	3	0.071	80	60	30	10
6.05	44	38.423	27.869	595	13.37	3.1	1.6	67	2.4	0.023	70	40	40	20
6.61	43	38.428	27.868	547	13.81	4.1	1.2	46	2.7	0.044	50	10	40	50
7.15	42	38.431	27.865	511	22.53	4.5	0.8	44	3.1	0.034	40	20	50	30
7.68	41	38.434		497	23.15	3.8	1.1	50	3.2	0.057	100	0	0	0
8.24	40	38.435	27.856	451	23.57	2.9	1.5	64	4.2	0.063	80	40	40	10
8.59	39	38.436	27.853	425	26.81	4.1	0.6	42	3.7	0.043	60	30	50	20
9.01	38	38.439	27.852	390	26.47	5.7	0.5	51	2.8	0.008	70	40	40	20
10.34	37	38.449	27.852	333	33.37	6.4	0.6	47	6.1	0.025	20	40	50	10
10.58	36	38.451	27.852	319	34.37	6.1	0.9	20	5.6	0.032	90	60	30	10
10.83	27	38.452	27.852	299	34.52	3.2	1.2	15	4.1	0.053	50	20	60	20
11.02	26	38.454	27.852	280	34.67	3.7	0.9	26	3.9	0.100	60	10	40	50
11.29	25	38.456	27.852	276	35.67	4.1	0.6	32	1.9	0.020	60	40	40	20
11.54	24	38.4584	27.85	264	35.28	3.7	0.8	26	3	0.070	90	0	70	30
11.74	23	38.46	27.9	258	35.54	4.1	0.7	30	2.7	0.038	10	30	60	10
12.03	22	38.462	27.9	240	35.83	3.2	0.6	21	3.1	0.043	20	10	70	20
12.26	21	38.464	27.9	220	35.98	3.6	0.6	23	2.7	0.085	100	0	0	0
12.52	20	38.466	27.9	215	41.76	9	0.4	29	4.8	0.019	0	80	10	10
12.83	19	38.468	27.9	188	42.01	4.3	0.9	74	3	0.025	90	70	20	10
13.03	18	38.468	27.9	167	42.71	4.9	0.9	27	5.4	0.048	50	20	50	30
13.32	28	38.47	27.8	164	42.95	5.2	0.8	34	4.7	0.013	60	30	40	30
13.77	16	38.474	27.8	157	43.52	5.6	0.5	35	4.1	0.017	10	20	50	30
14.12	17	38.476	27.8	149	43.71	5.6	0.6	43	3	0.010	0	40	50	10
14.6	30	38.48	27.8	131	44.38	4.8	0.5	62	3.2	0.013	100	0	0	0
14.98	29	38.483	27.8	123	46.5	8	1	78	1.4	0.067	0	0	10	90
15.04	13	38.485	27.8	121	46.6	6	3	78	0.1	0.013	0	40	40	20
15.35	34	38.487	27.8	116	46.7	7.6	0.9	82	2.1	0.036	50	40	40	20
15.49	35	38.488	27.8	110	46.71	8.9	0.6	202	0.4	0.000	75	50	40	10

Akcipinar River: stream power calculations part 1

	0.8	0.35	0.85	2									
	Finnegan prefactor	whittaker prefactor	prefactor	prefactor									
Down stream distance (km)	Predicted width Finnegan (m)	Predicted width Whittaker (m)	Predicted width: hydraulic scaling fitted to downstream of kp (m)	Predicted width: hydraulic scaling fitted to upstream of kp (m)	Velocity (m/s)	Cross-sectional area	Discharge (m3/s)	Discharge : Area (Q:A) ratio	Discharge scaled to drainage area (m3/s)	discharge scaled to regional Q:A ratio	Actual unit stream power (W/sqm)	Average actual stream power over ~2 km	error 1 standard deviation
0.94	1.41	1.43	0.77	1.82	0.52	0.225	0.12	7.11	0.12	0.18	194.78		
1.16	1.26	0.95	0.90	2.11	0.33	0.615	0.21	5.39	0.16	0.24	53.71		
1.49	2.04	2.35	1.11	2.62	0.14	0.57	0.08	20.73	0.25	0.37	108.62		
1.7	1.77	1.60	1.16	2.73	1.27	1.855	2.35	0.80	0.27	0.40	139.73		
1.86	1.84	1.75	1.18	2.77	0.21	0.405	0.09	22.25	0.28	0.41	98.20	119.01	26.19
2.12	1.62	1.16	1.31	3.09	3.01	2.1675	6.52	0.37	0.35	0.52	24.74		
2.44	2.22	2.34	1.35	3.18	0.94	1.19	1.12	2.27	0.37	0.55	49.11		
2.76	2.16	2.16	1.38	3.24	1.54	1.3175	2.03	1.30	0.38	0.57	17.92		
3.26	2.20	2.20	1.41	3.32	1.36	2.48	3.38	0.81	0.40	0.59	22.63		
3.55	3.82	4.72	2.35	5.54	1.13	2.07	2.34	3.28	1.12	1.65	195.65		
3.73	3.37	3.50	2.37	5.58	1.26	2.68	3.38	2.31	1.14	1.68	23.76	55.64	34.73
4.04	3.48	3.33	2.69	6.32	5.94	5.36	31.86	0.31	1.46	2.15	36.30		
4.3	3.65	3.69	2.70	6.36	6.00	4.59	27.54	0.37	1.48	2.18	39.56		
4.6	3.47	3.26	2.73	6.43	6.18	4.4	27.18	0.38	1.51	2.23	132.48		
4.9	3.69	3.53	2.90	6.82	4.55	4.13	18.79	0.62	1.70	2.51	94.09		
5.21	3.30	2.64	3.00	7.07	2.69	1.575	4.23	2.95	1.82	2.69	196.46		
5.67	3.68	3.37	3.03	7.13	6.51	2.96	19.27	0.66	1.86	2.74	515.91	169.13	90.11
6.05	3.92	3.79	3.11	7.31	5.82	2.48	14.44	0.93	1.95	2.88	211.46		
6.61	3.88	3.64	3.16	7.43	3.47	2.46	8.55	1.62	2.02	2.98	316.18		
7.15	4.55	4.12	4.03	9.49	1.65	1.8	2.98	7.56	3.29	4.86	359.13		
7.68	4.57	4.11	4.09	9.62	3.18	2.09	6.64	3.48	3.38	4.99	735.25	405.51	114.21
8.24	4.37	3.67	4.13	9.71	6.77	2.175	14.74	1.60	3.44	5.08	1079.01		
8.59	4.70	4.07	4.40	10.36	1.02	1.23	1.25	21.43	3.92	5.78	591.89		
9.01	4.93	4.59	4.37	10.29	0.61	1.425	0.88	30.24	3.87	5.70	73.75	581.55	251.36
10.34	4.64	3.55	4.91	11.55	1.31	1.92	2.51	13.29	4.87	7.19	275.31		
10.58	4.77	3.73	4.98	11.73	2.82	2.745	7.74	4.44	5.02	7.41	380.81		
10.83	5.07	4.29	4.99	11.75	4.28	1.92	8.22	4.20	5.04	7.44	1199.15		
11.02	5.13	4.39	5.00	11.78	2.35	1.665	3.91	8.86	5.06	7.47	1979.07		
11.29	5.94	6.09	5.08	11.94	0.73	1.23	0.90	39.81	5.21	7.69	367.50		
11.54	5.43	4.96	5.05	11.88	1.63	1.48	2.41	14.64	5.15	7.60	1409.72		
11.74	5.55	5.21	5.07	11.92	1.18	1.435	1.70	20.95	5.19	7.66	694.44	900.86	322.70
12.03	5.42	4.92	5.09	11.97	0.93	0.96	0.89	40.09	5.23	7.72	1028.20		
12.26	5.58	5.24	5.10	12.00	0.87	1.08	0.94	38.35	5.26	7.75	1786.14		
12.52	5.29	4.30	5.49	12.92	0.52	1.8	0.93	45.03	6.10	9.00	189.68		
12.83	5.80	5.30	5.51	12.96	2.06	1.935	3.99	10.54	6.14	9.05	515.86		
13.03	5.22	4.12	5.55	13.07	2.77	2.205	6.10	7.00	6.24	9.20	888.73		
13.32	5.37	4.39	5.57	13.11	2.04	2.08	4.24	10.13	6.27	9.26	232.60		
13.77	5.54	4.68	5.61	13.19	0.74	1.4	1.04	41.80	6.36	9.38	281.38	703.23	289.47
14.12	5.89	5.38	5.62	13.22	0.92	1.68	1.54	28.41	6.38	9.42	171.72		
14.6	5.85	5.26	5.66	13.32	0.66	1.2	0.79	56.31	6.48	9.56	256.95		
14.98	6.97	7.71	5.80	13.64	1.74	4	6.95	6.69	6.79	10.02	818.43		
15.04	11.51	24.64	5.80	13.65	4.18	9	37.60	1.24	6.81	10.04	211.66		
15.35	6.46	6.46	5.81	13.67	1.72	3.42	5.89	7.92	6.82	10.06	463.50	384.45	133.69
15.49	8.85	13.40	5.81	13.67	0.33	2.67	0.89	52.34	6.82	10.07	102.24	320.26	143.10
								6.846264					

Akcipinar River: stream power calculations part 2, stream powers calculated using different width prediction methods

Down stream distance (km)	(Finnegan) predicted Unit stream power (W/m^2)	(Whittaker) predicted Unit stream power (W/m^2)	(Hydraulic scaling, upstream of KP) predicted Unit stream power (W/m^2)	(Hydraulic scaling, downstream of KP) predicted Unit stream power (W/m^2)
0.94	230.32	366.02	55.79	23.71
1.16	817.63	1279.25	193.55	82.26
1.49	968.54	1591.47	209.73	89.14
1.7	811.92	1509.91	158.32	67.29
1.86	2040.97	2916.70	484.65	205.97
2.12	58.60	65.86	16.27	6.92
2.44	380.03	451.56	100.45	42.69
2.76	217.36	194.25	71.01	30.18
3.26	140.21	156.19	38.53	16.38
3.55	0.00	0.00	0.00	0.00
3.73	788.15	698.60	227.43	96.66
4.04	528.72	489.72	143.23	60.87
4.3	321.17	287.02	89.26	37.94
4.6	245.72	296.72	54.18	23.03
4.9	1108.40	1214.27	259.48	110.28
5.21	2004.07	2276.17	452.66	192.38
5.67	2460.51	3590.10	458.37	194.81
6.05	2304.50	2542.15	527.80	224.32
6.61	2068.92	2684.62	417.21	177.32
7.15	1055.07	1280.02	211.15	89.74
7.68	3683.35	5089.43	665.58	282.87
8.24	3429.93	4853.54	607.35	258.12
8.59	3875.04	4982.73	726.64	308.82
9.01	1420.46	1182.09	371.32	157.81
10.34	2804.37	3151.42	567.48	241.18
10.58	3598.60	3617.00	789.83	335.68
10.83	5543.40	7308.59	989.44	420.51
11.02	962.04	1556.46	146.90	62.43
11.29	2305.12	2449.84	482.78	205.18
11.54	1815.46	2639.04	300.08	127.53
11.74	3358.59	4188.82	623.14	264.84
12.03	4853.29	6263.10	876.55	372.54
12.26	1221.23	1861.43	194.26	82.56
12.52	4583.45	4831.43	947.84	402.83
12.83	5822.45	6542.99	1146.09	487.09
13.03	656.73	869.98	113.85	48.39
13.32	776.05	745.26	171.68	72.96
13.77	1205.91	1233.16	253.93	107.92
14.12	1804.63	1629.32	417.52	177.45
14.6	1069.15	1023.34	236.19	100.38
14.98	2474.48	3757.29	382.79	162.69
15.04	646.37	435.33	185.42	78.80
15.35	2000.16	1643.30	493.21	209.62

Akcipinar River: stream power calculations part 3, 2 km averages of stream powers calculated using different width prediction methods

Down stream distance (km)	Average unit stream power using widths from hydraulic scaling fitted to downstream of KP	error 1 standard deviation	Average unit stream power using widths from hydraulic scaling fitted to upstream of KP	error 1 standard deviation	Average unit stream power using widths from Finnegan width scaling	error 1 standard deviation	Average unit stream power using widths from Whittaker width scaling	error 1 standard deviation
0.94								
1.16								
1.49								
1.7								
1.86	231.23	59.71	98.27	25.38	144.21	40.39	154.99	46.27
2.12								
2.44								
2.76								
3.26								
3.55								
3.73	91.36	42.23	38.83	17.95	59.35	25.44	57.16	20.03
4.04								
4.3								
4.6								
4.9								
5.21								
5.67	167.87	68.27	71.35	29.01	137.29	56.87	151.22	63.16
6.05								
6.61								
7.15								
7.68	288.89	65.85	122.78	27.99	248.92	62.17	271.32	71.04
8.24								
8.59								
9.01	317.59	114.79	134.97	48.79	297.91	109.36	347.91	131.20
10.34								
10.58								
10.83								
11.02								
11.29								
11.54								
11.74	479.09	141.78	203.61	60.26	462.76	137.09	462.76	158.84
12.03								
12.26								
12.52								
12.83								
13.03								
13.32								
13.77	377.92	126.15	160.62	53.61	368.86	116.01	368.86	127.77
14.12								
14.6								
14.98								
15.04								
15.35								
15.49	264.63	140.02	112.47	59.51	222.43	119.13	209.99	110.60

Akcipinar River: Field Schmidt hammer readings

Downstream distance (km)	Location	Schmidt hammer readings																	
0.94	14	62	62	64	54	64	50	56	64	61	60	57	52	50	56	61	61	52	61
1.16	15	48	32	38	63	41	44	46	37	49	46	46	38	40	41	38	32	43	45
1.49	1	no data/ river/bed rock not accessible																	
1.7	2	69	60	67	68	68	68	70	66	68	68	71	65	67	69	66	68	65	69
1.86	3	60	59	57	66	58	52	60	65	59	68	63	66	63	63	62	50	65	65
2.12	4	57	61	60	54	58	57	60	60	60	58	58	60	56	51	61	59	59	58
2.44	5	no data/ river/bed rock not accessible																	
2.76	6	69	68	70	58	66	66	69	69	64	72	68	70	67	69	69	69	67	69
3.26	7	69	68	65	58	66	66	69	67	60	72	68	68	67	69	69	69	63	66
3.55	8	54	41	42	51	52	50	44	57	49	54	45	53	42	49	42	49	49	53
3.73	9	56	54	62	62	56	62	63	63	61	64	59	58	60	62	58	61	60	60
4.04	10	50	50	53	50	51	50	51	48	50	42	50	52	51	50	50	51	52	51
4.3	11	58	54	42	60	51	58	59	59	55	62	45	49	63	61	50	58	59	58
4.6	12	66	65	67	66	60	64	63	64	58	62	65	63	64	60	64	61	63	64
4.9	31	no data/ river/bed rock not accessible																	
5.21	32	40	37	45	35	46	42	31	42	49	39	49	46	33	46	33	46	39	36
5.67	33	57	56	51	54	58	60	62	60	59	64	64	59	56	61	61	52	61	52
6.05	44	no data/ river/bed rock not accessible																	
6.61	43	46	37	35	31	38	42	42	40	39	30	36	35	38	40	39	36	35	45
7.15	42	41	32	41	52	46	46	37	38	39	40	45	32	39	39	39	42	42	36
7.68	41	32	25	41	38	40	37	50	33	37	41	46	34	25	40	36	45	39	42
8.24	40	52	36	38	40	41	32	47	49	46	40	41	52	42	47	42	54	37	32
8.59	39	49	39	42	42	32	41	30	37	37	30	43	33	32	31	32	37	32	40
9.01	38	42	37	35	51	38	37	32	31	27	41	31	40	30	26	46	39	37	38
10.34	37	49	35	36	30	42	26	37	35	42	42	46	41	31	39	47	37	44	42
10.58	36	32	27	41	32	40	46	48	34	41	4	47	32	38	37	46	41	42	40
10.83	27	66	60	60	62	62	64	64	62	62	66	60	62	70	62	64	54	56	68
11.02	26	56	57	62	60	59	64	64	59	60	60	59	58	54	60	62	62	56	49
11.29	25	66	66	64	59	64	60	65	61	59	62	62	64	63	64	65	65	60	61
11.54	24	61	62	60	60	60	54	61	61	64	60	62	60	63	66	66	64	60	61
11.74	23	51	49	56	56	51	53	49	57	56	51	54	58	60	60	57	61	54	56
12.03	22	51	56	51	51	51	54	54	52	57	55	56	54	52	49	51	56	56	52
12.26	21	no data/ river/bed rock not accessible																	
12.52	20	48	52	52	49	56	46	45	51	56	61	49	60	59	54	52	54	60	60
12.83	19	65	62	67	68	66	64	67	64	56	63	60	66	66	62	60	62	58	63
13.03	18	41	38	46	51	46	47	56	49	48	42	52	45	56	47	38	39	44	42
13.32	28	60	62	58	63	67	60	62	67	68	66	64	67	60	62	62	64	64	62
13.77	16	35	34	42	21	32	40	35	37	35	51	52	37	42	40	40	31	43	35
14.12	17	30	37	42	28	38	40	35	35	31	38	28	42	30	37	32	38	22	42
14.6	30	41	38	37	37	36	38	40	45	31	34	34	40	42	32	34	37	42	37
14.98	29	31	36	36	35	39	30	40	36	41	37	41	36	38	31	42	40	33	36
15.04	13	38	34	24	36	38	38	32	24	34	58	38	32	32	24	26	37	41	36
15.35	34	no data/ river/bed rock not accessible																	
15.49	35	20	26	59	24	24	28	30	28	25	28	30	25	25	25	30	32	22	30

Akcipinar River: Selby Rock Mass Strength Index calculation

Downstream distance (km)	Location #	Schmidt hammer average	Hardness selby index number	Weathering selby index number	Joint spacing selby index number	Joint width selby index number	Joint orientation selby index number	Ground water selby index number	continuity of joints selby index numbers	Lithology	Selby rock mass strength rating
0.94	14	58	18	7	15	5	14	6	5	gneiss	70
1.16	15	43	14	5	8	5	20	6	5	schist	63
1.49	1										
1.7	2	67	20	9	8	6	18	6	5	mica schist	72
1.86	3	61	20	9	8	4	18	6	5	schist	70
2.12	4	58	18	9	8	5	18	6	5	schist	69
2.44	5										
2.76	6	68	20	9	8	5	18	6	5	schist	71
3.26	7	67	20	9	8	5	18	6	5	schist	71
3.55	8	49	14	9	8	4	18	6	5	schist	64
3.73	9	60	20	7	8	6	18	6	5	gneiss	70
4.04	10	50	18	7	8	4	18	6	5	schist	66
4.3	11	56	18	7	8	5	18	6	5	schist	67
4.6	12	63	20	8	8	2	18	6	6	schist	68
4.9	31										
5.21	32	41	14	9	8	5	18	6	6	schist	66
5.67	33	58	18	7	8	6	18	6	5	schist	68
6.05	44										
6.61	43	38	10	7	8	5	9	6	6	schist	51
7.15	42	40	14	9	15	4	20	6	5	schist	73
7.68	41	38	10	7	8	5	18	6	6	schist	60
8.24	40	42	14	9	8	5	18	6	5	gniess	65
8.59	39	37	10	7	15	5	20	6	5	schist	68
9.01	38	37		7	8	5	18	6	5	schist	49
10.34	37	39	10	7	8	6	20	6	6	schist	63
10.58	36	38	10	7	8	5	18	6	5	schist	59
10.83	27	63	20	9	15	6	18	6	5	gneiss	79
11.02	26	59	18	7	21	6	18	6	5	gneiss	81
11.29	25	62	20	9	21	6	18	6	5	gneiss	85
11.54	24	61	20	9	15	6	18	6	5	gneiss	79
11.74	23	54	18	7	15	6	18	6	5	gneiss	75
12.03	22	53	18	7	15	6	18	6	5	gneiss	75
12.26	21										
12.52	20	54	18	7	15	6	18	6	5	gneiss	75
12.83	19	64	20	7	8	6	18	6	5	gneiss	70
13.03	18	46	10	5	8	6	18	6	5	schist	58
13.32	28	64	20	9	8	6	18	6	5	gneiss	72
13.77	16	37	10	7	8	5	20	6	6	schist	62
14.12	17	35	10	5	15	5	18	6	6	schist	65
14.6	30	37	10	5	21	5	18	6	5	schist	70
14.98	29	36	10	5	8	6	18	6	5	schist	58
15.04	13	34	5	5	21	5	20	6	5	schist	67
15.35	34										
15.49	35	32	5	5	8	2	18	6	5	schists	49

Sart River: Field data

Down stream distance (km)	Field location	Lat	Long	elevation (m)	Upstream area (km2)	Bankfull channel width (m)	Bankfull depth (m)	Valley width (m)	Slope measured with range finder (°)	DEM y/x	% bedrock in channel	Sediment % coarse	Sediment % med.	Sediment % fine
0.44	8	38.375	27.971	959	1.79	6	0.5	181	2.7	0.007	0	0	0	0
0.90	9	38.378	27.969	957	2.22	1.1	0.3	236	1.2	0.065	0	20	60	20
0.96	10	38.379	27.969	957	2.23	1.7	0.5	240	2.5	0.037	0	30	40	30
1.26	11	38.382	27.970	953	2.79	1.5	0.5	35	1.7	0.028	90	0	0	100
1.62	12	38.384	27.971	941	3.41	2.2	0.6	47	1.4	0.006	10	10	70	20
2.12	13	38.388	27.972	936	3.72	2.7	0.5	33	2	0.007	80	60	20	20
2.56	14	38.391	27.972	912	4.03	5.5	0.9	56	4.2	0.017	0	40	40	20
2.97	15	38.394	27.971	911	4.32	3.7	0.5	22	1.4	0.010	0	40	20	40
3.29	16	38.397	27.972	909	5.31	5.6	0.85	72	1.7	0.020	50	20	30	50
3.68	17	38.400	27.973	899	5.51	6.2	0.5	32	1.2	0.016	5	40	20	20
4.06	18	38.403	27.974	886	5.79	3.2	0.45	29	1.1	0.018	0	10	70	20
4.43	19	38.406	27.974	880	6.98	1.7	1.5	16	1.4	0.034	20	20	30	50
4.67	20	38.408	27.974	870	7.15	6	0.5	39	1.8	0.005	20	10	70	20
5.04	21	38.411	27.973	886	7.67	5.2	0.9	12	3.4	0.018	25	30	40	20
5.42	22	38.413	27.970	838	8.05	7.1	0.4	22	1.9	0.016	5	10	60	30
5.91	29	38.416	27.967	825	8.51	4.5	0.7	70	1.9	0.021	100	0	0	0
6.49	30	38.420	27.964	800	8.81	3.6	1	72	0.9	0.019	40	10	70	20
7.02	31	38.424	27.962	770	11.31	3.9	1.9	64	1.9	0.018	30	20	40	40
7.63	32	38.429	27.962	739	11.96	4.8	0.6	36	1.6	0.008	0	40	30	30
8.11	33	38.433	27.965	711	12.31	5.2	0.7	61	2.9	0.034	60	10	60	30
8.80	34	38.438	27.968	657	13.19	5	0.6	41	6.7	0.076	20	30	60	10
9.32	35	38.442	27.971	594	15.20	6.2	0.5	36	3.2	0.026	0	10	70	20
9.74	36	38.445	27.973	558	15.38	3.2	1.8	54	4.4	0.038	0	30	50	20
10.24	37	38.449	27.975	526	17.11	4.8	1.6	52	3.6	0.011	70	20	60	20
11.99	41	38.459	27.987	402	20.45	3.7	1.7	48	2.1	0.078	0	30	40	30
12.22	40	38.466	27.988	363	21.69	2.1	1.3	10.2	1.8	0.043	100	0	0	0
12.74	39	38.463	27.991	320	21.88	1.9	2.6	12	2.5	0.039	100	0	0	0
13.25	38	38.465	27.996	256	22.60	2.6	1.8	69	3.6	0.046	90	0	100	0
13.95	23	38.466	28.002	210	29.48	1.8	2.4	21	4.2	0.053	100	0	0	0
14.40	24	38.467	28.006	182	32.34	3.5	0.9	52	3.3	0.017	70	50	40	10
14.87	25	38.468	28.010	172	33.53	3.9	2.5	84	1.3	0.006	0	25	60	15
15.37	26	38.470	28.015	161	35.45	5.9	1.4	109	1.1	0.006	0	10	60	30
15.72	27	38.470	28.018	154	35.92	4.9	1.4	119	1	0.010	0	5	70	25
16.22	6	38.471	28.022	146	67.38	4.8	1.4	162	0.7	0.011	0	20	40	40
16.58	5	38.473	28.025	138	69.41	4.6	1.3	158	0.6	0.006	0	20	20	60
16.92	4	38.476	28.027	135	70.58	4.8	1.4	258	1.2	0.006	0	30	30	40
17.28	3	38.478	28.029	133	71.70	5.3	1.25	342	0.4	0.005	0	20	20	60
17.67	2	38.481	28.030	127	72.63	5.6	1.4	332	0.5	0.003	0	15	20	65
18.00	1	38.483	28.032	121	72.98	5.9	1.5	307	0.4	0.003	0	10	30	60
18.30	28	38.487	28.034	114	73.20	5.9	1.5	540	0.2	0.010	0	10	60	30

Sart River: stream power calculations part 1

0.8	0.35	0.85	2
Finnegan prefactor	whittaker prefactor	prefactor	prefactor
0.52	0.14	0.6	1.35

Down stream distance (km)	Predicted width Finnegan (m)	Predicted width Whittaker (m)	Predicted width: hydraulic scaling fitted to downstream of kp (m)	Predicted width: hydraulic scaling fitted to upstream of kp (m)	Velocity (m/s)	Cross-sectional area	Discharge (m3/s)	Discharge: Area (Q:A) ratio	Discharge scaled to drainage area (m3/s)	discharge scaled to regional Q:A ratio	Actual unit stream power (W/sqm)	Average actual stream power over ~2 km	error 1 standard deviation
0.44	1.69	1.60	0.80	1.81	0.60	1.5	0.90	1.98	0.27	0.39	4.11		
0.90	1.18	0.63	0.89	2.01	0.14	0.165	0.02	92.87	0.34	0.48	276.21		
0.96	1.32	0.81	0.90	2.01	0.58	0.425	0.25	9.02	0.34	0.48	103.33		
1.26	1.52	1.00	1.00	2.26	0.48	0.375	0.18	15.57	0.43	0.60	109.35		
1.62	2.19	2.11	1.11	2.49	0.63	0.66	0.41	8.25	0.52	0.73	19.70		
2.12	2.22	2.08	1.16	2.60	0.52	0.675	0.35	10.61	0.57	0.80	19.58	88.71	51.23
2.56	1.92	1.43	1.21	2.71	2.44	2.475	6.04	0.67	0.62	0.87	26.32		
2.97	2.19	1.88	1.25	2.80	0.43	0.925	0.40	10.74	0.66	0.93	23.75		
3.29	2.06	1.47	1.38	3.11	1.38	2.38	3.29	1.61	0.81	1.14	40.23		
3.68	2.18	1.65	1.41	3.17	0.40	1.55	0.62	8.83	0.84	1.19	30.18		
4.06	2.16	1.58	1.44	3.25	0.31	0.72	0.22	25.81	0.89	1.25	70.75	38.25	9.61
4.43	2.06	1.29	1.58	3.57	3.91	1.275	4.98	1.40	1.07	1.50	298.10		
4.67	2.96	2.95	1.60	3.61	0.49	1.5	0.74	9.68	1.09	1.54	13.50		
5.04	2.41	1.76	1.66	3.74	2.19	2.34	5.13	1.49	1.17	1.65	57.52		
5.42	2.51	1.89	1.70	3.83	0.32	1.42	0.46	17.51	1.23	1.73	39.22		
5.91	2.45	1.74	1.75	3.94	0.99	1.575	1.56	5.45	1.30	1.83	82.37	98.14	57.29
6.49	2.53	1.84	1.78	4.01	1.39	1.8	2.51	3.51	1.35	1.90	96.50		
7.02	2.80	2.05	2.02	4.54	7.31	3.705	27.07	0.42	1.73	2.44	111.32		
7.63	3.32	2.97	2.07	4.67	0.67	1.44	0.96	12.42	1.83	2.58	43.42		
8.11	2.57	1.62	2.11	4.74	1.23	1.82	2.23	5.52	1.88	2.65	167.51	104.69	25.51
8.80	2.26	1.16	2.18	4.90	1.37	1.5	2.06	6.41	2.02	2.84	422.23		
9.32	2.93	1.96	2.34	5.26	0.66	1.55	1.02	14.93	2.32	3.27	134.58		
9.74	2.74	1.67	2.35	5.29	9.99	2.88	28.76	0.53	2.35	3.31	385.21		
10.24	3.58	2.95	2.48	5.58	7.13	3.84	27.40	0.62	2.62	3.69	85.84	256.96	85.64
11.99	2.66	1.35	2.71	6.11	6.15	3.145	19.34	1.06	3.13	4.41	915.19		
12.22	3.05	1.81	2.79	6.29	3.33	1.365	4.54	4.77	3.32	4.68	927.84		
12.74	3.11	1.89	2.81	6.31	15.69	2.47	38.77	0.56	3.35	4.72	947.38		
13.25	3.06	1.78	2.85	6.42	9.03	2.34	21.13	1.07	3.46	4.87	840.36	907.69	23.40
13.95	3.28	1.84	3.26	7.33	17.34	2.16	37.46	0.79	4.51	6.35	1844.86		
14.40	4.23	3.16	3.41	7.68	2.16	1.575	3.40	9.50	4.95	6.97	330.75		
14.87	5.22	5.05	3.47	7.82	10.46	4.875	51.00	0.66	5.13	7.23	109.11		
15.37	5.39	5.28	3.57	8.04	3.02	4.13	12.46	2.84	5.42	7.64	72.34		
15.72	4.85	4.11	3.60	8.09	2.88	3.43	9.87	3.64	5.49	7.74	157.11		
16.22	6.06	5.02	4.93	11.08	2.41	3.36	8.09	8.33	10.30	14.52	329.00	473.86	340.27
16.58	6.93	6.77	5.00	11.25	1.92	2.99	5.75	12.08	10.61	14.96	184.49		
16.92	7.04	6.94	5.04	11.34	3.15	3.36	10.59	6.66	10.79	15.21	171.91		
17.28	7.16	7.17	5.08	11.43	1.45	3.3125	4.81	14.92	10.96	15.45	149.25		
17.67	7.98	9.16	5.11	11.51	2.03	3.92	7.97	9.11	11.11	15.65	82.89		
18.00	7.86	8.81	5.13	11.53	2.09	4.425	9.24	7.90	11.16	15.73	86.60	135.03	23.81
18.30	6.38	5.43	5.13	11.55	1.48	4.425	6.54	11.20	11.19	15.78	262.04	156.20	33.55
								6.54					

Sart River: stream power calculations part 2, stream powers calculated using different width prediction methods

Down stream distance (km)	(Finnegan) predicted Unit stream power (W/m^2)	(Whittaker) predicted Unit stream power (W/m^2)	(Hydraulic scaling, upstream of KP) predicted Unit stream power (W/m^2)	(Hydraulic scaling, downstream of KP) predicted Unit stream power (W/m^2)
0.44	10.37	10.95	30.74	13.66
0.90	182.14	341.42	340.03	151.12
0.96	94.71	154.68	196.25	87.22
1.26	76.69	116.31	163.57	72.70
1.62	14.05	14.54	39.14	17.39
2.12	16.93	18.02	45.69	20.31
2.56	53.60	71.88	120.13	53.39
2.97	28.48	33.15	70.51	31.34
3.29	77.60	108.52	162.99	72.44
3.68	60.94	80.62	132.93	59.08
4.06	74.24	101.69	156.75	69.66
4.43	174.21	278.64	319.75	142.11
4.67	19.38	19.48	50.49	22.44
5.04	88.13	120.66	179.99	80.00
5.42	78.75	104.63	163.58	72.70
5.91	107.22	150.92	211.77	94.12
6.49	97.35	133.68	195.12	86.72
7.02	110.03	150.05	215.13	95.61
7.63	44.51	49.83	100.44	44.64
8.11	240.13	381.58	413.76	183.89
8.80	662.02	1290.10	968.76	430.56
9.32	202.35	301.79	356.74	158.55
9.74	319.76	524.22	523.89	232.84
10.24	81.69	99.15	166.04	73.80
11.99	904.65	1777.93	1247.89	554.62
12.22	453.19	764.40	697.22	309.88
12.74	410.41	677.21	641.36	285.05
13.25	507.43	871.80	766.04	340.46
13.95	717.65	1280.97	1019.36	453.05
14.40	194.24	260.32	339.27	150.78
14.87	57.83	59.80	122.47	54.43
15.37	56.23	57.39	119.48	53.10
15.72	112.60	132.74	214.08	95.15
16.22	184.98	223.00	320.64	142.51
16.58	86.86	89.00	169.77	75.46
16.92	83.21	84.30	163.70	72.75
17.28	78.43	78.31	155.70	69.20
17.67	41.28	35.96	90.78	40.35
18.00	46.15	41.13	99.68	44.30
18.30	172.05	202.09	301.17	133.85

Sart River: stream power calculations part 3, 2 km averages of stream powers calculated using different width prediction methods

Down stream distance (km)	Averages unit stream power using widths from hydraulic scaling fitted to downstream of KP	error 1 standard deviation	Averages unit stream power using widths from hydraulic scaling fitted to upstream of KP	error 1 standard deviation	Averages unit stream power using widths from Finnegan width scaling	error 1 standard deviation	Averages unit stream power using widths from Whittaker width scaling	error 1 standard deviation
0.44								
0.90								
0.96								
1.26								
1.62								
2.12	135.90	61.09	68.42	61.09	65.82	33.64	109.32	64.41
2.56								
2.97								
3.29								
3.68								
4.06	128.66	18.44	57.18	8.19	58.97	9.82	79.17	14.88
4.43								
4.67								
5.04								
5.42								
5.91	185.11	48.38	82.27	21.50	93.54	27.89	134.87	47.01
6.49								
7.02								
7.63								
8.11	231.11	65.82	102.72	29.25	123.01	41.54	178.78	71.07
8.80								
9.32								
9.74								
10.24	503.86	171.34	223.94	76.15	316.45	125.02	553.82	260.32
11.99								
12.22								
12.74								
13.25	1022.83	138.95	372.50	61.75	568.92	113.66	1022.83	254.82
13.95								
14.40								
14.87								
15.37								
15.72								
16.22	355.88	169.14	158.17	75.18	220.59	125.34	335.70	125.34
16.58								
16.92								
17.28								
17.67								
18.00								
18.30	163.47	37.69	72.65	16.75	84.67	23.50	88.47	23.50

Sart River: Field Schmidt hammer readings

Downstream distance (km)	Location	Schmidt hammer readings																			
0.44	8																				
0.90	9																				
0.96	10																				
1.26	11																				
1.62	12	53	46	48	52	51	48	48	53	49	47	40	46	52	42	45	49	55	50	49	49
2.12	13	52	48	48	45	51	51	50	46	50	48	55	53	50	49	55	48	48	42	51	43
2.56	14	20	20	17	27	28	20	22	25	20	26	16	20	13	20	20	20	16	17	22	16
2.97	15																				
3.29	16	34	46	40	20	42	20	47	48	45	44	20	30	47	39	28	36	46	45	40	42
3.68	17	38	35	30	48	47	30	34	38	42	37	26	32	38	31	50	47	38	40	53	58
4.06	18	30	38	42	46	40	39	41	42	47	41	35	40	39	37	37	45	44	41	40	36
4.43	19																				
4.67	20	34	25	43	50	20	42	49	51	25	41	46	54	35	41	40	48	27	30	46	42
5.04	21	51	58	50	55	48	53	47	53	56	56	50	53	63	57	54	49	60	52	59	49
5.42	22																				
5.91	29	30	32	36	32	34	32	31	44	26	30	40	30	40	33	30	36	30	20	26	39
6.49	30	41	41	40	36	30	31	36	35	34	40	37	42	45	39	46	41	43	43	37	42
7.02	31	38	34	24	36	38	38	32	26	28	34	28	38	32	24	32	30	26	36	30	32
7.63	32	36	46	41	47	41	40	41	41	40	37	44	46	44	51	36	37	41	44	42	45
8.11	33	44	30	41	37	46	42	41	39	36	41	42	51	32	41	46	47	43	43	46	45
8.80	34	41	43	46	51	49	50	48	48	46	50	51	52	55	40	55	47	43	42	28	41
9.32	35																				
9.74	36	41	46	44	37	34	37	46	41	41	38	44	31	34	48	49	39	45	42	41	46
10.24	37																				
11.99	41																				
12.22	40																				
12.74	39	70	64	65	60	61	66	69	65	72	64	65	60	62	63	59	67	70	64	66	58
13.25	38	64	62	57	62	58	54	60	59	64	66	62	63	54	58	64	64	60	61	59	66
13.95	23	66	66	68	64	69	72	58	59	62	62	66	64	66	58	59	66	60	71	65	62
14.40	24	55	62	64	54	60	64	52	61	62	52	62	58	51	62	49	59	64	61	51	48
14.87	25	75	65	65	69	71	71	72	70	69	71	68	72	72	65	68	70	62	66	64	66
15.37	26	32	36	32	34	32	31	44	37	26	32	38	31	50	47	38	40	40	39	37	37
15.72	27	35	42	35	37	37	30	42	35	41	38	40	54	36	49	32	31	44	40	36	31
16.22	6	36	24	39	46	41	20	39	41	36	30	33	42	36	41	41	37	45	30	34	32
16.58	5																				
16.92	4																				
17.28	3																				
17.67	2																				
18.00	1																				
18.30	28																				

Sart River: Selby Rock Mass Strength Index calculation

Down stream distance (km)	Location #	Schmidt hammer average	Hardness selby index number	Weathering selby index number	Joint spacing selby index number	Joint width selby index number	Joint orientation selby index number	Ground water selby index number	continuity of joints selby index numbers	Lithology	Selby rock mass strength rating
0.44	8	20	5	7	8	5	18	6	5	sediments	54
0.90	9	20	5	7	8	5	18	6	5	sediments	54
0.96	10	20	5	5	8	4	18	6	5	mica schists	51
1.26	11	49	14	7	8	5	18	6	5	schist	63
1.62	12	49	14	7	8	5	18	6	5	mica schist	63
2.12	13	20	5	5	15	5	18	6	5	mica schist	59
2.56	14										
2.97	15	38	10	5	8	4	18	6	5	schist	56
3.29	16	40	10	9	8	5	18	6	5	schist	61
3.68	17	40	14	7	8	5	9	6	5	schist	54
4.06	18										
4.43	19	39	10	7	8	5	9	6	5	schist	50
4.67	20	54	18	9	8	5	9	6	5	schit	60
5.04	21	20	5	5	8	5	18	6	5	schist	52
5.42	22	33	5	7	8	4	18	6	5	schist	53
5.91	29	39	10	7	8	5	18	6	5	schist	59
6.49	30	32	5	7	8	5	18	6	5	schist	54
7.02	31	42	14	5	8	5	9	6	5	schist	52
7.63	32	42	14	7	8	5	18	6	5	schist	63
8.11	33	46	14	7	8	5	18	6	5	schist	63
8.80	34									schist	
9.32	35	41	14	5	8	5	18	6	5	schist	61
9.74	36										
10.24	37										
11.99	41									gneiss	
12.22	40	65	20	9	15	6	9	6	5	gneiss	70
12.74	39	61	20	9	21	6	9	6	5	gneiss	76
13.25	38	64	20	7	8	6	9	6	5	gneiss	61
13.95	23	58	18	7	15	5	9	6	5	gneiss	65
14.40	24	69	20	9	15	6	9	6	5	schist	70
14.87	25	37	10	7	15	6	9	6	5	schist	58
15.37	26	38	10	7	15	5	18	6	5	schist	66
15.72	27	36	10	7	8	4	9	6	5	sediments	49
16.22	6	20	5	5	8	5	18	6	5	sediments	52
16.58	5	20	5	5	8	5	18	6	5	sediments	52
16.92	4	20	5	5	8	5	18	6	5	sediments	52
17.28	3	20	5	5	8	5	18	6	5	sediments	52
17.67	2	20	5	5	8	5	18	6	5	sediments	52
18.00	1	20	5	5	8	5	18	6	5	sediments	52
18.30	28	20	5	5	8	5	18	6	5	sediments	52

Bozdağ River: Field data

Down stream distance (km)	Field location	Lat	Long	elevation (m)	Upstream area (km2)	Bankfull channel width (m)	Bankfull depth (m)	Valley width (m)	Slope measured with range finder (°)	DEM y/x	% bedrock in channel	Sediment % coarse	Sediment % med.	Sediment % fine
1.04	1	38.327	28.069	1259	0.98	1	0.2	35.1	3.9	0.056	0	25	70	5
1.38	2	38.330	28.069	1245	1.52	3.1	1.2	22.1	2.3	0.046	0	20	50	30
1.66	3	38.332	28.069	1214	1.56	3.8	0.98	45.2	4.6	0.057	90	20	60	20
2.08	4	38.335	28.071	1178	2.48	6.3	0.53	160	2.2	0.021	0	85	55	10
2.95	5	38.342	28.074	1129	3.79	3.3	1.5	350	2	0.010	0	5	55	40
3.56	6	38.348	28.075	1120	7.27	3.6	1.3	650	0.9	0.013	0	15	70	15
3.64	7	38.357	28.075	1108	10.64	5.1	1.4	633	0.6	0.001	0	5	50	50
4.92	8	38.367	28.077	1100	10.63	7.2	1	460	0.3	0.008	0	5	50	45
6.16	9	38.372	28.079	1090	24.98	12	1.1	420	1.2	0.001	0	20	70	10
7.57	11	38.384	28.079	1073	30.28	18.4	0.7	23	2	0.006	0	25	50	25
8.19	12	38.390	28.078	1057	31.02	4.6	1.1	4.8	6.5	0.005	50	25	50	25
8.96	13	38.393	28.080	1037	34.06	9.2	0.9	19.3	3.2	0.035	10	40	40	20
9.33	27	38.393	28.079	1016	34.36	3.2	2.3	21	3.2	0.020	80	40	20	20
9.78	28	38.396	28.080	1000	35.67	5.6	0.9	16	2.8	0.056	60	40	40	20
9.94	10	38.383	28.079	998	27.68	6.9	1.25	11	2.1	0.020	0	40	20	40
10.09	29	38.399	28.081	996	35.87	5.8	1.4	18	2.6	0.032	0	30	40	50
10.46	30	38.399	28.081	969	36.53	4.8	1.9	17	4.6	0.044	60	50	30	20
10.91	31	38.406	28.083	936	37.46	4.1	1.6	20	5.2	0.017	50	30	40	30
11.57	32	38.411	28.087	875	37.89	6.2	0.3	16	2.4	0.049	0	30	40	30
12.56	33	38.417	28.091	686	39.6	18.7	0.6	32	2.5	0.039	100			
13.58	26	38.426	28.095	510	51.27	3.9	1.8	19	8	0.072	80	80	20	0
14.19	25	38.437	28.063	403	52.12	3.6	1.4	31	10.7	0.030	0	90	10	0
14.76	24	38.434	28.100	361	57.16	3.5	1.5	22	4.1	0.011	20	70	25	5
15.13	23	38.437	28.101	343	57.51	3.5	1.8	74	3	0.029	60	80	20	0
15.41	22	38.488	28.104	330	27.68	4.3	1.8	85	5	0.025	20	50	40	10
15.96	20	38.440	28.108	297	57.98	7.5	1.2	56	8.2	0.017	10	10	20	70
16.48	21	38.444	28.111	269	64.11	6.7	0.9	86	4.7	0.010	0	20	50	30
17.21	19	38.440	28.106	226	64.96	5.8	1.5	25	10	0.023	0	20	70	10
18.01	18	38.448	28.115	204	67.68	10.5	0.5	160	1.3	0.012	0	35	35	10
18.51	17	38.446	28.114	180	68.35	9.4	1	29	0.5	0.014	0	30	60	10
19.07	16	38.459	28.114	166	69.35	8	1.7	25	0.4	0.007	0	35	35	5
19.92	15	38.463	28.111	150	70.5	7.7	1.3	107	0.2	0.006	0	15	85	0
20.44	14	38.469	28.107	134	70.75	18.1	0.55	181	0.5	0.014	0	5	90	5

Bozdağ River: stream power calculations part 1

	0.8	0.23	0.85	1.7
	Finnegan prefactor	whittaker prefactor	prefactor	prefactor

Down stream distance (km)	Predicted width Finnegan (m)	Predicted width Whittaker (m)	Predicted width: hydraulic scaling fitted to downstream of kp (m)	Predicted width: hydraulic scaling fitted to upstream of kp (m)	Velocity (m/s)	Cross-sectional area	Discharge (m3/s)	Discharge : Area (Q:A) ratio	Discharge scaled to drainage area (m3/s)	discharge scaled to regional Q:A ratio	Actual unit stream power (W/sqm)	Average actual stream power over ~2 km	error 1 standard deviation
1.04	1.37	0.81	0.84	1.68	0.09	0.1	0.01	108.66	0.31	0.21	115.67		
1.38	1.68	1.04	1.05	2.10	5.32	1.86	9.90	0.15	0.47	0.33	48.08		
1.66	1.63	0.96	1.06	2.12	3.12	1.862	5.82	0.27	0.49	0.34	49.55		
2.08	2.36	1.79	1.34	2.68	0.74	1.6695	1.24	2.01	0.77	0.53	17.20	57.62	20.73
2.95	3.19	2.92	1.65	3.31	3.04	2.475	7.52	0.50	1.18	0.82	23.86		
3.56	3.91	3.36	2.29	4.58	7.27	2.34	17.02	0.43	2.27	1.57	53.32		
3.64	7.65	13.16	2.77	5.55	1.72	3.57	6.15	1.73	3.32	2.29	3.44	26.87	12.54
4.92	4.91	4.71	2.77	5.54	1.00	3.6	3.59	2.96	3.32	2.29	25.15		
6.16	9.45	14.00	4.25	8.50	1.48	6.6	9.74	2.56	7.80	5.38	6.24		
7.57	7.62	7.73	4.68	9.35	0.87	6.44	5.63	5.38	9.46	6.53	22.42		
8.19	8.02	8.58	4.73	9.47	2.17	2.53	5.48	5.66	9.69	6.69	73.99	31.95	14.62
8.96	5.78	3.84	4.96	9.92	2.14	4.14	8.88	3.84	10.64	7.34	274.73		
9.33	6.45	4.93	4.98	9.96	11.08	3.68	40.79	0.84	10.73	7.41	453.57		
9.78	5.38	3.17	5.08	10.15	1.01	2.52	2.54	14.07	11.14	7.69	756.74		
9.94	5.94	4.54	4.47	8.94	2.00	4.3125	8.65	3.20	8.65	5.97	169.46		
10.09	5.98	4.05	5.09	10.18	5.88	4.06	23.88	1.50	11.20	7.73	423.63	415.62	111.33
10.46	5.67	3.55	5.14	10.27	10.86	4.56	49.53	0.74	11.41	7.87	714.39		
10.91	6.90	5.52	5.20	10.40	8.65	3.28	28.36	1.32	11.70	8.07	321.62		
11.57	5.64	3.44	5.23	10.46	0.44	0.93	0.41	93.25	11.83	8.17	638.85	558.29	104.21
12.56	5.99	3.87	5.35	10.70	1.66	5.61	9.32	4.25	12.37	8.53	175.40		
13.58	5.89	3.27	6.09	12.17	15.08	3.51	52.92	0.97	16.01	11.05	2002.76		
14.19	7.00	4.85	6.14	12.27	5.91	2.52	14.90	3.50	16.28	11.23	911.98	1030.05	459.69
14.76	8.80	7.84	6.43	12.85	5.51	2.625	14.47	3.95	17.85	12.32	372.90		
15.13	7.33	5.13	6.45	12.89	7.76	3.15	24.43	2.35	17.96	12.39	991.55		
15.41	5.68	4.09	4.47	8.94	8.82	3.87	34.13	0.81	8.65	5.97	346.08		
15.96	8.09	6.41	6.47	12.94	3.71	4.5	16.71	3.47	18.11	12.50	282.59	498.28	165.51
16.48	9.40	8.64	6.81	13.61	2.18	3.015	6.59	9.73	20.02	13.82	193.79		
17.21	8.03	5.96	6.85	13.70	4.15	4.35	18.03	3.60	20.29	14.00	532.24		
18.01	9.20	7.99	6.99	13.99	0.61	2.625	1.60	42.37	21.14	14.59	163.37	296.47	102.38
18.51	8.93	7.43	7.03	14.05	1.76	4.7	8.26	8.28	21.35	14.73	219.39		
19.07	10.27	10.18	7.08	14.16	4.41	6.8	29.96	2.31	21.66	14.95	129.24		
19.92	10.73	11.20	7.14	14.27	3.29	5.005	16.49	4.28	22.02	15.19	111.56		
20.44	9.10	7.62	7.15	14.30	0.25	4.9775	1.25	56.74	22.10	15.25	114.66	143.71	25.52
								3.20					

Bozdağ River: stream power calculations part 2, stream powers calculated using different width prediction methods

Down stream distance (km)	(Finnegan) predicted Unit stream power (W/m^2)	(Whittaker) predicted Unit stream power (W/m^2)	(Hydraulic scaling, upstream of KP) predicted Unit stream power (W/m^2)	(Hydraulic scaling, downstream of KP) predicted Unit stream power (W/m^2)
1.04	122.06	206.42	199.21	99.60
1.38	128.52	207.50	206.12	103.06
1.66	167.21	284.36	257.00	128.50
2.08	66.54	87.77	117.33	58.66
2.95	35.72	39.13	68.95	34.48
3.56	71.16	82.76	121.37	60.68
3.64	3.33	1.93	9.18	4.59
4.92	53.46	55.72	94.68	47.34
6.16	11.48	7.75	25.53	12.76
7.57	78.45	77.33	127.84	63.92
8.19	61.53	57.46	104.19	52.09
8.96	634.12	954.92	738.38	369.19
9.33	326.08	426.52	422.16	211.08
9.78	1142.40	1935.14	1209.74	604.87
9.94	285.18	373.02	378.90	189.45
10.09	595.31	878.72	699.46	349.73
10.46	875.97	1398.97	967.30	483.65
10.91	276.92	346.08	367.32	183.66
11.57	1018.49	1670.94	1097.08	548.54
12.56	793.48	1228.18	888.64	444.32
13.58	1923.21	3466.73	1859.82	929.91
14.19	679.25	981.83	775.34	387.67
14.76	215.00	241.14	294.32	147.16
15.13	686.03	981.05	780.23	390.11
15.41	379.97	527.90	482.24	241.12
15.96	379.74	479.08	474.56	237.28
16.48	200.15	217.85	276.47	138.24
17.21	556.78	750.05	653.01	326.51
18.01	270.31	311.18	355.49	177.75
18.51	334.67	402.44	425.29	212.65
19.07	145.94	147.14	211.68	105.84
19.92	115.97	111.17	174.43	87.22
20.44	330.64	394.80	420.68	210.34

Bozdağ River: stream power calculations part 3, 2 km averages of stream powers calculated using different width prediction methods

Down stream distance (km)	Average unit stream power using widths from hydraulic scaling fitted to downstream of KP	error 1 standard deviation	Average unit stream power using widths from hydraulic scaling fitted to upstream of KP	error 1 standard deviation	Average unit stream power using widths from Finnegan width scaling	error 1 standard deviation	Average unit stream power using widths from Whittaker width scaling	error 1 standard deviation
1.04								
1.38								
1.66								
2.08	194.92	28.90	97.46	14.45	118.84	19.91	142.23	29.28
2.95								
3.56								
3.64	66.50	28.07	33.25	14.03	39.28	16.28	36.34	14.52
4.92								
6.16								
7.57								
8.19	88.06	21.98	44.03	10.99	67.57	21.24	75.17	31.08
8.96								
9.33								
9.78								
9.94								
10.09	689.73	166.03	344.86	83.02	594.09	146.44	679.17	169.75
10.46								
10.91								
11.57	810.57	194.65	405.28	97.33	737.15	163.39	898.07	186.14
12.56								
13.58								
14.19	1174.60	298.06	587.30	149.03	1241.58	353.95	1785.02	570.59
14.76								
15.13								
15.41								
15.96	507.84	100.64	253.92	50.32	500.30	90.40	650.83	109.45
16.48								
17.21								
18.01	428.33	99.28	214.16	49.64	448.46	141.35	619.54	260.93
18.51								
19.07								
19.92								
20.44	308.02	66.82	154.01	33.41	202.00	49.03	144.79	39.66

Bozdağ River: Field Schmidt hammer readings

Down stream distance (km)	Location	Schmidt hammer readings																			
1.04	1																				
1.38	2																				
1.66	3	34	41	60	42	42	38	65	52	33	39	47	40	36	60	36	48	39	63	46	47
2.08	4	32	34	33	33	39	38	28	30	32	27	32	30	27	34	31	32	33	31	29	32
2.95	5	54	60	49	59	59	56	62	57	59	46	61	48	59	54	66	53	54	61	55	55
3.56	6																				
3.64	7																				
4.92	8																				
6.16	9																				
7.57	11	56	56	58	63	54	58	54	58	54	64	63	65	50	50	44	54	64	64	63	57
8.19	12	30	41	40	42	32	40	37	40	43	36	26	38	36	22	46	42	47	39	34	35
8.96	13	41	37	37	33	41	38	35	34	38	36	32	30	39	38	37	39	32	36	39	37
9.33	27	33	34	48	40	53	48	48	50	52	51	46	48	50	52	49	50	52	51	46	54
9.78	28	40	38	46	42	41	39	39	41	42	46	38	38	42	43	45	42	43	45	41	43
9.94	10																				
10.09	29																				
10.46	30	41	42	48	49	36	36	37	40	42	39	39	45	40	37	42	41	37	42	45	32
10.91	31	41	48	37	37	34	50	43	49	42	40	43	48	42	37	47	45	46	46	51	43
11.57	32																				
12.56	33																				
13.58	26	61	56	52	48	60	54	50	60	55	57	53	49	48	57	53	61	49	48	61	64
14.19	25	46	48	48	51	48	52	48	50	50	49	46	50	52	43	46	49	49	50	47	51
14.76	24	48	56	48	49	52	44	59	51	49	47	52	46	51	50	53	46	50	43	49	49
15.13	23	52	43	48	50	43	48	44	50	41	46	44	48	52	52	49	51	50	47	43	50
15.41	22	56	57	48	48	50	52	54	43	50	42	48	49	56	54	43	48	47	43	47	51
15.96	20	32	34	28	28	44	28	30	28	23	40	24	46	24	24	32	52	56	30	28	28
16.48	21	42	45	46	40	38	42	52	56	48	52	52	48	49	41	47	51	50	42	38	59
17.21	19																				
18.01	18																				
18.51	17	44	55	30	34	47	38	44	46	47	39	58	60	41	44	56	50	59	59	56	54
19.07	16																				
19.92	15																				
20.44	14																				

Bozdağ River: Selby Rock Mass Strength Index calculation

Down stream distance (km)	Location #	Schmidt hammer average	Hardness selby index number	Weathering selby index number	Joint spacing selby index number	Joint width selby index number	Joint orientation selby index number	Ground water selby index number	continuity of joints selby index numbers	Lithology	Selby rock mass strength rating
1.04	1	20	5	5	8	6	14	6	6	sed	50
1.38	2	20	5	5	8	6	14	6	7	sed	51
1.66	3	45	14	7	21	6	9	6	5	gniess	68
2.08	4	32	5	7	15	4	18	6	5	gniess	60
2.95	5	56	18	9	21	5	18	6	5	gniess	82
3.56	6										
3.64	7										
4.92	8										
6.16	9										
7.57	11	57	18	9	21	5	18	6	5	gneiss	82
8.19	12	37	10	9	15	4	18	6	5	mica schist	67
8.96	13	36	10	9	15	5	18	6	5	mica schist	68
9.33	27	48	14	7	21	5	9	6	5	gniess	67
9.78	28	42	14	7	21	6	9	6	5	schist	68
9.94	10										
10.09	29										
10.46	30	41	14	7	8	5	18	6	5	schist	63
10.91	31	43	14	9	8	6	18	6	5	schist	66
11.57	32										
12.56	33										
13.58	26	55	18	9	15	6	9	6	5	gniess	68
14.19	25	49	14	9	15	6	9	6	5	gniess	64
14.76	24	50	14	7	21	5	9	6	5	gniess	67
15.13	23	48	14	7	21	6	9	6	5	gniess	68
15.41	22	49	14	7	21	5	9	6	5	gniess	67
15.96	20	33	5	7	21	4	9	6	5	gniess	57
16.48	21	47	14	9	15	5	9	6	5	gniess	63
17.21	19										
18.01	18										
18.51	17	48	14	7	15	5	18	6	5	gniess	70
19.07	16	20	5	5	8	5	18	6	6	sed	53
19.92	15	20	5	7	8	7	18	6	6	Breccia	57
20.44	14	20	5	5	15	7	18	6	6	sed	62

Kabazlı River: field data

Down stream distance (km)	Field location	Lat	Long	elev (m)	Upstream area (km2)	Bankfull channel width (m)	Bank full depth (m)	Valley width (m)	Slope measured with range finder (°)	DEM y/x	% bedrock in channel	Sediment % coarse	Sediment % med.	Sediment % fine
0.1	18 E	38.6360	28.1819	1462	0.05	1.08	0.3	67	1.8	0.056	0	20	60	20
0.64	18 D	38.3686	28.1826	1453	2.05	2.8	0.4	62	1.3	0.014	0	10	50	40
1.36	18 C	38.3748	28.1844	1415	2.77	3.2	0.5	97	1.2	0.051	50	30	40	30
1.71	18 B	38.3773	28.1852	1395	3.01	1.8	0.4	58	0.8	0.021	0	20	60	20
2.68	18 A	38.3849	28.1904	1297	5.62	6.2	1.2	42	3.3	0.034	60	10	60	30
3.21	18 F	38.3885	28.1944	1211	7.52	6.5	0.7	57	4.2	0.030	40	30	40	30
4.07	18 G	38.3959	28.1973	1124	7.84	6.2	1.2	71	3.7	0.156	60	10	60	30
4.23	18_32	38.4069	28.2007	1027	9.843	3.9	1.2	52	4.2	0.018	80	20	60	20
4.63	18_31	38.4042	28.2018	636	10.286	3.6	1.2	16.4	3.7	0.130	20	10	60	30
4.9	18_30	38.4064	28.2021	886	10.365	4.6	1.4	13.9	6	0.154	10	60	30	10
5.14	18_29	38.4083	28.3202	826	10.435	3.2	1.7	12.6	4.9	0.100	80	10	80	10
5.46	18_28	38.4109	28.2014	755	12.694	3.2	1.8	10.5	3.2	0.124	50	40	50	10
5.75	18_27	38.4132	27.2031	701	12.404	2.8	2.2	11	2.7	0.110	90	60	40	0
6.094	18_25	38.4159	28.2039	631	14.46	3.5	1.2	12.9	5.6	0.301	90	80	10	10
6.1604	18_23	38.4166	28.2045	618	14.494	4.5	5	24	4	0.318	90	0	20	80
6.261	18_22	38.4177	28.2046	596	14.522	9.8	1.7	103	7	0.075	90	60	30	10
6.6219	18_02	38.4199	28.2058	568	15.48	7.3	1.4	22	3.1	0.375	10	10	40	40
6.7339	18_01	38.4206	28.2061	567	16.029	9.4	1.6	13.7	6.1	0.117	100	0	0	0
7.1187	18_03	38.4224	28.2080	515	16.265	9.8	1	14.7	2.7	0.079	100	0	0	0
7.6503	18_04	38.4265	28.2089	194	17.019	10.5	1.1	45	8.5	0.050	100	0	0	0
8.275	18_05	38.4313	28.2073	372	19.156	3.2	1.9	61	8.9	0.078	100	0	0	0
8.429	18_26	38.4327	28.3207	333	19.206	3	2.2	2.5	2.1	0.099	0	10	65	25
8.4994	18_06	38.4332	28.2070	325	19.289	6.5	1.3	33	4.3	0.035	60	60	30	10
9.2337	18_07	38.4389	28.2048	277	21.869	6.9	0.8	60	1.3	0.061	0	20	50	30
9.625	18_08	38.4417	28.2022	253	22.442	3.2	1	90	2.2	0.028	0	40	50	10
10.119	18_09	38.4447	28.1997	239	23.394	2.7	1	55	1.5	0.027	0	10	60	30
10.645	18_21	38.4635	28.2001	211	24.568	3	0.4	78	0.8	0.017	0	30	40	30
11.238	18_20	38.4525	28.1998	192	24.834	11.7	0.7	64	1.5	0.015	0	20	50	30
11.832	18_11	38.4568	28.1996	173	26.311	7.4	0.8	271	0.7	0.007	0	30	50	20
12.674	18_10	38.4484	28.2067	152	26.463	9.6	0.7	150	0.8	0.008	0	45	35	20
14.088	18_12	38.4719	28.1996	177	27.223	18.9	0.5	1000	0.6	0.016	0	0	40	60

Kabazlı River: stream power calculations part 1

	1.17	0.45	1.1	1.75
	Finnegan prefactor	whittaker prefactor	prefactor	prefactor

Down stream distance (km)	Predicted width Finnegan (m)	Predicted width Whittaker (m)	Predicted width: hydraulic scaling fitted to downstream of kp (m)	Predicted width: hydraulic scaling fitted to upstream of kp (m)	Velocity (m/s)	Cross-sectional area	Discharge (m3/s)	Discharge : Area (Q:A) ratio	Discharge scaled to drainage area (m3/s)	discharge scaled to regional Q:A ratio	Actual unit stream power (W/sqm)	Average actual stream power over ~2 km	error 1 standard deviation
0.10	0.65	0.51	0.25	0.39	0.18	0.16	0.03	1.74	0.04	0.01	5.43		
0.64	3.46	3.88	1.57	2.51	0.27	0.56	0.15	13.67	1.75	0.44	21.48		
1.36	3.03	2.45	1.83	2.91	0.40	0.80	0.32	8.61	2.37	0.60	94.02		
1.71	3.72	3.77	1.91	3.04	0.21	0.36	0.08	39.80	2.57	0.65	72.82	48.44	20.91
2.68	4.29	3.84	2.61	4.15	3.84	3.72	14.29	0.39	4.80	1.21	65.02		
3.21	4.90	4.52	3.02	4.80	1.48	2.28	3.36	2.24	6.43	1.62	73.87		
4.07	3.64	2.23	3.08	4.90	4.07	3.72	15.14	0.52	6.70	1.69	417.30	185.40	100.44
4.23	6.02	6.36	3.45	5.49	4.34	2.34	10.15	0.97	8.41	2.12	93.28		
4.63	4.18	2.68	3.53	5.61	4.07	2.16	8.79	1.17	8.79	2.22	782.27		
4.90	4.06	2.49	3.54	5.63	7.06	3.22	22.73	0.46	8.86	2.23	733.69		
5.14	4.42	3.02	3.55	5.65	9.40	2.72	25.57	0.41	8.92	2.25	688.73		
5.46	4.57	2.96	3.92	6.24	8.51	2.88	24.52	0.52	10.85	2.74	1040.07		
5.75	4.63	3.09	3.87	6.16	11.68	3.08	35.97	0.34	10.60	2.67	1033.56		
6.09	4.06	2.11	4.18	6.65	5.01	2.10	10.52	1.37	12.35	3.12	2628.27	999.98	392.18
6.16	4.02	2.06	4.19	6.66	73.45	11.25	826.36	0.02	12.38	3.12	2163.89		
6.26	5.29	3.89	4.19	6.67	11.25	8.33	93.73	0.15	12.41	3.13	234.15		
6.62	3.99	1.96	4.33	6.89	5.07	5.11	25.90	0.60	13.23	3.34	1679.53		
6.73	5.05	3.32	4.40	7.01	9.30	7.52	69.93	0.23	13.70	3.45	421.18		
7.12	5.47	3.97	4.44	7.06	2.41	4.90	11.82	1.38	13.90	3.51	276.95		
7.65	6.08	4.95	4.54	7.22	5.20	5.78	30.02	0.57	14.54	3.67	169.88	824.26	433.85
8.28	5.20	3.25	4.81	7.66	15.87	3.04	48.25	0.40	16.37	4.13	1050.88		
8.43	5.03	3.01	4.82	7.67	10.30	3.30	33.98	0.57	16.41	4.14	1344.46	1197.67	103.80
8.50	6.80	6.03	4.83	7.69	5.15	4.23	21.75	0.89	16.48	4.16	221.92		
9.23	6.42	4.96	5.14	8.18	1.07	2.76	2.96	7.40	18.69	4.71	410.57		
9.63	7.51	7.04	5.21	8.29	2.18	1.60	3.48	6.44	19.17	4.84	419.78		
10.12	7.72	7.35	5.32	8.46	1.80	1.35	2.43	9.64	19.99	5.04	487.07	384.84	440.72
10.65	8.58	9.16	5.45	8.67	0.21	0.60	0.13	194.91	20.99	5.29	291.68		
11.24	8.79	9.64	5.48	8.72	0.88	4.10	3.61	6.88	21.22	5.35	67.92		
11.83	10.37	13.73	5.64	8.98	0.79	2.96	2.33	11.31	22.48	5.67	53.51	137.70	66.77
12.67	10.05	12.74	5.66	9.00	0.64	3.36	2.16	12.24	22.61	5.70	49.41	115.63	58.82
14.09	8.96	9.62	5.74	9.13	0.28	4.73	1.34	20.27	23.26	5.87	50.15	49.78	0.26
								1.17					

Kabazlı River: stream power calculations part 2, stream powers calculated using different width prediction methods

Down stream distance (km)	(Finnegan) predicted Unit stream power (W/m^2)	(Whittaker) predicted Unit stream power (W/m^2)	(Hydraulic scaling, upstream of KP) predicted Unit stream power (W/m^2)	(Hydraulic scaling, downstream of KP) predicted Unit stream power (W/m^2)
0.1	35.83	45.23	94.56	59.44
0.64	68.83	61.43	151.37	95.15
1.36	393.89	487.70	651.55	409.54
1.71	139.76	137.70	272.30	171.16
2.68	372.76	416.06	612.87	385.23
3.21	388.80	421.52	631.08	396.68
4.07	2817.29	4605.31	3330.28	2093.32
4.23	239.70	226.67	417.93	262.70
4.63	2669.44	4164.56	3164.68	1989.23
4.9	3296.63	5370.83	3778.13	2374.83
5.14	1977.76	2891.66	2458.94	1545.62
5.46	2888.59	4457.96	3366.71	2116.22
5.75	2478.31	3714.80	2961.48	1861.50
6.094	8992.06	17320.00	8718.63	5480.28
6.1604	9609.10	18762.65	9218.25	5794.33
6.261	1718.69	2337.04	2170.16	1364.10
6.6219	12174.87	24771.11	11231.02	7059.50
6.7339	3109.17	4727.29	3563.96	2240.20
7.1187	1967.47	2712.04	2425.46	1524.57
7.6503	1163.48	1427.76	1558.33	979.52
8.275	4406.27	7043.20	4759.45	2991.65
8.429	5445.71	9097.66	5686.29	3574.24
8.4994	841.45	949.03	1183.74	744.07
9.2337	1748.91	2262.91	2183.32	1372.37
9.625	709.13	756.48	1021.96	642.38
10.119	675.26	709.14	979.93	615.96
10.645	404.39	378.89	636.26	399.93
11.238	358.41	326.94	574.75	361.27
11.832	151.38	114.36	278.23	174.89
12.674	187.04	147.60	332.32	208.89
14.088	419.43	390.75	654.67	411.50

Kabazlı River: stream power calculations part 3, 2 km averages of stream powers calculated using different width prediction methods

Down stream distance (km)	Average unit stream power using widths from hydraulic scaling fitted to downstream of KP	error 1 standard deviation	Average unit stream power using widths from hydraulic scaling fitted to upstream of KP	error 1 standard deviation	Average unit stream power using widths from Finnegan width scaling	error 1 standard deviation	Average unit stream power using widths from Whittaker width scaling	error 1 standard deviation
0.10								
0.64								
1.36								
1.71	197.92	38.58	124.41	24.25	100.84	25.74	109.38	32.18
2.68								
3.21								
4.07	1317.24	125.91	827.98	79.14	914.42	133.91	1212.08	310.78
4.23								
4.63								
4.90								
5.14								
5.46								
5.75								
6.09	1947.87	291.55	1224.37	183.26	1652.39	352.30	1823.71	578.74
6.16								
6.26								
6.62								
6.73								
7.12								
7.65	2768.01	639.60	1739.89	402.03	2368.53	423.17	3629.42	512.81
8.28								
8.43								
8.50								
9.23								
9.63								
10.12	2018.56	839.27	1268.81	527.54	1676.85	800.24	2375.56	1339.37
10.65								
11.24								
11.83	665.74	142.39	418.47	89.51	404.61	94.90	358.28	94.24
12.67								
14.09	481.36	46.27	302.57	29.08	287.11	14.59	245.56	1.91

Kabazlı River: Field Schmidt hammer readings

Down stream distance (km)	Location	Schmidt hammer readings																			
0.10	18 E																				
0.64	18 D																				
1.36	18 C																				
1.71	18 B																				
2.68	18 A	42	56	52	50	50	51	56	47	51	48	56	55	57	61	49	49	60	62	56	52
3.21	18 F	56	41	47	57	64	57	51	48	62	57	59	68	55	57	52	47	57	64	57	60
4.07	18 G	54	62	57	57	64	61	52	56	61	65	50	52	49	51	60	51	47	49	58	55
4.23	18_32	61	52	49	51	56	56	42	51	61	46	47	50	53	49	49	51	56	49	51	60
4.63	18_31	48	52	49	56	48	49	56	49	56	48	52	51	48	54	55	60	57	50	56	48
4.90	18_30	48	47	52	49	56	61	49	49	52	47	53	56	58	41	49	45	45	51	46	51
5.14	18_29	52	43	51	56	56	58	57	56	49	48	53	56	54	56	61	49	60	60	57	54
5.46	18_28	48	56	61	58	47	52	53	44	56	51	52	61	50	59	58	60	51	51	56	52
5.75	18_27	58	58	55	61	65	60	60	65	60	60	62	62	60	66	58	62	65	62	60	66
6.09	18_25	51	56	56	42	51	65	51	60	45	57	58	51	56	56	63	61	55	54	53	59
6.16	18_23	61	50	52	40	46	55	46	44	57	59	46	41	50	46	47	38	54	55	55	51
6.26	18_22	57	61	61	68	59	67	64	64	60	68	66	57	61	59	60	62	61	57	64	59
6.62	18_02	36	26	36	48	45	49	48	32	33	39	44	34	28	47	44	35	50	55	51	46
6.73	18_01	50	55	56	55	51	54	48	61	54	53	61	56	52	60	55	63	53	63	61	64
7.12	18_03	31	50	48	58	47	43	42	45	45	46	46	56	46	39	42	29	52	49	53	48
7.65	18_04																				
8.28	18_05	42	43	48	48	32	30	33	47	46	48	48	35	48	35	30	46	49	54	30	40
8.43	18_26																				
8.50	18_06																				
9.23	18_07	22	24	19	19	17	22	15	19	21	24	17	19	20	25	21	18	15	17	20	19
9.63	18_08	25	29	25	29	26	35	31	29	32	33	30	34	33	27	30	33	30	26	27	33
10.12	18_09																				
10.65	18_21																				
11.24	18_20																				
11.83	18_11																				
12.67	18_10																				
14.09	18_12																				

Kabazlı River: Selby Rock Mass Strength Index calculation

Down stream distance (km)	Location #	Schmidt hammer average	Hardness selby index number	Weathering selby index number	Joint spacing selby index number	Joint width selby index number	Joint orientation selby index number	Ground water selby index number	continuity of joints selby index numbers	Lithology	Selby rock mass strength rating
0.10	18 E	20	5	5	8	5	18	6	5	sediments	52
0.64	18 D	20	5	5	8	5	18	6	6	sediments	53
1.36	18 C	20	5	5	8	5	18	6	5	sediments	52
1.71	18 B	20	5	5	8	4	20	6	5	sediments	53
2.68	18 A	53	18	7	15	5	18	6	6	gneiss	75
3.21	18 F	56	18	7	8	5	18	6	6	gneiss	68
4.07	18 G	56	18	9	15	6	9	6	5	gneiss	68
4.23	18_32	52	18	9	8	6	18	6	5	gneiss	70
4.63	18_31	52	18	9	15	6	14	6	5	gneiss	73
4.90	18_30	50	18	7	15	6	14	6	6	gneiss	72
5.14	18_29	54	18	9	21	6	18	6	5	gneiss	83
5.46	18_28	54	18	9	15	5	14	6	5	gneiss	72
5.75	18_27	61	20	9	8	6	18	6	6	gneiss	73
6.09	18_25	55	14	9	21	6	14	6	5	gneiss	75
6.16	18_23	50	14	9	4	6	18	6	5	gneiss	62
6.26	18_22	62	20	9	4	6	18	6	5	gneiss	68
6.62	18_02	41	14	7	4	5	14	6	5	schist	55
6.73	18_01	56	18	9	8	5	14	6	5	schist	65
7.12	18_03	46	14	7	8	5	14	6	5	schist	59
7.65	18_04									schist	
8.28	18_05	42	14	9	8	5	18	6	5	schist	65
8.43	18_26	20	5	5	8	6	9	6	5	sediments	44
8.50	18_06									schist	
9.23	18_07	20	5	5	8	5	9	6	5	sediments	43
9.63	18_08	30	5	5	8	5	9	6	5	sediments	43
10.12	18_09	20	5	5	8	4	9	6	6	conglomerate	43
10.65	18_21									sediments	
11.24	18_20									sediments	
11.83	18_11	20	5	5	8	5	9	6	6	sediments	44
12.67	18_10	20	5	5	8	4	14	6	5	conglomerate	47
14.09	18_12	20	5	5	8	5	14	6	6	sediments	49

Yeniköy River: Field data

Down stream distance (km)	Field location	Lat	Long	elevation (m)	Upstream area (km2)	Bankfull channel width (m)	Bankfull depth (m)	Valley width (m)	Slope measured with range finder (°)	DEM y/x	% bedrock in channel	Sediment % coarse	Sediment % med.	Sediment % fine
0	12_14	38.345	28.350	892	0.01	1	0.2	21	11.7	0.011				
0.28	12_15	38.348	28.351	839	0.21	1.2	0.2	14	9.7	0.050		vegetated		
0.52	12_16	38.349	28.352	785	0.39	1.3	0.4	15	12.2	0.083				
0.81	12_17	38.352	28.352	744	0.60	1.5	0.4	17	9.7	0.070				
1.112	12_01	38.355	28.353	660	0.75	2	0.5	14	10.2	0.085	0	40	40	20
1.489	12_02	38.357	28.355	613	1.24	3.2	1.2	15.2	11	0.086	0	60	20	20
1.78	12_03	38.359	28.356	568	1.89	7	1.2	33	6.7	0.077	10	60	20	20
2.13	12_04	38.362	28.356	479	2.07	3.7	0.6	75	4.9	0.070	70	20	60	20
2.59	12_05	38.366	28.358	431	2.76	2.1	0.7	250	5.5	0.036	100	0	0	0
3.337	12_06	38.372	28.360	374	4.11	1.2	0.7	204	6.8	0.041	0	40	10	50
3.92	12_07	38.376	28.362	348	7.12	6.5	0.75	197	2.5	0.008	10	60	20	20
5.195	12_09	38.387	28.361	292	11.14	14	0.4	317	0.8	0.032	0	10	30	60
5.51	12_08	38.381	28.361	301	9.76	12.3	0.6	230	1.7	0.072	0	10	10	80
5.719	12_10	38.390	28.363	272	12.18	13.2	0.5	310	0.6	0.015	0	20	30	50
6.33	12_11	38.396	28.136	254	13.54	14	0.5	352	0.6	0.012	0	20	5	75
6.847	12_12	38.400	28.365	239	14.08	12.6	0.6	315	0.7	0.009	0	20	10	70
7.841	12_13	38.406	28.368	211	14.54	12.7	0.5	347	0.6	0.032	0	30	10	60

Yeniköy River: stream power calculations part 1

2	0.7	3.7	1.95
Finnegan prefactor	whittaker prefactor	prefactor	prefactor

Down stream distance (km)	Predicted width Finnegan (m)	Predicted width Whittaker (m)	Predicted width: hydraulic scaling fitted to downstream of kp (m)	Predicted width: hydraulic scaling fitted to upstream of kp (m)	Velocity (m/s)	Cross-sectional area	Discharge (m3/s)	Discharge: Area (Q:A) ratio	Discharge scaled to drainage area (m3/s)	discharge scaled to regional Q:A ratio	Actual unit stream power (W/sqm)	Average actual stream power over ~2 km	error 1 standard deviation
0.00	0.36	0.19	0.26	0.14	0.20	0.1	0.02	0.25	0.00	0.00	0.11		
0.28	1.96	1.45	1.70	0.90	0.18	0.12	0.02	9.61	0.08	0.05	18.66		
0.52	2.25	1.47	2.32	1.22	0.83	0.26	0.21	1.82	0.14	0.08	52.71		
0.81	2.74	1.87	2.88	1.52	0.74	0.3	0.22	2.74	0.22	0.13	59.14		
1.11	2.87	1.86	3.21	1.69	1.18	0.5	0.59	1.27	0.27	0.16	67.32		
1.49	3.46	2.24	4.12	2.17	7.05	1.92	13.54	0.09	0.45	0.27	70.37		
1.78	4.14	2.75	5.09	2.68	5.48	4.2	23.03	0.08	0.69	0.41	43.99	44.61	13.09
2.13	4.37	2.98	5.32	2.80	1.17	1.11	1.30	1.59	0.75	0.45	82.08		
2.59	5.53	4.44	6.15	3.24	1.69	0.735	1.24	2.22	1.01	0.59	100.33		
3.34	6.27	4.87	7.50	3.95	1.88	0.42	0.79	5.20	1.50	0.89	297.65		
3.92	10.59	12.46	9.87	5.20	1.31	2.4375	3.18	2.24	2.60	1.53	18.14	124.55	60.33
5.20	9.63	7.98	12.35	6.51	0.21	2.8	0.59	18.94	4.07	2.40	53.35		
5.51	7.84	5.30	11.56	6.09	0.69	3.69	2.54	3.84	3.56	2.10	120.31		
5.72	11.52	11.58	12.91	6.80	0.28	3.3	0.94	12.98	4.44	2.62	28.69	67.45	23.70
6.33	12.55	13.39	13.61	7.18	0.28	3.5	0.99	13.61	4.94	2.92	23.71		
6.85	13.36	15.16	13.88	7.32	0.44	3.78	1.67	8.43	5.14	3.03	21.37		
7.84	10.63	8.80	14.11	7.44	0.28	3.175	0.90	16.11	5.31	3.13	77.50	40.86	15.88
								2.74					

Yeniköy River: stream power calculations part 2, stream powers calculated using different width prediction methods

Down stream distance (km)	(Finnegan) predicted Unit stream power (W/m^2)	(Whittaker) predicted Unit stream power (W/m^2)	(Hydraulic scaling, upstream of KP) predicted Unit stream power (W/m^2)	(Hydraulic scaling, downstream of KP) predicted Unit stream power (W/m^2)
0.00	0.53	1.03	0.73	1.39
0.28	19.35	26.14	22.26	42.24
0.52	51.59	79.07	50.10	95.07
0.81	54.83	80.45	52.26	99.15
1.11	79.57	122.71	71.13	134.96
1.49	110.21	170.48	92.54	175.59
1.78	125.85	189.50	102.55	194.58
2.13	117.63	172.61	96.71	183.50
2.59	64.57	80.44	58.06	110.17
3.34	96.46	124.14	80.68	153.08
3.92	18.85	16.03	20.23	38.39
5.20	131.41	158.48	102.45	194.39
5.51	319.64	472.69	216.83	411.42
5.72	55.68	55.42	49.70	94.30
6.33	44.78	42.00	41.29	78.35
6.85	34.15	30.10	32.85	62.34
7.84	156.78	189.54	118.17	224.22

Yeniköy River: stream power calculations part 3, 2 km averages of stream powers calculated using different width prediction methods

Down stream distance (km)	Average unit stream power using widths from hydraulic scaling fitted to downstream of KP	error 1 standard deviation	Average unit stream power using widths from hydraulic scaling fitted to upstream of KP	error 1 standard deviation	Average unit stream power using widths from Finnegan width scaling	error 1 standard deviation	Average unit stream power using widths from Whittaker width scaling	error 1 standard deviation
0.00								
0.28								
0.52								
0.81								
1.11								
1.49								
1.78	55.94	18.23	106.14	34.58	63.13	22.78	95.63	35.02
2.13								
2.59								
3.34								
3.92	63.92	16.58	121.28	31.46	74.38	21.48	98.30	33.26
5.20								
5.51								
5.72	122.99	42.72	233.37	81.06	168.91	12.43	228.87	108.68
6.33								
6.85								
7.84	64.11	23.51	121.64	44.60	78.57	33.97	87.21	44.41

Yeniköy River: Field Schmidt hammer readings

Down stream distance (km)	Location	Schmidt hammer readings																			
0.00	12_14	60	49	55	51	60	44	56	50	43	53	48	61	52	51	54	46	62	54	49	57
0.28	12_15	47	56	48	44	46	51	55	51	51	60	55	62	60	53	51	52	54	51	59	57
0.52	12_16	56	50	42	53	60	61	50	42	60	48	53	52	60	52	52	55	62	56	59	55
0.81	12_17	40	43	34	41	53	51	41	62	44	39	61	48	54	46	38	50	47	50	46	42
1.11	12_01	47	60	61	54	60		61	58	55	57	61	61	60	54	53	59	60	51	64	55
1.49	12_02	30	46	44	44	38	33	49	30	38	39	30	36	39	41	48	41	34	35	40	36
1.78	12_03	30	45	45	42	41	38	33	36	43	61	41	40	39	34	41	35	56	40	52	41
2.13	12_04	64	58	56	50	60	62	56	52	60	60	55	62	60	56	56	61	64	60	58	55
2.59	12_05	55	50	45	44	46	56	50	42	52	52	55	50	42	54	48	48	47	56	48	50
3.34	12_06																				
3.92	12_07	34	40	42	43	42	43	41	42	42	40	37	38	40	37	41	39	42	40	42	38
5.20	12_09																				
5.51	12_08																				
5.72	12_10																				
6.33	12_11																				
6.85	12_12																				
7.84	12_13																				

Yeniköy River: Selby Rock Mass Strength Index calculation

Down stream distance (km)	Location #	Schmidt hammer average	Hardness selby index number	Weathering selby index number	Joint spacing selby index number	Joint width selby index number	Joint orientation selby index number	Ground water selby index number	continuity of joints selby index numbers	Lithology	Selby rock mass strength rating
0.00	12_14	53	5	9	15	5	18	6	5	gniess	63
0.28	12_15	53	18	7	8	6	9	6	5	gneiss	59
0.52	12_16	54	18	7	15	6	9	6	5	gneiss	66
0.81	12_17	47	18	7	21	6	9	6	5	gneiss	72
1.11	12_01	57	5	7	21	6	9	6	5	gniess	59
1.49	12_02	39	10	7	15	6	9	6	5	gneiss	58
1.78	12_03	42	10	7	15	6	9	6	5	gneiss	58
2.13	12_04	58	18	9	15	6	18	6	5	granite	77
2.59	12_05	50	14	9	8	5	9	6	5	gneiss	56
3.34	12_06										
3.92	12_07	40	14	5	8	6	9	6	6	granite	54
5.20	12_09	20	5	5	8	6	9	6	6	sed	45
5.51	12_08	20	5	5	8	6	9	6	6	sed	45
5.72	12_10	20	5	5	8	6	9	6	6	sed	45
6.33	12_11	20	5	9	8	5	9	6	6	sed	48
6.85	12_12	20	5	7	15	5	18	6	5	sed	61
7.84	12_13	20	5	7	8	6	9	6	5	sed	46

Badınca River: field measurements

Down stream distance (km)	Field location	Latitude	Longitude	Upstream area (km2)	Bankfull channel width (m)	Bankfull depth (m)	Valley width (m)	Slope measured with range finder (°)	DEM y/x	% bedrock in channel	Sediment % coarse	Sediment % med.	Sediment % fine
0.9	E30	38.252	28.495	0.4	1.1	0.3	104	1.4	0.044	0	20	50	30
1.6	E18	38.257	28.503	1.568	1.2	0.4	94	1.2	0.062	0	10	50	40
1.94	E19	38.259	28.498	1.894	1.4	0.4	89	1.8	0.067	0	20	50	30
2.39	E20	38.261	28.501	2.105	2.4	0.5	74	1.1	0.065	10	20	70	10
2.87	E21	38.265	28.504	2.492	3	0.5	84	2.4	0.059	20	20	60	20
3.41	E22	38.269	28.504	2.859	3.6	0.7	57	2.3	0.044	40	30	50	20
3.98	E17	38.274	28.503	4.523	3.8	0.8	46	4.6	0.028	40	20	60	20
4.51	E7	38.278	28.502	7.548	4.1	0.6	26	6.7	0.046	20	40	40	20
4.79	E8	38.280	28.500	7.946	4.1	0.8	79	2.5	0.019	10	20	30	50
5.22	E9	38.284	28.500	8.374	4.5	0.5	125	1.9	0.069	40	10	60	30
5.54	E10	38.286	28.498	8.624	6.7	0.7	162	2.7	0.014	0	60	20	20
5.96	E11	32.289	28.500	15.706	6.5	1	182	3.1	0.097	0	40	30	30
6.28	E12	38.291	28.502	15.919	3.2	1.9	16	5.2	0.122	40	60	30	10
6.46	E13	38.291	28.503	15.996	4.9	0.4	108	3.1	0.079	0	15	60	25
6.7	E14	38.292	28.505	16.874	3.2	0.6	97	2.4	0.047	10	10	50	40
7.04	E15	38.293	28.508	17.237	3.6	0.7	62	3.1	0.062	0	10	70	20
7.33	E16	28.295	28.510	17.832	4.2	0.6	32	4.6	0.013	30	30	40	30
7.88	E26	38.298	28.514	18.952	3.6	0.9	45	4.1	0.018				
8.21	E1	38.300	28.516	19.331	3.2	1	19	6	0.040	100			
8.56	E2	38.303	28.517	19.851	7.2	0.4	28	2.6	0.031	100			
9.01	E3	38.305	28.520	20.89	3.7	1.3	45	4.3	0.042	80	10	70	20
9.37	E4	38.307	28.522	21.189	5.3	0.8	57	3.9	0.017	100			
9.72	E5	38.310	28.523	21.546	2.4	1.2	52	3.1	0.063	30	40	50	10
9.99	E6	38.311	28.525	21.739	3.8	0.6	61	4.2	0.047	20	60	30	10
10.33	E23	38.313	28.527	22.129	5	0.7	43	2.4	0.043	10	40	30	30
10.7	E24	38.315	28.353	21.651	3.1	0.5	72	3.1	0.006	0	20	50	30
11.51	E25	38.317	28.528	25.126	4.1	0.8	82	3.9	0.005	10	30	40	30
12.62	E28	38.320	28.548	26.382	4.6	1.4	32	1	0.015	0	10	50	40
13.02	E29	38.319	28.551	26.506	8	1	124	0.8	0.008	0	20	60	20
14.03	E27	38.321	28.5614	28.782	6.9	0.7	206	1.2	0.018	0	20	40	40

Badınca River: stream power calculations part 1

	Finnegan prefactor	whittaker prefactor	prefactor	prefactor
	0.8	0.35	0.9	1.35

Down stream distance (km)	Predicted width Finnegan (m)	Predicted width Whittaker (m)	Predicted width: hydraulic scaling fitted to downstream of kp (m)	Predicted width: hydraulic scaling fitted to upstream of kp (m)	Velocity (m/s)	Cross-sectional area	Discharge (m3/s)	Discharge: Area (Q:A) ratio	Discharge scaled to drainage area (m3/s)	discharge scaled to regional Q:A ratio	Actual unit stream power (W/sqm)	Average actual stream power over ~2 km	error 1 standard deviation
0.9	1.14	1.26	0.57	0.85	0.16	0.165	0.03	15.51	0.06	0.086	34.01		
1.6	1.98	2.28	1.13	1.69	0.26	0.24	0.06	25.39	0.22	0.338	170.46		
1.94	1.97	2.04	1.24	1.86	0.32	0.28	0.09	21.46	0.27	0.408	190.49		
2.39	2.25	2.64	1.31	1.96	0.38	0.6	0.23	9.11	0.30	0.454	119.64	128.65	34.89
2.87	2.07	2.00	1.42	2.13	0.57	0.75	0.43	5.84	0.35	0.537	103.97		
3.41	2.20	2.15	1.52	2.28	1.09	1.26	1.37	2.08	0.41	0.616	73.57		
3.98	2.29	1.88	1.91	2.87	2.02	1.52	3.07	1.48	0.64	0.975	71.15		
4.51	2.59	1.94	2.47	3.71	1.37	1.23	1.69	4.48	1.07	1.627	180.53	107.30	25.52
4.79	3.19	3.05	2.54	3.81	1.49	1.64	2.44	3.26	1.13	1.713	76.15		
5.22	3.43	3.51	2.60	3.91	0.51	1.125	0.57	14.71	1.19	1.805	270.21		
5.54	3.24	3.04	2.64	3.96	1.18	2.345	2.77	3.11	1.22	1.859	38.84		
5.96	3.96	3.60	3.57	5.35	2.59	3.25	8.40	1.87	2.23	3.385	494.39		
6.28	3.61	2.88	3.59	5.39	12.10	3.04	36.79	0.43	2.26	3.431	1284.17	432.75	254.64
6.46	3.99	3.62	3.60	5.40	0.41	0.98	0.41	39.45	2.27	3.447	545.84		
6.7	4.28	4.14	3.70	5.55	0.82	0.96	0.79	21.46	2.39	3.637	524.10		
7.04	4.11	3.72	3.74	5.60	1.27	1.26	1.60	10.80	2.45	3.715	627.69		
7.33	3.86	3.17	3.80	5.70	1.13	1.26	1.43	12.47	2.53	3.843	114.13		
7.88	4.04	3.41	3.92	5.88	2.41	1.62	3.90	4.86	2.69	4.084	202.16		
8.21	3.78	2.91	3.96	5.94	3.60	1.6	5.76	3.35	2.74	4.166	510.36	420.71	104.64
8.56	4.48	4.25	4.01	6.01	0.38	1.44	0.55	36.39	2.82	4.278	181.16		
9.01	4.15	3.47	4.11	6.17	5.15	2.405	12.38	1.69	2.96	4.502	496.86		
9.37	4.25	3.64	4.14	6.21	1.86	2.12	3.94	5.38	3.01	4.567	144.75		
9.72	4.47	4.05	4.18	6.27	3.72	1.44	5.36	4.02	3.06	4.644	1193.85		
9.99	4.23	3.56	4.20	6.29	1.08	1.14	1.24	17.59	3.08	4.685	568.60	517.04	211.03
10.33	4.74	4.58	4.23	6.35	1.11	1.75	1.95	11.34	3.14	4.769	404.22		
10.7	4.48	4.06	4.19	6.28	0.65	0.775	0.50	43.22	3.07	4.666	91.06		
11.51	4.54	3.88	4.51	6.77	1.86	1.64	3.05	8.25	3.57	5.415	69.96	188.41	93.60
12.62	5.99	7.21	4.62	6.93	2.88	3.22	9.26	2.85	3.74	5.686	181.70		
13.02	6.26	7.96	4.63	6.95	1.31	4	5.25	5.05	3.76	5.713	55.43		
14.03	5.98	6.87	4.83	7.24	0.79	2.415	1.90	15.12	4.08	6.203	157.32	131.48	33.49
								7.05					

Badınca River: stream power calculations part 2, stream powers calculated using different width prediction methods

Down stream distance (km)	(Finnegan) predicted Unit stream power (W/m^2)	(Whittaker) predicted Unit stream power (W/m^2)	(Hydraulic scaling, upstream of KP) predicted Unit stream power (W/m^2)	(Hydraulic scaling, downstream of KP) predicted Unit stream power (W/m^2)
0.9	25.73	35.41	65.73	43.82
1.6	89.18	133.37	181.50	121.00
1.94	109.79	167.37	215.31	143.54
2.39	112.88	170.71	219.89	146.60
2.87	113.13	167.46	219.53	146.35
3.41	86.11	118.22	174.04	116.02
3.98	67.95	83.61	141.25	94.17
4.51	168.22	234.26	299.34	199.56
4.79	58.49	64.81	123.07	82.05
5.22	286.24	439.71	466.88	311.25
5.54	44.94	46.61	98.45	65.63
5.96	635.78	1064.09	900.97	600.65
6.28	1126.37	2122.15	1456.50	971.00
6.46	505.71	804.75	743.04	495.36
6.7	281.49	393.32	453.64	302.43
7.04	396.53	593.77	604.74	403.16
7.33	61.45	61.92	126.12	84.08
7.88	97.56	107.47	185.75	123.83
8.21	210.09	271.21	353.76	235.84
8.56	206.54	264.75	348.53	232.35
9.01	438.53	654.10	655.47	436.98
9.37	78.46	81.38	154.32	102.88
9.72	803.23	1355.06	1089.30	726.20
9.99	404.11	589.44	611.45	407.63
10.33	392.73	568.10	596.73	397.82
10.7	29.30	24.64	67.40	44.94
11.51	27.43	22.32	63.59	42.39
12.62	95.26	100.01	180.81	120.54
13.02	44.68	39.99	95.70	63.80
14.03	123.73	135.69	224.82	149.88

Badınca River stream power calculations part 3, 2 km averages of stream powers calculated using different width prediction methods

Down stream distance (km)	Averages unit stream power using widths from hydraulic scaling fitted to downstream of KP	error 1 standard deviation	Averages unit stream power using widths from hydraulic scaling fitted to upstream of KP	error 1 standard deviation	Averages unit stream power using widths from Finnegan width scaling	error 1 standard deviation	Averages unit stream power using widths from Whittaker width scaling	error 1 standard deviation
0.9								
1.6								
1.94								
2.39	170.61	35.99	113.74	23.99	65.72	15.40	59.01	14.26
2.87								
3.41								
3.98								
4.51	208.54	34.26	139.03	22.84	111.13	26.13	132.56	39.97
4.79								
5.22								
5.54								
5.96								
6.28	546.75	233.12	364.50	155.41	326.81	152.86	376.17	190.96
6.46								
6.7								
7.04								
7.33								
7.88								
8.21	421.00	118.51	280.67	79.01	257.71	69.12	293.79	140.65
8.56								
9.01								
9.37								
9.72								
9.99	431.63	84.89	287.75	63.21	272.00	59.64	311.01	68.30
10.33								
10.7								
11.51	202.79	118.90	135.19	79.27	121.26	69.02	128.21	70.17
12.62								
13.02								
14.03	167.11	32.82	111.41	21.88	86.05	18.40	72.33	16.92

Badınca River: Field Schmidt hammer readings

Down stream distance (km)	Location	Schmidt hammer readings																			
0.9	E30																				
1.6	E18																				
1.94	E19	40	47	39	45	47	36	34	52	42	40	46	42	39	42	47	45	40	43	49	32
2.39	E20	46	51	57	46	46	42	42	32	34	36	42	39	47	59	50	42	40	35	31	40
2.87	E21	38	35	42	36	37	29	36	42	30	36	42	38	30	35	34	32	32	24	36	32
3.41	E22	48	46	42	42	38	45	32	26	44	32	35	42	36	37	35	38	30	32	29	31
3.98	E17																				
4.51	E7	36	34	30	32	32	34	29	36	39	40	36	43	44	30	41	37	44	30	43	47
4.79	E8	50	60	64	64	40	52	60	50	66	60	54	58	42	42	58	56	60	48	52	56
5.22	E9	50	44	38	40	56	46	50	40	34	50	42	42	36	42	52	47	50	56	43	42
5.54	E10	50	52	40	54	46	30	52	46	46	42	42	56	55	52	43	54	56	42	56	48
5.96	E11	52	44	45	55	59	60	42	40	54	42	40	53	37	46	53	42	32	58	48	38
6.28	E12	50	47	53	55	46	55	51	40	46	51	57	50	56	46	49	48	52	41	50	58
6.46	E13	37	42	47	38	34	34	46	49	38	46	35	35	47	37	40	32	39	35	31	40
6.7	E14	34	42	40	40	39	34	33	29	34	36	41	40	45	32	37	40	37	29	36	38
7.04	E15																				
7.33	E16	46	45	39	47	36	34	51	46	40	47	39	54	52	59	57	46	44	40	50	47
7.88	E26																				
8.21	E1	28	32	41	45	32	26	44	45	37	30	32	41	43	31	37	29	36	42	49	46
8.56	E2	43	42	36	31	42	49	30	29	42	37	36	34	33	32	42	47	30	41	39	45
9.01	E3	56	42	30	46	64	62	51	54	46	47	53	48	62	60	53	52	47	59	51	51
9.37	E4	51	46	60	43	48	49	65	52	40	52	52	42	60	52	47	49	49	51	62	42
9.72	E5	53	46	64	60	56	56	58	62	52	44	50	48	48	51	46	60	49	53	56	59
9.99	E6	48	46	42	42	37	43	51	49	46	43	49	51	38	41	47	46	37	39	42	46
10.33	E23	50	32	40	54	46	30	32	46	46	42	38	34	37	35	29	30	37	34	30	38
10.7	E24	38	42	34	38	39	40	42	34	30	46	38	42	47	30	29	36	34	34	37	36
11.51	E25	34	46	28	34	42	40	22	36	46	42	29	36	42	30	36	29	36	42	30	32
12.62	E28																				
13.02	E29																				
14.03	E27	25	23	29	24	26	27	24	22	22	26	30	27	24	26	22	24	21	26	28	28

Badınca River: Selby Rock Mass Strength Index calculation

Down stream distance (km)	Location #	Schmidt hammer average	Hardness selby index number	Weathering selby index number	Joint spacing selby index number	Joint width selby index number	Joint orientation selby index number	Ground water selby index number	continuity of joints selby index numbers	Lithology	Selby rock mass strength rating
0.9	E30										
1.6	E18	20	5	5	8	6	9	6	5	gneiss	44
1.94	E19	42	14	7	15	5	18	6	5	gneiss	70
2.39	E20	43	14	7	15	6	18	6	5	gneiss	71
2.87	E21	35	10	9	8	5	18	6	6	schist	62
3.41	E22	37	10	9	8	5	14	6	6	schist	58
3.98	E17		5	5	8	6	9	6	5	gneiss	44
4.51	E7	37	10	5	8	6	18	6	5	schist	58
4.79	E8	55	18	9	21	6	14	6	6	quartzite	80
5.22	E9	45	14	7	8	6	14	6	5	gneiss	60
5.54	E10	48	14	5	15	5	14	6	6	gneiss	65
5.96	E11	47	14	7	8	5	18	6	5	gneiss	63
6.28	E12	50	18	7	8	4	14	6	5	gneiss	62
6.46	E13	39	10	5	8	5	18	6	5	travertine	57
6.7	E14	37	10	7	15	5	18	6	6	travertine	67
7.04	E15									travertine	
7.33	E16	46	14	5	21	6	18	6	5	gneiss	75
7.88	E26	20	5	5	8	5	14	6	5	sediments	48
8.21	E1	37	10	7	8	5	18	6	5	schist	59
8.56	E2	38	10	7	8	5	18	6	5	schist	59
9.01	E3	52	18	9	8	5	18	6	5	granite	69
9.37	E4	51	18	7	15	6	18	6	5	granite	75
9.72	E5	54	18	9	8	6	20	6	5	gneiss	72
9.99	E6	44	14	7	8	5	20	6	5	schist	65
10.33	E23	38	10	7	8	6	14	6	6	travertine	57
10.7	E24	37	10	7	15	6	18	6	5	travertine	67
11.51	E25	36	10	5	15	6	14	6	5	travertine	61
12.62	E28	20	5	5	8	5	18	6	5	sediments	52
13.02	E29	20	5	5	8	5	18	6	5	sediments	52
14.03	E27	25	5	5	8	5	18	6	5	sediments	52

Percentage bedrock in the channel field data

Akcipinar

Down stream distance (km)	% bedrock in the channel
0.9	0
1.2	40
1.5	40
1.7	30
1.9	40
2.1	100
2.4	10
2.8	20
3.3	60
3.6	10
3.7	25
4.0	70
4.3	80
4.6	50
4.9	90
5.2	80
5.7	80
6.1	70
6.6	50
7.2	40
7.7	100
8.2	80
8.6	60
9.0	70
10.3	20
10.6	90
10.8	50
11.0	60
11.3	60
11.5	90
11.7	10
12.0	20
12.3	100
12.5	0
12.8	90
13.0	50
13.3	60
13.8	10
14.1	0
14.6	100
15.0	0
15.0	0
15.4	50
15.5	75

Sart

Down stream distance (km)	% bedrock in the channel
0.4	0
0.9	0
1.0	0
1.3	90
1.6	10
2.1	80
2.6	0
3.0	0
3.3	50
3.7	5
4.1	0
4.4	20
4.7	20
5.0	25
5.4	5
5.9	100
6.5	40
7.0	30
7.6	0
8.1	60
8.8	20
9.3	0
9.7	0
10.2	70
12.0	0
12.2	100
12.7	100
13.3	90
14.0	100
14.4	70
14.9	0
15.4	0
15.7	0
16.2	0
16.6	0
16.9	0
17.3	0
17.7	0
18.0	0
18.3	0

Bozdağ

Down stream distance (km)	% bedrock in the channel
1.0	0
1.4	0
1.7	90
2.1	0
3.0	0
3.6	0
3.6	0
4.9	0
6.2	0
7.6	0
8.2	50
9.0	10
9.3	80
9.8	60
9.9	0
10.1	0
10.5	60
10.9	50
11.6	0
12.6	100
13.6	80
14.2	0
14.8	20
15.1	60
15.4	20
16.0	10
16.5	0
17.2	0
18.0	0
18.5	0
19.1	0
19.9	0
20.4	0

Kabazlı

Down stream distance (km)	% bedrock in the channel
0.1	0
0.6	0
1.4	50
1.7	0
2.7	60
3.2	40
4.1	60
4.2	80
4.6	20
4.9	10
5.1	80
5.5	50
5.8	90
6.1	90
6.2	90
6.3	90
6.6	10
6.7	100
7.1	100
7.7	100
8.3	100
8.4	0
8.5	60
9.2	0
9.6	0
10.1	0
10.6	0
11.2	0
11.8	0
12.7	0
14.1	0

Yeniköy

Down stream distance (km)	% bedrock in the channel
0.0	0
0.3	0
0.5	0
0.8	0
1.1	0
1.5	0
1.8	10
2.1	70
2.6	100
3.3	0
3.9	10
5.2	0
5.5	0
5.7	0
6.3	0
6.8	0
7.8	0

Badınca

Down stream distance (km)	% bedrock in the channel
0.9	0
1.6	0
1.9	0
2.4	10
2.9	20
3.4	40
4.0	60
4.5	20
4.8	10
5.2	40
5.5	20
6.0	0
6.3	60
6.5	0
6.7	10
7.0	50
7.3	30
7.9	0
8.2	100
8.6	100
9.0	80
9.4	100
9.7	30
10.0	20
10.3	10
10.7	0
11.5	10
12.6	0
13.0	0
14.0	0

REFERENCES

Adamiec, G., & Aitken, M.J. (1998). Dose-rate conversion factors: new data. Ancient TL. 16, 37-50.

Ağırbaş, H., (2006). Alkan köyü (Alaşehir) ve yakın çevresinde Gediz grabeni' nin stratigrafisi ve yapısal özellikleri. [B.Sc. thesis] İstanbul University, İstanbul.

Aitken, M. J. (1985). Thermoluminescence Dating. Academic Press, London.

Aitken, M. J. (1992). Optical dating. Quaternary Science Reviews 11, 127-131.

Aitken, M. J. (1998). An Introduction to Optical Dating. Oxford University Press, Oxford.

Akçar, N., Yavuz, V., Ivy-Ochs, S., Kubik, P. W., Vardar, M., & Schlüchter, C. (2007). Paleoglacial records from Kavron Valley, NE Turkey: field and cosmogenic exposure dating evidence. Quaternary International, 164, 170-183.

Akkök, R. (1983). Structural and metamorphic evolution of the northern part of the Menderes massif: new data from the Derbent area and their implication for the tectonics of the massif. The Journal of Geology, 342-350.

Aktug, B., Nocquet, J. M., Cingöz, A., Parsons, B., Erkan, Y., England, P., Lenk, O., GürdaL, M. A., Kilicoglu, A., Akdeniz, H., & Tekgül, A. (2009). Deformation of western Turkey from a combination of permanent and campaign GPS data: Limits to block-like behavior. Journal of Geophysical Research: Solid Earth (1978–2012), 114(B10).

Allen, G. H., Barnes, J. B., Pavelsky, T. M., & Kirby, E. (2012). Bedrock Channel Adjustment to Variations in Tectonics and Lithology at the Himalayan Front in Northwest India. In AGU Fall Meeting Abstracts (Vol. 1, p. 0992).

Allen, G. H., Barnes, J. B., Pavelsky, T. M., & Kirby, E. (2013). Lithologic and tectonic controls on bedrock channel form at the northwest Himalayan front.Journal of Geophysical Research: Earth Surface, 118(3), 1806-1825.

Alley, R. B., Mayewski, P. A., Sowers, T., Stuiver, M., Taylor, K. C., & Clark, P. U. (1997). Holocene climatic instability: A prominent, widespread event 8200 yr ago. Geology, 25(6), 483-486.

Alley, R. B., & Ágústsdóttir, A. M. (2005). The 8k event: cause and consequences of a major Holocene abrupt climate change. Quaternary Science Reviews, 24(10), 1123-1149.

Alto, R., Dunne, T., & Guyot, J. L. (2006). Geomorphic controls on Andean denudation rates. The Journal of Geology, 114(1), 85-99.

Ambraseys, N. N., & Jackson, J. A. (1998). Faulting associated with historical and recent earthquakes in the Eastern Mediterranean region. Geophysical Journal International, 133(2), 390-406.

Ambraseys, N. N. (2009). Earthquakes in the Mediterranean and Middle East: A multidisciplinary study of seismicity up to 1990. Cambridge Univeristy Press. Cambridge.

Amos, C. B., Burbank, D. W., Nobes, D. C., & Read, S. A. (2007). Geomorphic constraints on listric thrust faulting: Implications for active deformation in the Mackenzie Basin, South Island, New Zealand. Journal of Geophysical Research: Solid Earth (1978–2012), 112(B3).

Anthony, D. M., & Granger, D. E., (2007). An empirical stream power formulation for knickpoint retreat in Appalachian Plateau fluviokarst. Journal of Hydrology 343(3), 117-126.

Ariztegui, D., Asioli, A., Lowe, J. J., Trincardi, F., Vigliotti, L., Tamburini, F., Chondrogianni, C., Acrossi, C. A., Mazzanti, M., Mercuri, A. M., Van der Kaars, S., McKenzie, J. A., & Oldfield, F. (2000). Palaeoclimate and the formation of sapropel S1: inferences from Late Quaternary lacustrine and marine sequences in the central Mediterranean region. Palaeogeography, Palaeoclimatology, Palaeoecology,158(3), 215-240.

Armijo, R., Meyer, B. G. C. P., King, G. C. P., Rigo, A., & Papanastassiou, D. (1996). Quaternary evolution of the Corinth Rift and its implications for the Late Cenozoic evolution of the Aegean. Geophysical Journal International, 126(1), 11-53.

Arpat, E., & Bingöl, E. (1969). Ege Bölgesi graben sisteminin gelişimi üzerine düşünceler. MTA Dergisi, 73, 1-8.

Arrowsmith, J. R., & Zielke, O. (2009). Tectonic geomorphology of the San Andreas Fault zone from high resolution topography: an example from the Cholame segment. Geomorphology, 113(1), 70-81.

ASTER GDEM Validation Team. 2009. ASTER Global DEM Validation Summary Report

Attal, M., Tucker, G. E., Whittaker, A. C., Cowie, P. A., & Roberts, G. P. (2008). Modeling fluvial incision and transient landscape evolution: Influence of dynamic channel adjustment. Journal of Geophysical Research: Earth Surface (2003–2012), 113(F3).

Attal, M., Cowie, P. A., Whittaker, A. C., Hobley, D., Tucker, G. E., & Roberts, G. P. (2011). Testing fluvial erosion models using the transient response of bedrock rivers to tectonic forcing in the Apennines, Italy. Journal of Geophysical Research: Earth Surface (2003–2012), 116(F2).

Attal, M., Mudd, S. M., Hurst, M. D., & Crickmore, B. A. (2013). Quantifying Holocene Coastal Retreat From River Morphology in Southern England and Wales. In AGU Fall Meeting Abstracts,1, 905.

Azamathulla, H. M., & Jarrett, R. D. (2013). Use of gene-expression programming to estimate Manning's roughness coefficient for high gradient streams. Water resources management, 27(3), 715-729.

Baldwin, J. A., Whipple, K. X., & Tucker, G. E. (2003). Implications of the shear stress river incision model for the timescale of postorogenic decay of topography. Journal of Geophysical Research: Solid Earth (1978–2012), 108(B3).

Banerjee, D., Murray, A. S., Bøtter-Jensen, L., & Lang, A. (2001). Equivalent dose estimation using a single aliquot of polymineral fine grains. Radiation Measurements, 33(1), 73-94.

Bard, E., Rostek, F., Turon, J. L., & Gendreau, S. (2000). Hydrological impact of Heinrich events in the subtropical northeast Atlantic. Science, 289(5483), 1321-1324.

Barka, A. & Reilinger, R. (1997). Active tectonics of the Eastern Mediterranean region: deduced from GPS, neotectonic and seismicity data. Annals of Geophysics, 40(3).

Barnett, J. A., Mortimer, J., Rippon, J. H., Walsh, J. J., & Watterson, J. (1987). Displacement geometry in the volume containing a single normal fault. AAPG Bulletin, 71(8), 925-937.

Benda, L. (1971). Principles of the palynologic subdivision of the Turkish Neogene. Newsletters on Stratigraphy, 23-26.

Benda, L., Meulenkamp, J. E., Zachariasse, W. J. (1974). Biostratigraphic correlations in the Eastern Mediterranean Neogene: 1. Correlation between planktonic foraminiferal, uvigerinid sporomorphal, and mammal zonations of the Cretan and Italian Neogene. Newsletter on Stratigraphy, 3, 205–217.

Benda, L., & Meulenkamp, J. E. (1979). Biostratigraphic correlations in the Eastern Mediterranean Neogene. 5. Calibration of sporomorph associations, marine microfossils and mammal zones, marine and continental stages and the radiometric scale. In Ann. Géol. Pays Hellén., Tome hors ser (Vol. 1, pp. 61-70).

Berger, G. W., & Luternauer, J. J. (1987). Preliminary fieldwork for thermoluminescence dating studies at the Fraser River delta, British Columbia.Geological Survey of Canada Paper, 87, 901-904.

Berlin, M. M., & Anderson, R. S. (2007). Modelling of knickpoint retreat on the Roan Plateau, western Colorado. Journal of Geophysical Research: Earth Surface (2003–2012), 112(F3).

Berlin, M. M., & Anderson, R. S. (2009). Steepened channels upstream of knickpoints: Controls on relict landscape response. Journal of Geophysical Research: Earth Surface (2003–2012), 114(F3).

Berryman, K., Marden, M., Eden, D., Mazengarb, C., Ota, Y., & Moriya, I. (2000). Tectonic and paleoclimatic significance of Quaternary river terraces of the Waipaoa River, east coast, North Island, New Zealand. New Zealand Journal of Geology and Geophysics, 43(2), 229-245.

Bilham, R., Gaur, V. K., & Molnar, P. (2001). Himalayan seismic hazard. Science Washington), 293(5534), 1442-1444.

Bishop, P., Hoey, T. B., Jansen, J. D., & Artza, I. L. (2005). Knickpoint recession rate and catchment area: the case of uplifted rivers in Eastern Scotland. Earth Surface Processes and Landforms, 30(6), 767-778.

Bishop, P. (2007). Long-term landscape evolution: linking tectonics and surface processes. Earth Surface Processes and Landforms, 32(30) 329-365.

Blong, R. J., & Gillespie, R. (1978). Fluvially transported charcoal gives erroneous 14C ages for recent deposits. Nature 271, 739 - 741

Blum, M. D., and Valastro, S. Jr. (1994). Late Quaternary sedimentation, lower Colorado River, Gulf Coastal Plain of Texas; with Suppl. Data 9420: Geological Society of America Bulletin, 106, 1002-1016.

Blum, M. D., & Törnqvist, T. E. (2000). Fluvial responses to climate and sea-level change: a review and look forward. Sedimentology, 47(s1), 2-48.

Blumetti, A. M., Dramis, F., & Michetti, A. M. (1993). Fault-generated mountain fronts in the central Apennines (Central Italy): Geomorphological features and seismotectonic implications. Earth Surface Processes and Landforms, 18(3), 203-223.

Bøtter-Jensen, L. (1997). Luminescence techniques: instrumentation and methods. Radiation Measurements, 27(5), 749-768.

Bøtter-Jensen, L., Bulur, E., Duller, G. A. T., & Murray, A. S. (2000). Advances in luminescence instrument systems. Radiation Measurements, 32(5), 523-528.

Bøtter-Jensen, L., Andersen, C. E., Duller, G. A. T., & Murray, A. S. (2003). Developments in radiation, stimulation and observation facilities in luminescence measurements. Radiation Measurements, 37(4), 535-541.

Boulton, S. J., Robertson, A. H., & Ünlügenç, U. C. (2006). Tectonic and sedimentary evolution of the Cenozoic Hatay Graben, Southern Turkey: a two-phase model for graben formation. Geological Society, London, Special Publications, 260(1), 613-634.

Boulton, S. J., & Whittaker, A. C. (2009). Quantifying the slip rates, spatial distribution and evolution of active normal faults from geomorphic analysis: Field examples from an oblique-extensional graben, southern Turkey. Geomorphology, 104(3), 299-316.

Bowen, D. Q., Sykes, G. A., Maddy, D., Bridgland, D. R., & Lewis, S. G. (1995). Aminostratigraphy and amino acid geochronology of English lowland valleys: the Lower Thames in context. The Quaternary of the lower reaches of the Thames, 61-63.

Bozkurt, E., (2000). Timing of extension on the Büyük Menderes Graben, western Turkey, and its tectonic implications, in: E. Bozkurt, J. A. Winchester, J. D. A. Piper (Eds.), Tectonics and Magmatism in Turkey and the Surrounding Area, 173, Special Publications, Geological Society, London, 2000, pp. 385–403.

Bozkurt, E. (2001). Neotectonics of Turkey–a synthesis. Geodinamica Acta, 14(1), 3-30.

Bozkurt, E., (2003). Origin of NE-trending basins in western Turkey, Geodinamica Acta 16, 61-81.

Bozkurt, E., & Satir, M. (2000). The southern Menderes Massif (western Turkey): geochronology and exhumation history. Geological Journal, 35(3-4), 285-296.

Bozkurt, E., & Mittwede, S. K. (2001). Introduction to the geology of Turkey—a synthesis. International Geology Review, 43(7), 578-594.

Bozkurt, E., & Oberhänsli, R. (2001). Menderes Massif (Western Turkey): structural, metamorphic and magmatic evolution–a synthesis. International Journal of Earth Sciences, 89(4), 679-708.

Bozkurt, E., & Sözbilir, IR, H. (2004). Tectonic evolution of the Gediz Graben: field evidence for an episodic, two-stage extension in western Turkey. Geological Magazine, 141(01), 63-79.

Bozkurt, E., & Mittwede, S. K. (2005). Introduction: Evolution of continental extensional tectonics of western Turkey. Geodinamica Acta, 18(3-4), 153-165.

Braun, J., & Sambridge, M. (1997). Modelling landscape evolution on geological time scales: a new method based on irregular spatial discretization. Basin Research, 9(1), 27-52.

Bridgland, D. R., & Maddy, D. (1995). River terraces as records of Quaternary climate oscillation. Abstracts INQUA XIV, Berlin, 37.

Bridgland, D. R. (2000). River terrace systems in north-west Europe: an archive of environmental change, uplift and early human occupation. Quaternary Science Reviews, 19(13), 1293-1303.

Bridgland, D. R., Philip, G., Westaway, R., & White, M. J. (2003). A long quaternary terrace sequence in the Orontes River valley, Syria: a record of uplift and of human occupation. Current science., 84(8), 1080-1089.

Bridgland, D. R., Demir, T., Seyrek, A., Pringle, M., Westaway, R., Beck, A. R., Rowbotham, G., & Yurtmen, S. (2007). Dating Quaternary volcanism and incision by the River Tigris at Diyarbakır, southeast Turkey. Journal of Quaternary Science, 22(4), 387-393.

Bridgland, D. R., & Westaway, R. (2008a). Preservation patterns of Late Cenozoic fluvial deposits and their implications: results from IGCP 449.Quaternary International, 189(1), 5-38.

Bridgland, D., & Westaway, R. (2008b). Climatically controlled river terrace staircases: a worldwide Quaternary phenomenon. Geomorphology, 98(3), 285-315.

Bridgland, D. R., Westaway, R., Romieh, M. A., Candy, I., Daoud, M., Demir, T., Galiatsatos, N., Schreve, D. C., Seyrek, A., Shaw, A. D., White, T. S., & Whittaker, J. (2012). The River Orontes in Syria and Turkey: Downstream variation of fluvial archives in different crustal blocks.Geomorphology, 165, 25-49.

Brinkmann, R. (1976). Geology of Turkey (p. 153). Ferdinand Enke Veriag, Stuttgart.

Brocard, G. Y., & Van der Beek, P. A. (2006). Influence of incision rate, rock strength, and bedload supply on bedrock river gradients and valley-flat widths: Field-based evidence and calibrations from western Alpine rivers (southeast France). Geological Society of America Special Papers, 398, 101-126.

Brook, G. A., Srivastava, P., & Marais, E. (2006). Characteristics and OSL minimum ages of relict fluvial deposits near Sossus Vlei, Tsauchab River, Namibia, and a regional climate record for the last 30 ka. Journal of Quaternary Science, 21(4), 347-362.

Brown, E. T., Bourlés, D. L., Raisbeck, G. M., Yiou, F., Burchfiel, B. C., Molnar, P. Qidong, D. & Jun, L. (1998). Estimation of slip rates in the southern Tien Shan using cosmic ray exposure dates of abandoned alluvial fans. Geological Society of America Bulletin, 110(3), 377-386.

Brunnacker, K., & Boenigk, W. (1983). The Rhine valley between the Neuwied Basin and the lower Rhenish Embayment. In Plateau Uplift (pp. 62-72). Springer Berlin Heidelberg.

Buddensiek, M. L., Sheng, J., Crosby, T., Schuster, G. T., Bruhn, R. L., & He, R. (2008). Colluvial wedge imaging using traveltime and waveform tomography along the Wasatch Fault near Mapleton, Utah. Geophysical Journal International, 172(2), 686-697.

Bull, W. B. (1991). Geomorphic responses to climatic change. Oxford University Press, Oxford.

Burbank, D. W., Leland, J., Fielding, E., Anderson, R. S., Brozovic, N., Reid, M. R., & Duncan, C. (1996). Bedrock incision, rock uplift and threshold hillslopes in the northwestern Himalayas. Nature, 379(6565), 505-510.

Burbank, D. W., & Anderson, R. S. (2001a). Establishing Timing in the landscape: dating methods. Tectonic Geomorphology, Second Edition, 45-70.

Burbank, D. W., & Anderson, R. S., (2001b). Tectonic geomorphology. Wiley-Blackwell.

Buscher, J. T., Hampel, A., Hetzel, R., Dunkl, I., Glotzbach, C., Struffert, A., Akal, C., & Rätz, M. (2013). Quantifying rates of detachment faulting and erosion in the central Menderes Massif (western Turkey) by thermochronology and cosmogenic 10Be. Journal of the Geological Society, 170(4), 669-683.

Byrd, J. O., Smith, R. B., & Geissman, J. W. (1994). The Teton fault, Wyoming: Topographic signature, neotectonics, and mechanisms of deformation. Journal of Geophysical Research: Solid Earth (1978–2012), 99(B10), 20095-20122.

Candan, O., Dora, O., Oberhänsli, R., Çetinkaplan, M., Partzsch, J., Warkus, F., & Dürr, S. (2001). Pan-African high-pressure metamorphism in the Precambrian basement of the Menderes Massif, western Anatolia, Turkey. International Journal of Earth Sciences, 89(4), 793-811.

Carcaillet, J., Mugnier, J. L., Koçi, R., & Jouanne, F. (2009). Uplift and active tectonics of southern Albania inferred from incision of alluvial terraces. Quaternary Research, 71(3), 465-476.

Carretier, S., & Lucazeau, F. (2005). How does alluvial sedimentation at range fronts modify the erosional dynamics of mountain catchments?. Basin research,17(3), 361-381.

Castillo-Rodríguez, Miguel E. (2011) Base-level fall, knickpoint retreat and transient channel morphology: The case of small bedrock rivers on resistant quartzites (Isle of Jura, western Scotland). PhD thesis, University of Glasgow.

Castillo, M., Bishop, P., & Jansen, J. D. (2013). Knickpoint retreat and transient bedrock channel morphology triggered by base-level fall in small bedrock river catchments: The case of the Isle of Jura, Scotland. Geomorphology, 180, 1-9.

Catlos, E. J., & Çemen, I. (2005). Monazite ages and the evolution of the Menderes Massif, western Turkey. International Journal of Earth Sciences, 94(2), 204-217.

Çemen, I., Catlos, E. J., Göğüs, O., & Özerdem, C. (2006). Postcollisional extensional tectonics and exhumation of the Menderes massif in the Western Anatolia extended terrane, Turkey. Geological Society of America Special Papers, 409, 353-379.

Chang, W. L., Smith, R. B., Meertens, C. M., & Harris, R. A. (2006). Contemporary deformation of the Wasatch Fault, Utah, from GPS measurements with implications for interseismic fault behavior and earthquake hazard: Observations and kinematic analysis. Journal of Geophysical Research: Solid Earth (1978–2012), 111(B11).

Chen, Y. W., Chen, Y. G., Murray, A. S., Liu, T. K., & Lai, T. C. (2003). Luminescence dating of neotectonic activity on the southwestern coastal plain, Taiwan. Quaternary Science Reviews, 22(10), 1223-1229.

Cheong, C. S., Hong, D. G., Lee, K. S., Kim, J. W., Choi, J. H., Murray, A. S., Chwae, U., Im, C.B., Chang, C.J. & Chang, H. W. (2003). Determination of slip rate by optical dating of fluvial deposits from the Wangsan fault, SE Korea. Quaternary Science Reviews,22(10), 1207-1211.

Childs, C., Watterson, J., & Walsh, J. J. (1995). Fault overlap zones within developing normal fault systems. Journal of the Geological Society, 152(3), 535-549.

Çiftçi, N. B., (2007). Geological evolution of the Gediz graben, SW Turkey: Temporal and spatial variation of the graben. Ph. D. thesis, Middle East Technical University, Ankara, Turkey.

Çiftçi, N. B., & Bozkurt, E. (2007). Anomalous stress field and active breaching at relay ramps: a field example from Gediz Graben, SW Turkey. Geological Magazine, 144, 687-699.

Çiftçi, N. B., & Bozkurt, E. (2009a). Pattern of normal faulting in the Gediz Graben, SW Turkey. Tectonophysics, 473(1), 234-260.

Çiftçi, N. B., & Bozkurt, E. (2009b). Evolution of the Miocene sedimentary fill of the Gediz Graben, SW Turkey. Sedimentary Geology, 216(3), 49-79.

Çiftçi, N. B., & Bozkurt, E. (2010) Structural evolution of the Gediz graben, SW Turkey: Temporal and spatial variation of the graben basin: Basin Research, 22, 846–873.

Çiner, A. (2004). Turkish glaciers and glacial deposits. Developments in Quaternary Sciences, 2, 419-429.

Çiner, A., Doğan, U., Yıldırım, C., Akçar, N., Ivy-Ochs, S., Alfimov, V., & Schlüchter, C. (2015). Quaternary uplift rates of the Central Anatolian Plateau, Turkey: insights from cosmogenic isochron-burial nuclide dating of the Kızılırmak River terraces. Quaternary Science Reviews, 107, 81-97.

Clarke, P. J., Davies, R. R., England, P. C., Parsons, B., Billiris, H., Paradissis, D., Vies, G., Cross, P. A., Denys, P. H., Ashkenazi, V., Bingley, R., Kahle, H. G., Muller, M. V. & Briole, P. (1998). Crustal strain in central Greece from repeated GPS measurements in the interval 1989–1997. Geophysical Journal International, 135(1), 195-214.

Cohen, H. A., Dart, C., Akyüz, H. S., & Barka, A. (1995). Syn-rift sedimentation and structural development of the Gediz and Büyük Menderes graben, western Turkey: Geological Society of London Journal, 152, 629-638.

Cohen, S., Willgoose, G., & Hancock, G. (2009). The mARM spatially distributed soil evolution model: A computationally efficient modeling framework and analysis of hillslope soil surface organization. Journal of Geophysical Research: Earth Surface (2003–2012), 114(F3).

Collettini, C. (2011). The mechanical paradox of low-angle normal faults: Current understanding and open questions. Tectonophysics, 510(3), 253-268.

Combourieu-Nebout, N., De Beaulieu, J. L., Bout-Roumazeilles, V., Colombaroli, D., Desprat, S., Francke, A., Joannin, S., Peyron, O., Revel, M., Sadori, L., Siani, G., Samartin, S., Simonneau, A., Vannière, B., Wagner, B., Zanchetta, G., Anselmetti, F., Brugiapaglia, E., Chapron, E., Debret, M., Desmet, M., Didier, J., Essallami, L., Galop, D., Gill, A., Haas, J., Kallel, N., Millet, L., Stock, A.,Turon, J., & Wirth, S. (2013). North-south palaeohydrological contrasts in the central Mediterranean during the Holocene: tentative synthesis and working hypotheses. Climate of the Past Discussions,9, 1901-1967.

Cook, K. L., Turowski, J. M., & Hovius, N. (2014). River gorge eradication by downstream sweep erosion. Nature Geoscience, 7(9), 682-686.

Cook, K. L., Whipple, K. X., Heimsath, A. M. & Hanks, T. C., (2009). Rapid incision of the Colorado River in Glen Canyon–insights from channel profiles, local incision rates, and modelling of lithologic controls. Earth Surface Processes and Landforms, 34(7), 994-1010.

Coppersmith, K. J., & Youngs, R. R. (1989). Issues regarding earthquake source characterization and seismic hazard analysis within passive margins and stable continental interiors. In Earthquakes at North-Atlantic Passive Margins: Neotectonics and Postglacial Rebound (pp. 601-631). Springer Netherlands.

Coulthard, T. J. (2001). Landscape evolution models: a software review. Hydrological processes, 15(1), 165-173.

Coulthard, T. J., Macklin, M. G., & Kirkby, M. J. (2002). A cellular model of Holocene upland river basin and alluvial fan evolution. Earth Surface Processes and Landforms, 27(3), 269-288.

Cowie, P. A. (1998). A healing–reloading feedback control on the growth rate of seismogenic faults. Journal of Structural Geology, 20(8), 1075-1087.

Cowie, P. A., & Roberts, G. P. (2001). Constraining slip rates and spacings for active normal faults. Journal of Structural Geology, 23(12), 1901-1915.

Cowie, P. A., Attal, M., Tucker, G. E., Whittaker, A. C., Naylor, M., Ganas, A., & Roberts, G. P. (2006). Investigating the surface process response to fault interaction and linkage using a numerical modelling approach. Basin Research,18(3), 231-266.

Cowie, P. A., Whittaker, A. C., Attal, M., Roberts, G., Tucker, G. E., Ganas, A., (2008). New constraints on sediment-flux-dependent river incision: Implications for extracting tectonic signals from river profiles. Geology, 36(7), 535-538.

Croissant, T. and Braun, J. (2014). Constraining the stream power law: a novel approach combining a landscape evolution model and an inversion method Earth Surface Dynamics 2, 155–166.

Crone, A. J., & Harding, S. T. (1984). Relationship of late Quaternary fault scarps to subjacent faults, eastern Great Basin, Utah. Geology, 12(5), 292-295.

Crosby, BT, & Whipple, KX, (2006). Knickpoint initiation and distribution within fluvial networks: 236 waterfalls in the Waipaoa River, North Island, New Zealand. Geomorphology, vol. 82, pp. 16-38.

Cunha, P. P., Martins, A. A., Huot, S., Murray, A., & Raposo, L. (2008). Dating the Tejo river lower terraces in the Ródão area (Portugal) to assess the role of tectonics and uplift. Geomorphology, 102(1), 43-54.

Cyr, A. J., Granger, D. E., Olivetti, V., & Molin, P. (2010). Quantifying rock uplift rates using channel steepness and cosmogenic nuclide–determined erosion rates: Examples from northern and southern Italy. Lithosphere, 2(3), 188-198.

Cyr, A. J., Granger, D. E., Olivetti, V., & Molin, P. (2014). Distinguishing between tectonic and lithologic controls on bedrock channel longitudinal profiles using cosmogenic 10 Be erosion rates and channel steepness index.Geomorphology, 209, 27-38.

Dadson, S. J., Hovius, N., Chen, H., Dade, W. B., Hsieh, M. L., Willett, S. D., Hu, J. C., Horng, M. J., Chen, M. C., Stark, C. P., Lague, D., & Lin, J. C. (2003). Links between erosion, runoff variability and seismicity in the Taiwan orogen. Nature, 426(6967), 648-651.

Daëron, M., Benedetti, L., Tapponnier, P., Sursock, A., & Finkel, R. C. (2004). Constraints on the post~ 25-ka slip rate of the Yammoûneh fault (Lebanon) using in situ cosmogenic36Cl dating of offset limestone-clast fans. Earth and Planetary Science Letters, 227(1), 105-119.

Dansgaard, W., Johnsen, S. J., Clausen, H. B., Dahl-Jensen, D., Gundestrup, N. S., Hammer, C. U., ... & Bond, G. (1993). Evidence for general instability of past climate from a 250-kyr ice-core record. Nature, 364(6434), 218-220.

Dean, J. R., Jones, M. D., Leng, M. J., Sloane, H. J., Roberts, C. N., Woodbridge, J., Swann, G. E. A., Metcalf, S. E., Eastwood, W. J., & Yiğitbaşıoğlu, H. (2013). Palaeo-seasonality of the last two millennia reconstructed from the oxygen isotope composition of carbonates and diatom silica from Nar Gölü, central Turkey. Quaternary Science Reviews,66, 35-44.

Demir, T., Seyrek, A., Westaway, R., Bridgland, D., & Beck, A. (2008). Late Cenozoic surface uplift revealed by incision by the River Euphrates at Birecik, southeast Turkey. Quaternary International, 186(1), 132-163.

Demir, T., Westaway, R., Bridgland, D. R., & Seyrek, A. (2007). Terrace staircases of the River Euphrates in southeast Turkey, northern Syria and western Iraq: evidence for regional surface uplift. Quaternary Science Reviews,26(22), 2844-2863.

Demir, T., Yeşilnacar, İ., & Westaway, R. (2004). River terrace sequences in Turkey: sources of evidence for lateral variations in regional uplift. Proceedings of the Geologists' Association, 115(4), 289-311.

Densmore, A. L., Ellis, M. A., Li, Y., Zhou, R., Hancock, G. S., & Richardson, N. (2007). Active tectonics of the Beichuan and Pengguan faults at the eastern margin of the Tibetan Plateau. Tectonics, 26(4).

Densmore, A. L., Ellis, M. A., & Anderson, R. S. (1998). Landsliding and the evolution of normal-fault-bounded mountains. Journal of Geophysical Research: Solid Earth (1978–2012), 103(B7), 15203-15219.

Densmore, A. L., Dawers, N. H., Gupta, S., Allen, P. A., & Gilpin, R. (2003). Landscape evolution at extensional relay zones. Journal of Geophysical Research: Solid Earth (1978–2012), 108(B5).

Densmore, A. L., Dawers, N. H., Gupta, S., Guidon, R., & Goldin, T. (2004). Footwall topographic development during continental extension. Journal of Geophysical Research: Earth Surface (2003–2012), 109(F3).

Dewey, J. F. (1988). Extensional collapse of orogens. Tectonics, 7(6), 1123-1139.

Dewey, J. F., & Sengör, A. C. (1979). Aegean and surrounding regions: complex multiplate and continuum tectonics in a convergent zone. Geological Society of America Bulletin, 90(1), 84-92.

Dietrich, W. E., Bellugi, D. G., Sklar, L. S., Stock, J. D., Heimsath, A. M., & Roering, J. J. (2003). Geomorphic transport laws for predicting landscape form and dynamics. Prediction in geomorphology, 103-132.

Dilek, Y., & Pavlides, S. (Eds.). (2006). Postcollisional tectonics and magmatism in the Mediterranean region and Asia (Vol. 409). Geological Society of America.

Doglioni, C., Agostini, S., Crespi, M., Innocenti, F., Manetti, P., Riguzzi, F., & Savascin, Y. (2002). On the extension in western Anatolia and the Aegean sea. Journal of the Virtual Explorer, 8, 169-183.

Dorsey, R. J., & Roering, J. J. (2006). Quaternary landscape evolution in the San Jacinto fault zone, Peninsular Ranges of Southern California: transient response to strike-slip fault initiation. Geomorphology, 73(1), 16-32.

Duller, G. A. (1994). Luminescence dating of poorly bleached sediments from Scotland. Quaternary Science Reviews, 13(5), 521-524.

Duller, G. A. (2006). Single grain optical dating of glacigenic deposits.Quaternary Geochronology, 1(4), 296-304.

Duvall, A., Kirby, E., & Burbank, D. (2004). Tectonic and lithologic controls on bedrock channel profiles and processes in coastal California. Journal of Geophysical Research: Earth Surface (2003–2012), 109(F3).

Eastwood, W. J., Leng, M. J., Roberts, N., & Davis, B. (2007). Holocene climate change in the eastern Mediterranean region: a comparison of stable isotope and pollen data from Lake Gölhisar, southwest Turkey. Journal of Quaternary Science, 22(4), 327-341.

Ediger, V., Bati, Z. & Yazman, M., (1996). Palynology of possible hydrocarbon source rocks of the Alasehir-Turgutlu area in the Gediz graben (western Anatolia). Turkish Association of Petroleum Geologists Bulletin 8, 94–112.

England, P., & Molnar, P. (1990). Surface uplift, uplift of rocks, and exhumation of rocks. Geology, 18(12), 1173-1177.

Erinç, S. (1978). Changes in the physical environment in Turkey since the end of the last glacial. The environmental history of the Near and Middle East since the last Ice Age, 87-110. In Brice, W. C. (1978). Environmental history of the Near and Middle East since the last ice age.

Erol, O. (1978). The Quaternary history of the lake basins of central and southern Anatolia. The environmental history of the Near and Middle East since the last Ice Age, 111-139. In Brice, W. C. (1978). Environmental history of the Near and Middle East since the last ice age.

Eronen, J. T., Fortelius, M., Micheels, A., Portmann, F. T., Puolamäki, K., & Janis, C. M. (2012). Neogene aridification of the Northern Hemisphere. Geology, 40(9), 823-826.

Eyidoğan, H., & Jackson, J. (1985). A seismological study of normal faulting in the Demirci, Alaşehir and Gediz earthquakes of 1969–70 in western Turkey: implications for the nature and geometry of deformation in the continental crust. Geophysical Journal International, 81(3), 569-607.

Fairbridge, R. W. (1968). Terraces, fluvial —Environmental controls. In Geomorphology (pp. 1124-1138). Springer Berlin Heidelberg.

Ferrier, K. L., Huppert, K. L., & Perron, J. T. (2013). Climatic control of bedrock river incision. Nature, 496(7444), 206-209.

Finnegan, N. J., Roe, G., Montgomery, D. R., & Hallet, B. (2005). Controls on the channel width of rivers: Implications for modeling fluvial incision of bedrock.Geology, 33(3), 229-232.

Finnegan, N. J., Schumer, R., & Finnegan, S. (2014). A signature of transience in bedrock river incision rates over timescales of 104-107 years. Nature,505(7483), 391-394.

Fisher, G. B., Bookhagen, B., & Amos, C. B. (2013). Channel planform geometry and slopes from freely available high-spatial resolution imagery and DEM fusion: Implications for channel width scalings, erosion proxies, and fluvial signatures in tectonically active landscapes. Geomorphology, 194, 46-56.

Fleitmann, D., Cheng, H., Badertscher, S., Edwards, R. L., Mudelsee, M., Göktürk, O. M., Frankhauser, A., Pickering, R., Raible, C. C., Matter, A., Kramers, J., & Tüysüz, O. (2009). Timing and climatic impact of Greenland interstadials recorded in stalagmites from northern Turkey.Geophysical Research Letters, 36(19).

Fletcher, R. C., Buss, H. L., & Brantley, S. L. (2006). A spheroidal weathering model coupling porewater chemistry to soil thicknesses during steady-state denudation. Earth and Planetary Science Letters, 244(1), 444-457.

Fouke, B. W., Farmer, J. D., Des Marais, D. J., Pratt, L., Sturchio, N. C., Burns, P. C., & Discipulo, M. K. (2000). Depositional facies and aqueous-solid geochemistry of travertine-depositing hot springs (Angel Terrace, Mammoth Hot Springs, Yellowstone National Park, USA). Journal of Sedimentary Research,70(3), 565-585.

Fossen, H. (2010) Structural geology. Cambridge University Press, Cambridge.

Frankel, K. L., Brantley, K. S., Dolan, J. F., Finkel, R. C., Klinger, R. E., Knott, J. R., Machette, M., Owen, L. A., Phillips, F. M. Slate, J. L. & Wernicke, B. P. (2007). Cosmogenic 10Be and 36Cl geochronology of offset alluvial fans along the northern Death Valley fault zone: Implications for transient strain in the eastern California shear zone. Journal of Geophysical Research: Solid Earth (1978–2012), 112(B6).

Gansecki, C. A., Mahood, G. A., & McWilliams, M. O. (1996). 40Ar39Argeochronology of rhyolites erupted following collapse of the Yellowstone caldera, Yellowstone Plateau volcanic field: implications for crustal contamination. Earth and Planetary Science Letters, 142(1), 91-107.

Garbrecht, J., & Martz, L. W. (1997). The assignment of drainage direction over flat surfaces in raster digital elevation models. Journal of hydrology, 193(1-4), 204-213.

Gasparini, N. M., Bras, R. L., & Whipple, K. X. (2006). Numerical modelling of non–steady-state river profile evolution using a sediment-flux-dependent incision model. Geological Society of America Special Papers, 398, 127-141

Gawthorpe, R. L., Sharp, I., Underhill, J. R., & Gupta, S. (1997). Linked sequence stratigraphic and structural evolution of propagating normal faults. Geology, 25(9), 795-798.

Giardini, D., Grünthal, G., Shedlock, K. M. and Zhang, P. (2003) The GSHAP Global Seismic Hazard Map. In: Lee, W., Kanamori, H., Jennings, P. and Kisslinger, C. (eds.): International Handbook of Earthquake & Engineering Seismology, International Geophysics Series 81 B, Academic Press, Amsterdam, 1233-1239.

Gibbard, P. L., & Lewin, J. (2002). Climate and related controls on interglacial fluvial sedimentation in lowland Britain. Sedimentary Geology, 151(3), 187-210.

Gibbard, P. L., & Lewin, J. (2009). River incision and terrace formation in the Late Cenozoic of Europe. Tectonophysics, 474(1), 41-55.

Gilbert, G. K., (1877), Report on the geology of the Henry Mountains: Geographical and geological survey of the Rocky Mountain region: Washington, D.C., Government Printing Office.

Gillespie, R., Prosser, I. P., Dulgokencky, E., Sparks, R. J., Wallace, G., & Chappell, J. (1992). AMS dating of alluvial sediments on the southern tablelands of New South Wales, Australia. Radiocarbon, 34(1), 29-36.

Giraudi, C. (1995). Considerations on the significance of some post-glacial fault scarps in the Abruzzo Apennines (Central Italy). Quaternary International, 25, 33-45.

Giraudi, C., & Frezzotti, M. (1997). Late Pleistocene glacial events in the central Apennines, Italy. Quaternary Research, 48(3), 280-290.

Godfrey-Smith D. I., Huntley D. J. and Chen W. H. (1988). Optical dating studies of quartz and feldspar sediment extracts. Quaternary Science Reviews 7, 373-380.

Göktürk, O. M., Fleitmann, D., Badertscher, S., Cheng, H., Edwards, R. L., Leuenberger, M., Frankhauser, A., Tüysüz, O., & Kramers, J. (2011). Climate on the southern Black Sea coast during the Holocene: implications from the Sofular Cave record.Quaternary Science Reviews, 30(19), 2433-2445.

Goldrick, G, Bishop, P, (1995). Differentiating the roles of lithology and uplift in the steepening of bedrock river long profiles: An example from southeastern Australia. The Journal of Geology, pp. 227-231.

Goldrick, G, Bishop, P, (2007). Regional analysis of bedrock stream long profiles: evaluation of Hack's SL form, and formulation and assessment of an alternative (the DS form). Earth Surface Processes and Landforms, vol. 32, no. 5, pp. 649-671.

Gosse, J. C., & Phillips, F. M. (2001). Terrestrial in situ cosmogenic nuclides: theory and application. Quaternary Science Reviews, 20(14), 1475-1560.

Granger, D. E., Kirchner, J. W., & Finkel, R. (1996). Spatially averaged long-term erosion rates measured from in situ-produced cosmogenic nuclides in alluvial sediment. The Journal of Geology, 249-257.

Grootes, P. M., & Stuiver, M. (1997). Oxygen 18/16 variability in Greenland snow and ice with 10− 3-to 105-year time resolution. Journal of Geophysical Research: Oceans (1978–2012), 102(C12), 26455-26470.

Guidoboni, E., Bernardini, F., & Comastri, A. (2004). The 1138–1139 and 1156–1159 destructive seismic crises in Syria, south-eastern Turkey and northern Lebanon. Journal of Seismology, 8(1), 105-127.

Guidoboni, E., & Comastri, A. (2005). Catalogue of Earthquakes and Tsunamis in the Mediterranean Area from the 11th to the 15th Century. Istituto nazionale di geofisica e vulcanologia.

Gupta, A., & Scholz, C. H. (2000). A model of normal fault interaction based on observations and theory. Journal of Structural Geology, 22(7), 865-879.

Hack, J. T. (1957). Dynamic equilibrium and landscape evolution in: Theories Of Landform Development. In: Melhorn, WN, Flemal, RC, Allen, Unwin, C. eds. Winchester, Massachusetts. 87-102.

Hack, J. T. (1960). Interpretations of erosional topography in humid temperate regions. American Journal of Science, 158(A), 80-97.

Hack, J. T. (1973). Stream-profile analysis and stream-gradient index. Journal of Research of the US Geological Survey, 1(4), 421-429.

Hancock, G. S., & Anderson, R. S. (2002). Numerical modeling of fluvial strath-terrace formation in response to oscillating climate. Geological Society of America Bulletin, 114(9), 1131-1142.

Hancock, G. R., Willgoose, G. R., & Evans, K. G. (2002). Testing of the SIBERIA landscape evolution model using the Tin Camp Creek, Northern Territory, Australia, field catchment. Earth Surface Processes and Landforms,27(2), 125-143.

Hancock, P. L. (1994). Continental deformation. Pergamon Press.

Hancock, G. S., Anderson, R. S., Chadwick, O. A., & Finkel, R. C. (1999). Dating fluvial terraces with 10Be and 26Al profiles: Application to the Wind River, Wyoming. Geomorphology, 27(1), 41-60.

Hanfmann, G. M. A., Mierse, W. E., & Foss, C. (1983). Sardis from prehistoric to Roman times: results of the Archaeological Exploration of Sardis, 1958-1975. Harvard University Press.

Hansen, L., Funder, S., Murray, A. S., & Mejdahl, V. (1999). Luminescence dating of the last Weichselian glacier advance in East Greenland. Quaternary science reviews, 18(2), 179-190.

Harbor, D. J. (1998). Dynamic equilibrium between an active uplift and the Sevier River, Utah. The Journal of geology, 106(2), 181-194.

Harden, J. W., & Matti, J. C. (1989). Holocene and late Pleistocene slip rates on the San Andreas fault in Yucaipa, California, using displaced alluvial-fan deposits and soil chronology. Geological Society of America Bulletin, 101(9), 1107-1117.

Harkins, N., Kirby, E., Heimsath, A., Robinson, R., & Reiser, U. (2007). Transient fluvial incision in the headwaters of the Yellow River, northeastern Tibet, China. Journal of Geophysical Research: Earth Surface (2003–2012),112(F3).

Harris, R. A., & Day, S. M. (1993). Dynamics of fault interaction: Parallel strike-slip faults. Journal of Geophysical Research: Solid Earth (1978–2012), 98(B3), 4461-4472.

Hart, E. W., & Bryant, W. A. (1997). Fault-rupture hazard zones in California. California Department of Conservation Division of Mines and Geology.

Haviv, I., Enzel, Y., Whipple, K. X., Zilberman, E., Matmon, A., Stone, J., & Fifield, K. L. (2010). Evolution of vertical knickpoints (waterfalls) with resistant caprock: Insights from numerical modeling. Journal of Geophysical Research: Earth Surface (2003–2012), 115(F3).

Hayakawa, Y., & Matsukura, Y. (2003). Recession rates of waterfalls in Boso Peninsula, Japan, and a predictive equation. Earth Surface Processes and Landforms, 28(6), 675-684.

Hetzel, R., Romer, R. L., Candan, O., & Passchier, C. W. (1998). Geology of the Bozdag area, central Menderes massif, SW Turkey: Pan-African basement and Alpine deformation. Geologische Rundschau, 87(3), 394-406.

Holdsworth, R. E., & Turner, J. P. (Eds.). (2002). Extensional Tectonics. Geological Society of London.

Hovius, N. (1998). Controls on sediment supply by large rivers. In Shanley, K.W., and McCabe, P.J., eds., Relative Role of Eustasy, Climate, and Tectonism in Continental Rocks: Society for Sedimentary Geology (SEPM) Special Publication 59, 3–16.

Hovius, N. (2000). Macroscale process systems of mountain belt erosion.Geomorphology and global tectonics, 77-105.

Hovius, N., & von Blanckenberg, F. (2007). Constraining the denudational response to faulting.

Howard, A. D. (1980). Thresholds in river regimes. Thresholds in geomorphology, 227-258.

Howard, A. D., & Kerby, G. (1983). Channel changes in badlands. Geological Society of America Bulletin, 94(6), 739-752.

Howard, A. D. (1987). Modelling fluvial systems: rock, gravel and sand bed channels. In Richards K. S., ed. River Channels, Basil Blackwell, Oxford, 69-94.

Howard, A. D. (1994). A detachment-limited model of drainage basin evolution. Water resources research, 30(7), 2261-2285.

Howard, A. D., Dietrich, W. E., & Seidl, M. A. (1994). Modeling fluvial erosion on regional to continental scales. Journal of Geophysical Research: Solid Earth (1978–2012), 99(B7), 13971-13986.

Howard, A. D. (1998). Long profile development of bedrock channels: Interaction of weathering, mass wasting, bed erosion, and sediment transport. Rivers over rock: In: Tinkler, K, & Wohl, EE, eds. Rivers over rock: Fluvial processes in bedrock channel. Washington, D.C., American Geophysical Union, Geophysical Monograph, 297-319.

Hsieh, M. L., & Knuepfer, P. L. (2001). Middle–late Holocene river terraces in the Erhjen River Basin, southwestern Taiwan—Implications of river response to climate change and active tectonic uplift. Geomorphology, 38(3), 337-372.

Huntley, D. J., Hutton, J. T., Prescott, J. R. (1993). The stranded beach±dune sequence of south-east South Australia: a test of thermoluminescence dating, 0±800 ka. Quaternary Science Reviews 12, 1±20

Hurtrez, J. E., Lucazeau, F., Lavé, J., Avouac, J. P., 1999. Investigation of the relationships between basin morphology, tectonic uplift, and denudation from the study of an active fold belt in the Siwalik Hills, central Nepal. Journal of Geophysical Research, vol. 104, no. B6, pp. 12,77

Ingersoll, R. V. & Busby, C.J. (1995). Tectonics of sedimentary basins, In Tectonics of Sedimentary Basins, edited by Busby, C. J. & Ingersoll, R. V. Blackwell Science, Cambridge, 1–51.

Iredale, L. J., Teyssier, C., & Whitney, D. L. (2013). Cenozoic pure-shear collapse of the southern Menderes Massif, Turkey. Geological Society, London, Special Publications, 372(1), 323-342.

Iztan, H. & Yazman M. (1991). Geology and hydrocarbon potential of the Alaşehir (Manisa) area, western Turkey. Proceedings of the International Earth Sciences Congress on Aegean Regions, 327–338.

Jackson, J. A. (1987). Active normal faulting and crustal extension. Geological Society, London, Special Publications, 28(1), 3-17.

Jackson, J. A., & White, N. J. (1989). Normal faulting in the upper continental crust: observations from regions of active extension. Journal of Structural Geology, 11(1), 15-36.

Jackson, M., & Bilham, R. (1994). Constraints on Himalayan deformation inferred from vertical velocity fields in Nepal and Tibet. Journal of Geophysical Research: Solid Earth (1978–2012), 99(B7), 13897-13912.9–12,796.

Jacobs, Z., Duller, G. A., & Wintle, A. G. (2003). Optical dating of dune sand from Blombos Cave, South Africa: II—single grain data. Journal of Human Evolution, 44(5), 613-625.

Jansen, J. D. (2006). Flood magnitude–frequency and lithologic control on bedrock river incision in post-orogenic terrain. Geomorphology, 82(1), 39-57.

Jansen, J. D., Fabel, D., Bishop, P., Xu, S., Schnabel, C., & Codilean, A. T. (2011). Does decreasing paraglacial sediment supply slow knickpoint retreat?. Geology, 39(6), 543-546.

Jenson, S. K., & Domingue, J. O. (1988). Extracting topographic structure from digital elevation data for geographic information system analysis. Photogrammetric engineering and remote sensing, 54(11), 1593-1600.

Johnson, M. O., Mudd, S. M., Pillans, B., Spooner, N. A., Keith Fifield, L., Kirkby, M. J., & Gloor, M. (2014). Quantifying the rate and depth dependence of bioturbation based on optically-stimulated luminescence (OSL) dates and meteoric 10Be. Earth Surface Processes and Landforms, 39(9), 1188-1196.

Jones, M. D., Leng, M. J., Eastwood, W. J., Keen, D. H., & Turney, C. S. (2002). Interpreting stable-isotope records from freshwater snail-shell carbonate: a Holocene case study from Lake Gölhisar, Turkey. The Holocene,12(5), 629-634.

Karlstrom, K. E., Crow, R., Crossey, L. J., Coblentz, D., & Van Wijk, J. W. (2008). Model for tectonically driven incision of the younger than 6 Ma Grand Canyon. Geology, 36(11), 835-838.

Karner, D. B., & Renne, P. R. (1998). 40Ar/39Ar geochronology of Roman volcanic province tephra in the Tiber River valley: Age calibration of middle Pleistocene sea-level changes. Geological Society of America Bulletin, 110(6), 740-747.

Kayseri, M. S., Akgün, F., & Kapan-Yeşilyurt, S. (2008). Palaeoclimate and Palaeoecology of the Chattian in the Milas-Ören Basin: Based on the Palynological and 13C–18O Isotopic Analysis Results. In 62nd Geological Congress of Turkey, MTA, Ankara (pp. 740-741).

Keller, E. A., & Pinter, N. (1996). Active tectonics. Upper Saddle River: Prentice Hall.

Kent E. J. (2011). Towards defining the extent of climatic influence on alluvial fan sedimentation in semi-arid Sonoran and Mojave Deserts, southern California, USA and Baja California, northern Mexico. MS thesis, University of Cincinnati.

Khayyun, Y. S. (2008) The Effects of Changes in Manning's Roughness Coefficients and Eddy Viscosity on a Constrained Flume. Journal of Engineering and Development, 12 (2).

Kidden, P. & Törnqvist, T. E. (1998) Can river terrace flights be used to quantify Quaternary tectonic uplift rates. Journal of Quaternary science, 13(6), 573-575.

Kim, Y. S., & Sanderson, D. J. (2005). The relationship between displacement and length of faults: a review. Earth-Science Reviews, 68(3), 317-334.

Kirby, E., & Whipple, K. (2001). Quantifying differential rock-uplift rates via stream profile analysis. Geology, 29(5), 415-418.

Kirby, E., Whipple, K. X., Tang, W., & Chen, Z. (2003). Distribution of active rock uplift along the eastern margin of the Tibetan Plateau: Inferences from bedrock channel longitudinal profiles. Journal of Geophysical Research, 108(B4), 2217.

Kirby, E., & Whipple, K. X. (2012). Expression of active tectonics in erosional landscapes. Journal of Structural Geology, 44, 54-75.

Kissel, C., & Laj, C. (1988). The Tertiary geodynamical evolution of the Aegean arc: a paleomagnetic reconstruction. Tectonophysics, 146(1), 183-201.

Knighton, A. D. (1998). Fluvial Forms and Processes A New Perspective. Arnold, London.

Knighton, A. D. (1999). Downstream variation in stream power. Geomorphology, 29(3), 293-306.

Koçyigit, A., Yusufoglu, H., & Bozkurt, E. (1999). Discussion on evidence from the Gediz Graben for episodic two-stage extension in western Turkey. Journal of the Geological Society, London, 156, 1240-1242.

Koons, P. O., & Kirby, E. (2007). The Role of Surface Processes in Fault Evolution. Tectonic Faults: Agents of Change on a Dynamic Earth, 95, 205.

Kotthoff, U., Müller, U. C., Pross, J., Schmiedl, G., Lawson, I. T., van de Schootbrugge, B., & Schulz, H. (2008a). Lateglacial and Holocene vegetation dynamics in the Aegean region: an integrated view based on pollen data from marine and terrestrial archives. The Holocene, 18(7), 1019-1032.

Kotthoff, U., Pross, J., Müller, U. C., Peyron, O., Schmiedl, G., Schulz, H., & Bordon, A. (2008b). Climate dynamics in the borderlands of the Aegean Sea during formation of sapropel S1 deduced from a marine pollen record.Quaternary Science Reviews, 27(7), 832-845.

Küçükuysal, C., Türkmenoğlu, A. G., & Kapur, S. (2013). Multi-proxy evidence of Mid-Pleistocene dry climates observed in calcretes in Central Turkey. Turkish Journal of Earth Sciences, 22(3), 469-483.

Kurter, A., & Sungur, K. (1980). Present glaciation in Turkey. World Glacier Inventory, International Association of Hydrological Sciences, 126, 155-160.

Lancaster, S. T., Hayes, S. K., & Grant, G. E. (2001). Modeling sediment and wood storage and dynamics in small mountainous watersheds. Geomorphic processes and riverine habitat, 85-102.

Lavé, J., & Avouac, J. P. (2000a). Active folding of fluvial terraces across the Siwaliks Hills, Himalayas of central Nepal. Journal of Geophysical Research: Solid Earth (1978–2012), 105(B3), 5735-5770.

Lavé, J., & Avouac, J. P. (2001b). Fluvial incision and tectonic uplift across the Himalayas of central Nepal. Journal of Geophysical Research: Solid Earth (1978–2012), 106(B11), 26561-26591.

Le Pichon, X., & Angelier, J. (1979). The Hellenic arc and trench system: a key to the neotectonic evolution of the eastern Mediterranean area. Tectonophysics, 60(1), 1-42.

Leigh, D. S., Srivastava, P., & Brook, G. A. (2004). Late Pleistocene braided rivers of the Atlantic coastal plain, USA. Quaternary Science Reviews, 23(1), 65-84.

Leng, M. J., Jones, M. D., Frogley, M. R., Eastwood, W. J., Kendrick, C. P., & Roberts, C. N. (2010). Detrital carbonate influences on bulk oxygen and carbon isotope composition of lacustrine sediments from the Mediterranean. Global and Planetary Change, 71(3), 175-182.

Leopold, L. B., & Maddock, T. (1953). The hydraulic geometry of stream channels and some physiographic implications. U. S. Geological Survey Professional Paper 252, 1–57.

Limerinos, J.T. (1970) Determination of the Manning coefficient from measured bed roughness in natural channels: U.S. Geological Survey Water-Supply Paper 1898 (B) 47.

Lips, A. L., Cassard, D., Sözbilir, H., Yilmaz, H., & Wijbrans, J. R. (2001). Multistage exhumation of the Menderes massif, western Anatolia (Turkey). International Journal of Earth Sciences, 89(4), 781-792.

Litchfield, N., & Berryman, K. (2006). Relations between postglacial fluvial incision rates and uplift rates in the North Island, New Zealand. Journal of Geophysical Research: Earth Surface (2003–2012), 111(F2).

Litchfield, N., Van Dissen, R., Heron, D., & Rhoades, D. (2006). Constraints on the timing of the three most recent surface rupture events and recurrence interval for the Ohariu Fault: trenching results from MacKays Crossing, Wellington, New Zealand.

Litchfield, N., Ellis, S., Berryman, K., & Nicol, A. (2007). Insights into subduction-related uplift along the Hikurangi Margin, New Zealand, using numerical modeling. Journal of Geophysical Research: Earth Surface (2003–2012), 112(F2).

Livermore, R. A., & Smith, A. G. (1985). Some boundary conditions for the evolution of the Mediterranean region. In Geological evolution of the Mediterranean Basin (pp. 83-98). Springer New York.

Loget, N., Davy, P., & Van Den Driessche, J. (2006). Mesoscale fluvial erosion parameters deduced from modeling the Mediterranean sea level drop during the Messinian (late Miocene). Journal of Geophysical Research: Earth Surface (2003–2012), 111(F3).

Lowe, M., Personius, S., Bradley, L. A., Forman, S. L., Klauk, R., & Garr, J. (2006). Holocene earthquake history of the northern Weber segment of the Wasatch fault zone, Utah. Utah Geological Survey.

Macklin, M. G., Passmore, D.G., (1995). Pleistocene environmental change in the Guadalope basin, northeast Spain: fluvial and archaeological records. In: Lewin, J., Macklin, M.G., & Woodward, J.C. (Eds.), Mediterranean Quaternary River Environments. Balkema, Rotterdam, 103–113.

Macklin, M. G., Fuller, I. C., Lewin, J., Maas, G. S., Passmore, D. G., Rose, J., Woodward, J. C., Black, S., Hamlin, R. H. B., & Rowan, J. S. (2002). Correlation of fluvial sequences in the Mediterranean basin over the last 200ka and their relationship to climate change. Quaternary Science Reviews, 21(14), 1633-1641.

Maddy, D. (1997). Uplift-driven valley incision and river terrace formation in southern England. Journal of Quaternary Science, 12(6), 539-545.

Maddy, D., Lewis, S. G., Scaife, R. G., Bowen, D. Q., Coope, G. R., Green, C. P., Hardaker, R., Keen, D.H., reEES-Jones, J., Parfitt, S. & Scott, K. (1998). The Upper Pleistocene deposits at Cassington, near Oxford, England. Journal of Quaternary Science, 13(3), 205-231.

Maddy, D., Bridgland, D. R., & Green, C. P. (2000). Crustal uplift in southern England: evidence from the river terrace records. Geomorphology, 33(3), 167-181.

Maddy, D., Bridgland, D., & Westaway, R. (2001). Uplift-driven valley incision and climate-controlled river terrace development in the Thames Valley, UK.Quaternary International, 79(1), 23-36.

Maddy, D., Demir, T., Bridgland, D. R., Veldkamp, A., Stemerdink, C., van der Schriek, T., & Westaway, R. (2005). An obliquity-controlled Early Pleistocene river terrace record from Western Turkey? Quaternary Research, 63(3), 339-346.

Maddy, D., Demir, T., Bridgland, D. R., Veldkamp, A., Stemerdink, C., van der Schriek, T., & Westaway, R. (2008). The Early Pleistocene development of the Gediz River, Western Turkey: An uplift-driven, climate-controlled system? Quaternary International, 189(1), 115-128.

Mahan, S., Sohn, M., Knott, J., and Bowman, D., (2006). Slip Rates, Recurrence Intervals and Earthquake Event Magnitudes for the southern Black Mountains Fault Zone, southern Death Valley, California. Sesmological Research Letters, 77, 245.

Mallinson, D., 2008. A Brief Description of Optically Stimulated Luminescence Dating

Manning, R. (1891). On the flow of water in open channels and pipes. Transactions of the Institution of Civil Engineers of Ireland, 20, 161-207.

Mark, R. K. (1977). Application of linear statistical models of earthquake magnitude versus fault length in estimating maximum expectable earthquakes. Geology, 5(8), 464-466.

Martins, A. A., Cunha, P. P., Huot, S., Murray, A. S., & Buylaert, J. P. (2009). Geomorphological correlation of the tectonically displaced Tejo River terraces (Gavião–Chamusca area, central Portugal) supported by luminescence dating.Quaternary International, 199(1), 75-91.

Mason, D. P., Little, T. A., & Van Dissen, R. J. (2006). Rates of active faulting during late Quaternary fluvial terrace formation at Saxton River, Awatere fault, New Zealand. Geological Society of America Bulletin, 118(11-12), 1431-1446.

Mathew, G., Singhvi, A. K., & Karanth, R. V. (2006). Luminescence chronometry and geomorphic evidence of active fold growth along the Kachchh Mainland Fault (KMF), Kachchh, India: seismotectonic implications.Tectonophysics, 422(1), 71-87.

Mattson, A. (2004). Tomographic imaging of late Quaternary faulting, Oquirrh Mountains, Utah. Journal of Geophysical Research: Solid Earth (1978–2012), 109(B11).

Mayya, Y. S., Morthekai, P., Murari, M. K., & Singhvi, A. K. (2006). Towards quantifying beta microdosimetric effects in single-grain quartz dose distribution.Radiation Measurements, 41(7), 1032-1039.

McCalpin, J., (1985). Quaternary fault history and earthquake potential of the Hansel Valley area, north central Utah: Final Technical Report, U.S. Geological Survey.

McCalpin, J. P. (2009). Paleoseismology. International Geophysics, 95, 171-269.

McCalpin, J. P., Forman, S. L., & Lowe, M. (1994). Reevaluation of Holocene faulting at the Kaysville site, Weber segment of the Wasatch fault zone, Utah.Tectonics, 13(1), 1-16.

McGill, S., Weldon, R., & Owen, L. (2010, May). Latest Pleistocene slip rates along the San Bernardino strand of the San Andreas fault. In Geological Society of America Abstracts with Programs (Vol. 42, No. 4, p. 69).

McKenzie, D. (1978). Some remarks on the development of sedimentary basins. Earth and planetary science letters, 40(1), 25-32.

McLeod, A. E., & Underhill, J. R. (2000). The propagation and linkage of normal faults: insights from the Strathspey–Brent–Statfjord fault array, northern North Sea. Basin Research, 12(3-4), 263-284.

Mejdahl, V. (1979). Thermoluminescence dating: beta-dose attenuation in quartz grains. Archaeometry. 21, 61-72.

Merritts, D. & Vincent, K. R. (1989). Geomorphic response of coastal streams to low, intermediate, and high rates of uplift, Medocino triple junction region, northern California. Geological Society of America Bulletin, 101(11), 1373-1388.

Merritts, D., & Bull, W. B. (1989). Interpreting Quaternary uplift rates at the Mendocino triple junction, northern California, from uplifted marine terraces. Geology, 17(11), 1020-1024.

Meshkova, L. V., Carling, P. A., & Buffin-Bélanger, T. (2012). Nomenclature, Complexity, Semi-Alluvial Channels and Sediment-Flux-Driven Bedrock Erosion. Gravel-Bed Rivers: Processes, Tools, Environments, 424-431.

Meulenkamp, J. E., Wortel, M. J. R., Van Wamel, W. A., Spakman, W., & Hoogerduyn Strating, E. (1988). On the Hellenic subduction zone and the geodynamic evolution of Crete since the late Middle Miocene. Tectonophysics, 146(1), 203-215.

Meulenkamp, J. E., Van der Zwaan, G. J., & Van Wamel, W. A. (1994). On Late Miocene to recent vertical motions in the Cretan segment of the Hellenic arc. Tectonophysics, 234(1), 53-72.

Michetti, A. M., Brunamonte, F., Serva, L., & Vittori, E. (1996). Trench investigations of the 1915 Fucino earthquake fault scarps (Abruzzo, Central Italy): geological evidence of large historical events. Journal of Geophysical Research: Solid Earth (1978–2012), 101(B3), 5921-5936.

Miller, J. R. (1991). The influence of bedrock geology on knickpoint development and channel-bed degradation along downcutting streams in south-central Indiana. The Journal of Geology, 591-605.

Miller, R. D., Steeples, D. W., & Myers, P. B. (1990). Shallow seismic reflection survey across the Meers fault, Oklahoma. Geological Society of America Bulletin, 102(1), 18-25.

Mirabella, F., Ciaccio, M. G., Barchi, M. R., & Merlini, S. (2004). The Gubbio normal fault (Central Italy): geometry, displacement distribution and tectonic evolution. Journal of Structural Geology, 26(12), 2233-2249.

Mitchell, W. A. (1976). Reconstruction after disaster: the Gediz earthquake of 1970. Geographical Review, 296-313.

Monaco, C., Tapponnier, P., Tortorici, L., & Gillot, P. Y. (1997). Late Quaternary slip rates on the Acireale-Piedimonte normal faults and tectonic origin of Mt. Etna (Sicily). Earth and Planetary Science Letters, 147(1), 125-139.

Montgomery, D. R., & Foufoula-Georgiou, E. (1993). Channel network source representation using digital elevation models. Water Resources Research,29(12), 3925-3934.

Montgomery, D. R., & Gran, K. B. (2001). Downstream variations in the width of bedrock channels. Water Resources Research, 37, no. 6, pp. 1841-1846.

Morewood, N. C., & Roberts, G. P. (1997). Geometry, kinematics and rates of deformation in a normal fault segment boundary, central Greece. Geophysical Research Letters, 24(23), 3081-3084.

Morthekai, P., & Reddy, D. V. (2012). Applications of TL and OSL in terrestrial and extra-terrestrial materials: recent developments and challenges.International Journal of Luminescence and Applications, 2(3), 96-108.

Mudd, S. M., Attal, M., Milodowski, D. T., Grieve, S. W., & Valters, D. A. (2014). A statistical framework to quantify spatial variation in channel gradients using the integral method of channel profile analysis. Journal of Geophysical Research: Earth Surface, 119(2), 138-152.

Mueller, S., Kahle, H. G., & Barka, A. (1997). Plate tectonic situation in the Anatolian-Aegean region. Active Tectonics of Northwestern Anatolia-the Marmara Poly-Project, 13-28.

Mukul, M., Jaiswal, M., & Singhvi, A. K. (2007). Timing of recent out-of-sequence active deformation in the frontal Himalayan wedge: Insights from the Darjiling sub-Himalaya, India. Geology, 35(11), 999-1002.

Murray, A. S., & Wintle, A. G. (2000). Luminescence dating of quartz using an improved single-aliquot regenerative-dose protocol. Radiation measurements,32(1), 57-73.

NASA https://wist.echo.nasa.gov/api/

Nelson, A. R., & Personius, S. F. (1993). Surficial geologic map of the Weber segment. Wasatch fault zone, Weber and Davis Counties, Utah: US Geological Survey Miscellaneous Investigations Series Map I-2199, 22.

Nicol, A., Gillespie, P. A., Childs, C., & Walsh, J. J. (2002). Relay zones between mesoscopic thrust faults in layered sedimentary sequences. Journal of Structural Geology, 24(4), 709-727.

Nicol, A., Walsh, J. J., Watterson, J., & Underhill, J. R. (1997). Displacement rates of normal faults. Nature, 390(6656), 157-159.

Nicol, K., & Küçükuysal, C. (2013). Emerging multi-proxy records of Late Quaternary Palaeoclimate dynamics in Turkey and the surrounding region.Turkish Journal of Earth Sciences, 22(1), 126-142.

Niemi, T. M., & Hall, N. T. (1992). Late Holocene slip rate and recurrence of great earthquakes on the San Andreas fault in northern California. Geology,20(3), 195-198.

Nissen, E., Walker, R., Molor, E., Fattahi, M., & Bayasgalan, A. (2009). Late Quaternary rates of uplift and shortening at Baatar Hyarhan (Mongolian Altai) with optically stimulated luminescence. Geophysical Journal International, 177(1), 259-278.

Norton, K. P., von Blanckenburg, F., Schlunegger, F., Schwab, M., & Kubik, P. W. (2008). Cosmogenic nuclide-based investigation of spatial erosion and hillslope channel coupling in the transient foreland of the Swiss Alps.Geomorphology, 95(3), 474-486.

Okay, A. I. (2008). Geology of Turkey: a synopsis. Anschnitt, 21, 19-42.

Okay, A. I., Tansel, I., & Tueysuez, O. K. A. N. (2001). Obduction, subduction and collision as reflected in the Upper Cretaceous–Lower Eocene sedimentary record of western Turkey. Geological Magazine, 138(02), 117-142.

Olig, S. S., McDonald, G., Black, B., Duross, C., & Lund, W. R. (2005). Evidence from the Mapleton Megatrench for more frequent Holocene earthquakes on the Provo segment of the Wasatch fault zone, Utah. In 2005 Salt Lake City Annual Meeting.

Olley, J., Caitcheon, G., & Murray, A. (1998). The distribution of apparent dose as determined by optically stimulated luminescence in small aliquots of fluvial quartz: implications for dating young sediments. Quaternary Science Reviews, 17(11), 1033-1040.

Oner, Z. (2012). Supradetachment Basin Tectonics and The Exhumation History of The Menderes Core Complex, Western Anatolia-Turkey (Doctoral dissertation, Miami University).

Oner, Z., & Dilek, Y. (2011). Supradetachment basin evolution during continental extension: The Aegean province of western Anatolia, Turkey. Geological Society of America Bulletin, 123(11-12), 2115-2141.

Ouimet, W. (2007). Dissecting the Eastern Margin of the Tibetan Plateau: A Study of Landslides, Erosion and River Incision in a Transient Landscape Ph.D. thesis, Massachusetts Institute of Technology.

Ouimet, W. B., Whipple, K.X., & Granger, D.E., (2009). Beyond threshold hillslopes: Channel adjustment to base-level fall in tectonically active mountain ranges. Geology, 37(7), 579-582.

Özkaymak, Ç., Sözbılır, H., Uzel, B., & Akyüz, H. S. (2011). Geological and Palaeoseismological Evidence for Late Pleistocene− Holocene Activity on the Manisa Fault Zone, Western Anatolia. Turkish Journal of Earth Sciences, 20(4), 449-474.

Pantosti, D., Collier, R., D'Addezio, G., Masana, E., & Sakellariou, D. (1996). Direct geological evidence for prior earthquakes on the 1981 Corinth fault (central Greece). Geophysical Research Letters, 23(25), 3795-3798.

Papanikolaou, I. D., & Roberts, G. P. (2007). Geometry, kinematics and deformation rates along the active normal fault system in the southern Apennines: Implications for fault growth. Journal of Structural Geology, 29(1), 166-188.

Papanikolaou, I. D., Foumelis, M., Parcharidis, I., Lekkas, E. L., & Fountoulis, I. G. (2010). Deformation pattern of the 6 and 7 April 2009, MW= 6.3 and MW= 5.6 earthquakes in L'Aquila (Central Italy) revealed by ground and space based observations. Natural Hazards and Earth System Sciences, 10, 73-87.

Papoulia, J. E., & Gülkan, P. (2001). Seismic hazard parameter estimation for north-western Turkey based on combination of disparate catalogues. Bolletino di Geofisica Teorica ed Applicata, 42(1-2), 75-88.

Paton, S. (1992). Active normal faulting, drainage patterns and sedimentation in southwestern Turkey. Journal of the Geological Society, 149(6), 1031-1044.

Pazzaglia, F. J., & Brandon, M. T. (2001). A fluvial record of long-term steady-state uplift and erosion across the Cascadia forearc high, western Washington State. American Journal of Science, 301(4-5), 385-431.

Pazzaglia, Frank J., (2013). Fluvial Terraces, in Schroder, F., ed., Treatise of Geomorphology. New York, NY: Elsevier.

Peacock, D. C. P. (2002). Propagation, interaction and linkage in normal fault systems. Earth-Science Reviews, 58(1), 121-142.

Peacock, D. C. P., & Sanderson, D. J. (1994). Geometry and development of relay ramps in normal fault systems. AAPG bulletin, 78(2), 147-165.

Pederson, J. L., Anders, M. D., Rittenhour, T. M., Sharp, W. D., Gosse, J. C., & Karlstrom, K. E. (2006). Using fill terraces to understand incision rates and evolution of the Colorado River in eastern Grand Canyon, Arizona. Journal of Geophysical Research: Earth Surface (2003–2012), 111(F2).

Pederson, J. L., & Tressler, C. (2012). Colorado River long-profile metrics, knickzones and their meaning. Earth and Planetary Science Letters, 345, 171-179.

Pelton, J. R., Meissner, C. W., Waag, C. J., & Wood, S. H. (1985). Shallow seismic refraction studies across the Willow Creek fault rupture zone and the Chilly Buttes sand boils. In Workshop XXVIII on the Borah Peak, Idaho, Earthquake,, A, US Geol. Surv. Open File Rep,85-290.

Perillo, G. M. (Ed.). (1995). Geomorphology and sedimentology of estuaries (Vol. 53). Elsevier.

Personius, S. F. (1995). Late Quaternary stream incision and uplift in the forearc of the Cascadia subduction zone, western Oregon. Journal of Geophysical Research: Solid Earth (1978–2012), 100(B10), 20193-20210.

Peyron, O., Goring, S., Dormoy, I., Kotthoff, U., Pross, J., De Beaulieu, J. L., Drescher-Schneider, R., Vannière, B., & Magny, M. (2011). Holocene seasonality changes in the central Mediterranean region reconstructed from the pollen sequences of Lake Accesa (Italy) and Tenaghi Philippon (Greece). The Holocene, 21(1), 131-146.

Piccardi, L., Gaudemer, Y., Tapponnier, P., & Boccaletti, M. (1999). Active oblique extension in the central Apennines (Italy): evidence from the Fucino region. Geophysical Journal International, 139(2), 499-530.

Preece, R. R., Scourse, J. D., Houghton, S., Knudsen, K. I. and Penney, D. N. (1990). The Pleistocene sea-level and neotectonic history of the eastern Solent, southern England. Philosophical Transactions of the Royal Society of London, 328, 425–477

Prescott, J. R., & Hutton, J. T., (1994). Cosmic ray contributions to dose rates for luminescence and ESR dating: large depths and long-term time variations. Radiation Measurements. 23, 497–500.

Purvis, M. & Robertson, A. (2005). Sedimentation of the Neogene–Recent Alaşehir (Gediz) continental graben system used to test alternative tectonic models for western (Aegean) Turkey. Sedimentary Geology, 173, 373-408.

Reneau, S. L. (2000). Stream incision and terrace development in Frijoles Canyon, Bandelier National Monument, New Mexico, and the influence of lithology and climate. Geomorphology, 32(1), 171-193.

Richards, D. A., & Smart, P. L. (1991). Potassium–argon and argon–argon dating. Quaternary Dating Methods–A User's Guide. Technical Guide, 4, 37-44.

Richardson-Bunbury, J. M. (1996). The Kula volcanic field, western Turkey: the development of a Holocene alkali basalt province and the adjacent normal-faulting graben. Geological Magazine, 133(03), 275-283.

Rittenour, T. M. (2008). Luminescence dating of fluvial deposits: applications to geomorphic, palaeoseismic and archaeological research. Boreas, 37(4), 613-635.

Rittenour, T. M., Goble, R. J., & Blum, M. D. (2005). Development of an OSL chronology for Late Pleistocene channel belts in the lower Mississippi valley, USA. Quaternary Science Reviews, 24(23), 2539-2554.

Rittenour, T. M., Blum, M. D., & Goble, R. J. (2007). Fluvial evolution of the lower Mississippi River valley during the last 100 ky glacial cycle: Response to glaciation and sea-level change. Geological Society of America Bulletin, 119(5-6), 586-608.

Ritter, J. B., Miller, J. R., and Husek-Wulforst, J., 2000, Environmental controls on the evolution of alluvial fans in Buena Vista Valley, north central Nevada, during late Quaternary time: Geomorphology, 36, 63-87.

Ritz, J. F., Brown, E. T., Bourles, D. L., Philip, H., Schlupp, A., Raisbeck, G. M. Yiou, F. & Enkhtuvshin, B. (1995). Slip rates along active faults estimated with cosmic-ray–exposure dates: Application to the Bogd fault, Gobi-Altaï, Mongolia. Geology, 23(11), 1019-1022.

Roberts, G. P., Cowie, P., Papanikolaou, I., & Michetti, A. M. (2004). Fault scaling relationships, deformation rates and seismic hazards: an example from the Lazio–Abruzzo Apennines, central Italy. Journal of Structural Geology, 26(2), 377-398.

Roberts, G. P., & Michetti, A. M. (2004). Spatial and temporal variations in growth rates along active normal fault systems: an example from The Lazio–Abruzzo Apennines, central Italy. Journal of Structural Geology, 26(2), 339-376.

Roberts, N., Black, S., Boyer, P., Eastwood, W. J., Griffiths, H. I., Lamb, H. F., Leng, M. J., Pariah, R., Reed, J. M., Twigg, D., & Yiğitbaşioğlu, H. (1999). Chronology and stratigraphy of Late Quaternary sediments in the Konya Basin, Turkey: results from the KOPAL Project.Quaternary Science Reviews, 18(4), 611-630.

Roberts, N., Eastwood, W. J., Kuzucuoğlu, C., Fiorentino, G., & Caracuta, V. (2011). Climatic, vegetation and cultural change in the eastern Mediterranean during the mid-Holocene environmental transition. The Holocene, 21(1), 147-162.

Robertson, A. H., & Mountrakis, D. (2006). Tectonic development of the Eastern Mediterranean region: an introduction. Geological Society, London, Special Publications, 260(1), 1-9.

Rockwell, T. K., Keller, E. A., Clark, M. N., & Johnson, D. L. (1984). Chronology and rates of faulting of Ventura River terraces, California. Geological Society of America Bulletin, 95(12), 1466-1474.Bogd fault, Gobi-Altaï, Mongolia.Geology, 23(11), 1019-1022.

Rockwell, T., Loughman, C., & Merifield, P. (1990). Late Quaternary rate of slip along the San Jacinto fault zone near Anza, southern California. Journal of Geophysical Research: Solid Earth (1978–2012), 95(B6), 8593-8605.

Rodnight, H., Duller, G. A., Wintle, A. G., & Tooth, S. (2006). Assessing the reproducibility and accuracy of optical dating of fluvial deposits. Quaternary Geochronology, 1(2), 109-120.

Rodrigues, K. (2013). Evaluating OSL equivalent dose distributions in a sandy ant disturbed environment: Apalachicola Forest, Florida.

Rose, J., Whiteman, C. A., Allen, P., & Kemp, R. A. (1999). The Kesgrave sands and gravels:‘pre-glacial’Quaternary deposits of the River Thames in East Anglia and the Thames Valley. Proceedings of the Geologists' Association, 110(2), 93-116.

Şan O. (1998) Ahmetli (Manisa) guneyinde Menderes masifi ve Tersiyer ortu kayalarinin jeolojisi [Geology of the basement and Tertiary cover rocks of Menderes massif in the south of Ahmetli (Manisa)] MSc thesis, Ankara University.

Sancho, C., Peiia, J.L., Lems, C., McDonald, E., Rhodes, E., 2003. Preliminary dating of glacial and fluvial deposits in the Cinca River valley (NE Spain): chronological evidences for the Glacial Maximum in the Pyrenees? In: Ruiz-Zapata, M.B., Dorado, M., Valdeolmillos, A., Gil Garcia, M.J., Bardaji, T., de Bustamante, Martinez Mendizabal, (Eds.), Quaternary climatic changes and environmental crises in the Mediterranean region, Univ. Alcala/INQUA, pp. 169-173.

Sancho, C., Peiia, J.L., Lems, c., McDonald, E., Rhodes, E., 2004. Registros fluviales y glaciares cuaternarios en las cuencas de los rios Cinca y Gallego (Pirineos y depresion del Ebro). In: Colombo, F., Iesa, C.L., Melendez, G., Pocovi, A., Sancho, c., Soria, A.R. (Eds.), VI Congreso Geologico de Espaiia. Geo-Guias 1. Itinerarios Geologicos por Aragon, pp. 181-205.

Santisteban, J. I., & Schulte, L. (2007). Fluvial networks of the Iberian Peninsula: a chronological framework. Quaternary Science Reviews, 26(22), 2738-2757.

Sarica, N. (2000). The Plio-Pleistocene age of Bueyuek Menderes and Gediz grabens and their tectonic significance on N-S extensional tectonics in West Anatolia: mammalian evidence from the continental deposits. Geological Journal, 35, 1-24.

Sarıkaya, M. A , (2009). Late quaternary glaciation and paleoclimate of Turkey inferred from cosmogenic 36Cl dating of moraines and glacier modelling. PhD thesis, University of Arizona, Tuscon, AZ. USA.

Sarıkaya, M. A., Zreda, M., Çiner, A., & Zweck, C. (2008). Cold and wet Last Glacial Maximum on Mount Sandıras, SW Turkey, inferred from cosmogenic dating and glacier modeling. Quaternary Science Reviews, 27(7), 769-780.

Sbaffi, L., Wezel, F. C., Curzi, G., & Zoppi, U. (2004). Millennial-to centennial-scale palaeoclimatic variations during Termination I and the Holocene in the central Mediterranean Sea. Global and Planetary Change, 40(1), 201-217.

Schmiedl, G., Kuhnt, T., Ehrmann, W., Emeis, K. C., Hamann, Y., Kotthoff, U., Dulski, P., & Pross, J. (2010). Climatic forcing of eastern Mediterranean deep-water formation and benthic ecosystems during the past 22 000 years. Quaternary Science Reviews, 29(23), 3006-3020.

Schokker, J., Cleveringa, P., Murray, A. S., Wallinga, J., & Westerhoff, W. E. (2005). An OSL dated middle and late quaternary sedimentary record in the Roer Valley Graben (southeastern Netherlands). Quaternary Science Reviews,24(20), 2243-2264.

Schorghofer, N., & Rothman, D. H. (2002). A causal relations between topographic slope and drainage area. Geophysical Research Letters, 29(13), 11-1.

Schulte, L. (2002). Climatic and human influence on river systems and glacier fluctuations in southeast Spain since the Last Glacial Maximum. Quaternary International, 93, 85-100.

Schulte, L., Julià, R., Burjachs, F., & Hilgers, A. (2008). Middle Pleistocene to Holocene geochronology of the River Aguas terrace sequence (Iberian Peninsula): fluvial response to Mediterranean environmental change.*Geomorphology*, *98*(1), 13-33.

Schumm, S. A. (1977). The fluvial system (Vol. 338). New York: Wiley.

Schumm, S. A., Dumont J. F., & Holbrook J. M. (2002). Active Tectonics and Alluvial Rivers. Cambridge University Press, Cambridge.

Schwartz, D. P., & Coppersmith, K. J. (1984). Fault behavior and characteristic earthquakes: Examples from the Wasatch and San Andreas fault zones.Journal of Geophysical Research: Solid Earth (1978–2012), 89(B7), 5681-5698.

Scumm, S. A. (1993) River response to base level change: implications for sequance stratigraphy. Journal of Geology, 101, 279-294.

Sdrolias, M., & Müller, R. D. (2006). Controls on back-arc basin formation. Geochemistry, Geophysics, Geosystems, 7(4).

Sébrier, M., Ghafiri, A., & Bles, J. L. (1997). Paleoseismicity in France: fault trench studies in a region of moderate seismicity. Journal of geodynamics, 24(1), 207-217.

Seeber, L., & Gornitz, V. (1983). River profiles along the Himalayan arc as indicators of active tectonics. Tectonophysics, 92(4), 335-367.

Seidl, M. A., & Dietrich, W. E. (1992). The problem of channel erosion into bedrock. Catena Supplement, vol. 23. pp. 101-124.

Seidl, M. A., Dietrich W. E., & Kirchner J. W. (1994). Erosion by rivers into bedrock: An analysis of Hawaiian channels. Journal of Geology.

Selby, M. J. (1980). A rock mass strength classification for geomorphic purposes: with tests from Antarctica and New Zealand. Zeitschrift für Geomorphologie, 24(1), 31-51.

Sen, S., & Seyitoğlu, G. (2009). Magnetostratigraphy of early–middle Miocene deposits from east–west trending Alaşehir and Büyük Menderes grabens in western Turkey, and its tectonic implications. Geological Society, London, Special Publications, 311(1), 321-342.

Şenel, M., & Aydal, N. (2002). Geological map of Turkey, Izmir no.7, 1:500,000. MTA, Ankara.

Sengör, A. M. C., Satir, M., & Akkök, R. (1984). Timing of tectonic events in the Menderes Massif, western Turkey: Implications for tectonic evolution and evidence for Pan-African basement in Turkey. Tectonics, 3(7), 693-707.

Sengör, A. M., & Yilmaz, Y. (1981). Tethyan evolution of Turkey: a plate tectonic approach. Tectonophysics, 75(3), 181-241.

Serpelloni, E., Bürgmann, R., Anzidei, M., Baldi, P., Mastrolembo Ventura, B., & Boschi, E. (2010). Strain accumulation across the Messina Straits and kinematics of Sicily and Calabria from GPS data and dislocation modeling. Earth and Planetary Science Letters, 298(3), 347-360.

Seyítoğlu, G., Scott, B. C., & Rundle, C. C. (1992). Timing of Cenozoic extensional tectonics in west Turkey. Journal of the Geological Society, 149(4), 533-538.

Seyítoğlu, G., & Scott, B. C. (1994). Late Cenozoic basin development in west Turkey: Gördes basin tectonics and sedimentation. Geological Magazine, 131(05), 631-637.

Seyitoğlu, G., & Scott, B. C. (1996). Age of the Alaşehir graben (west Turkey) and its tectonic implications. Geological Journal, 31(1), 1-11.

Seyitoğlu, G. & Benda, L. (1998). Neogene palynologicaland isotopic age data from Selendi and Usak-Gure basins, western Turkey: A contribution to the upper limit of Eskihisar sporomorph association. Newsletters on Stratigraphy, 36, 105–115.

Seyitoglu, G., Tekeli, O., Çemen, I., Sen, S., & Isik, V. (2002). The role of the flexural rotation/rolling hinge model in the tectonic evolution of the Alasehir graben, western Turkey. Geological Magazine, 139(01), 15-26.

Seyrek, A., Demir, T., Pringle, M., Yurtmen, S., Westaway, R., Bridgland, D., Beck, A., & Rowbotham, G. (2008). Late Cenozoic uplift of the Amanos Mountains and incision of the Middle Ceyhan river gorge, southern Turkey; Ar–Ar dating of the Düziçi basalt. Geomorphology, 97(3), 321-355.

Sharp, W. D., Ludwig, K. R., Chadwick, O. A., Amundson, R., & Glaser, L. L. (2003). Dating fluvial terraces by230Th/U on pedogenic carbonate, Wind River Basin, Wyoming. Quaternary Research, 59(2), 139-150

Sheley, D., Crosby, T., Zhou, M., Giacoma, J., Yu, J., He, R., & Schuster, G. T. (2003). 2-D seismic trenching of colluvial wedges and faults. Tectonophysics, 368(1), 51-69.

Shyu, J. B. H., Sieh, K., Avouac, J. P., Chen, W. S., & Chen, Y. G. (2006). Millennial slip rate of the Longitudinal Valley fault from river terraces: Implications for convergence across the active suture of eastern Taiwan. Journal of Geophysical Research: Solid Earth (1978–2012), 111(B8).

Sieh, K. E. (1981). A review of geological evidence for recurrence times of large earthquakes. American Geophysical Union, 181-207.

Sierralta, M., Kele, S., Melcher, F., Hambach, U., Reinders, J., van Geldern, R., & Frechen, M. (2010). Uranium-series dating of travertine from Süttő: implications for reconstruction of environmental change in Hungary. Quaternary International, 222(1), 178-193.

Simpson, G., & Schlunegger, F. (2003). Topographic evolution and morphology of surfaces evolving in response to coupled fluvial and hillslope sediment transport. Journal of Geophysical Research: Solid Earth (1978–2012), 108(B6).

Sklar, L., & Dietrich, W. E. (1998). River longitudinal profiles and bedrock incision models: Stream power and the influence of sediment supply, In Tinkler, K. J., & Wohl, E. E. eds., (1998). Rivers over rock: Fluvial processes in bedrock channels: Washington, D.C., American Geophysical Union, Geophysical Monograph, 107, 237–260.

Sklar, L. S., & Dietrich, W. E. (2001). Sediment and rock strength controls on river incision into bedrock. Geology, 29(12), 1087-1090.

Sklar, L. S., & Dietrich, W. E. (2004). A mechanistic model for river incision into bedrock by saltating bed load. Water Resources Research, 40(6).

Sklar, L. S., & Dietrich, W. E. (2006). The role of sediment in controlling steady-state bedrock channel slope: Implications of the saltation–abrasion incision model. Geomorphology, 82(1), 58-83.

Snyder, N. P., Whipple, K. X., Tucker, G. E., Merritts, D. J. (2000). Landscape response to tectonic forcing: Digital elevation model analysis of stream profiles in the Mendocino triple junction region, northern California. Geological Society of America Bulletin, 112(8), 1250-1263.

Snyder, N. P., Whipple, K. X., Tucker, G. E., Merritts, D. J. (2003). Channel response to tectonic forcing: field analysis of stream morphology and hydrology in the Mendocino triple junction region, northern California. Geomorphology, 53(1), 97-127.

Snyder, N. P., Castele, M. R., & Wright, J. R. (2009). Bedload entrainment in low-gradient paraglacial coastal rivers of Maine, USA: Implications for habitat restoration. Geomorphology, 103(3), 430-446.

Sohn, M. F., Mahan, S. A., Knott, J. R., & Bowman, D. D. (2007). Luminescence ages for alluvial-fan deposits in Southern Death Valley: Implications for climate-driven sedimentation along a tectonically active mountain front. Quaternary International, 166(1), 49-60.

Solheim, A., Russwurm, L., Elverhøi, A., & Berg, M. N. (1990). Glacial geomorphic features in the northern Barents Sea: direct evidence for grounded ice and implications for the pattern of deglaciation and late glacial sedimentation. Geological Society, London, Special Publications, 53(1), 253-268.

Sólyom, P. B., & Tucker, G. E. (2004). Effect of limited storm duration on landscape evolution, drainage basin geometry, and hydrograph shapes. Journal of Geophysical Research: Earth Surface (2003–2012), 109(F3).

Sowers, J. M. (2000). Rock varnish chronometry. Quaternary Geochronology: Methods and Applications, 241-260.

Srivastava, P., & Misra, D. K. (2008). Morpho-sedimentary records of active tectonics at the Kameng river exit, NE Himalaya. Geomorphology, 96(1), 187-198.

Stanley, D. J., & Hait, A. K. (2000). Deltas, radiocarbon dating, and measurements of sediment storage and subsidence. Geology, 28(4), 295-298.

Stein, R. S., & Barrientos, S. E. (1985). Planar high-angle faulting in the basin and range: Geodetic analysis of the 1983 Borah Peak, Idaho, earthquake. Journal of Geophysical Research: Solid Earth (1978–2012), 90(B13), 11355-11366.

Stein, R. S., King, G. C. P., and Rundle, J. B. (1988). The growth of geological structures by repeated earthquakes. Field examples of continental dip slip faults, J. Geophysical Research, 95, 13319–1333.

Stock, J. D., & Montgomery, D. R. (1999). Geologic constraints on bedrock river incision using the stream power law. Journal of Geophysical Research, 104, 4983-4994.

Stokes, M., Cunha, P. P., & Martins, A. A. (2012). Techniques for analysing Late Cenozoic river terrace sequences. Geomorphology, 165.

Stokes, S. (1994). The timing of OSL sensitivity changes in a natural quartz.Radiation Measurements, 23(2), 601-605.

Stokes, S. (1999). Luminescence dating applications in geomorphological research. Geomorphology, 29(1), 153-171.

Strahler, A. N. (1952). Hypsometric (area-altitude) analysis of erosional topography. Geological Society of America Bulletin, 63(11), 1117-1142.

Strahler, A. N. (1957). Quantitative analysis of watershed geomorphology. Civil Engeneering, 101, 1258-1262.

Sutherland, R., Berryman, K., & Norris, R. (2006). Quaternary slip rate and geomorphology of the Alpine fault: Implications for kinematics and seismic hazard in southwest New Zealand. Geological Society of America Bulletin,118(3-4), 464-474.

Swan, F. H., Schwartz, D. P., & Cluff, L. S. (1980). Recurrence of moderate to large magnitude earthquakes produced by surface faulting on the Wasatch fault zone, Utah. Bulletin of the Seismological Society of America, 70(5), 1431-1462.

Syvitski, J. P., & Shaw, J. (1995). Sedimentology and geomorphology of fjords. In Perillo, G. M. (Ed.). (1995). Geomorphology and sedimentology of estuaries 53, 113-178.

Tahir, E. (1996). Geology and the Tectonics of the Gediz Graben. Turkish Journal of Earth Sciences, 5(3), 171-185.

Taylor Perron, J., & Fagherazzi, S. (2012). The legacy of initial conditions in landscape evolution. Earth Surface Processes and Landforms, 37(1), 52-63.

Taylor, R. E. (1997). Radiocarbon dating. Springer US, 65-96.

Ten Veen, J. H., Boulton, S. J., & Alçiçek, M. C. (2009). From palaeotectonics to neotectonics in the Neotethys realm: The importance of kinematic decoupling and inherited structural grain in SW Anatolia (Turkey). Tectonophysics, 473(1), 261-281.

Tinkler, K. J., & Wohl, E. E., editors (1998). Rivers over rock: Fluvial processes in bedrock channels: American Geophysical Union Geophysical Monograph, 107, 323.

Tooth, S., Rodnight, H., Duller, G. A., McCarthy, T. S., Marren, P. M., & Brandt, D. (2007). Chronology and controls of avulsion along a mixed bedrock-alluvial river. Geological Society of America Bulletin, 119(3-4), 452-461.

Törnqvist, T. E. (1998). Longitudinal profile evolution of the Rhine-Meuse system during the last deglaciation: interplay of climate change and glacio-eustasy? TERRA NOVA-OXFORD-, 10, 11-15.

Törnqvist, T. E., Wallinga, J., Murray, A. S., De Wolf, H., Cleveringa, P., & De Gans, W. (2000). Response of the Rhine–Meuse system (west-central Netherlands) to the last Quaternary glacio-eustatic cycles: a first assessment. Global and Planetary Change, 27(1), 89-111.

Tucker, G. E. (2004). Drainage basin sensitivity to tectonic and climatic forcing: Implications of a stochastic model for the role of entrainment and erosion thresholds. Earth Surface Processes and Landforms, 29(2), 185-205.

Tucker, G. E., & Slingerland, R. L. (1994). Erosional dynamics, flexural isostasy, and long-lived escarpments: A numerical modeling study. Journal of Geophysical Research: Solid Earth (1978–2012), 99(B6), 12229-12243.

Tucker, G. E. & Bras, R. L. (1998). Hillslope processes, drainage density and landscape morphology. Water Resources Research, 34(10) 2751.

Tucker, G. E., & Whipple, K. X. (2002). Topographic outcomes predicted by stream erosion models: Sensitivity analysis and intermodel comparison. Journal of Geophysical Research, 107(B9), 2179.

Tucker, G. E., & Bras, R. L. (2000). A stochastic approach to modelling the role of rainfall variability in drainage basin evolution. Water Resources Research, 36(7), 1953-1964

Tucker, G., Lancaster, S., Gasparini, N., & Bras, R. (2001). The channel-hillslope integrated landscape development model (CHILD). In Landscape erosion and evolution modeling, Springer US. 349-388.

Tucker, G. E., & Hancock, G. R. (2010). Modelling landscape evolution. Earth Surface Processes and Landforms, 35(1), 28-50.

Turowski, J. M., Hovius, N., Wilson, A., & Horng, M. J. (2008). Hydraulic geometry, river sediment and the definition of bedrock channels.Geomorphology, 99(1), 26-38.

Turowski, J. M., & Rickenmann, D. (2009). Tools and cover effects in bedload transport observations in the Pitzbach, Austria. Earth Surface Processes and Landforms, 34(1), 26-37.

Twiss, R. J. (1992). Structural geology. W.H. Freeman, New York.

Vaks, A., Woodhead, J., Bar-Matthews, M., Ayalon, A., Cliff, R. A., Zilberman, T. & Frumkin, A. (2013). Pliocene–Pleistocene climate of the northern margin of Saharan–Arabian Desert recorded in speleothems from the Negev Desert, Israel. Earth and Planetary Science Letters, 368, 88-100.

Valla, P. G., Van Der Beek, P. A., & Lague, D. (2010). Fluvial incision into bedrock: Insights from morphometric analysis and numerical modeling of gorges incising glacial hanging valleys (Western Alps, France). Journal of Geophysical Research: Earth Surface (2003–2012), 115(F2).

Van De Wiel, M. J., Coulthard, T. J., Macklin, M. G., & Lewin, J. (2007). Embedding reach-scale fluvial dynamics within the CAESAR cellular automaton landscape evolution model. Geomorphology, 90(3), 283-301.

Van den Berg, M. W. (1996). Fluvial sequences of the Maas: Ph.D. dissertation, Landbouw universiteit.

Van den Berg, M. W. and Van Hoof, T. (2001) The Maas Terrace sequence at Maastricht, SE Netherlands; evidence for 200 m of late Neogene and Quaternary surface uplift in, Maddy, D., Macklin, M. G., Woodward, J. C., eds., River basin sediment systems; archives of environmental change: A.A. Balkema Publishers, Netherlands, 45-86.

Van den Berghe, J. & Maddy, D. (2001). The response of river systems to climate change.Quaternary International, 79, 1-121.

Van den Berghe, J. (2008). The fluvial cycle at cold–warm–cold transitions in lowland regions: a refinement of theory. Geomorphology, 98(3), 275-284.

Van Der Woerd, J., Klinger, Y., Sieh, K., Tapponnier, P., Ryerson, F. J., & Mériaux, A. S. (2006). Long-term slip rate of the southern San Andreas fault from 10Be-26Al surface exposure dating of an offset alluvial fan. Journal of Geophysical Research: Solid Earth (1978–2012), 111(B4).

Van Laningham, S, Meigs, A, Goldfinger, C, 2006. The effects of rock uplift and rock resistance on river morphology in a subduction zone forearc, Oregon, USA. Earth Surface Processes and Landforms, vol. 31, no. 10, pp. 1257-1279.

Van Raden, U. J., Colombaroli, D., Gilli, A., Schwander, J., Bernasconi, S. M., van Leeuwen, J., Leuenburger, M. & Eicher, U. (2013). High-resolution late-glacial chronology for the Gerzensee lake record (Switzerland): δ 18 O correlation between a Gerzensee-stack and NGRIP. Palaeogeography, Palaeoclimatology, Palaeoecology, 391, 13-24.

Viles, H., Goudie, A., Grab, S., & Lalley, J. (2011). The use of the Schmidt Hammer and Equotip for rock hardness assessment in geomorphology and heritage science: a comparative analysis. Earth Surface Processes and Landforms, 36(3), 320-333.

Von Blanckenburg, F. (2005). The control mechanisms of erosion and weathering at basin scale from cosmogenic nuclides in river sediment. Earth and Planetary Science Letters, 237(3), 462-479.

Wagner, G. A. (1998). Age Determination of Young Rocks and Artifacts: physical and chemical clocks in Quaternary geology and archaeology. Springer Science & Business Media.

Walker, R., & Jackson, J. (2002). Offset and evolution of the Gowk fault, SE Iran: a major intra-continental strike-slip system. Journal of Structural Geology,24(11), 1677-1698.

Wallace, R. E. (1984). Patterns and timing of late Quaternary faulting in the Great Basin province and relation to some regional tectonic features. Journal of Geophysical Research: Solid Earth (1978–2012), 89(B7), 5763-5769.

Wallace, R. E. (1988). Faulting related to the 1915 earthquakes in Pleasant Valley, Nevada. Volume 1274 of Geological Survey United States: Geological Survey professional paper. U.S. Government Printing Office.

Wallace, R. E., & Moxham, R. M. (1967). Use of infrared imagery in study of the San Andreas fault system, California. Geological Survey Research 1967, 147-156.

Wallinga, J. (2002a). Optically stimulated luminescence dating of fluvial deposits: a review. Boreas, 31(4), 303-322.

Wallinga, J. (2002b). On the detection of OSL age overestimation using single-aliquot techniques. Geochronometria, 21(1), 17-26.

Wallinga, J., Murray, A. S., Duller, G. A., & Törnqvist, T. E. (2001). Testing optically stimulated luminescence dating of sand-sized quartz and feldspar from fluvial deposits. Earth and Planetary Science Letters, 193(3), 617-630.

Wegmann, K. W., & Pazzaglia, F. J. (2002). Holocene strath terraces, climate change, and active tectonics: The Clearwater River basin, Olympic Peninsula, Washington State. Geological Society of America Bulletin, 114(6), 731-744.

Wegmann, K. W., & Pazzaglia, F. J. (2009). Late Quaternary fluvial terraces of the Romagna and Marche Apennines, Italy: Climatic, lithologic, and tectonic controls on terrace genesis in an active orogen. Quaternary Science Reviews,28(1), 137-165.

Wernicke, B., Axen, G. J., & Snow, J. K. (1988). Basin and Range extensional tectonics at the latitude of Las Vegas, Nevada. Geological Society of America Bulletin, 100(11), 1738-1757.

Westaway, R. (2004). Kinematic consistency between the Dead Sea Fault Zone and the Neogene and Quaternary left-lateral faulting in SE Turkey. Tectonophysics, 391(1), 203-237.

Westaway, R., Pringle, M., Yurtmen, S., Demir, T., Bridgland, D., Rowbotham, G., & Maddy, D. (2003). Pliocene and Quaternary surface uplift of western Turkey revealed by long-term river terrace sequences. Current Science Bangalore, 84(8), 1090-1101.

Westaway, R., Pringle, M., Yurtmen, S., Demir, T., Bridgland, D., Rowbotham, G., & Maddy, D. (2004). Pliocene and Quaternary regional uplift in western Turkey: the Gediz river terrace staircase and the volcanism at Kula.Tectonophysics, 391(1), 121-169.

Westaway, R., Guillou, H., Yurtmen, S., Beck, A., Bridgland, D., Demir, T., Scaillet, S., Rowbotham, G. (2006a). Late Cenozoic uplift of western Turkey: Improved dating of the Kula Quaternary volcanic field and numerical modelling of the Gediz river terrace staircase. Global and Planetary Change, 51(3), 131-171.

Westaway, R. C., Bridgland, D.R. & White, M.J. (2006b). The Quaternary uplift history of central southern England: evidence from the terraces of the Solent River system and nearby raised beaches. Quaternary Science Reviews 25(17-18), 2212-2250.

Westaway, R., Bridgland, D. R., Sinha, R., & Demir, T. (2009). Fluvial sequences as evidence for landscape and climatic evolution in the Late Cenozoic: a synthesis of data from IGCP 518. Global and Planetary Change,68(4), 237-253.

Whipple, K. X. (2004). Bedrock rivers and the geomorphology of active orogens. Annual Review of Earth and Planetary Sciences, 32, 151-185.

Whipple, K. X., & Tucker, G. E. (1999). Dynamics of the stream-power river incision model: Implications for height limits of mountain ranges, landscape response timescales, and research needs. Journal of Geophysical Research: Solid Earth (1978–2012), 104(B8), 17661-17674.

Whipple, K. X., Hancock, G. S., & Anderson, R. S. (2000a). River incision into bedrock: Mechanics and relative efficacy of plucking, abrasion, and cavitation.Geological Society of America Bulletin, 112(3), 490-503.

Whipple, K. X., Snyder, N. P., and Dollenmayer, K., (2000b), Rates and processes of bedrock incision by the Upper Ukak River since the 1912 Novarupta ash flow in the Valley of Ten Thousand Smokes, Alaska: Geology, 28, 835–838.

Whipple, K. X., & Tucker, G. E. (2002). Implications of sediment-flux-dependent river incision models for landscape evolution. Journal of Geophysical Research: Solid Earth (1978–2012), 107(B2), ETG-3.

Whittaker, A. C., (2007). Investigating controls on bedrock river incision using natural and laboratory experiments. P.hD. Theis, University of Edinburgh.

Whittaker, A. C. (2012). How do landscapes record tectonics and climate? Lithosphere, 4, 160-164.

Whittaker, A. C., Cowie, P. A., Attal, M., Tucker, G.E., Roberts, G.P. (2007a). Bedrock channel adjustments to tectonic forcing: Implications for predicting river incision rates. Geology, 35 (2), 103-106.

Whittaker, A. C., Cowie, P. A., Attal, M., Tucker, G. E., & Roberts, G. P. (2007b). Contrasting transient and steady-state rivers crossing active normal faults: New field observations from the Central Apennines, Italy. Basin Research, 19(4), 529-556.

Whittaker, A. C. & Boulton, S. J. (2012). Tectonic and climatic controls on knickpoint retreat rates and landscape response times. Journal of Geophysical Research,117.

Whittaker, A. C., Cowie, P.A., Attal, M., Tucker, G.E., Roberts, G.P. (2008). Decoding temporal and spatial patterns of fault uplift using transient river long profiles. Geomorphology,100, 506-526.

Whittaker, A. C., Attal, M., & Allen, P. A. (2010). Characterising the origin, nature and fate of sediment exported from catchments perturbed by active tectonics. Basin Research, 22(6), 809-828.

Whittaker, A. C., & Walker, A. S. (2014). Geomorphic constraints on fault throw rates and linkage times: Examples from the Northern Gulf of Evia, Greece.Journal of Geophysical Research: Earth Surface.

Willgoose, G. (2005). Mathematical modelling of whole landscape evolution.Annu. Rev. Earth Planet. Sci., 33, 443-459.

Willgoose, G., Bras, R. L., & Rodriguez-Iturbe, I. (1991). A coupled channel network growth and hillslope evolution model: 1. Theory. Water Resources Research, 27(7), 1671-1684.

Wintle, A. G., & Murray, A. S. (2006). A review of quartz optically stimulated luminescence characteristics and their relevance in single-aliquot regeneration dating protocols. Radiation Measurements, 41(4), 369-391.

Wohl, E. (2004). Limits of downstream hydraulic geometry. Geology, 32(10), 897-900.

Wohl, E., Kuzma, J. N., & Brown, N. E. (2004). Reach-scale channel geometry of a mountain river. Wohl, E., Kuzma, J. N., & Brown, N. E. (2004). Reach-scale channel geometry of a mountain river. Earth Surface Processes and Landforms, 29(8), 969-981.Earth Surface Processes and Landforms, 29(8), 969-981.

Wolkowinsky, A. J., & Granger, D. E. (2004). Early Pleistocene incision of the San Juan River, Utah, dated with 26Al and 10Be. Geology, 32(9), 749-752.

http://www.turkstat.gov.tr/ (2013) Address Based Population Registration System (ABPRS) Database. Turkish Statistical Institute.

Yazman, M. K., & Iztan, H. (1990). Alaşehir'in (Manisa) Jeolojisi ve Petrol Olanakları. TPAO Exploration Group, unpublished technical report, 18.

Yerli, B. (2005) Tectonics and Lithofacies of the Igneada Peninsula, Strandja Massif, NW Turkey. MSc-thesis, University of Bremen, Faculty of Geosciences.

Yilmaz, Y., Genç, Ş. C., Gürer, F., Bozcu, M., Yilmaz, K., Karacik, Z., Altunkaynal, Ş., & Elmas, A. (2000). When did the western Anatolian grabens begin to develop? Geological Society, London, Special Publications, 173(1), 353-384.

Yin, H., & Groshong Jr, R. H. (2007). A three-dimensional kinematic model for the deformation above an active diapir. AAPG bulletin, 91(3), 343-363.

Yilmaz, Y., & Avşar. (2013) Structural damages of the May 19, 2011, Kütahya–Simav earthquake in Turkey.Natural Hazards, 69 (1), 981-1001.

Zahno, C., Akçar, N., Yavuz, V., Kubik, P. W., & Schlüchter, C. (2009). Surface exposure dating of late Pleistocene glaciations at the Dedegöl Mountains (Lake Beyşehir, SW Turkey). Journal of Quaternary Science, 24(8), 1016-1028.

Zahno, C., Akçar, N., Yavuz, V., Kubik, P. W., & Schlüchter, C. (2010). Chronology of Late Pleistocene glacier variations at the Uludağ mountain, NW Turkey. Quaternary Science Reviews, 29(9), 1173-1187.

Zimmerman, D. W. (1971). Thermoluminescent dating using fine grains from pottery. Archaeometry, 13, 29-50.

Zreda, M., Zweck, C., & Sarikaya, M. A. (2006). Early Holocene glaciation in Turkey: large magnitude, fast deglaciation and possible NAO connection. In AGU Fall Meeting Abstracts 1, 1232.

Zreda, M., Çiner, A., Sarikaya, M. A., Zweck, C., & Bayarı, S. (2009). Remarkably extensive early Holocene glaciation in Turkey. Late Quaternary Glaciation and Paleoclimate of Turkey Inferred from Cosmogenic Chlorine-36 Dating of Moraines and Glacier Modeling, 136.

Zuchiewicz, W., Cuong, N. Q., Bluszcz, A., & Michalik, M. (2004). Quaternary sediments in the Dien Bien Phu fault zone, NW Vietnam: a record of young tectonic processes in the light of OSL-SAR dating results. Geomorphology,60(3), 269-302.